NCRP REPORT No. 144

RADIATION PROTECTION FOR PARTICLE ACCELERATOR FACILITIES

NCRP

National Council on Radiation Protection and Measurements

Radiation Protection for Particle Accelerator Facilities

Recommendations of the
NATIONAL COUNCIL ON RADIATION
PROTECTION AND MEASUREMENTS

Issued December 31, 2003
Revised March 4, 2005

National Council on Radiation Protection and Measurements
7910 Woodmont Avenue, Suite 400/Bethesda, Maryland 20814-3095

LEGAL NOTICE

This Report was prepared by the National Council on Radiation Protection and Measurements (NCRP). The Council strives to provide accurate, complete and useful information in its documents. However, neither the NCRP, the members of NCRP, other persons contributing to or assisting in the preparation of this Report, nor any person acting on the behalf of any of these parties: (a) makes any warranty or representation, express or implied, with respect to the accuracy, completeness or usefulness of the information contained in this Report, or that the use of any information, method or process disclosed in this Report may not infringe on privately owned rights; or (b) assumes any liability with respect to the use of, or for damages resulting from the use of any information, method or process disclosed in this Report, *under the Civil Rights Act of 1964, Section 701 et seq. as amended 42 U.S.C. Section 2000e et seq. (Title VII) or any other statutory or common law theory governing liability.*

Preface

The National Council on Radiation Protection and Measurements (NCRP) Report No. 51, *Radiation Protection Design Guidelines for 0.1–100 MeV Particle Accelerator Facilities*, was published in 1977. Since then, NCRP has issued two reports that discuss specific radiological protection issues at particle accelerators: NCRP Report No. 72, *Radiation Protection and Measurements for Low-Voltage Neutron Generators* and NCRP Report No. 79, *Neutron Contamination from Medical Electron Accelerators*. NCRP Report No. 88, *Radiation Alarms and Access Control Systems* is also of interest for those who operate accelerators, but until now, there has been no recent attempt to readdress the entire issue of accelerator radiological protection in a single report.

In light of the significant experience with the operation and design of accelerator facilities and the increased understanding of accelerator radiation environments obtained over the past 25 y, it was considered appropriate to revise NCRP Report No. 51 while maintaining its extremely valuable practical utility.

Accordingly, Scientific Committee 46-8 was established and given the general charge to "review and update Report No. 51 to include: new shielding data, extension of the energy range up to the giga-electron volt region, skyshine radiation, transmission of radiation through ducts and labyrinths, induced radioactivity, and environmental considerations such as radioactive airborne and liquid effluents."

Some of the material in this Report is historical and refers to studies performed many decades ago. In such cases, the quantities, units and references as formatted are retained in their original form.

Those who served on Scientific Committee 46-8 were:

Ralph H. Thomas, *Chairman*
University of California

Members

W. Robert Casey
Brookhaven National Laboratory
Upton, New York

J. Donald Cossairt
Fermi National Accelerator
  Laboratory
Batavia, Illinois

Keran O'Brien
Northern Arizona State
  University
Flagstaff, Arizona

Norman Rohrig
National Engineering and
  Environmental Laboratory
Idaho Falls, Idaho

Lester A. Slaback, Jr.
National Institute of
  Standards and Technology
Gaithersburg, Maryland

Geoffrey B. Stapleton
Thomas Jefferson National
  Accelerator Facility
Newport News, Virginia

William P. Swanson*
Lawrence Berkeley National
  Laboratory
Berkeley, California

Consultants

Lutz E. Moritz
TRIUMF, National Laboratory
  for Particle and Nuclear
  Physics
Vancouver, Canada

Vaclav Vylet
Duke University Medical
  Center
Durham, North Carolina

Advisor

David R. Perry
Rutherford Appleton Laboratory
Chilton, Oxon, United Kingdom

NCRP Secretariat

Constantine J. Maletskos, *Consultant* (1998–2003)
Thomas M. Koval, *Senior Staff Scientist* (1993–1998)
James A. Spahn, *Senior Staff Scientist* (1986–1993)
Cindy L. O'Brien, *Managing Editor*

The Council wishes to express its appreciation to the Committee members for the time and effort devoted to the preparation of this Report.

Thomas S. Tenforde
President

*deceased

Contents

Executive Summary

The National Council on Radiation Protection and Measurements (NCRP) Report No. 51, published in 1977 and entitled, *Radiation Protection Design Guidelines for 0.1–100 MeV Particle Accelerator Facilities*, was one of the first comprehensive treatments of accelerator radiological-protection concerns. The present Report is a substantial revision and expansion of that earlier report and includes new information on source intensities, shielding, dosimetry, and the environmental aspects of particle accelerator operation. It is primarily concerned with radiological safety aspects that are special to the operation of particle accelerators having energies above about 5 MeV up to the highest energies available, while not neglecting low-energy neutron generators.

The purpose of this Report is to provide design guidelines for radiation protection, and to identify those aspects of radiological safety that are of major, or even unique, importance to the operation of particle accelerator installations and to suggest methods by which safe operation may be achieved. The Report is written from an engineering physics viewpoint and is intended to be useful to those engaged in the design and operation of accelerators particularly in smaller institutions and organizations that do not have a large radiological-protection staff. Managers of institutional and industrial accelerator installations, health physicists, hospitals, radiological physicists, research scientists, government regulators, project engineers, and other similar specialists will also find the information contained in this Report useful.

Since 1977, NCRP has issued two reports that discuss specific radiological-protection issues at particle accelerators: NCRP Report No. 72, *Radiation Protection and Measurements for Low-Voltage Neutron Generators* and NCRP Report No. 79, *Neutron Contamination from Medical Electron Accelerators*. NCRP Report No. 88, *Radiation Alarms and Access Control Systems* is also of interest for those who operate accelerators. The International Atomic Energy Agency has issued three reports that specifically deal with the radiological safety aspects of the operation of low-energy neutron generators, electron linear accelerators, and proton accelerators. In 1988, the U.S. Department of Energy issued its *Health Physics Manual for Good Practices for Accelerator Facilities*. In 1990, the European

1

Organisation for Nuclear Research (CERN) published a comprehensive volume on shielding against high-energy radiation. One aim of this Report was to revise NCRP Report No. 51 in such a way that access to much of this new material was brought together in one volume.

The first of this Report's seven sections provides a general introduction, sets out the scope of the Report, and provides information on radiological-protection standards, and international, national and state regulatory agencies.

The second section of the Report, Particle Accelerators and Accelerator Facilities, defines and classifies particle accelerators by their functional and radiological characteristics. A brief historical review of accelerator development is followed by a discussion of the ionizing radiation produced by the separate components of accelerator systems. The special problems of ion sources, radiofrequency (RF) systems, beam-handling systems, beam stops and auxiliary systems, such as high-voltage and microwave power supplies, and cooling and vacuum systems are briefly described. Guidance for the siting and layout of accelerator facilities is provided.

Section 3, entitled The Sources of Ionizing Radiations from Accelerators, provides a fundamental overview of the production of ionizing radiations by accelerated particles. After a brief review of the basic atomic and nuclear-physics concepts, the radiations produced by energetic electrons, protons and ions are separately described. Radiation yield data are presented in analytical and graphical form. The Section ends with a discussion of the production of radioactivity in materials. Bremsstrahlung yields, including angular distribution data, from thick and thin targets bombarded by electrons from the lowest energies up to the giga-electron volt region are given. Similar data are given for neutron production. Muon yields, important at the higher energies, are briefly discussed. The electron subsection ends with a description of the transport of the initial particle energy *via* the electromagnetic cascade. At energies above ~10 MeV, neutrons usually present the dominant source of occupational radiation exposure at proton accelerators. Neutron yields and angular distribution data for materials bombarded by proton beams are provided from the lowest energies up to the multi-giga-electron volt energy region, usually in graphical form. For proton energies above ~10 GeV muon production becomes important and is discussed. Muon range-energy data are given. The degradation of the primary proton energy *via* the hadronic cascade is described and the radiation environment outside the shield of high-energy proton accelerators, particularly neutron spectra, is discussed. Neutron yields for ions

of energies up to ~100 MeV amu^{-1} are provided for a variety of targets and ions.

Section 4 is entitled Radiation Shielding at Accelerators and provides a description of shielding of electron, proton and ion accelerators up to the multi-giga-electron volt energy region. A special section is devoted to synchrotron radiation facilities. Theoretical and experimental aspects of shield design are discussed. Information is given on the properties of shielding materials. The efficient design of penetrations through shielding and the design of shield doors are also described. Specimen shield calculations are provided.

Section 5 is entitled Special Techniques of Radiation Measurement at Particle Accelerators. Personal and environmental monitoring, as well as field surveys are discussed. After a preliminary review of the purposes for which accelerator-radiation measurements are made and the quantities in which these measurements are expressed, radiation detectors are classified as *active (real time)*, *e.g.*, Geiger-Mueller (GM) counters, proportional counters, fission chambers, counter telescopes; and *passive*, *e.g.*, thermoluminescence dosimeters (TLD), nuclear emulsions, track-etch techniques, bubble dosimeters, and activation measurements. The special problems of operating active real-time detectors in the pulsed radiation fields of accelerators are discussed. Above primary energies of a few mega-electron volts the radiation environments of electron, proton and ion accelerators are of a "mixed" character, consisting primarily of photons and neutrons. At the highest energies neutrons are often the most significant component of the radiation environment and much attention is, therefore, given to neutron detection techniques. The determination of neutron spectra from field survey data is described.

The environmental impact of the operation of particle accelerators is discussed in detail in Section 6, Environmental Radiological Aspects of Particle Accelerators, and includes descriptions of skyshine and the production of radioactivity. The mechanisms of the transport of prompt radiation to distances far from the accelerator, generally known as skyshine, are described for both photons and neutrons. Simple examples of the calculation of appropriate overhead shielding to reduce radiation intensities due to skyshine are provided. Second only to skyshine, but several times smaller in magnitude, the potential for the exposure of members of the public to radioactivity produced by accelerator operation is an important concern. Exposure to the public to accelerator produced radioactivity might result from three pathways: air activation, groundwater activation, and radioactive accelerator components. The mechanisms for the production and migration of radionuclides are described in detail. Illustrative data tables and calculations are provided. Methods of evaluating estimates

of the population collective dose equivalent from these potential sources of exposure are given. Finally, in this Section, there is a brief discussion of the production of nonradioactive toxic gases, such as ozone, and the oxides of nitrogen.

The seventh and final section outlines the basic needs for an Operational Radiation Safety Program for Accelerators. Much of the safety program includes elements common to other radiological installations and this Section draws attention only to those special elements required at accelerators. For example, the conflicts between the requirements for easy access and the need to limit radiation leakage through the external shielding are discussed. Differences between the types of radionuclides produced at accelerators (more positron emitters) compared with nuclear reactors and their spatial distribution in surrounding materials, are described. Contamination control requires radiation detection techniques capable of detecting positron and low-energy beta emitters.

The Report has two appendices, the first tabulating importance functions for both neutrons and photons, the second giving tabulations of kinematic data for electrons, muons, kaons, protons, deuterons and selected heavier particles up to ^{238}U. Finally, a detailed Glossary and a comprehensive list of references are provided.

Some of the material in this Report is historical and refers to studies made many decades ago. In such cases, the then contemporary quantities, units and references as formatted are retained. Some of the figures reproduced from older references are somewhat impaired in quality.

1. Introduction

Accelerators, first designed and constructed as research instruments, have now entered the very fabric of our life. In addition to their continued application to fundamental research in cosmology and particle physics, they are now widely applied in, *e.g.*, medicine (diagnosis, therapy, radiopharmaceutical production), materials science and solid-state physics (ion implantation, radiation damage studies, microlithography), polymerization of plastics, sterilization of toxic biological wastes, and food preservation.

In the future, accelerators and accelerator-like devices may be used to generate energy by nuclear fusion, to incinerate radioactive waste to produce fissionable material for use in energy production, and in plasma heating (Barbalat, 1991; Thomas, 1992). Particle accelerators, then, will continue to be designed, constructed and operated for the foreseeable future. The radiological protection aspects of these facilities are extremely important aspects of their design and it is, therefore, appropriate that a volume such as this address these issues.

NCRP Report No. 51, *Radiation Protection Design Guidelines for 0.1 − 100 MeV Particle Accelerator Facilities* (NCRP, 1977), was one of the first comprehensive treatments of accelerator radiological protection concerns. The present Report is both a substantial revision and expansion of that earlier report, including new information on source intensities, shielding, dosimetry and environmental aspects of accelerator operation.

The radiological aspects of accelerators encompass most of the issues found in the entire discipline of health physics. In fact, there is a strong case to be made that radiological protection began at accelerator laboratories. Since the time of Thomson's cathode ray tube, circa 1894 (Thomson, 1897) and the discovery of Roentgen rays in 1895 (Roentgen, 1895), accelerators have been associated with many of the major discoveries in radiological protection. Accelerators were the first to produce the symptoms of the acute radiation syndrome, induced radioactivity (although not properly understood at the time), radiopharmaceuticals, transuranic elements, and tritium. It was by an instrument based on accelerator technology, the calutron, that fissile and fissionable materials were first made in substantial quantities. It was at an accelerator laboratory that the first

5

studies of the radiotoxicity of alpha-emitting transuranic elements were made.

Although the radiological aspects of accelerators encompass nearly all those issues found in the entire discipline of health physics, in some respects the discipline is unique. It is at accelerators "that the science and technology of radiation (protection) dosimetry are at their most sophisticated. In only one other class of radiation environments, those met in extraterrestrial exploration, do such novel and diverse dosimetric challenges need to be faced. Even here the dosimetrist does not encounter the range of particle intensities, variety of radiation environments, or pulsed characteristics of radiation fields" (Swanson and Thomas, 1990).

1.1 Purpose

The purpose of this Report is to provide design guidelines for radiation protection, and to delineate those aspects of radiological safety that are of major, or even unique, importance in the operation of particle-accelerator installations and to suggest methods by which safe operation may be achieved. The Report is intended to assist as a guide, both, to the planning and operation of all types of accelerators above an energy of a few mega-electron volts.

1.2 Scope

The Report is written from an engineering physics viewpoint. It should prove useful to those engaged in the design and operation of accelerators, particularly in smaller institutions and organizations that do not have a large radiological protection staff. Managers of institutional and industrial accelerator installations, health physicists, hospital physicists, radiological physicists, research scientists, government regulators, project engineers, and other similar specialists will also find the information contained in this Report useful.

This Report defines a particle accelerator as a device that imparts sufficient kinetic energy to charged particles to initiate nuclear reactions. Therefore, the Report is concerned with the radiological safety of accelerators of energy above ~5 MeV. The choice of this low-energy cutoff is somewhat arbitrary but was determined on the following basis: charged particles with an energy between 5 and 10 MeV can produce neutrons through nuclear interactions, with the concomitant induction of radioactivity in accelerator structures

and components. An exception to the 5 MeV lower limit, but included in this Report, are D-D and D-T devices and the use of low-mass-number targets such as lithium and beryllium. In such cases, charged particles with energies lower than 5 MeV may produce neutrons. It was decided to have no upper-energy cutoff. The very highest-energy accelerators in operation, or even being planned at the present time, have radiation environments that have many features in common with those of low-energy accelerators.

Some of the material in this Report is historical and refers to studies made many decades ago. In such cases, the then contemporary quantities, units and references as formatted are retained. Some of the figures reproduced from older references are somewhat impaired in quality.

1.3 Particle Accelerator Safety

It is important to emphasize that particle-accelerator radiological safety has much in common with other broad and diverse radiological safety programs. The primary difference lies in the complex nature of the particle-accelerator-radiation source term, particularly in the pulsed and unusual nature of the radiation fields. This Report stresses these essential differences beginning with general introductory material and comprises seven sections, two appendices, and a bibliography. The Report begins with a review of the diverse nature of accelerators and accelerator facilities in Section 2. A comprehensive accelerator radiological safety program consists of characterization of prompt and residual radiation fields (Section 3), shielding of these sources (Section 4), radiation monitoring (Section 5), determination of any environmental impact (Section 6), and other specific operational radiation requirements of accelerator facilities (Section 7).

1.4 Regulatory and Advisory Agencies

In the United States, the regulation of the manufacture, distribution and operation of particle accelerators in a manner that does not jeopardize public health and safety is a complex matter shared by several government agencies. What follows is intended only as a rough guide. Because the specific authority of regulatory agencies and their regulations that are ever-changing, it is most important that current information be obtained.

1.4.1 *Federal Regulation*

The U.S. Food and Drug Administration has the statutory authority to adopt performance standards for accelerators under the provision of the Radiation Control for Health and Safety Act of 1968 (RCHSA, 1968).

The U.S. Department of Energy exercises statutory authority for the radiological safety (and often for most matters of environmental protection, safety and health) of particle accelerators under its jurisdiction by way of specific contractual requirements (Casey *et al*., 1988) and the requirements of the orders it issues (DOE, 1992; 1993; 1994).

The U.S. Environmental Protection Agency (EPA) has the responsibility to develop guidance on radiological protection for all federal agencies. Such guidance is normally, although not necessarily, based on recommendations of the International Commission on Radiological Protection (ICRP) and NCRP. After Presidential approval, EPA guidance is implemented in the regulations of all federal agencies.

In addition to its statutory responsibility to provide guidance on radiological protection, EPA has several other responsibilities and authorities regarding the regulation of radiation exposures. Under authority of the Clean Air Act (CAA, 1963), radioactive emissions into the air are limited. Similarly, under the authority of the Safe Drinking Water Act (SDWA, 1974), EPA has set standards for the control of radioactive contaminants in community water systems (EPA 1976; 1989a; 1989b).

In implementing many of its regulations, EPA can defer to the separate states. Thus, for example, in its requirements for the establishment of water quality standards, EPA requires that states "develop and adopt a statewide anti-degradation policy and identify the methods for implementation of such a policy . . ." (EPA, 1987a; 1987b; 1987c). General guidelines for minimum compliance are given, but individual states may adopt more restrictive policies.

There is a complex interrelationship of regulations between several agencies of both the federal government and the separate states. This interrelationship, besides being complex, is fluid and always subject to change. As will be discussed in Section 6, these environmental regulations influence the design of new accelerators.

1.4.2 *State Regulation*

Uniformity between the regulations of the separate states is encouraged by the Conference of Radiation Control Program Directors,

Inc. This organization has published a *Suggested State Regulations for Control of Radiation* (CRCPD, 1991) which includes model regulations for accelerators. It is important to consider the specific uses of particle accelerators, particularly those used in research, when writing such regulations.

1.4.3 *Local (County, City) Regulation*

Local authorities may choose to adopt more restrictive policies than those of either the state or the federal government, particularly in the area of environmental regulations. It is most important to seek out current information when accelerator installations are planned.

1.4.4 *Advisory Organizations*

In addition to the regulatory agencies, there are a substantial number of organizations that offer advice which is important for the operation of particle accelerators. Several of these are listed below.

1.4.4.1 *International Agencies.* At the international level, three organizations are extremely important: the International Atomic Energy Agency (IAEA), International Commission on Radiological Protection (ICRP), and the International Commission on Radiation Units and Measurements (ICRU).

IAEA has issued three reports which deal with the radiological safety operations of electron accelerators, neutron generators, and proton accelerators (IAEA, 1976; 1979a; 1988).

ICRP, in addition to its basic recommendations on radiological protection (ICRP, 1977; 1991), has issued Publication 75, *General Principles for the Radiation Protection of Workers* (ICRP, 1997a) and Publication 76, *Protection from Potential Exposures: Application to Selected Radiation Sources* (ICRP, 1997b). Both publications contain concepts that are very useful for the design of accelerator facilities. A joint ICRP and ICRU report has been issued under the title *Conversion Coefficients for Use in Radiological Protection Against External Radiation* (ICRP, 1996; ICRU, 1998a). This Report contains particle fluence-to-dose-equivalent conversion coefficients of great utility in radiation dosimetry.

ICRU has issued Report 28, *Basic Aspects of High-Energy Particle Interactions and Radiation Dosimetry* (ICRU, 1978) and Report 46, *Photon, Electron, Proton and Neutron Interaction Data for Body Tissues* (ICRU, 1992a). Other reports of interest to accelerator radiological protection include Report 25, *Conceptual Basis for the*

Determination of Dose Equivalent (ICRU, 1976a); Report 47, *Measurement of Dose Equivalents from External Photon and Electron Radiations* (ICRU, 1992b); Report 51, *Quantities and Units in Radiation Protection Dosimetry* (ICRU, 1993a); Report 60, *Fundamental Quantities and Units for Ionizing Radiation* (ICRU, 1998b); and Report 40, *The Quality Factor in Radiation Protection* (ICRU, 1986). Two reports defining the operational dose-equivalent quantities, the ambient and directional dose equivalents, are also of interest for accelerator-radiation dosimetry (ICRU, 1985; 1988).

1.4.4.2 *National Organizations.*   There are also a number of national organizations that have issued reports relevant to accelerator facilities. These include the American National Standards Institute, the American Society for Testing Materials, the Institute of Electrical and Electronic Engineers, the American Nuclear Society, and the American Association of Physicists in Medicine (AAPM). AAPM Report No. 16 and No. 19 are particularly helpful (AAPM, 1986a; 1986b). NCRP also has prepared other reports that should be considered by operators of accelerator facilities [*e.g.*, NCRP Report No. 49, No. 51, No. 72, No. 79, No. 88, No. 102, No. 116, and No. 127 (NCRP, 1976a; 1977; 1983; 1984; 1986; 1989; 1993; 1998)].

1.5   Radiological Protection Standards

The basic considerations of radiation protection were stated by ICRP in Publication 26, and reiterated in Publication 60 (ICRP, 1977; 1991). ICRP Publication 26 recommended a system of dose limitation that has three interrelated components:

- justification—no practice shall be adopted unless its introduction produces a positive net benefit
- optimization (ALARA)—all exposures shall be kept as low as reasonably achievable, economic and social factors being taken into account
- compliance with dose limits—the dose equivalent to individuals shall not exceed the appropriate limits recommended by ICRP

When the processes of justification and optimization have been implemented to demonstrate that there is a net benefit from the use of ionizing radiation and that the protection has been optimized, the individual doses that result from the operation must be compared with the appropriate dose limits to ensure that no unacceptable doses occur. The present dose limits recommended by NCRP for

different segments of the population are listed in NCRP Report No. 116, *Limitation of Exposure to Ionizing Radiation* (NCRP, 1993).

When ICRP, in its Publication 26 (ICRP, 1977), presented new radiation protection recommendations, the whole philosophy of radiation protection changed in emphasis from one of *maximum permissible* to one of *as low as reasonably achievable* (ALARA) below an administratively or legally prescribed limit. The limit is to be considered as a legally acceptable ceiling above which there may be a penalty, but management must review operations to maintain radiation exposures ALARA below the limit. The degree attainable below the limit is a judgment based on many factors that can be different for the same situation at different organizations.

ICRP Publication 60, *1990 Recommendations of the International Commission on Radiological Protection* (ICRP, 1991) states in Paragraph S26: "Subject to medical advice in individual cases, there need be no special restrictions applied to the exposure of an individual following a control period in which the exposure of the individual has exceeded a dose limit. Such events should call for a thorough examination, usually by the regulatory agency, of the design and operational aspects of protection in the installation concerned, rather than for restrictions or penalties applied to the exposed individual."

It is clear from the above that both ICRP and NCRP consider control of exposure at the source and not at the individual to be most important. This is particularly true in the design of a new facility. For example, the dose criteria for shielding design in a new facility should be placed at a small fraction of the dose limit. For facilities already in operation, the inclusion of additional shielding or other methods for controlling the source will fall under the "as reasonable achievable" portion of the ALARA principle. For a more complete discussion of the ALARA principle, the reader is referred to various publications of ICRP and NCRP.

Terms used in the Report are defined in the Glossary. Because, however, recommendations throughout the Report are expressed in terms of *shall* and *should*, the use of these terms is also explained here:

- *shall* indicates a recommendation that is necessary to meet the currently accepted standards of radiation protection
- *should* indicates an advisory recommendation that is to be applied when practicable

2. Particle Accelerators and Accelerator Facilities

2.1 Particle Accelerators—Definitions

A review of the scientific literature suggests that there is no adequate definition of the term "*particle accelerator*." Many of the so-called definitions are tautological; many others are specific descriptions of particular instruments (Flugge, 1959). There is even uncertainty as to whether particle accelerators are "apparatuses," "instruments," "devices" or "machines."

One of the most apt definitions has been given by Persico *et al*. (1968): "Particle accelerators are machines built with the aim of accelerating charged particles to kinetic energies sufficiently high that they can be used to produce nuclear reactions."

This definition includes the particle accelerators discussed in this Report but it is incomplete because it excludes those particle accelerators not capable of producing charged particles with sufficient energy to produce nuclear reactions, and neither does it include those accelerators not specifically designed to produce nuclear reactions that, nevertheless, do so as an inevitable consequence of their operation, *e.g*., synchrotron-light sources. Furthermore, scholars would properly insist that x-ray tubes are particle accelerators, as are many other instruments utilizing high voltages and evacuated accelerating tubes (Thomas, 1992). All accelerators of energy below ~5 MeV that generate neutrons are included within the general purview of this Report.

2.2 Classification of Particle Accelerators

There are many parameters by which particle accelerators may be classified. For example, they may be classified in terms of the technology by which acceleration is achieved, such as power source

12

or acceleration path geometry (Table 2.1). Also, they may be classified by their application (Table 2.2), but the classifications of greatest relevance in radiological physics are the types of particles accelerated, the maximal energy, the maximal intensity, the duty factor of the accelerated particle beams, and the types of media in the vicinity of locations struck by the beams (Swanson and Thomas, 1990).

2.3   Brief Historical Review

The earliest scientific instruments which technically may be classified as accelerators, such as the Crooke's tube and the x-ray tube which accelerated electrons to several thousand or several tens-of-thousand electron volts were invented at the latter end of the nineteenth century. However, it was not until nearly 30 y later,

TABLE 2.1—*Particle accelerators classi ed by technology.*

Direct (potential-drop) accelerators
   [single stage for acceleration of either ions or electrons; two stage (tandem) for acceleration of ions]

Electrostatic high-voltage generators:
   Belt-charging system (*e.g.*, Van de Graaff, Peletron)
   Rotating-cylinder charging system

High-voltage transformers:
   Transformer-rectifier set (*e.g.*, Cockcroft-Walton, dynamitron)
   Voltage-multiplying system (*e.g.*, insulating-core transformer)
   Cascaded-transformer system

Indirect (RF, plasma) accelerators

Linear-beam trajectory:
   Radiofrequency quadrupole
   Ion linear accelerator
   Electron linear accelerator

Circular- or spiral-beam trajectory:
   Cyclotron (ions only)
   Synchrotron (ions or electrons)
   Betatron (electrons only)
   Microtron (electrons only)

Combined/complex accelerators:
   Race track microtron (electrons only)
   Colliding beam, storage rings

TABLE 2.2—*Accelerator-produced radiation classified by routine application.*[a]

	Electron	X ray	Ion	Neutron
Diagnostic radiology		*		
Radiotherapy	*	*	*	*
Industrial radiography		*		*
Analysis of materials				
Activation analysis			*	*
Microscopy, electron or ion	*		*	
X-ray fluorescence analysis	*	*	*	
Geological well-logging	*	*		*
Neutron scattering			*	*
Synchrotron light sources	*	*		
Ion separation			*	
Ion implantation, polishing			*	
Surface conditioning, roughening	*	*		
Radioisotope production			*	*
Radiation processing	*	*		
Radiation sterilization	*	*		
Research and training				
Nuclear structure physics	*	*	*	*
Neutron physics	*	*	*	*
Atomic and solid state physics	*	*	*	*
Biology, chemistry	*	*	*	*
Radiation effects on materials	*	*	*	*
Particle physics	*		*	*

[a] Augmented and adapted from NCRP Report No. 51 which summarized applications of particle accelerators in the energy range 0.1 to 100 MeV (NCRP, 1977).

towards the end of the 1920s, that particle accelerators, as we now know them, were invented.

The year 1932 is usually attributed to the invention of modern accelerators. In that year, both Cockcroft and Walton (1932a; 1932b; 1934) at Cambridge, and Lawrence and his colleagues at Berkeley (Lawrence and Livingston, 1932; Lawrence *et al.*, 1932), independently designed, constructed and operated particle accelerators as research instruments to investigate nuclear structure. However, as with most inventions, there was considerable technological

development that preceded this event, and it is not truly possible to identify any particular year which uniquely defines the creation of such accelerators.

Since the development of the engineering principles of particle accelerators towards the end of the 1920s and their practical realization in the early 1930s, there has been a steady increase in both the energy and intensity of particles accelerated. In 1962, Livingston and Blewitt presented a series of graphs showing the energies achieved by several types of particle accelerators plotted against the year in which the energy was first obtained. They concluded that "An envelope enclosing all the curves shows a tenfold increase every six to seven years" (Livingston and Blewett, 1962). Some 20 y later, Panofsky confirmed their general conclusions and his revised version of the "Livingston plot" is shown in Figure 2.1 (Panofsky, 1980). Five distinct phases of particle accelerator development have been recognized (IAEA, 1988: Livingston, 1966):

- direct voltage acceleration
- resonant acceleration
- synchronous acceleration
- alternate gradient focusing
- colliding beam technology

It is not our purpose here to give a detailed review of the history of development of particle accelerators. That has been done with great thoroughness elsewhere, and the interested reader is referred to the literature. Comprehensive bibliographies may be found in IAEA (1988) and Livingston (1966).

Medical electron accelerators are described by Karzmark *et al*. (1993). This book includes chapters on microwave structures and power sources, modulators and beam optics. It contains detailed discussions on beam monitoring, controls and interlocks, as well as on facility design.

Particle accelerators operating at energies above 100 MeV are generally synchrotrons, cyclotrons, or linear accelerators. Information on the design and operation of high-energy particle accelerators may be found in a variety of excellent texts, including Lapostolle and Septier (1970) and Livingood (1961). Machine development is set forth in international conference proceedings (CERN, 1971; FNAL, 1983a) and summer schools organized by CERN (1977; 1985), and the Fermi National Accelerator Laboratory (FNAL, 1982; 1983a; 1983b; 1985). A complementary series of proceedings was sponsored by the Institute of Electrical and Electronic Engineers (IEEE, 1975; 1977; 1979; 1981; 1983; 1985). An overview is also given by Lawson and Tigner (1984).
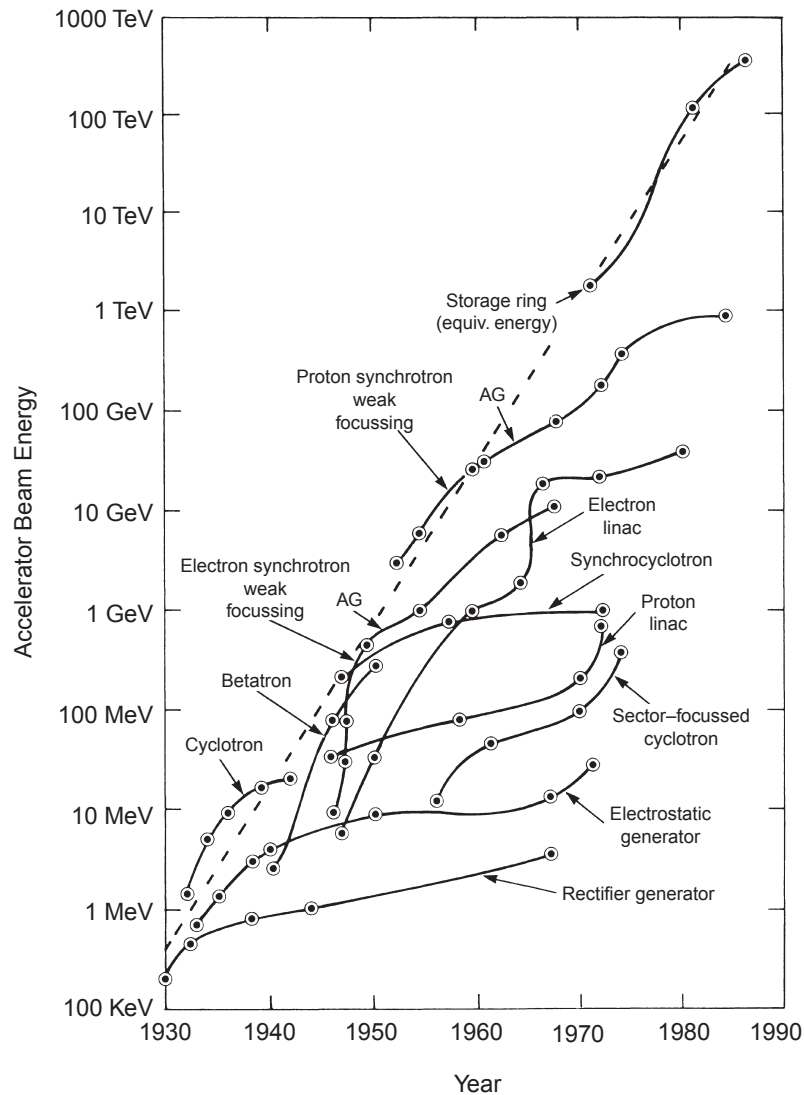
Fig. 2.1. A revised version of the "Livingston plot," first prepared in 1962 (Livingston and Blewett, 1962), in which the maximum particle energy achieved in the laboratory is shown, plotted against the date of attainment. The dashed line shows that about every 7 y, an increase of a factor of 10 in energy has been obtained. Thus far, new technologies have appeared when previous technologies appear to have saturated (Panofsky, 1980).

The development of superconducting materials was an important innovation, and these materials were quickly applied in magnet windings and for RF accelerating cavities. The use of superconducting systems has made possible the construction of ever-larger facilities, greatly extending the upper energy limit. Examples of accelerators utilizing "state-of-the-art" superconducting technology are the Tevatron in operation at FNAL (Edwards, 1985), the Continuous Electron Beam Accelerator Facility at the Thomas Jefferson National Accelerator Facility, Newport News, Virginia (CEBAF, 1986), and the Superconducting Super Collider which was proposed but never constructed (DOE, 1984; SSC, 1986). The concept of continuous wave acceleration has been successfully realized in a number of facilities using both superconducting and normally conducting technology (Herminghaus, 1984). The 100 percent duty factor[1] of such facilities eliminates the gross pulsed structure of the radiation that usually needs to be considered, although, the dosimetrist must be aware of the RF micropulse structure which is present on all continuous wave machines.

Recent decades have been marked by steady development in particle-physics research toward higher energies, higher intensities, and larger duty factors. At present, there is a vigorous accelerator construction program around the world, and several technological advances, especially in superconductivity, make for growth in both complexity and reliability of particle accelerators. Steady progress and expansion of their capabilities and applications are clearly characteristic of the types of high-energy facilities addressed in this Section, as well as the new technologies and applications of low-energy accelerators (Scharf, 1986). The recent trend has been to develop the capability of colliding particle beams. This has the advantage of making the full accelerated energy available in the reaction center-of-mass system in studying particle-to-particle collisions.

One of the consequences of all these developments has been the ability to manufacture reliable and economic accelerators in the low-energy range, which have a variety of applications in industry and medicine. Such accelerators comprise the majority of accelerators in current operation.

2.4 Accelerator Radiation

Particle accelerators use electromagnetic forces to place particles in a chosen region of phase space, where phase space in this context

---

[1]Duty factor is defined as the percentage of the total time that beam is actually delivered. For example, a beam that is on for 1 ms of each second of operation has a duty factor of 0.1 percent. Within the "beam-on time," the beam may have a time structure, *e.g.*, consisting of a string of pulses uniformly spaced in time, but this microstructure is not considered in determining the duty factor.

is a particular energy or range of energies at a specified location moving in a desired direction. None of the various means engineered to accomplish this goal do so perfectly. For example, particle types other than those required may be accelerated, arriving at other locations with other energies; not all the chosen particles will gain the chosen energies or arrive at the desired location and travel in the desired direction; and particles arriving at the wrong region of phase space may present a radiation hazard. These stray particles may also generate secondary radiations by collisions with the materials that make up the accelerator hardware and its surroundings and, at the same time, make these materials radioactive (Section 7). Both the secondary radiations and the radioactivity so generated, as well as the primary beam, can result in radiation hazards. Accelerator personnel and the general public must be protected from these radiations, both stray and direct, and one of the chief means of doing so is to interpose sufficient shielding between the sources of radiation and the occupied environment (Sections 4 and 6). In order to provide adequate protection, it is necessary to understand the various potential sources of ionizing radiations associated with particle accelerator configurations.

Particle accelerators often comprise several smaller accelerators. For the purpose of describing their radiological properties or subsystems, it is convenient to regard the accelerator as separated into several compartments: the ion or electron source, the accelerator structure, beam-delivery systems, user facilities, beam stops, and, finally, auxiliary systems (*e.g.*, cooling system, vacuum system, RF, and high-voltage power-delivery systems).

Substantial shielding is often required around the beam-delivery systems, user facilities, and beam stops, as well as around the accelerator itself. Depending on the intensity of the accelerated beam and the extent of beam losses, it may be also necessary to provide shielding for some or all of the subsystems given in the previous paragraph (Table 2.3).

2.5 Ion and Electron Sources

At all accelerators, the source of the accelerated beam consists of a device producing ions combined with a beam-forming and pre-acceleration apparatus, often referred to as the *pre-injector* or the *injector*, depending on the complexity of the accelerator system. In the simplest electron accelerators, the injector may be nothing more than a pulsed or time-gated heated filament. In the case of the

TABLE 2.3—*Potential for radiation exposure from particle accelerator component systems.*

	Particles Accelerated					
	Electron Energy (MeV)			Proton, Heavy Ion Energy (MeV)		
	10–100	100–1,000	>1,000	<10	10–100	>100
Ion source	low	mod.	mod.	low	low	mod.
Accelerator	mod.	mod.	high	low	mod.	high
Beam delivery	high	high	high	mod.	mod.	high
Target/user	high	high	high	mod.	high	high
Beam stop	mod.	high	high	mod.	high	high

simplest positive ion accelerators, the injector is a gas plasma with an extraction device. RF radiation is commonly used to ionize the gas in the ion source and may cause interference in instruments used in ionizing-radiation surveys. High-power ion sources are often complex systems presenting special problems such as, heat dissipation, maintenance, and possible x-ray production.

If the output energy of the ion source is less than several mega-electron volts, radiological protection concerns are usually minimal and often limited to the control of occupancy of certain areas during accelerator operation. Electron sources are, in essence, high-power triode vacuum tubes. As such, these tubes and the rest of the pre-injector primarily represent an x-ray hazard. Proton and heavy particle accelerators generally use an ionized gas as an ion source. Where such sources incorporate high voltages for extraction, back-streaming electrons can similarly present x-ray risks. In the case of accelerators, electrons may coincidentally be extracted from the ion source at substantial energy (a few 100 keV) and result in significant x-ray sources.

Photocathode RF guns can present particular safety challenges. These guns achieve a "super-charged" state in which currents can be generated in high RF field gradients after the last pulse is extinct. In this state, the gun output can be much higher than in normal operation.

Most high-energy accelerators ($E > 200$ MeV) use a lower-energy accelerator as a source of beam. In this instance, the injector should generally be evaluated as a separate device.

2.6 Particle Accelerating Schemes

There is a wide variety of acceleration schemes that differ in the nature of the field-particle interaction that is in use. These differ

more in terms of the method of delivering energy to the particle than by type of particle accelerated. Cyclotrons are the major exception to this generalization in that they accelerate only heavy particles. However, these acceleration schemes have only a second-order influence on radiation-protection programs that are most strongly influenced by particle type accelerated, energy and current.

The requirement to transfer megawatts of energy in a very short distance controls the design of these structures: typical voltage gradients for electron accelerators are $\sim$5 to 10 MV m^{-1}, but at accelerators used for research the gradients may be much higher. Waveguides and other power systems now are achieving gradients in excess of 50 MV m^{-1}. The radiological protection implications of the various structures lie in the quality of the beam produced in terms of energy and spatial definition. All accelerating systems represent a compromise between beam quality and the ability to deliver high current or energy. Accelerator technology is extremely volatile; new concepts and technologies are constantly being developed permitting both improved beam definition and higher beam currents (Lawson and Tigner, 1984; Sessler, 1988).

Electrostatic and high-voltage transformers, although economical, tend to have the poorest energy and spatial definition and are also limited to energies below $\sim$10 MeV, or in the case of tandem Van de Graaff accelerators, below $\sim$50 MeV. The stray radiations from these are bremsstrahlung from parasitically accelerated electrons and, in the case of positive-ion accelerators, back-streaming electrons. Neutrons may be produced unintentionally. Radiation levels from the accelerating structures can be greater than 10 mSv h^{-1}.

The beam definition produced by linear and cyclic accelerators is improved over that produced by the simple potential drop accelerators. Linear accelerators generally are capable of higher currents than are cyclic accelerators, *i.e.*, higher power for the same energy capability. Differences in accelerating structures because of particle types are seen primarily in the indirect accelerator types. Electrons reach relativistic velocities, (*i.e.*, nearly a constant velocity), at much lower energies than do protons and heavier particles. Consequently, for a given accelerator type, the accelerating structure can be simpler than that for protons. In an electron linear accelerator, all the accelerating sections beyond the first can be identical while those of proton and heavier particle accelerators must differ in physical dimensions in order to account for the changing velocity of the particle.

Cyclic accelerators are designed in a variety of ways (Table 2.4). Mixtures of the linear and cyclic configurations are commonplace, *e.g.*, where a linear accelerator is used as an injector for a cyclic accelerator or where a linear accelerator is the acceleration leg

TABLE 2.4—*Characteristics of cyclic accelerators.*

Accelerator	Particles Accelerated	Orbit Radius	RF	Magnetic Field	Output	Energy Limit	Reason for Limit
Betatron	Electrons	Constant	Not applicable	Increasing	Pulsed	<300 MeV	Cost
Cyclotron	Ions	Increasing	Constant	Constant	Continuous	<1 GeV	Magnet cost
Synchrocyclotron	Ions	Increasing	Modulated	Constant	Pulsed	<1 GeV	Magnet cost
Synchrotron	Electrons and ions	Constant	Constant and modulated	Increasing	Pulsed	$\sim 10^5$ GeV for protons	Radiative loss
Microtron	Electrons	Increasing	Constant	Constant	Continuous	<300 MeV	Cost

of a cyclic accelerator. A somewhat complex example of the latter arrangement occurs in the racetrack microtron, that combines one or more linear accelerating sections with a cyclic arrangement to return the particles to the accelerator. These accelerator systems combine the benefit of the beam power-delivery characteristics of a linear accelerator with the high-particle energy and economy in size of a cyclic device.

The various cyclic accelerators also differ in the time definition of the beam. When accelerating conditions are constant, the device is capable of a continuous beam output (continuous wave). When some condition must be varied in order to achieve the final energy, *e.g.*, RF or magnetic field strength, then by definition a packet of particles must be of a certain energy to be in phase with the accelerating process. This means that particles of lesser energy cannot be present until the structure is returned to its starting condition. Hence, the output beam is pulsed. It is this gross time structure to which the term duty factor refers.

Most, but not all, RF linear accelerators are pulsed. Maximal duty factors range from 10^{-6} to rarely greater than 4×10^{-3}. The primary radiation safety implication of the pulsed nature of these beams is in the response of real-time radiation detectors. It is also important to note that for indirect RF accelerators, there is a micropulse structure reflecting the frequency of the RF used to accelerate the particles. Such structure may exist in the accelerating cycle of even those accelerators that appear to be continuous wave on longer time scales. For radiological protection purposes, this micropulse structure is generally only of academic interest, but should not be confused with what is meant by the term "pulsed beam."

Usually, for convenience of operation, RF power generating components are placed external to the shielding of the accelerator, enhancing the potential for the exposure of support personnel to both x rays and the RF itself (nonionizing radiation). Such an exposure may be controlled by assuring the integrity of the conductive cabinets enclosing this equipment. Care must be taken in the use of radiation survey instruments in the vicinity of such equipment to be sure that readings are not perturbed by RF.

The radiofrequency quadrupole, a version of the linear accelerator, in which both the acceleration and transverse focusing are performed by RF fields has been developed (Humphries, 1986; Stokes *et al.*, 1979). This device is very efficient at low energies compared with Cockcroft-Walton accelerators and can provide almost continuous acceleration of ions of average beam currents up to tens of milliamperes; *e.g.*, a 2.5 MeV radiofrequency quadrupole can be less than 2 m long.

Dependent on the intensity of the accelerated beam, accelerators of all energies considered in this Report have the potential to produce substantial radioactivity by nuclear reactions in their components and shielding. Effective dose-equivalent rates of tens of millisieverts per hour can result even at low energies (tens of mega-electron volts for ion accelerators). The radionuclides produced are distributed over large regions of the periodic table in components containing a mixture of materials. Removable contamination may present a potential source of internal exposure. However, in the case of many electron accelerators of energies below 30 MeV used in industry and medicine, induced radioactivity is generally not a problem. For further discussion of this topic, see Section 3.6.

Radiological protection problems of linear accelerating structures tend to be minimal relative to other portions of the facility, because of the critical need to avoid the damage caused by inadvertent beam losses. The greatest losses occur during the low-energy phase of acceleration and, hence, are of least importance. For the shield designer, the greatest constraint may be a catastrophic beam loss of the high-energy beam caused either by design or system failure. Losses during startup and tuning are limited by operating at reduced intensities. However, for the higher energy accelerators even small losses can pose significant problems.

2.7 Beam Delivery Systems

Beam delivery systems consist of current and position monitors, generally very sensitive to radiation damage, beam focusing devices (quadrupoles and sextupole magnets), beam bending devices (dipole magnets), and devices that limit beam size and protect equipment (collimators). Beam loss and, hence, radiation production and radioactivation is most likely to occur at collimators and at magnets.

An essential fact is that a particle in the beam does not simply travel down the geometric center of the vacuum beam pipe. It must periodically be redirected back towards the centerline. The overall path is thus one of oscillation about the centerline. The smaller the spatial definition of the beam packet, the smaller the fraction of the beam that is lost to the beam-delivery system components. Further, because the steering process is tuned to a particular energy, particles of slightly different energy will cause the packet to enlarge thereby increasing losses.

In general, the vacuum structure, *i.e.*, beam pipe is not designed to absorb much power from the beam. Consequently, collimators are

typically positioned at locations where beam loss is most likely, *e.g.*, at the points of greatest divergence from the optimum orbit and where sensitive equipment is located, *e.g.*, near current monitors. These collimators are designed for their power absorption capability. Because the primary beam strikes collimators, it is important to consider their design carefully to reduce both heating and induced radioactivity. Collimators are sometimes air cooled but in those cases where the energy density is sufficiently high water-cooled systems are frequently used. It is desirable to minimize both the prompt radiation production efficiency and the residual activation characteristics. The choice of materials is controlled by the power and power density to be dissipated in the collimator. Possible choices are graphite, copper, brass and tungsten, each with its own particular advantages and disadvantages.

Magnets are used to direct the beam along a new path. A single magnet will bend a beam to a new direction, but also acts as a beam spreading device, much like a prism for light. Again, the better the energy definition of the beam, the less spread and, hence, the less loss to beam-line structures. Several magnets can be placed in sequence as a limited achromatic beam bending system. In general, dipole magnets are used to bend the beam and quadrupole magnets are used for focusing. Locations near bending magnets are typically significant beam-loss points and, hence, potential activation and radiation producing locations.

2.8 Beam Stops

The design of beam-stopping devices is largely determined by the incident beam power and particle type. Beam power places constraints on the choice of materials to be used in the construction of the beam stop because of the need to dissipate heat, often at very high power densities. The power densities to be dissipated in beam stops designed for electron accelerators are larger than for proton accelerators because of respective differences in the physical characteristics of the deposition of energy.

The choice of material also is influenced by the types of secondary radiations produced in the beam stop by the interaction of the primary beam. For incident particle energies up to several giga-electron volts, the controlling secondary radiations produced by incident electrons are photons and photo-produced neutrons, while those produced by incident protons are neutrons. At higher energies (for incident electron energies above several giga-electron volts and for

incident proton energies above several tens of giga-electron volts) muons can become the controlling secondary radiations, especially in the forward direction with respect to the incident beam.

For incident energies in the giga-electron volt region, it is necessary for designers to fully understand the complications resulting from the fact that secondary cascades may give rise to power deposition far downstream from the point of beam loss. For example, the accelerator structures, such as magnets, may themselves give rise to secondary sources of radiation or inadvertently act as beam stops.

Materials used for beam stops are typically water, iron, concrete, graphite or earth, all of which can be made radioactive. Special attention must be given in beam-stop design to the control of any contamination which might arise. In the particular case of beam stops using water to dissipate the thermal energy special considerations apply because of the greater potential for leaks and spills of radioactive material. In water the dominant radionuclides in terms of radiological hazard are ^{3}H and ^{7}Be (because of their long half-life), but ^{11}C, ^{13}N and ^{15}O are also produced in greater quantities (for more detailed discussion of these matters see Section 7). The induced radioactivity in beam stops of higher-energy accelerators may be controlled by appropriate material selection; *e.g.*, the use of graphite is often preferable to that of tungsten for this reason.

2.9   Auxiliary Systems

Several auxiliary systems of particle accelerators are potential sources of ionizing radiation including high-voltage systems, microwave power systems (in particular klystrons), cooling systems, and, under certain circumstances, vacuum systems.

2.9.1   *High-Voltage and Microwave Power Supplies*

Klystrons are microwave power amplifiers used to generate the RF accelerating fields required for electron accelerators. When used for accelerators, klystrons operate with pulsed beam voltages in the range of 100 to 250 kV and currents in the range of 100 to 300 A. The corresponding average power is in the region of tens of kilowatts, but average power levels of megawatts are now possible. Very intense x-ray emissions are possible and shielding will almost certainly be necessary. Typically, 2 to 5 cm of lead shielding is sufficient to reduce radiation levels to adequately protect operating and maintenance personnel.

Because of the irregular geometry of klystron tubes, particularly in the region around the RF output waveguides and the beam collimator cooling connections, special care must be taken to avoid radiation leakage through gaps in poorly fitting shields. It is strongly recommended that adequate radiation surveys be made with ionization chambers that can function in the pulsed radiation field and in the presence of RF power and high magnetic fields. Large sheets of photographic film may be exposed while wrapped around the casing of the klystron tube to identify radiation leaks through small holes and cracks.

When maintenance necessitates the removal of shielding, it is essential that adequate procedures be followed to ensure correct reassembly, followed by assurance of the shield's performance. The following excerpts from Swanson and Thomas (1990) illustrate the various radiation problems that can arise from RF power sources.

"In addition to the familiar production of x rays from klystrons and similar RF generators, Swanson has reported, 'Any vacuum containing high-power microwave fields, such as an RF separator or accelerator cavity, can produce x-ray emissions which may be intense. This radiation is unpredictable and may be erratic, depending on microscopic surface conditions which change with time. The x-ray output is a rapidly increasing function of RF power.'

"Measurements have been reported from several laboratories. At SLAC [Stanford Linear Accelerator Center] measurements at 90 degrees to a test cavity to be used on PEP [Positron-Electron-Proton Collider] showed that the absorbed dose D due to x rays was proportional to the fifth power of the RF power P [$D(90°) \sim P^5$].

"Tesch has reported that at DESY [Deutsches Electronen Synchrotron] measurements on the axis of a single cavity showed dose-equivalent rates as high as 100 rem h^{-1} [1 Sv h^{-1}], at a distance of 10 cm from the axis, with an RF pulse power of 200 kW and a duty factor of eight percent. Here the dose-equivalent rate was said to be proportional to the tenth power of the RF power applied to special copper cavities.

"The exposure rates around RF sources are not entirely predictable and depend strongly on specific designs. Users are strongly advised to make adequate measurements before routine use. Ionization chambers that are sensitive to low-energy x rays should be used; thermoluminescent dosimeters are valuable integrating devices."

The behavior of RF cavities depends strongly on conditioning of the vacuum system. Initial operation with poor vacuum may lead to multipactoring with high yields of x rays that diminish as the vacuum improves and all surfaces outgas.

2.9.2 *Cooling Systems*

The importance of cooling systems for radiological protection is in direct proportion to the potential of the accelerator to generate radioactivity. Design considerations should take account of direct radiation from the system due to the decay of short-lived radionuclides, such as ^{13}N and ^{15}O and the increasing concentration of longer-lived radionuclides in the cooling fluids and filtration systems (*e.g.*, resin beds); the decay-radiations characteristic of the materials of the system components; and the beam-energy of the accelerator. The materials used in cooling systems are varied: stainless steel and copper are used in great quantities and their induced radioactivity is well understood. Sections 3 and 6 discuss the radionuclides that are produced in water or may appear in cooling-water systems.

Provision must be made for venting radioactive and other gases from cooling systems. Some of these gases may be chemically reactive or toxic (*e.g.*, oxides of nitrogen), or even flammable or explosive (*e.g.*, hydrogen). These considerations are particularly important at electron accelerators.

2.9.3 *Vacuum Systems*

A particularly important consideration for any evacuated enclosure is whether any high voltages are associated with it. The possibility of generating x rays in such assemblies must always be considered.

In addition, the accelerator vacuum system can be a means by which radioactive products may leave the accelerator. In general, this does not present a serious problem unless gaseous targets are used, although Taka (1984) has observed activation products in diffusion-pump oil. Activation products, especially volatile species, are also transported through the vacuum at isotope separator on line facilities.

The principal use of gaseous targets is at neutron generators where tritium or deuterium, usually adsorbed on titanium, is often used. Tritium released from such targets can be a potential source of contamination of the vacuum system. Particular care must be taken

to control the exhaust from diffusion and mechanical pumps and to control waste products, particularly pump oil which can act as a scavenger of tritium (Pollock, 1981).

2.10 Summary of the General Specifications and Parameters of Accelerators

The two essential descriptive parameters of any accelerator are the output beam energy and average beam power. These dictate the major characteristics of health physics interest, *e.g.*, activation and radiation characteristics. Sometimes, however, a single set of numbers does not adequately describe a particular accelerator. The accelerator may be capable of several modes of operation that result in very different energy and power parameters, and particularly for positive ion accelerators may be capable of accelerating several, or a wide range of particles. A characteristic of electron linacs is that they can be tuned to different final electron energies, albeit by sacrificing beam power. For high-energy linacs, the energy of the maximal power condition is the parameter of interest, but, in the energy range from 10 to 30 MeV, the set of operating conditions of greatest concern depends upon the specific mechanism being evaluated, *e.g.*, photon production, photon shielding, activation, or neutron production.

Of secondary concern is the accelerator's duty factor, pulse repetition rates, pulse lengths, physical characteristics (number of accelerator sections, number of klystrons, orbit diameter, accelerator length), RF, type of vacuum systems, facility usage, etc. Many of these impact on the design of the health-physics support program and the selection of instrumentation. Nevertheless, beam energy and power are the starting point for all considerations of radiological protection.

2.11 Applications of Accelerators

Although many accelerators are still devoted to fundamental research, particularly in the disciplines of nuclear physics and particle physics, most are used in the applied sciences, in industry, and in medicine. While electron accelerators may currently have wider application than positive ion accelerators, the latter have been increasingly applied in many areas, *e.g.*, to problems in "atomic physics, astrophysics, archaeology, mineralogy, environmental science, nuclear structure, surface physics, solid state physics, radiological physics, the

production of radionuclides for use in medicine and fusion research. Applications in industry include oil well logging, ion implantation, trace element studies in environmental samples, aerosol composition studies and radiation sterilization. In medicine, small accelerators have been used for radiotherapy, trace element studies, body calcium assays, *in vivo* neutron activation and radiography" (IAEA, 1988).

Electron accelerators are used in a wide variety of industrial applications including radiography and various areas of radiation processing (polymer modification, sterilization of medical devices, preservation of foods, waste treatment). Future applications include the use of electron-accelerator-based, free-electron lasers and the wealth of applications from such devices (far infrared spectroscopy, isotope separation, chemical physics, and materials surface processing).

Synchrotron radiation, produced by high-energy electron storage rings and circular accelerators, is used in physics, chemistry, materials science, metrology, and microelectronics, and has been successfully used for diagnostic imaging. A growing application is the production of integrated circuits by lithography. Many circular electron machines (synchrotrons, storage rings) are fully dedicated to utilization of their synchrotron radiation. A review of e^+e^- storage rings is given by Kohaupt and Voss (1983). An extensive treatment of synchrotron radiation and its sources is given by Winick (1989; 1994). All modern aspects are addressed in the *Handbook on Synchrotron Radiation* edited by Koch (1983-1991) (see also Brown and Moncton, 1991).

2.12 Future Developments in Accelerators

New, large accelerator complexes, such as the Large Hadron Collider, linear electron-positron colliders, muon colliders, and free electron lasers, bring with them new and intriguing radiological problems. Beyond these concepts, future progress may be possible only by the development of new accelerator principles that will permit higher energies to be reached without increasing the areas of land required for accelerator construction.

2.13 Siting and Layout

The great diversity of the particle accelerators discussed in this Report makes it impossible to develop criteria for the siting and

layout of accelerator facilities which are both comprehensive and, yet, sufficiently detailed in most respects. For example, it is clear that the criteria for siting and layout of a neutron-generator operated by a university department will be quite different from those for a large state-of-the-art accelerator such as the Large Hadron Collider near Geneva (Brianti and Hubner, 1984). IAEA (1979a) described typical installations using electron linear accelerators including those used for medicine (diagnosis and therapy), industrial radiography, and research. IAEA (1988) described several positive-ion accelerators covering the energy range 20 to 400 MeV used in research or medicine. The accelerator facilities include a 30 MeV electrostatic generator, an 800 MeV proton linear accelerator, an 800 MeV rapid cycling proton synchrotron, a multi-giga-electron volt heavy ion facility, a 12 GeV strong focusing synchrotron, and the 400 GeV Super Proton Synchrotron (SPS).

Several factors play an important role in determining the optimum location of an accelerator facility. These factors include:

- radiological protection limits: workers and the general population
- environmental impacts
- accessibility
- availability of existing buildings and facilities

There is no typical "accelerator site" but it is often the case that the cost of radiological protection systems, particularly shielding, for accelerators may represent a significant fraction of the total cost.

It is, therefore, extremely important to pay particular attention to the selection of an appropriate location for any new accelerator. It is preferable to develop site criteria concurrently with the design of the accelerator and its facilities. This will provide effective and prompt interaction with those responsible for the design of safety features. Costly design modifications may be avoided if a site is selected which satisfies well-developed site criteria.

The steps needed to arrive at a preliminary understanding of the radiological impact of an accelerator may be summarized as:

- specification of design parameters
- specification of assumptions on expected operation
- estimation of radiation source strengths
- determination of applicable or desired radiological protection goals
- specification of shield-wall thicknesses, beam-line dimensions, distances between facilities, and site features required to accommodate the measures necessary for radiological protection

Although it is possible for the accelerator site criteria and accelerator design to be developed independently, the accelerator site is often already known and the installation must be accommodated to the constraints of the available location. Such might be the case, *e.g.*, when an accelerator intended for therapy is added to an existing hospital radiotherapy department or when a university department wishes to install a research accelerator on campus.

The U.S. Department of Energy's *Health Physics Manual of Good Practices for Accelerator Facilities* (Casey *et al.*, 1988) describes general procedures for developing site criteria, and a brief summary is given here:

- specify the accelerator parameters
- estimate the radiation source strengths
- estimate prompt radiation transmitted through shielding, and skyshine, considering both normal operations and unusual conditions of excessive beam loss
- in some cases, it will be necessary to develop an environmental impact statement to satisfy National Environmental Policy Act (NEPA, 1969) requirements

Calculations of collective population dose equivalent, due to accelerator operation, should include the contribution from airborne radioactivity, either in the form of radioactive gases or radioactive aerosols, which is usually trivial (Thomas, 1978a; 1978b).

Induced radioactivity of the soil and groundwater outside the accelerator buildings may be important, particularly because the regulatory criteria are more restrictive for such pathways than for direct exposure. Radionuclides produced directly in the groundwater and those leached from the earth may be transported to surface waters or an aquifer. Other sources of radioactive water include routine discharges and spills from closed cooling-water loops or water collected in sumps. Hydrogeological information may be needed to predict the concentrations of radionuclides that might appear in drinking water supplies (CEBAF, 1987; Gollon, 1978). For a discussion of the estimation of radioactivity in air, earth and water, see Section 6, Environmental Radiological Aspects of Particle Accelerators of this Report.

Because the storage and movement of radioactive accelerator components around the accelerator site can contribute to the dose equivalent, both at the site boundary and within the accelerator facility, it may be important to consider the location of storage areas, maintenance workshops, laboratories, and office areas with a view of minimizing radiation exposures, especially in areas of high occupancy or areas where members of the general public are present.

Particle accelerators do not, in general, have profound environmental radiological consequences (Section 6). Nevertheless, increasingly strict regulation of environmental radiation levels is leading to designs that minimize both radiation dose-equivalent rates at the facility boundary and the population dose equivalent to the neighboring community. These constraints could be of greater importance in determining the cost of the radiological-protection system than that for protection of radiation workers.

3. Sources of Ionizing Radiation from Accelerators

3.1 Introduction

In order to fully understand the ionizing radiation environments of particle accelerators, the details of secondary particle production at the first interaction of the primary particles (*i.e.*, those particles intentionally produced by the accelerator) must first be known. The intensity of these secondary particles resulting from the first interaction is often referred to as the *source term*. This Section describes our understanding of the energy and angular distributions of these source terms. The subsequent interactions of the source particles through the accelerator components, shielding and other material generate the "*prompt-radiation elds*" that are observed around accelerators.[2]

In Section 2, the various types of particle accelerators and how they may produce ionizing radiations were briefly described. The production of ionizing radiations by particle accelerators may be classified by many schemes: for example, in terms of the accelerator type, in terms of the particle being accelerated or by the particle energy, or in terms of the operational characteristics of the accelerator. Any particular choice is to some extent arbitrary. The classification of particle yields used throughout this Section is by accelerator type.

Some of the devices employed to produce the electromagnetic fields used to accelerate charged particles in an accelerator may be operated for test and maintenance purposes while the accelerator itself is not fully operational. This condition potentially can result in radiation exposures to personnel involved in maintenance activities as discussed in Section 2.9.1.

---

[2] There is some unavoidable overlap between this Section and Section 4: Section 3 largely deals with the particles that make up the source term while Section 4 discusses radiation transport.

33

Any accelerated beam of particles may produce radiation as a consequence of an interaction between the particle beam and the material it strikes. Radiations of many types may be produced by such interactions. In general, the higher the kinetic energy of the incident particle, the greater the yield and the number of types of secondary radiations.

Those radiations of most concern for radiological protection at low and intermediate energies are:

- bremsstrahlung x radiation due to the transfer of energy from the moving charged particle to a photon in the electromagnetic field of an atom[3]
- characteristic x radiation due to the transfer of energy from the moving charged particle to an electron in a bound atomic state followed by the subsequent decay of that state by photon emission
- prompt gamma radiation from the interactions of ions or neutrons with matter
- neutron, charged particles, ions, and nuclear fragments emitted as a result of the transformation of energy from the moving charged particle to an atomic nucleus
- delayed radiation due to the de-excitation of radioactive nuclei (*i.e.*, induced radioactivity) that have been produced by means of nuclear reactions of the moving particle with atomic nuclei

In addition to those radiations listed above, muons and other particles, such as pions and kaons, may be of concern.

At electron accelerators, the primary radiological issues are generally created by the production of photons, while at proton and other positive-ion accelerators the radiological problems usually result from the production of hadrons. Hadrons are particles subject to the nuclear (strong) interaction most prominently exemplified by neutrons and protons. The higher the energy of the particles accelerated, the more complex the character of the *prompt-radiation eld*—the radiation field that exists only while the accelerator is in operation.

The prompt-radiation field is one of two somewhat different external fields at accelerators that are of concern for radiological protection; the other is identified as *residual*. The former exists only while

---

[3] The term "x ray" is commonly used to denote this kind of radiation field when produced by radiation generating devices. "Bremsstrahlung" is more descriptive and more often used in relation to high-energy accelerators to denote both the radiation itself and the underlying physical process by which it occurs. In the case of bremsstrahlung, the photons have a very broad energy spectrum and spatial distribution.

the accelerator is in operation while the latter persists after operation has ceased and is due to induced radioactivity. The characteristics of the prompt-radiation field are determined by the energy and type of particle accelerated, the beam duty factor, the target material, and shielding around the accelerator.

It is the interaction with matter of the particles that comprise the prompt-radiation field that leads to the induction of radioactivity. The rate of radioactivity production is greatest in accelerator components located near points of interaction such as targets, beam absorbers, beam pipes, and certain types of beam diagnostic instrumentation, but may be detected in the accelerator shield, in structural components of the accelerator and in the environment. The decay of this induced radioactivity gives rise to the *residual-radiation eld* (Sections 3.6 and 6).

3.2 General Considerations

It is necessary to know the radiation yields from particle accelerators for many purposes other than radiological protection. Indeed, at research establishments or laboratories, the determination of secondary particle yields in terms of angular and energy distribution is often one of the principal purposes of the accelerator. In radiological protection, particle yield data are often needed to determine how possible changes in accelerator operation or shielding may modify external radiation environments. Particle yields from accelerators are reported in terms of physical distributions such as particle type, energy, fluence and angle of emission. The intensities of radiation fields are often characterized in terms of fluence rate (ICRU, 1980).[4] In order for the accelerator health physicist to understand the radiological-protection issues applicable to particle beams and secondary particles, specification of radiation fields in this manner is usually necessary.

The radiation-yield data necessary for the health physicist are usually published in scientific journals, and, to understand these published measurements of secondary particle yields, one must be conversant with the terminology generally used to describe nuclear reactions. Figure 3.1 shows a typical geometry for studying the angular distribution of particles produced by the interaction of the primary particle beam with a target. The target in which the particles interact is chosen, for convenience, to be at the origin of a spherical-

---

[4] Fluence is often referred to in the literature as flux density or even flux.
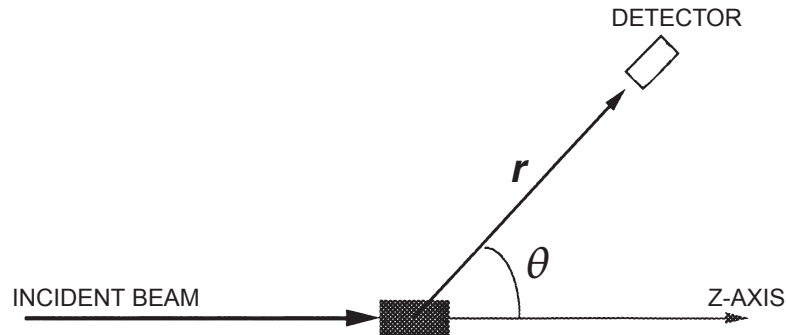
Fig. 3.1. Typical geometry of an angular distribution measurement of particle yield at angle Θ relative to the direction of an incident beam of particles striking a target.

coordinate system. Scattered reaction products are detected at radius (r) and polar angle (Θ) relative to the direction of the incident particle along the positive z-axis. In general, both the rate of detection of the desired reaction products and their energy spectra are a strong function of both Θ and the incident particle energy (E_0). On the other hand, such quantities are, with one exception, independent of the azimuthal angle in this spherical coordinate scheme.[5]

After striking such a target, the incident particle will lose energy as it passes through the target material. If the target is sufficiently thin so that the loss of energy in the target is negligible, then suitable detectors arranged as shown in Figure 3.1 may be used to measure the differential cross section for production of a given secondary particle as a function of primary particle energy $[d\sigma(\Theta,E)/d\Omega]$ where $\sigma(E)$ is the cross section as a function of energy of the reaction product and Ω is the solid angle into which the secondary particles are produced. In this simple case, the total cross section or angle-integrated energy spectrum may be determined in a straightforward way by performing the appropriate integration of the differential cross sections over the angle (Θ). Extensive measurements of this type are reported in the scientific literature. Under such "thin target" conditions, only a tiny fraction of the particles in the incident beam actually interacts with the target nuclei. On the other hand, in most applications of interest to the accelerator health physicist, the beam of particles does not interact with such a thin target, but instead

---

[5] The single exception is the case in which the spins of the target nuclei and/or the incident particle are oriented along some chosen direction in a "polarization" experiment.

interacts with rather thick objects such as the walls of beam pipes, vacuum-system flanges, or Faraday cups. These situations are usually described as "thick-target conditions." A comparison of the ionization range of the primary charged particles with their interaction mean-free path in material may be used to assess the probability of an interaction before the charged particles are stopped by ionization. The electromagnetic cascade is discussed further in Section 3.3.6.

The ionization range of charged secondary particles increases as their kinetic energy increases, while their interaction mean-free path becomes approximately constant at sufficiently high energies. For electrons, the ionization range (R) in the region $2 < E_0 < 10$ MeV, where E_0 is the kinetic energy of the electron in mega-electron volts, is approximately given by $R = 0.6\,E_0$ g cm^{-2}. This relationship is only weakly dependent upon the absorbing material. Above 10 MeV, radiative processes begin to dominate over such collision ionization energy loss.

For protons, Figure 3.2 (Janni, 1982; Tesch, 1985) shows both the ionization range in various materials as well as the probability of having an inelastic nuclear collision within that value of range as a function of energy. For proton energies even as high as 100 MeV, the range is less than $\sim$10 cm in solid materials. Thus "thick" target yields are needed in order to take into account the variation of the cross section with energy, and to be able to account for secondary particle effects such as the initiation of hadronic cascades or "showers." Such thick target yields have been measured directly in some cases; in other cases, thick target yields have been calculated from thin target cross-section data by integrating over the range of the incident proton.

For many applications, such as shielding design, the details of the angular distributions of total secondary particle yield, d$Y(\Theta)$/dΩ, and the angular and energy dependence, d$^2Y(\Theta,E)$/dEdΩ, of the emitted particle spectra are very important. Often, the particle fluence is needed at a particular location at coordinates (r,Θ) from a known "point source" of beam loss. Energy spectra and particle yields can be rather strongly dependent upon Θ. Knowledge of the secondary particle yield at specific angles is useful for both personnel protection and equipment protection. Unfortunately, angular distribution data for secondary-particle production in thick targets are quite sparse. This is so even for neutrons for which most measurements have been made. Representative data given in this Section are to be used as *guides*; calculations made for radiation protection purposes should be made *conservatively*.

The data presented later in this Section are derived from a number of original sources that vary considerably in their choice of physical
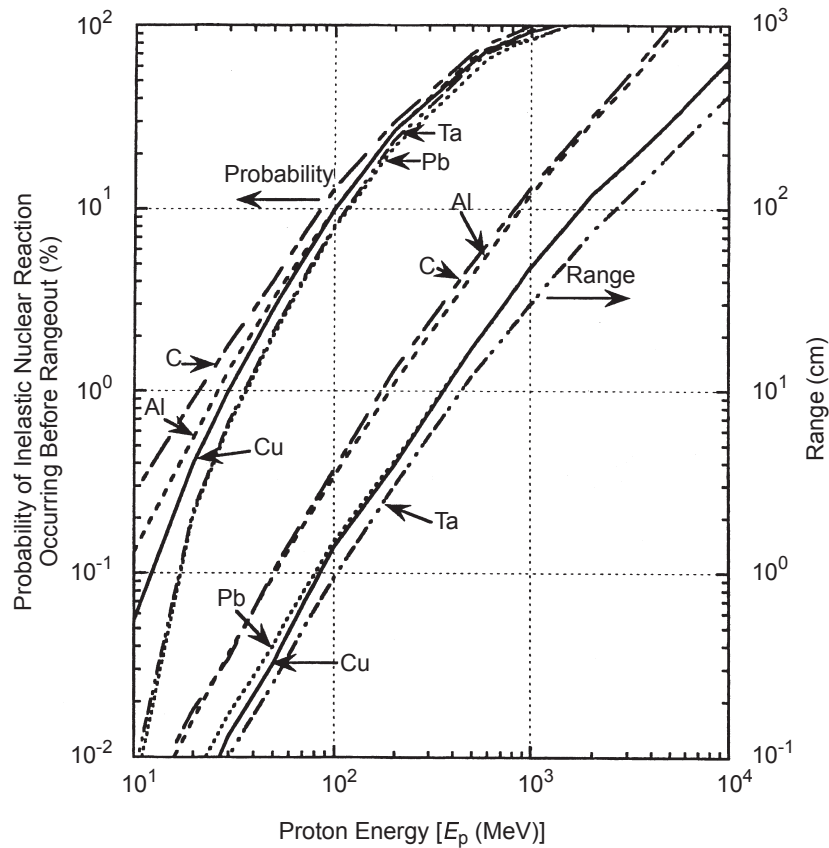
Fig. 3.2. Range of protons (right-hand scale) and probability of inelastic nuclear interaction within the range (left-hand scale) [Tesch (1985) adapted from Janni (1982)].

units to express the quantities measured. For example, some normalize to the integrated beam current, while others normalize directly to the number of incident particles. For the convenience of the reader, angular distributions of energy spectra have been plotted in units of secondary particles/(MeV steradian incident primary particle). Angular distributions of $dY/d\Omega$ are normalized in the same way. To find the total fluence $\phi(\Theta)$ [secondary particles/(cm^2 incident primary particle)], or differential fluence $d\phi(E,\Theta)/dE$ [secondary particles/(cm^2 MeV incident primary particle)] at a given distance r (centimeters) at a specified angle Θ, the plotted values must be divided by r^2 (cm^2):

$$\phi(\Theta) = \frac{\mathrm{d}Y(\Theta)}{r^2\mathrm{d}\Omega} \qquad\qquad (3.1a)$$

and

$$\frac{\mathrm{d}\phi(E,\Theta)}{\mathrm{d}E} = \frac{\mathrm{d}^2Y(E,\Theta)}{r^2\mathrm{d}E\mathrm{d}\Omega} \; . \qquad\qquad (3.1b)$$

3.3   Radiation Production at Electron Accelerators[6]

3.3.1   *General*

At electron accelerators of all energies, bremsstrahlung photons dominate the secondary radiation field. For primary electron energies above 100 MeV, a description of the radiation field is best approached through a discussion of the electromagnetic cascade. In this process, electrons and photons repeatedly interact, each time losing energy until the degraded electrons are brought to rest by ionization and, finally, the photons are attenuated at a rate close to the minimum attenuation coefficient for the material. For a more complete discussion of the electromagnetic cascade, see Section 3.3.6.

For tables of electron energy loss, extensive data are presented by Berger and Seltzer (1964; 1966; 1982), Pages *et al.* (1972), and Seltzer and Berger (1982a; 1982b). Report 37 of ICRU (1984) contains extensive discussion and tabulations on stopping powers for electrons and positrons. The theory of electron bremsstrahlung has been summarized by Heitler (1954) and Jauch and Rohrlich (1976). A compendium of bremsstrahlung formulae is given by Koch and Motz (1959). Data on photon mass attenuation coefficients and related parameters are well explained and tabulated by Hubbell (1969; 1977; 1982), Hubbell *et al.* (1980), Plechaty *et al.* (1975), and Storm and Israel (1967; 1970). These tabulations emphasize the lower-energy behavior of electrons and photons and, therefore, provide the essential information necessary for a complete understanding of dosimetry of high-energy electron beams. This is so because the electromagnetic cascade contains electrons and photons of essentially all energies from zero up to the maximum energy possible; and it is indeed the particles of lower energy that dominate the deposition of energy in matter.

---

[6]This Section draws heavily upon the report *Radiological Safety Aspects of the Operation of Electron Linear Accelerators* (IAEA, 1979a).

Concise descriptions of the electromagnetic cascade may be found in Section 3.3.6 of this Report and in ICRU Report 28 (ICRU, 1978). The electromagnetic cascade is copiously populated with low-LET (linear energy transfer) particles, and the quality factor for related absorbed doses is accepted as $Q = 1$. Metrology is, therefore, considerably simpler than, say, for neutron fields.[7] In most cases, readily-available standard instruments can be used for radiological-protection measurements in photon fields. An outstanding body of work has been compiled for accelerators that operate below 100 MeV (*e.g*, NCRP, 1977), but the approach presented here also includes higher-energy facilities.

In contrast to the situation at electron facilities, bremsstrahlung is a negligible effect at proton (or heavy ion) accelerators except at the highest tera-electron-volt energies. The radiative energy loss by protons is less than that by electrons by approximately the ratio $(m_e/m_p)^4$, where m_e is the electron mass and m_p is the proton mass.

3.3.2 *Electron Beams*

Electron beams for acceleration are typically produced by emission from a cathode in the form of a hot filament or an indirectly heated surface. In a few instances, electrons are drawn from the plasma of an ion source, *e.g.*, in certain direct (electrostatic) accelerators that can produce either ions or electrons. Very high currents of electrons may be drawn from cathode material by field emission, *e.g.*, in flash electron/x-ray machines. Electrons can also be produced by the interaction of other electrons or ions with matter, by field emission in high electric-field gradients, or from photocathode guns. These phenomena are often of importance within the evacuated acceleration region and beam-transport structure. Secondary electrons usually proceed along different paths than that of the impinging particles, thereby giving rise to other possible sources of x rays. Photocathode guns are also used in which lasers produce useful electron beams, in particular polarized beams in which the spins of the electrons are aligned with some particular coordinate.

In many applications, the electron beam emerges from the accelerator vacuum system into the atmosphere through a thin, low-

---

[7] This simplicity would disappear if Q were not held constant at a value of one. For example, ICRU Report 40 recommended that Q for photons and electrons as a function of lineal energy vary by as much as a factor of three (ICRU, 1986). Under those circumstances, photon dosimetry would become as difficult as neutron dosimetry! The introduction, in ICRP Publication 60 (ICRP, 1991), of radiation weighting factors (w_R) to replace Q does not change the logical basis for this conclusion.

energy-loss membrane or "window." Because air has a density of $\sim 1.2 \times 10^{-3}$ g cm^{-3} at normal room temperatures and pressures, the maximal range in air of such electrons, in meters, is approximately five times the electron energy in mega-electron volts $[R(E) = 5 E$ m].

Electrons are scattered by all materials on which they impinge (including air), and may, therefore, constitute a problem in accelerator facility design. Scattering may occur along the entire path of the electron beam. A conservative estimate of shielding requirements may be made by assuming that the energy of the scattered electrons is identical to that of the accelerated electrons.

Accelerated electron beams are a potential source of very high absorbed-dose rates. Electrons that are scattered out of the beam are present at very much smaller fluence rates than those present in the direct beam, but, nevertheless, may still present serious hazards in relatively short exposure times. Radiation safety interlocks are of primary importance in the safe handling of such beams (Casey *et al.*, 1988; NCRP, 1986) (see also Section 7 of this Report).

3.3.3 *Photon Fields*

3.3.3.1 *External Bremsstrahlung.* The type of *secondary* radiation with the greatest potential hazard at all energies consists of the photons produced by bremsstrahlung. Photons are radiated from any object struck by the primary electrons (such as a target designed for that purpose) and form an external secondary-radiation field.

At low energies, the electrons incident on a target lose their energy primarily by ionization in the stopping medium: most of this energy reappears in the form of heat and only a small fraction is radiated as external bremsstrahlung. As the electron energy is increased, an increasing fraction is converted to bremsstrahlung (Berger and Seltzer, 1964; 1966; Koch and Motz, 1959; Pages *et al.*, 1972) until at very high energies this mechanism predominates. Figure 3.3 shows the bremsstrahlung efficiency for electrons stopped in various materials [see also ICRU Report 37 (ICRU, 1984)]. The percentage of kinetic energy of the incident electrons converted to radiation is plotted as a function of incident energy E_0.

The "critical energy," (E_c), for a given material is the electron energy at which the energy losses from the emission of radiation, $[(dE/dx)_{rad}]$ which increases with energy, equals the energy losses from the electron collisions $[(dE/dx)_{col}]$. Values of E_c in mega-electron volts are given approximately by:
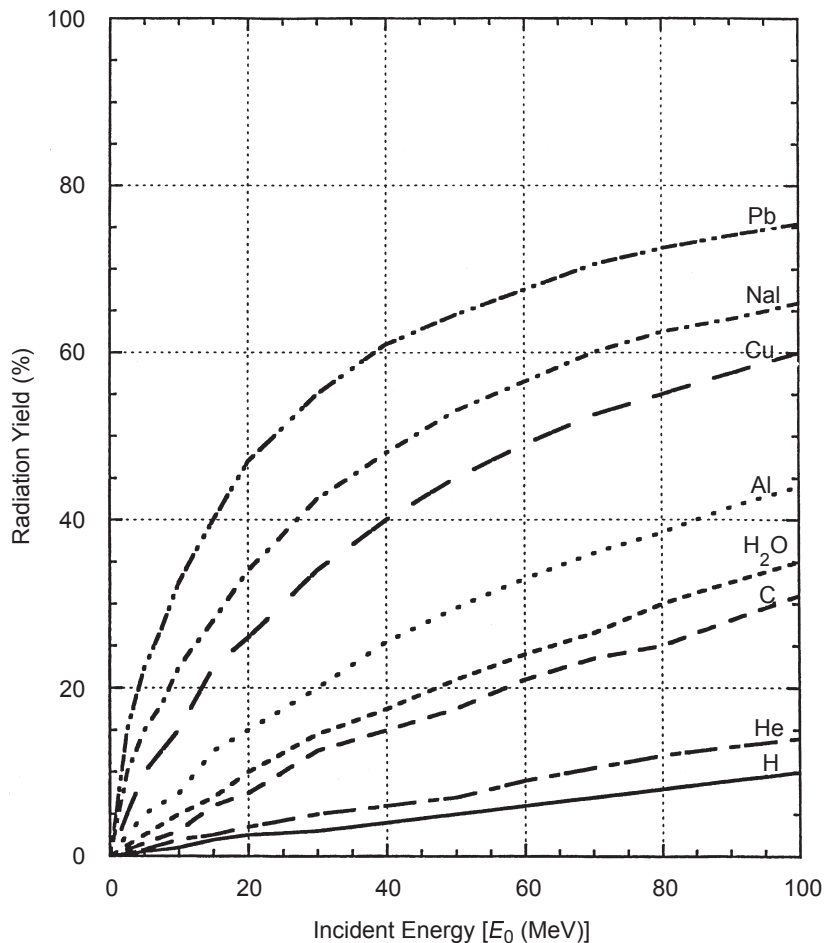
Fig. 3.3. Bremsstrahlung efficiency for electrons stopped in various materials. Fraction (in percent) of kinetic energy of incident electrons (E_0) converted to radiation, as a function of incident energy (E_0). The remainder is transferred to the medium by ionization and manifests itself ultimately as heat (adapted from IAEA, 1979a).

$$E_c = 800/(Z + 1.2), \qquad (3.2)$$

where Z is the atomic number of the material medium. E_c is plotted in Figure 3.4 as a function of Z (IAEA, 1979a).

The radiation length (X_0) is a parameter of great significance in describing the slowing down of electrons. X_0 is defined as the mean thickness of material over which the energy of an electron is reduced
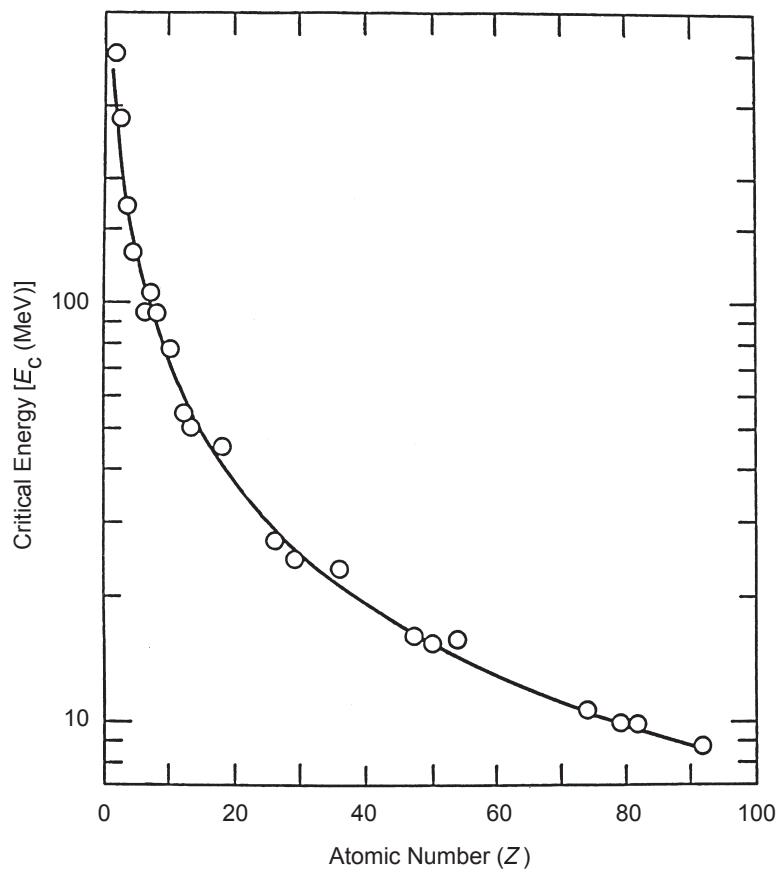
Fig. 3.4. Critical energy (E_c) as a function of atomic number (Z). The curve represents the approximation E_c(mega-electron volt) = 800/(Z + 1.2) (adapted from Berger and Seltzer, 1964; IAEA 1979a).

by a factor (e), because of bremsstrahlung, and is the approximate scale length for describing electromagnetic cascades in the high-energy limit. This distance is approximated by:

$$X_0 = \frac{716.4\,A}{Z(Z\,+\,1)\ln(287/\sqrt{Z})}\ \text{g cm}^{-2}, \qquad (3.3)$$

where Z and A are the atomic number and weight of the material medium. The energy deposited by radiative effects per unit length, $(\mathrm{d}E/\mathrm{d}x)_\mathrm{rad}$ is given approximately by:

$$\left(\frac{\mathrm{d}E}{\mathrm{d}x}\right)_{\mathrm{rad}} = -\frac{E}{X_0}, \tag{3.4}$$

so that at high energies (where ionization may be neglected):

$$E = E_0 \mathrm{e}^{-x/X_0}, \tag{3.5}$$

where E is the energy at depth x in the material. Accurate values of X_0 have been calculated by Knasel (1970), Seltzer and Berger (1982a; 1985), and Tsai (1974).

The development of external bremsstrahlung as a function of target thickness is described by the so-called "transition curve": as the target thickness increases the radiation first increases until reabsorption modifies this growth to produce a broad maximum followed by a decline that becomes approximately exponential with depth at very great thicknesses. The photon spectrum emanating from a target that is sufficiently thick to allow full development of the electromagnetic cascade is described as a *"thick-target" bremsstrahlung spectrum*.

In radiation protection planning, it is conservative practice to assume that the yields of all bremsstrahlung sources arise from targets of optimum thickness, regardless of the actual thickness of the source.

Some salient properties of thick-target bremsstrahlung are summarized by the three "rules of thumb" proposed by IAEA (1979a) that are based on the following analyses:

1. For constant beam current, the absorbed dose in the forward direction ($\Theta = 0$ degrees) varies rapidly with incident electron beam energy (E_0). Below ~10 MeV, the absorbed dose varies approximately as E_0^2, and above 10 MeV as E_0. This behavior is illustrated in Figure 3.5, in which the absorbed dose is plotted as a function of E_0, for constant beam power. Up to ~20 MeV, the absorbed-dose rate ($\mathrm{d}D/\mathrm{d}t$) per unit beam power in kilowatts at zero degrees from an optimum high-Z target is, to within a factor of two, given by **Rule of Thumb 1**:

$$\frac{\mathrm{d}D}{\mathrm{d}t} \approx 20 \, E_0^2 \left[(\mathrm{Gy \ h^{-1}}) \, (\mathrm{kW \ m^{-2}})^{-1}\right],$$

$$\Theta = 0°, E_0 < 20 \ \mathrm{MeV} \tag{3.6}$$

where E_0 is in mega-electron volts. Above 20 MeV, Equation 3.6 will begin to overestimate the dose rate substantially.

For $E_0 > 20$ MeV, **Rule of Thumb 2** reflects the change in slope seen in Figure 3.5:
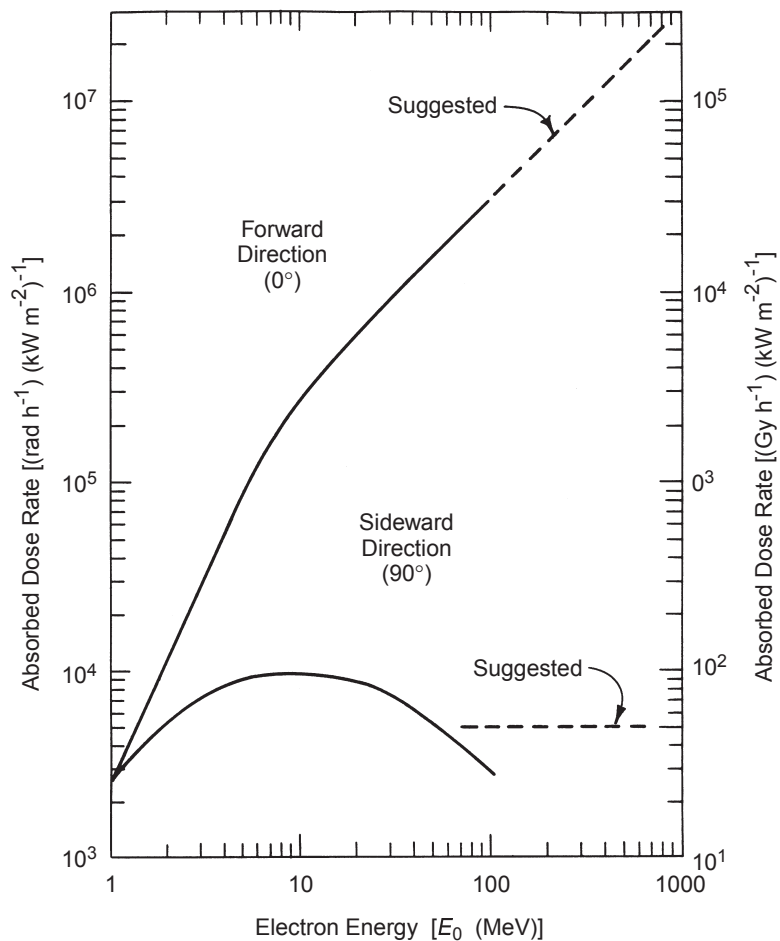
Fig. 3.5.   Thick-target bremsstrahlung yield from a high-Z target. Absorbed dose rate at 1 m per unit incident electron beam power (kilowatt) as a function of incident electron energy (E_0). The dashed line at zero degrees represents a reasonable extrapolation of the measured values. The dose rates measured in the sideward direction (smoothed for this figure) depend strongly on target and detector geometry and vary by more than a factor of two. The dashed line at 90 degrees represents the more penetrating radiation component to be considered in room shielding (IAEA, 1979a).

$$\frac{\mathrm{d}D}{\mathrm{d}t} \approx 300\, E_0 \left[(\mathrm{Gy\ h^{-1}})\, (\mathrm{kW\ m^{-2}})^{-1} \right],$$

$$\Theta = 0°,\ E_0 > 20\ \mathrm{MeV}. \tag{3.7}$$

2. At $\Theta = 90$ degrees (also shown in Figure 3.5), the absorbed dose rate at high energy is approximately proportional to beam power, independent of beam energy. Therefore, **Rule of Thumb 3** suggests that the behavior at high energy is constant at:

$$\frac{\mathrm{d}D}{\mathrm{d}t} \approx 50 \left[(\mathrm{Gy\ h^{-1}})\, (\mathrm{kW\ m^{-2}})^{-1} \right],$$

$$\Theta = 90°,\ E_0 > 100\ \mathrm{MeV}. \tag{3.8}$$

The dose rates given by these Rules of Thumb represents the more penetrating radiation component to be considered in shielding design. Dose rates at 90 degrees to an *unshielded* target may be significantly higher because of the contribution of softer radiation components.

The three Rules of Thumb expressed by Equations 3.6, 3.7, and 3.8 can be used to provide a source term when thick shielding is employed, *e.g.*, at 90 degrees to a target. It should be noted that the data of Fasso *et al.* (1984a; 1984b) agree with the Rule of Thumb for zero degrees, for target thicknesses between 2 and 4 X_0, but at a thickness of 10 X_0 the Rule of Thumb would exceed the data of Fasso *et al.* by an order of magnitude.

3. For materials of medium to high Z at a given electron energy E_0 the intensity in the forward direction is a slowly varying function of target material. However, for materials of very low Z, the intensity is considerably lower than that for materials with medium Z. This implies that use of Equation 3.8 for radiation protection purposes will not be overly conservative, regardless of the target material used.

4. At electron energies above ~1.5 MeV, the intensity of bremsstrahlung peaks in the forward direction. This trend increases markedly with increasing energy, as can be seen in the comparison of the perpendicular ($\Theta = 90$ degrees) and forward ($\Theta = 0$ degrees) intensities shown in Figure 3.5. Figure 3.6 shows a curve of the relative angular distribution, plotted as a function of $E_0\Theta$ (where Θ is the angle at which the bremsstrahlung intensity is measured, relative to the incident beam direction, multiplied by the incident electron energy) (Brynjolfsson and Martin, 1971). Measurements in the range $E_0 = 2$ to 20 MeV can be adequately described by a single curve to ~$E_0\Theta = 400$ MeV degrees, and a qualitatively similar behavior is obtained at higher energies. The angular width of the forward
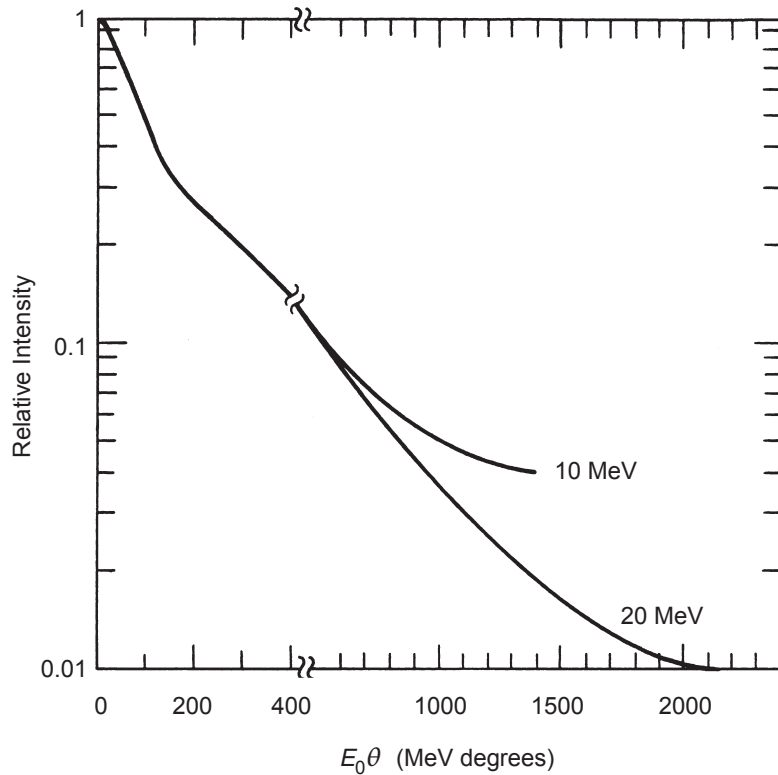
Fig. 3.6. Angular distribution of bremsstrahlung intensity from thick high-Z targets (relative units), plotted as a function of the variable $E_0\Theta$ (the angle at which the bremsstrahlung intensity is observed relative to the incident beam direction, multiplied by the incident electron energy) (IAEA, 1979a).

lobe may be expressed in terms of the angle of half-intensity ($\Theta_{1/2}$). E_0, and $\Theta_{1/2}$ are related approximately by the equation:

$$E_0\ \Theta_{1/2} \cong 100 \text{ MeV degrees,} \qquad (3.9)$$

when E_0 is in mega-electron volts and $\Theta_{1/2}$ is expressed in degrees.

5. At lower energies, where energy loss by ionization dominates, the width of the forward lobe varies approximately as the square root of Z of the target material. At higher energies ($E_0 \geq 20$ MeV), in materials of high Z the width is almost independent of Z.

6. The hardest radiation (*i.e.*, that containing the greatest proportion of the most energetic photons) occurs in the forward direction. The radiation towards the sides becomes progressively

softer as the angle is increased. This shift in spectrum may permit economies in shielding at large angles to the incident beam.

7. The spectra from thick targets have a more complicated dependence on energy than the well-known "thin-target spectra."

For thin targets ($X \ll X_0$), the photon spectrum is approximately given by:

$$\frac{\mathrm{d}N}{\mathrm{d}k} \cong X\,X_0^{-1}\,k^{-1}, \qquad (3.10)$$

where:

k = photon energy[8]
X = target thickness
X_0 = radiation length both in the same units

For thick targets, the photon spectrum declines more rapidly from low photon energies to the limit E_0 than is the case for thin targets. Representative measured spectra are shown in Figure 3.7 from the
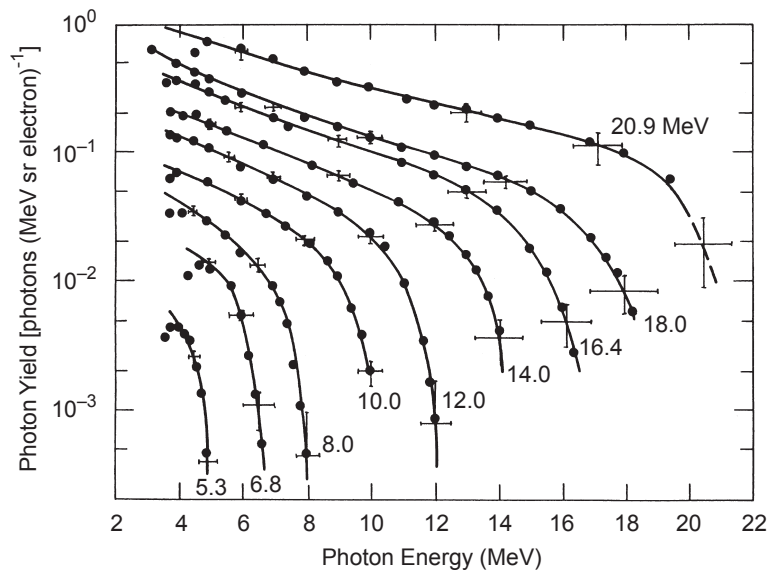
Fig. 3.7. Bremsstrahlung spectra measured at zero degrees from intermediate-thickness (0.2 X_0) targets of high-Z material. The data points are measurements of O'Dell *et al.* (1968) (adapted from IAEA, 1979a).

---

[8] For this discussion, the conventional use of the symbol k for photon energy is retained.

work of O'Dell *et al.* (1968) (also see Dickinson and Lent, 1968 for calculations in this energy range).

The radiation spectra emerging from thick targets depend on target shape and material. Filtration by the target itself or by separate filters will alter the spectrum. The most satisfactory spectral calculations are made using Monte-Carlo methods. Figure 3.8 shows representative spectra from the work of Berger and Seltzer (1970).

References to earlier work on thick-target bremsstrahlung may be found in NBS Handbook No. 85 (NBS, 1964a). Other calculations and measurements can be found in IAEA (1979a).

**3.3.3.2** *High Energies.* The photon field in the environment of a high-energy electron accelerator is produced as a result of the electromagnetic cascade, and modified by the effects of passing through the accelerator components and any intervening shielding. Assuming that a substantial amount of material has been traversed, two distinct radiation fields, the "broad field" and the "forward spike," are observed.

Broad Field. The broad photon field is forward-peaked in the direction of the electron beam but extends to backward angles as well with decreasing intensity. This field is due to bremsstrahlung generated by multiple Coulomb scattering of electrons. A large fraction of these photons must therefore come from electrons present in the maximum of the shower. This radiation field at large values of Θ will be dominated by photons near the *Compton minimum*,[9] and the attenuation is controlled by the attenuation coefficient near that energy. As commonly used, the term refers to the minimum mass attenuation coefficient for photons in a given material. It occurs at a photon energy at which the cross sections for the Compton effect and electron-positron pair production are about equal. The energy at which it occurs (E_{Compt}) is less than the critical energy (E_{c}) for all materials. The *critical energy* is the energy above which the radiative losses of energy exceed those due to ionization for electrons interacting in matter. At the critical energy, the losses of energy through the mechanisms of ionization (dominant at low energies) and the emission of photons (dominant at high energies) are approximately equal. Values of critical energy in various materials can be found in IAEA (1979a).

---

[9] The expression "Compton minimum" is conventionally used here but does not accurately describe the physical phenomenon. The Compton cross section is not a minimum at the so-called "Compton minimum." It would be more accurate to describe the phenomenon as "the photon attenuation minimum."
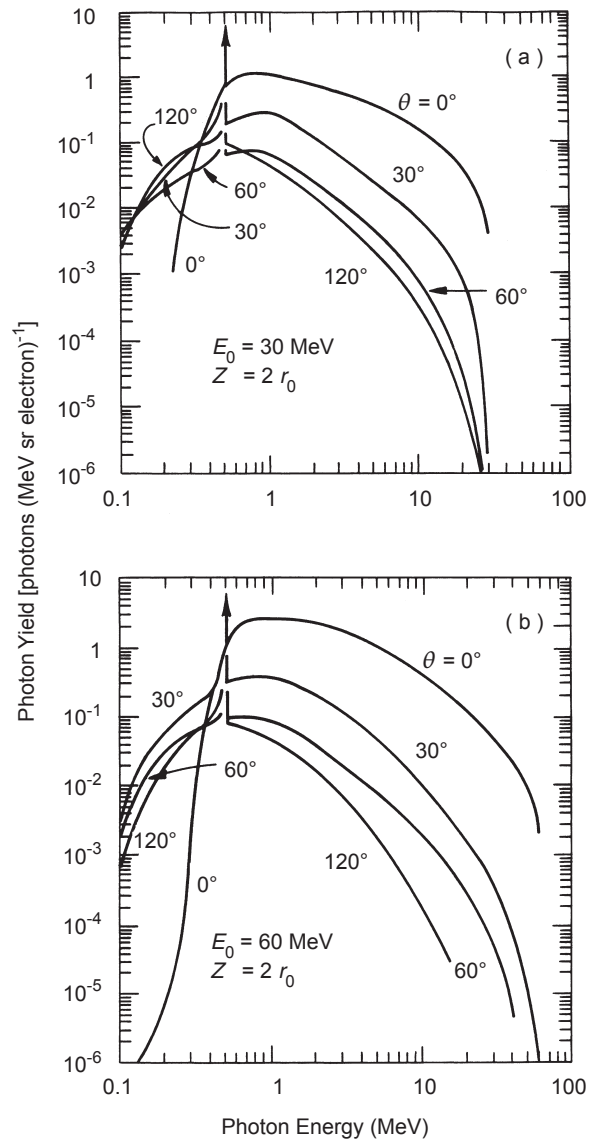
Fig. 3.8.   Spectra of bremsstrahlung photons emerging in various directions from thick tungsten targets irradiated by normally incident, monoenergetic electron beams. The target thickness in both cases is 2 r_0, or twice the mean electron range given by the continuous slowing down approximation. The arrows indicate positron annihilation radiation at 0.511 MeV. (a) Kinetic energy 30 MeV, thickness $z = 24$ g cm^{-2} (3.6 X_0); (b) 60 MeV, $z = 33$ g cm^{-2} (4.9 X_0) (adapted from Berger and Seltzer, 1970 by IAEA, 1979a).

Forward Spike. The very sharp forward spike is a remnant of the radiation produced by the incident electrons and contains photons of the highest energy possible for that primary energy. The characteristic angle (Θ_c) of this radiation is given by:

$$\Theta_c = m_0/E_0 \text{ (radians)}, \qquad (3.11)$$

where m_0 is the rest energy of the electron (0.511 MeV). In the limit of very thin targets ($X/X_0 \ll 1$), the spike of photons in the forward direction will have the spectrum and other characteristics of thin-target bremsstrahlung (Koch and Motz, 1959). For thick targets, this spike persists above a background of photons from subsequent shower generations. The angular width of the forward spike is somewhat wider for thick targets than for thin targets and is approximately given by Equation 3.9.

Absorbed Doses Related to the Forward Spike. The spike in the direction of the initial electron beam was analyzed by Tesch (1966), who compared doses from thin-target bremsstrahlung with doses from monoenergetic photons and electrons. Analyses of this type have received renewed attention because this radiation might be produced in the "maximum credible accident" at electron storage rings. Two examples are:

- An errant electron beam, if it were to strike an internal component of the machine, could produce a large dose confined to a small solid angle.
- A less-likely, but not far-fetched scenario, would result if a sudden vacuum leak occurred in a portion of the ring. In this case, it would take some time before air could diffuse to fill the vacuum chamber uniformly and, during the time that the pressure in the beam tube remained low, the beam would continue circulating until virtually every electron had interacted with air in a limited region at the air leak. Such an occurrence would produce the forward spike of thin-target bremsstrahlung already described. This phenomenon has been studied at several accelerator laboratories including Adone at Frascati (Esposito and Pelliccioni, 1982; 1986; Esposito *et al.*, 1978; Pelliccioni and Esposito, 1987; Rindi, 1982), the National Synchrotron Light Source at Brookhaven (Blumberg and Perlman, 1980)[10] and Aladdin at Wisconsin (DeLuca *et al.*, 1987; Otte *et al.*, 1987; Schilthelm *et al.*, 1985; Swanson *et al.*, 1985). Although there

---

[10] Blumberg, L. and Perlman, M.L. (1980). "Maximum credible radiation accident," unpublished National Synchrotron Light Source memo dated May 15, 1980 (Brookhaven National Laboratory, Upton, New York).

is disagreement over the magnitude of the maximum dose that might be delivered, all the studies agree that such an occurrence could have severe consequences with the beam intensities commonly achieved.

Bremsstrahlung Doses at Large Angles. Absorbed doses due to thick-target bremsstrahlung at large angles are important because of the large areas at high-energy electron accelerators that generally must be protected by radiation shielding. De Staebler *et al.* (1968) presented the first significant information for the Stanford Linear Accelerator Center (SLAC) 20 GeV electron accelerator. Their data have been used for conceptual designs of several accelerator facilities. Figure 3.9 shows the photon dose rate, normalized to a distance of 1 m from the source and for 990 MeV and 7 GeV electrons incident on targets of various materials. This work at SLAC has been extended by Jenkins (1979), who expressed the photon dose at 15 GeV in a form in which all factors are explicit assuming cylindrical geometry:

$$D = E_0 C \left(\frac{\sin \Theta}{a + d} \right)^2 \left(\frac{1}{E_0} \frac{\mathrm{d}N}{\mathrm{d}\Omega} \right) B \exp \left[-\frac{\mu}{\rho} \left(\frac{\rho d}{\sin \Theta} \right) \right],$$

$$\text{Gy electron}^{-1}, \tag{3.12}$$

where:

- D = the absorbed dose per incident electron in gray per electron
- E_0 = incident electron energy in giga-electron volts
- C = fluence to absorbed-dose conversion coefficient, which is assumed constant after the depth of shower maximum within the shield. When the absorbed dose is in gray, the electron energy is in giga-electron volts, and the distances a and d are in meters, the value of C is 2.14×10^{-15} Gy m^2 photon^{-1}
- a = internal radius, *e.g.*, of a tunnel (meters)
- d = transverse shield thickness around the tunnel (meters)
- Θ = angle with respect to the beam direction
- μ = mass attenuation coefficient
- ρ = density of material
- B = photon dose buildup factor, dependent on energy and material. In this context, the value is not significantly different from unity and this factor is omitted in the discussion that follows
- $\frac{1}{E_0} \frac{\mathrm{d}N}{\mathrm{d}\Omega}$ = the yield of photons of all energies
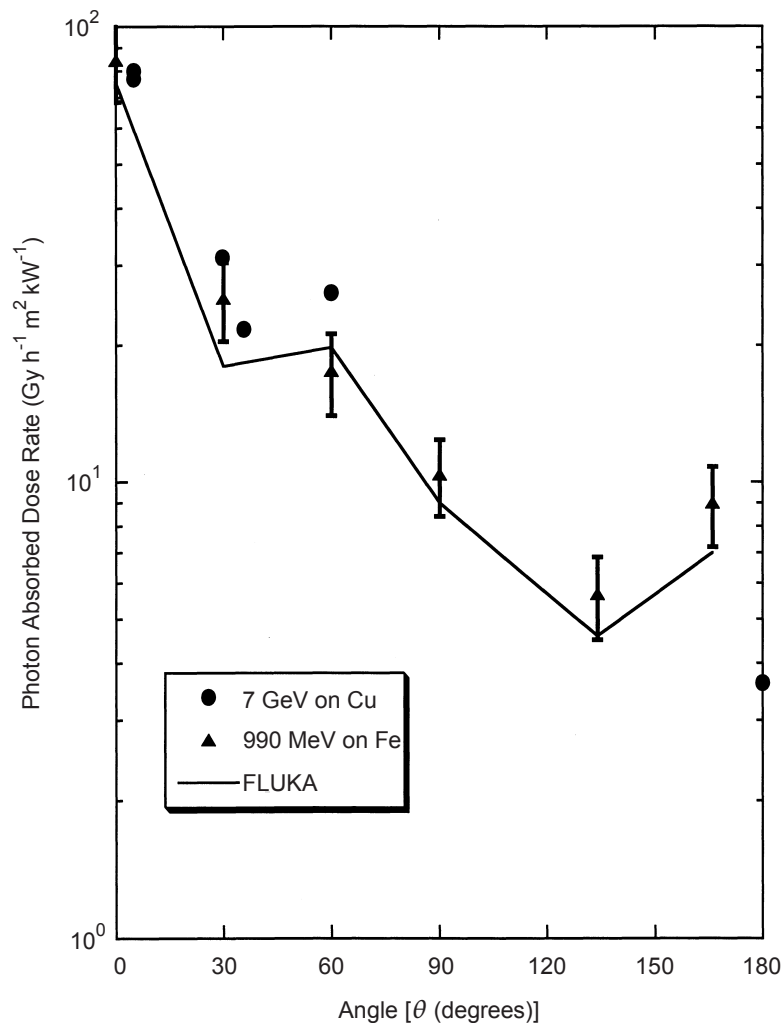
Fig. 3.9. Photon absorbed dose rate from a typical beam absorber as a function of the angle (Θ) from the beam direction. These are normalized to 1 kW of beam power and to a source-to-detector distance of 1 m for 990 MeV and 7 GeV electrons incident on a cylindrical target having a length of approximately 15 radiation lengths. The results for 7 GeV (solid circles) are for a radial distance (R_0) approximately three times the Moliere radius (X_M) (Equation 3.16a) (De Staebler *et al.*, 1968). Results at 990 MeV (solid triangles) are given by Neet (1965). Mao *et al.* (2000) provided corrections to the plots of De Staebler *et al.* incorporated in the figure. Ferrari *et al.* (1993) provided a theoretical calculation labeled "FLUKA." The errors shown for the 990 MeV data are representative of those of all the measurements and of the calculation.

The yield expression, $\frac{1}{E_0}\frac{dN}{d\Omega}$, is well-fit by the expression:

$$\frac{1}{E_0}\frac{dN}{d\Omega} = 4.76\,E_0\,\exp(-\Theta^{0.6}) + 1.08\,\exp(-\Theta/72),$$

$$\text{photons sr}^{-1}\,\text{GeV}^{-1}\,\text{electron}^{-1}. \tag{3.13}$$

The first term corresponds to yield at small angles, zero to five degrees, from targets of several radiation lengths thickness. The second fits the remaining angular range to 180 degrees. Combining Equations 3.12 and 3.13 gives:

$$D(\Theta) = 10^{-15}\big[10.2\,E_0\,\exp(-\Theta^{0.6}) + 2.3\,\exp(-\Theta/72)\big]$$

$$E_0\left(\frac{\sin\Theta}{a+d}\right)^2 \exp\left[-\frac{\mu}{\rho}\left(\frac{\rho d}{\sin\Theta}\right)\right], \text{Gy electron}^{-1}. \tag{3.14}$$

At 90 degrees, the above formulation gives:

$$D(90°) = \frac{6.95 \times 10^{-16}E_0}{(a+d)^2}\exp\left(-\frac{\mu}{\rho}\rho d\right). \tag{3.15a}$$

Expressing this in terms of total incident electron energy (U) (in joules) when D is in gray and a and d are in meters we have:

$$D(90°) = \frac{4.11 \times 10^{-6}U}{(a+d)^2}\exp\left(-\frac{\mu}{\rho}\rho d\right). \tag{3.15b}$$

In a detailed study, Dinter and Tesch (1977) measured the absorbed dose from electromagnetic radiation around iron plates of thickness t = 0.2, 1, 5 and 10 cm (0.11, 0.57, 2.84 and 5.68 X_0, respectively), placed at various orientation angles (ϕ) to electron beams of E_0 = 3, 5 and 7.2 GeV. The target was struck by 5 GeV electrons and data are normalized to an incident beam energy of 1 J. Some of their measurements, obtained with ^{7}LiF TLDs, are shown in Figure 3.10 for E_0 = 5 GeV. At this energy, shower maximum is at $\sim X_{\text{max}}$ = 7.6 cm (4.3 X_0). More recent results have also been reported by Ferrari *et al.* (1993).

In Figures 3.10a through 3.10d, the angle of observation Θ increases in the clockwise direction and the detector is on the opposite side of the target from the point of beam incidence. For Figures 3.10e through 3.10h, Θ is measured in same sense as ϕ; dips in curves occur when the detector (TLD) is nearly in the target plane (*i.e.*, $\Theta \approx \phi$; see insets in Figures 3.10a and 3.10d). Note that 1 cm = 0.568 X_0 and that the step line at ϕ = 2 degrees in Figure 3.10a shows the result of a Monte-Carlo calculation. Several general
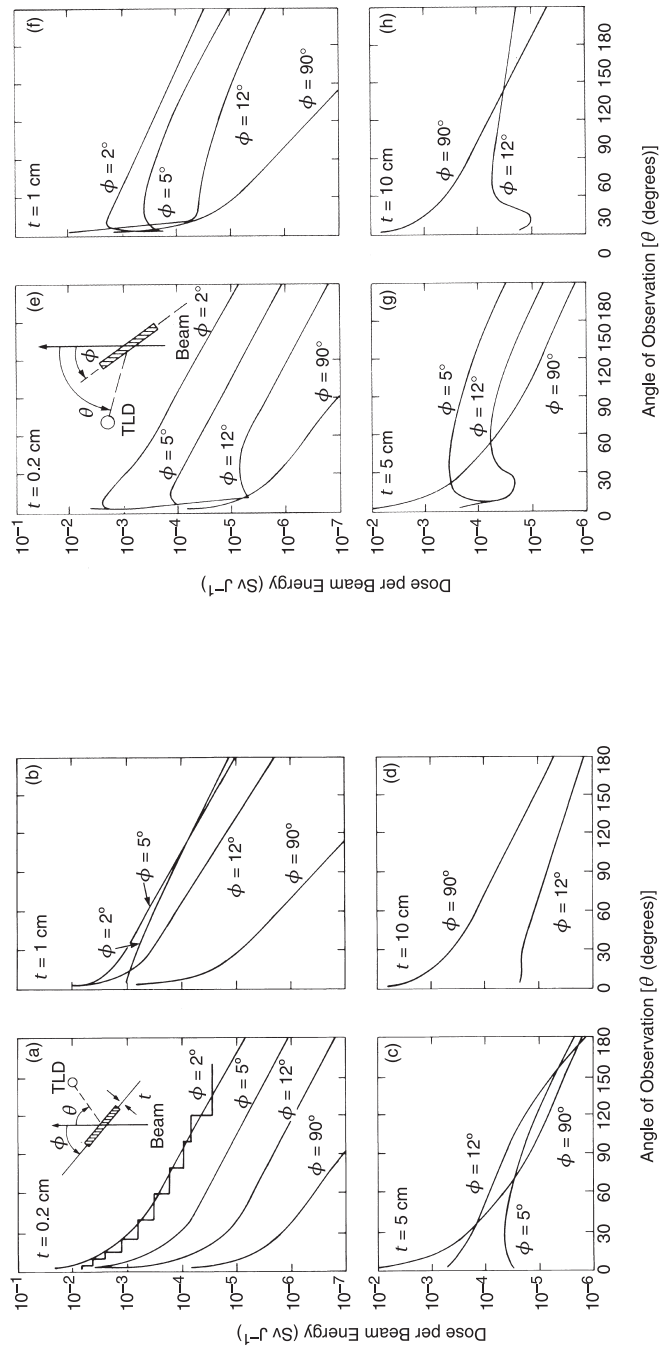
Fig. 3.10.   Absorbed dose of electron-photon stray radiation at a distance of 1 m from an iron target at various orientation angles (ϕ) as function of the angle of observation (Θ) and for an electron beam of $E_0 = 5$ GeV (Dinter and Tesch, 1977). In the case of electron irradiation, the quantities Sv J^{-1} and Gy J^{-1} are numerically identical because the absorbed dose and dose equivalent are identical.

conclusions can be drawn from these data which may be applied to a wide range of energy. The strong dependence on target geometry is obvious:

- The absorbed doses decline with detector angle (Θ) for all geometries. This is manifestly true for those orientations for which the detector is on the opposite side of the target from the point of beam incidence (Figures 3.10a through 3.10d). The dips seen in Figures 3.10e through 3.10h are due to self-absorption in the target when the plane of the target nearly coincides with the direction of observation; thus, they can be considered as artifacts. Around $\Theta = 90$ degrees, the reduction in dose with angle can be approximately described by exponentials of the form: $D \, e^{-\beta\Theta}$. For glancing incidence, (2 degrees $\leq \phi \leq$ 12 degrees), on thin targets the slopes of the curves at 90 degrees correspond to values of β between 1.6 and 1.7 radians^{-1}. For thicker targets, smaller values of β are found and for all target thicknesses, the rate of decline with observation-angle is strongest for perpendicular incidence ($\phi \sim 90$ degrees).
- For effective target thicknesses, t cosec $\phi < 15$ cm, the highest absorbed doses were found in the forward direction ($\Theta = 0$ degrees).

Analysis of the absorbed dose rates, as a function of incident beam energy (not shown here), led to the following generalizations by Dinter and Tesch:

- For "thick" targets (t cosec $\phi > 8$ cm), absorbed-dose rates were proportional to incident electron energy over the range 3 GeV $\leq E_0 \leq$ 7 GeV.
- For "thin" targets ($t = 0.2$ cm and t cosec $\phi < 2$ cm), absorbed dose rates were independent of incident electron energy over the range 3 GeV $\leq E_0 \leq$ 7 GeV.

Dinter and Tesch also made the following observations concerning the dose attenuation in representative shielding materials (lead, iron, heavy concrete, ordinary concrete, and sand):

- For "thin" targets, as defined above, 99 percent of the absorbed dose was from very low-energy particles, as evidenced by rapid initial attenuation by relatively thin layers of shielding. For perpendicular incidence ($\phi \sim 90$ degrees), the initial transmission factor for these materials ranged from 0.007 to 0.004 for target thicknesses 0.2 cm $\leq t \leq$ 5 cm.
- The attenuation coefficient for the subsequent exponential attenuation μ_0/ρ, was independent of target arrangement.

Observed values of μ_0/ρ were consistent with the minimum photon attenuation coefficients μ_{min}/ρ, for the shielding materials investigated.

Another parameter of importance for describing the electromagnetic cascade is the Moliere radius (X_M) given by:

$$X_M = X_0 E_s / E_c, \tag{3.16a}$$

where:

$$E_s = \left(\sqrt{4\pi/\alpha}\right) m_e c^2 = 21.2 \text{ MeV}, \tag{3.16b}$$

and α is the fine structure constant and m_e is the mass of the electron (Moliere, 1948). The parameter X_M serves as a good "characteristic" width with which to describe the radial distributions of electromagnetic showers.

Fasso *et al.* (1984a) reported Monte-Carlo studies using the program EGS (Ford and Nelson, 1978) which gave the dose distribution about a tungsten target of 0.5 cm radius (1.43 X_0 or 0.69 X_M) and three thicknesses ($t = 2, 4$ and 10 X_0) struck by 200 MeV electrons. For this energy, *shower maximum* occurs at $X_{max} = 2 X_0$. The shower maximum is that point at which the number of particles involved in an electromagnetic cascade is the largest. This distribution is shown in Figure 3.11, where the dose as a function of angle about the target can be seen.

Calculations using the EGS code have subsequently been extended to cover the energy range from 0.15 to 500 GeV. These have been tabulated by Schopper *et al.* (1990). The electron-photon cascades in concrete, iron and lead were studied and their dependence on primary energy, target configuration, and angle of observation determined. Comparisons between calculation and experimental observation were made at 5 GeV (Dinter *et al.*, 1988) and considerable agreement obtained. The EGS code provides accurate data up to very high energies.

A comparison with Equations 3.15a and 3.15b shows consistency with measurements. The data of Fasso *et al.* (1984a) give absorbed doses about a factor of two higher than Equation 3.15 for the target radius used in the calculations. The data of Dinter and Tesch (1977) lie a factor of two to five higher at 90 degrees than predicted by Equation 3.15. However, after correction for the low-energy component, which is quickly absorbed, the data of Dinter and Tesch lie within a factor of three to five below those given by Equation 3.15.

Scaling of Doses from Thick-Target Bremsstrahlung. Absorbed-dose rates from thick-target bremsstrahlung at large angles (45 to 180 degrees) scale linearly with initial beam power
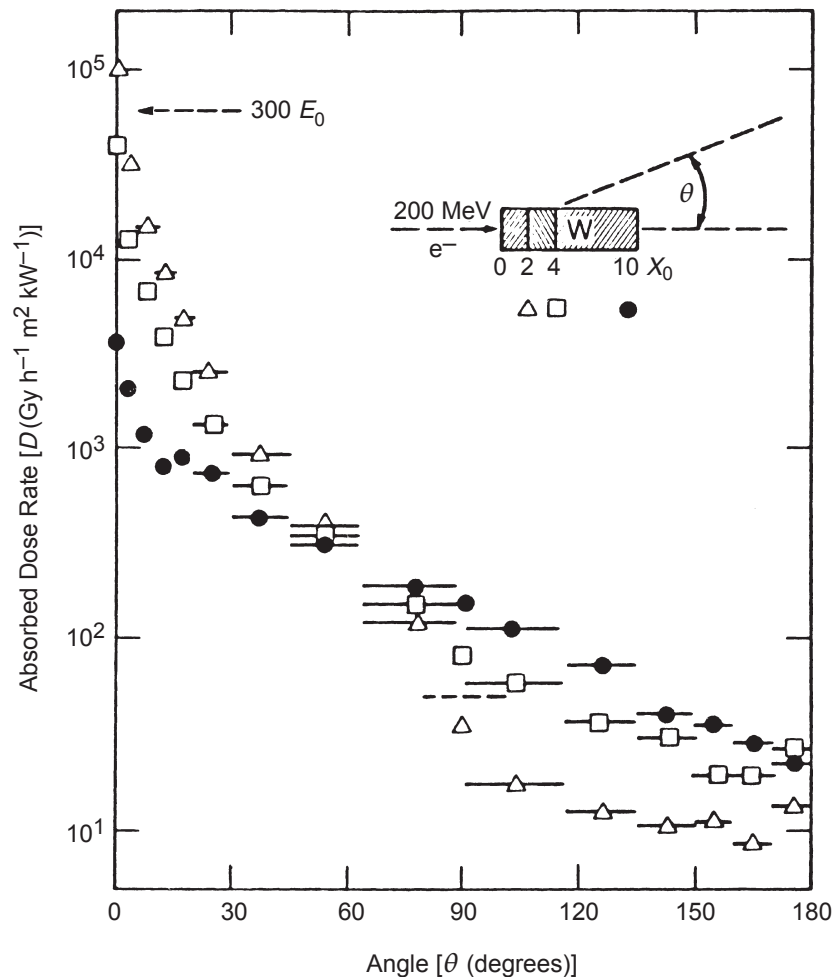
Fig. 3.11. Normalized absorbed dose rate at a distance of 1 m from a 1 cm diameter tungsten target struck by 200 MeV electrons, as a function of angle (Θ). Target thicknesses used: 2 ($\triangle$), 4 ($\square$) and 10 X_0 ($\bullet$) (Fasso *et al.*, 1984a).

and within limits is independent of energy. The reason for this is that the photon doses at large angles are mainly due to radiation from electrons of relatively low energy that have been scattered to large angles. The number of such degraded particles, at energies near E_c, increases with initial particle energy, for constant beam current. This rule was confirmed by Dinter and Tesch (1977) for thick targets (see above). The careful reader will notice that the

results presented in Figures 3.5, 3.9, and 3.10 together with the use of Equation 3.15 are not self-consistent to high accuracy. For example, at $\Theta = 90$ degrees, the following values of dose per unit beam energy are found:

Figure 3.5: $\sim 1.4 \times 10^{-5}$ Gy J^{-1} for optimal radius target
Figure 3.9: $\sim 4 \times 10^{-6}$ Gy J^{-1} for large radius of 5 X_M
Figure 3.10: 1×10^{-5} to 7×10^{-5} Gy J^{-1} for unknown radius
Figure 3.11: 4.1×10^{-6} Gy J^{-1} for large radius of X_M

These differences most likely arise from the differences in radius of the target but there are also differences in the material used. This topic has been studied in detail by Mao *et al.* (2000).

3.3.4 *Neutron Production*

The production of neutrons by electron beams incident on thick targets has been discussed in detail by Swanson (IAEA, 1979a; Swanson, 1978; 1979). The principal yield of neutrons arises from photonuclear reactions.

Total photoneutron production is obtained by integration of the photoneutron-production cross section multiplied by the photon track length distribution of the electromagnetic cascade shower. The results for several materials are summarized in Figure 3.12, which shows that, at $E_0 = 100$ MeV, the neutron production rate per unit beam power is nearly saturated for high-Z target materials, whereas it is still rising for $Z < 50$. However, the production rate per unit beam power for $E_0 \geq 500$ MeV is almost constant for all materials.

The variation of photoneutron source strength (N) with target material is indicated by an approximate formula suggested by Swanson (1979) which fits the behavior over a large range of Z and energies (Section 4):

$$N = 1.21 \times 10^8 \, Z^{0.66} \qquad \text{neutrons J}^{-1}. \qquad (3.17)$$

This formula is reliable over most of the range of Z for electron energies above ~ 200 MeV, but underestimates the source for very light materials (especially ^{3}H, lithium and beryllium) and for transuranic materials in which photofission processes become important.

In discussing photoneutron production mechanisms, it must be borne in mind that the electromagnetic cascade shower contains photons of all energies from zero up to the primary particle energy. The thin-target photon spectrum behaves approximately as k^{-1}, where k is the photon energy. Because of the preponderance of lower energy photons and because of the large absorption cross sections
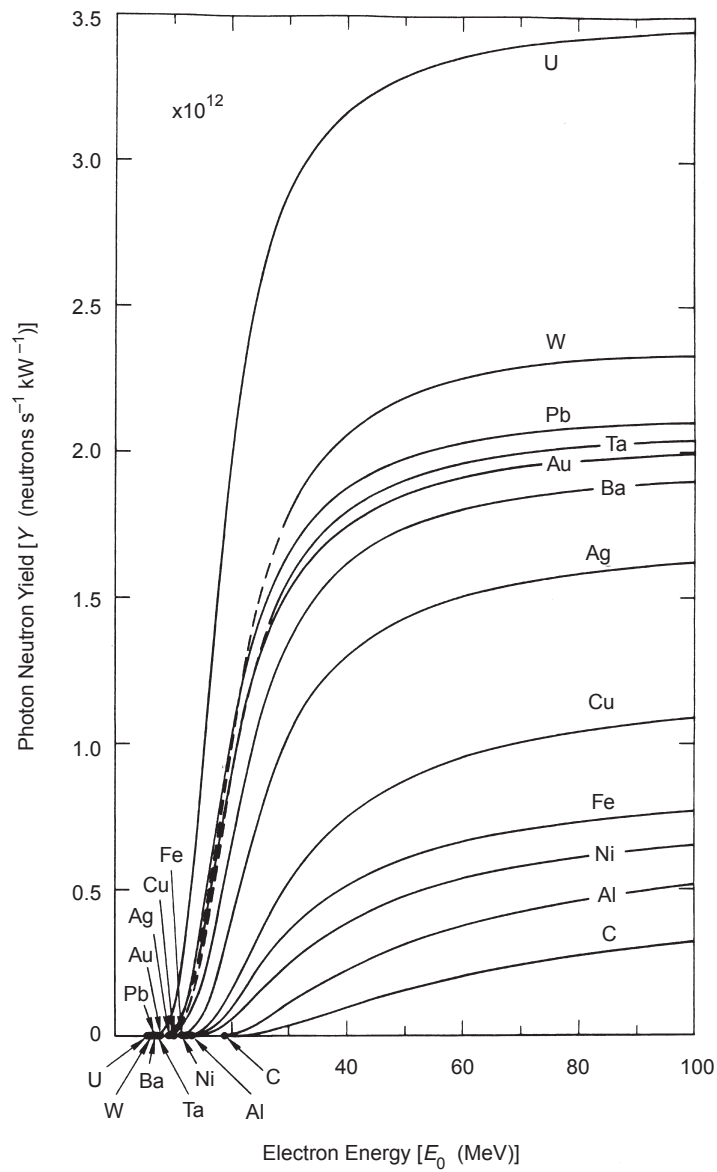
Fig. 3.12. Yield of photoneutrons produced in electromagnetic cascades initiated by electron incident on thick targets per unit beam power, as a function of incident energy (Swanson, 1979).

at low photon energies, the dominant neutron source mechanism at all primary energies is the giant photonuclear resonance. Other mechanisms play an important role when high-energy photons are present in the electromagnetic cascade shower. These secondary mechanisms are the *quasi-deuteron* effect, which is more important for photon energies in the range 30 to 300 MeV (De Staebler *et al.*, 1968; IAEA, 1979a), and neutrons released as a product of *photopion* reactions (threshold at 150 MeV), which are more important at photon energies above 300 MeV (De Staebler *et al.*, 1968). The *quasi-deuteron* effect refers to the absorption of a photon by a proton-neutron pair in the nucleus with the possible subsequent emission of a neutron. *Photopion* reactions are those in which the absorption of a photon is followed by the emission of a pion, possibly accompanied by one or more neutrons.

Photoneutron spectra from the giant dipole resonance[11] process are often compared to a fission spectrum and are well described by a Maxwellian distribution, having a "temperature" in the range $0.5 \text{ MeV} \leq T \leq 1.5 \text{ MeV}$. The Maxwellian energy spectrum is expressed by the equation:

$$\frac{\mathrm{d}\phi}{\mathrm{d}E_n} = \frac{E_n}{T^2}\, \mathrm{e}^{-E_n/T}, \tag{3.18}$$

which is normalized to unit fluence. For this distribution, the peak ($\hat{E}_n$) and average ($\overline{E}_n$) energies lie respectively in the range:

$$\hat{E}_n = T \approx 0.5 - 1.5 \text{ MeV} \tag{3.19}$$

and

$$\overline{E}_n = 2\,T \approx 1 - 3 \text{ MeV}. \tag{3.20}$$

The Maxwellian distribution does not account for the high-energy tail produced by the secondary mechanisms described above. The behavior at photoneutron energies higher than ~10 MeV is summarized by IAEA (1979a) and has been described by a simple exponential behavior:

$$\frac{\mathrm{d}N}{\mathrm{d}E_n} \approx E_n^{-\alpha}, \tag{3.21}$$

where α is in the range 1.7 to 3.6. However, as the secondary neutron energy approaches the primary photon-beam energy, the spectrum becomes steeper (*i.e.*, if Equation 3.21 is still used, the value of α increases with neutron energy).

---

[11] The giant dipole resonance is hereafter referred simply as the "giant resonance."

Although many more photoneutrons are produced *via* the giant resonance than from the higher-energy mechanisms, it is the neutrons above 100 MeV that are most capable of penetrating thick shields. Except for limited regions where muons may predominate, it is the high-energy neutrons (*i.e.*, $E_n > 150$ MeV) that propagate the radiation field for shielding thicknesses greater than $\sim$2 m of concrete. In so doing, they continually regenerate a "satellite" field: neutrons of lower energy and neutron-capture gamma rays.

3.3.5 *Muon Production*

The two principal sources of muons are, first, by pair production and second from pion and kaon decay. Muon pair-production (μ^+, μ^-) by photons becomes possible at energies above $\sim$211 MeV (the dimuon rest mass). This is a process analogous to (e^+, e^-) pair production, except that the production cross sections for electron pair production are higher by a factor that is approximately the square of the ratio of the particle masses $(m_\mu/m_e)^2$ (*i.e.*, $\sim$40,000).

Muons also are produced by the decay of $\pi^\pm$ and $K^\pm$ mesons in flight. The magnitude of the fluences produced depends on the length of the decay path[12] available but is generally small compared to the magnitude of the fluences from direct muon pair production. At both electron and hadron accelerators, the photo-produced muon fluence is very highly peaked in the forward direction. Outside thick accelerator shielding, the fluence distribution typically may have diameters (at half intensity) of 10 to 30 cm. Stevenson (1983) has provided a complete analysis of the dosimetry of muons and has found that over the muon energy domain from 100 MeV to 200 GeV, the dose equivalent per unit fluence may be taken to be 4×10^{-8} μSv m^2 (4×10^{-4} μSv cm^2).

Both the photo-production and transport of muons, with specific application to electron accelerators, have been discussed by Clement and Kessler (1965), Nelson (1968), and in the companion papers by Nelson and Kase (1974), Nelson *et al.* (1974), and Alsmiller and

---

[12] The term "decay path" refers to the available flight path in which the pions and kaons can decay in flight to produce muons. Such decay paths may be comprised of vacuum or gases but not solids or liquids since solids or liquids absorb the pions or kaons by means of nuclear interactions after flight times insufficient to allow for the decay into significant numbers of muons.

Barish (1969). Figure 3.13 shows an example of calculated integral energy spectra of muons produced in a thick target of iron at various angles (Θ) by 20 GeV electrons. Figure 3.14 shows the $\mu^{\pm}$ fluence at zero degrees integrated over all muon energies, as a function of primary electron energy (E_0). The fluence rate at zero degrees per kilowatt of primary electron-beam power is approximately proportional to E_0 at energies up to ~30 GeV.

The photoproduction of muons from targeted electron beams has been described by Nelson (1968), and the expression for generating the differential muon fluence rate ($d\phi/dE$) at distance R in the direction Θ is:
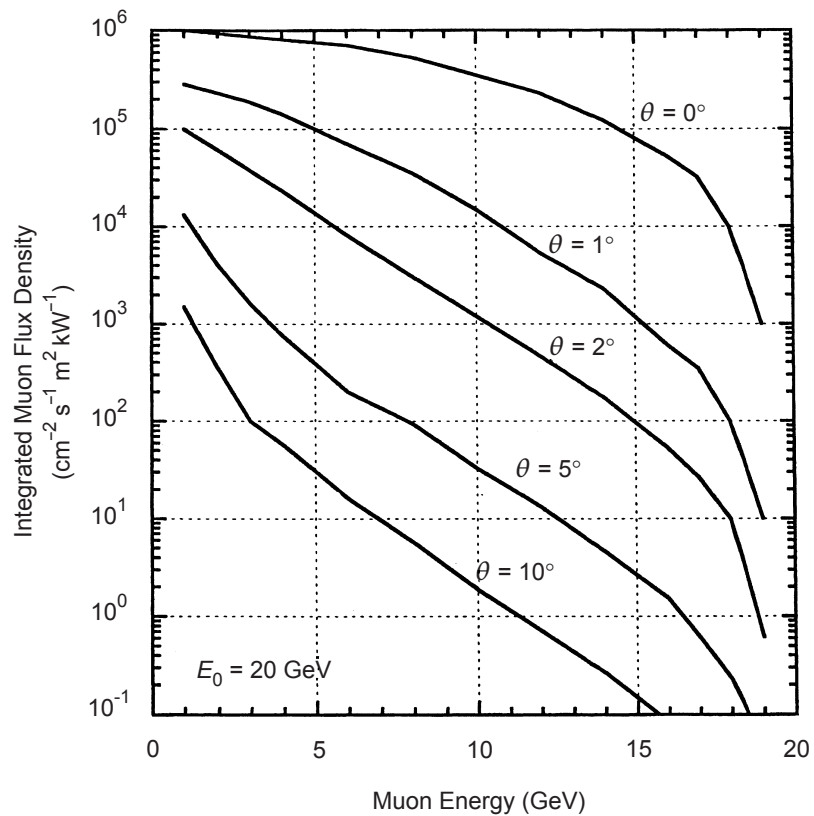
Fig. 3.13. Integrated muon flux density at 1 m kW^{-1} of electron beam power as a function of muon energy for 20 GeV electrons incident on a thick iron target at several values of Θ. The integral of the flux density over energy includes all muons that have energies that exceed the value of the abscissa at the specified value of Θ (after Nelson, 1968 as adapted by IAEA, 1979a).
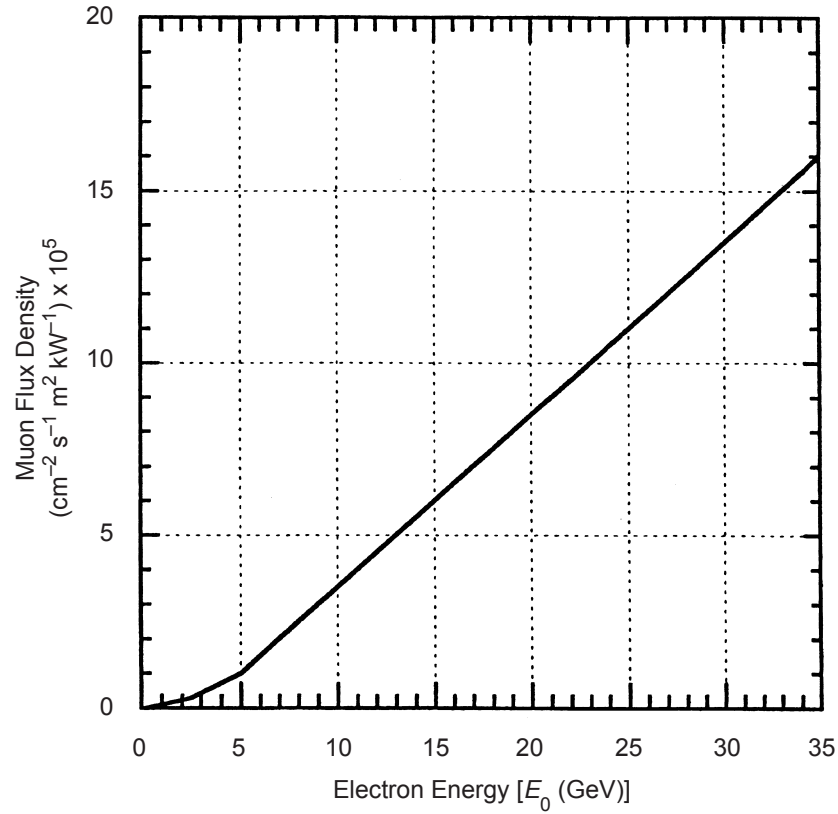
Fig. 3.14. Muon flux density at zero degrees at 1 m from an unshielded iron target per kilowatt of electron beam power as a function of electron energy (E_0) (Nelson, 1968).[13]

$$\frac{\mathrm{d}\phi}{\mathrm{d}E}(E,\Theta;E_0) = \frac{2\,I}{R^2}\int_{E+\mu}^{E_0-m}\frac{\mathrm{d}^2\sigma}{\mathrm{d}\Omega\mathrm{d}E}(k,E,\Theta)\frac{\mathrm{d}\ell}{\mathrm{d}k}\,\mathrm{d}k$$

$$\mathrm{cm}^{-2}\ \mathrm{s}^{-1}\ \mathrm{GeV}^{-1}, \tag{3.22}$$

where:

I = electron current (e s^{-1})
R = distance from target (centimeters)
Θ = laboratory production angle

---

[13] The scale factor 10^5, which has been correctly applied to the ordinate of Figure 3.14, has not appeared in several manifestations of this figure in the literature.

E_0 =   total energy of an electron in the beam (giga-electron volt)

E =   total muon energy (giga-electron volt)

k =   energy of photon in shower (giga-electron volt)

m, μ =   rest mass of electron (0.000511 GeV) and rest mass of muon (0.1057 GeV)

$\mathrm{d}\ell/\mathrm{d}k$ =   differential photon track length

The factor two in the equation results from taking into account the production of the μ^+, μ^- as a pair.

For a thick-electron target, we can use the Clement and Kessler (1965) equation for the photon differential track length ($\mathrm{d}\ell/\mathrm{d}k$) which agrees quite well with Monte-Carlo results over most of the photon energy range. Alternatively, Tsai and Whitis (1966) provide an equation for targets of limited thickness.

The muon pair production cross section $\mathrm{d}^2\sigma/\mathrm{d}\Omega\mathrm{d}E$ as derived by Tsai (1971) permits a reasonably straightforward solution of Equation 3.22. The integral muon fluence rate is given by:

$$\phi(E_0, E, \Theta) = \int_E^{E_0 - m - \mu} (\mathrm{d}\phi/\mathrm{d}E')\mathrm{d}E' \quad \mathrm{cm}^{-2}\ \mathrm{s}^{-1} \qquad (3.23)$$

and the dose rate:

$$\frac{\mathrm{d}D}{\mathrm{d}t} = \int_E^{E_0 - m - \mu} \mathrm{f}(E')\ (\mathrm{d}\phi/\mathrm{d}E')\mathrm{d}E' \quad \mathrm{Gy}\ \mathrm{s}^{-1}, \qquad (3.24)$$

where $\mathrm{f}(E') = 1.6 \times 10^{-10}(1/\rho)\mathrm{d}T(E')/\mathrm{d}x$, and $(1/\rho)\mathrm{d}T(E')/\mathrm{d}x$ is the unrestricted mass stopping power formula given by Barkas and Berger (1964). Thus, to arrive at the dose rate from photo-produced muons using Tsai's expression for $\mathrm{d}\ell/\mathrm{d}k$, a routine for numerically integrating this function is required. This is reasonably straightforward, using one of the many routines available from math libraries.

3.3.6   *Electromagnetic Cascade*

For the cascade processes to be possible, the energy of the primary beam must be well above the critical energy of the material struck by the beam.[14] For electron energies greater than the critical energy (E_c) the radiation losses will dominate those from ionization so that showering can occur more readily, whereas, at energies below E_c,

---

[14] For the sake of continuity, definitions of some of the parameters defined in previous sections are repeated here.

bremsstrahlung production, and therefore showering, is increasingly suppressed. Although the electromagnetic cascade is in detail an exceedingly complicated stochastic phenomenon, it is nevertheless possible to describe it through generalizations that describe its average behavior. An intuitive picture is very helpful: An electron travels about one radiation length (X_0) and emits a photon with which it shares its energy about equally. The emitted photon then travels approximately one radiation length (actually $\sim$9/7 X_0), within which distance it produces an electron-positron pair. The pair members share the photon's energy about equally. Meanwhile, the original electron radiates a new photon. In each such encounter, the number of particles approximately doubles and the average energy per particle is similarly halved. This multiplication process results in a rapid rise in particle number (and absorbed dose to the medium) until the average electron energy is near the critical energy. When this occurs, the shower "tops out" at a maximal dose deposition. Thereafter the electrons, having too low an energy, cannot actively participate in maintaining the shower. Thus, photons remain as the particles that principally propagate the cascade. The photon energy at which the minimal attenuation coefficient occurs, called the "Compton minimum," is typically one-third to one-half E_c for all materials. Below this energy, the probability for Compton scattering and resulting energy degradation becomes larger than for electron-positron pair production" (Swanson and Thomas, 1990). The concepts and units by which an electromagnetic shower may be characterized are summarized below:

- radiation length (X_0);
- Moliere length (X_M);
- critical energy (E_c);
- Compton minimum occurs at energy (E_{Compt}), which is less than the critical energy (E_c) for all materials. Values can be found in IAEA (1979a);
- interaction length for pair-production (λ_p). When the photon energy is much greater than the Compton minimal energy (E_{Compt}), the interaction length for pair-production (λ_p) is given by 9/7 X_0;
- attenuation coefficient (μ_c) used to describe the exponential attenuation of the "tail" of the electromagnetic cascade (see, for example, Bathow *et al.*, 1970; Dinter and Tesch, 1977) according to the functional form for intensity of:

$$I = I_0 e^{-\mu_c x} \tag{3.25}$$

is a good approximation at values of the coordinate x beyond that of the shower maximum. Due to inclusion of other effects,

values of μ_c are somewhat larger than the inverse of the photon mass-attenuation length at the Compton minimum; *e.g.*, for aluminum, copper and lead, μ_c is smaller by factors of 0.73, 0.83 and 0.95, respectively;

- the equivalent quantum energy for thin-target bremsstrahlung is equal to the total energy radiated by all incident electrons divided by the incident energy of one electron (E_0). It is approximately equal to the thickness of the radiating target, measured in radiation lengths, multiplied by the number of incident electrons.

The dosimetric properties of an electromagnetic cascade shower may be summarized in curves that show the quantities of interest (*e.g.*, fluence of particles, the absorbed dose) as functions of shower depth or of distance from the shower axis. An example is the curve in Figure 3.15 that shows the fraction of total energy deposited versus depth, from the work of Bathow *et al.* (1970 as adapted by Van Ginneken and Awschalom, 1974). Energy deposition is integrated over all radii about the shower axis. Van Ginneken and Awschalom generalized this curve by defining a new parameter (λ_ℓ) as:

$$\lambda_\ell = 325 \, (\ln Z)^{-1.73} \, (\ln E_0), \tag{3.26}$$

where λ_ℓ is in g cm^{-2}, and E_0 is in mega-electron volts. When depths are expressed in units of λ_ℓ, all curves approximately merge into a universal curve. The energy dependence of λ_ℓ shows that the location of the dose maximum moves deeper into the medium, proportional to the logarithm of the incident energy. This is because each doubling of incident energy adds approximately one unit of distance to that needed to reduce the average particle energy to E_c.

The so-called *Approximation B* of analytic shower theory (Rossi, 1952; Rossi and Greisen, 1941) predicts that the number of negative and positive electrons at the shower maximum (N) should be nearly proportional to E_0/E_c in the following manner:

$$N = \frac{0.31 \, (E_0/E_c)}{[\ln(E_0/E_c) - 0.37]^{1/2}} . \tag{3.27}$$

This conclusion is consistent with the intuitive picture outlined above where, at the shower maximum, the energy of the incident electron (E_0) is divided among a number of particles having energy near E_c. As discussed, the location of shower maximum (X_{max}) should depend on the logarithm of the incident energy. Approximation B gives:
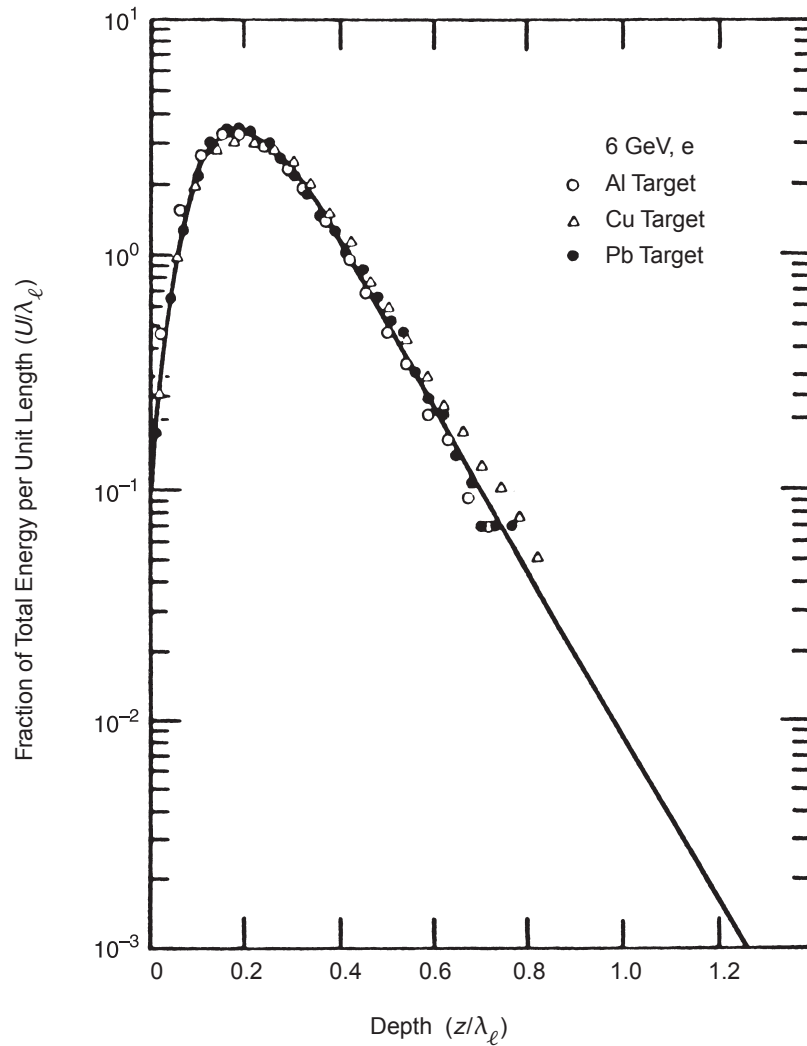
Fig. 3.15. Fraction of total energy per unit length (U/λ_ℓ) deposited by an electromagnetic cascade versus depth [z (in units of λ_ℓ)], integrated over all radii about the shower axis (Bathow *et al.*, 1970; Van Ginneken and Awschalom, 1974).

$$X_{max}/X_0 = 1.01 \, [\ln(E_0/E_c) - 1]. \qquad (3.28)$$

Experimentally, Bathow *et al.* (1967) found:

$$X_{max}/X_0 = \ln(E_0/E_c) - C, \qquad (3.29)$$

where C takes the values 0.77 for copper and 0.47 for lead.

Figure 3.16 shows the fraction (U/E_0) of incident energy that escapes as a function of cylinder radius for showers caused by electrons of various energies (De Staebler *et al.*, 1968; Nelson *et al.*, 1966). The abscissa is the cylinder radius in units of Moliere length. There is obviously a transition in this distribution from a steeper slope to a constant smaller slope at larger radii. The curve has been parameterized as:

$$U/E_0 = 0.8 \exp(-3.45 \, R/X_M) + 0.2 \exp(-0.889 \, R/X_M), \quad (3.30)$$

where X_M is the Moliere length previously defined. While there is no simple derivation for the first term of this expression, the second
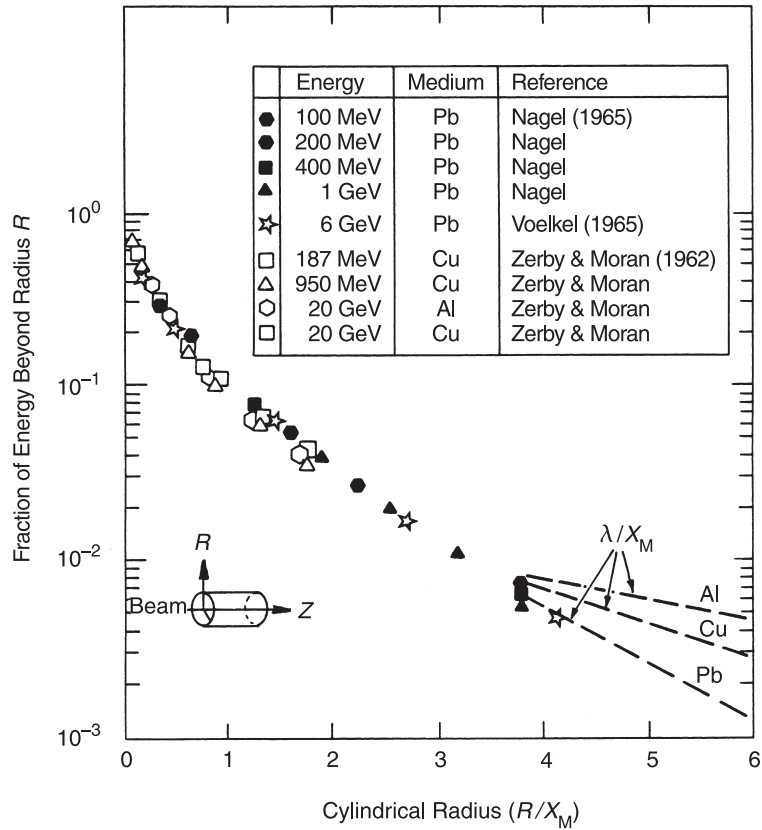
Fig. 3.16. Fraction of total energy (U) deposited outside a cylindrical radius (R/X_M) as a function of radius for showers caused by 0.1 to 20 GeV electrons incident on various materials (De Staebler *et al.*, 1968).

term, describing the radial "tail," is related to the attenuation of photons near the Compton minimum.

Although these empirical observations are useful, the Monte-Carlo approach to calculations of the electromagnetic cascade is the most satisfactory in several ways (see, for example, Ford and Nelson, 1978; Nelson *et al.*, 1985). Particular advantages are, first, that all of the several elementary physical processes of electrons and photons can be taken into account accurately, and second, that geometrical details can be modeled with utmost flexibility. Monte-Carlo calculations of the electromagnetic cascade, published in the literature, are summarized in Table 3.1.

Experimental studies of the electromagnetic cascade go back several decades, having received early impetus from cosmic-ray research. References to earlier experimental work can be found, for example, in Bathow *et al.* (1967; 1970). Additional experimental work has been described by Brockmann *et al.* (1971), Hirayama *et al.* (1987), Jakeways and Calder (1970), Mueller (1972), Nakamura *et al.* (1987), and Yuda *et al.* (1970).

3.4 Radiation Protection at Proton Accelerators

3.4.1 *General*

Section 2 of this Report has described the wide variety of proton accelerators currently in operation.

Of the accelerator types described in Section 2, those used to accelerate protons include direct-voltage accelerators, linear accelerators, cyclotrons, and synchrotrons. Many of these proton accelerators also accelerate light, intermediate-mass, or even heavy ions. This is particularly true at lower energies and at proton accelerators used in research. (The special considerations for accelerators of ions heavier than protons are discussed in Section 3.5.) Although many accelerator types may be used to accelerate many species of ions, the use of hydrogen ions dominates the use of the other light ions in importance with respect to radiation safety. The reason for this is that the proton beam intensities are usually higher and protons generally have the highest energy per nucleon (specific energy), and therefore the longest ionization range in a given material.

TABLE 3.1—*Monte-Carlo calculations of the electromagnetic cascade.*

Authors and Dates	Data[a]	Medium	Type[b]	Initial Particle Energy
Wilson (1952)	I	Pb	e, γ	20, 50, 100, 200, 300, 500 MeV
Alsmiller and Moran (1966)	D, Y	Ta	e	30, 100, 150, 200 MeV
Alsmiller and Moran (1966)	Y	Pb	e	34, 100 MeV
Varfolomeev and Drabkin (1966)	D	Pb	e	6 GeV
Alsmiller and Moran (1967)	E	H_2O	e	0.1, 0.02, 0.5, 1, 5.2, 10, 20 GeV
Alsmiller and Moran (1967)	E	H_2O	γ	0.01, 0.02, 0.05, 0.1, 0.2, 0.5, 1, 5.2, 10, 20 GeV
Burfeindt (1967)	D	Pb	e	3 GeV
Voelkel (1967)	D	Cu	γ	1, 3, 6 GeV
Voelkel (1967)	D	Cu	B	6 GeV
Alsmiller and Moran (1968)	D	Pb	γ	15, 25, 35, 45, 60, 75, 100 MeV
Alsmiller and Moran (1970a)	E	H_2O, Al	e	1 GeV
Cioni and Treves (1969)	I	Pb-glass	e	50, 150, 300, 500 MeV; 1 GeV
Gabriel and Alsmiller (1969)	D, Y	Cu	e	50, 100, 200, 300, 400 MeV
Alsmiller and Moran (1970a)	E	H_2O, Al	e	1 GeV
Alsmiller and Moran (1970b)	E	Be, Al	γ	45 GeV
Beck (1970a)	E	H_2O	e, γ	100, 200, 500 MeV; 1, 5.2, 10, 20 GeV
Beck (1970b)	E	H_2O, Al	e	1 GeV
Berger and Seltzer (1970)	D, Y	Ta, W	e	2, 5, 10, 15, 20, 30, 60 MeV
Messel and Crawford (1970)	D	Air	e, γ	500 MeV; 1, 10, 50 GeV
Messel and Crawford (1970)	D	Cu	e, γ	50, 100, 200, 500 MeV; 1, 2 GeV
Messel and Crawford (1970)	D	Pb	e, γ	50, 100, 200, 500 MeV; 1, 2, 10 GeV
Beck (1971)	E	Pb + H_2O[c]	e	1 GeV
Beck (1971)	I	Air + Al[c]	e	200, 500 MeV; 1 GeV
Beck (1971)	I	Air + Fe[c]	e	200, 500 MeV; 1 GeV

TABLE 3.1—*Monte-Carlo calculations of the electromagnetic cascade.* (continued)

Authors and Dates	Data[a]	Medium	Type[b]	Initial Particle Energy
Alsmiller *et al.* (1974)	E	H_2O	e	50, 100, 150, 200 MeV
Ford and Nelson (1978)	D	Various	e, γ	Various
Nelson *et al.* (1985)	D	Various	e, γ	Various
Nakamura *et al.* (1987)	D	Cu	e	900 MeV
Ferrari *et al.* (1993)	E	Fe, Sn, W	e, γ	100, 250, 510, 800, 1,000 MeV

[a]Type of cascade data given:
  D = data on electron and/or photon track length, differential in energy or in such a form that some information on differential track length can be derived
  E = distribution of energy deposition (absorbed dose) in medium only
  I = data on electron and/or photon track length, but integrated over energy
  Y = yield of some type of secondary particle is given, in addition to cascade data
[b]Particle type:
  e = electron (or positron)
  γ = monoenergetic photon
  B = bremsstrahlung beam of indicated endpoint energy
[c]Two-material medium.

3.4.2 *Proton Beams*

It is essential to avoid human exposure to high intensities of the primary proton beams now available.[15] This topic is discussed more completely in Section 7 and is of particular concern at high-energy proton accelerators used in research.

At proton accelerators with energies above ~500 MeV, secondary beams of various particles, such as pions ($\pi^\pm$), kaons ($K^\pm$), muons ($\mu^\pm$), and electrons of both charge ($e^\pm$), become available. Operation of these accelerators is extremely flexible: several beams may be available at any one time and a wide range in beam energy and intensity is possible. Frequent safe access may be required to some beam lines while the accelerator continues to provide beam to other beam lines. It cannot, therefore, be too strongly emphasized that the design of radiation-safety interlocks is of prime importance (Casey *et al.*, 1988; NCRP, 1986; see also Section 7 of this Report). Ingenious solutions are often needed to accommodate these various conditions in order to provide for sufficient operational flexibility that includes reasonable accessibility of areas along with an acceptable level of safety.

3.4.3 *Neutron Yields*

Except in unusual circumstances, neutrons constitute the greatest prompt radiation hazard at proton accelerators above ~10 MeV. Modern accelerators are capable of producing high proton intensities, and the subsequent production of neutrons almost always requires the provision of shielding around the accelerator to produce dose-equivalent rates acceptable in areas occupied by personnel.

Because of the detailed interaction mechanisms of the electromagnetic and hadronic cascades (Sections 3.3.6, 3.4.5, and 4), photons and charged particles are preferentially removed by the shield so that they usually account for only a small contribution to the total effective dose or dose-equivalent rate outside the shield, which is largely due to neutrons (special circumstances apply for thin shielding). At proton accelerators at nearly all energies, therefore, it is important to understand the phenomenology of neutron production.

A detailed understanding of accelerator operation is helpful in identifying potential beam-loss mechanisms, both deliberately planned (such as with beam-target interactions) and accidental beam losses. A knowledge of neutron fields and their energy and angular

---

[15] With the exception of patients being exposed for medical purposes.

distribution may be important in selecting the orientation of shielding and the location of adjacent facilities that are to be occupied. Energy spectra are needed to estimate the effectiveness of shielding and, incidentally, to determine radiological protection parameters, *e.g.*, radiation weighting factors (w_R) or quality factor (Q).[16]

3.4.3.1 *Neutron Production at Low Energies (E < 200 MeV).* At energies below ~10 MeV, (p,n) reactions are extremely important sources of neutrons. Madey (1968) has summarized some of the more important (p,n) reaction sources:

The $^7Li(p,n)^7Be$ Reaction. The ^{7}Li(p,n)^{7}Be reaction has been widely used as a source of neutrons with energies in the kilovolt region. Gibbons and Newson (1960) have tabulated the neutron energy as a function of the proton energy and the emission angle in the laboratory coordinate system. Neutrons with energies below 80 keV must be taken from thin targets at angles greater than 90 degrees to the direction of the proton beam. The neutron energy and the relative yield at an angle of 120 degrees are shown in Figure 3.17 as a function of proton energy. Curves c and d in Figure 3.18 give the energy of neutrons at 0 and 180 degrees, respectively, for proton bombarding energies up to 4 MeV. Figure 3.19 depicts the total cross section for the ^{7}Li(p,n)^{7}Be reaction as a function of proton energy from threshold to 5.5 MeV. The cross section rises steeply above the threshold to a plateau which is interrupted by a strong resonance at a proton energy of 2.25 MeV. Macklin and Gibbons (1958a) measured a cross section of ~570 mb (millibarns) at the peak of this resonance. The cross section has another broad resonance at a proton energy of ~5 MeV.

The reaction ^{7}Li(p,n)^{7}Be* produces a second group of neutrons when the proton energy bombarding the lithium target exceeds the threshold energy of 2.378 MeV for this excited state reaction. The excited state ^{7}Be* decays to the ground state by the emission of a 430 keV gamma ray.

The $T(p,n)^3He$ Reaction. The total cross section for the T(p,n)^{3}He reaction is shown in Figure 3.20 as a function of bombarding proton energy from the threshold of 1.019 to ~5 MeV. The yield of neutrons is substantial near the threshold energy. The absence of an excited state of ^{3}He in the observed energy region means that the T(p,n)^{3}He

---

[16] In Publication 60, ICRP introduced the concept of radiation weighting factor to replace quality factor for the evaluation of the protection quantities. The use of the quality factor was retained for the evaluation of the ICRU operational quantities but with a revised $Q(L)$ relationship (ICRP, 1991; 1996; ICRU, 1998a).
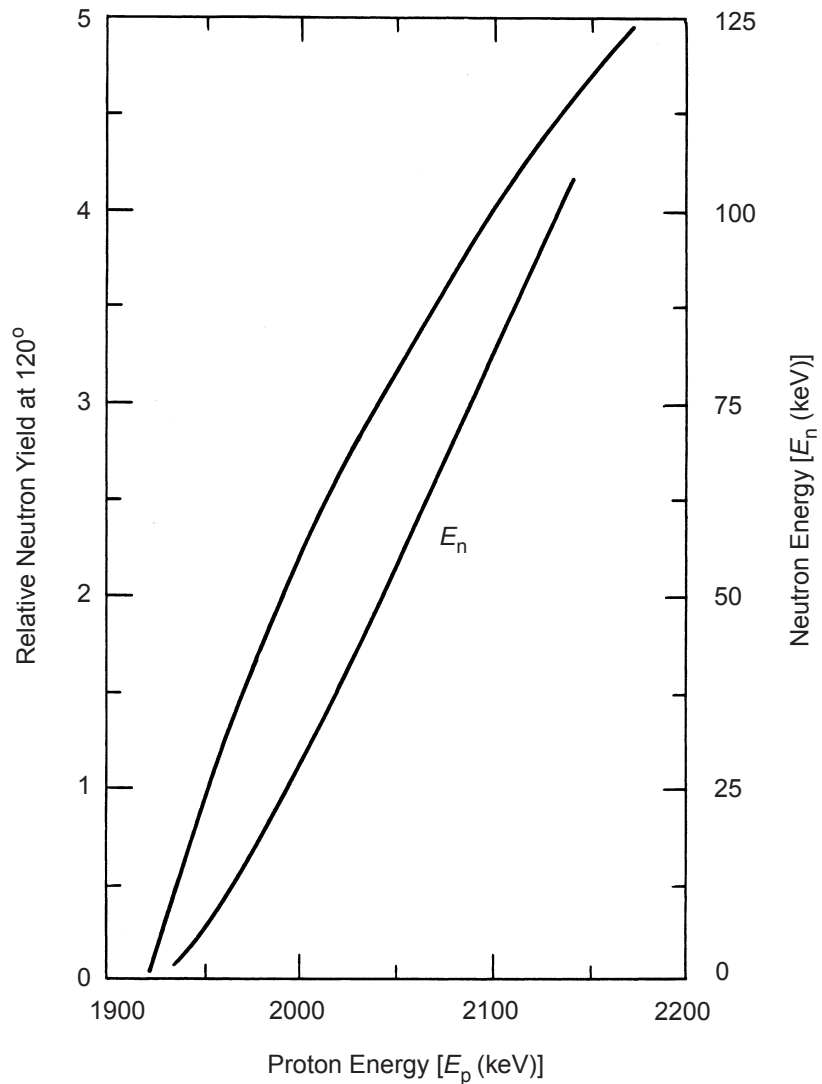
Fig. 3.17. Energy and relative yield of neutrons at an angle $\Theta = 120$ degrees from the ^{7}Li(p,n)^{7}Be reaction versus proton bombarding energy (Gibbons, 1956; Hanna, 1955; IAEA, 1968; Madey, 1968).

reaction is not complicated by a second group of neutrons as arises in the ^{7}Li(p,n)^{7}Be* reaction. The relativistic tables of Blumberg and Schlesinger (1956) give the energy and angle relationships for this reaction in both the laboratory and center-of-mass coordinate systems as a function of proton bombarding energy.
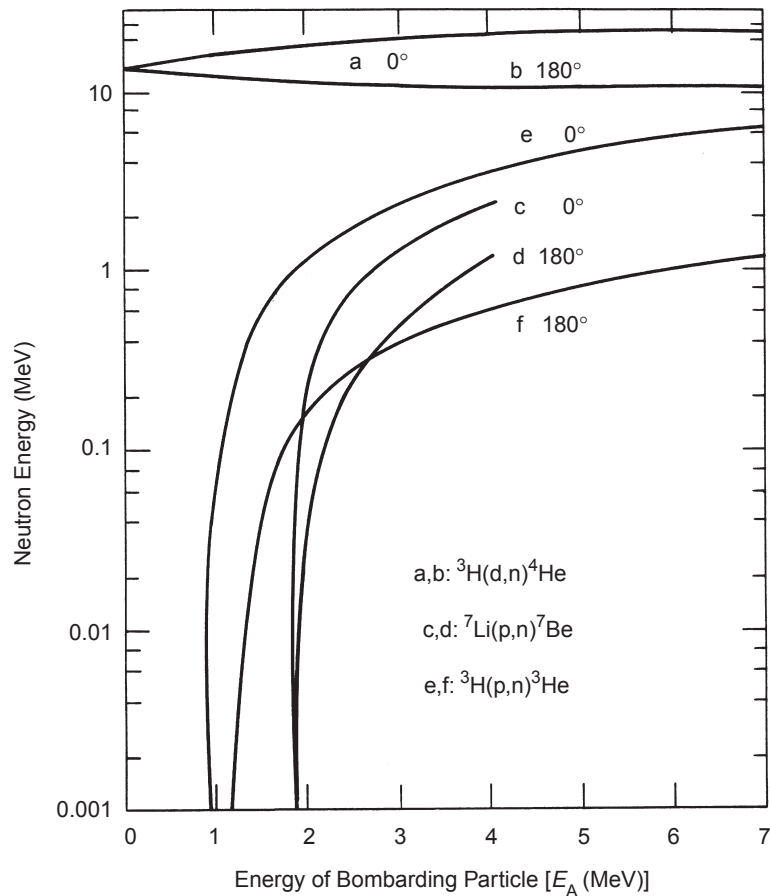
Fig. 3.18.   Neutron energy in the forward direction ($\Theta = 0$ degrees) and backward direction ($\Theta = 180$ degrees) for the ^{3}H(p,n)^{3}He, ^{7}Li(p,n)^{7}Be, and ^{3}H(d,n)^{4}He reactions versus energy of the bombarding particle (IAEA, 1968; Madey, 1968).

The (p,n) Reactions in Medium-Weight Nuclei. Several (p,n) reactions with medium-weight nuclei are used as sources of monoenergetic neutrons in the low-energy region from 5 to 150 keV in the forward direction. Table 3.2 lists the minimum energies of monoenergetic neutrons at $\Theta = 0$ degrees from reactions with medium-weight nuclei.

The cross sections for (p,n) reactions in medium-weight nuclei are smaller than for the ^{7}Li(p,n)^{7}Be cross section. For example, in the
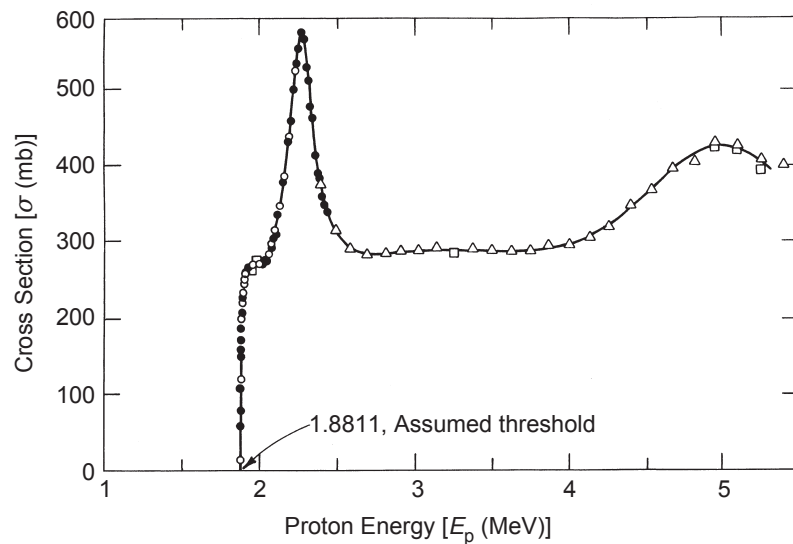
Fig. 3.19. Total cross section for ^{7}Li(p,n)^{7}Be reaction versus bombarding proton energy from threshold to 5.5 MeV (Gibbons and Macklin, 1959; IAEA, 1968; Madey, 1968).

energy region just above the threshold, the cross sections for ^{45}Sc and ^{63}Cu targets average 1 to 3 mb per steradian in the forward direction, whereas those for ^{51}V and ^{65}Cu are somewhat smaller because of their lower threshold energy. The energy of the first excited state in the residual nucleus corresponds approximately to the maximal energy of monoenergetic neutrons that can be produced. Copper-65 is limited in its ability to produce monoenergetic neutrons up to an energy of 50 keV, whereas ^{45}Sc, ^{51}V, and ^{63}Cu have much higher energy limitations.

Proton beams from synchrocyclotrons have been used to generate neutron beams with energies in the neighborhood of the bombarding energy.

Figure 3.21 summarizes the total yields per incident proton for selected materials spanning the periodic table and a large range of incident proton kinetic energies (Tesch, 1985). This figure is the result of an extensive literature search of both measurements and calculations. Except at the highest energies, these data are for targets longer than the range of the incident protons. The plotted values are maximal, and, above ~300 MeV, include some multiplicity effects due to secondary particle production in thick targets for proton
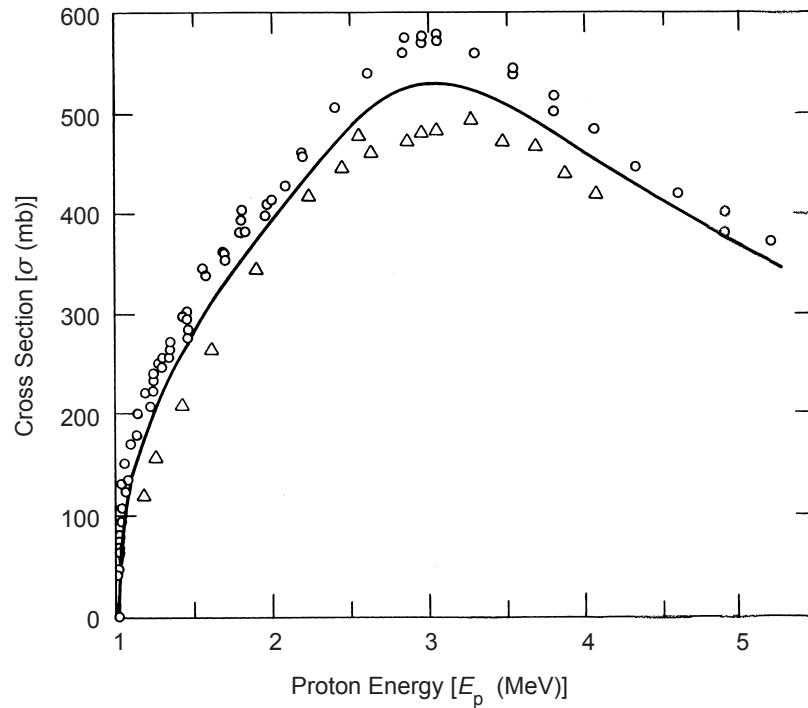
Fig. 3.20. Total cross section of the $T(p,n)^3He$ reaction versus energy of the bombarding proton from threshold to 5 MeV (Gibbons and Macklin, 1958; Macklin and Gibbons, 1958a; 1958b).

TABLE 3.2—*A comparison of the energy characteristics of (p,n) reactions in nuclei of low- and medium-mass number.*

| Reaction	Minimum Energy of Neutrons at 0° (keV)	Threshold Energy (MeV)	Required Bombarding Energy Above Threshold (keV)	First Excited State (MeV)
$^3T(p,n)^3He$	288	1.019	128	—
$^7Li(p,n)^7Be$	120	1.882	39	0.478
$^{45}Sc(p,n)^{45}Ti$	5.6	2.908	1.46	0.743
$^{51}V(p,n)^{51}Cr$	2.36	1.5656	0.61	0.775
$^{63}Cu(p,n)^{63}Zn$	4.2	4.214	1.08	0.191
$^{65}Cu(p,n)^{65}Zn$	2.03	2.1646	0.52	0.054
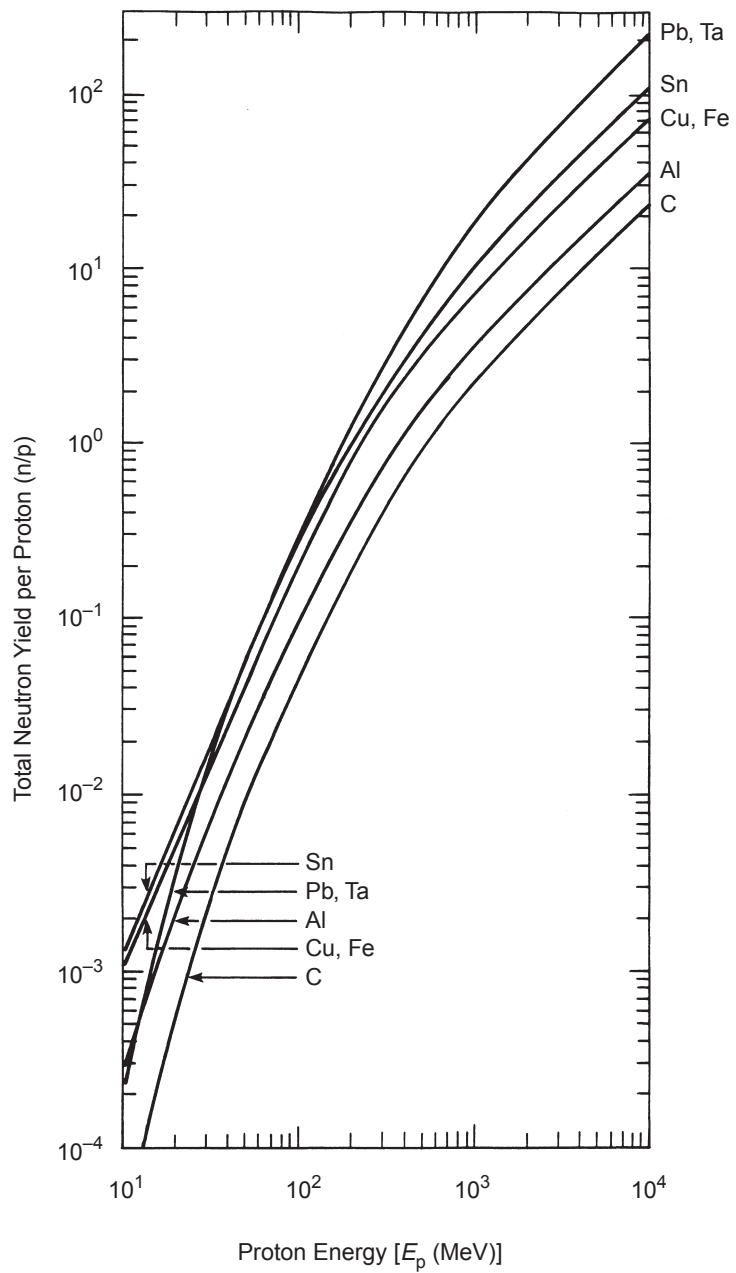
Fig. 3.21. Total neutron yield per proton for different target materials (Tesch, 1985).

energies above ~300 MeV. An important feature is that, between 50 and 500 MeV, the neutron yield increases as E_p^2, while above 1 GeV it is approximately linear in E_p. In using these curves, it is important to recognize that the geometrical configuration of the target may have a profound effect on the actual neutron yield encountered. Comparisons with the original references cited by Tesch reveal that the smoothed curves through all the data given in Figure 3.21 agree with individual measurements and calculations to within about a factor of two.

A sample of the angular distribution information for proton energies up to 231 MeV (calculations and measurements) is plotted in Figures 3.22 to 3.28. Figures 3.22, 3.24, 3.26, 3.27 and 3.28 are plots of $d\phi(E,\Theta)/dE$, while Figures 3.23 and 3.25 are plots of $\phi(\Theta)$. These data were obtained using a rather wide variety of experimental techniques and methods best described in the original references.

3.4.3.2 *Neutron Production at Intermediate Energies (200 MeV $\leq$ E $\leq$ 1 GeV).* For our purpose here, the intermediate-energy region is taken to extend from 200 MeV up to ~1 GeV. In this energy region, calculations of particle yield begin to be sensitive to the increased number of nuclear reactions which are energetically possible. The production of highly excited compound nuclear states giving rise to copious quantities of "evaporation neutrons" proceeds along with the development of hadronic cascades. (Other particles and light nuclei are emitted by the "evaporation" process but these are even more readily absorbed by shielding than are the protons.) An extensive discussion of these mechanisms is given elsewhere (IAEA, 1988; Patterson and Thomas, 1973). Extensive calculations of both cascade and evaporation neutrons from protons bombarding an aluminum target have been performed. Figures 3.29 and 3.30 show the energy spectra of all *nucleons* (protons and neutrons) arising from these collisions calculated from the results of Metropolis *et al.* (1958a; 1958b). Protons and neutrons are produced in nearly equal numbers. At intermediate and high energies, protons emitted from a target are of increasing importance from the standpoint of radiation protection. The spectra of emitted neutrons at energies below the primary energy (E_0) are rather insensitive to the bombarding energy.

3.4.3.3 *Neutron Production at High Energies (E $\geq$ 1 GeV).* At high energies ($E \geq 1$ GeV), both calculations and measurements of neutron yields, angular distributions and spectra are more difficult than for the low and intermediate-energy regions. Calculations are complicated by the increased number of nuclear reactions which are energetically allowed and by the need to incorporate relativistic effects. Measurements
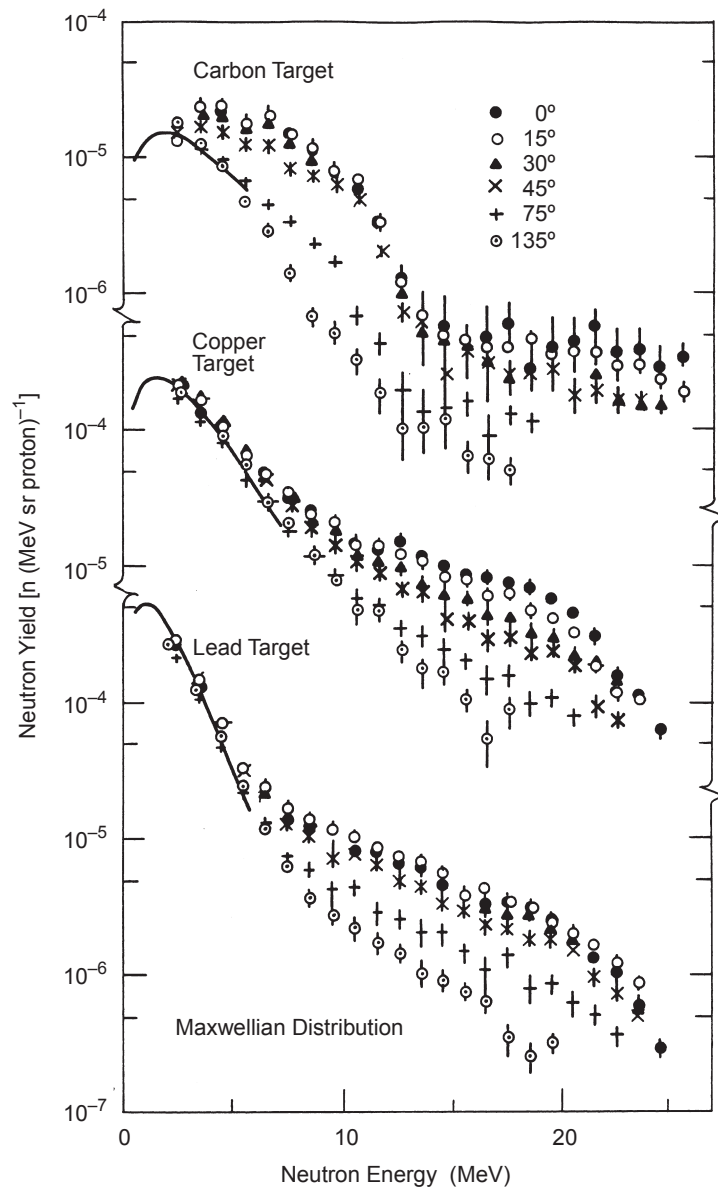
Fig. 3.22. Differential yield of neutrons emitted by different materials bombarded by 30 MeV protons at a number of angles. The symbols represent measurements while the curves represent a Maxwellian fit to the measured spectra (Nakamura *et al.*, 1983).
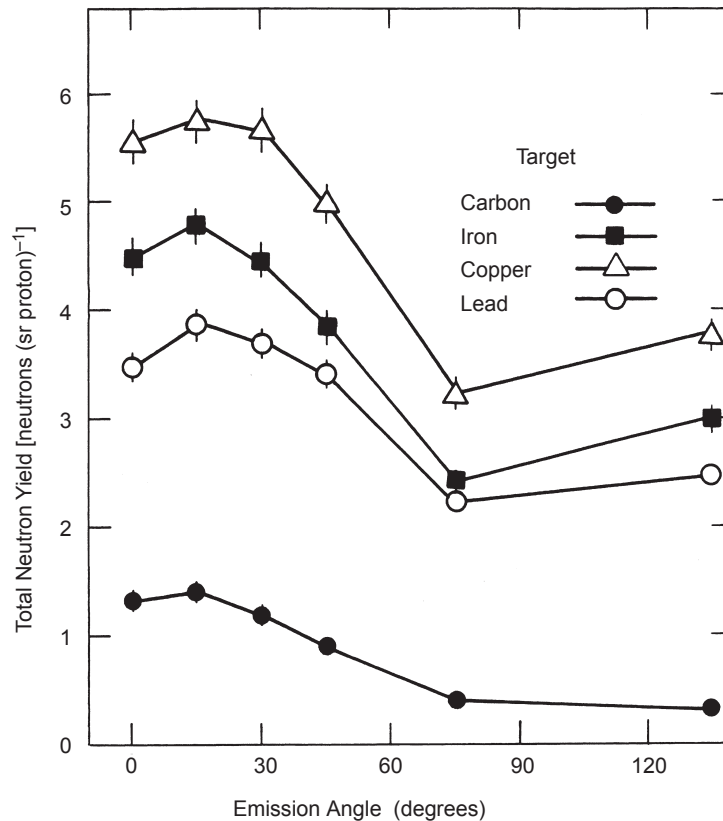
Fig. 3.23. Angular distributions of total neutron yield above 3 MeV for four targets bombarded by 30 MeV protons (Nakamura *et al.*, 1983).

are made difficult by the enhanced production of secondary particles, the more exotic detection techniques required, and the limited beam time available on the relatively smaller number of high-energy proton accelerators. For purposes of shielding localized beam losses at high-energy, a simplistic calculation of neutron yield from a "point" target can readily lead to incorrect assessment of shielding requirements because neutrons emitted even at large angles are sufficiently energetic to develop cascades in the shielding and, therefore, to produce radiation sources that are extended in space.[17]

[17] The concept of "point" sources or beam losses "at a point" is misleading. Both the physical interaction mechanisms of high-energy particles and the operation of particle accelerators ensure that radiation sources are extended in space. For practical purposes of shield design, a point source is taken to be one whose spatial distribution is small compared with the distance from which it is viewed.
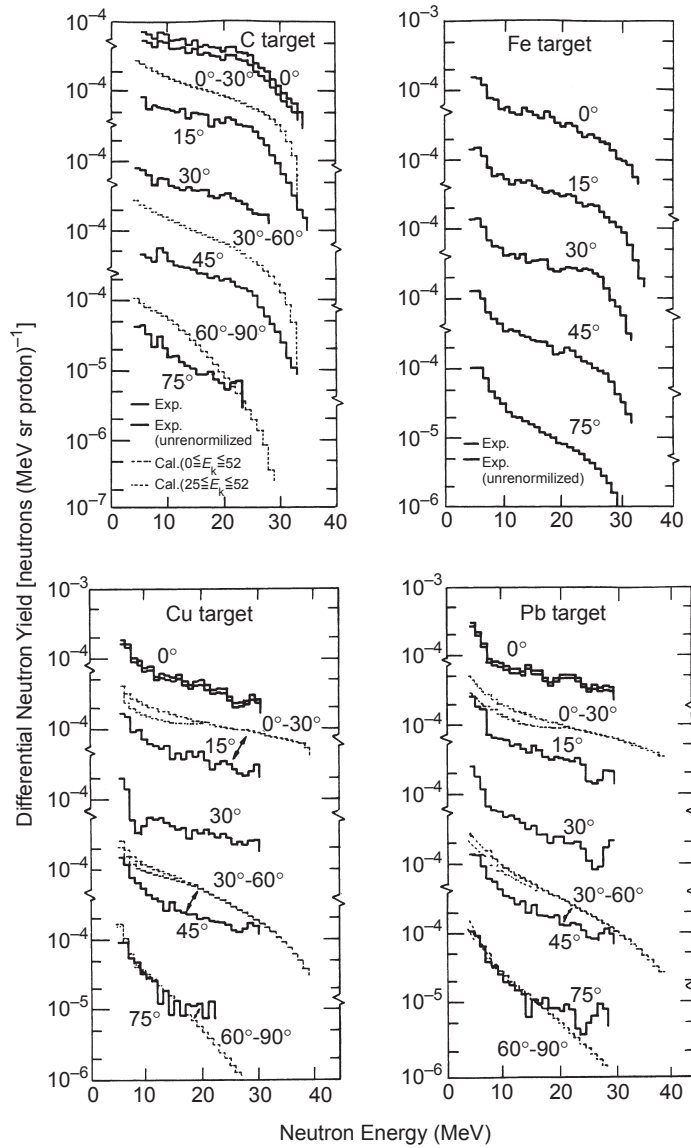
Fig. 3.24.   Differential yield of neutrons emitted by different materials bombarded by 52 MeV protons at a number of angles for carbon, iron, copper, and lead (Nakamura *et al.*, 1978). The solid histograms represent measurements while the dashed histograms represent theoretical calculations. The variation between the histograms labeled "exp" and "exp (unrenormalized)" result from uncertainties in the measurements in the vicinity of $\Theta = 0$ degrees.
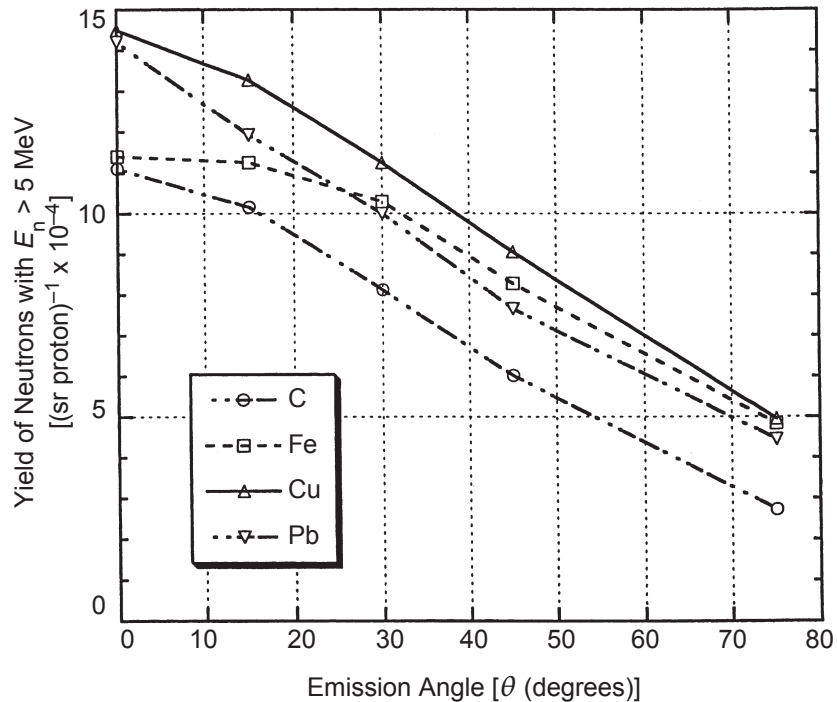
Fig. 3.25. Measured angular distributions of total neutron yield above 5 MeV for carbon, iron, copper and lead bombarded by 52 MeV protons. The measurements were normalized at $\Theta = 15$ degrees. The curves are drawn to guide the eye (Nakamura *et al.*, 1978).

In the region of a few tens of giga-electron volts, measurements of the angular distributions of hadrons (principally neutrons, protons, and pions of crudely equal contributions) produced by bombarding targets with 14 and 26 GeV protons have been made by Gilbert *et al.* (1968). The results are displayed in Figures 3.31 and 3.32 where $g(\Theta)$ is the value of $dY/d\Omega$ integrated above a threshold energy corresponding to that of a chosen nuclear reaction used as a detector for the emitted hadrons. Such threshold reactions are commonly used at high-energy accelerators to measure the yield of neutrons and other hadrons having energies above such a threshold. This technique is valid to the extent that the cross section of the chosen reaction is approximately independent of the bombarding energy at energies significantly above its threshold. The results using different thresholds indicate that the higher the energy of the detector threshold, the more forward-peaked will be the measured angular distribution.
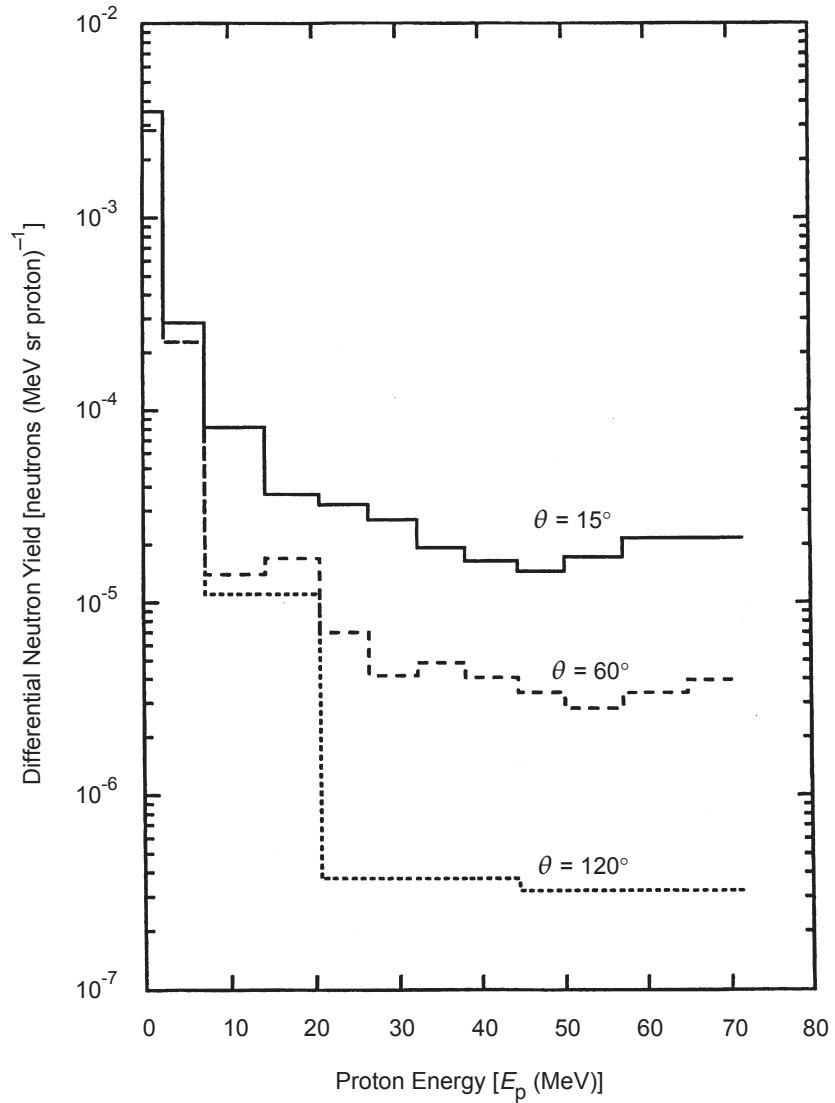
**Fig. 3.26.** Measured differential yield of neutrons emitted by a copper target bombarded by 72 MeV protons at three values of Θ (Broome *et al.*, 1983).

"Thin" target here means a target thickness less than the removal mean free path for high-energy neutrons for the material. Table 3.3 summarizes removal mean free paths (collision lengths), *i.e.*, the inelastic "attenuation length," for protons in several common
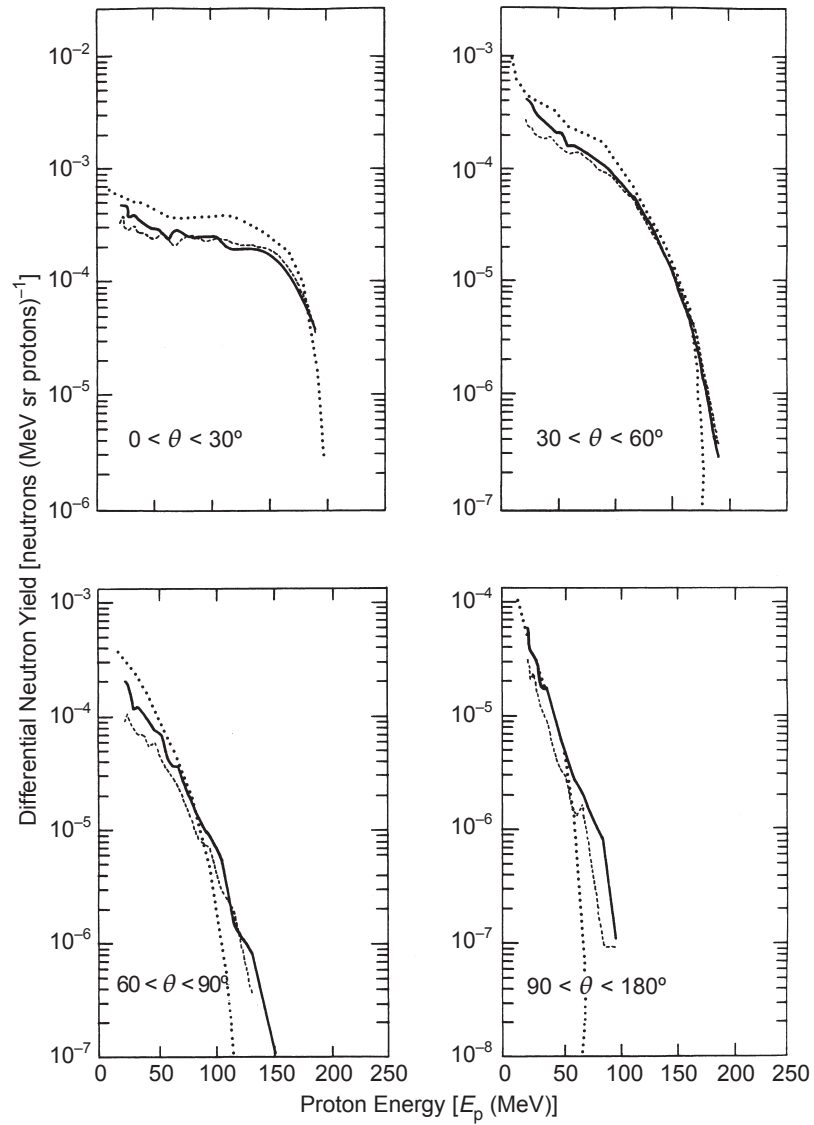
Fig. 3.27. Calculated differential yield of neutrons emitted by water (- - - -), iron (—) and aluminum (⋯⋯) targets bombarded by 200 MeV protons for four ranges of Θ. The iron and water calculations are from Hagan *et al.* (1988) while the aluminum results are from Alsmiller *et al.* (1975).
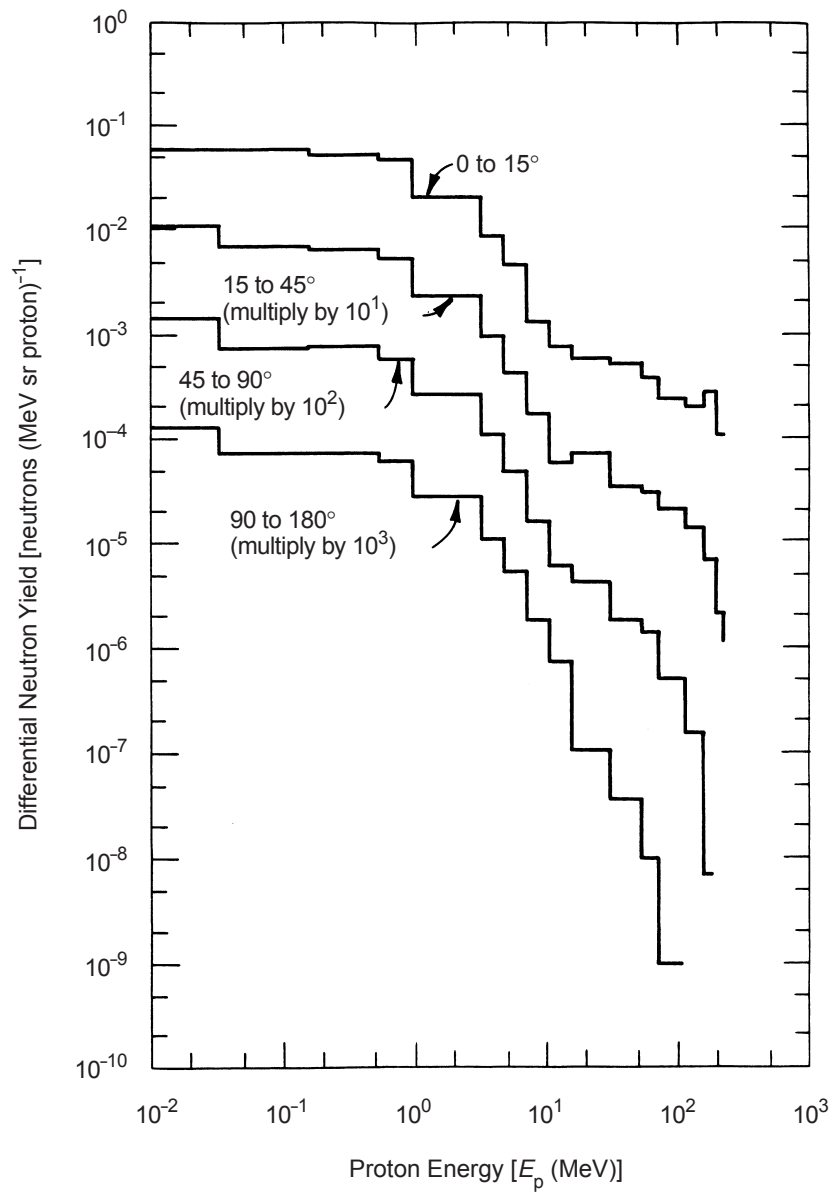
Fig. 3.28. Calculated differential yield of neutrons emitted by a tantalum target bombarded by 231 MeV protons for four ranges in Θ (Alsmiller *et al.*, 1981a).
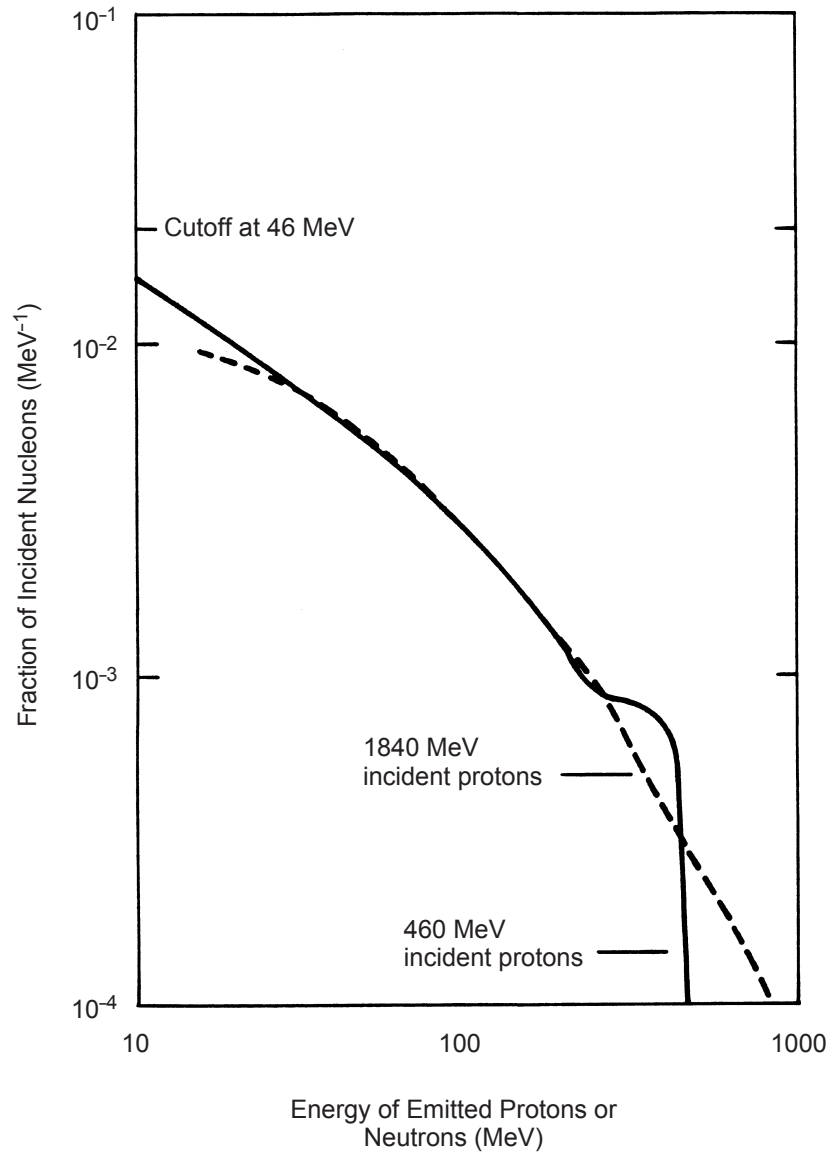
Fig. 3.29. Energy spectra of cascade nucleons emitted from aluminum (Metropolis *et al.*, 1958a; 1958b).
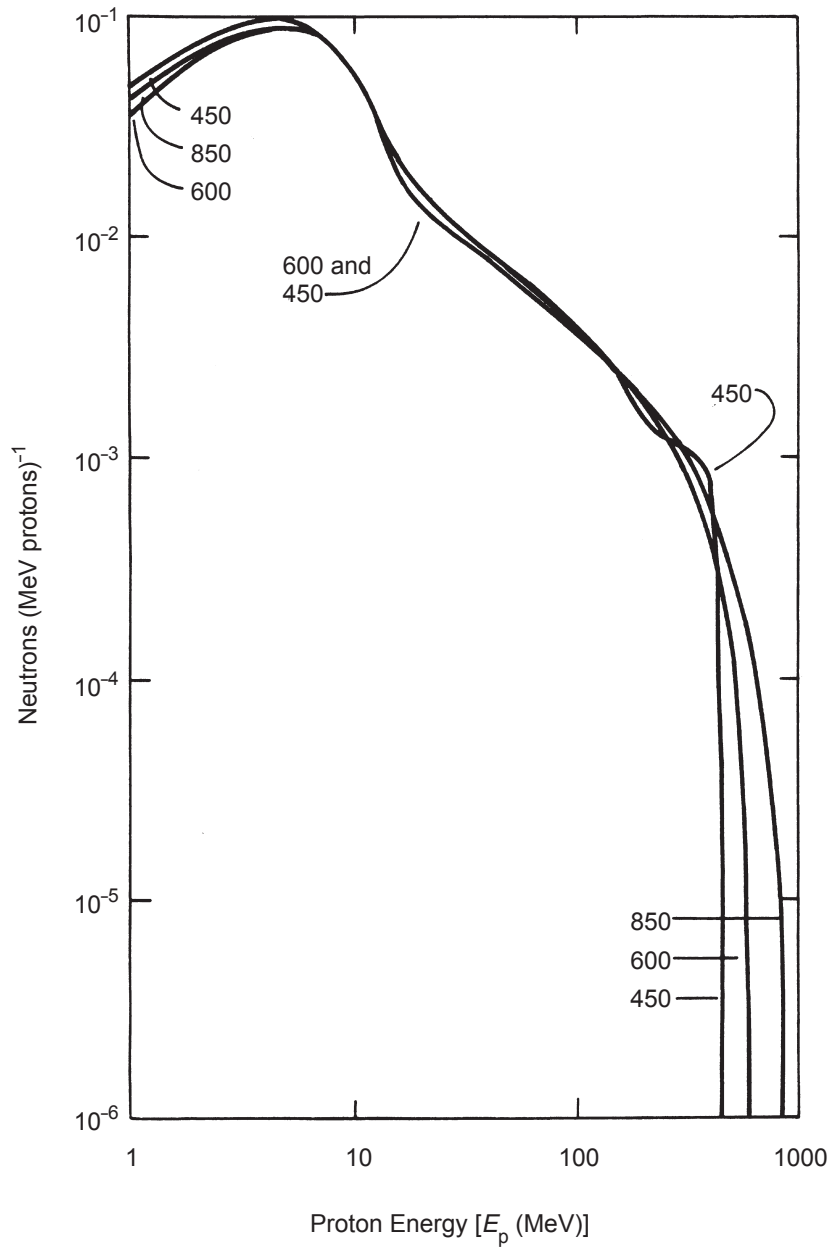
Fig. 3.30. Cascade and evaporation neutron emission per incident proton from 450, 600 and 850 MeV protons on aluminum (Metropolis *et al.*, 1958a; 1958b).
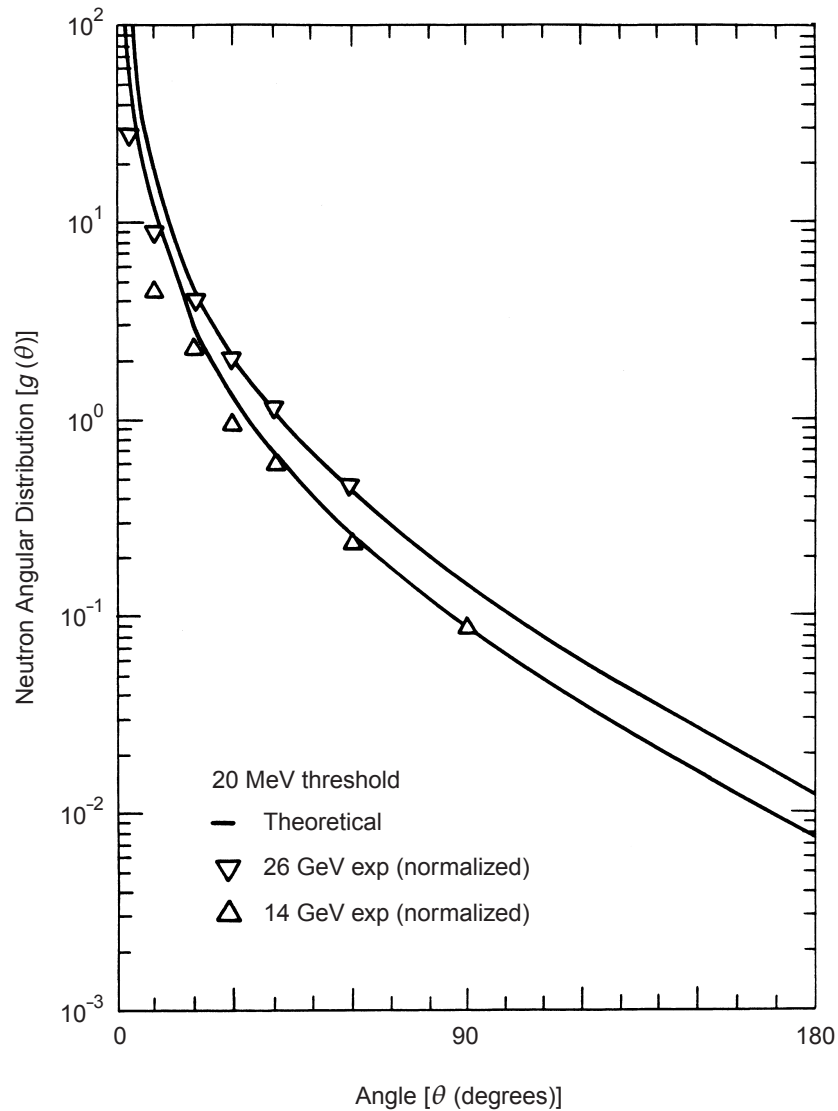
Fig. 3.31. The neutron angular distribution $g(\Theta) = \mathrm{d}Y(\Theta)/\mathrm{d}\Omega$ of neutrons above 20 MeV produced by 14 and 26 GeV protons incident on a thin beryllium target (see Section 3.2) (Gilbert *et al.*, 1968).

materials. At high energies, removal mean free paths for incident protons are approximately equal to those of neutrons.

Figure 3.33 shows the angular distributions of the total hadron fluence (principally neutrons, protons, and pions in roughly equal
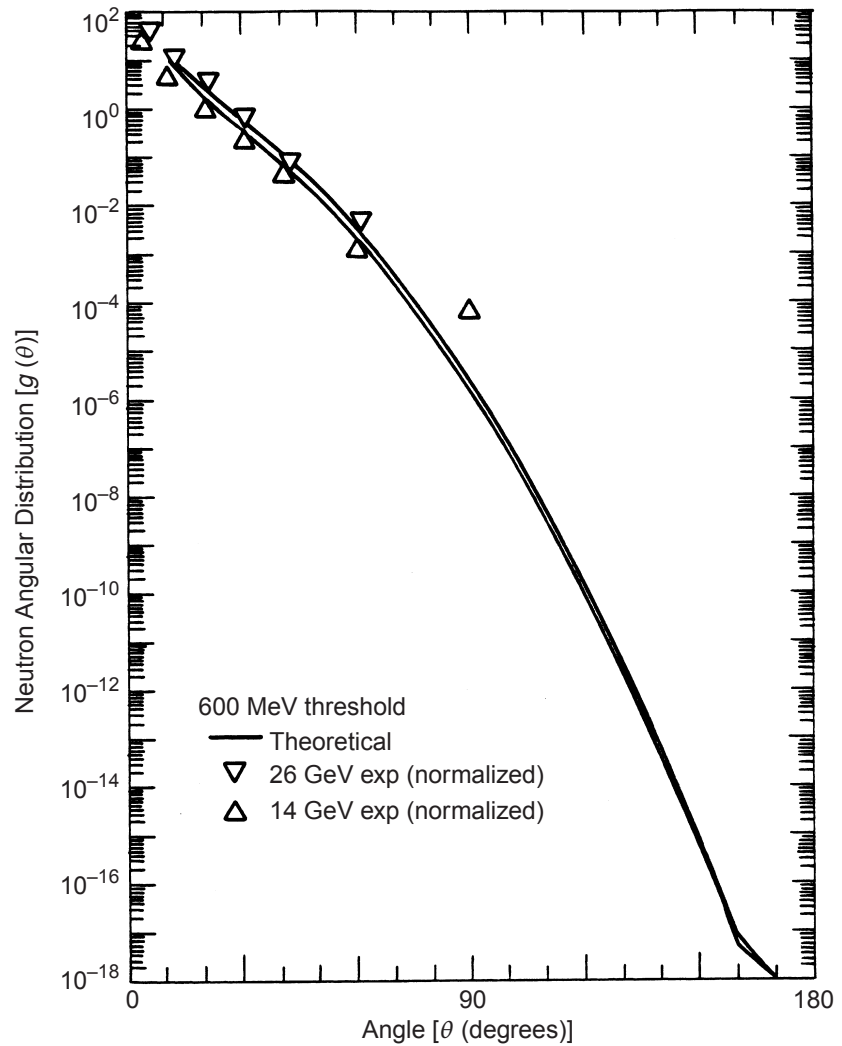
Fig. 3.32.   The neutron angular distribution $g(\Theta) = dY(\Theta)/d\Omega$ of neutrons above 600 MeV produced by 14 and 26 GeV protons incident on a thin beryllium target (see Section 3.2) (Gilbert *et al.*, 1968).

contributions) due to 22 GeV protons bombarding an 8 cm-long copper target (measured by Levine *et al.*, 1972; reported by Ranft and Routti, 1972). The measurements represent total hadron yields per *interacting* proton. In the 8 cm-thick target, about 41 percent of the incident protons will interact, thus, the plotted values of fluence need to be multiplied by a factor of 0.41 to obtain corresponding

TABLE 3.3—*Proton removal mean free paths at high energies.*

Material	Density (g cm^{-3})	Removal Mean Free Path (g cm^{-2})	Removal Mean Free Path (cm)
Hydrogen gas	9.0×10^{-5}	43.3	4.81×10^5
Beryllium	1.85	55.5	30.03
Carbon	2.27	60.2	26.58
Aluminum	2.7	70.6	26.15
Iron	7.87	82.8	10.52
Copper	8.96	85.6	9.55
Lead	11.35	116.2	10.24
Uranium	18.95	117	6.17
Air	1.29×10^{-3}	62	4.81×10^4
Water	1	60.1	60.10
Concrete (typical)	2.5	67.4	26.96
Silicon dioxide (quartz)	2.64	67	25.38
Plastics (polyethylene)	0.93	56.9	61.51

yields per *incident* particle. This figure shows the forward-peaking of the emitted particles. For both measurements and calculations, the variation of the angular distributions with the hadron energy threshold selected for the "detector" is clearly evident. Conversion from hadron fluence to differential yield shows consistency in the magnitudes of the measurements with those given in Figures 3.31 and 3.32.

Both measurements and calculations of the hadron fluence also exist for 225 GeV protons incident on a 15 cm-long copper target at the CERN SPS (Stevenson *et al.*, 1986). The measurements were also based on threshold activation techniques and are displayed, along with corresponding Monte-Carlo calculations, in Figure 3.34 for a number of choices of energy threshold. In the higher-energy realm, Monte-Carlo calculations are of vital importance for estimating these quantities.

Tesch and Dinter (1986) have produced a summary of some analytical approaches which approximate the quantities of interest in this energy region. Sullivan (1989) has given a formula that fits the measured angular distributions of the fluence of hadrons of energy greater than 40 MeV at 1 m from a copper target struck by protons in the energy region of $5 < E_p < 500$ GeV. The fluence (cm^{-2}) per *interacting proton* as a function of energy, E_p (giga-electron volt), measured at angle Θ (degrees), $\phi(\Theta)$, is given by:
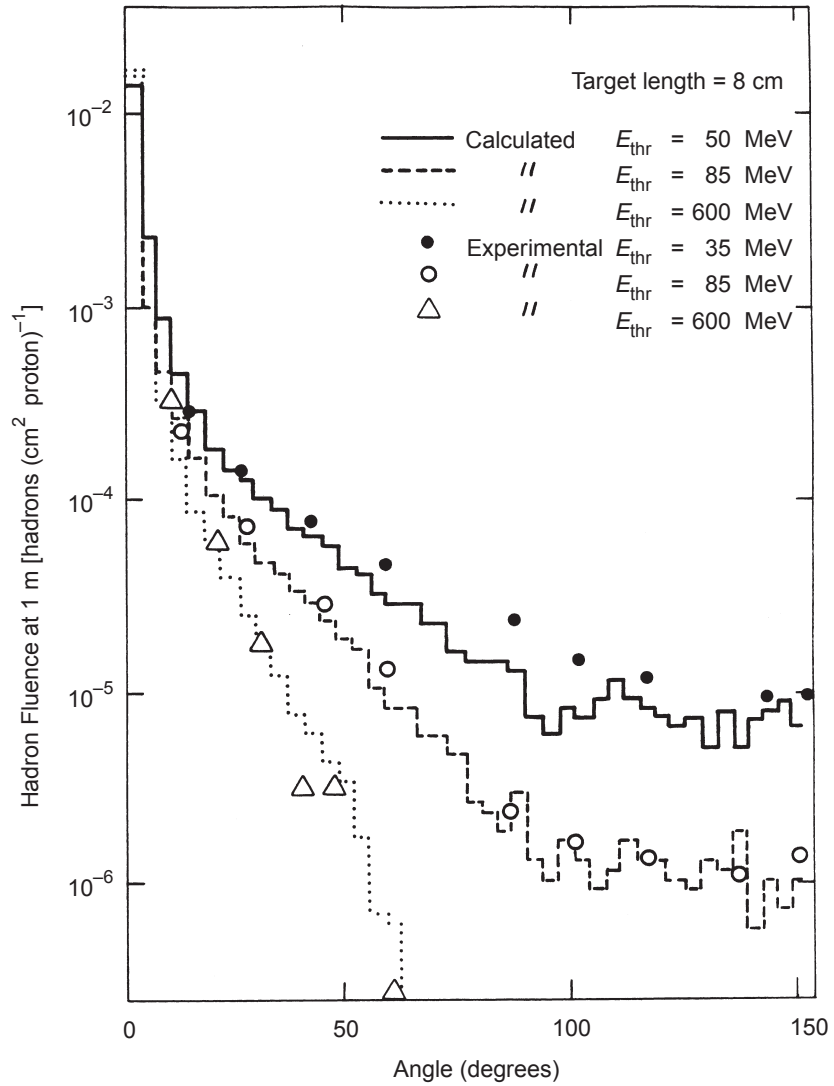
Fig. 3.33. Comparison of calculated (Ranft and Routti, 1972) and measured (Levine *et al.*, 1972) angular distributions of hadron fluence (particles cm^{-2}) at 100 cm from a copper target bombarded by 22 GeV c^{-1} protons. Several choices of hadron energy thresholds (E_{thr}) are shown.

$$\phi(\Theta) = \frac{1}{2\,[\Theta + (35/\sqrt{E_{\mathrm{p}}})]^2} \,. \tag{3.31}$$

If the fluence per interacting proton is doubled, then Equation 3.31 also well represents the neutron distributions per *incident proton*
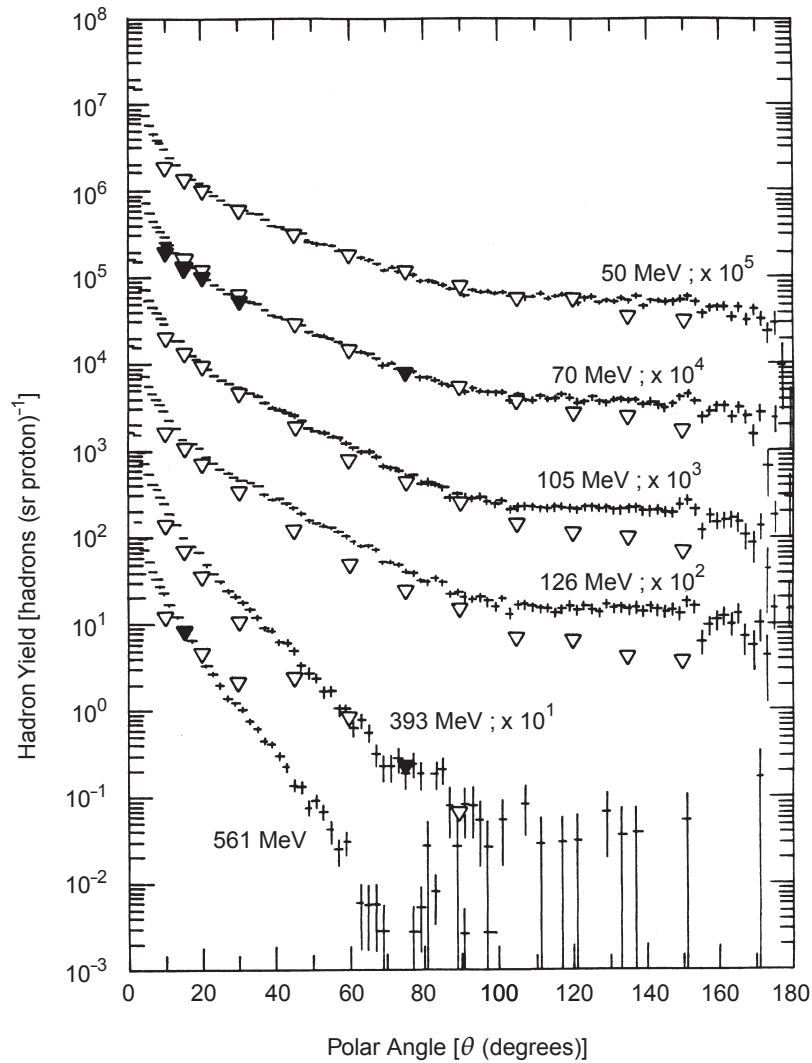
Fig. 3.34. Comparison of the experimental (open and closed triangles) and calculated (+) hadron fluences above different energy thresholds as a function of polar angle Θ around a 15 cm long copper target bombarded by 225 GeV protons (Stevenson *et al.*, 1986). The data have been multiplied by the indicated factors prior to plotting and represent the number of hadrons (incident proton per steradian).

produced in targets struck by protons in the energy region $0.025 < E_p < 1$ GeV. Numerical integration of Equation 3.31 yields a fairly good approximation to the total hadron or neutron fluence emitted. For a target that is much shorter than one attenuation length, the fluence will be proportional to the target thickness.

Absorbed dose or dose equivalent, rather than neutron fluence, may be of more immediate interest to the operational health physicist particularly in determining compliance with radiation-protection standards. However, if the neutron energy spectrum in a given situation is known, either from direct measurement or from information of the type presented in this Section, the absorbed dose or dose equivalent may be determined by application of appropriate conversion coefficients to each portion of the spectrum in an integration:

$$H_d = \int_{E_{min}}^{E_{max}} g(E)\phi(E)\mathrm{d}E. \tag{3.32}$$

In Equation 3.32, the dose equivalent H_d is related to the neutron fluence as a function of energy $\phi(E)$ through the conversion coefficient $g(E)$. The limits of integration, E_{min}; E_{max}, span the region of concern. In a mixed radiation field, the absorbed doses or dose equivalents from each radiation component must be added. [The absorbed dose (D) would be related to the function $\phi(E)$ through a similar integral]. Given the discrete nature of experimental measurements and the limitations on the number of energy groups (bins) allowable in a feasible calculation, this integral is often evaluated numerically, selecting the number of energy bins to be appropriate for the desired accuracy:

$$H = \sum_{j=1}^{m} g_j \, \phi_j \, (\Delta E_j), \tag{3.33}$$

where the summation in index j is over the m energy bins ΔE_j selected. Often for *approximate* calculations, the few energy bins of the most obvious importance may be selected. Figure 3.35 is a plot of the data collected by Tesch of the dose equivalent due to energetic neutrons at 1 m from a copper target ($\Theta = 90$ degrees) bombarded by protons of various energies (Tesch, 1985), along with an analytical fit. In many cases, the principal concern is not directly with the dose equivalent due to the neutrons emitted from a bare target, but instead with doses outside shielding. Figure 3.36 shows a plot of r^2H as a function of concrete shield thickness for several intervals of Θ and for 200 MeV protons incident on an aluminum target (Alsmiller *et al.*, 1975). Figure 3.37 is a similar plot of r^2H as a function of angle at a depth of 1 m in a concrete shield for two different irradiation
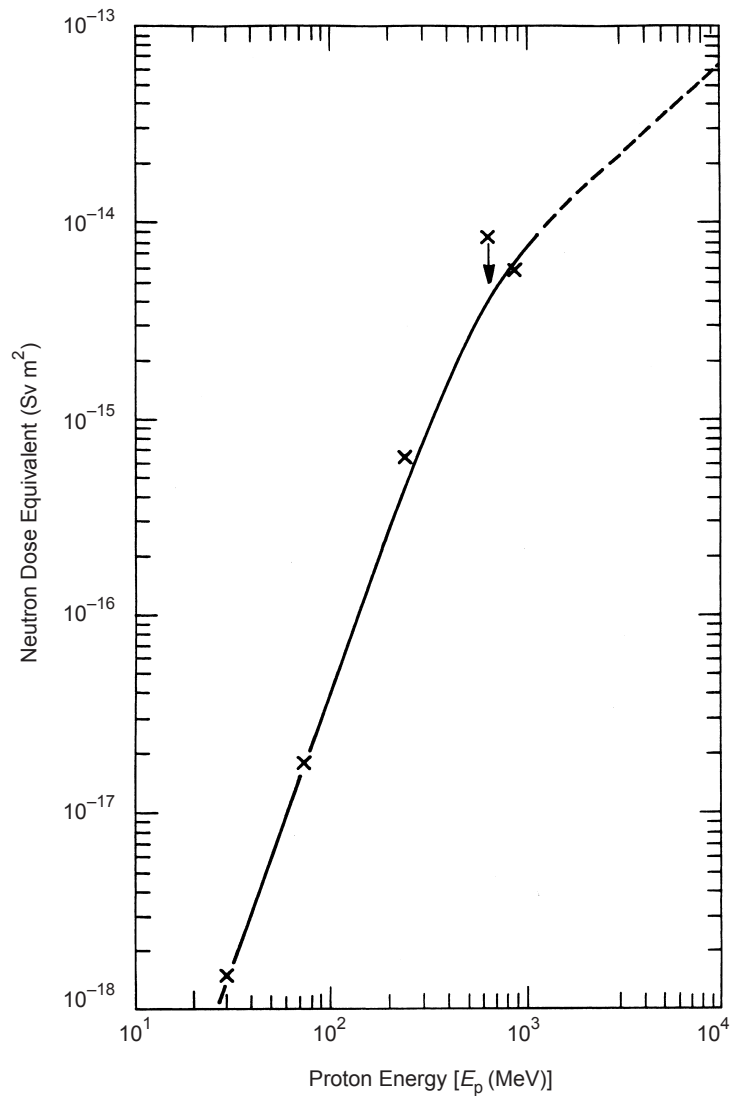
Fig. 3.35. Dose equivalent per proton due to neutrons with ener-
gies higher than 8 MeV at a distance of 1 m from a copper target at
Θ = 90 degrees (Tesch, 1985). The $\times$ symbols represent measurements
taken from the literature and the curve represents an analytical fit.
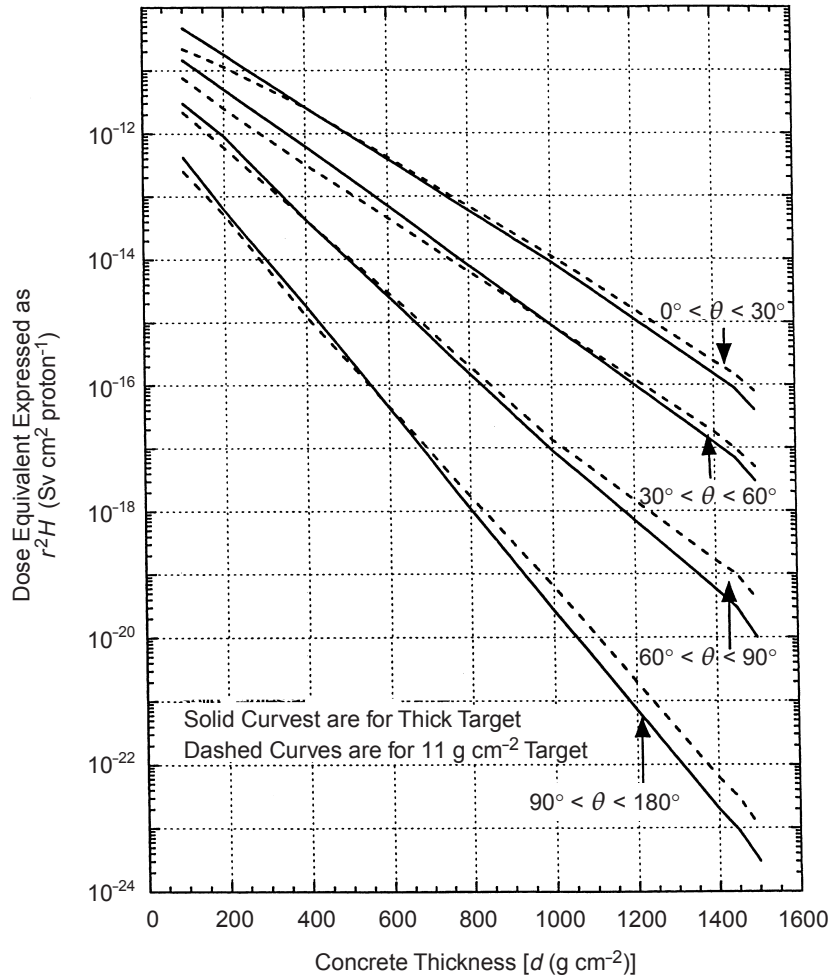
Fig. 3.36. Calculations of dose equivalent per incident proton multiplied by distance squared (r^2H) as a function of concrete shield thickness (d) averaged over several intervals of Θ for 200 MeV protons incident on an aluminum target of two different thicknesses (Alsmiller *et al.*, 1975).

conditions of the case of bombardment of an iron target by 200 MeV protons (Hagan *et al.*, 1988). These calculations are in agreement to better than a factor of two.

Figure 3.38 shows the measured angular distribution of absorbed dose due to hadrons at 1 m from a 5 cm thick copper target struck by 24 and 8 GeV protons (Levine *et al.*, 1972). Comparison with a theoretical calculation is also included. In this case, about 28 percent
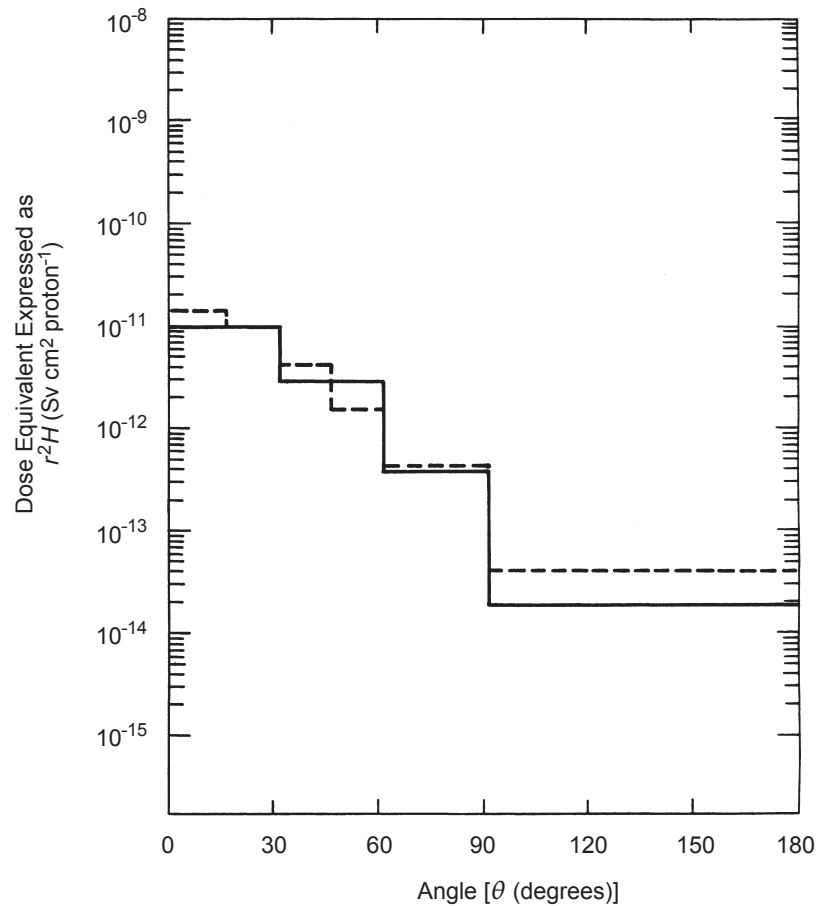
Fig. 3.37. Calculations of r^2H per 200 MeV proton versus angle (Θ) following a 100 cm thick concrete shield (Hagan *et al.*, 1988) (1 cm^2 rem = 10^{-8} m^2 Sv). The solid lines correspond to the results of Alsmiller *et al.* (1975), while the dashed lines are alternative theoretical calculations of Hagan *et al.* (1988).

of the incident protons interact in the target, so the results must be multiplied by a factor of 0.28 to be normalized per *incident* proton.

3.4.4 *Muon Production*

At proton accelerators exceeding ~300 MeV in energy, the production of charged pions (rest energy = 140 MeV) becomes important. Above 1 GeV, the production of charged kaons (rest energy =
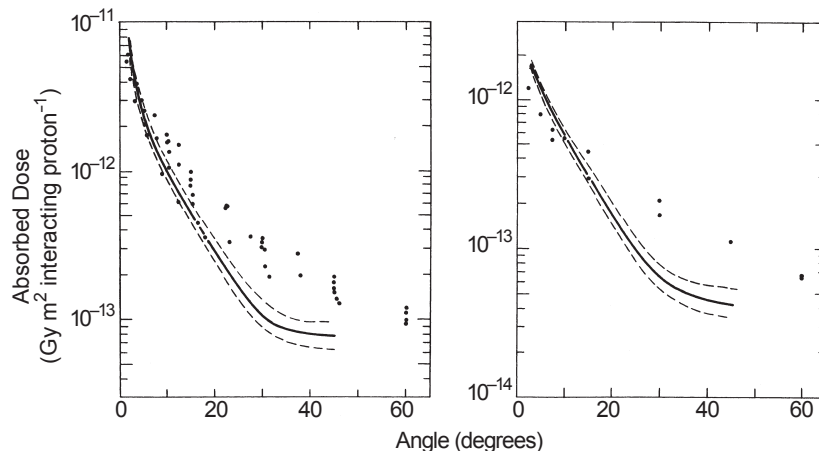
Fig. 3.38. Absorbed dose per interacting proton at a distance of 1 m from a 5 cm thick copper target bombarded by 24 GeV c^{-1} (left) and 8 GeV c^{-1} (right) protons. The solid points are measurements while the curves are calculations (experimental Trilling model). Multiply the plotted values by a factor of 0.28 to obtain the approximate results per incident proton (Levine *et al.*, 1972).

494 MeV) ensues. As the proton energy increases above these thresholds, pions and kaons also can be produced by both the primary particles and by energetic secondary particles present in the hadronic cascade.

Because the mean lives of pions and kaons are short (26 and 12 ns, respectively), they quickly decay with high probability into a muon (rest energy = 106 MeV) plus a neutrino. The muons from pion decay can have a momentum ranging from 57 to 100 percent of that of the parent. Muons, which are leptons, are not subject to the strong (nuclear) interaction and hence to first order can only be attenuated by being "ranged out" by ionization. Figure 3.39 shows range-energy curves for muons in various materials (Schopper *et al.*, 1990). For high energies, the range becomes quite long, longer in fact than feasible shields constructed of materials other than earth.

Because decay muons from pions with an energy of as little as 3 GeV easily penetrate the typical beam stop (~2 m long, made of steel), they may present especially serious problems at facilities where pion beams operate. The decay length for a pion beam is approximately 55 m GeV^{-1} c of pion momentum. Thus, in a decay path of ~20 m, a 10 GeV c^{-1} pion has a decay probability of about four percent. Consequently, in this case, a muon intensity of about
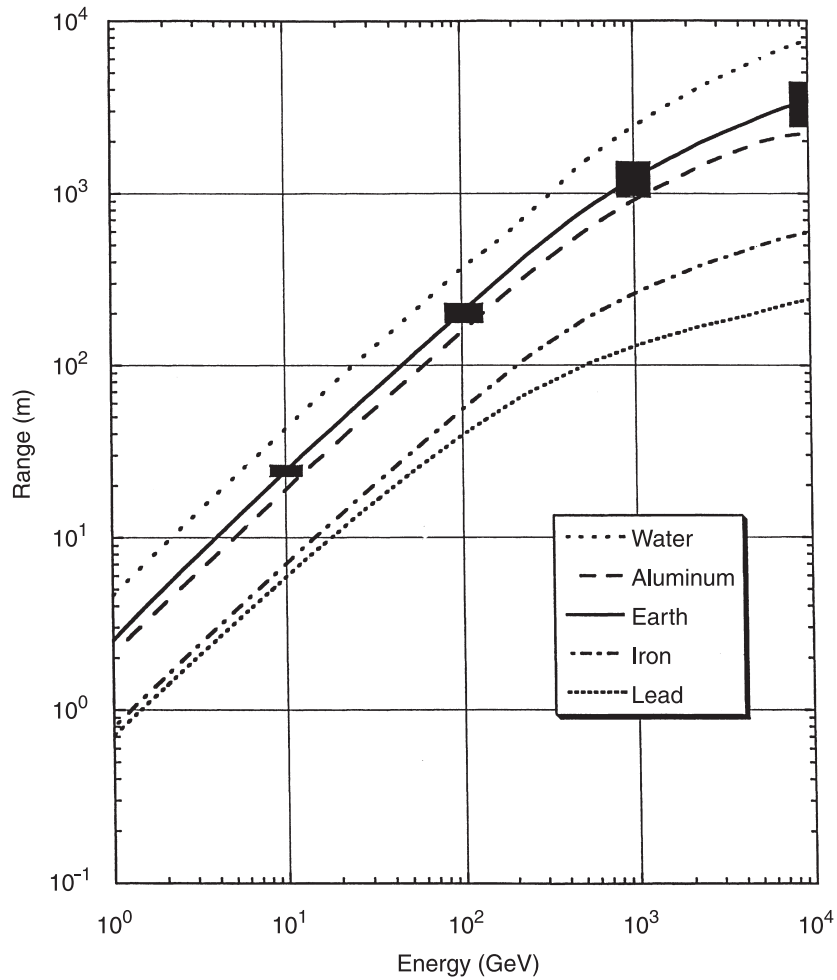
Fig. 3.39. Range-energy curves for muons in various materials. On the curve labeled "earth," the boxes are indicative of the approximate spread (± 1 standard deviation) in the range due to range-straggling at the indicated muon energy. The density of "earth" was taken to be 2 g cm^{-2}. The data values were taken from those of Schopper *et al.* (1990). The straggling results are those of Van Ginneken *et al.* (1987).

four percent of the incident pion intensity can escape from the pion beam stop. Such muons are strongly forward peaked; the great majority of the fluence is within a few degrees of the incident beam direction, unless magnetic fields are encountered.

Muons can also be produced by direct interactions in targets. Muons produced by direct interactions in the targets and beam stops will be less sharply forward-peaked than those resulting from decays, because of scattering within the target material, and consequently will be more likely to increase overall radiation levels. At very high energies (exceeding a few hundred giga-electron volts), the range-energy relation for muons gradually becomes dominated by statistical fluctuations and departs from the "Bragg" peak familiar for low-energy particles. This "range straggling" implies that significant numbers of muons can have ranges much larger than the mean of the range (Van Ginneken *et al.*, 1987).

Beam stops for proton beams at large accelerators are typically 4 to 5 m long. Hadron interactions in the beam stop are most likely to produce cascade muons of a somewhat softer spectrum than found in the case of pion decay. In this case, the depth of shielding required to reduce muon fluence rates to acceptable levels corresponds to the range of a muon having a momentum of about 75 percent of that of the incident proton (Keefe and Noble, 1968). Muons can be expected to dominate longitudinal shielding considerations at proton energies above ~20 GeV. This problem has been seen at all accelerators above this energy. Monte-Carlo calculations are now quite capable of making reliable estimates of muon radiation patterns (Cossairt *et al.*, 1988; Maslov *et al.*, 1983; Van Ginneken *et al.*, 1987). The fluence-to-dose conversion coefficients for muons has been determined to be 40 fSv m^2 over the muon energy range from 100 MeV to 100 GeV (Stevenson, 1983). The interested reader is referred to texts by Fasso *et al.* (1990) and by IAEA (1988).

3.4.5 *Hadronic (Nuclear) Cascade*

3.4.5.1 *General.* The nuclear cascade is of major importance in determining the shielding of both high-energy nucleon and high-energy, high-intensity electron accelerators (De Staebler, 1965). In either case, the nuclear cascade is the most important means of transporting radiation through matter (*i.e.*, the shield).

At proton accelerators, the hadronic cascade is initiated when the beam interacts with components of the accelerator or the extraction system. At electron accelerators, high-energy electrons produce energetic hadrons, principally, by photodisintegration of pseudodeuterons within the nucleus and by photoproduction of energetic pions which are then reabsorbed within the nucleus. The resultant high-energy neutrons and protons also can then generate a hadronic cascade.

Because knowledge of the characteristics of nuclear interactions in the laboratory is limited to energies below 1,000 GeV for incident protons and 100 GeV for electrons, our only available source of information at very high energies is obtained from cosmic-ray studies. These data, coupled with the more precise data obtained at high-energy accelerators, have allowed assembly of a fairly detailed description of the nuclear cascade.

3.4.5.2 *Qualitative Description of the Hadronic Cascade*. The collision of a high-energy nucleon with a nucleus gives rise to a large number of particles, principally nucleons, pions and kaons. A substantial fraction of the incident energy may be vested in a single nucleon, which in crude terms may be thought of as propagating the cascade. At high energies above 1 GeV, something like 20 to 30 percent of the primary energy is radiated as pions (Perkins, 1963), but since the pion production cross sections fall steeply with increasing energy, they do not play an important part in the cascade penetration. The production of rare particles at high energies is unimportant in the propagation of the cascade.

Thus the main means of energy transfer is due to the interaction of high-energy nucleons, and it is those particles, whose energies are above ~150 MeV, that serve to propagate the cascade. Nucleons in the energy range 20 to 150 MeV also transfer their energy predominantly by nuclear interactions, but at these incident energies, the energy is transferred to a large number of nucleons, each receiving on the average a small fraction of the total energy and thus having a rather low kinetic energy (below ~10 MeV). Charged particles at these energies are rapidly stopped by ionization and thus, neutrons predominate at low energies. Charged π mesons (and K mesons that are produced only about one-tenth as frequently as π mesons) decay into muons (μ) and neutrinos (ν_μ), for example:

$$\pi^+ \rightarrow \mu^+ + \nu_\mu \text{ and } K^+ \rightarrow \mu^+ + \nu_\mu. \tag{3.34}$$
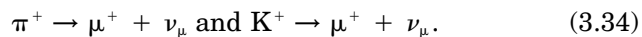
Muons are not subject to the strong interaction and thus are primarily stopped in material only by ionization energy losses at most energies of interest for radiological protection. However, it should be noted that at energies above 100 GeV, where pair production, bremsstrahlung, and the effects of nuclear interactions become significant, the energy-loss mechanisms for muons become more complex. The effective attenuation length of these muons depends upon the energy spectrum of the parent pion and kaons (and thus upon the energy of the incident nucleon). As early as 1964, Keefe predicted that muons would represent an increasing problem as the intensity of then existing 30 GeV accelerators increased and at the newer

accelerators at Serpukhov (70 GeV), Batavia (200 GeV), and CERN (300 GeV) (Keefe, 1964). Subsequently, following the successful operation of these accelerators, Keefe's prediction has been verified by observation.

Energetic gamma rays produced by the decay of π^0 mesons initiate electromagnetic cascades, but the attenuation length of these cascades is, in general, much shorter than the absorption length for the strongly interacting particles. Hence, they contribute little to the energy transport.

Deep in the shield, therefore, neutrons take on the dominant role in cascade propagation because the rate of energy loss is significant for protons and pions of energy less than ~450 MeV.[18] Production of evaporation and low-energy cascade particles is then controlled by the most penetrating particles.

Figure 3.40 schematically represents the components of the hadronic cascade and indicates the interrelationships between its separate components (ICRU, 1978). The problem can be simplified by neglecting all those radiation components that are produced in relatively small numbers, have short lifetimes, or are rapidly attenuated. Of the latter, only components produced in the outermost layer of a thick shield actually emerge; these are fewer in variety and number than in the early stages of the cascade, since the average energy of the cascade particle is reduced to a fraction of the primary radiation incident on the shield. At any point outside the shield, the high-energy neutrons that are present have either come directly from the source without scattering, or have undergone only small angle scattering *via* quasi-elastic interactions. The other (charged) particles are everywhere rapidly attenuated. Thus, those particles outside the shielding have been produced by the high-energy neutrons *via* nonelastic interactions in the outer layers of the shield.

3.4.6 *Radiation Environment*

An understanding of the radiation environment of high-energy proton accelerators, although complex, is necessary and of major concern for several reasons, *e.g.*:

- personnel protection from prompt radiation
- equipment degradation because of radiation damage (with consequent *human* exposure to effect repairs)
- component radioactivation with its impact on the radiation exposure of maintenance personnel and the generation of radioactive waste

---

[18] At this energy the ionization range becomes roughly equal to the interaction length. Below this energy the ionization range is less than the interaction length.

	Most Numerous Participants	Time Scale (s)	Typical Energy per Particle (MeV)	Percent of Energy Deposition
π^+_- → μ^+_- Muons	π, K → μ	10^{-8}	any	10
π^o → γ, e^-, e^+, γ, n Electro-magnetic Cascade	π^o → e,γ	10^{-16}	any	20
Intranuclear Cascade	p, n, π, K	10^{-22}	<200	30
Incoming Hadron A → A, A Extranuclear Cascade	p, n, π, K	10^{-23}	>200	30
n, n, α, p Evaporation of Nucleons and Fragments	p, n, d, α	10^{-19}	<30	10
β, γ, α Induced Activity	α, β, γ	seconds to years	<10	<1

Fig. 3.40. Schematic representation of the components of the six levels of the hadronic cascade as the incoming hadron strikes the nucleus (ICRU, 1978). Note that typically 30 percent of the energy is deposited by the extranuclear cascade.

At some research installations, especially those that utilize hadron colliders (Section 2), the prompt radiation fields within the beam enclosures may present significant limitations to the potential for the scientific exploitation of the facility. For a discussion of this topic, see Swanson and Thomas (1990).

An understanding of neutron spectra is of crucial importance towards providing solutions to all the problems mentioned above. This is true both inside the accelerator enclosure and outside the enclosure shielding. The spectra span a wide range in energies (from thermal energies up to the energy of the accelerated protons), thus

presenting a formidable challenge to both spectrometrist and dosimetrist alike. The following description of our current understanding of neutron energy spectra, both inside and outside the accelerator enclosure, is largely taken from the work of Swanson and Thomas (1990).

3.4.6.1 *Neutron Energy Spectra.* The materials struck by the primary accelerator beam (targets, beam dumps, magnets), as well as the material of the accelerator enclosure (generally concrete or earth), will significantly modify the neutron spectrum. The neutron spectrum is softened by both multiple elastic scattering (particularly with light materials) and by inelastic scattering. As a result, the neutron angular distribution becomes nearly isotropic. Studies by Eisenhauer *et al.* (1982), McCall *et al.* (1979), McCaslin and Stephens (1976), and McCaslin *et al.* (1983), following on earlier work by Patterson and Wallace (1958), demonstrated the importance of scattered neutrons within a concrete enclosure.

It is often stated, that the neutron spectrum is relatively soft within the accelerator enclosure, but it must be remembered that there are nevertheless many high-energy particles present, at least as many as in the shielding. It is just that the unattenuated neutrons in the evaporation spectrum outnumber the high-energy neutrons.

By calculations, Alsmiller and Barish (1973; 400 MeV electrons on copper) and Gabriel and Santoro (1971; 500 GeV protons) predicted a very soft component of the neutron spectrum, caused by moderation by hydrogenous materials, namely concrete and earth. The particular spectral form, $1/E$, for these neutrons results from the "slowing-down" process and is known by that name. Figure 3.41 shows calculated energy spectra of neutrons and other hadrons within a volume of earth at the end of a concrete tunnel. The primary neutron source, in this case, is the cascade initiated by a 500 GeV proton beam incident on an iron target inside the tunnel. Alsmiller and Barish (1973) also predicted a substantial moderating effect of iron (used in magnet yokes and beam stops) as well as an enhancement in the spectrum between 10 keV and 1 MeV due to selective filtration by the iron shielding. This effect had previously been observed at several particle accelerators (see, for example, Patterson, 1957; Perry and Shaw, 1965). Elwyn and Cossairt (1986; 1987) have experimentally confirmed the existence of a peak in the distribution of neutrons leaking through an iron shield at the Tevatron. This peak in the energy spectrum, in the range from ~0.01 to 1 MeV, was removed by the addition of 0.9 m concrete.

A definitive experiment by McCaslin *et al.* (1986; 1988) is very instructive in this regard. Measurements of the neutron fluence and
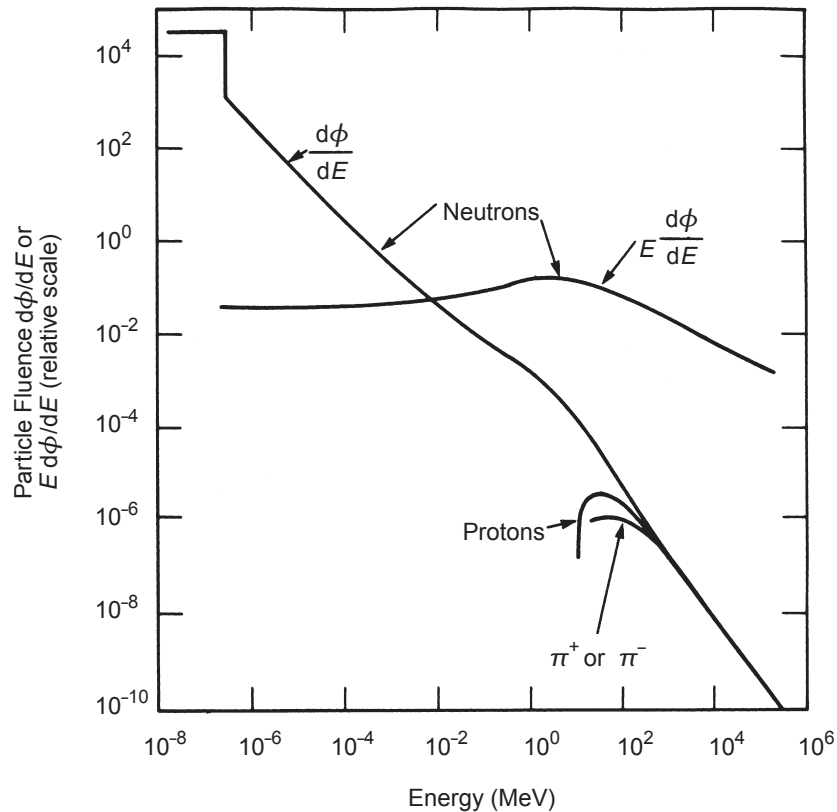
Fig. 3.41.   The energy spectra of neutrons and other hadrons in a volume of earth at the end of a concrete tunnel. The primary source is the cascade generated within an iron target bombarded by 500 GeV protons (Gabriel and Santoro, 1971).

spectrum were made inside the Fermilab Tevatron tunnel during operation by use of Bonner spheres and other instruments. At the location of the experiment, which was at a lateral distance of ~2 m from the beamline against the tunnel wall, there were no significant differences between spectra determined for operation at 800 or 150 GeV, or for Main-Ring[19] acceleration from 8 to 120 to 150 GeV. Five different spectra shown in Figure 3.42 correspond to different operating conditions of the accelerators. When the unfolded spectra

---

[19] The "Main Ring" is a separate accelerator that occupied the same tunnel and was used for injection of protons into the Tevatron.
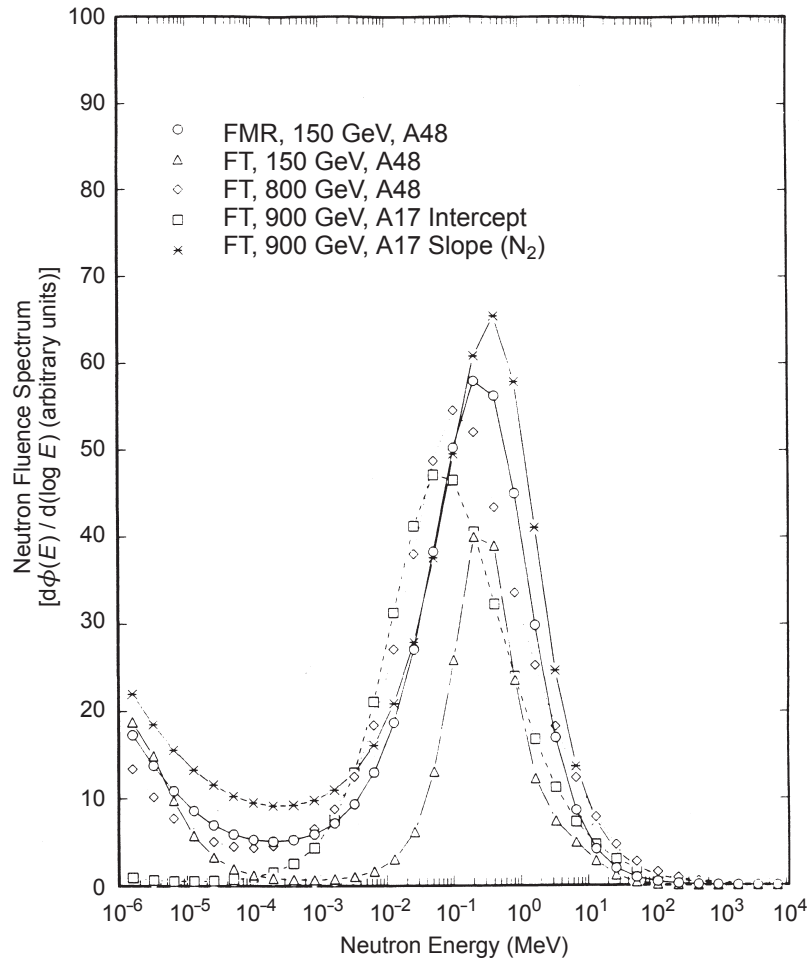
Fig. 3.42. Unfolded neutron fluence spectrum at 2 m from the beam line for four different types of operating conditions of the Fermilab Tevatron (FT) and one operating condition of the Fermilab Main Ring (FMR) (for precise details, see McCaslin *et al.*, 1988).

were plotted in lethargy units,[20] dominant peaks between 0.2 and 1.3 MeV were evident in addition to the expected slowing-down component and enhancement of thermal neutrons. Hadron cascades in the surrounding iron of the accelerator structure, initiated by primary

---

[20] Lethargy is defined as $\log(E_0/E)$, where E_0 is an arbitrary energy. Thus, plotting $E[d\phi(E)/dE] = [d\phi(E)/d(\log E)]$ versus the logarithm of E allows the spectrum to be displayed over a large range of energies in a way that preserves area representation of fluence rates and gives a clear indication of the relative contributions of source neutrons, slowing down neutrons, and thermal neutrons.

beam interactions with nitrogen gas in the vacuum chamber, identi-fied by "Slope-(N_2)" in Figure 3.42, were analyzed separately from others at a location designated A17. Random beam events in acceler-ator component materials were compared at a remote location desig-nated A48. For typical neutron spectra filtered through iron, about 30 percent of the fluence was contained between 100 keV and 1 MeV, and there was a notable lack of high-energy neutrons (four percent above 10 MeV) (Figure 3.43).[21] The median energy was ~0.06 MeV and the mean quality factor close to seven.[22]

3.4.6.2 *Spectra Outside Accelerator Shielding.* Experience at the highest-energy proton synchrotrons has shown that it is possible to find radiation fields in which any single energy component (*e.g.*, thermal neutrons, intermediate-energy neutrons, or fast neutrons) may dominate (Antipov *et al.*, 1978; McCaslin and Thomas, 1981; McCaslin *et al.*, 1988). These differences between the neutron radia-tion fields very much depend upon the thickness of shielding and the number and type of penetrations in the shielding between the primary source and the point of observation.

The neutron field reaches equilibrium through transverse shield thicknesses of ~500 g cm^{-2}, and the properties of the field were studied in some detail at the early proton synchrotrons. Perry (1967; Perry and Shaw, 1965) was one of the first to give a detailed descrip-tion of the field outside the concrete shield (1.5 to 3 m thick) for a 7 GeV, weak-focusing proton synchrotron, and his results are given in Table 3.4.

As the energy of available accelerated particles increased, there were many unexplained differences between dosimetric assess-ments. For example, at CERN, it was reported that the importance of fast neutrons relative to intermediate and thermal neutrons could significantly differ from what was indicated by earlier data (Baarli and Sullivan, 1965a; 1965b; Capone *et al.*, 1965). It became clear that it would be necessary to determine neutron spectra before the dosimetric data could be fully understood.

---

[21] At the particular location in which the measurements were made, the detector array was shielded from direct view of the beam line by a chain of magnets having iron yokes ~11 cm thick. The picture suggested by these results is that very little remained of the high-energy particles of the hadronic cascade (predominantly $\pi^{\pm}$ and $K^{\pm}$) or electromagnetic cascade (photons and $e^{\pm}$), but rather that the radiation field at the location of the detector was dominated by fast neutrons from the iron dipole magnets, subsequently scattered within the enclosure.

[22] This estimate of quality factor was based on the data and recommendations given in ICRP Publication 21 (ICRP, 1973).
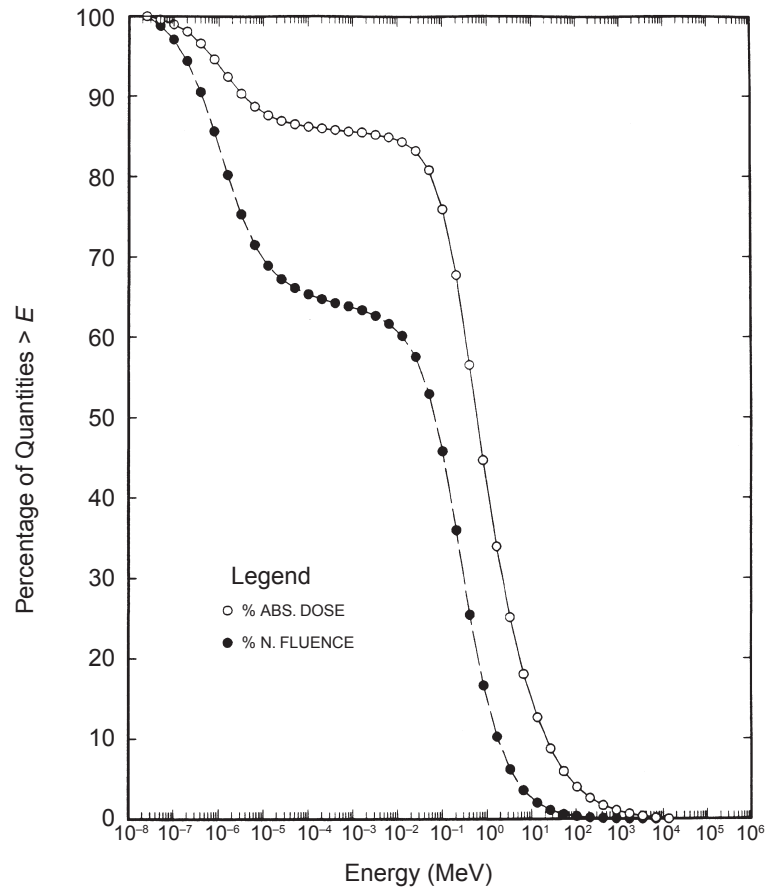
Fig. 3.43. Fraction of absorbed dose and neutron fluence above energy
E for the 800 GeV spectrum of Figure 3.42 (McCaslin *et al.*, 1988).

Over the past 30 y, neutron spectra have been determined at
several accelerators under different conditions of shielding. The spec-
tra were obtained by using a variety of experimental techniques
including nuclear emulsions, activation detectors, Bonner spheres,
and fission counters (Cossairt *et al.*, 1989; Gilbert *et al.*, 1968;
Thomas, 1974; Thomas and Stevenson, 1985).

Figure 3.44 shows neutron energy spectra measured at the Law-
rence Berkeley Laboratory in the 1960s, as reported by Gilbert *et al.*

TABLE 3.4—*Radiation spectrum above Nimrod extracted proton beam shielding (Perry, 1967).*

Type of Radiation	Energy Range	Estimated Percentage of Neutron Fluence Rate	Estimated Percentage of Total Dose Equivalent
Neutrons	<1 eV	7	<1
Neutrons	1 eV – 0.7 MeV	70	20
Neutrons	0.7 – 3 MeV	15	35
Neutrons	3 – 7 MeV	7	25
Neutrons	7 – 20 MeV	1.5	5
Neutrons + protons	20 – 100 MeV	1	5
Neutrons + charged particles	>100 MeV	0.5	4
Other particles + gammas	—	—	<2
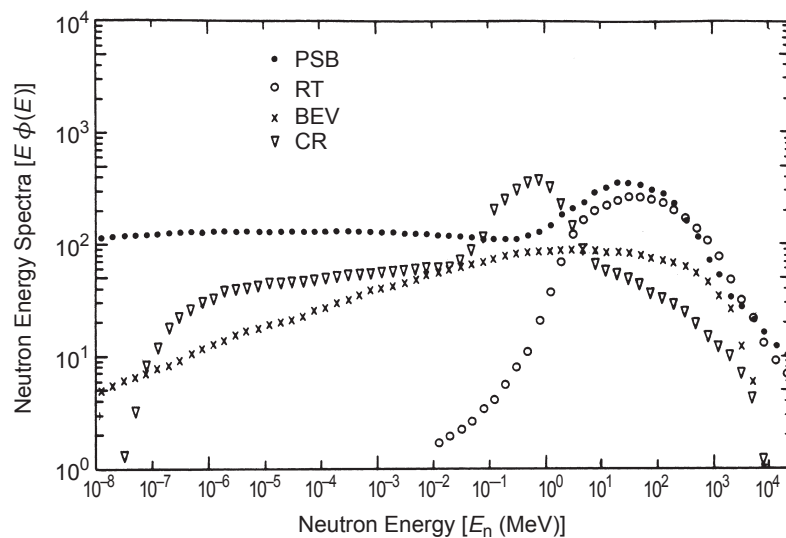
Fig. 3.44. Neutron energy spectra measured by the Health Physics Group of the Lawrence Berkeley Laboratory in the mid-1960s (see text for the explanation of the designations PSB, RT, BEV and CR).

(1968).[23] The same experiment yielded upper limits to the absorbed dose due to photons and minimum-ionizing particles. These measurements showed that the absorbed dose (in tissue) from photons is comparable to, or less than, the absorbed dose from the neutron

[23] The spectra shown were measured many years ago. Other, more recent, data could have been presented. The older data, however, have been presented because, apart from their historical value, they still define the range in types of spectra to be observed outside high-energy proton accelerator shielding.

field, and the absorbed dose from minimum-ionizing particles from the beam line is lower than that from neutrons by at least an order of magnitude.

Figures 3.44 through 3.46 show several of these spectra[23] identified by the following symbols:

RT: neutron spectrum determined at the CERN 29 GeV Proton Synchrotron above the earth shielding with a target intercepting the beam as a primary radiation source

PSB: measured at the CERN 29 GeV Proton Synchrotron above a concrete shield, again with a target acting as the primary source

BEV: measured at the University of California Radiation Laboratory 6.3 GeV Proton Synchrotron, outside thick-concrete shielding

X2: measured at the 7 GeV Proton Synchrotron of the Rutherford Laboratory (now called the Rutherford Appleton Laboratory), outside concrete shielding

P1: measured as for X2, but outside steel shielding

PLA: the ambient neutron spectrum around the 50 MeV proton linac of the Rutherford Laboratory, largely from skyshine

CR: cosmic-ray neutron spectrum measured by Hess *et al.* (1959)
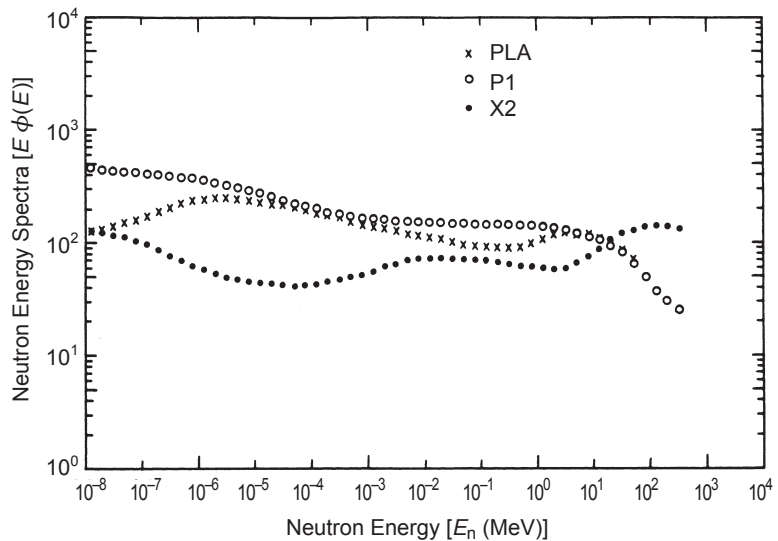
Fig. 3.45. Neutron energy spectra measured at the 7 GeV proton synchrotron (Nimrod) of the Rutherford Laboratory using Bonner spheres (see text for the explanation of the designations PLA, P1 and X2) (Perry, 1967).
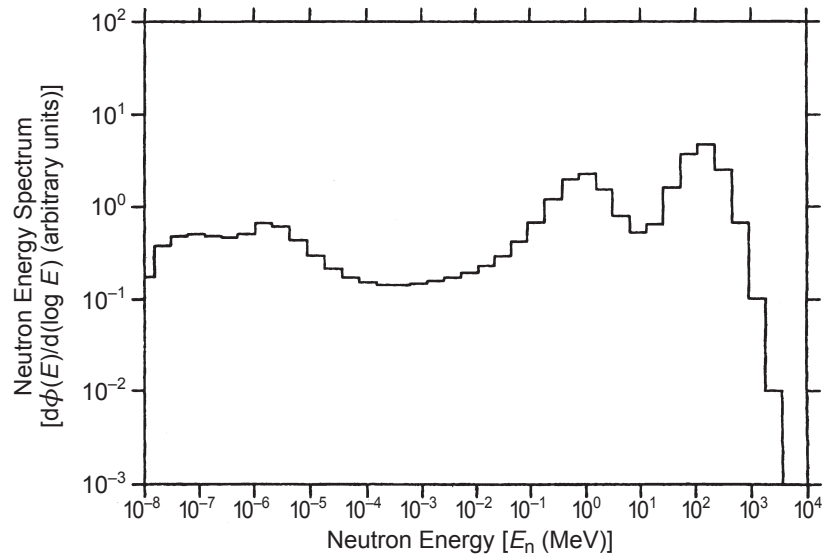
Fig. 3.46. Typical neutron energy spectrum measured at the 12 GeV Japanese (KEK) proton synchrotron external to thick shielding (Moritz *et al.*, 1990). This spectrum is based on the Bonner sphere technique supplemented with the use of the $^{12}C(n,2n)^{11}C$ reaction to improve the sensitivity to neutrons having energies greater than 20 MeV.

In addition to the measured spectra shown, Figure 3.47 shows an early calculation of the neutron energy spectrum of neutrons emerging from the shield of a 500 MeV proton linear accelerator. These calculations were made during the design of the Los Alamos Meson Physics Facility (O'Brien, 1971a). Other, more recent, measurements have been reported by Cossairt *et al.* (1989) and Dinter and Tesch (1992).

3.5 Radiation Production at Accelerators of Positive Ions

3.5.1 *General*

As we have seen in Sections 1 and 2 of this Report, a large number of accelerators produce ion beams. For medium and heavy ions, the yield parameters are nearly continuous functions of ion mass. However, there are sometimes dramatic differences between the neutron yields resulting from targets bombarded by different species
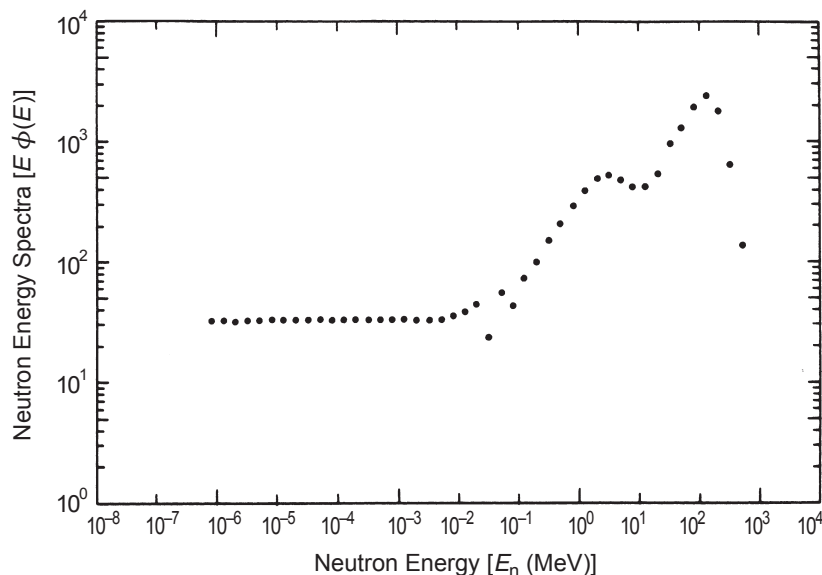
Fig. 3.47. Energy spectrum of neutrons emerging from the shield of a 500 MeV proton linear accelerator. These calculations were made during the design of the Los Alamos Meson Physics Facility and used the method of spherical harmonics (O'Brien, 1971a).

of light ions such as deuterons, tritons or alpha particles. Because the ionization range for ions of a given kinetic energy decreases as a function of ion mass, targets become effectively thicker in terms of d/R, where d is the target thickness and R is the range of the ion, as the ions become heavier.

Ion reactions are often used to produce intense neutron sources. Light ions are often the projectiles of choice for this purpose. This is because in certain cases at least one neutron may be quite loosely bound in the projectile; *e.g.*, the binding energy of the deuteron is only 2.2 MeV to be compared with a value of 6 to 8 MeV for medium- and heavy-mass nuclei.

3.5.2 *Light Ions*

Figures 3.48a and 3.48b summarize stopping power and range-energy relations for protons up to 1,000 MeV (Enge, 1966). These curves can be used to obtain approximate values for other light ions. Total neutron yields from these ions and protons have been
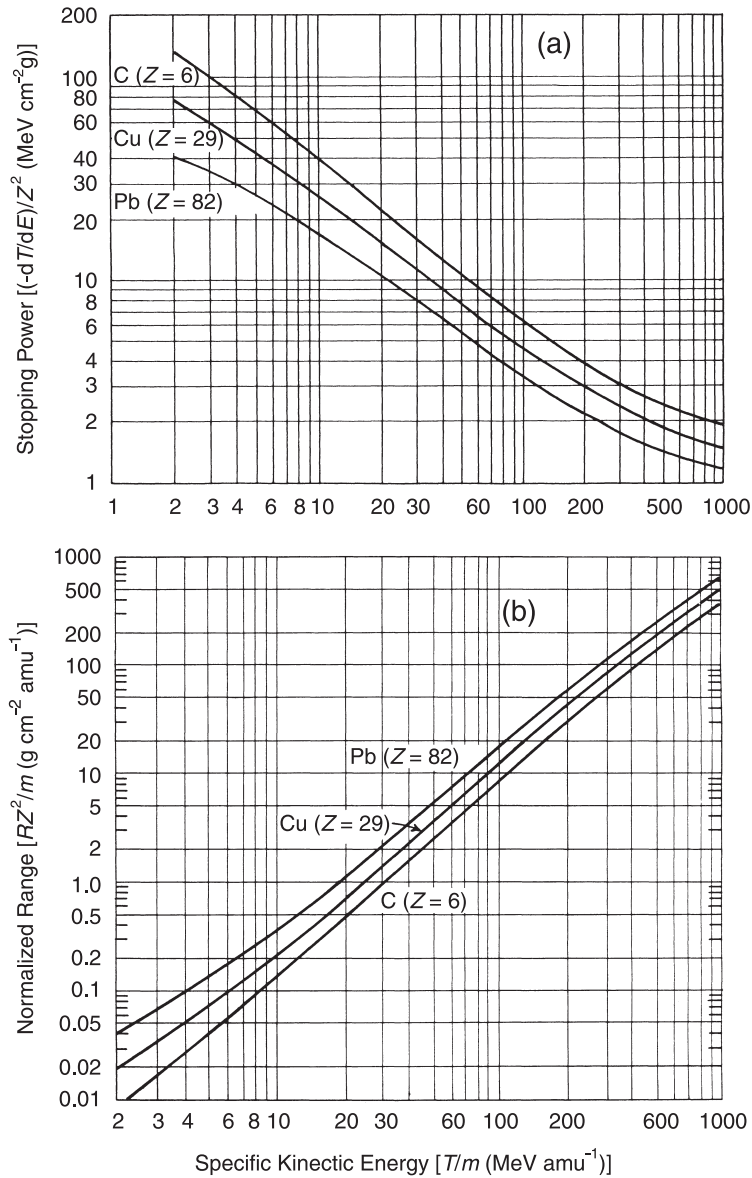
Fig. 3.48. Stopping power (a) and ranges (b) for protons in three materials. These curves can be used for other incident particles by adjusting for their atomic number (Z) and mass [m (amu)]. The incident energy is thus expressed as the specific kinetic energy (T/m). The curves are approximately correct except at the very lowest energies where charge exchange effects can be important and are probably most valid for $m \leq 4$ (Enge, 1966; ICRU, 1993b).

summarized and are plotted as a function of kinetic energy from 10 MeV to 10 GeV in Figure 3.49 (Stephens and Miller, 1969).

Figure 3.50 shows a polar plot of the angular distribution of neutrons emitted from 40 MeV alpha particles incident on a thick tantalum target. The distributions are normalized to unity at Θ = 0 degrees and represent an estimate of total neutron yields above the indicated reaction thresholds. In general, the emitted neutrons are forward-peaked, with angular distributions similar to those for protons of equivalent specific energy (energy/atomic mass in units
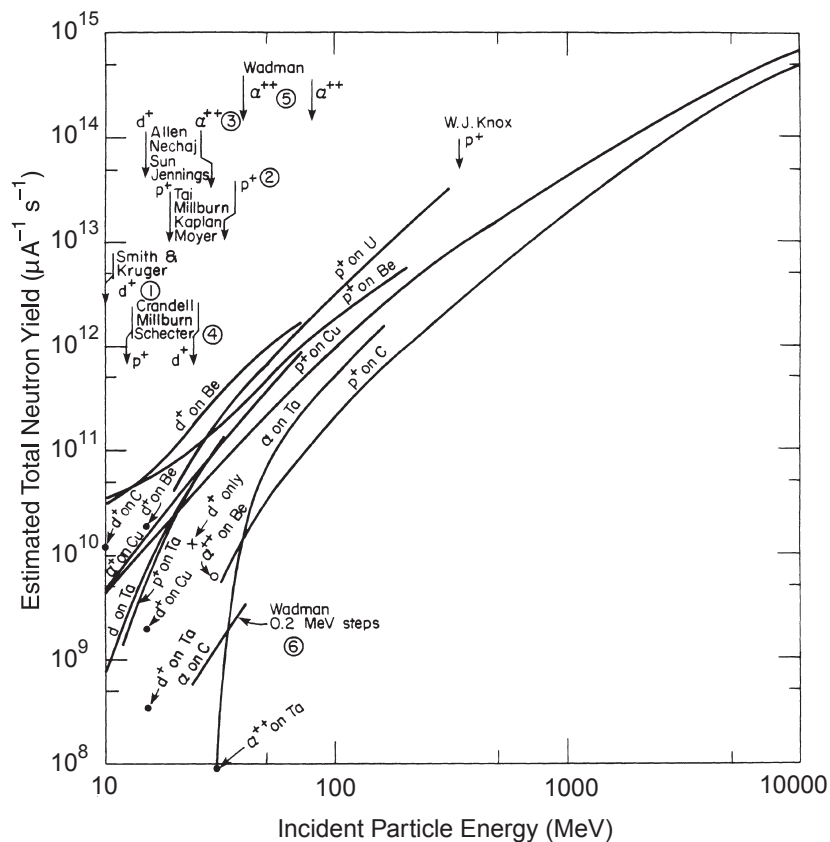
Fig. 3.49. Plots of total neutron yields for various light ions on a number of materials (Stephens and Miller, 1969). The names associated with the circled numbers ① to ⑥ are references that can be found in the Stephens and Miller reference. 1 μA s [1 μC (microcoulomb) of electric charge] corresponds to 6.25×10^{12} incident singly charged particles; 3.125×10^{12} doubly charged particles; etc.
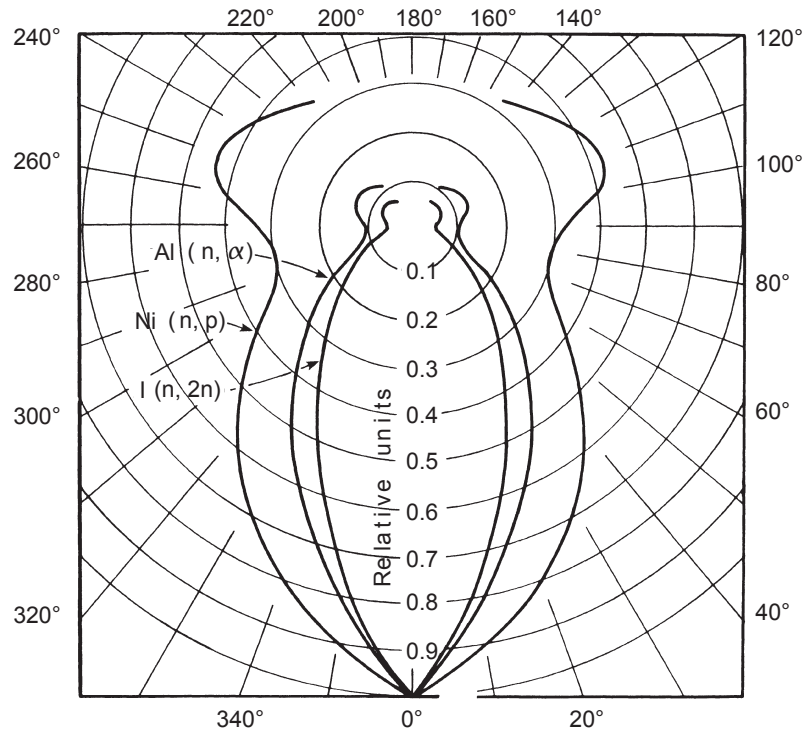
Fig. 3.50. Angular distributions of neutrons emitted from a thick tantalum target struck by 40 MeV alpha particles. The distributions are normalized to unity at $\Theta = 0$ degrees and represent neutrons above the indicated nuclear reaction thresholds: 1.1 MeV for the ^{58}Ni(n,p)^{58}Co; 6.7 MeV for the ^{27}Al(n,α)^{24}Na; and 8.5 MeV for ^{127}I(n,2n)^{126}I (Stephens and Miller, 1969).

of MeV amu^{-1}). A detailed study of the total neutron yields resulting from alpha-particle bombardment of various materials over the energy range 3 to 9 MeV is summarized in Table 3.5 (Bair and del Campo, 1979).

The neutron yield from the bombardment of low-mass targets by light ions may be enhanced greatly for those reactions that are exothermic and, at the same time, have large cross sections. The exothermic reactions can produce neutrons more energetic than the projectile. Noteworthy examples (followed by their reaction Q-values in parentheses) are D(d,n)^{3}He ($Q = 3.266$ MeV); ^{9}Be(α,n)^{12}C ($Q = 5.708$ MeV); and T(d,n)^{4}He ($Q = 17.586$ MeV).

In some cases quasi-monoenergetic beams of neutrons are possible using these or the following slightly endothermic reactions:

TABLE 3.5—*The yield of neutrons from infinitely thick targets of various materials when bombarded by alpha particles in the energy range 3 to 9 MeV (yield given in neutrons per 10^6 alpha particles).*

Energy (MeV)	^{6}Li	^{7}Li	^{NAT}Li	^{9}Be	^{10}B	^{11}B	^{NAT}B	^{19}F	^{NAT}Mg	^{27}Al	^{NAT}Si	^{238}U^{NAT}O$_2$	^{238}U^{NAT}C
3.00				9.790									0.00468
3.50		0.001	0.001	12.97	0.331	3.803	3.150	0.31		0.0012		0.00091	0.00810
4.00		0.002	0.002	19.88	0.758	7.618	6.238	0.879	0.077	0.0169		0.00208	0.00842
4.50		0.030	0.028	33.27	1.924	12.64	10.63	2.159	0.263	0.0802	0.016	0.00593	0.00943
5.00		0.680	0.629	49.43	3.522	18.43	15.64	4.394	0.644	0.2643	0.052	0.0107	0.0119
5.50		2.325	2.150	71.81	5.674	24.05	20.59	7.746	1.262	0.6967	0.114	0.0164	0.0193
6.00	0.000	5.268	4.873	99.16	8.578	29.24	25.35	12.26	2.141	1.438	0.231	0.0236	0.0295
6.50	0.000	11.26	10.41	126.2	12.29	33.92	29.85	17.95	3.250	2.780	0.385	0.0321	0.0423
7.00	0.294	23.42	21.68	154.8	16.78	37.52	33.62	24.84	4.600	4.657	0.602	0.0416	0.0574
7.50	1.733	40.03	37.16	185.5	20.67	42.27	38.21	32.95	6.352	7.131	0.872	0.0520	0.0747
8.00	4.054	51.71	48.14	221.3				42.17	8.349	10.13	1.226	0.0631	0.0939
8.50	7.428	63.32	59.13	259.1					10.55	13.77	1.666		0.114
9.00	11.80	74.99	70.25	302.5					13.29	17.99	2.191		0.136

^{12}C(d,n)^{13}N ($Q = -0.281$ MeV); T(p,n)^{3}He ($Q = -0.764$ MeV); and ^{7}Li(p,n)^{7}Be ($Q = -1.646$ MeV). The energies of such neutrons can range from 0 to 27 MeV for bombarding energies up to 10 MeV. An understanding of these reactions is of great importance to the health physicist responsible for a radiation safety program at a low-energy accelerator, and the interested reader is referred to the text by Patterson and Thomas (1973, pages 118 to 127) where a detailed discussion is given. In general, the so-called "deuteron stripping" reactions (d,n) have large neutron yields because the neutron inside the deuteron is only weakly bound (the binding energy of the deuteron is 2.225 MeV) and is rather easily released. On average, the emitted neutrons carry off half the energy of the incident particle. Their angular distributions are forward-peaked with the energy spectrum centered on roughly half of the incident kinetic energy. Another reaction of interest in producing neutrons is (α,n) because, though the reaction cross sections are typically small, the available accelerated beam currents can be exceptionally large.

3.5.3 *Heavy Ions*

In discussing ion-induced reactions, it is conventional to use the *specific energy*, defined to be the total kinetic energy divided by the atomic mass number (MeV amu^{-1}). It is generally taken to be equivalent to the kinetic energy per nucleon. An extensive tabulation of range-energy and stopping-power relations for energies up to 12 MeV amu^{-1} is that of Northcliffe and Schilling (1970). It spans the entire periodic table for both target and projectile. Figure 3.51 shows plots of the range-energy relation for three different ions bombarding five different materials (Hubbard *et al.*, 1960). The abscissa in these curves is in units of total kinetic energy.

Neutron yields were measured for targets slightly more than one range thick by Hubbard *et al.* (1960) for beams of ^{12}C, ^{14}N, and ^{20}Ne ions of specific energy of 10 MeV amu^{-1} incident on targets of various mass numbers. Figure 3.52 shows the results as a function of target mass number (the uncertainties are estimated to range from 6 to 50 percent). The yields from carbon and neon ions of approximately 5.8 to 10 MeV amu^{-1} incident on other targets are plotted in Figure 3.53 as a function of specific energy. It is clear that for target materials of intermediate mass number, at least at this specific energy of the bombarding ion, the neutron yield is nearly independent of the mass number of both the target nuclei and the projectile. Figure 3.54 shows neutron dose equivalent measured as a function of Θ around a stainless-steel beam stop bombarded by ^{14}N ions having
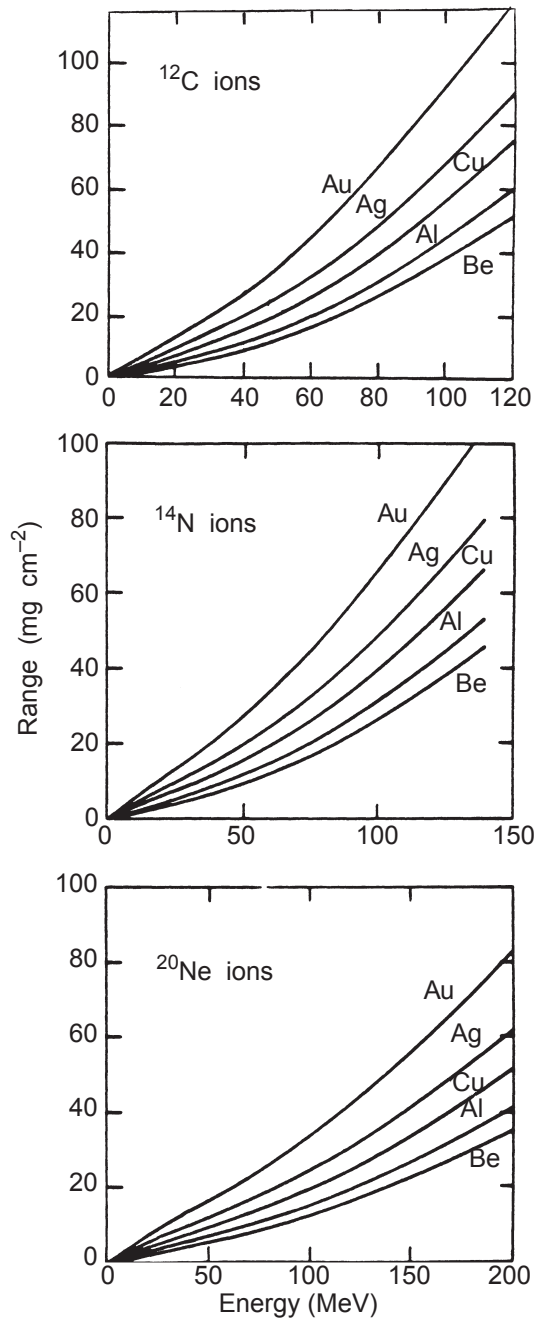
Fig. 3.51. Range versus energy for several different ions in five different materials (Hubbard *et al.*, 1960).
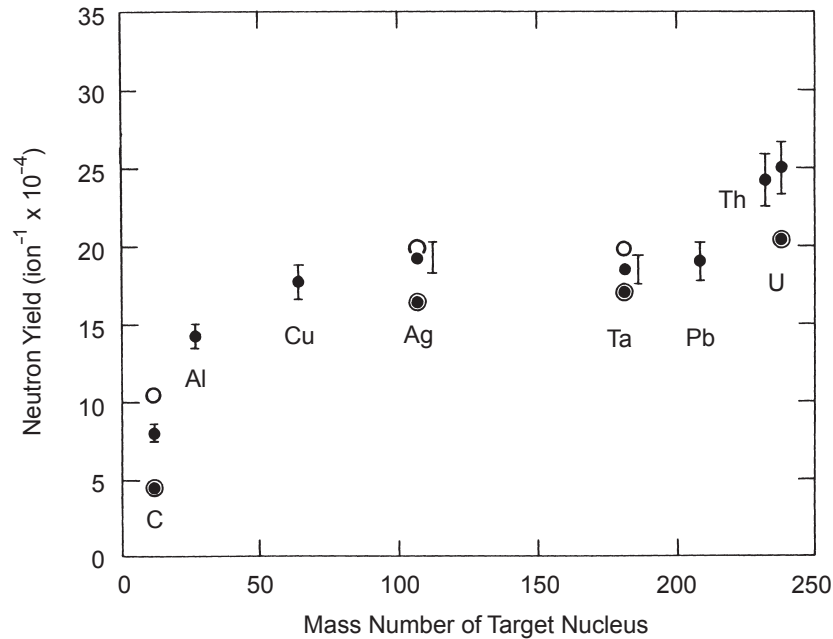
Fig. 3.52. Total neutron yields as a function of target mass number for 10 MeV amu^{-1} ions [^{12}C (small solid circles), ^{14}N (open circles), and ^{20}Ne (large solid circles)] bombarding a number of thick targets with a range of $Z = 6$ to 92 (Hubbard *et al.*, 1960).

a specific energy of 10.5 MeV amu^{-1} (Ohnesorge *et al.*, 1980). The same workers also measured the energy dependence of the dose-equivalent rate at $\Theta = 90$ degrees at 1 m from thick (longer than one range of the bombarding ion) targets of iron, nickel or copper with the results shown in Figure 3.55. Room-scattered neutrons (perhaps up to 33 percent of the total dose equivalent) are included in the measurements. From these measurements, it may be inferred tentatively that the dose equivalent is not strongly dependent on the bombarding ion at a given value of the specific energy, at least up to perhaps 20 MeV amu^{-1} for targets near iron in the periodic table.

Measurements of angular distributions of dose equivalent and neutron energy spectra have been made for 6.6 MeV amu^{-1} ^{58}Ni ions incident on a thick-copper target at the Joint Institute for Nuclear Research cyclotron at Dubna (Aleinikov *et al.*, 1985). Figure 3.56 contains three energy spectra taken at the indicated values of Θ at a radius of 1 m. The ordinate is shown as the fluence per incident ion multiplied by the neutron energy (E). Also shown is the percentage of the dose equivalent [$R(E)$] due to neutrons having energy greater
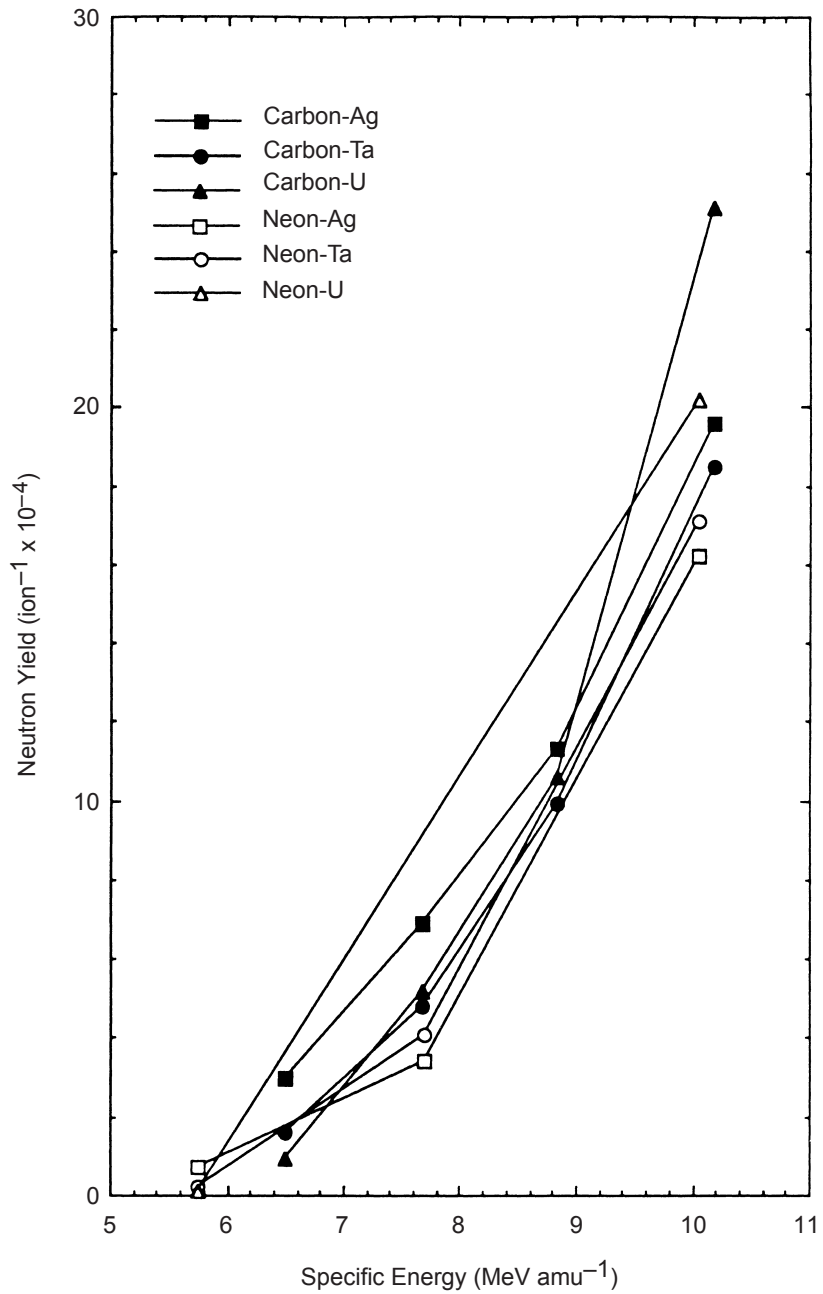
Fig. 3.53.   Neutron yields from thick-target (silver, tantalum and uranium) bombardments by carbon and neon ions having specific energies from approximately 5.8 to 10 MeV amu^{-1} (Hubbard *et al.*, 1960).
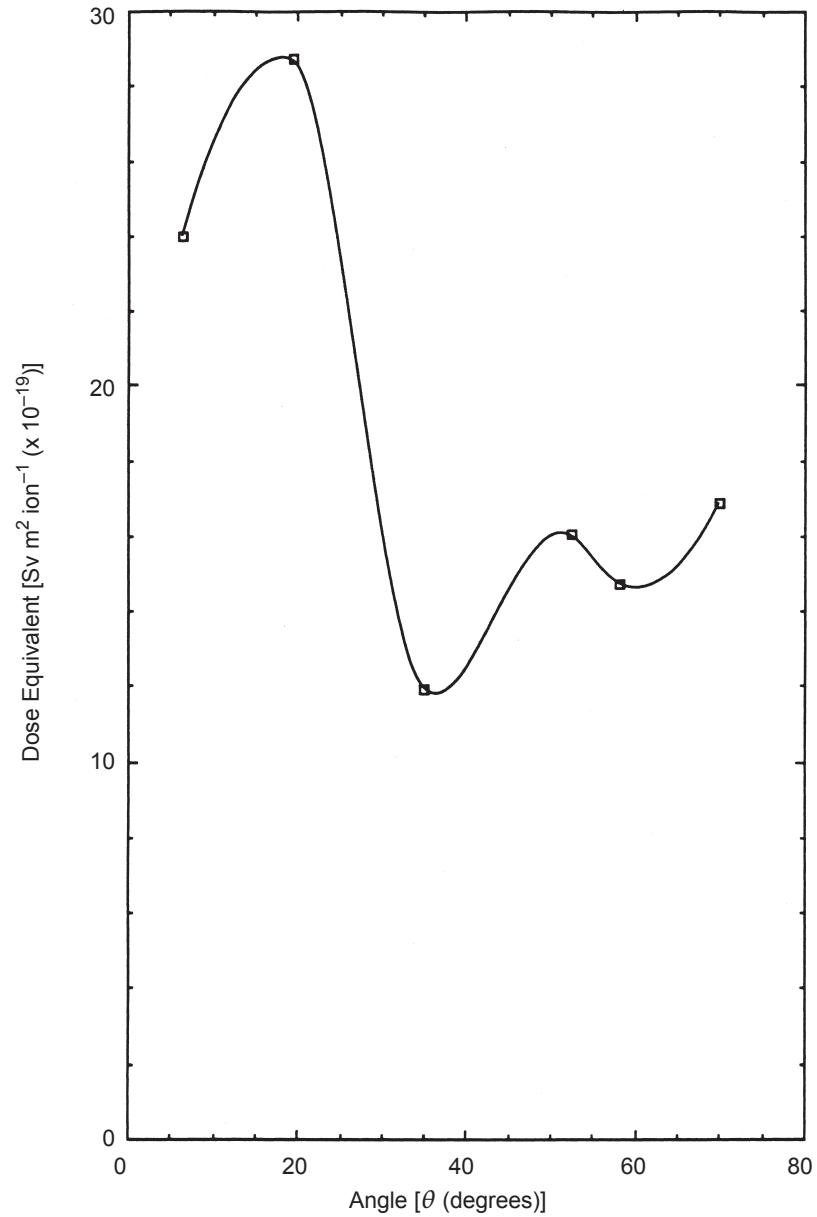
**Fig. 3.54.** Angular distribution of dose equivalent around a stainless steel beam stop bombarded by 10.5 MeV amu^{-1} ^{14}N ions (Ohnesorge *et al.*, 1980). The curve is an interpolation meant to guide the eye. The value at $\Theta = 6.5$ degrees may be partially shadowed by the beam stop in the experimental setup.
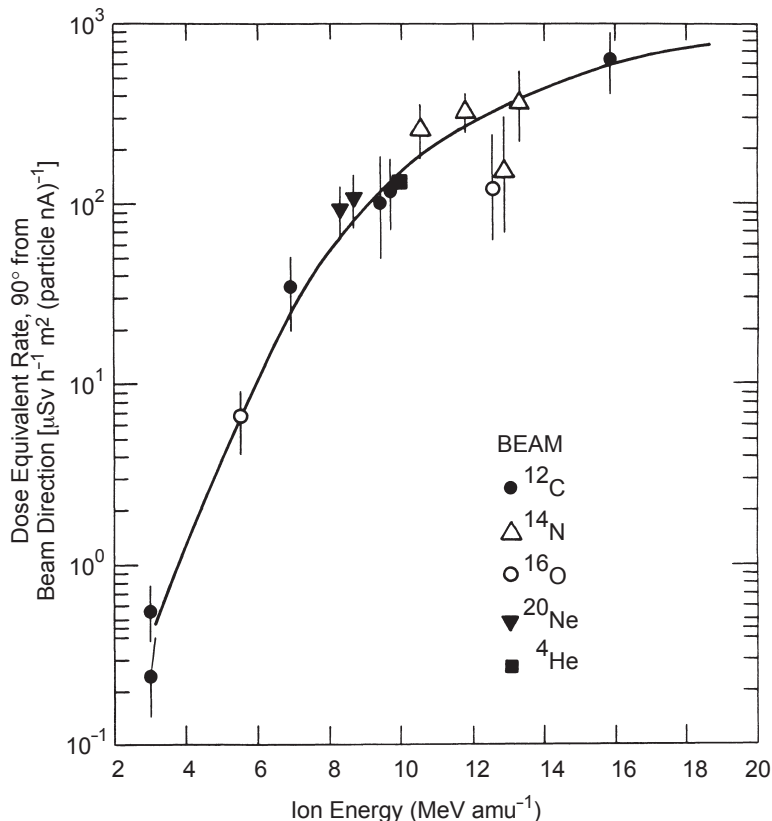
Fig. 3.55.   Fast neutron dose-equivalent rates at 1 m from thick targets of iron, nickel or copper and at $\Theta = 90$ degrees. The ^{16}O and ^{14}N points near 13 MeV amu^{-1} were ignored in drawing the smooth curve (Ohnesorge *et al.*, 1980). One particle nanoampere is 6.25×10^9 particles s^{-1}. 1 μSv h^{-1} per particle nanoampere is equivalent to 4.44×10^{-20} Sv per incident ion.

than E. These experiments show that neutrons directed forward are produced both at greater intensity and with greater energy. In all cases, neutrons with energy greater than 2.5 MeV represent more than 50 percent of the dose equivalent. The total neutron yield was estimated to be $(1.6 \pm 0.4) \times 10^{-3}$ neutrons per incident ion which is comparable to values obtained for much lighter ions (*e.g.*, Figure 3.53). A determination of Q and the energy-integrated neutron yield resulted in the values in Table 3.6.

Aleinikov *et al.* (1985) also determined the normalized angular distribution of dose equivalent shown in Figure 3.57. A successful phenomenological fit was obtained using the formula:
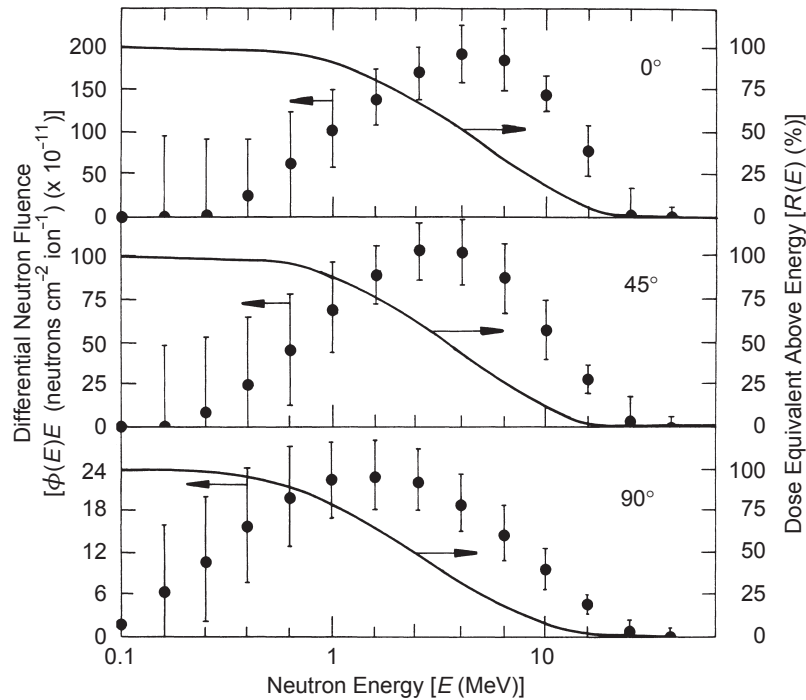
Fig. 3.56. Differential neutron fluence $\phi(E)E$ and percent of dose equivalent above energy (E), $[R(E)]$, as functions of neutron energy measured, at three values of Θ, 1 m from a thick copper target bombarded by 6.6 MeV amu^{-1} ^{58}Ni ions (Aleinikov *et al.*, 1985).

TABLE 3.6—*The total neutron   uence and neutron quality factor measured at three angles for a thick-copper target bombarded by 6.6 MeV amu^{-1} ^{58}Ni ions (Aleinikov et al., 1985).*

Angle to the Beam Direction (Θ) (degrees)	Neutron Fluence (ϕ)[a] $(n\ cm^{-2})$	Quality Factor[b] (Q)
0	$(5.4 \pm 1.4) \times 10^{-9}$	5.2 ± 1.0
45	$(2.9 \pm 0.8) \times 10^{-9}$	5.1 ± 0.4
90	$(0.8 \pm 0.12) \times 10^{-9}$	5.4 ± 2.7

[a] Neutron fluence integrated over the entire energy spectrum per incident ion measured at a distance of 1 m from the target.

[b] These estimates of Q were based on the data and recommendations given in ICRP Publication 21 (ICRP, 1973).
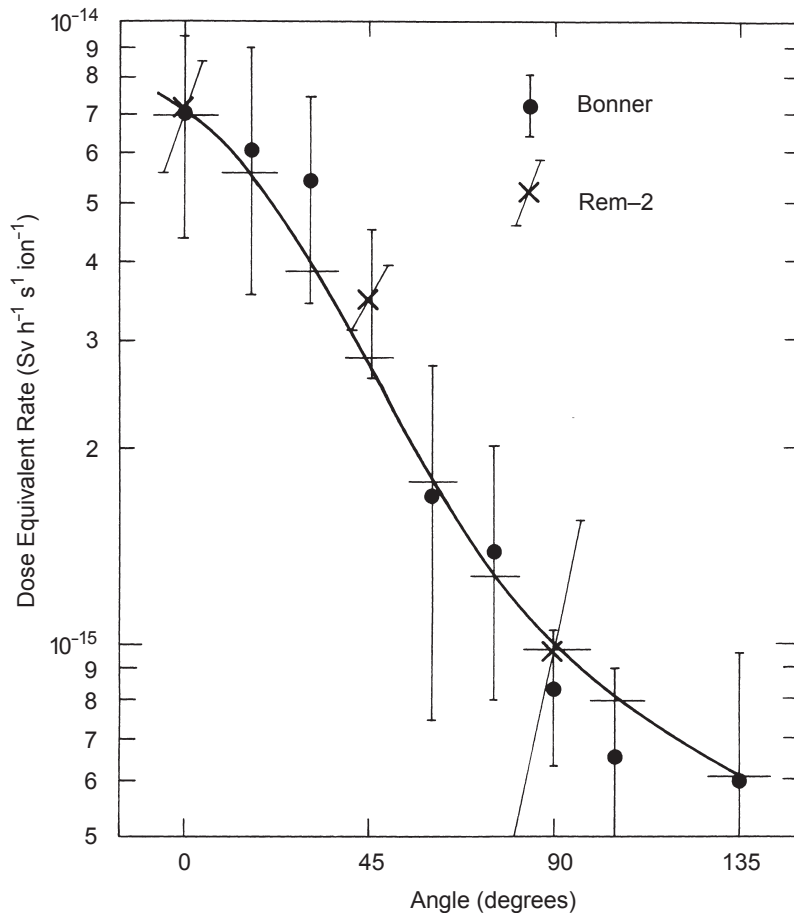
Fig. 3.57. Angular distribution of the dose equivalent rate at 1 m from a thick copper target bombarded by 6.6 MeV amu^{-1} ^{58}Ni ions (Aleinikov *et al.*, 1985). The data points labeled "Bonner" use the multisphere technique (Bramblett *et al.*, 1960) while those labeled "Rem-2" use a recombination chamber technique (Zielczynski, 1963) (1 Sv h^{-1} s^1 ion^{-1} = 2.77 $\times$ 10^{-4} Sv ion^{-1}).

$$f(\Theta,\xi) = \frac{1}{4\pi}\left[\frac{1}{\log\,(1\,+\,1/\xi)}\right]\left[\frac{1}{\xi\,+\,\sin^2\,(\Theta/2)}\right], \qquad (3.35a)$$

where:

$$\xi = \frac{f(90°)}{f(0°)\,-\,f(90°)} \qquad (3.35b)$$

and f(Θ) is either the value of the fluence or the dose equivalent at Θ. This formulation also has been confirmed as valid over a much larger domain of specific energy (Clapier and Zaidins, 1983).

Clapier and Zaidins (1983) also have given a few examples of the parameter (ξ) in Equations 3.35a and 3.35b for fitting the angular distribution. They report values of ξ = 0.07 for uranium incident on uranium at 9 MeV amu^{-1}, ξ = 0.025 for neutrons of energy <20 MeV produced by 86 MeV amu^{-1} ^{12}C incident on iron, and ξ = 3×10^{-4} for neutrons of energy >20 MeV produced by 86 MeV amu^{-1} ^{12}C incident on iron.

Only limited information exists about the neutron yields from intermediate- and high-energy heavy ions. Tuyn *et al.* (1984) have reported studies with 86 MeV amu^{-1} ^{12}C ion incident on iron targets slightly longer than the range. Threshold detectors were used to measure neutron angular distributions and compare them with calculations using the computer code of Bertini *et al.* (1976). The results of measurements of the yield (dY/dΩ) are given in Figure 3.58 (for neutron energies below 20 MeV) and in Figure 3.59 (for neutron energies greater than 20 MeV). Calculations for iron, aluminum and carbon targets agree with one another to within 20 percent.

Clapier and Zaidins (1983) have surveyed the experimental results of heavy-ion yield measurements for the specific-energy region from 3 to 86 MeV amu^{-1}. These studies have verified the validity of the above empirical parameterization of the angular distribution in terms of f(Θ,ξ) for a number of different spectral conditions. These authors have parametrically fitted existing data and have found that the total neutron yield [Y (neutrons/ion)], can be approximately fitted as a function of the atomic number of the target material (Z) and the specific energy [W (MeV amu^{-1})]. There does not appear to be strong dependence upon the Z of the target. The expressions that result are:

$$Y\,(W,Z) \,=\, \mathrm{C}(Z)\, W\eta(Z) \tag{3.36a}$$

with

$$\eta(Z) \,=\, 1.22\sqrt{Z} \tag{3.36b}$$

and

$$\mathrm{C}(Z) \,=\, \frac{1.95 \times 10^{-4}}{Z^{2.75}}\, \exp\!\left[-0.475\,(\ln Z)^2\right]. \tag{3.36c}$$

Results are shown in Figure 3.60 for incident ions ranging from protons to very heavy ions up to the mass region of lead. The shaded region is an estimate of the probable error one might expect in the
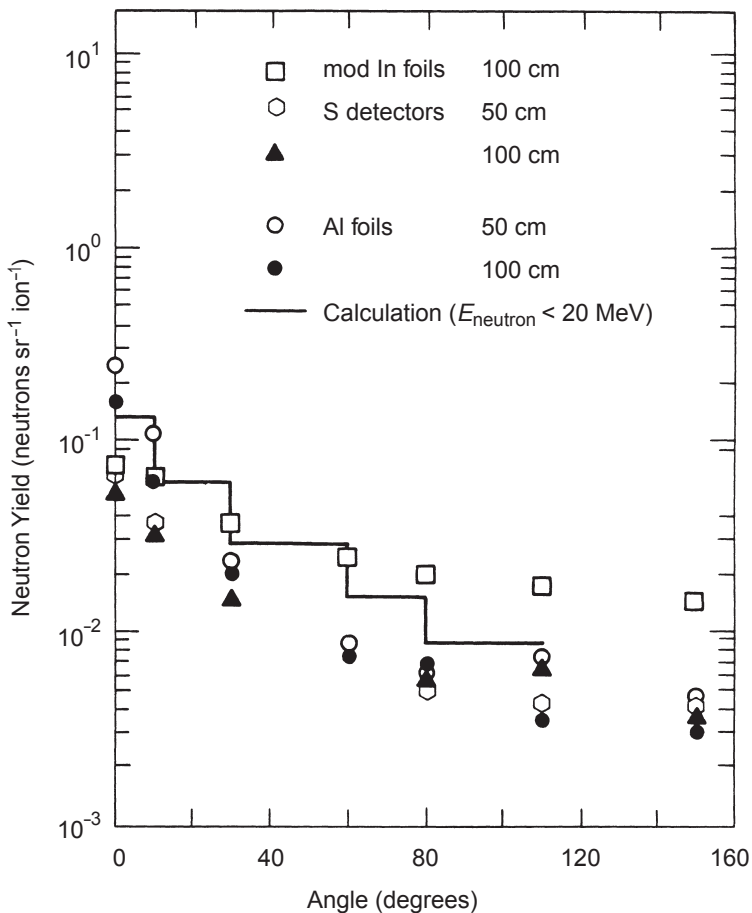
Fig. 3.58. Comparison between measured and calculated neutron yields as a function of angle at 86 MeV amu^{-1} ^{12}C ions incident on an iron target for neutron energies below 20 MeV. Activation detectors with the following sensitive regions in neutron energy (E_n) were used: moderated indium foils ($0.4 < E_n < 10^7$ eV); ^{32}S(n,p)^{32}P ($E_n > 3$ MeV); and ^{27}Al(n,α)^{24}Na ($E_n > 7$ MeV). Measurements were made at the indicated radial distances (Tuyn *et al.*, 1984).

use of this equation. The authors also tabulated the individual values of C(Z) and $\eta(Z)$ used to obtain the fitting parameters in the above equations. These are given in Table 3.7. For these particular materials, a reasonable method for making crude estimates of the neutron yield is to calculate it using both the values from Table 3.7 and those obtained from the above equation. The difference in the results
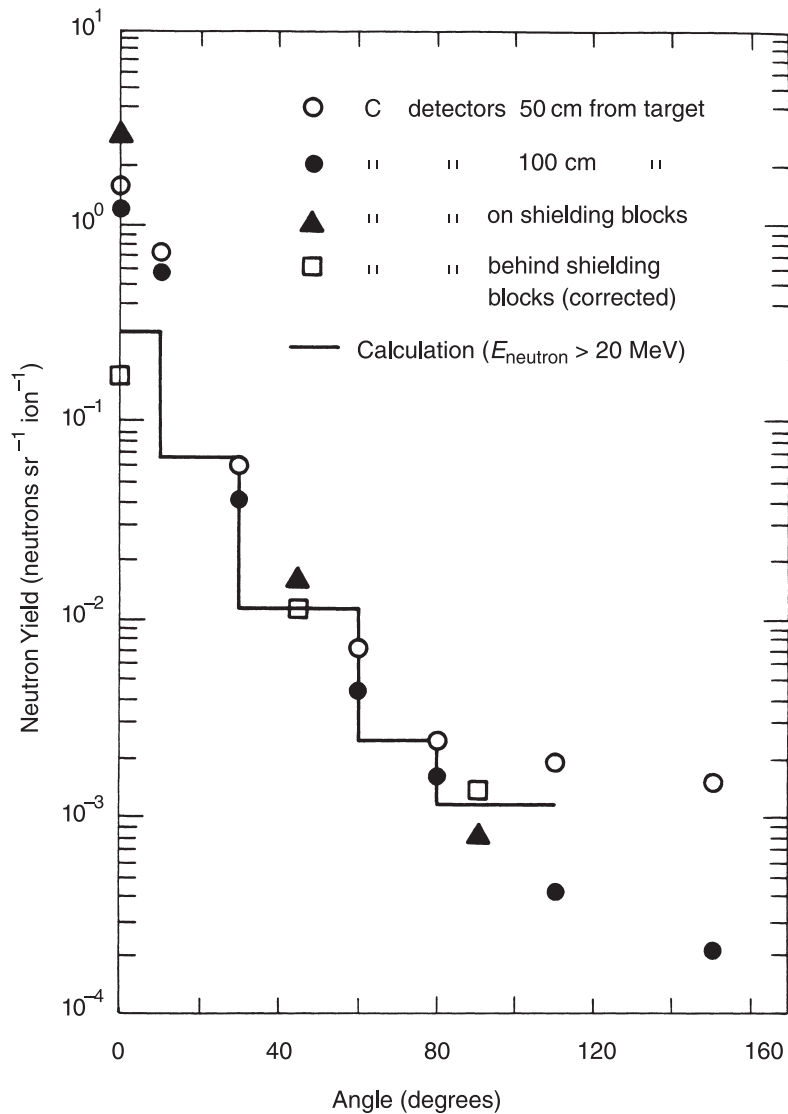
Fig. 3.59. Comparison between measured angle and calculated neutron yields as function of angle at 86 MeV amu^{-1} ^{12}C ions incident on an iron target for neutron energies above 20 MeV using the ^{12}C(n,2n)^{11}C reaction. Measurements were made at the indicated radial distances (Tuyn *et al.*, 1984).
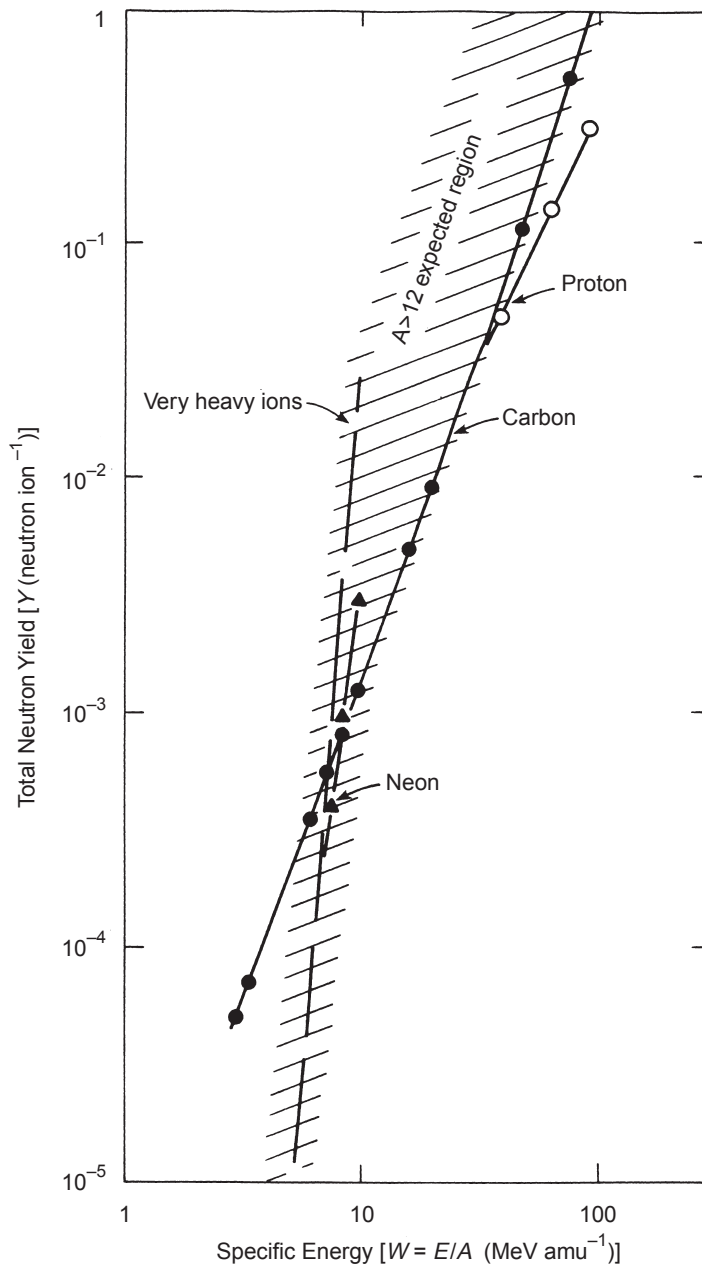
Fig. 3.60. Total neutron yield as a function of specific energy for a variety of ions (Clapier and Zaidins, 1983). The shaded region is representative of the errors in the associated parametric fit to these data given in the text.

TABLE 3.7—*Values of the functions C(Z) and η(Z) in Equation 3.36.*

Element	Z	η(Z)	C(Z)
Hydrogen	1	1.5	1.7×10^{-4}
Helium	2	2.6	3.9×10^{-6}
Carbon	6	2.7	2.5×10^{-6}
Oxygen	8	3.6	3.6×10^{-7}
Neon	10	7.0	2.7×10^{-10}
Argon	18	7.0	5.1×10^{-11}
Krypton	36	7.9	6.0×10^{-12}
Lead	82	11.0	1.7×10^{-13}

obtained can be used as an indicator of the uncertainty involved in this approach.

McCaslin *et al.* (1985a) have studied neutron yields for incident neon and silicon ions at a specific energy of 670 MeV amu^{-1}. Radioactivation produced by several nuclear reactions, listed with the corresponding effective thresholds in Table 3.8, were used to obtain spectral information at 1 m from a thick copper target. Figure 3.61 shows the measured angular distributions for incident silicon ions. Similar results were obtained for neon ions. These authors were able to parameterize the neutron yield for several of the threshold reactions with the following empirical relationship, where $\phi(\Theta)$ is the fluence.

For incident ^{20}Ne ions including all neutrons above 6.5 MeV:

$$\phi(\Theta) = 372 \ \Theta^{-1} \text{ neutrons m}^{-2} \text{ ion}^{-1}$$

$$\text{(for } 2° < \Theta < 180°, \Theta°). \tag{3.37}$$

TABLE 3.8—*Neutron detectors used for yield measurements with 670 MeV amu^{-1} neon and silicon ions.*

| Type of Detector	Reaction	Energy Range
Indium	n capture	Thermal
BF$_3$ (moderated)	^{10}B(n,α)^{7}Li	0 – 15 MeV
Aluminum	^{27}Al → ^{24}Na	>6.5 MeV
Teflon	^{19}F → ^{18}F	>10 MeV
Polyethylene (CH$_2$)$_n$	^{12}C → ^{11}C	>20 MeV
Aluminum	^{27}Al → ^{22}Na	>25 MeV
Aluminum	^{27}Al → ^{18}F	>50 MeV
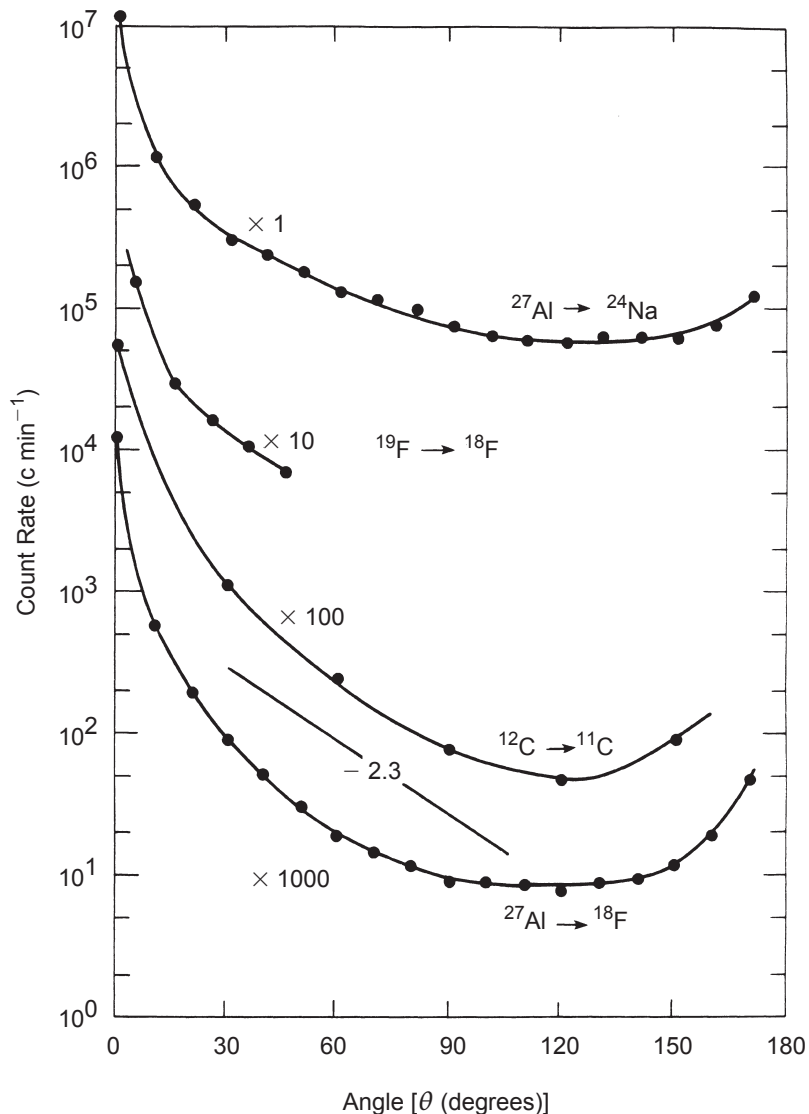
Fig. 3.61.   Angular distributions (count rate) measured at 1 m by four types of activation detectors having different thresholds in the range 6.5 to 50 MeV (see text). The beam was 2.5×10^8 Si ions s^{-1} having a specific energy of 670 MeV amu^{-1} incident on a thick copper target. The normalization is arbitrary (McCaslin *et al.*, 1985a). The line labeled "-2.3" corresponds to an exponential slope which successfully fit the angular distribution derived for high-energy proton distributions (Levine *et al.*, 1972).

For incident ^{20}Ne ions including all neutrons above 20 MeV:

$$\phi(\Theta) = 248\ e^{-0.2\,\theta}\ \text{neutrons m}^{-2}\ \text{ion}^{-1}$$

$$(\text{for }0° < \Theta < 20°, \Theta°) \qquad (3.38a)$$

and

$$\phi(\Theta) = 10\ e^{-0.038\theta}\ \text{neutrons m}^{-2}\ \text{ion}^{-1}$$

$$(\text{for }20° < \Theta < 120°, \Theta°). \qquad (3.38b)$$

The neutron yields for heavy ions at this high specific energy are quite large as compared with yields for protons of comparable specific energy. This is due to the fact that, for example, for silicon ions there are some 28 nucleons comprising the incident particle in the nuclear reactions.

3.6 Radioactivation at Accelerators

3.6.1 *General*

All accelerators that can produce heavy charged particles or neutrons having a specific energy above $\sim$10 MeV amu^{-1}, either directly or by interaction of the primary beam, can produce radioactivity. In some special cases (see discussion below), radioactivity can be produced at much lower energies by exothermic nuclear reactions that either produce radionuclides directly or that emit neutrons capable of inducing radioactivity through their secondary interactions (Sections 3.6.2 and 3.6.3).

At electron accelerators, the activation results indirectly through the production of neutrons and other particles and ions that participate in the nuclear interaction in the course of the development of the electromagnetic cascade. The giant-resonance photonuclear reactions, in particular, copiously produce neutrons that are available to further initiate nuclear reactions that result in the production of radioactivity. At higher energies, some of these photon-induced reactions continue to be of importance. These mechanisms have been described in detail by Barbier (1969) and IAEA (1979a) and summarized by Swanson and Thomas (1990).

For many accelerators, provided the shielding against prompt radiation is properly designed and provided proper access controls are implemented to avoid direct beam-on exposure to people, the radioactivity induced in accelerator components is very likely to be the dominant source of radiation exposure. Experience at accelerators

world-wide is that the largest cause of the radiation exposure incurred by accelerator workers arises from operations on and maintenance of radioactivated components, handling and moving of activated items, radiation surveys, and radioactive waste handling (Section 7). An understanding of the production of radionuclides provides background information that may be applied to the reduction of personnel exposures by, *e.g.*, the selection of more appropriate machine component materials or the optimization of decay times recommended after the beam has been turned off.

3.6.2 *Activation by Low-Energy Particles*

At lower incident energies at proton and ion accelerators ($E < 30$ MeV), radionuclide production by such processes as (p,γ) and single- and multi-nucleon transfer reactions are of principal concern. The systematics and *approximate* energy dependencies of these processes are generally well understood. The majority of reactions of concern are endothermic nuclear reactions that have a *threshold* (E_{th}) below which the process is forbidden by conservation of energy. E_{th} is related to the mass of the projectile ion (m), the mass of the target nucleus (M), and the energy released in the reaction (Q):

$$E_{th} = \frac{m + M}{M} Q \qquad (3.39)$$

(see, for example, Livesey, 1966). In an endothermic reaction, Q is negative for reactions having a positive value of E_{th}.

Yields of radionuclides from thick targets having different Z have been systematically plotted for numerous reaction processes (Cohen, 1978). A brief summary of these plots for the more significant reactions is given in Figure 3.62. It is assumed that the target thickness exceeds the range of the incident ions and that the irradiation period greatly exceeds the half-life of the radionuclide of interest. If shorter bombarding periods are used, one can correct by multiplying the plotted value by $(1 - e^{-\lambda T})$ where λ is the decay constant for the radionuclide of interest and T is the irradiation period. The values shown for the yield should be accurate to within a factor of about three. More accurate values can be obtained from the original reference from which these curves were derived (Keller *et al.*, 1974). It should be emphasized that these are plots of radionuclide yield as a function of the energy above threshold ($E - E_{th}$). As one can see, a general feature is that the yield rises as the threshold energy is exceeded by the bombarding energy by a few mega-electron volts. At higher energies, the yield increases more slowly and, in some
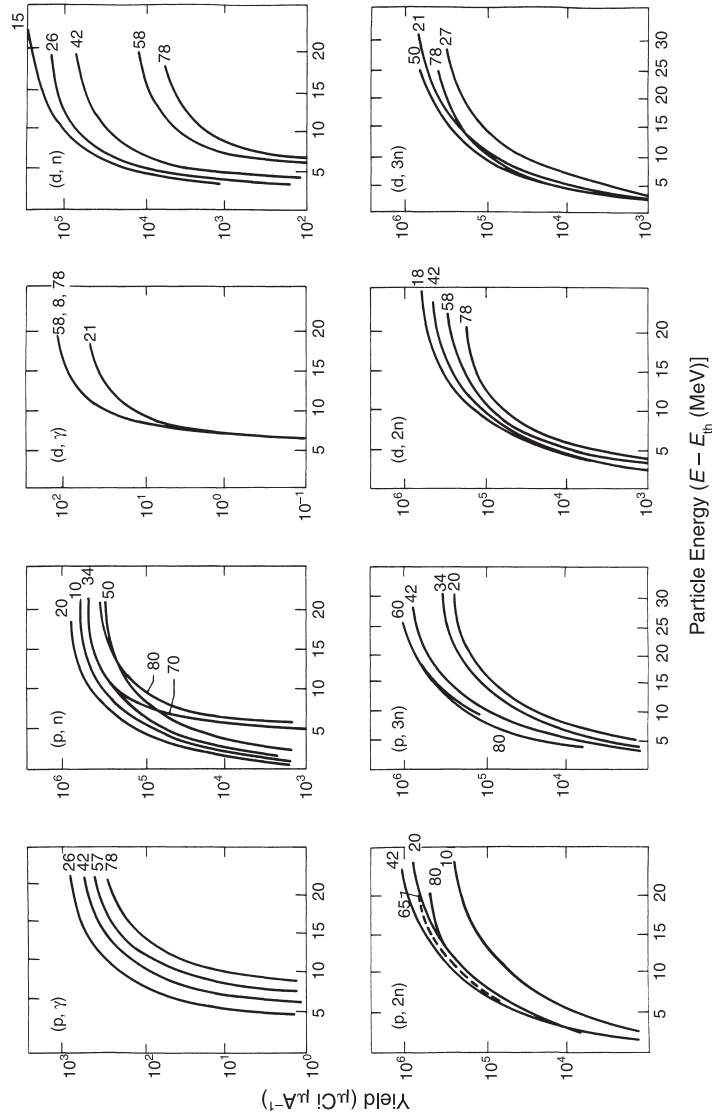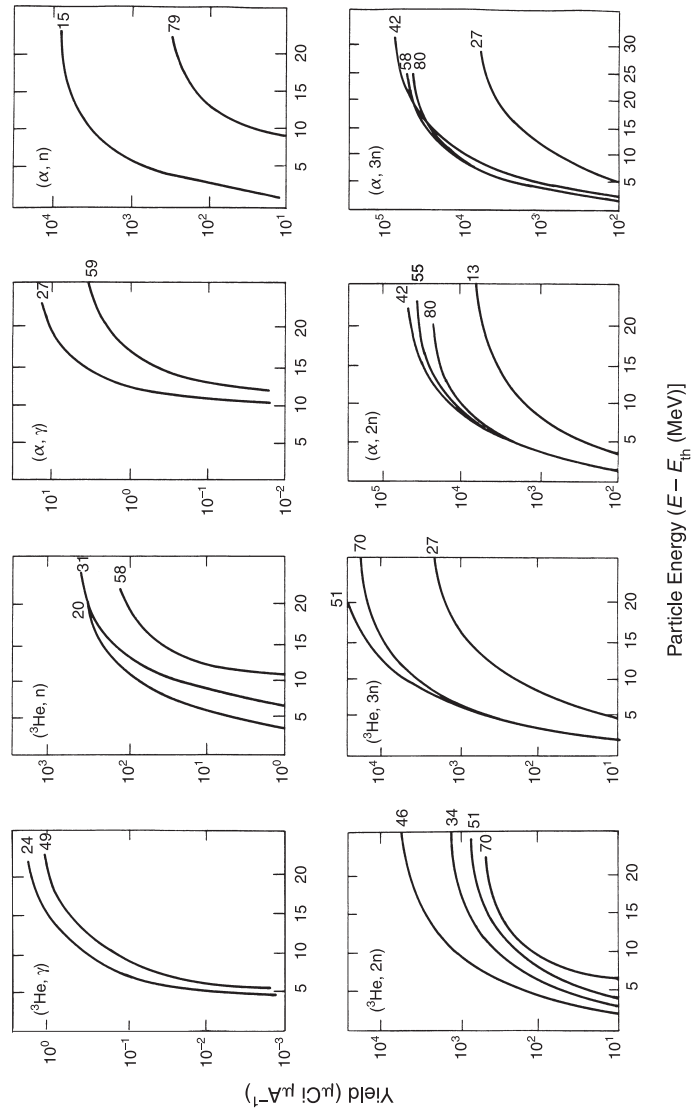
Fig. 3.62. Thick target yields from charged particle reactions (Cohen, 1978). Curves show the yield in microcuries per microamp for elements of given atomic number (Z) as a function of particle energy (E) minus the threshold energy (E_{th}) for the reaction. Nuclides of the same Z have about the same approximate yield (order of magnitude) for the same value of ($E − E_{th}$).

cases, appears to level off to a "saturation" value. Over the energy range of the curves in Figure 3.62, the importance of activation by secondary particles is small compared to that encountered at higher energies.

It is also quite common for thermal neutrons (*i.e.*, those neutrons that are in thermal equilibrium with the ambient temperature) to produce significant levels of induced radioactivity in the accelerator room. Such radioactivity results from thermal neutron capture reactions that sometimes can have relatively large cross sections. In particular, it has been demonstrated that thermal neutrons tend to uniformly fill a room surrounded by the concrete walls that comprise the radiation shield (Kimura *et al*, 1994). Of particular concern is the production of ^{24}Na which has a 15 h half-life and can be produced copiously in concrete walls that might typically contain about one percent natural sodium, an effect described by Armstrong and Barish (1970) and Cossairt (1996). In medical facilities, the production of this radionuclide in the tissues of patients being given therapeutic treatments of protons or neutrons can be significant.

3.6.3 *Activation by High-Energy Particles*

As the energy of the incident radiation increases, the number of possible reaction channels increases, with a corresponding increase in the number of radionuclides produced. An example of this is shown in Figure 3.63 for the case of bismuth when bombarded by protons. The number of radionuclides increases with increased proton energy. At 40 MeV, only few nucleon transfer reactions are available, while at 3 GeV the entire periodic table is essentially available for the production of nuclei lighter than the target. The variety of radionuclides that can be produced increases as one increases the bombarding energy because more reaction thresholds are exceeded.

Table 3.9 lists radionuclides typically encountered in accelerator installations and their half-lives (adapted from Patterson and Thomas, 1973). In this table only nuclides with half-lives between 10 min and 5 y are listed. "Pure" $\beta^\pm$ emitters (*i.e.*, those that emit no photons) are not included in this table due to the difficulty of their identification by means of gamma-ray spectroscopy. While these radionuclides are not listed here, it is clear that beta radioactivity at accelerators can sometimes represent a significant source of exposure to personnel by way of exposures to the skin of individuals engaged in maintenance activities. Also, these radionuclides can result in photon exposures due to bremsstrahlung by the stopping electrons and positrons and also through the pair of 0.511 MeV
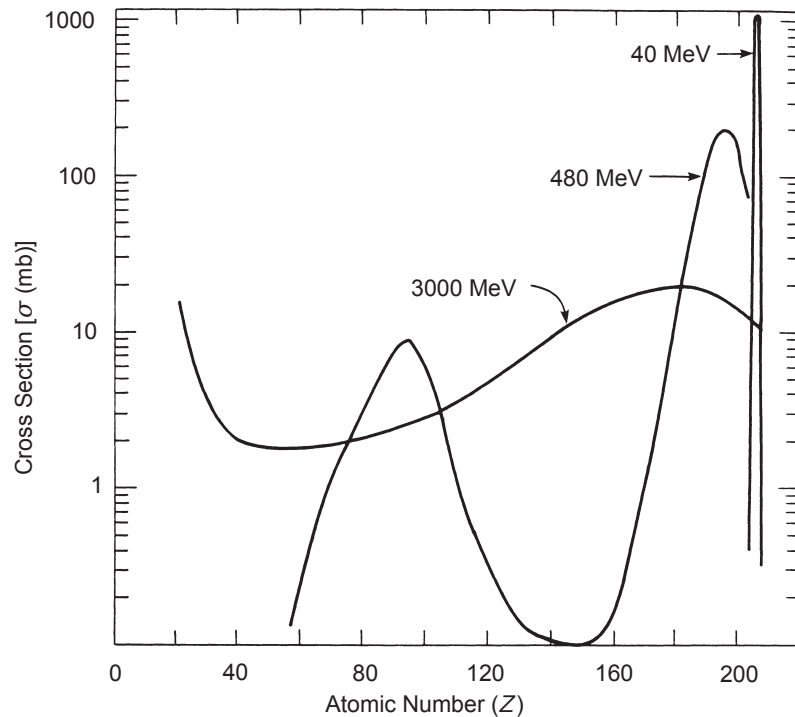
Fig. 3.63. Mass-yield curves (cross section versus Z) for the bombard-
ment of bismuth by protons of the indicated bombarding energies (Patterson
and Thomas, 1973).

photons produced by the annihilation of each positron. However, in
general, at medium- or high-energy accelerators, the "whole-body"
radiation exposures of personnel due to work with or in proximity
to activated components dominates over that due to beta particles.
This result arises from the fact that due to the relatively large mean
free paths of the beam particles comprising the prompt radiation
field, the components tend to be nearly uniformly irradiated, and
hence uniformly activated over considerable volumes of space. The
mean free paths of the gamma rays from the decaying nuclei in a
material of interest are larger than the extrapolated ranges of the
beta particles. Thus, the photons from throughout a given accelerator
component contribute to the dose equivalent at its surface while only
beta particles near the surface contribute to the dose equivalent just
outside of the surface.

An extensive treatise on this subject dealing with the multitude
of complications has been written by Barbier (1969), in which

TABLE 3.9—*A summary of the radionuclides commonly identi ed in materials irradiated in radiation environments.*

Irradiated Material	Radionuclides Produced	Half-Life	
Water, plastics, oils	^{7}Be	53.3	d
	^{11}C	20.3	min
Aluminum	All of those above plus:		
	^{18}F	110	min
	^{22}Na	2.60	y
	^{24}Na	15.0	h
Steel	All of those above plus:		
	^{42}K	12.4	h
	^{43}K	22.3	h
	^{44}Sc	3.93	h
	^{44m}Sc	2.44	d
	^{46}Sc	83.8	d
	^{47}Sc	3.35	d
	^{48}Sc	1.82	d
	^{48}V	16.0	d
	^{51}Cr	27.7	d
	^{52}Mn	5.59	d
	^{52m}Mn	21.1	min
	^{54}Mn	312	d
	^{56}Co	77.3	d
	^{57}Co	272	d
	^{58}Co	70.9	d
	^{55}Fe	2.73	y
	^{59}Fe	44.5	d
Stainless steel	All of those above plus:		
	^{60}Co	5.27	y
	^{57}Ni	35.6	h
	^{60}Cu	23.7	min
Copper	All of those above plus:		
	^{65}Ni	2.52	h
	^{61}Cu	3.35	h
	^{62}Cu	9.74	min
	^{64}Cu	12.7	h
	^{63}Zn	38.5	min
	^{65}Zn	244	d

methods for systematizing the large body of nuclear physics data are described. The reader is encouraged to refer to this extensive discussion of the mechanisms, including excitation functions for many nuclides of interest. A very useful summary of the production of radioactivity at particle accelerators has been given by Gollon (1976).

The extranuclear hadron-cascade process produces the major fraction of the induced activity at high-energy accelerators. In this process, many nuclei are produced in excited states and de-excite by emitting "evaporation neutrons." As de-excitation proceeds, both stable and radioactive nuclides are produced. Particles in the hadron cascade will continue to produce radionuclides in this way until their energies drop below the thresholds for the nuclear reactions involved or, in the case of exothermic reactions, until they are captured.

One exothermic reaction of great importance is thermal-neutron capture in sodium; ^{23}Na(n,γ)^{24}Na. ^{24}Na has a half-life of 15 h and can be the principal source of exposure in a concrete accelerator enclosure during the first few hours after cessation of operations (Patterson and Thomas, 1973).

Four simple rules developed by Gollon are extremely useful for *approximate* radioactivity estimates.

- **Rule 1:** The absorbed-dose rate, dD/dt (Gy h^{-1}), at a distance r (meters) from a "point" source of typical activation gamma rays is given in terms of the source strength [S (bequerel)] and the photon energy [E_γ (mega-electron volt)] by:

$$\frac{\mathrm{d}D}{\mathrm{d}t} = \Gamma \Sigma E_\gamma \left(\frac{S}{r^2}\right),$$ (3.40)

  where the summation is over all gamma rays present, including appropriate branching fractions if more than one photon is emitted per decay. The constant, Γ, has the value of 1.08×10^{-13} m^2 Gy h^{-1} MeV^{-1} Bq. {If dD/dt is desired as an approximate absorbed-dose rate in rad h^{-1} at a distance [r (meters)] from a source strength (S) in curies, then $\Gamma = 0.4$ m^2 rad h^{-1} MeV^{-1} Ci.}
- **Rule 2:** In many common materials, about 50 percent of the nuclear interactions produce a nuclide with a half-life longer than a few minutes, with about 50 percent of these having a half-life longer than 1 d.
- **Rule 3:** For most common shielding materials, the approximate dose rate dD/dt due to a constant irradiation is given by (Sullivan and Overton, 1965) as:

$$\frac{\mathrm{d}D}{\mathrm{d}t} = \mathrm{b}\phi \ln[(t_\mathrm{i} + t_\mathrm{c})/t_\mathrm{c}].$$ (3.41)

In Equation 3.41, b is a factor that depends on geometry and target material (b can often be determined either empirically or by using Rule 2), ϕ is the fluence rate of incident particles, the variable t_i is the irradiation time, while t_c is the cooling time since the cessation of the irradiation. There is considerable experience at proton accelerators that suggests that the formula is valid for $t_i > 0.2$ h and for $(t_i + t_c) < 500$ d. Tuyn *et al.* (1984) have shown Equation 3.41 to be reliable in the case of irradiation by heavy ions of 86 MeV amu^{-1}.

- **Rule 4:** In a hadronic cascade, a proton produces about four interactions for each giga-electron volt of energy.

The application of these four rules may be made clear by the following example:

The activity (S) produced in a target bombarded by particles is given by:

$$S = f_1 f_2 I, \qquad (3.42)$$

where:

f_1 = fraction of the beam interacting in the target
f_2 = fraction of radionuclides produced with half-life longer than a day
I = beam intensity

For the example, assume that a target of thickness one-tenth of an interaction length is irradiated by an intensity (I) of 10^{11} protons s^{-1}. In other words, only about 10 percent of the incident protons interact in the target (10^{10} s^{-1}) and therefore $f_1 = 0.1$. Further, assume this irradiation has been occurring for several months (long enough to reach saturation production for many radionuclides).

Rule 2 then gives $f_2 = 0.5 \times 0.5 = 0.25$. Thus, the decay rate within 1 d of the shutdown (S) is ~$0.1 \times 0.25 \times 10^{11} = 2.5 \times 10^9$ Bq. If each of these decays produces a 1 MeV gamma ray, then Rule 1 indicates an absorbed dose rate of ≈ 0.27 mGy h^{-1}.

Rule 3 can be used together with calculations of the type shown above to predict the absorbed-dose rate at some future time, after beam shutdown from a point source, if one knows the irradiation and cooling times. Furthermore, Rule 3 is not restricted to "point" sources but can be used for extended sources. Sometimes one can estimate this product of bϕ or can use a measurement of the exposure or absorbed-dose rate at some definite value of t_i and t_c in order to determine the product empirically for the purpose of using the formula to predict the "cooldown." In this way, Rule 3 is also useful

for extended shields irradiated by secondary particles from a well-developed cascade.

Rule 4, coupled with Rule 2, can be used to roughly estimate the activation of a beam dump by incident high-energy particles.

Finally, the absorbed dose rate (dD/dt) at the surface of a thick target may be estimated by use of the danger parameter (Δ) introduced by Barbier (1969). If radioactivity produced in a thick object, irradiated by a fluence rate ($\dot{\phi}$) subtends solid angle (Ω) at the point of concern, then:

$$\frac{\mathrm{d}D}{\mathrm{d}t} = \frac{\Omega}{4\pi}\,\dot{\phi}\Delta. \tag{3.43}$$

(For contact with a semi-infinite slab of *uniformly* irradiated material, the fractional solid angle factor obviously becomes 0.5.) The physical meaning of Δ is equal to the absorbed-dose rate actually existing inside a cavity of arbitrary form embedded in an infinite volume of radioactive substance with uniform distribution of activity which has been irradiated by a unit flux density (one particle per second per square centimeter).

Figure 3.64 shows representative examples of plots of the danger parameter (Δ) for four different materials: carbon, silver, tungsten and lead. More extensive data have been given by Barbier (1969). These curves can readily be used to predict the relative "cooling" rates of various components around accelerators with a fair degree of accuracy. Their use in the prediction of absolute dose-equivalent rates due to activated accelerator components requires additional care. To do this, the geometric configuration should be simple and well-defined, the flux density of thermal neutrons should be a small component of the prompt radiation field, and the activation of other materials in proximity such as the enclosure walls should be taken into account. Cracks through the shielding materials can sometimes result in higher dose-equivalent rates that are difficult to quantify. The importance of understanding the contribution due to thermal neutrons interacting with shielding concrete has been discussed by Armstrong and Alsmiller (1969) and by Cossairt (1996).
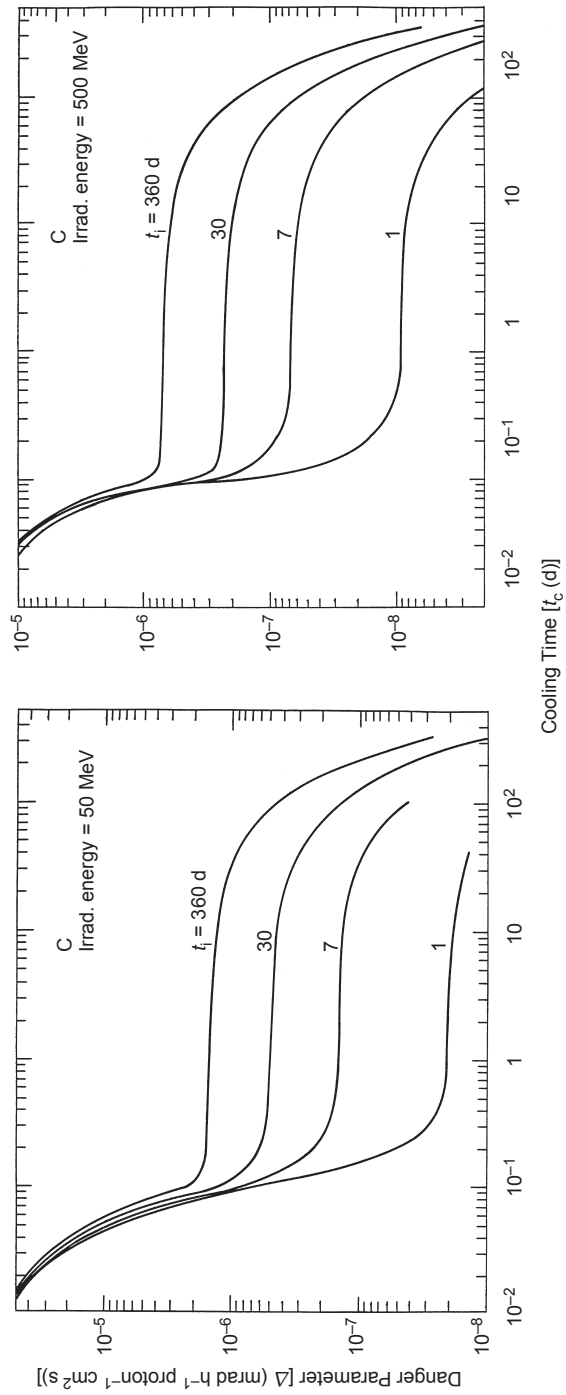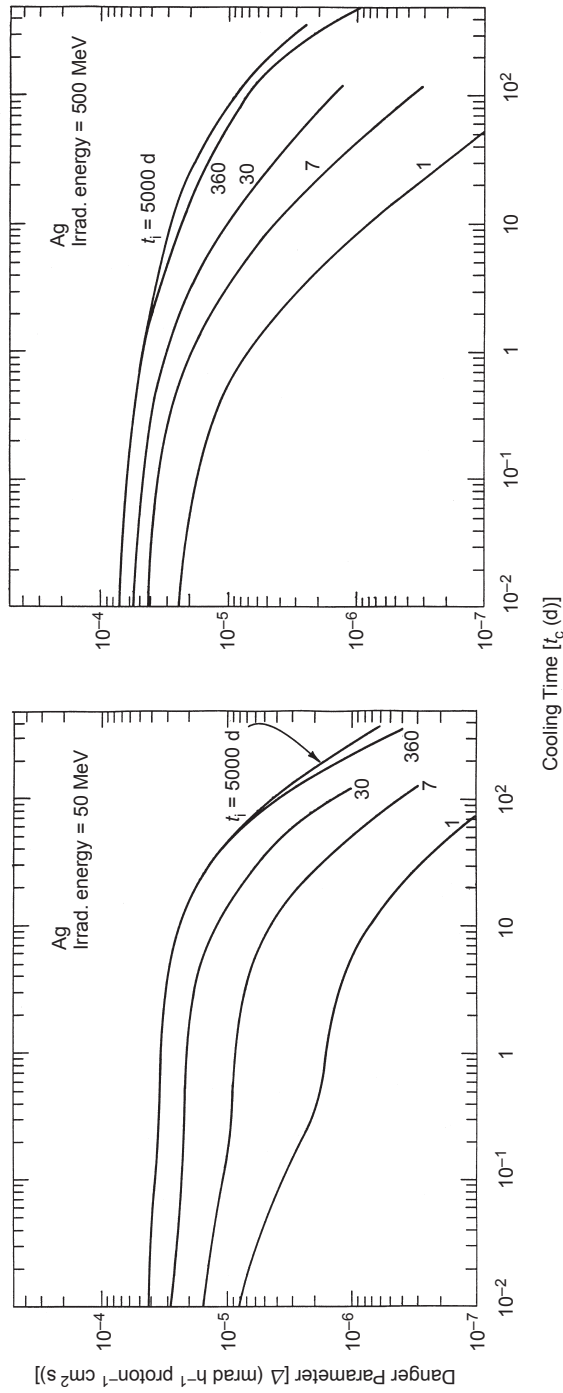
Fig. 3.64. Plots of the Barbier danger parameter (Δ) for carbon, silver, tungsten and lead irradiated by protons of 50 and 500 MeV for different irradiation times (t_i) as a function of cooling times since cessation of the irradiation (t_c) (1 mrad h^{-1} = 10 μGy h^{-1}) (Barbier, 1969).

Cooling Time [t_c (d)]

Danger Parameter [Δ (mrad h^{-1} proton^{-1} cm^2 s)]
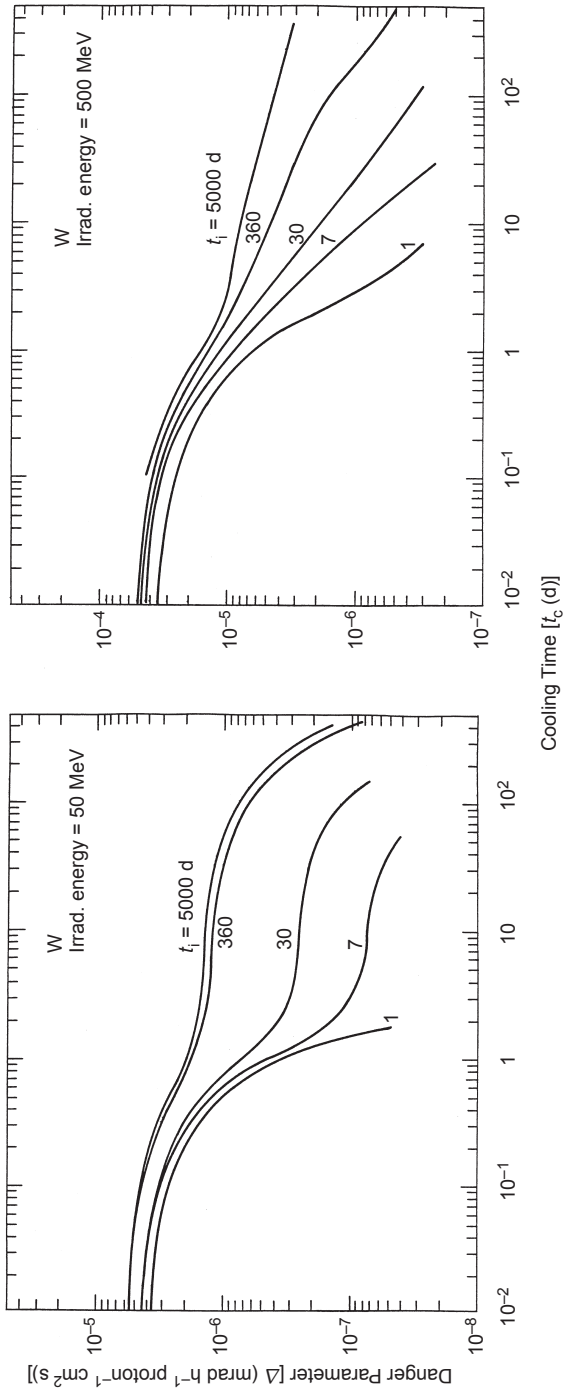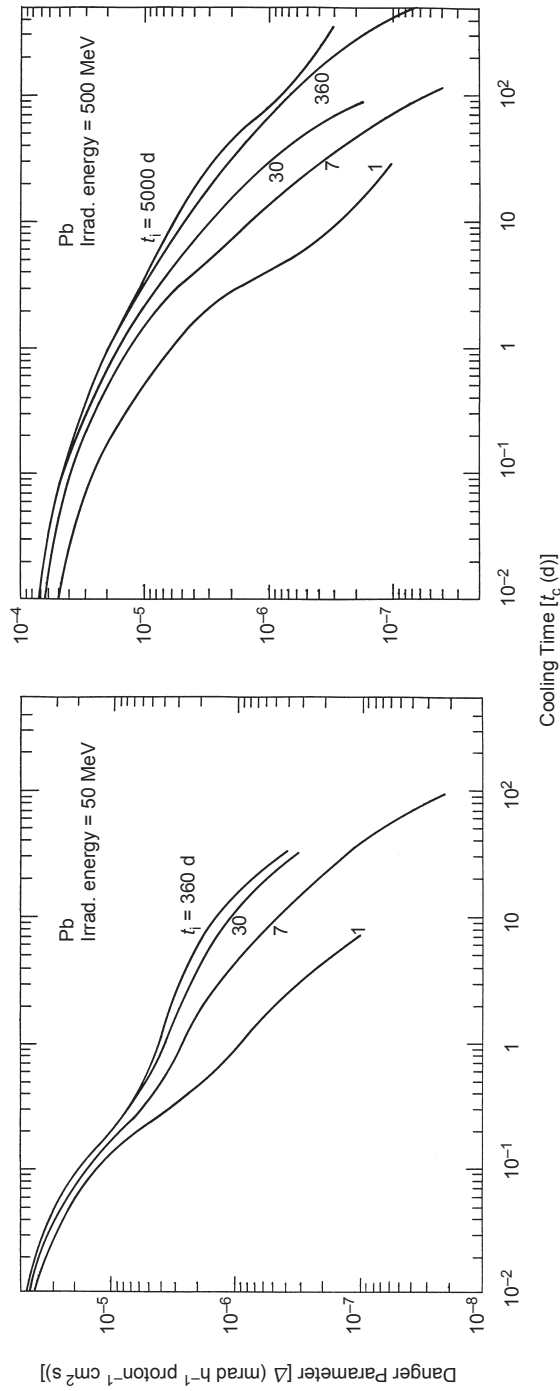
Fig. 3.64. (*continued*) Plots of the Barbier danger parameter (Δ) for carbon, silver, tungsten and lead irradiated by protons of 50 and 500 MeV for different irradiation times (t_i) as a function of cooling times since cessation of the irradiation (t_c) (1 mrad h^{-1} = 10 μGy h^{-1}) (Barbier, 1969).

4. Radiation Shielding at Accelerators

4.1 Introduction

A shield has been defined as "a physical entity interposed between a source of ionizing radiation and an object to be protected such that the radiation level at the position of that object will be reduced. . . The object to be protected is most often a human being, but can be anything that is sensitive to ionizing radiation" (Chilton *et al.*, 1984)."

It is important that structural shielding be properly designed and installed in the original construction because corrections or additions, after facilities are completed, are usually expensive. For the same reason, planning should also include consideration of possible future needs for new equipment, higher radiation energies, increased beam intensities, different species of accelerated particles, and increased workloads.

To ensure that the required degree of radiation protection is achieved in the most economical fashion, it is recommended that the shielding be designed by a qualified expert (see definition given in Glossary). This objective will be furthered by providing the qualified expert with all pertinent information regarding the proposed radiation equipment and its use, type of building construction, and occupancy of nearby areas. The expert should be consulted during the early planning stages; often the shielding requirements affect the choice of location of radiation facilities and type of building construction. Final shielding drawings and specifications should be reviewed and approved by the qualified expert and by the pertinent federal, state or local agency (if applicable) before construction begins.

The final assessment of the design and construction of structural shielding should be based on the radiation survey of the completed installation when it first operates. If the radiation survey is inconsistent with the preconstruction analysis, the cause of the discrepancy should be determined so that corrective actions can be knowledgeably

146

taken. Table 4.1 summarizes the factors that must be considered in accelerator-shield design.

Modern accelerators are capable of producing extremely high radiation intensities. The goal of efficient accelerator-shield design is to attenuate these high radiation intensities to acceptable levels outside the shield and to do so at reasonable cost and, insofar as is practical, without compromising the utility of the accelerator for its designed purpose. Three separate stages may be identified in achieving this goal:

- specification of required dose equivalent (rates) outside the shielding
- determination of the source term(s)
- design of the shield with adequate attenuation to achieve the required dose equivalent (rate) limitation

This Section discusses basic radiation transport, practical shield design for both electron and proton accelerators, and radiation leakage through labyrinths, ducts and voids. Special consideration is given in the final sections to radiation leakage through labyrinths and ducts, and through voids and leaks in shielding.

Space limitations necessarily limit this discussion of accelerator shielding. For broader discussions on radiation shielding, the reader is referred to Chilton *et al.* (1984), Price *et al.* (1957), Shultis and Faw (1996), and to the IAEA *Engineering Compendium on Radiation Shielding* (IAEA, 1968; 1970; 1975) which largely discuss nuclear reactor shielding. Particle accelerator shielding is specifically discussed in Freytag and Ranft (1971), IAEA Technical Reports 188 and

TABLE 4.1—*Factors to be considered in accelerator-shielding design.*

- ALARA
- available space
- comparison with other facilities
- construction techniques
- environmental radiation
- induced radioactivity
- quality and radiation weighting factors
- radiation exposure history at the institution
- regulatory limits
- shielding materials
- source terms
- trends in regulatory limits with time

283 (IAEA, 1979a; 1988), Patterson and Thomas (1973), Schopper *et al.* (1990), Sullivan (1992), and Zaitsev *et al.* (1971).

4.2 Theory of Radiation Transport

4.2.1 *Introduction*

Ideally, the shield designer wishes to know the energy and angular distributions of all particles throughout the entire shield whatever its composition or geometry. Stray and direct radiations at any location are distributed in particle type, direction and energy, and the radiation field may be specified by a multi-dimensional quantity named the angular fluence, $\phi_i(\mathbf{x},E,\mathbf{\Omega},t)$ and defined as the number of particles of type i per unit area, per unit energy, per unit solid angle, per unit time at a location $\mathbf{x}$, with an energy E, at a time t, and traveling in a direction $\mathbf{\Omega}$. The angular fluence [$\phi_i(\mathbf{x},E,\mathbf{\Omega},t)$] may be related to the scalar fluence rate [$\phi_i(\mathbf{x},t)$] by integrating over direction and energy:

$$\phi_i(\mathbf{x},t) = \int_{4\pi} \mathrm{d}\mathbf{\Omega} \int \mathrm{d}E \; \phi_i(\mathbf{x},E,\mathbf{\Omega},t). \tag{4.1}$$

The fluence [$\phi_i(\mathbf{x})$] is determined by integrating [$\phi_i(\mathbf{x},t)$] over the intervening period of time:

$$\phi_i(\mathbf{x}) = \int \mathrm{d}t \; \phi_i(\mathbf{x},t) = \int \mathrm{d}t \int_{4\pi} \mathrm{d}\mathbf{\Omega} \int \mathrm{d}E \; \phi_i(\mathbf{x},E,\mathbf{\Omega},t). \tag{4.2}$$

The energy spectrum at point $\mathbf{x}$ at time t, [$\phi_i(\mathbf{x},E,t)$] is obtained by integrating the angular fluence over direction:

$$\phi_i(\mathbf{x},E,t) = \int_{4\pi} \mathrm{d}\mathbf{\Omega} \; \phi_i(\mathbf{x},E,\mathbf{\Omega},t). \tag{4.3}$$

When the radiation field is specified in this manner, the magnitude of radiation protection quantities {$H(\mathbf{x},t)$ [such as, *e.g.*, absorbed dose, dose equivalent, effective dose equivalent, and effective dose (or rates)]}, may be readily determined at any location by integrating the product of fluence (or fluence rate) and the appropriate coefficient converting fluence (rate) to a radiation protection quantity [$g(E)$] over energy and angle and summing over all particle types (i):

$$H(\mathbf{x},t) = \sum_i \int_{4\pi} \mathrm{d}\mathbf{\Omega} \int_0^\infty \mathrm{d}E \; \phi_i(\mathbf{x},E,\mathbf{\Omega},t)g_i(E), \tag{4.4}$$

where **x** is the coordinate vector of the point in space where the radiation-protection quantity is to be calculated and $g_i(E)$ is the appropriate conversion coefficient as a function of energy and particle type, and the outer integral is over all spatial directions which contribute to the radiation field at the location specified by **x**.

Values of conversion coefficients may be found in ICRP Publications 51 and 74 (ICRP, 1988; 1996) and ICRU Report 57 (ICRU, 1998a).

Design or analysis of the performance of accelerator shielding requires that the amount of radiation (expressed in terms of the dose-equivalent quantities) which penetrates the shield and reaches locations of interest must be calculated. This quantity must be compared with the dose-equivalent limits. If the calculated dose or dose equivalent is too large, either the shield dimensions or the conditions associated with the source of the radiation must be changed (*e.g.*, the amount of beam loss allowed by the beam control instrumentation, the amount of residual gas in the vacuum system, or the amount of beam allowed to be accelerated).

The precise and exact description of radiations and all their interactions with shielding materials, often in complex geometries, is within the mandate of transport theory, which, in its turn, is a sub-discipline of statistical mechanics. The interested reader who wishes to understand these topics is referred to standard texts such as *Principles of Radiation Shielding* (Chilton *et al.*, 1984), *Neutron Transport Theory* (Davison, 1957), or *Radiation Shielding* (Shultis and Faw, 1996) and by O'Brien (1980).

There are several methods which may be used to obtain approximate solutions to this problem, particularly at low energies and for simple geometries, such as, *e.g.*, ray-analysis techniques and point-kernel methods. Some special techniques and concepts used in these simplified methods (*e.g.*, radiation buildup, diffusion theory, removal cross sections, the concepts of radiation albedo and importance) are discussed later in this Section and elsewhere in this Report. The interested reader is referred to the text by Chilton *et al.* (1984) and Shultis and Faw (1996) for further details.

Nowadays, the principle method of solving radiation transport problems for accelerator-shield design is by the application of Monte-Carlo techniques which are briefly described in Section 4.2.2. Nevertheless, because of the physical insight obtained, it is of interest to study several of the analytical methods used to determine the amount of radiation reaching a given location. Furthermore, the rigorous analytical treatment of radiation transport problems provides a sound theoretical foundation for many of the intuitive and empirical methods used for shielding design described in this Section

[*e.g.*, exponential attenuation, diffusion approximations, multi-energy-group approximations (see Chilton *et al.*, 1984 for further details)].

The fundamental tool for solving radiation transport problems is the Boltzmann equation which, when solved, yields the angular fluence, $\phi_i(\mathbf{x},E,\mathbf{\Omega},t)$, the distribution in energy and angle for each particle type as a function of position and time. In many instances, and almost always for the purposes of radiological protection, it is sufficient to assume that the time dependence of the radiation field is that of the primary radiation source, the finite velocity of the heavier particles (*e.g.*, neutrons, protons, helium ions, etc.) having no significance. However, one important influence of the finite velocity of unstable particles is in determining their decay times in the laboratory frame.

4.2.1.1 *Construct of the Boltzmann Equation.* The Boltzmann equation is an integro-differential equation describing the behavior of a dilute assemblage of "corpuscles" originally derived by Ludwig Boltzmann in 1872, to study the properties of gases. The method has been extended to describe the behavior of those corpuscular ionizing radiations (*e.g.*, Davison, 1957).

The theory yields the distribution of radiation in matter and may be used to obtain numerical values for elements of this distribution such as particle fluence, or related quantities, such as dose, activation or instrument response. The basis for this theory is the stationary form of the Boltzmann equation (henceforth, referred to simply as the Boltzmann equation) that describes the interaction processes of all the various types of radiation that make up the radiation field.

Boltzmann's equation is a continuity equation of the angular flux [$\phi_i(\mathbf{x},E,\mathbf{\Omega},t)$] in the phase space consisting of the three space coordinates of Euclidean geometry, the three corresponding direction cosines, and the kinetic energy. The equation may be derived by considering the mechanisms by which particles leave or enter any small volume in space. The density of radiation in a volume of phase space may be changed in five ways:

1. *Collisions*: as a result of which the energy-angle coordinates change, but the spatial coordinates remain unchanged, or the particle may be absorbed and disappear altogether from that region of phase space; absorption for particles of type (i) is expressed by the absorption cross section (σ_i).
2. *Uniform translation*: where the spatial coordinates change, but the energy-angle coordinates remain unchanged, which is expressed by the invariance of the operator $\nabla\cdot\mathbf{\Omega}$ with respect to the coordinate system.

3. *Continuous slowing down*: in which uniform translation is combined with continuous energy loss expressed by the term $\partial S_i/\partial E$ where S_i is the stopping power for particles of type i (taken to be zero for uncharged particles).

4. *Decay*: where particles are transmuted into particles of another kind (*e.g.*, muons or pions); expressed by the probability for decay (d_i) per unit flight path of particles of type i and is given by:

$$d_i = \frac{\sqrt{(1 - \beta^2)}}{\tau_i \beta_i c} , \qquad (4.5)$$

where:

  c =   the velocity of light
  β_i =   the velocity of a particle of type i in units of c
  τ_i =   the mean life of a radioactive particle of type i in the particle's rest frame

5. *Introduction*: involving the direct emission of a particle from a source into the volume of the phase space of interest; alpha particles, electrons or photons from radioactive materials, neutrons from alpha-neutron sources, expressed by source terms (Y_i); or particles emitted from a collision at another (usually higher) energy expressed by the "scattering-down" integral (Q_{ij}). Y_i is the number of particles of type i introduced, for example by a source per unit area, time, energy and solid angle. Q_{ij}, the "scattering-down" integral, is the production rate of particles of type i, with a direction $\mathbf{\Omega}$, an energy E at a location $\mathbf{x}$, by collisions with nuclei or decay of j-type particles having a direction $\mathbf{\Omega}'$ at a higher energy E_B defined by the equation:

$$Q_{ij} = \sum_j \int_{4\pi} d\mathbf{\Omega}' \int_E^{E_{max}} dE_B \; \sigma_{ij}(E_B \rightarrow E, \; \mathbf{\Omega}' \rightarrow \mathbf{\Omega}) \; \phi_j(\mathbf{x}, E_B, \mathbf{\Omega}', t); \quad (4.6)$$

where σ_{ij} is the doubly-differential inclusive cross section for the production of type-i particles with energy E and a direction $\mathbf{\Omega}$ from nuclear collisions or decay of type-j particles with energy E_B and a direction $\mathbf{\Omega}'$.

In order to simplify the final result, we define the mixed differential and integral Boltzmann operator for particles of type i (B_i) by the equation:

$$B_i = \nabla \cdot \mathbf{\Omega} + \sigma_i + d_i + \left(\frac{\partial S_i}{\partial E}\right). \qquad (4.7)$$

Combining this simplification with particle balance, we obtain the Boltzmann equation:

$$B_i \phi_i(\mathbf{x}, E, \mathbf{\Omega}, t) = Q_{ij} + Y_i . \qquad (4.8)$$

4.2.1.2 *Approximate Solutions of the Boltzmann Equation.* The Boltzmann equation is, in general, extremely difficult to solve, and several special techniques have been devised to yield useful results, all of which, however, are limited in application to some degree. It is important to understand both the strengths and weaknesses of all such approximate methods. Reference to only a few of these methods can be given here and the reader interested in understanding these techniques in greater depth is referred to the standard works cited in this Section. These methods are as follows:

1. *The Method of Moments (Spherical-Harmonics Method).* In the design of accelerator shields, it is usually important to have detailed knowledge of the energy spectrum of particles emerging from the shield because the conversion coefficients $g_i(E)$ of Equation 4.4 are strongly energy-dependent. In simple shield geometries, the Spherical-Harmonics Method is capable of obtaining detailed information on the spatial and energy distribution of radiations. The method represents the angular distributions in a continuous manner as a series of Legendre polynomials (Margenau and Murphy, 1943) and, then uses the orthogonal properties of these functions to generate Legendre moments (Chilton *et al.*, 1984).

   The method provides a very powerful process of calculating energy spectra in infinite media, but this process also has an intrinsic weakness because it is less powerful for the design of small shields. The results of calculations close to the radiation source are not as reliable as those calculations far from the source.

2. *The Diffusion Equation.* Diffusion theory is an important tool in the evaluation of the behavior of dilute fluids, but it has been adapted to provide an important alternative description of the behavior of radiation in matter. The classical diffusion equation, in which the current is proportional to the gradient of the concentration (Fick's Law), appears quite naturally as the lowest order solution produced by the application of the method of spherical harmonics (Davison, 1957).

3. *The Method of Discrete Ordinates.* Those several methods of solving the Boltzmann equation that approximate the angular distributions of particles by a number of discrete directions, rather than all directions possible in practice, are collectively known under the title of the "Method of Discrete Ordinates." The method can be extremely powerful for finite and heterogeneous shield design, but is limited in the geometries that may be used. The radiation intensity penetrating irregular shield

boundaries is difficult to calculate accurately, and the spatial distribution of radiation emitted from the shield is subject to large fluctuations.

4. *A Note on the Concept of Importance*. In the calculation of angular particle fluence or some integral of the angular fluence such as the current, scalar fluence density, or detector response, some domains of the problem are more "important" (*i.e.*, significant) than others in that they contribute more of the particle trajectories that lead to the desired result. For example, in the calculation of the dose absorbed by a dosimeter in a medium, those electrons intersecting the detector region are more important than those electrons outside the region. Because those hadrons emitted from a hadron-nucleus collision in essentially the same direction as the incident particle are much more energetic than hadrons emitted at large angles, the forward-directed elements of the cross section are those most important for the propagation of the hadronic cascade. Thus, the "straight-ahead approximation," which assumes that all secondaries travel in the direction of the primary, gets its ease and power by the technique of "importance-weighting" the emission angle of the emerging secondary particles. The use of importance is discussed in Sections 6.2.2 and 6.2.3 on neutron and photon skyshine, respectively, and values for importance are tabulated in Appendix A.

This concept can be used in both analytical techniques, such as the discrete-ordinates method, or in the Monte-Carlo method. A common approach to determining Importance in Monte-Carlo methods is described by Carter and Cashwell (1975). The objective is to reduce the number of histories necessary to calculate the value of the quantity desired with some specified variance.

5. *Comparison of Calculations using Alternative Techniques*. O'Brien (1969; 1970) has reported comparisons of the results of calculations of neutron transport in a concrete slab irradiated by normally incident 400 MeV neutrons. The three methods of calculation used were: the spherical harmonics method [in the P3 approximation (O'Brien, 1970)], the method of discrete ordinates, and the Monte-Carlo method (Alsmiller *et al.*, 1969a; 1969b). The results obtained for scalar fluence rate with energies higher than thermal, higher than 0.1 MeV, and higher than 20 MeV indicate generally good agreement and suggest the general validity of all three very different approaches for the conditions of the calculation.

O'Brien has also compared the results of calculations of neutrons produced by the interaction of cosmic rays with the atmosphere. This is of importance for accelerator-shield design

because the behavior of atmospheric cosmic rays has been used as a model to estimate the properties of high-energy radiation incident on accelerator shields (Moyer, 1957). Various aspects of the cosmic-ray interactions with the atmosphere were calculated including the cosmic-ray neutron spectrum and the hadron collision density in air and soil, the vertical nucleon and pion spectra, and the angular muon fluence rate in the vertical direction. The calculations were made using the straight-ahead approximation to the Boltzmann equation and, in some cases, the discrete-ordinates code DTF-IV to propagate the low-energy neutrons (O'Brien, 1971b; 1972; O'Brien *et al.*, 1978). Comparisons with experimental data show fair to excellent agreement [hadron collision density (Yamashita *et al.*, 1966), vertical neutron and pion energy spectra (Ashton and Coats, 1968; Brooke and Wolfendale, 1964; Brooke *et al.*, 1964), and vertical muon energy spectra (Kiraly and Wolfendale, 1970; Osborne *et al.*, 1964)].

4.2.2 *Computer Codes for Shielding Calculations*

4.2.2.1 *The Monte-Carlo Method.* Because the Boltzmann equation is often difficult to solve by analytical means, particularly for complicated shielding geometries, recourse to computational methods is usually necessary. The most frequently used computational techniques are based on the Monte-Carlo method. The general Monte-Carlo technique provides a computational framework for the description of an analog method for the solution of radiation-transport problems. The Monte-Carlo method is based on the use of random sampling to obtain the solution of the Boltzmann equation. It is one of the most useful methods for evaluating radiation hazards for those realistic geometries which, in general, are not readily modeled by analytical techniques. The calculation proceeds by constructing a series of trajectories, each segment of which is randomly chosen from a distribution of applicable processes. By this method, the values of energy, direction and path length are randomly selected from probability distributions. Thus, it is possible with this technique to track the interactions of individual particles in their passage through matter and to obtain distributions of many desired physical quantities by tracing a large number of particle histories. The particle history is then established through the shield as the particle undergoes various interactions and ends when the particle becomes absorbed, leaves the region of interest, or loses energy to a significant degree.

In the simplest and most widely used form of the Monte-Carlo technique, a history is obtained by calculating travel distances between collisions, then sampling from distributions in energy and angle made up from the cross sections (*e.g.*, Carter and Cashwell, 1975).

Even with the availability of high-speed digital computers and general Monte-Carlo codes (which also facilitate the calculation of radiation transport in complex geometries), this approach makes heavy demands on computer time. It is not possible to chart an infinite number of particle histories; thus, various methods are adopted to minimize statistical uncertainties. Variance reduction techniques are used to reduce this demand (Lux and Koblinger, 1991; Spanier and Gelbard, 1969). The Monte-Carlo result is the number of times the event of interest occurred for the random steps through the relevant processes. As a counting process, it has a counting uncertainty, and the variance will tend to decrease as the square root of the run time. Thus, high-probability processes can be more accurately estimated than low-probability processes such as passage through a thick shield.

Several adaptations of the general Monte-Carlo technique have been developed to allow for different interactions of charged and uncharged particles. In addition, approximations to the description of some of the atomic and nuclear processes (*e.g.*, the continuous slowing down approximation or the kerma approximation) may have been used.

Absorbed dose is usually calculated by summing the energy deposited inside a region. Consequently, it is necessary to account properly for the energy transferred in the region that subsequently escapes. This is done using the restricted energy loss (dE/dx) with the proper threshold energy, rather than the unrestricted energy loss [$(dE/dx)_\infty$]. Using $(dE/dx)_\infty$ would give incorrect results because it ignores the energy lost when high-energy delta rays escape from the region. The interactions of all types of particles resulting from secondary and tertiary processes, as well as the primary radiation must be included.

Calculation of the transport of charged radiations is both complex and time-consuming. Fortunately, for those radiations and energies considered in this Report, the transport of charged particles may be facilitated by using the continuous slowing down approximation and multiple scattering theory. The continuous slowing down approximation assumes that slowing-down is a smooth process as a function of energy, yielding the concepts of projected ranges and stopping powers. Multiple scattering accounts for the spatial and angular spread of the particles. The two processes taken together (*i.e.*, the

energy loss plus the scattering angle) are normally referred to as the "condensed history approximation."

Charged particles undergo many more interactions along their path than do uncharged particles, such as photons or neutrons. Interactions may be described in terms of stopping power, range, and range-straggling. This description enables the reduction of computation time for electron transport calculations using the "condensed history" (or "path-segment") approximation. In this technique, the particle paths are divided into path segments along which many elastic and inelastic Coulomb collisions occur. This allows for treatment of the combined effects of many collisions occurring along each path segment without having to sample a very large number of individual interactions. Energy losses are accounted for using the continuous slowing down approximation and, in some cases, energy-loss-straggling distributions; angular scattering is accounted for using multiple-scattering distributions. For a basic text on these topics, see Berger (1963).

Several codes used to calculate the transport of electrons, photons, muons and neutrons through matter are available. Many of these codes are continually being improved. The following sections give a brief description of some of these Monte-Carlo codes.

4.2.2.2 *MARS*.   This code, originally written by Mokhov (1995) at Serpukhov, USSR, has been updated and maintained at FNAL. It is a general purpose multi-particle Monte-Carlo code that handles complex geometries. It accounts for hadron interactions from 1 MeV to 100 TeV, and includes a pre-equilibrium model for neutron production, deuteron and photonuclear interactions. MARS interfaces to MCNP (Section 4.2.2.6) for low-energy neutron transport. It uses a point kernel technique to calculate dose rate from radionuclide production. Extensive biasing is available for deep penetration calculations. It can include magnetic fields and multi-turn particle tracking in the accelerator lattice. MARS applications include shielding design of proton and electron accelerators, dosimetry, simulation of high-energy physics experiments, cosmic-ray physics, and activation. MARS has replaced the code CASIM described by Van Ginneken and Awschalom (1974) as the program of choice for general use at FNAL.

4.2.2.3 *EGS4 Code System*. EGS (Electron Gamma Shower) is a computer program package that has gone through several modifications. Originally developed at SLAC, the most recent version (EGS4) contains many improvements at low energies that were developed in a collaborative effort with KEK (Japan) and the National Research Council of Canada (Nelson *et al.*, 1985). EGS4 provides a Monte-Carlo

analysis of electron and photon scattering including electromagnetic shower generation. The lower limit of energy is approximately 1 keV and the upper limit is 100 GeV. Prior to running EGS4, an off-line code called PEGS4 must be run in order to create a media data file representing any of 100 elements, or any compound/mixture of these elements. EGS4 has been extensively benchmarked by the medical physics community, to the extent, that it oftentimes has provided a standard by which other electron-photon codes and methods are judged.

4.2.2.4 *FLUKA*. Originally, a high-energy hadron transport code written by J. Ranft, FLUKA has been completely rewritten and extended, mainly by Ferrari (Fasso *et al.*, 2001; Ferrari *et al.*, 2001). Using the Monte-Carlo method, FLUKA can transport more than 30 different particles including neutrons from thermal energies to ~20 TeV, electrons and photons from 1 keV to thousands of tera-electron volts, muons of any energy, and also optical photons. Older versions of its high-energy hadron interaction model have been included in other codes (*e.g.*, HETC, CALOR, HERMES, GEANT, LAHET, MCNPX). Additional features in FLUKA, include a special treatment of multiple scattering, photonuclear reactions, polarized photons, fluorescence, and very high-energy effects. FLUKA is a multi-purpose code that can handle complex geometries, magnetic fields, and deep penetration problems (several biasing techniques are available). It has application for shielding design of proton and electron accelerators (including synchrotron radiation beam lines), radiotherapy (with electrons, photons, protons and neutrons), dosimetry, cosmic-ray physics, activation, nuclear transmutation, and simulation of high-energy physics experiments.

4.2.2.5 *NMTC/HETC*. NMTC is an intranuclear cascade-evaporation Monte-Carlo code written by Coleman and Armstrong (1970). It can transport nucleons below 3.5 GeV and charged pions below 2.5 GeV. The High-Energy Transport Code (HETC) (Armstrong, 1978; Gabriel, 1985) is an Oak Ridge National Laboratory (ORNL) version of NMTC that has been extended to higher energies. Its applications are primarily for proton accelerator shielding and activation; whereas, another version called CALOR is designed mainly for high-energy physics calorimetry (Gabriel *et al.*, 1989) and is linked to EGS4 (for transporting photons/electrons) and to MICAP (for transporting low-energy neutrons). HETC can be obtained as part of the CALOR package from the ORNL Radiation Safety Information Computational Center. In the original ORNL version of HETC, neutrons below 20 MeV must be transported by a separate

code (MORSE-CG, or more recently MCNP). Combinatorial geometry and scoring routines must be written by the user. Several different versions of HETC also exist outside ORNL, each with one or more different physical models including:

- *LAHET*: An extended version by Prael and Lichtenstein (1989) that is now the most widely used. When used together with MCNP it is known as the LAHET Code System (LCS). LAHET is a general purpose code and, with the exception of electron accelerator shielding, its applications are the same as for FLUKA. It does not include photonuclear reactions. Recently LAHET and MCNP have been fully merged as a single code and given the name MCNPX.
- *HERMES*: A version by Cloth *et al.* (1988) that includes an improved intranuclear cascade and evaporation model. It has additional applications in calorimetry and spallation source calculations.
- *HETC-3STEP*: A version from Japan by Yoshizawa *et al.* (1995) that includes a pre-equilibrium model for neutron production, with specific applications for dosimetry.

4.2.2.6 *MCNP*. MCNP was developed by a large group of specialists at the Los Alamos National Laboratory (Briesmeister, 2000) and is a general purpose Monte-Carlo code that simulates the transport of neutrons, photons and electrons below 100 MeV (the electron transport module is that of the Integrated Tiger Series). MCNP contains very sophisticated geometry, biasing and scoring options and is now the most widely used code for low-energy neutron shielding and dosimetry. It has been carefully benchmarked with experiments and is regularly submitted to a quality assurance procedure.

4.2.2.7 *Integrated Tiger Series*. The Integrated Tiger Series (ITS) was developed at the Sandia National Laboratories by Halbleib *et al.* (1992), and is a series of electron-photon Monte-Carlo codes (*e.g.*, TIGER, ACCEPT, CYLTRAN) functioning in the energy range from 1 keV to 10 GeV. Derived originally from the ETRAN code of Berger and Seltzer (1968), ITS incorporates the multiple-scattering algorithm of Goudsmit and Saunderson (1940). The ITS, as are many of these codes, is also available from the Nuclear Energy Agency of France.

4.2.2.8 *MORSE-CGA*. MORSE was originally developed at ORNL by Straker *et al.* (1976), and was one of the first Monte-Carlo transport codes to be widely distributed. MORSE-CGA (Emmett, 1985) has as its geometry module, MARS (not to be confused with the

MARS code itself), which is a multiple array system that uses combinatorial geometry; hence, the CGA suffix indicates combinatorial geometry array. The combinatorial geometry scheme has also been incorporated into many other codes.

4.2.2.9 *TOMCAT*.   Written at CERN by Stevenson (1981), TOMCAT is a coupled analytic-Monte-Carlo code developed to meet the need for a fast and simple way of determining the fluence of muons through simple slab geometry. The muon transport, itself, is determined analytically, whereas the incident muons are sampled from secondary beam characteristics supplied by the user. TOMCAT can handle incident muons, or pions and kaons (that decay to muons), and up to 20 slabs made of four different materials (iron, concrete, soil, air). Fermi-Eyges theory is used to predict the radial distribution of muons at different depths, taking into account Coulomb scattering, bremsstrahlung and nuclear collisions according to a method developed by Alsmiller. The program uses biasing techniques such as forced pion decay and weighted sampling from the muon parent spectrum. A comparison of TOMCAT with experiment and with other code methods is summarized in Chapter 4, Muon Transport, of Fasso *et al.* (1990).

4.2.2.10 *MUSTOP*.   Derived from the work of Keefe and Noble (1968), MUSTOP is an analytic program by Stevenson (1979) at CERN to aid in the design of shielding against muons produced in high-energy proton accelerators with energies up to 1,000 GeV. The muons are assumed to be the decay products of pions produced in the interaction of a high-energy proton beam with a target and/or dump in cylindrical geometry (kaon decay is ignored). The decay length available for muon production is taken to be the target-to-shield distance in the direction under study. Three choices are available for the pion production model (Cocconi-Koester-Perkins, Trilling, or Ranft). Only Coulomb scattering is considered for the prediction of the lateral dimensions of the muon cone, but several energy-loss mechanisms are taken into account.

4.2.2.11 *MUCARLO*.   MUCARLO is an undocumented SLAC Monte-Carlo code written by Feldman (1988)[24] to study muon background in the MKII detector at the final focus of the Stanford Linear Collider. Improvements have been made to the code in applications by Keller (1991; 1993) and by Rokni *et al.* (1996), but the only documentation is in the form of extensive comments made throughout the

---

[24]Feldman, G. (1988). *Muon Background at the Stanford Linear Collider*, internal presentation (Stanford Linear Accelerator Center, Menlo Park, California).

code itself. Nevertheless, MUCARLO is a viable code for transporting muons through complicated beam-line components (*i.e.*, magnets, dumps, shields, etc.). By default, the muons are pair-produced (coherent Bethe-Heitler) at a point within a fully-developed electromagnetic shower initiated by an electron beam striking a thick target. The muons are then transported through the various beam components, taking into account continuous energy loss and (Moliere) scattering.

4.2.2.12 *MUON89*. This is a fully analytic program, originally called GREEN and written by Nelson and Kase (1974), that determines the fluence of muons through thick shields after they have been produced by a high-energy electron beam striking an upstream beam dump. The production kernel takes into account a variety of photo-produced sources (*e.g.*, coherent and incoherent Bethe-Heitler pairs, charm-related contributions, etc.). The convolution integration is based on Fermi-Eyges multiple scattering theory with continuous energy loss applied along the path of the muon. Documentation for MUON89 consists only of extensive commenting throughout the code itself. The code has been used for many years in the design of muon shielding at SLAC.

4.2.2.13 *SHIELD11*. Written at SLAC by Jenkins and Nelson in the early 1970s, SHIELD11 is a simple analytic code based on the scaling of experimental data taken with electron beams striking thick targets. The empirical model has three neutron components (giant-resonance excitation, quasideuteron, high-energy) and two photon components (electromagnetic shower escape, direct gammas from neutron interactions). The code (model) has been used with great success in the design of shielding at SLAC, KEK and JLAB. Currently, the only documentation for SHIELD11 is in the form of extensive comments within the code itself.

4.2.2.14 *PHOTON*. This is an x-ray shielding code written by Chapman *et al.* (1988) that is based on an analytic model. The program has been experimentally verified (Brauer and Thomlinson, 1988). The primary application of PHOTON is in determining the radiation levels associated with beamlines at synchrotron light facilities. A version called PHOTON2 by Dejus *et al.* (1992) extends the model to include wiggler magnets.

4.2.2.15 *STAC8*. Written by Asano and Sasamoto (1994), STAC8 was developed from the PHOTON code with specific application around beamlines at synchrotron light facilities. It contains improvements for undulator radiation, angular-dependent coherent and

incoherent scattering, photon polarization, buildup factors, and self-shielding by scatterers (including inclined scatterers).

4.2.2.16 *SKYSHINE-KSU*.   This is a package of codes developed at Kansas State University for calculating skyshine dose. SKYNEUT (Shultis *et al.*, 1997a) evaluates the neutron and neutron-induced secondary gamma-ray skyshine doses from an isotropic, point neutron source collimated by three simple geometries: an open silo, a vertical black (perfectly absorbing) wall, and a rectangular building. The source may emit monoenergetic neutrons or neutrons with an arbitrary multi-group spectrum of energies. SKYDOSE (Shultis *et al.*, 1998) evaluates the gamma-ray skyshine dose from an isotropic, monoenergetic, point gamma-photon source collimated by three simple geometries: (1) a source in a silo; (2) a source behind an infinitely long, vertical, black wall; and (3) a source in a rectangular building. In all three geometries, an optional overhead slab shield may be specified. MCSKY (Shultis *et al.*, 1997b) evaluates the gamma-ray skyshine dose from an isotropic, monoenergetic, point gamma-photon source collimated into either a vertical cone (*i.e.*, silo geometry) or into a vertically oriented structure with an N-sided polygon cross section. An overhead laminate shield composed of two different materials is assumed, although shield thicknesses of zero may be specified to model an unshielded skyshine source.

4.2.2.17 *SKYSHINE III*.   SKYSHINE was designed (Price *et al.*, 1976) to aid the evaluation of the effects of structure geometry on the gamma-ray dose rate at given detector positions outside of a building housing [16]N gamma-ray sources. The program considers a rectangular structure enclosed by four walls and a roof. Each of the walls and the roof of the building may be subdivided into up to nine different areas representing different materials, or different thicknesses of the same material for those positions of the wall or roof. SKYSHINE-III (Lampley *et al.*, 1988) provides an increase in versatility over the original SKYSHINE code, in that it addresses both neutron and gamma-ray point sources. In addition, the emitted radiation may be characterized by an energy emission spectrum defined by the user.

4.2.2.18 *TRIPOLI*.   Written at Saclay (Baur *et al.*, 1980), this is a low-energy neutron and photon transport code. It contains sophisticated biasing features and qualities similar to MCNP.

4.3 Practical Shield Design

4.3.1 *General*

Over a fairly-wide range of shield thicknesses, it has been found sufficiently accurate to estimate shielding with simple point kernel equations of the form:

$$H(d,\Theta) = r^{-2}H_\theta e^{-d(\theta)/\lambda} \qquad (4.9)$$

which combines the inverse square law and an exponential attenuation through the shield. This equation applies to a point source of a specified radiation where:

$H(d,\Theta) =$ dose equivalent at depth (d), angle (Θ) in the shield

$H_\theta \quad =$ constant that may be described as the dose equivalent extrapolated to zero depth in the shield, and corresponding to angle (Θ), at unit distance from the point source

$r \quad =$ distance from the source to the point of interest outside the shield

$\lambda \quad =$ effective attenuation length for dose equivalent through the shield

A point kernel equation form is used in the Moyer model for calculating secondary radiation shielding for high-energy accelerators. This model is discussed in detail in Section 4.8.3.

Over a limited range of shield thicknesses, approximating the radiation transmission by an exponential function works well. For shields of thickness, less than ~100 g cm², the value of λ changes with increasing depth in the shield because the more easily absorbed ("softer") radiations are attenuated more rapidly. This process is often described as "spectrum-hardening."

Under idealized circumstances, the transmission factor (T)[25] of a barrier of thickness, x may be expressed in the following equivalent ways:

$$T(x) = 10^{-x/\lambda_T} = 2^{-x/\lambda_H} = e^{-x/\lambda}. \qquad (4.10)$$

Equation 4.10 assumes that each additional equal increment of barrier thickness reduces the radiation by a constant factor. The tenth-value layer (λ_T) is the thickness which attenuates the radiation in question by a factor of 10; the half-value layer (λ_H) is the thickness which attenuates it by a factor of two; and the attenuation length (λ) is the thickness which attenuates it by a factor of e. When

---

[25] The terms attenuation and transmission are often confused in literature. In proper use, almost always, an attenuation factor is greater than one, and a transmission factor is less than one. Thus, *e.g.*, when a shield reduces the radiation intensity by a factor of 10, the attenuation factor is 10 and the transmission factor is 10^{-1}. The frequently used symbol, A, for the transmission factor is confusing.

expressed as in Equation 4.10 and plotted on a semi-log graph as a function of x, $T(x)$ appears as a straight line.[26]

Significant deviations from this ideal behavior may occur in the shielding layers closest to the radiation source. Depending on the material and energy, there may be a transition region (a change in slope in the attenuation curves) which can be taken into account by using a value for the attenuation length over the first tenth-value layer (TVL), designated as λ_{T_n} in the shield nearest the radiation source which is different from TVL used for thick shields (λ_T).[27] Use of a value for λ_{T_1} different from λ_T is similar to using a buildup factor for the radiation. For a desired barrier transmission factor (T) the total barrier thickness is determined from the number of TVLs (n_{λ_T}) required:

$$n_{\lambda_T} = - \log_{10}(T). \tag{4.11}$$

If λ_{T_1} is significantly different from the equilibrium value of the attenuation length (λ), the total thickness x is given by:

$$x = \lambda_{T_1} + (n_{\lambda_T} - 1)\lambda_T. \tag{4.12}$$

The use of λ_T facilitates simple calculation. If the total shielding barrier is to consist of more than one material, it is necessary to adjust only the material thicknesses such that the number of λ_T of all the materials combined is equal to n_{λ_T} (similar arguments apply both to half-value layers and attenuation lengths).

4.3.2 *Photon Transmission*

Figure 4.1 gives values of the tenth-value layer ($\rho\lambda_T$) in g cm^{-2} (where ρ is the material density) for the dose equivalent produced by thick-target bremsstrahlung incident upon the most commonly used shielding materials: concrete, iron (steel), and lead. Interpolation to

---

[26] The nomenclature which is widely used in the literature is repeated here but is nevertheless confusing. The attenuation length (λ), tenth-value layer (λ_T), and the half-value layer (λ_H) are related by the equations: $\lambda_T = \lambda \ln 10 = 2.3026\,\lambda$ and $\lambda_H = \lambda \ln 2 = 0.6931\,\lambda$. To add further confusion, the value of the tenth-value layer at equilibrium is often denoted by λ_e, where the "e" denotes equilibrium—not to be confused with λ, that reduces the radiation intensity by a factor of $e^{2.713}$. Yet more inconsistency is introduced by the symbols λ_1, λ_2, λ_3, etc., for the first, second, and third tenth-value layers. In this form, the subscripts indicate the depth in the shield and not the factor by which the radiation is attenuated.

[27] This procedure may be continued indefinitely. Some authors have reported values for first, second and third TVLs (λ_{T_1}, λ_{T_2}, λ_{T_3}). As equilibrium is approached the values of λ_{T_n} will approach λ_T.

other materials, based on Z, can be made from these data. Values of λ_{T_1} are also shown as dashed lines in Figure 4.1. Alternatively, one can read the necessary barrier thickness directly from attenuation curves given in Figure 4.2 for ordinary concrete (2.35 g cm^{-3}), iron (steel), and lead.

The TVLs plotted in Figure 4.1 are given in units of g cm^{-2} to facilitate comparison and interpolation to other materials. Presumed high-energy values are indicated at the right. The curves shown represent an average of data from several sources and are believed sufficiently accurate for most room-shielding calculations. There is
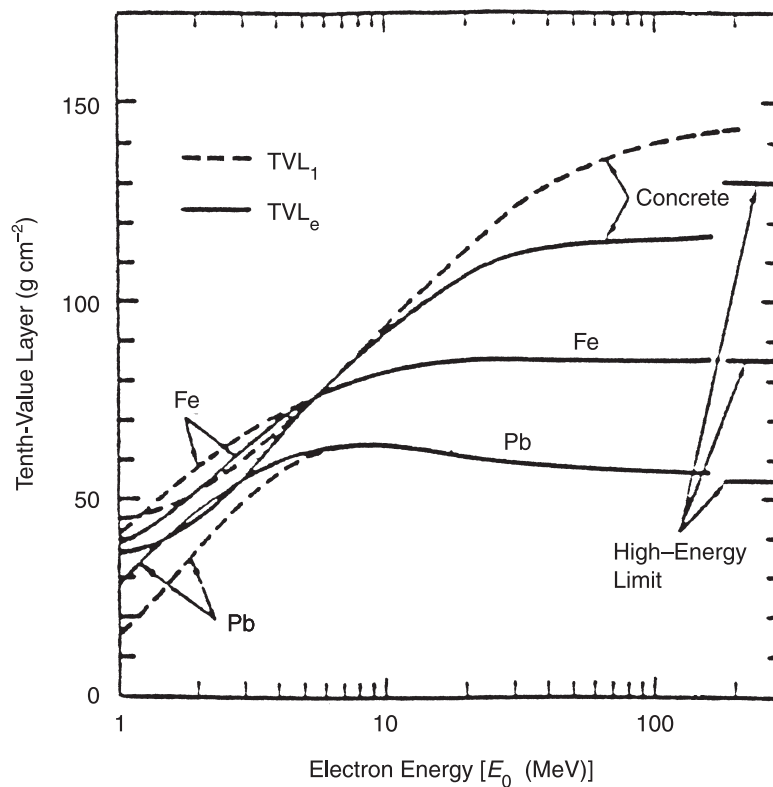
Fig. 4.1. Values of dose-equivalent TVLs $\rho\lambda_T$ in ordinary concrete, iron (steel) and lead, for thick-target bremsstrahlung under broad-beam conditions at zero degrees, as a function of the energy E_0 of electrons incident of high-Z target. The solid curves show the "equilibrium" TVL ($\rho\lambda_T$), the dashed curves the "first" TVL ($\rho\lambda_{T_1}$) or the thickness closest to the radiation source needed to reduce the dose equivalent by a factor of 10.
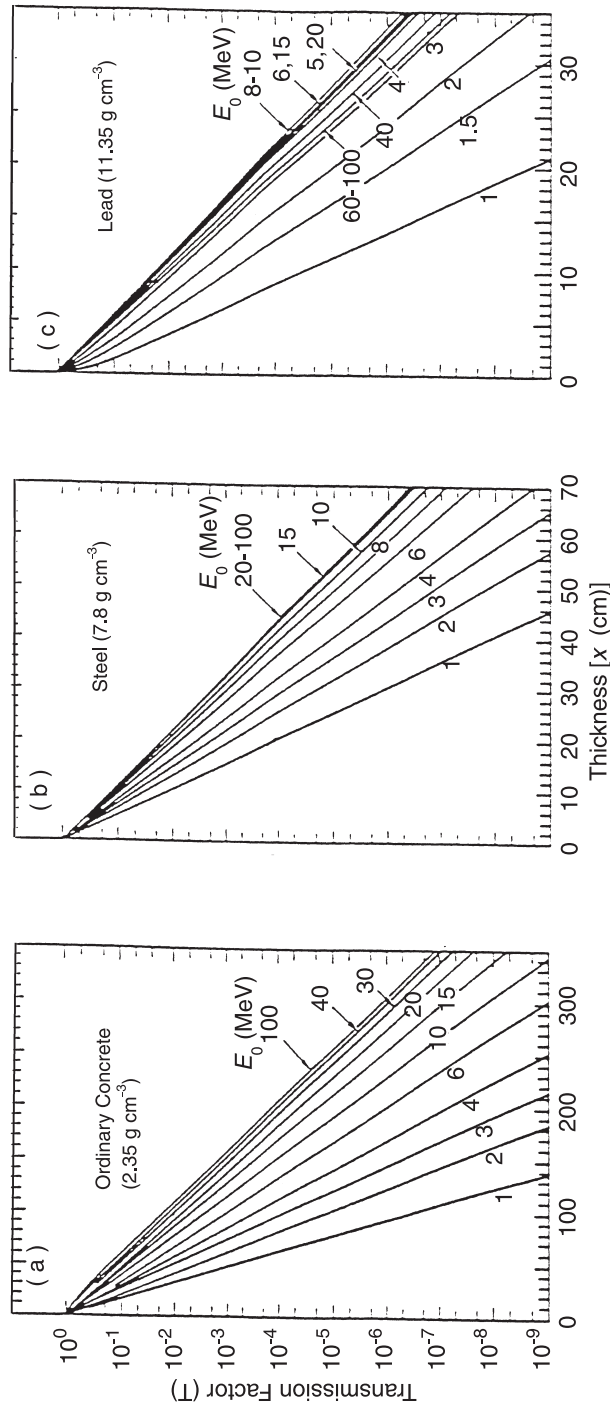
Fig. 4.2. Transmission factor (T) of thick-target bremsstrahlung by selected materials under broad-beam conditions at zero degrees with respect to the incident electron beam, as a function of shielding thickness (x). The energy designation for each curve refers to the monoenergetic electron energy E_0 incident on a thick, high-Z target. The curves are for (a) ordinary concrete (2.35 g cm^{-3}); (b) iron (steel, 7.8 g cm^{-3}); and (c) lead (11.35 g cm^{-3}).

a surprising lack of consistency among the reported shielding measurements (*e.g.*, deviations as large as 20 percent from the curves shown in the case of iron and lead). These variations may indicate that the effective $\rho\lambda_T$ for these materials is geometry and/or spectrum dependent. In critical applications, it is suggested that the chosen shielding thickness be based on measurements for the specific radiation source and geometry at hand.

Sources of data are:

- concrete, steel, lead: 1 to 50 MeV (DIN, 1975)
- concrete, lead: <1, 2, 3, 4 MeV and Steel: <1, 4, 6 MeV (NCRP, 1970)
- concrete, steel, lead: 4, 8, 15 MeV (Varian, 1975)
- concrete, heavy concrete, steel, lead: 4, 6, 10, 20, 30, 32 MeV (Maruyama *et al.*, 1971)
- concrete, steel, lead: 5, 8, 16 MeV (Coleman, 1975)
- concrete, steel, lead: 6 MeV (Karzmark and Capone, 1968)
- concrete: 6, 10, 20, 30, 38 MeV (Kirn and Kennedy, 1954)
- concrete, lead: 86, 178 MeV (Miller and Kennedy, 1956)
- steel: 1, 2 MeV (Buechner *et al.*, 1948)
- steel: 3 MeV (Goldie *et al.*, 1954)
- steel: 6 to 90 MeV (Scag, 1954)
- steel: 10 MeV (O'Connor *et al.*, 1949)
- steel: 4 to 100 MeV; lead: 10 to 100 MeV (Westendorp and Charlton, 1945)

Similar adaptations, involving mostly the same data sources, are published by Bly and Burrill (1959), Burrill (1968), and IAEA (1975) [see also NBS Handbooks 55 and 97 (NBS, 1954; 1964b)]. Shielding data, specifically for heavy concretes, are given by Lokan *et al.* (1972) and Maruyama *et al.* (1971).

Nelson and LaRiviere (1984) have calculated the primary spectra (leakage spectra) of radiation for electron accelerators operating at 6, 10 and 25 MeV and have transported them through concrete shields. Figures 4.3 and 4.4 and Table 4.2 summarize these calculations. Figure 4.3 shows the calculated primary spectra and the leakage spectra from a simulated therapy head at 45, 90, and 135 degrees. Figure 4.4 shows transmission calculated with MORSE and with EGS for the primary and the leakage radiations. Table 4.2 provides the λ_T for the transmission curves. The leakage radiation is more easily attenuated than the primary radiation, particularly for the 25 MeV operation. Experimental measurements made by LaRiviere (1984), which are also given in Table 4.2, at 24 MeV through 1.32 m of concrete agreed well with the calculations.
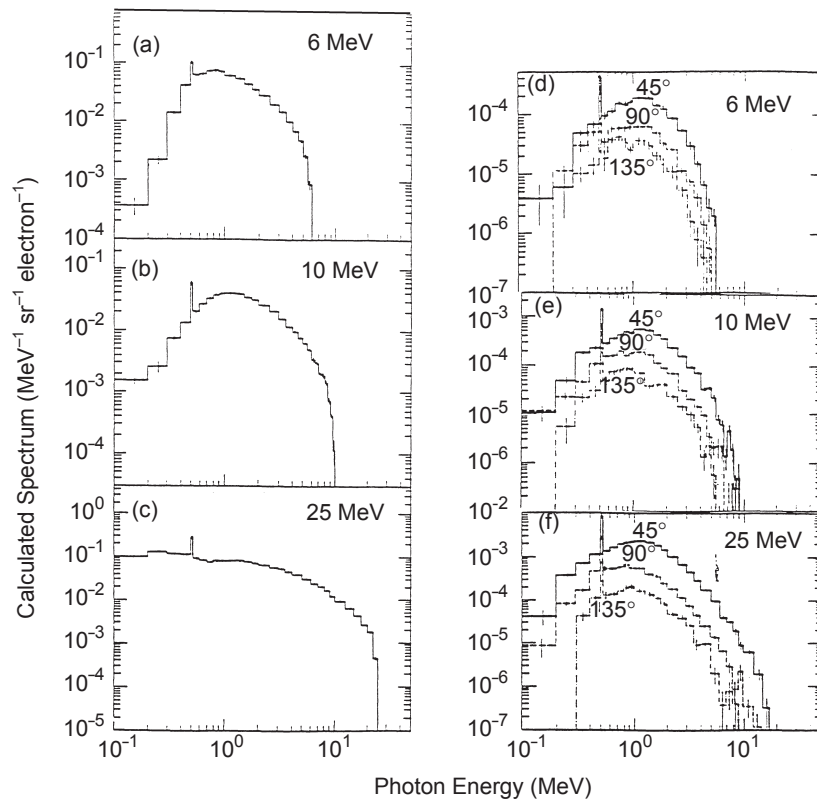
Fig. 4.3. (a)–(c): Primary x-ray beam spectra calculated by EGS at 6, 10 and 25 MeV, respectively, 0 to 15 degrees (d)–(f): Leakage x-ray spectra calculated by EGS at 6, 10, and 25 MeV, and for angular groups centered around 45, 90 and 135 degrees.

Caution must be used when applying these values of λ_T to a specific accelerator source because the TVL will depend on the shielding surrounding the target and the emerging photon energy spectrum. Additional calculations of bremsstrahlung angular distribution and energy spectra can be found in de Marco *et al.* (1995), Faddegon *et al.* (1990; 1991), Ferrari *et al.* (1993), Landry and Anderson (1991), Mao *et al.* (2000), and Mohan *et al.* (1985).

4.3.3 *Neutron Transmission*

The shielding thickness for proton accelerators of moderately high energy, up to ~400 MeV, is determined by the neutron-attenuation
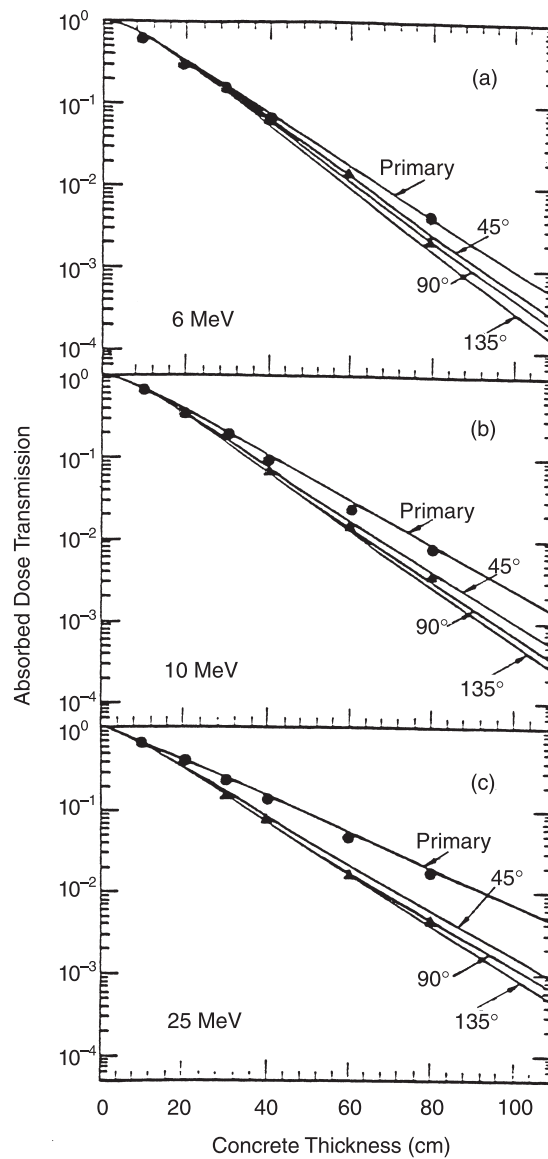
Fig. 4.4. Broad-beam absorbed dose transmission curves in ordinary concrete ($\rho = 2.35$ g cm^{-3}) for both primary and leakage components produced by electron beams of 6, 10 and 25 MeV, respectively. The lines are calculated using the EGS/LEAKAGE computer codes. The data points are calculated by MORSE for the primary-beam case and for leakage radiation at 45 degrees.

TABLE 4.2—*First, second and third TVLs* $(\lambda_{T_1}, \lambda_{T_2}, \lambda_{T_3})$ *in ordinary concrete* $(\rho = 2.35 \text{ g cm}^{-3})$ *and for photon spectra produced by 6, 10 and 25 MeV monoenergetic electrons.*

Spectrum	Angular Range (degrees)	Electron Energy $(\lambda_{T_1}, \lambda_{T_2}, \lambda_{T_3})$ (cm)		
		6 MeV	10 MeV	25 MeV
Primary	0 – 15	36.7/31.3/32.3	41.0/36.6/37.6	48.2/45.4/45.6
Leakage	35 – 55	35.3/28.6/29.3	36.6/31.1/32.8	37.7/33.8/36.7 34.9[a]
Leakage	80 – 100	34.1/27.5/28.4	34.9/29.3/31.1	35.9/31.9/34.7 34.7[a]
Leakage	125 – 145	33.3/26.1/26.9	34.7/28.6/29.9	35.5/30.5/32.5 34.4[a]

[a] Measured value of λ_T at 24 MeV (LaRiviere, 1984).

characteristics of the shielding material(s). The basic methods of neutron-transport calculations to solve the Boltzmann transport equation, the method of discrete ordinates, and the Monte-Carlo methods of O'Brien (1970) and Alsmiller *et al.* (1969a), have shown that these three methods give essentially equivalent results. Values of the attenuation lengths needed for the TVL method of shield design previously described may be derived from such calculations.

Curves of dose equivalent for monoenergetic, unidirectional broad neutron beams perpendicularly incident on concrete barriers are shown in Figure 4.5 as functions of shielding thickness ρx (g cm^{-2}). The quantity dose equivalent contains the fluence-to-dose-equivalent conversion (including the gamma-ray contribution), based on the spectrum at the shielding depth in question.[28] The intercept at $\rho x = 0$ is equivalent to the fluence-to-dose conversion coefficient for no shielding. The changing slopes of the attenuation curves (for $\rho x < 200$ g cm^{-2}, Figure 4.5) result in a large variation in λ_{T_1}, whereas those for λ_e show less variation.

The calculations for these three methods may be conveniently expressed as an exponential function of the form:

$$H(z) = H_0 \, e^{-z/\lambda}, \qquad (4.13)$$

[28] Estimates of conversion coefficients were based on the data and recommendations given in NCRP Report No. 38 (NCRP, 1971).
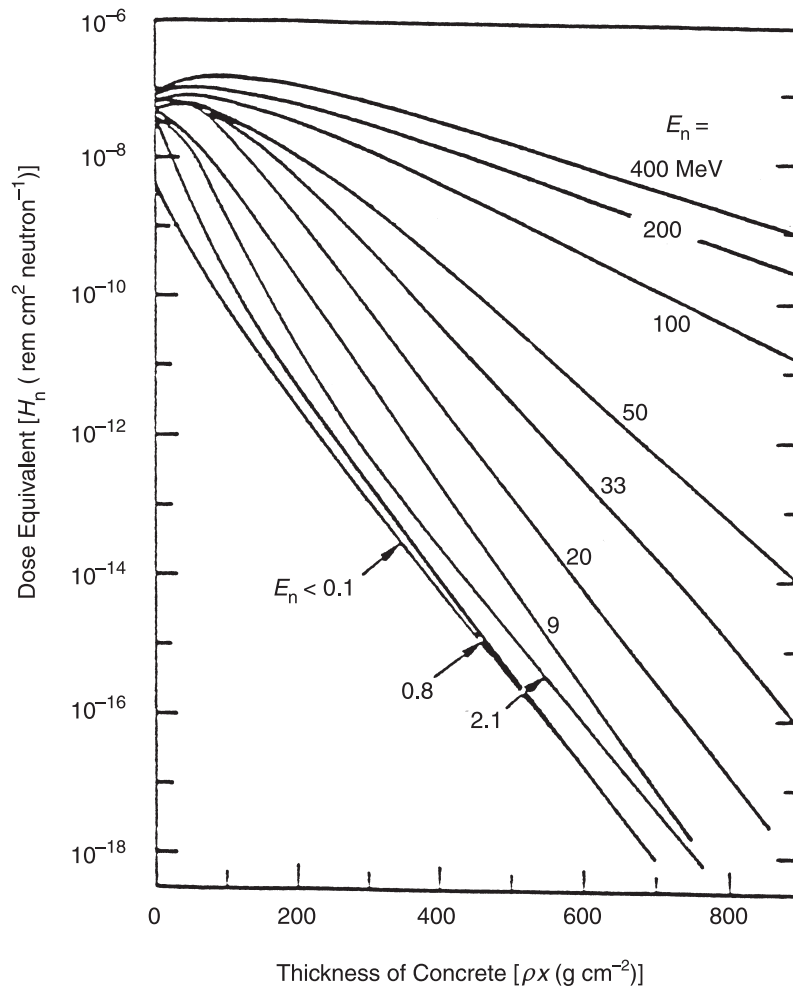
Fig. 4.5. Attenuation of broad beams of monoenergetic, unidirectional neutrons perpendicularly incident on ordinary concrete. The abscissa is the thickness of concrete (ρx) in g cm^{-2}, and the ordinate is the ratio H_n of dose equivalent in rem at shielding thickness ρx to unshielded neutron fluence in neutrons cm^{-2}. The dose-equivalent contribution of gamma rays is included. The curves are based on discrete-ordinate calculations of Alsmiller *et al.* (1969b), Roussin and Schmidt (1971), and Roussin *et al.* (1973).

where:

$H(z)$ = dose equivalent at depth z in the shield
λ = attenuation length
H_0 = dose equivalent extrapolated to zero depth

Figures 4.6 and 4.7 show the variation of the parameters λ and H_0 with neutron energy. The values of λ and H_0 shown have been selected to give a satisfactory representation of the data by Alsmiller *et al.* (1969b) and by Wyckoff and Chilton (1973) at depths greater than 1 m in concrete. The values of these parameters used for subsequent analysis are indicated by the solid line in Figures 4.6 and 4.7. The value of $\rho\lambda$, at energies above 200 MeV, has been chosen to agree with the limiting value of 1,170 kg m^{-2} found at high energies (see Section 4.8 which describes the Moyer model).

In the case of electron accelerators with a primary beam energy E_0 above the peak of the target's giant-resonance energy (k_0), the selection of shielding data for a monoenergetic energy equal to $E_n = (E_0 - k_0)/2$ would be conservative. The attenuation in concrete of radiation incident from a variety of photoneutron spectra emitted from thin targets bombarded by bremsstrahlung beams is shown in Figure 4.8. These curves were derived by Wyckoff and Chilton (1973) by folding the monoenergetic neutron dose-equivalent attenuation data (Figure 4.7) together with measured photoneutron spectra.
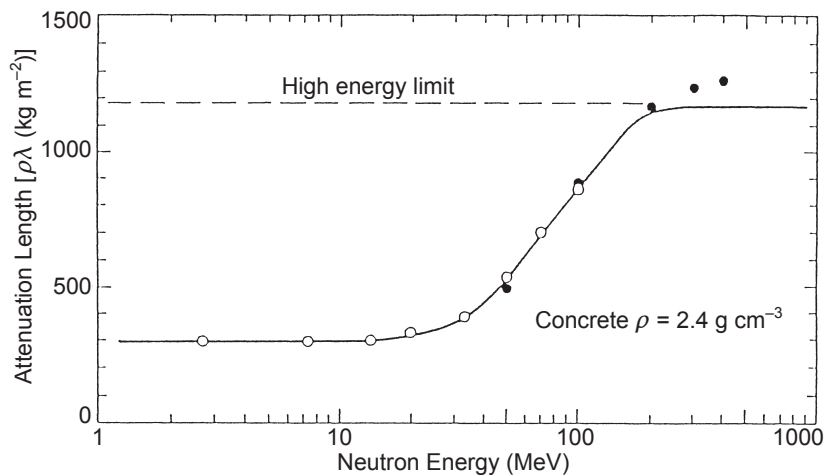
Fig. 4.6. The variation of the attenuation length ($\rho\lambda$) for monoenergetic neutrons in concrete as a function of neutron energy. Solid circles indicate the data of Alsmiller *et al.* (1969a) and open circles those of Wyckoff and Chilton (1973). The solid line shows recommended values of $\rho\lambda$ and the dashed line shows the high-energy limiting value of 1,170 kg m^{-2}.
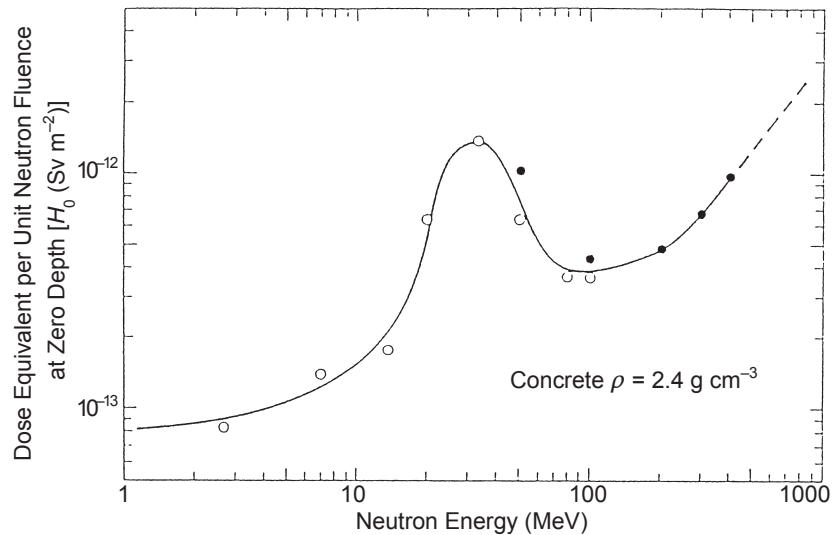
Fig. 4.7. The variation of the parameter (H_0) as a function of monoenergetic neutron energy. H_0 is the value of the dose equivalent per unit neutron fluence extrapolated from deep in the shield back to zero depth. Solid circles indicate values calculated by Alsmiller *et al.* (1969a) and open circles indicate values calculated by Wyckoff and Chilton (1973). The solid line indicates recommended values of H_0.

Because these curves are based on photoneutron production from thin targets, they assume a spectrum richer in high-energy neutrons than is often observed in practice. They, therefore, represent a conservative choice of attenuation curve, if used together with a neutron fluence for a thick target.

The curves shown are predominantly for materials of medium or high Z and for neutron emission at 90 degrees to the incident beam direction. The trend is for a more penetrating neutron spectrum at higher energy E_0, lower Z, and more forward angles. Thus, the three curves at a somewhat more forward angle (67 degrees) lie highest in Figure 4.8. Curves for light elements ($Z < 10$) will be relatively richer in fast neutrons from direct emission and will, therefore, show less attenuation.

For comparison with the curves for low-energy photo neutrons, Figure 4.8 also shows the attenuation of neutrons from an isotopic plutonium-beryllium source, and for the behavior at very high energies (beam energy $\gg$ 150 MeV); also the attenuation curve for neutrons from a copper target struck by a 400 MeV electron beam is given.
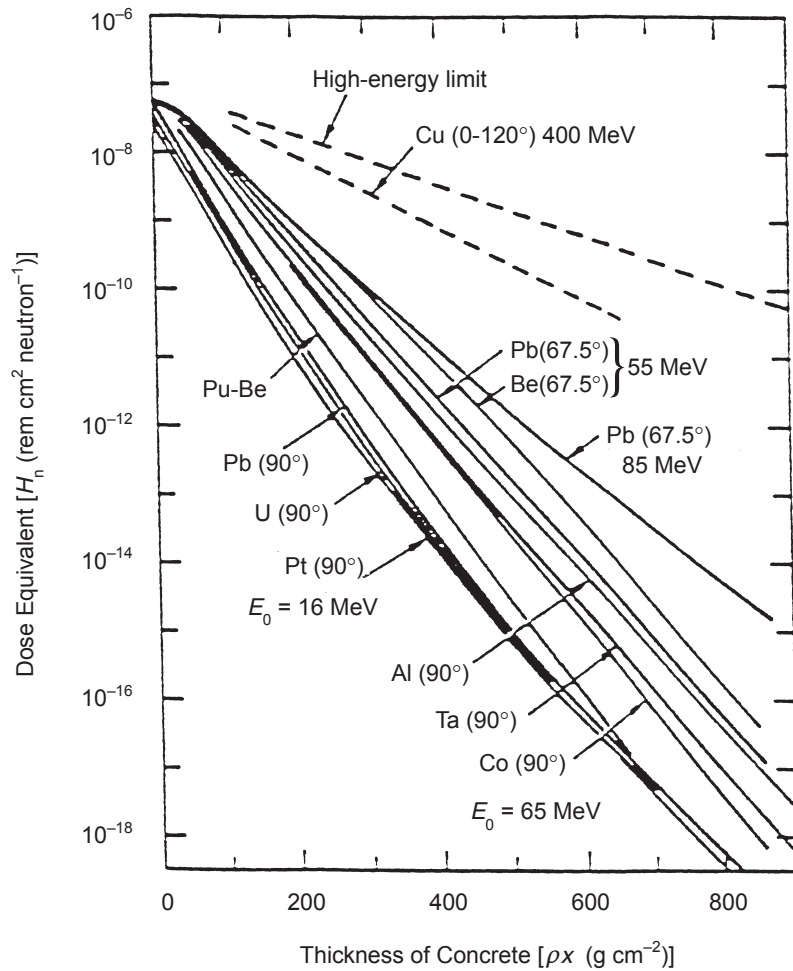
Fig. 4.8. Attenuation of unidirectional broad beams of neutrons, for representative photoneutron spectra, perpendicularly incident on ordinary concrete. The abscissa is the thickness of concrete (ρx) in g cm^{-2}, and the ordinate (H_n) is the ratio of dose equivalent to unshielded neutron fluence. The labels indicate target material, laboratory angle of neutron emission and endpoint energy (E_0) of the bremsstrahlung beam. The dose equivalent from gamma rays is included.

Production and transport of photo-neutrons is discussed in detail in NCRP Report No. 79 (NCRP, 1984). Report No. 79 is directed at the evaluation and measurement of neutrons produced by electron accelerators used for medical purposes and operating with electrons

in the energy range from 10 to 50 MeV. However, the principles related to the production and transport, energy spectra and shielding are applicable to electron accelerators of all energies.

Information concerning photo-neutron production and transport calculations can be found in a number of recent publications. Mao *et al.* (1996), have calculated electro- and photo-neutron yields produced by electrons with energies up to 10 GeV as a function of target material and thickness. Examples of neutron production and transport are shown in Figure 4.9. Calculations and measurements of photo-neutron leakage fluence and energy spectra from medical electron accelerators are found in Agosteo and Froglio Para (1994), Kase *et al.* (1998), Mao *et al.* (1997), and Uwamino *et al.* (1986).
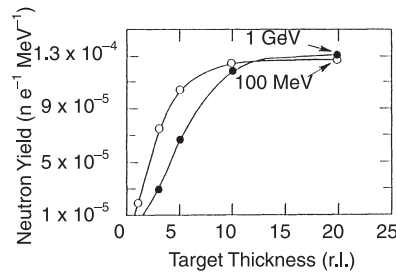
Fig. 4.9a. Neutron yield as a function of iron target thickness for 100 MeV and 1 GeV electron beams.
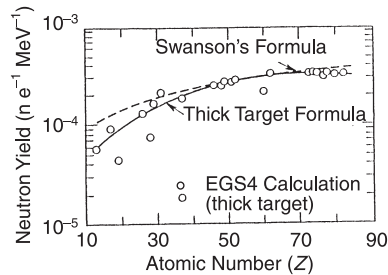
Fig. 4.9b. Neutron yields produced in thick targets struck by 100 MeV electrons as a function of Z.
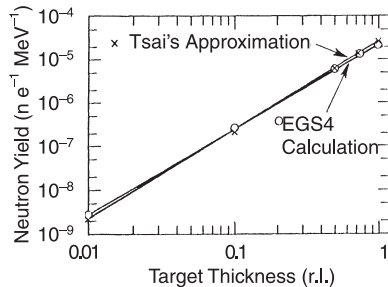
Fig. 4.9c. Neutron yields produced by bremsstrahlung in thin iron targets struck by 100 MeV electrons as a function of the target thickness.
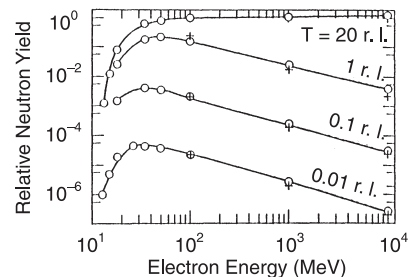
Fig. 4.9d. Relative neutron yields produced by bremsstrahlung in thick and thin iron targets as a fuction of the electron energy. The yield at 10 GeV for curve 20, r.1. is used as a normalizing point. The + symbol shows the results of calculations using a scaling function (Equation 15 of Mao *et al.*, 1996). The ○ symbol shows the reults of EGS4 calculations with a solid line drawn through them.

Fig. 4.9. Examples of neutron production and transport (Mao *et al.*, 1996) ("r.l." in the figures stands for radiation length.)

McGinley (1992a; 1992b) reported on the production of neutrons when a photon beam is directed at a metal or concrete slab.

When materials other than concrete are to be used for the shielding of neutrons of energy less than 30 MeV, and provided the outer material of the shield contains some hydrogenous material, the "removal cross-section" method is convenient and usually sufficiently accurate. This method is neatly summarized in NCRP Report No. 38 (NCRP, 1971) and treated in detail by Shultis and Faw (1996). Original removal cross-section data are given by Chapman and Storrs (1955). Comprehensive discussions can be found in the general references on shielding (Blizard and Abbott, 1962; IAEA, 1968; Price *et al.*, 1957; Schaeffer, 1973). To use the removal cross-section method, the material of the shield must either be hydrogenous, mixed intimately with hydrogenous material, or followed by 20 to 30 cm of water or its equivalent in hydrogen content. An obviously useful combination of materials satisfying these conditions is, *e.g.*, a steel or lead shield followed by concrete. The removal cross-section method may be used to advantage, *e.g.*, in cases where it is required to estimate the enhancement of existing concrete shielding by the addition of lead or steel inside the concrete. In composite shields, the hydrogenous material serves greatly to enhance the effectiveness of the nonhydrogenous portion. In optimizing the design of shields, a useful rule of thumb is that 30 cm of water (or its equivalent) is sufficient to remove the low-energy portion of the neutron spectrum not efficiently removed by the nonhydrogenous portion of the shield.

The trend of λ_{T_R} (the tenth-value layer for removal) with atomic weight A is shown in Figure 4.10. For $A > 8$, the λ_{T_R} in g cm^2 is given approximately by:

$$\lambda_{T_R} = 4.76 \ (\ln 10) \ A^{0.58} = 11 \ A^{0.58}. \qquad (4.14)$$

These values of λ_{T_R} apply to a fission spectrum, but are also suitable for neutrons from thick targets at installations operating at energies E_0 ranging from the photoneutron threshold k_{th} to somewhat above the giant-resonance energy k_0.

The enhancement of the effectiveness of shields of steel and lead as a function of thickness of an outer layer of hydrogenous material has been studied by Dudziak (1968), Dudziak and Schmucker (1968), and Shure *et al.* (1969) (see also Stevens *et al.*, 1973). Their results should be used when it is necessary to evaluate the effect of a hydrogenous layer of less than ~20 cm of water or its equivalent.

The spectrum of giant-resonance neutrons is not very different from that of either an americium-beryllium source or of a fission spectrum. Experimental λ_T values for these neutrons for several materials are given in Table 4.3. These data, which are useful for designing shielding for those accelerators which produce neutrons
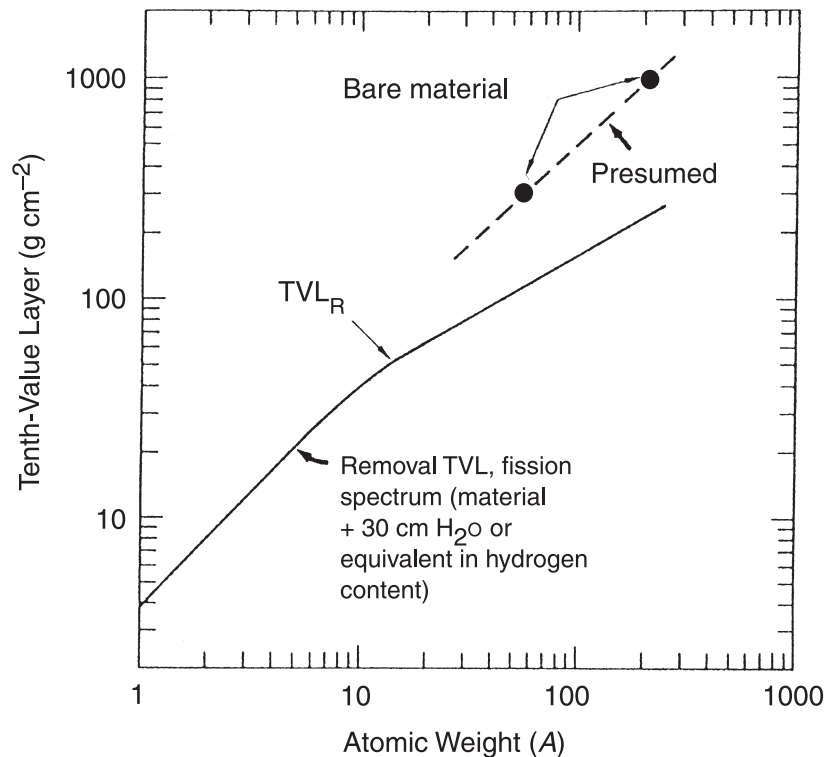
Fig. 4.10. Neutron removal TVL as a function of atomic weight (*A*) of shielding material. The solid curve is for a fission spectrum, assuming a backing of 30 cm of water or the equivalent in hydrogen content (Chapman and Storrs, 1955). For comparison, the two points above the curve joined by the interpolated dashed line show TVLs for a fission spectrum incident on iron and lead, without hydrogenous backing (adapted from Shure *et al.*, 1969).

predominantly close to the giant resonance, clearly show the greater effectiveness of low-*Z* (especially hydrogenous) materials. The variability of shielding effectiveness of bare nonhydrogenous materials is explained, in part, by the experimental sensitivity of the detector type. These data are meant to be indicative only and should be used with caution.

The energy spectrum of neutrons emerging from the target region of an electron accelerator will be influenced by the materials surrounding the target. For a typically well-shielded target in a medical accelerator, *e.g.*, the mean energy of the leakage neutrons is less than 1 MeV. The TVL for a typical leakage neutron spectrum is much smaller than that given in Table 4.3. Figure 4.11 shows the

TABLE 4.3—*Values of neutron dose-equivalent TVLs (λ_T), for representative low-energy neutron spectra.*[a,b]

Material	Neutron Spectrum	λ_T (g cm^{-2})	Reference
Paraffin (solid)	AmBe	23	
Wood	AmBe	28	
Water	Fission	22	NCRP (1971)
Sand (SiO$_2$)	AmBe	74	
Ordinary concrete	AmBe	96	
Heavy concrete	AmBe	110	
Iron (steel)	Fission	280 – 330	Shure *et al.* (1969)
Lead	Fission	900 – 1,070	Shure *et al.* (1969)

[a] Based on data from ICRP Publication 21 (ICRP, 1973) and NCRP Report No. 38 (NCRP, 1971).

[b] Fire safety advice should be obtained when any flammable material is being considered.
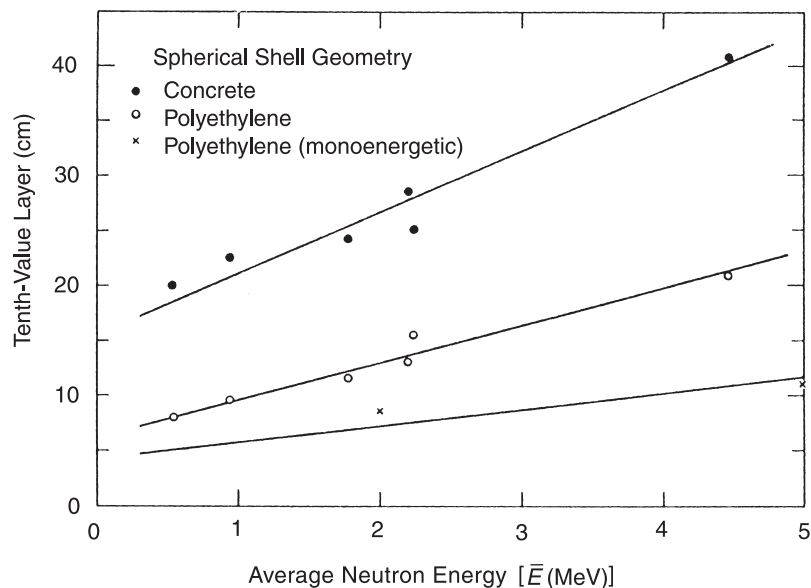
Fig. 4.11. The dose-equivalent TVL for spherical shell shielding as a function of the average energy of the neutron source (McCall *et al.*, 1979). The lines are least-square fits to the calculated points (Figure 33 in NCRP, 1984).

TVL as a function of mean neutron energy from 0 to 5 MeV, taken from NCRP Report No. 79 (NCRP, 1984).

There are only very limited reports of measurements of the attenuation of dose equivalent in shielding of the neutrons produced by the interaction of energetic heavy ions. McCaslin *et al.* (1985a) provide limited data for dose-equivalent rates measured in concrete shields at various distances and angles from a thick-copper target bombarded by neon ions of specific energy 670 MeV amu^{-1}.

In recent years, acceleration of heavy ions up to energies of 100 GeV per nucleon has been achieved at the Relativistic Heavy Ion Collider at Brookhaven National Laboratory. The shielding in the transverse and forward directions for this facility has been designed using methodology developed for high-energy proton accelerators. To first order, a high-energy, heavy-ion particle can be treated as an independent collection of high-energy neutrons and protons. As such, the calculational techniques developed through the Moyer model and through Monte-Carlo codes such as CASIM have been demonstrated by Stevens (1992; 1994a; 1994b) to be directly applicable to the design of the shield for the Relativistic Heavy Ion Collider. CASIM was utilized by Stevens to design the transverse and forward shielding, as well as internal beam dumps by assuming that ^{197}Au accelerated to 100 GeV per nucleon was an assemblage of 197 nucleons with an average energy of 100 GeV.

4.3.4 *Scattering—Albedo*

The amount of radiation back scattered is proportional to the radiation fluence incident on the surface and on the area of the surface irradiated, and it is inversely proportional to the square of the distance (d_s) from the irradiated surface to the location in question. These factors are multiplied by the differential dose albedo (α) (the fraction of the incident radiation reflected), which depends on the photon or neutron incident energy spectrum, the type of material irradiated, the angle of scattering (Θ_s), and the orientation of the surface.

For photons, the differential dose albedo (α) may be regarded as a combination of two terms whose relative importance depends on irradiation conditions; one term contains the angular dependence of Compton scattering and the second, which is essentially isotropic, is dominated by positron-annihilation photons (0.511 MeV) for incident photon energies above 7 MeV. Both terms are modified by absorption within the scattering material in a way that depends on the angles of incident and outgoing radiation relative to the surface. For example,

for perpendicular incidence, the albedo for Θ_s close to 180 degrees is larger than for sideward directions, because the outgoing radiation has less material to penetrate.

Chilton and his colleagues have developed parameterization which adequately describe the scattering of photons and neutrons up to energies of 10 MeV (Chilton, 1965; Chilton and Huddleston, 1963; Chilton *et al.*, 1965). These methods are discussed in detail by Shultis and Faw (1996). Figures 4.12 and 4.13 give albedo coefficients for monoenergetic photons (α_x) and for monoenergetic neutrons (α_n), respectively. These are based on an irradiated area of 1 m² and a distance of 1 m. Inspection of these curves shows that the reflectivity or albedo of neutrons is typically larger than and less energy-dependent than that of photons.

Values of the differential dose albedo (α) are given in Figure 4.14 for the scattering of bremsstrahlung beams of endpoint energy (E_0) incident on selected materials. These data, based on the parameterization used in Figure 4.13, are obtained as a simple average of the albedo over the photon energy range 0.5 MeV to E_0. Although parameters are available only for photon energies up to 10 MeV, this energy range dominates the effective bremsstrahlung albedo from primary photons at all higher energies. The effective bremsstrahlung albedo at higher E_0 is, therefore, relatively insensitive to the behavior at high photon energies, and extrapolations to higher bremsstrahlung energies are given. These extrapolations are consistent with measurements of total energy albedo at high energies (Kruglov and Lopatin, 1960; Pruitt, 1964; Sugiyama and Tomimasu, 1967).

4.3.5 *Scatter Paths*

In addition to the direct paths from the source points to the dose point, shielding studies must also consider scatter paths. A common pitfall of point-kernel calculations, illustrated in Figure 4.15, is associated with slant-incidence geometry (Lahti, 1986). The detector would "see" a response dominated by collisions at Regions A or B, over those that would be generated by the line-of-sight pathway. The subject has been studied and results published by Fournie and Chilton (1980) and Price *et al.* (1957).

The scatter paths are often important when considering roof shielding because the roof is usually thinner than the side walls. The roof is usually not as accessible and it is more expensive to build than side walls. Two important paths are scatter from the air above the roof and from the roof itself. Because neutrons are not readily
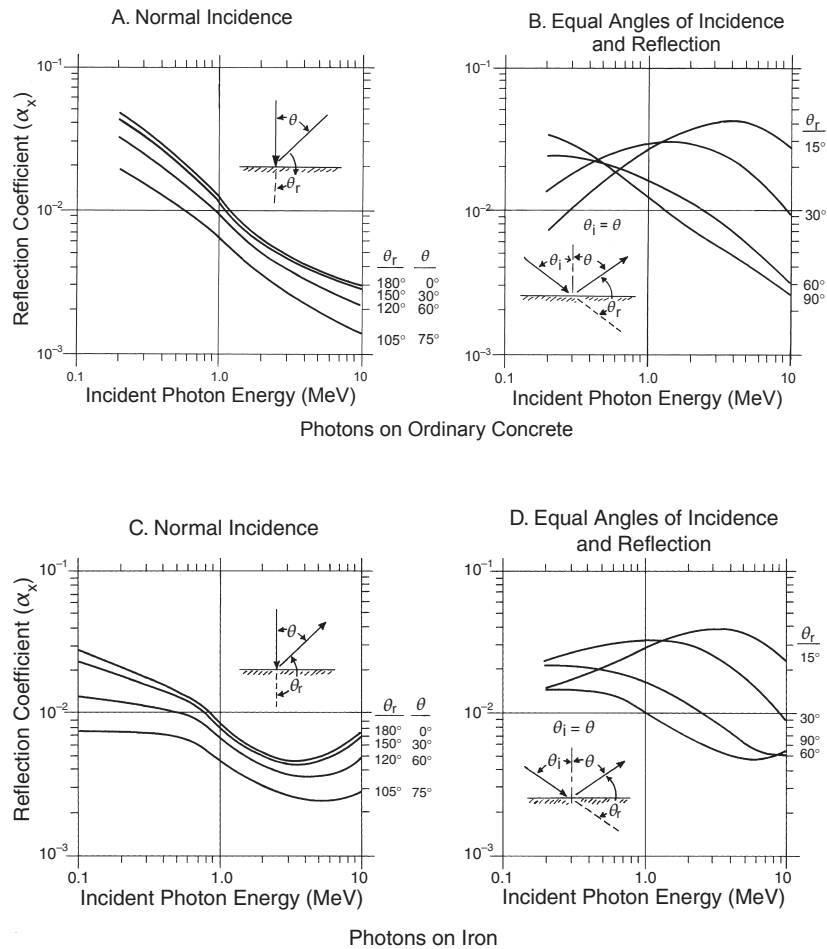
Fig. 4.12. Reflection coefficients (α_x) for monoenergetic photons incident on ordinary concrete, iron and lead as a function of incident photon energy, for several reflection angles assuming normal incidence and equal angles of incidence and reflection. The values are given for ordinary concrete and iron, based on theoretical and experimental information (Chilton, 1965; Chilton and Huddleston, 1963; Chilton *et al.*, 1965). Use of the 10 MeV values for α_x above 10 MeV is expected to be safe. Values of α_x for photons on lead are not as readily calculable, but a conservative upper limit is 5×10^{-3} for any curve and scattering angle. The values of α_x for $\Theta_r = 180$ degrees in Curve A are the same as for $\Theta_r = 180$ degrees in Curve B (NCRP, 1977).
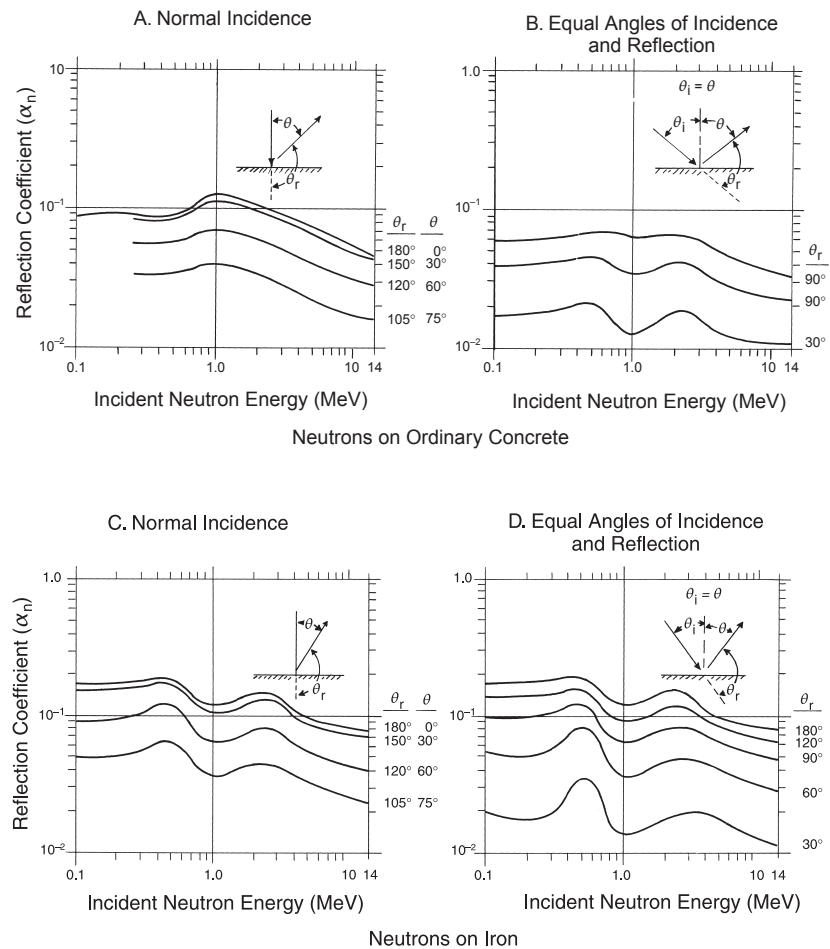
Fig. 4.13. Reflection coefficients (α_n) for monoenergetic neutrons incident on ordinary concrete, iron and lead as a function of incident neutron energy, for several angles of reflection assuming normal incidence and equal angles of incidence and reflection. Values are given for ordinary concrete and iron, based on existing available information, both theoretical and experimental (Chilton, 1965; Chilton and Huddleston; 1963; Chilton *et al.*, 1965). Values for neutrons incident on lead are probably an order of magnitude higher than those given above, indicating that thick lead barriers are not desirable for capturing neutrons. The values of α_n for $\Theta_r = 180$ degrees in Curve A are the same as for $\Theta_r = 180$ degrees in Curve B (NCRP, 1977).
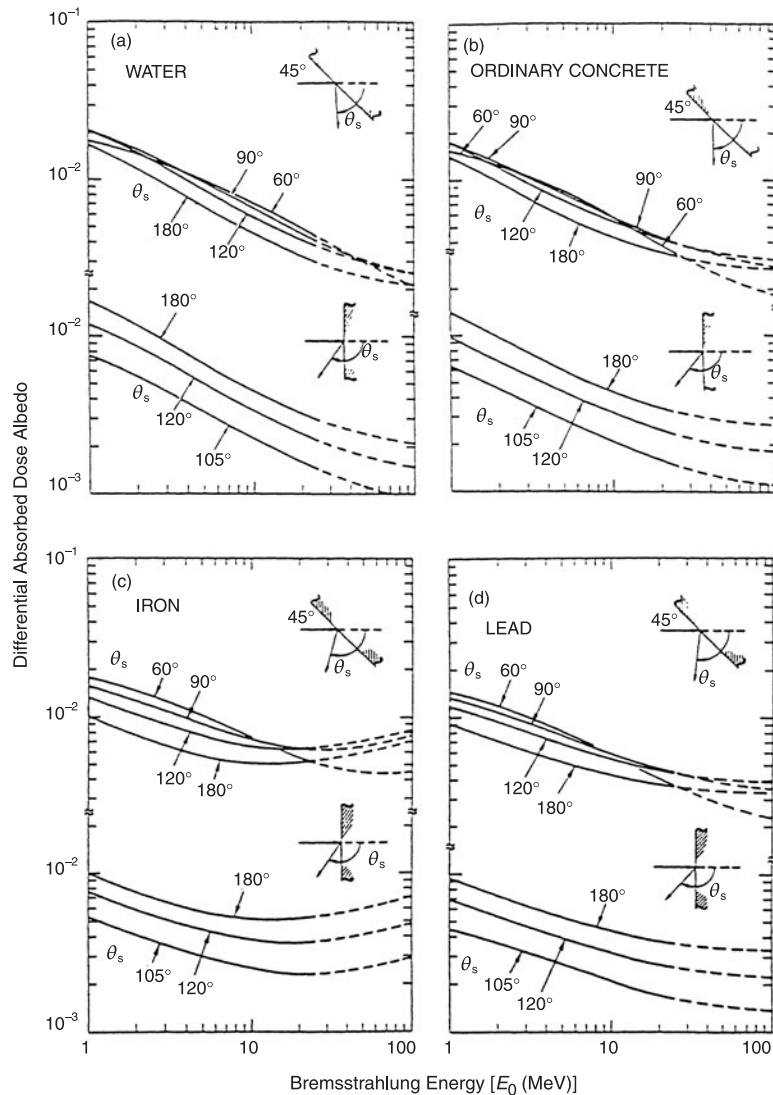
Fig. 4.14. Effective differential absorbed-dose albedo for bremsstrahlung beams of endpoint energy (E_0) incident on selected materials, for 45 degrees incidence (upper curves) and perpendicular incidence (lower curves), for representative scattering angles (Θ_s). For 45 degrees incidence, the albedo given is for scattered radiation in the plane containing the normal to the surface and the direction of incident radiation. The data are interpolated using the Chilton-Huddleston parameterization (Chilton and Huddleston, 1963). Extensions to higher energies are suggested extrapolations. (a) water (this may also be used for tissue), (b) ordinary concrete, (c) iron (steel), and (d) lead.
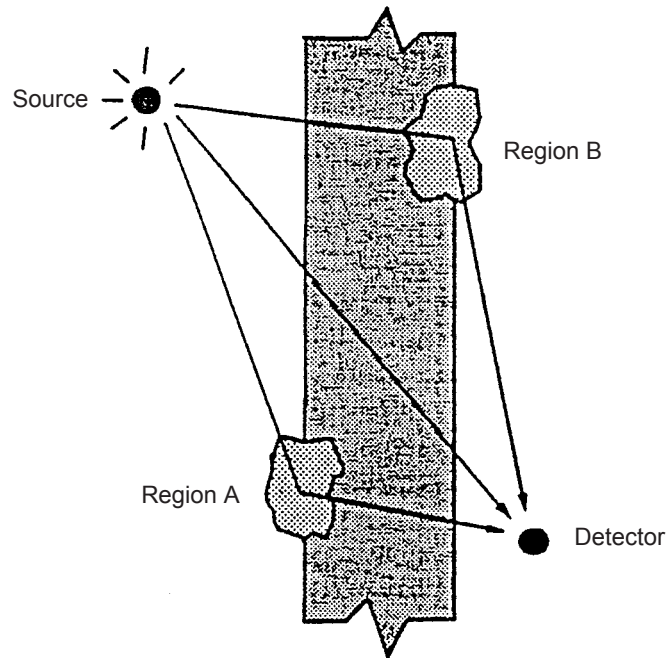
Fig. 4.15. A diagram indicating a potential problem when point kernel calculations are used in the case of slant incidence. The response of the detector located as shown with respect to the point radiation source would be influenced by collisions at Regions A or B more than those generated by the line-of-sight pathway.

absorbed above thermal energies, neutron scattering is more important than photon scattering, particularly if the shield is designed so that the neutron and photon fields are comparable. Scattered radiation inside the shielding, from near the shield surface, and from skyshine are more important for a large facility (Section 6).

4.4 Radiation Goals and Area Occupancy and Use Factors

Radiological protection standards and dose limits have been discussed in Section 1. The design of an efficient radiation shield for an accelerator, however, goes beyond compliance with legal protection limits. ICRP (1991) has recommended a system of radiation protection which has three interrelated components:

- justification
- optimization of radiation protection
- individual dose limitation

The principle that guides optimization of radiation protection is often described by the acronym "ALARA," an abbreviation for "as low as reasonably achievable." In ensuring a proper optimization of radiation protection, it is most important to set up a proper relationship between dose limits and radiation protection goals.

In setting up this relationship, four principal regions of potential exposure should be considered:

- areas routinely occupied by workers directly involved with accelerator operation
- areas such as laboratories and offices routinely occupied by workers not directly involved with accelerator operation
- areas infrequently occupied
- areas accessible to members of the general public

NCRP and ICRP have made recommendations of effective dose limits for both occupationally exposed individuals and for members of the general public. These are discussed in ICRP Publication 60 (ICRP, 1991) and NCRP Report No. 116 (NCRP, 1993). Because the detailed implementation of these recommendations and the philosophy behind them are rather sophisticated, the reader is encouraged to study these reports carefully.

When planning new facilities, the ALARA principle should be applied to control radiation dose both to individuals who are occupationally exposed and to members of the public. NCRP recommends that facilities should be designed to limit dose to occupationally exposed individuals to a fraction of the annual dose limit (NCRP, 1993). NCRP also recommends that reference dose levels be established for purposes of design and control. With regard to exposure of members of the public, NCRP recommends that the facility be designed so that no individual member of the public receive more than 25 percent of the recommended annual dose limit. The management of the facility shall determine the administrative dose-control values for its various employee categories and the required radiation safety training for each category (NCRP, 2000).

For design purposes, the relevant annual reference dose can be expressed as a maximal, 40 h, weekly-dose rate (H_m). To take into account the average time per week spent by an individual in the areas that may be occupied, an area occupancy factor (T) (defined in Section 4.6.1.3), and use factor (U), can be used so that the shield is designed to allow dose rates no greater than H_m/TU. U expresses the fraction of operating time that the primary radiation beam is directed at the particular occupied area. If the data are available, actual values for T, as observed in operation, can be used. In the

absence of such information, the values given in Table 4.4 may be used. Some of the values for T recommended in Table 4.4 may be found to be unduly conservative in certain practical situations, but they are recommended in the absence of alternatives firmly based on appropriate information.

For 40 h week^{-1} operation, the value T = 1 is used for the entire controlled area, including adjacent irradiation rooms if designed to be occupied during accelerator operation. Frequently occupied areas outside the controlled area, such as offices, laboratories, shops, and nearby buildings, are also ascribed the value T = 1. When accelerator operation exceeds 40 h week^{-1}, the value of T may be less than one, because it is not likely that a single individual will be present during the entire operating period.

Areas expected to be occasionally used by individuals, such as corridors, waiting rooms, and elevators, may be ascribed T = 1/4. For areas outside the controlled area, but within the institution's bounds when it can be assured that no individual remains more than a small fraction of the time, an occupancy factor T = 1/16 is suggested. Public areas where it is unreasonable to expect that any individual would consistently linger more than, say, 2 h week^{-1} (such as streets, sidewalks, parking lots, or lawns) may also be ascribed T = 1/16.

Calculations are normally based on a 40 h work week. If an accelerator operates for more, or less, than a 40 h week, or if the particle or photon beam can be directed to several locations, a use factor different from U = 1 can be applied. The use factor is the time (t) in hours per week that the accelerator operates, or that the beam is directed to a particular location divided by 40 (U = t/40).

4.5   Determination and Specification of the Beam-Loss Terms

The source term is a specification of the distribution and type of the radiation source(s) caused by the accelerated beam, whether

TABLE 4.4—*Suggested occupancy factors.*

Type and Occupancy of Area	Occupancy Factor (T)
Full occupancy	1
Controlled area	1
Nearby buildings	1
Work areas	1
Offices and laboratories	1
Partial occupancy	1/2 to 1/5
Occasional occupancy	1/8 to 1/40

deliberately (*e.g.*, in targets) or otherwise, and must be specified before any shield design is attempted. This specification should be based on particle type and reasonable estimates of the upper limits of beam energy, current, operating time, beam losses, and the magnitude and frequency of conditions of high beam loss such as start-up, abnormal or accident conditions.

Except at targets and beam stops, the radiation field is caused not by the primary beam intensity but by the *beam-loss intensity,* which designers strive to minimize but is never zero. In an accelerator which produces useful beam, it is self-evident that the sum of generally distributed beam losses will be lower than the accelerator primary beam intensity. These losses can be characterized by their expected location in the facility and whether they are expected to be routine or to arise from some accidental situation, which might be expressed, *e.g.*, as a maximum credible beam loss. The production of secondary radiations/particles, by the interaction of the primary beam with targets, has been discussed in Section 3 of this Report.

For a facility with a single radiation room, the precise location of the stopped beam, whether on the target or on an aperture a short distance from the target, is not usually of great importance in determining shielding requirements. This case is discussed explicitly in Section 4.6.

For more complex facilities that may have, *e.g.*, many different operating modes and several loss points spread over several rooms, tunnels, or caves; the burden of determining responsible loss scenarios for facility design falls upon those who design the facility and those who review their designs. Before accelerator operation, the actual location and the amount of beam losses may not be known. In the design phase, there needs to be considerable discussion of these matters between all knowledgeable persons—particularly so for a new type of facility. Several credible loss scenarios should be considered, based both on good and on bad operating experience. For example, the constituent accelerators of a large accelerator complex may not all work efficiently at the same time.

Targets, to which the accelerator beam is intentionally directed, are not the only sources of penetrating secondary radiation and particles. Some primary particles will interact with residual gas and solid objects such as accelerator structures. Estimation of the location and magnitude of such interactions should be made during the design of an accelerator. In accelerators that efficiently extract the useful beam, the magnitude of the loss in the accelerator itself will usually be much less than that from the beam striking the target and beam stop.

At a large facility, beam losses usually may be localized by design of lost-beam collectors (dumps) or collimators, etc. When this is done correctly, the demands on the shielding over much of the facility are reduced, particularly at higher energies. Of course, undesirable radiation levels can occur if the assumptions are incorrect.

The provision of internal shielding or barriers around these areas of high beam loss to separate the activated material from the work force is often desirable. The choice of material for local shielding should be optimized with regard to both secondary and residual radiation levels. If credit is given for such local shielding in the shield design, controls should be established to ensure that the shielding remains in place during operation and cannot unknowingly be removed.

Losses of stored particles must be low to prolong beam lifetime. This is particularly important if cryogenic magnets are used because quenching must not occur. Operational considerations may impose an upper limit to the beam intensity (and therefore source strength) striking accelerator or beam transport components to prevent their destruction or damage, when energy deposition is too high.

If, in the shield design, it is assumed that beam losses at full beam intensity will not occur at predictable loss points (*e.g.*, beam-splitters, extraction septa), or elsewhere; it may be necessary to install special monitors inside the shield or to place area radiation monitors outside the shield so that both the accelerator and personnel are protected in the event of malfunction. In some cases, these monitors will need to be combined with interlocks to maintain radiation intensities below desired administrative or regulatory limits. In a well operated accelerator facility, these interlocks will rarely be activated but it is *most important* that their reliable operation be regularly tested. At start-up and during beam tuning, it is important to confirm that such tests have taken place recently.

At experimental facilities with a projected program requiring only a limited fraction of the available beam intensity, the design of shielding for the full available intensity is nevertheless prudent, even though it may be more expensive than shielding the beam intensities required for the projected program. By their very nature, experimental programs need to be flexible to respond to rapid changes in need and are, therefore, somewhat volatile. The provision of shielding adequate for any reasonably foreseeable use of the accelerator is almost always a good investment. If multiple-beam operation is planned, either by the development of several independent particle beams or by the steering of a single beam into several experimental areas, the specification of source terms is more difficult. In

such a case, it may also be prudent to require that each target station be built to receive the full intensity of the accelerator.

In some cases, the basic specification of the loss term will be difficult. The use of an accelerator in a fundamental research program will not be reliably predictable. At high-energy accelerators, there will be many experimental facilities used at a variety of beam energies and intensities, and even particle type. Over a given period, there may be several major radiation sources, each with a different radiation characteristic, and the future use of such an accelerator will be determined by the "as yet" unknown research interests at that future time.

For large and/or complicated facilities, it is particularly important that intensities and losses on which a shield design is based should be well-defined and agreed to by the shield designer, management and, possibly, the national or regional regulatory authority before the facility design is completed. Limiting conditions of operation may need to be established if the shield design is based on less than full accelerator output. Critical review of the beam-loss assumption, which forms the basis for shield design, is essential.

4.6 Shielding of Electron Accelerators in the Energy Range from 1 to 100 MeV

Many, if not most, of the accelerators that operate with energies in the range from 1 to 50 MeV are manufactured commercially and are used for radiation therapy, industrial processing, and radiography. Accelerators that have energies extending to 100 MeV are generally small research units. Usually, the electron beam is stopped in a target that is made of high-Z material, such as tungsten. Photons (and, for incident electron energies above 10 MeV, neutrons as well) are emitted in all directions. Photon emission becomes more anisotropic, as the incident electron energy increases, with the photons being increasingly directed in the forward direction. On the other hand, the neutrons are emitted almost isotropically throughout this energy range. The size of the beam is typically limited by adjustable collimators. In directions outside the useful beam, local shielding around the target, collimators and filters attenuate the photon radiation by a large factor (typically of the order of 1,000). However, this local shielding, which typically is of high-Z material, will reduce the energy of the neutrons by inelastic scattering but will not significantly reduce the number of neutrons.

Some accelerators are designed so that they can be used to provide both photon and electron beams. In such "bi-modal accelerators,"

when the electron-irradiation operating mode is required, the bremsstrahlung target is removed and the electron beam is permitted to emerge through a thin vacuum window. When operating in the electron-beam mode, the local dose rate is much higher than in the bremsstrahlung photon beam for the same accelerator beam current.

In dual-mode therapy accelerators, the accelerator beam current is greatly reduced when operating in the electron-beam therapy mode. Radiation therapy treatments or industrial processing may be performed using the direct electron beam. Large area irradiation fields are produced by two methods, either by scattering the electrons or by scanning the beam using a variable magnetic field. In accelerators designed solely for electron irradiation, no target is installed and the electron beam emerges through a thin vacuum window.

For accelerators designed to produce either photon or electron beams, the shielding that is required for photon beam operation will suffice for the electron beam mode. In the sterilization of foods, pharmaceuticals and other such industrial operations that use only the electron beam, the current is much higher than for therapy applications. X rays produced in the materials irradiated by the electron beam must be considered in the shield design. Because massive local shielding may not be practical, the irradiation-room walls may need to be rather thick, even if the materials being irradiated are not efficient photon production targets.

4.6.1 *Source Term for Simple Accelerators*

For accelerators located in a single room (Figure 4.16), specification of the source term may be fairly simple. For example, in the case of an accelerator routinely used in a hospital for radiotherapy, there will be only a limited number of beam ports and consequently, only a limited number of primary radiation sources, even perhaps only one. The accelerator and the target may be in the same heavily-shielded room, so beam-losses in the accelerator may not need to be known. Furthermore, the number of patients and/or treatments and the radiation doses required (the workload) will be well known. The facility may not operate at the full potential output of the accelerator because a significant fraction of the time in radiotherapy is necessarily devoted to patient positioning and setup.

In assessing shielding requirements, it is appropriate to take into account the accelerator operating schedule or workload (W), together with the beam orientation (use) factor (U) that will affect the average weekly dose equivalent to individuals in areas that may be occupied.
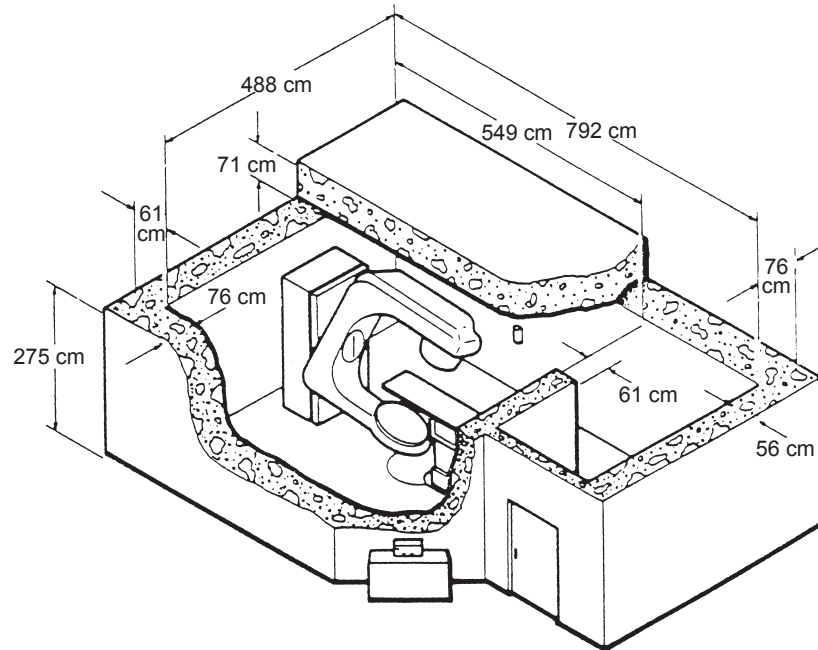
Fig. 4.16. Cutaway view of a clinical accelerator arrangement for rotational therapy. The dimensions will vary with the workload and the accelerator energy. The lower therapy-unit member is a beam stopper which permits a reduction in primary barrier thickness. Without the beam stopper, the primary barriers (the ceiling and two 76 cm walls) would have to be augmented by ~85 cm of concrete or the equivalent of other materials (original data in inches) (adapted with permission of Varian Medical Systems, Palo Alto, California).

4.6.1.1 *Workload.* The radiation output of electron accelerators designed for radiotherapy is fairly standard for all manufacturers, and it is customary to express the equipment workload (W) in dose equivalent per week at 1 m from the x-ray target (*e.g.*, Sv m^2 week^{-1}). Typical workloads for modern equipment and therapy-facility operations are currently being evaluated. A new NCRP report on the design of radiation therapy facilities is in preparation. Until such time as the new report is published, the recommendations given in NCRP Report No. 49 (NCRP, 1976a) should be followed.

The output of industrial accelerators is likely to be more variable than that for radiation therapy units and has not been evaluated. It is recommended that the radiation-protection shielding be planned assuming that the accelerator is operated for 10 h in a 40 h work week. Typical workloads lie in the range of 10^2 to 5 $\times$ 10^4 Gy m^2 week^{-1}.

4.6.1.2 *Primary and Secondary Barriers and the Orientation (Use) Factor.* In this application, the orientation (use) factor (U) provides an estimate of the average fraction of the accelerator operation when the radiation beam is directed toward a given shielding barrier. When the accelerator has a fixed orientation and there is no provision for changing the direction of the beam, there is a single primary barrier (Section 4.6.2) with U = 1 for that orientation. The remaining (secondary) barriers (Section 4.6.3) are designed to shield the stray (leakage and scattered) radiation, and for these, a value of U = 1 is also used. When the beam orientation can be changed, as is the case for radiation therapy accelerators that are mounted on a rotating gantry, orientation factors for primary barriers may be less than one. For secondary barriers, however, U is always assigned a value of unity. Orientation factors for modern radiotherapy accelerators are currently being evaluated. Until new guidance is issued, the values of U recommended in NCRP Report No. 49 (NCRP, 1976a) should be used.

4.6.1.3 *Occupancy Factor.* The occupancy factor (T) is used to describe the fraction of the accelerator operating time that an individual is likely to be in an area outside, but next to the shielded room. Recommended values of T are given in Section 4.4.

4.6.2 *Primary Barriers for Photons*

The primary electron beam can be stopped in a short distance in an absorbing material. Photons and neutrons, however, do not have discrete ranges and are attenuated exponentially in absorbing material. Typically, photon radiation controls the shielding requirements. If adequate shielding is provided for the primary and secondary photon radiation, the direct and scattered electrons will be completely stopped and need not be considered further for radiation protection. This is true, even for those accelerators that operate with only electron beams. If the shielding provided for the photon radiation is concrete, the accompanying neutrons will also be adequately shielded because concrete contains sufficient hydrogen to thermalize the neutrons which are then readily absorbed (Section 4.10.2). However, if composite shields containing a significant thickness of materials with high-Z, such as steel or lead are used, the penetration of the neutrons must be evaluated. In addition, the production of neutrons by photonuclear interactions in the shield must be examined.

The primary barrier may be defined by that area on the outer surface of the shield that is illuminated by the useful bremsstrahlung

beam with the beam collimator fully opened, so as to provide the largest possible field size, and for any feasible orientation of the treatment head or collimator. In specifying the primary barrier, an adequate margin should be provided around this area (Figure 4.17).
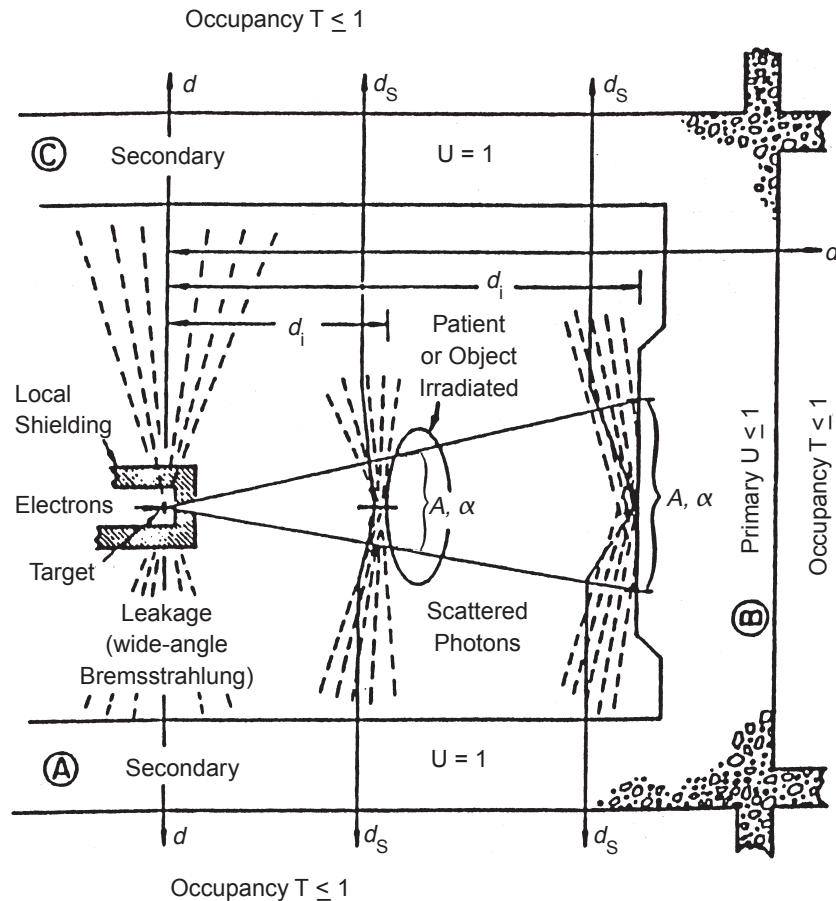
Fig. 4.17. Conceptual plan of a radiation room for one accelerator orientation, showing the relationship of primary (U ≤ 1) and secondary (U = 1) barriers to radiation sources (not to scale). Each barrier is ascribed an orientation (use) factor (U), and each occupied area an occupancy factor (T). The distances (d_i) are measured from the electron target to each scattering surface, and d_s from each such surface to the nearest point of each occupied area. Each source of scattered photons is characterized by its area (A) (in a plane perpendicular to the beam direction) and differential dose albedo (α), depending on the material, its orientation, the scattering angle, and primary energy (E_0).

In the calculation of shielding, scale drawings that show the radiation area in relation to other areas in the facility and to the public areas outside the facility should be used. The types of activities that are expected in the surrounding areas should be identified. The shielding for radiation protection should be determined based on the distance (d) to the nearest point that needs protection. However, in determining d, it can be assumed that individuals will be at least 30 cm from the shielding wall and 50 cm above a floor that is over the accelerator room. For areas that are beneath an accelerator room, d should be measured to a point that is 2 m above the floor. In facilities that have several accelerators, account should be taken for the radiation dose from each unit.

For many applications, accelerators are mounted on rotational gantries, or are otherwise designed so that the distance from the source (target) to the barriers depends on orientation or position. For units that rotate about a fixed axis, the distance (d) in the primary beam is fixed and U can be utilized to take into account the fraction of time that the beam is directed at any single barrier. For other mountings, such as crane-mounted radiography units or robotically controlled units, the distance (d) in the primary beam may be highly variable, and the determination of an effective value may be very uncertain. In this case, the shield thickness should be based on the minimum distance (d) that can be achieved.

The approach to designing an adequate shield is detailed in NCRP Report No. 49 (NCRP, 1976a) and is summarized here. If no shielding is provided, the average weekly dose at a distance (d) from the target in the direction of the useful beam is:

$$H_{\text{unshielded}} = \text{WUT}/d^2. \tag{4.15}$$

A barrier of thickness (x) that is interposed between the target and an observer reduces the dose in accordance with a transmission factor [T(x)] (reciprocal of the attenuation factor), associated with that barrier:

$$H_{\text{shielded}} = \text{T}(x)\, H_{\text{unshielded}}. \tag{4.16}$$

If the design goal for the weekly dose is H_{m}, the required transmission factor for the shield barrier is:

$$\text{T}(x) = H_{\text{m}}d^2/(\text{WUT}). \tag{4.17}$$

The required shield thickness can be determined from T(x) by using the information found in Figures 4.2 and 4.4, and in Table 4.2. An additional safety factor may be applied to the results of these calculations to reflect the uncertainties in the assumptions and the radiation-protection philosophy of the facility management.

4.6.3 *Secondary Barriers for Photons*

Secondary barriers are those toward which the useful beam cannot be directed. Two sources of photon radiation must be considered in the design of these barriers: bremsstrahlung at wide angles (leakage radiation) and photons that are scattered from objects that are placed in the direct beam.

4.6.3.1 *Leakage Radiation.* For accelerators that are manufactured for use in radiation therapy or industrial radiography, shielding is installed around the electron target to reduce the leakage radiation to a small fraction of the radiation in the primary beam (measured at the same distance from the target). The manufacturer will usually provide information about the dose rate from leakage radiation.

The energy spectrum of the leakage photons is generally of lower average energy than that of the primary-beam spectrum, but considerably higher than that for the spectrum of scattered photons. A conservative assumption is that the transmission of photons at 90 degrees to the primary beam is the same as the transmission of photons produced by electrons of $2 E_0/3$ (Coleman, 1975) (Table 4.2). However, in the absence of information about the specific accelerator, it is prudent to assume that the leakage radiation transmission factors are the same as those for the primary radiation.

For research and industrial installations, the characteristics of unshielded large-angle bremsstrahlung can be estimated from the data given in Figures 3.5 and 3.6. Although these figures are now quite old, there are no more recent data that would change the values given.

4.6.3.2 *Scattered Photons.* Photons scattered by objects in the direct bremsstrahlung beam should be considered when estimating the thickness of the shielding barrier, as well as in the design of labyrinths and ducts (Section 4.11). In general, photons scattered at large angles relative to the primary beam will have energies that are much lower than the leakage radiation, while their intensity will be of the same order of magnitude, or less. Consequently, the scattered photons will seldom determine the shield thickness.

A practical expression for the unshielded dose-equivalent rate of radiation scattered from objects in the direct bremsstrahlung beam is:

$$H_{\text{unshielded}} = \alpha A W T/(d_i d_s)^2 \qquad (4.18)$$

in which the factor, W/d_i^2, expresses the photon dose rate at the scattering surface. It is convenient to express H in Sv week^{-1}, W in Sv m^2 week^{-1}, d_i and d_s both in meters, and the area of the beam at

the scattering surface A in m². The differential dose albedo (α) is dimensionless (Figure 4.12). Two scattering surfaces must be considered in the specification of A, the patient or irradiated object and the wall behind the patient. Regardless of the orientation of the irradiated surface, the beam area (A) is determined in the plane perpendicular to the incident beam direction. For a therapeutic facility, a field size of 0.030 m² (corresponding, *e.g.*, to a 15 × 20 cm² treatment field) at d_i = 1 m is adequately conservative for typical use (Figure 4.17). For a radiographic unit, the largest area obtainable from the equipment at the distance in question should generally be assumed.

4.6.4 *Shielding Against Neutrons*

The dose-equivalent rate from photoneutrons produced in an unshielded target is significantly less than that from the bremsstrahlung photons. Furthermore, the equilibrium attenuation length ($\rho\lambda$) in concrete lies in a narrow range (30 to 35 g cm⁻²) for neutron energies up to 30 MeV (Figure 4.8). Thus, the tenth-value layer ($\rho\lambda_T$) for neutrons has a value between 75 and 85 g cm⁻², whereas $\rho\lambda_T$ for the bremsstrahlung photons lies between 90 and 130 g cm⁻² for the spectra produced by incident electron energies above 10 MeV (Figure 4.3). For this reason, and because of the relative production dose rates of bremsstrahlung and neutrons, conventional electron accelerator facilities in this energy region that are adequately shielded with concrete for bremsstrahlung photons will also generally be adequately shielded for neutrons. However, the following reservations must be added:

1. If materials such as steel or lead are used in the structural shielding, the shield configuration and the concrete thickness should be evaluated for adequate protection against neutrons.
2. In a situation where the electron target is sufficiently well shielded for bremsstrahlung, it may also be necessary to evaluate the shield thickness for protection against neutrons.
3. Neutrons may stream through labyrinths and other openings in otherwise well-designed shielding.
4. For facilities with roofs which are significantly thinner than the walls, neutron skyshine should be evaluated.
5. Radiation doors of materials other than concrete should be evaluated for neutron leakage.

At installations operating above ~10 MeV, the labyrinth door (Section 4.11) should be designed for protection against neutrons.

NCRP Report No. 79 (NCRP, 1984) is a good resource for the design of radiation-therapy facilities for protection against neutron radiation.

Neutrons, like photons, are attenuated approximately exponentially through thick shielding barriers. Capture gamma rays, released within the shielding material when neutrons are absorbed, contribute to the dose equivalent at the outside surface of the barrier. Information about these capture gamma rays may be found in NCRP Report No. 38 (Appendix D, Table 6 of NCRP, 1971).

The photonuclear interaction in the giant-resonance region is the most important source of neutrons for electron accelerators operating at energies <100 MeV. Neutron yields may be estimated from data given in Figure 3.12 for the energy, target material, and beam power anticipated. The production of photoneutrons is nearly isotropic. However, the energy spectrum and intensity of the neutrons in the primary photon beam is different from that of the neutrons outside the beam because of the shielding that is usually installed in the head of the accelerator around the target and collimators.

For bremsstrahlung energies above ~15 MeV, a conservative estimate of neutron yield is 2×10^{12} s^{-1} kW^{-1} of electron beam power incident on a high-Z target (IAEA, 1979a). Therapy machine manufacturers can provide the ratio of neutron dose equivalent to useful beam dose. The neutron contribution to the absorbed dose at 1 m from the target can be as much as 0.05 percent of that due to the useful photon beam. If a Q of 10 is assumed, this contribution could be as much as 0.5 percent, *i.e.*, five times the usual photon leakage specification.

In order to treat the neutron component in a manner consistent with the method outlined previously for photons, it is convenient to begin with an estimate of the neutron fluence rate ($d\phi/dt$) at a distance of 1 m from the electron target in units of cm^{-2} week^{-1} m^2, where the unit, m^2, implies an inverse-square dependence of the unshielded neutron fluence rate on distance. This should be estimated for the direction in question and for the average accelerator operating schedule per 40 h work week. In the following, the estimate of ϕ plays a role analogous to that of the workload (W).

The required dose-equivalent transmission factor for neutrons can be derived using:

$$H_n = H_m/(T\Sigma \ [(d\phi/dt)U_i/d^2], \qquad (4.19)$$

where:

H_n =   coefficient (Sv cm^2 n^1) relating the neutron dose-equivalent at the location in question to the unshielded neutron fluence

$\mathrm{d}\phi/\mathrm{d}t$ = neutron fluence rate at the standard distance of 1 m from the target in the direction in question (n cm^2 week^{-1} m^2)

d = distance between the neutron source and the location to be protected (meters)

H_m = maximal permissible dose-equivalent rate for the type of area (Sv week^{-1})

U = orientation (use) factor, the summation is over all machine orientations

Equation 4.19 resembles Equation 4.17 except that $\mathrm{d}\phi/\mathrm{d}t$ is used in place of the workload (W) and, therefore, H_n has a different meaning than the transmission factor [T(x)] of Equation 4.17; H_n contains the fluence-to-dose-equivalent conversion based on the spectrum at the shielding depth in question.

The thickness of concrete required to achieve the desired neutron transmission can be determined from graphs such as those in Figures 4.7 and 4.10. Alternatively, the TVL can be used to estimate the thickness of material needed to achieve the desired reduction in dose equivalent (Figures 4.6 and 4.10, Table 4.3).

4.7 Shielding of Large Electron Accelerator Facilities at Higher Energies (E > 100 MeV)

The shielding data for electron accelerators, which operate above 100 MeV, are not so well-known as those for energies below 100 MeV. However, at these high energies where the electromagnetic cascade plays an important role in the transport of energy, the attenuation parameters for shielding materials vary rather slowly with incident electron energy and eventually become almost independent of energy. From a shielding perspective, the most important radiation sources are bremsstrahlung photons and neutrons. It is most important that Section 3, The Sources of Ionizing Radiation from Accelerators, be read in conjunction with Section 4.

4.7.1 *Review of Source Terms*

4.7.1.1 *Electromagnetic Cascade.* When a high-energy electron beam strikes a target, an electromagnetic cascade develops (Section 3.3). Extensive experimental studies and Monte-Carlo calculations have been carried out. Figure 3.15 shows the fraction of total energy deposited by a cascade shower versus depth integrated over all radii.

The parameters used to specify the electromagnetic cascade are the radiation length (X_0) and the Moliere length (X_M) applicable to scattering of the cascade to the side (Section 3.3.6). If the incident electron energy is increased by a factor of e, the peak of the longitudinal distribution moves deeper into the shield by about one radiation length. The fraction of energy escaping the sides of finite radius cylinders (which are essentially infinitely long) can be estimated from Figure 3.16 (De Staebler *et al.*, 1968) for all materials and energies, where the radius is given in Moliere units.

Bathow *et al.* (1970) have performed precise TLD measurements of both the longitudinal and lateral development of 6 GeV electromagnetic cascades in aluminum, copper and lead. As an example of the use to which these data may be put, the isopleths of absorbed dose shown in Figure 4.18 were applied to the design of lead apertures along the beamlines of the Brookhaven National Laboratory National Synchrotron Light Source. Based on expected loss scenarios, shields which enclosed the 30 fGy electron^{-1} isopleth for the smaller storage ring and the 16 fGy electron^{-1} isopleth for the larger storage ring were required.

4.7.1.2 *Neutron Source Terms and Attenuation.* At electron accelerators, neutrons are produced by interactions of the bremsstrahlung photons with the shielding material. The cross sections for the production of neutrons are schematically shown as a function of photon energy in Figure 4.19. The variation of cross sections with energy may be conveniently explained by considering the three energy realms identified in the figure.

Above the threshold of ~4 MeV for heavy nuclei and ~12 MeV for light nuclei, evaporation neutrons are produced through the giant-resonance process wherein a photon interacts with a nucleus producing an excited compound nucleus that de-excites by the evaporation of a neutron the energy of which follows a Maxwellian energy distribution up to ~8 MeV. Figure 3.12 gives the giant-resonance neutron yield which is isotropic in the laboratory system for different thick targets for the energy range from ~10 to 100 MeV. Above 100 MeV, for thick targets this yield (Y) is independent of energy and can be calculated from Equation 3.17 as modified by Mao *et al.* (1996):

$$Y = 8 \times 10^{-6}(Z^{1/2} + 0.12\ Z^{3/2}$$
$$-\ 0.001\ Z^{5/2})\ \text{n electron}^{-1}\ \text{MeV}^{-1}. \qquad (4.20)$$

For thin targets in the same energy range, Mao *et al.* (1996) propose the following relationship:

$$Y = 8 \times 10^{-4}(1 + 0.12\ Z$$
$$-\ 0.001\ Z^2)\ (T^2/E_0)(1 + 0.04/T), \qquad (4.21)$$
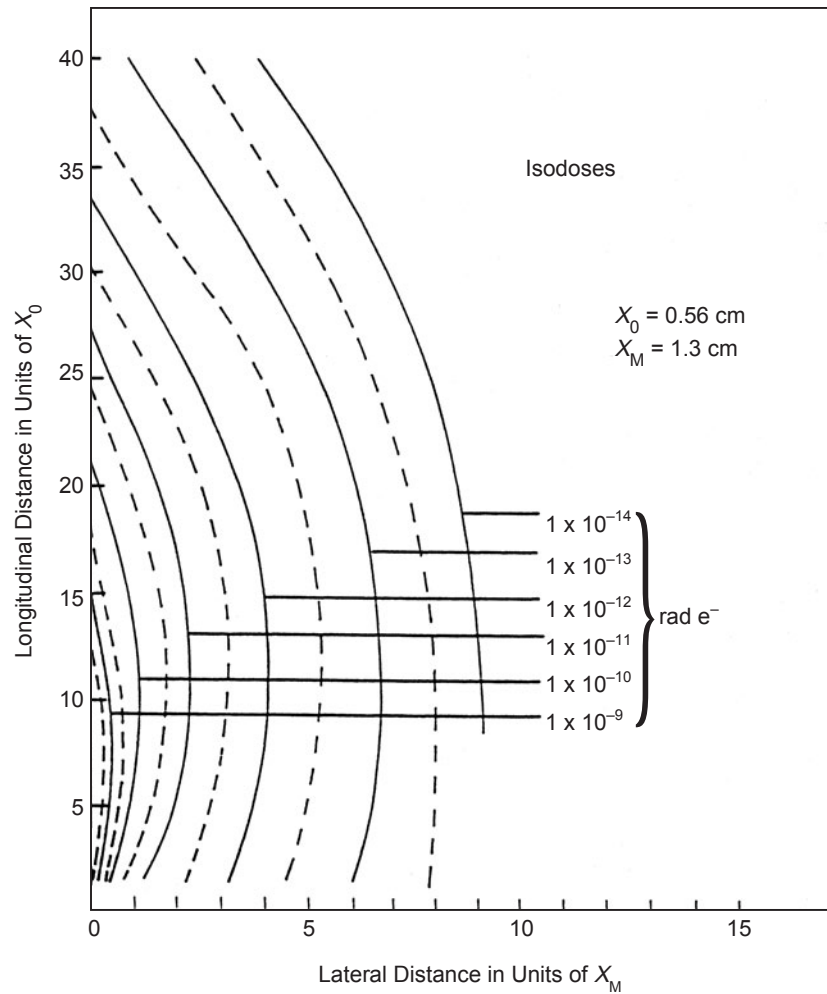
Fig. 4.18. Isopleths for absorbed dose (in units of rad per incident electron) in lead based on measurements of the longitudinal and lateral development of 6 GeV electromagnetic cascades (Bathow *et al.*, 1969). The ordinate is the longitudinal distance parallel to the incident beam direction in units of radiation length (X_0). The abscissa is the lateral distance from the incident beam direction in units of Moliere length (X_M).

where:

E_0 = electron energy in mega-electron volts
T = target thickness in numbers of relaxation lengths
Z = atomic number
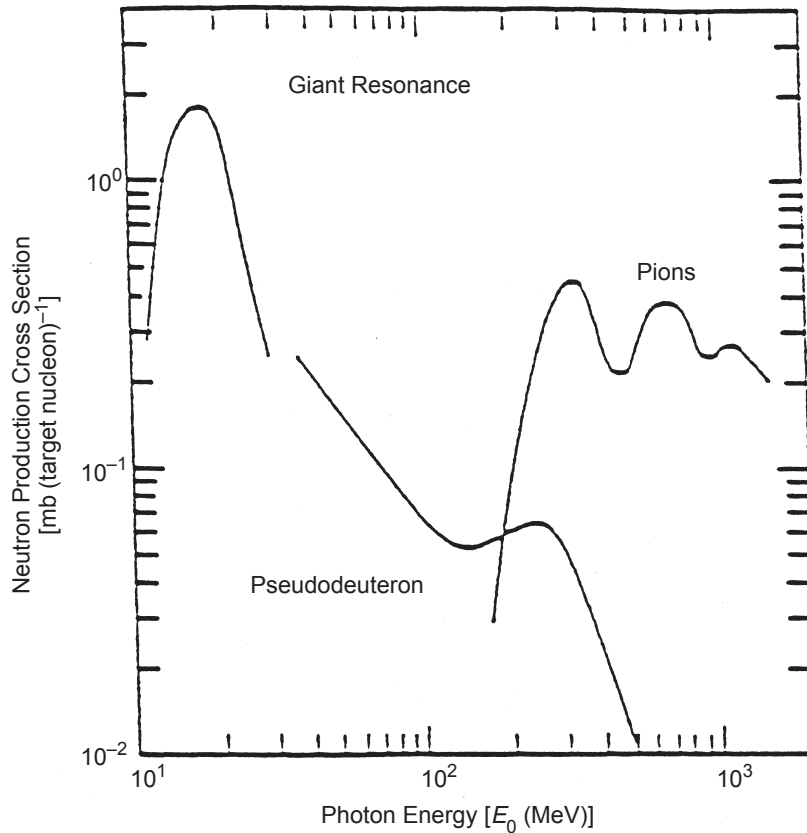
Fig. 4.19. The neutron production cross section versus photon energy. The three principal production mechanisms are separately shown (Section 4.7.1.2).

Above photon energies of ~25 MeV, the absorption of the photon by a proton-neutron pair in the nucleus (the quasi-deuteron model) produces neutrons with energy between 10 and 100 MeV.

At photon energies above ~200 MeV, a photon can interact with a nucleon to produce a pion plus a high-energy neutron while above 400 MeV, the photon may interact with a nucleon pair to produce two pions and a neutron. In addition, a photon interacting with a nucleon pair may eject two nucleons, either or both of which may be neutrons.

In many cases, it is not necessary to calculate the source strength of the neutrons produced by the quasi-deuteron process because the shielding is usually dominated by photons and by giant-resonance

neutrons at small shield thicknesses, and by high-energy neutrons at large shield thicknesses. However, this mid-energy term could be important for concrete shields about a meter thick or for sandwich shields involving lead for photon attenuation and for completeness it is given here. This term is often taken into account by making small adjustments in the low- and high-energy source terms. The neutron yield at high electron energy (~10 GeV) is given by:

$$Y = \left(\frac{3.1 \times 10^{-3}}{1 - 0.75 \cos \Theta} \right) \text{sr}^{-1} \text{ GeV}^{-1} \text{ electron}^{-1}. \qquad (4.22)$$

The yield of high-energy neutrons from a copper target as a function of production angle (Jenkins, 1979) is shown in Figure 4.20. For targets other than copper, the yield can be estimated by multiplying by the production cross section of the material relative to that of copper, $14.9/A^{0.65}$, where A is the atomic mass of the target material. For example:

$$Y = \frac{1.5 \times 10^{-4}}{(1 - 0.72 \cos \Theta)^2} \left(\frac{14.9}{A^{0.65}} \right) \text{sr}^{-1} \text{ GeV}^{-1} \text{ electron}^{-1}. \qquad (4.23)$$

This equation will estimate the yield within 10 percent for elements between aluminum and lead.

Most shielding studies for high-energy electron accelerators have concentrated on the high-energy neutron component because it is the most penetrating (Figure 4.6). Deep in the shield, the neutron spectrum will reach an equilibrium level that is driven and maintained by the interactions of these high-energy neutrons. Under equilibrium conditions, a single fluence-to-dose conversion coefficient can be used. At electron accelerators, there will be cases where thin shields are adequate to reduce overall radiation intensities to an acceptable level, but not thick enough for the neutron spectrum to have reached equilibrium. Experience shows that in such cases, the neutrons may be treated in only two or three neutron energy groups.

After losing energy and having been slowed down, neutrons are absorbed often emitting so-called "capture" gamma rays. Based on his measurements at SLAC, Jenkins (1979) has suggested the addition of a term to the bremsstrahlung formula which accounts for the most penetrating neutron component that gives rise to these "capture" gamma rays, but which is of importance only for very thick shields.

The neutron yields given in Equations 4.22 and 4.23 apply to electrons with energy above 10 GeV. In planning for the LEP facility at CERN, the intermediate- and high-energy neutron yields as a function of electron energy were summarized (Figure 4.21) (Goebel,
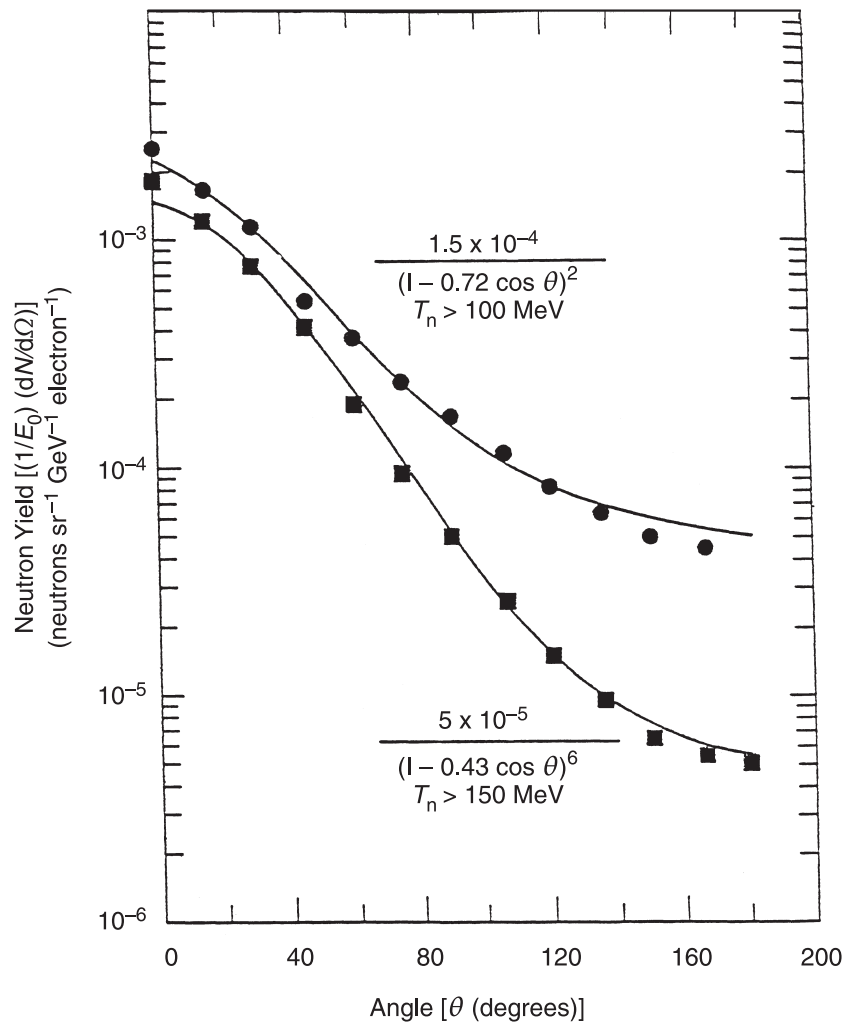
Fig. 4.20. Yield of photo-produced neutrons from a copper target per steradian as a function of angle (Θ). Refer to text for calculation of neutron yields from other targets.

1987). For lower-energy electron beams, these source terms can be scaled using the relative yield data of Figure 4.21. At high energy (>10 GeV), the yield depends only on beam power and is, thus, directly proportional to electron energy.

4.7.2 *Design of High-Intensity Beam Stops and Walls*

The following approximate procedure is suggested for planning the shielding of a target or beam dump for high-energy electrons.
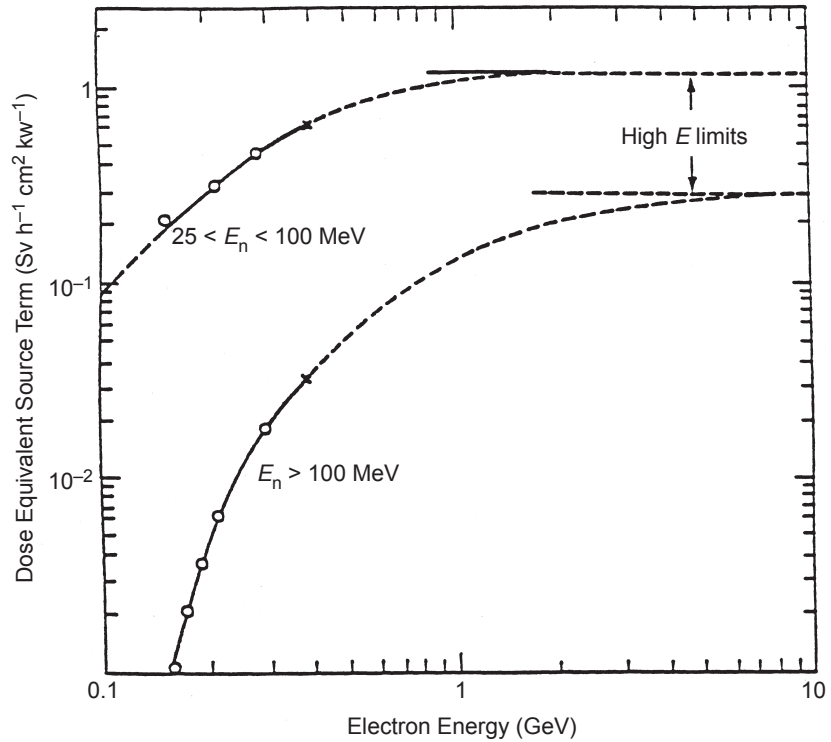
Fig. 4.21. Effective source terms as a function of electron energy for a thick-copper target for neutrons of energy 25 to 100 MeV and for neutrons of energy greater than 100 MeV.

1. Design the beam dump to be capable of thermally dissipating the entire power in the electron beam. The dump should be at least 15 radiation lengths $(15\,X_0)$ long and provide an adequate radial margin about the beam area.
2. For bremsstrahlung in the forward (zero degrees) direction, extrapolate the absorbed dose curve shown in Figure 3.5 to the desired energy [E_0 (in mega-electron volts)], by scaling the absorbed dose per unit beam power as if it were proportional to E_0:

$$(\mathrm{d}D/\mathrm{d}t) \sim 300\,E_0\ \mathrm{Gy}\quad \mathrm{m^2\,h^{-1}\,kW^{-1}}. \tag{4.24}$$

3. Determine the total shielding requirements in terms of TVLs (n_{λ_T}) by means of Equation 4.17 after substituting $\mathrm{d}D/\mathrm{d}t$ in the appropriate units for W.

4. In determining the effective length of the beam dump, the distance required to achieve shower maximum, ~5 to 6 X_0 should be subtracted from the total length of the dump. Convert the length of the beam dump into multiples of λ_T, assuming the values shown in Figure 4.1 (dashed curve). Call this value $n_{\lambda_{BD}}$.

5. Determine the necessary amount of additional shielding of the chosen material or combination of materials using the equation $n_{BARRIER} = n_{\lambda_T} - n_{\lambda_{BD}}$, assuming values taken from Figure 4.1 (dashed curve).

6. For shielding at 90 degrees, the absorbed-dose rate is essentially constant (Figure 3.5) at:

$$(\mathrm{d}D/\mathrm{d}t) = 50 \text{ Gy} \quad \mathrm{m^2 \ h^{-1} \ kW^{-1}}. \qquad (4.25)$$

Follow the same procedure as used for the calculation of shielding in the forward direction. To account approximately for the absorption of the beam dump, use the beam-dump radial margin about the beam as in the manner described in Step 5.

If the same beam dump is not always used, it is conservative to assume $n_{\lambda_{BD}} = 0$ for Steps 5 and 6, regardless of what is actually installed. Any location where the beam can strike should be shielded in the same manner.

4.7.3 *Distributed Loss Issues*

There are two tasks in specifying source strengths. The first is to determine the location and extent of accelerator beam losses. The second is to characterize the source itself by the nature and intensity of the interactions of the lost beam with any material surrounding the point of loss.

The approach of Section 4.7.2 is quite useful for a point-loss situation such as a beam stop. However, not all beam is lost at the beam stops. For much of an accelerator facility, the beam lost in a section is usually a small fraction of that which passes through it. Moreover, some beam will be lost in places not surrounded by accelerator hardware, and we may not describe the loss region as a "thick target." Thus the issue at many facilities is how to deal with many sources of relatively low intensity, which are characterized as "thin" or "intermediate" sources and distributed over large spatial regions. This is particularly true for the latest generation of electron accelerators/storage rings which are used to produce synchrotron radiation between the infrared and x-ray frequency ranges.

4.7.3.1 *Synchrotron-Radiation Facilities.* Over the past 30 y, many electron storage rings have been constructed and applied to studies using synchrotron radiation (Winick, 1994). A synchrotron radiation facility is typically composed of an injector and a storage ring. The injector consists of one or more electron accelerators—a common setup is a linac followed by a synchrotron. The injector supplies electrons to the storage ring where they are re-circulated or "stored." A storage ring is configured as a set of curves connected by straight sections. When a bending magnet deflects the stored electron beam, synchrotron radiation is emitted tangentially to the electron (or positron) path, creating a "fan" of radiation in the plane of the ring. This radiation is channeled to experimental areas using beam lines that are tangential to the storage ring. A small section of a storage ring with a schematic representation of major components is presented in Figure 4.22.

In addition to bending magnets, new generations of synchrotron facilities use "insertion devices," so-called wigglers or undulators. An insertion device consists of a linear array of magnets with alternating polarities that make electrons wiggle or undulate along the axis of the device, tremendously enhancing the intensity of synchrotron
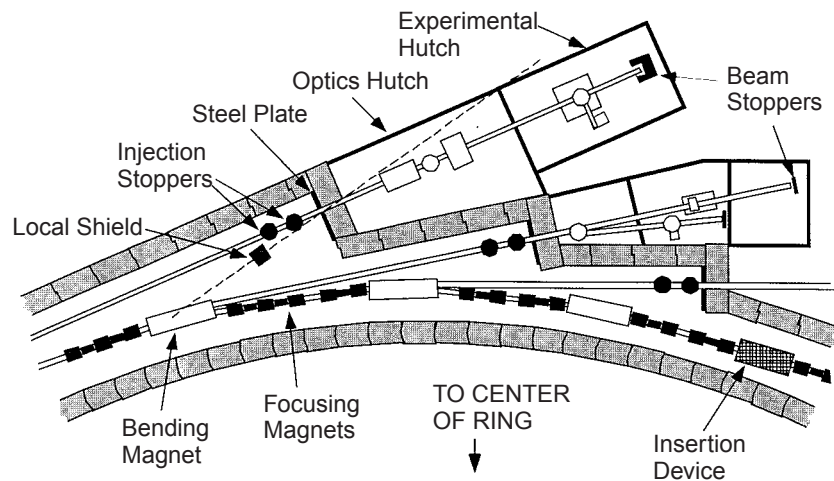
Fig. 4.22. Schematic view of a section of a storage ring with three synchrotron-light beam lines. The dashed indicates a possible path for bremsstrahlung from a beam loss through the penetration in the shielding that is mitigated by a local shield mask. Optics hutches contain mirror and crystal optical devices, such as monochromators, while experimental hutches or shacks contain user instrumentation. More massive beam stoppers are required where gas bremsstrahlung is present.

radiation emitted in that direction. Many electron storage rings operate in the electron energy range from hundreds of mega-electron volts to a few giga-electron volts. High-energy facilities such as ESRF (6 GeV) in France, APS (7 GeV) in the United States, or SPRING-8 (8 GeV) in Japan are capable of producing hard x rays up to approximately 100 keV.

The lifetime of the stored beam in a modern storage ring can exceed 24 h. A typical operational pattern, therefore, consists of long periods of circulating stored beam alternating with short injection events. When designing shielding for a synchrotron facility, one must consider beam-loss scenarios and other sources of radiation under these two distinct modes of operation. However, shielding is more likely to be dictated by injection losses than by stored-beam operations. In both cases, normal operations as well as mis-steering and accident scenarios need to be considered.

Only a portion of the injected current is captured in the ring. The capture-to-injection ratio will depend on the facility, and partially on operator skills, 50 percent is a realistic first-order estimate. Major injection beam losses usually occur in the injector-to-ring beam line. Devices such as injection septa or pulsed injection magnets are the usual culprits and may require additional local shielding. The same applies to insertable diagnostic devices, *e.g.*, Faraday cups and screens that need to be used for a fraction of the injection time.

Additional injection losses occur in the ring while the beam orbit is being tuned. These losses are distributed around the ring, often unevenly, due to variations in apertures of the beam-line devices and specific features of beam-line optics.

Dose rates resulting from normal injection losses or mis-steering of the injection beam can be protracted in time, as long as the injector supplies electrons. In the stored-beam mode, the amount of electron loss is inherently limited by the storage capacity of the ring. Typical values of stored current at synchrotron facilities range between 100 to 300 mA. A 200 mA stored beam in a medium-size ring with a circumference of 120 m is maintained by a circulating charge of only 8 nC, or 5×10^{10} electrons. During the slow decay of the stored beam, the low and distributed electron losses result in negligible dose rates. If the stored charge is lost instantaneously in a distributed fashion, the integrated dose at any single point behind shielding of the ring is also likely to be negligible. It is useful to remember that an approximately equal charge is lost, often in a more localized fashion, during the short injection time. Shielding designed to attenuate dose rates from injection losses will, therefore, be adequate for a stored beam loss.

Bremsstrahlung yields in the forward direction are substantially higher than at 90 degrees. This may be somewhat compensated by the fact that a forward ray will hit the straight lateral section of the ring shielding (Figure 4.22) at a greater distance from the source and pass through a considerably higher thickness of concrete than a ray at 90 degrees. However, the latter effect is not true for the short portion of the ratchet wall design that is perpendicular to the synchrotron beam line. This section usually requires a thicker shielding. Because space is very precious in these areas, steel or lead shielding is often used in front of the concrete wall, rather than adding more concrete. It should be noted that simple geometric shield models may prove quite inadequate for design of storage-ring shielding (Moe, 1991). Monte Carlo codes discussed in Section 4.2.2 would be best suited for complex geometries.

Among specific shielding constraints at synchrotron storage rings is the need for straight penetrations for synchrotron-light beam lines. Local shielding masks may be necessary to shadow these penetrations from forward bremsstrahlung and neutrons, as indicated in Figure 4.22. In the injection mode, injection stoppers, typically preceded by a massive water-cooled copper heat mask, protect the penetration against accidental mis-steering of the electron beam into the synchrotron light pipe and against forward bremsstrahlung from beam losses. However, in stored-beam operation, injection stoppers are removed to allow the synchrotron light through. The synchrotron light pipe is, therefore, open also to gas bremsstrahlung generated by interaction of the stored electron beam with residual air in the ring vacuum chamber. The intensity of gas bremsstrahlung is proportional to the length of the air column in the straight section of the ring, which is in line with the synchrotron beam line. Therefore, the problem of gas bremsstrahlung is more acute for linear insertion devices. Gas bremsstrahlung is substantially more penetrating than any kind of synchrotron light. It, therefore, must be considered when designing shielding for the optics and experimental hutches. If the synchrotron light is not sufficiently deflected in the optics hutch and the beam pipe remains in line with bremsstrahlung, a massive beam stop for bremsstrahlung is needed in the experimental hutch. When mirrors or monochromators deflect synchrotron light horizontally or vertically, local lead shielding behind these devices in the optics hutch may be needed to stop gas bremsstrahlung. In either case, high-intensity gas bremsstrahlung may generate measurable levels of photo-neutrons in the high-Z stopper material.

Problems with straight penetrations are further escalated if the facility uses the "top-off" injection mode. In this mode, the stored-beam operation is not interrupted to allow injection. Instead, the

stored charge is replenished by frequent (or continuous) injections as needed while synchrotron lines are open. In this case, there are no injection stoppers to protect against mis-steering of electrons into the synchrotron beam line and against zero-degree bremsstrahlung from accidental beam loses. Both of these scenarios would lead to substantially higher radiation levels behind the shielding penetration than those from gas bremsstrahlung. Consequently, the "top-off" mode will likely require a more conservative approach to shielding design, coupled with a higher degree of redundancy in safety systems.

Another specific feature of synchrotron storage rings is the high occupancy in the immediate vicinity of the outer shielding wall. Experiment control, data acquisition and analysis are performed from stations located near the beam lines, often against the outside shielding walls of the ring or experimental and optics hutches. Modern storage rings are extremely bright sources of synchrotron light. Around soft and hard x-ray beam lines, very high radiation levels may be present in the optics and experimental hutches from radiation scattered off optical elements and instrumentation. Extreme care must be taken in shielding design to avoid streaming through ventilation and cable penetrations and under doors. Two codes specifically designed for synchrotron radiation shielding are available: PHOTON (Chapman, 1988) and the more recent STAC8 (Asano and Sasamoto, 1994), which includes buildup factors and polarization.

In space-saving optimized shielding designs, the concrete walls, used in combination with high-Z materials or alone, may not be thick enough to fully attenuate giant-resonance neutrons. This component needs to be explicitly considered in shielding calculations, because the assumption of an equilibrium spectrum is no longer valid. Nonequilibrium neutron spectra around the Stanford Synchrotron Radiation Laboratory have been measured by Vylet *et al.* (1997a; 1997b).

4.7.3.2 *Photon Shielding Experiments.* Jenkins (1979) at SLAC has provided empirical equations to describe the results important for shielding high-energy electron accelerators. The angular yield of photons from a thick-copper target ($15\,X_0$) bombarded by an electron beam is shown in Figure 3.9. For normally incident electrons with energies above a few hundred mega-electron volts, an empirical fit for the large angles of the form $e^{-\Theta/72}$ with Θ in degrees, can be used.

For thick targets (*i.e.*, beyond the shower maximum), the energy in the electromagnetic cascade is predominantly carried by photons at the minimum of the mass energy absorption curve, as shown in Figure 4.23. Thus, to a first approximation, the bremsstrahlung yield in the forward direction can be scaled to target thicknesses greater
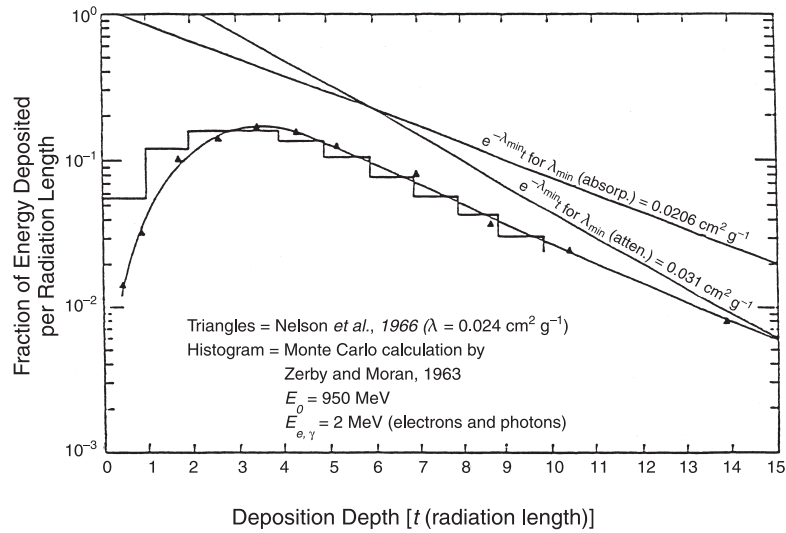
Fig. 4.23. Longitudinal energy deposition in lead. Comparison of the results of Nelson *et al.* (1966) with a Monte-Carlo calculation; $X_0 = 6.4$ g cm^{-2}, $\rho = 11.35$ g cm^{-3}.

than 15 X_0 using the value of the minimum absorption coefficient for the material.

Dinter and Tesch (1977) have measured the angular distributions of electron and photon stray radiation with ^{7}LiF TLD around 0.2, 1, 5 and 10 cm thick iron targets at various angles to the beam (Section 3.3.3.2).

The distributions shown in Figure 3.10 have a strong forward peak, particularly for thin targets. Absorption in the target causes a sharp dip at some angles. Dinter and Tesch also measured the attenuation of this radiation for lead and iron, as shown in Figure 4.24, and showed that it could be described by:

$$D(\Theta,t) = D_{\mathrm{t}}(\Theta) \, A_{\mathrm{t}} \, \mathrm{e}^{-\lambda t} \qquad (4.26)$$

where the parameters Θ and ϕ are shown in Figure 3.10 and their values and those of t and A_{t} are shown in Table 4.5.

Because the energy deep in an electromagnetic cascade is carried by photons at the minimum of the absorption curve, shielding should be designed for photons of those energies. A removal mean-free-path of 38 and 42 g cm^{-2} can be assigned to steel and concrete, respectively. The fast drop for the small thicknesses and severe attenuation by the target observed in Figure 3.10, is explained by low-energy electrons and positrons coming from the target. A Monte-Carlo simulation using the EGS code for electrons incident on a thick target
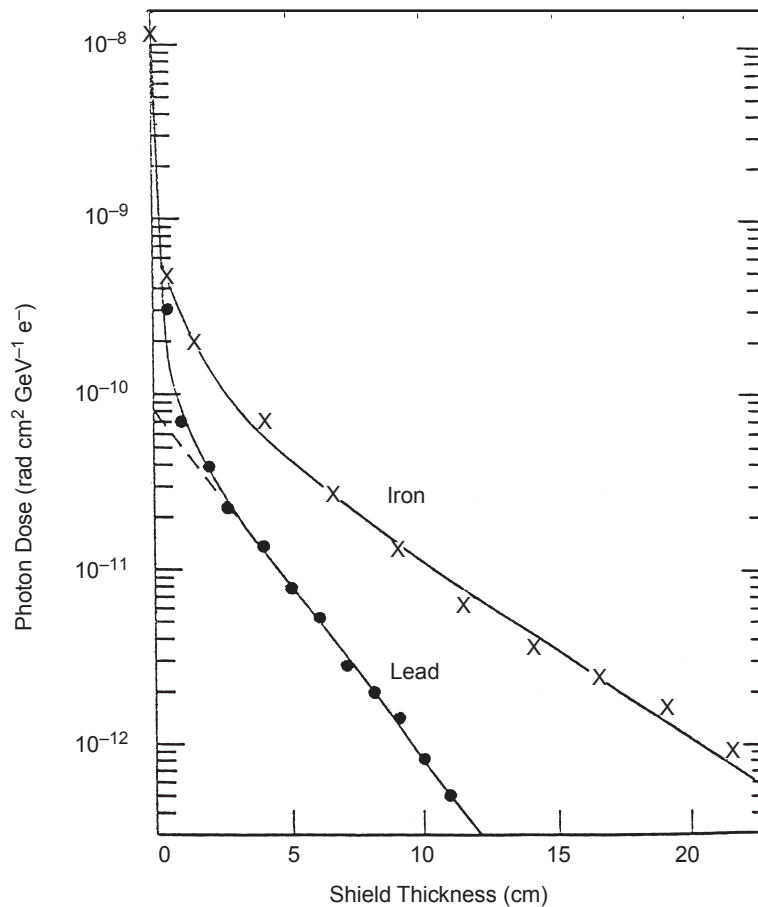
Fig. 4.24. Photon dose in the forward direction for iron and lead as a function of shield thickness for 5 GeV incident electrons (Dinter and Tesch, 1977).

clearly demonstrates that electron-positron pairs are the major contributor to dose in unshielded geometries (Figure 4.25).

As part of the design for LEP at CERN, the EGS calculations shown in Figure 3.11 were carried out for 200 MeV electrons striking 1 cm diameter tantalum targets 2, 4 or 10 radiation lengths long. These calculations of dose in 5 cm thick polyethylene use a thick target to provide scatter, but provide little side shielding and are consistent with the measurements of Dinter and Tesch (1977). The large-angle bremsstrahlung radiation depends very much on the

TABLE 4.5—*Shielding parameters measured by Dinter and Tesch (1977) for use in Equation 4.26.*

(a) *Attenuation Coefficients (cm⁻¹)*

Shielding Material	Density (g cm⁻²)	Shielding to Absorb Low-Energy Component x_A (cm)	$d = 0.2$ cm $\phi = -2°$ $\theta = -90°$	$d = 0.2$ cm $\phi = -2°$ $\theta = +30°$	$d = 10$ cm $\phi = 90°$ $\theta = -90°$	Minimal Absorption Coefficient	Recommended Value
Lead	11.3	2	0.47	0.46		0.47	0.47
Iron	7.8	6	0.23	0.23		0.23	0.23
Heavy concrete	3.7	20	0.086	0.085	0.089	0.093	0.080
Ordinary concrete	2.4	25	0.056	0.061		0.048	0.055
Sand	1.3	50	0.025			0.026	0.025

(b) *Absorption Factor (A_t)*

t (cm)	ϕ (degrees)	A_t	
		$\theta = +30°$	$\theta = +90°$
0.2	−1	0.053	0.0077
	−5	0.036	0.012
	−12	0.037	0.007
	90		
	Mean	0.04	0.009
1	−2	0.24	0.023
	−5	0.11	0.013
	−12	0.07	~0.01
	Mean	0.1	0.02
5	−5	1.0	0.18
	+5	0.51	0.038
	+12	1.0	0.18
	90	0.8	0.1
	Mean	0.17	0.040
10	−12	1.0	0.42
	+12	1.0	0.11
	12	1.0	0.3
	90		
	Mean	0.24	0.027

Fig. 4.25. Angular distribution of absorbed dose about a thick target irradiated by 2 GeV electrons. The solid and open circles show experimental data at glancing incidence angles of 1.5 and 3 degrees, respectively. The three histograms show a comparison with Monte-Carlo calculations using the EGS code.

target/shield arrangement. For the thinnest target, the zero degree peak is evident and the large-angle scatter is fairly weak.

4.7.3.3 *Generalized Loss Model.* The previous information can be combined into a shielding recipe. For a point loss, the point kernel technique of Equation 4.9 is used for each type of radiation. The total dose equivalent is, then, the sum over all radiation types and the integral over all losses. Table 4.6 lists the neutron radiation

TABLE 4.6—*Attenuation lengths for different neutron energy-groups (adapted from Swanson, 1979).*

Shielding Material	Giant-Resonance Neutrons (g cm^{-2})	Mid-Energy Neutrons (g cm^{-2})	High-Energy Neutrons (g cm^{-2})	Scattered Neutrons (g cm^{-2})
Iron	100	138	138	NU[a]
Lead	NU	NU	NU	—
Concrete	30	55	120	20
Polyethylene	7	20	70	5

[a] NU = not useful.

attenuation lengths (λ_i) used for the different materials. In a sandwich shield of several materials, each material will contribute an exponential attenuation term.

The source terms H_i [(Sv m^2 e^{-1}) $\times$ 10^{-17}] are:

$$H_{gr} = 90\ E,\ \text{giant-resonance neutrons} \tag{4.27}$$

$$H_{ni} = 10\ \text{R}\ E/(1 - 0.75\ \cos \Theta),$$
$$\text{intermediate-energy neutrons} \tag{4.28}$$

$$H_{nh} = \text{R}\ E/(1 - 0.72\ \cos \Theta)^2,\ \text{high-energy neutrons} \tag{4.29}$$

$$H_{br} = E\ [(1.33 \times 10^6)\ E\ e^{-1000\ E\Theta/2.51}$$
$$+\ (1.33 \times 10^5)\ e^{-\Theta/0.159}$$
$$+\ (3 \times 10^3)\ e^{-\Theta/0.834}],\ \text{bremsstrahlung} \tag{4.30}$$

where:
   E = primary electron energy (giga-electron volt)
   Θ = angle between the electron momentum and the dose point (radian)
   R = ratio of neutron yield at this energy to the value at the high-energy limit taken from Figure 4.21

The first term of the dominating bremsstrahlung term has a very large forward spike. The bremsstrahlung formula (Equation 4.30), parameterized by Swanson (1985), has been modified to fit the 100 Sv m^2 h^{-1} kW^{-1} source term at 90 degrees used for LEP (Fasso *et al.*, 1984a; 1984b) and the Monte-Carlo calculations with EGS shown in Figure 3.11.

The neutron source is divided into three terms following the work at SLAC by Jenkins (1979). The giant-resonance term of 1 to 25 MeV neutrons is assumed to be generated in lead, to be isotropic in the laboratory system, and to depend only on the electron power lost. The strengths at lower electron energy of the intermediate-energy term (25 to 100 MeV) and the high-energy term (above 100 MeV), assumed to be generated in steel, are reduced from that observed at 15 GeV, by the factor R.

4.8.   Proton Accelerators—Transverse Shielding

The principal concern in lateral shielding of proton accelerators is to attenuate to an acceptable level the neutrons produced by the interaction of the high-energy protons with experimental targets, beam-transport components, the accelerator structure, and the

shield itself. Published experimental and theoretical data in this energy range are mostly for neutrons of energy less than 400 MeV.

The energy region between 400 MeV and 3 GeV is difficult to treat theoretically, because hadron cascade processes have not yet stabilized and experimental data are meager. It is convenient to resort to interpolation between 400 MeV and the "high-energy limit" achieved at proton energies of several giga-electron volts. Estimation of shielding for proton accelerators in this energy range requires a detailed understanding of the production of particles by the interaction of the primary protons, their transport through the shield, and the determination of the energy spectrum of the radiations that penetrate the shield.

At proton energies above 1 to 3 GeV, the lateral shielding (at 90 degrees to the proton beam) and to some extent the longitudinal shielding (*i.e.*, in the direction of the proton beam), may be determined by means of simple models. At these higher energies, simplifications are possible because the attenuation length of high-energy neutrons is independent of neutron energy above ~100 MeV and the yield of high-energy neutrons is roughly proportional to the primary proton energy (E_p) (Thomas and Thomas, 1984). Below 100 MeV, neither of these simplifications may be made: hadron cross sections change rapidly with energy and total high-energy particle yields are no longer even approximately proportional to E_p (Tesch, 1985).

This Section first discusses the particle yields from the proton-nucleus interaction followed by a description of the nuclear processes involved and the angular and energy distributions of the neutrons produced (see also Section 3 for a discussion of particle yields). Finally, methods of calculating shielding in the transverse directions are summarized.

4.8.1 *Particle Yields from the Proton-Nucleus Interaction*

Two nuclear processes are important in determining the yield of particles following proton-nucleus interactions: nuclear evaporation and intranuclear cascades.

At low proton energies, the interaction of a proton with a nucleus is best explained by a compound nucleus model, in which the incident particle is absorbed into the target nucleus to create a new compound nucleus. This compound nucleus is in an excited state with a number of allowed decay channels and with the entrance channel preferred. As the energy of the incident particle increases, the number of levels available to the incident channel becomes very large; there are no longer discrete levels in the quasi-stationary states of the compound

nucleus but rather a complete overlapping of levels inside the nucleus. Under these circumstances, the emission of particles is best described by an evaporation process analogous to the evaporation of a molecule from the surface of a liquid. The energy distribution of emitted neutrons can be described by an equation of the form:

$$n(E) \, dE = a \, E \, e^{-E/\tau}, \tag{4.31}$$

where "a" is a constant and τ is a so-called nuclear temperature (usually having a value between 0.5 and 5 MeV). These evaporated particles are emitted isotropically in the laboratory system, and the energy distribution of the evaporated neutrons extends up to ~8 MeV. Similar equations describe the emission of protons, deuterons, and heavier particles, but the Coulomb barrier suppresses the emission of low-energy charged particles and, if emitted, they are in any event readily stopped near their point of emission. Charged particles produced by evaporation are, therefore, unimportant in determining shielding thickness.

Evaporation neutrons produced by interactions near the source contribute to dose inside the shield or to leakage dose through doorways or openings. Because they are more strongly attenuated (Figure 4.8), they do not usually contribute to dose outside a shield. Tesch (1985) points out that, for 75 MeV protons incident upon 40 cm of concrete, a 3 MeV neutron will be attenuated a factor of 10 more than the cascade neutrons. However, it is important to note that, while the energy of the nuclear cascade is predominantly transported by the higher-energy neutrons, it is the lower-energy radiations produced by the interaction of these high-energy particles that are important in depositing a large fraction of the absorbed dose, even outside thick shields.

At higher incident energies (above 50 MeV), the development of an intranuclear cascade, in which an incident proton interacts with individual nucleons rather than with the nucleus as a whole, becomes important. The angular distribution of the neutrons from this process is forward-peaked, rather than isotropic and the neutrons generated are higher in energy resulting in longer attenuation lengths and are, thus, more important in shielding considerations.

Bertini (1963) has reported calculations of the production of particles from protons interacting with several target nuclei: carbon, oxygen, aluminum, chromium, copper, ruthenium, cerium, tungsten, lead and uranium. Protons of energy 25 MeV and 50 to 400 MeV were selected, and both evaporation and intranuclear cascades were included in the calculations. The particle yields were determined for four angular ranges: 0 to 30, 30 to 60, 60 to 90, and 90 to 180 degrees. Alsmiller *et al.* (1967) have conveniently summarized the calculated

spectra of Bertini by fitting them with fifth- and sixth-order polynomials. This parameterized version of yields is still the most amenable form for calculation of shielding requirements by computer. Bertini *et al.* (1974) have also published extensive intranuclear cascade calculations for 39 and 72 MeV protons incident upon several materials. These calculated yields have been compared with experimental data from carbon, aluminum, and copper targets by Fasso and Hoefert (1976) who found good agreement.

Tesch (1985) has reviewed the literature on the total number of cascade neutrons produced per proton interacting in various target materials (carbon, aluminum, copper, iron, tin, tantalum and lead) over the energy range from 10 MeV to 1.45 GeV. For the most part, these data were obtained with targets thick enough to completely stop the incident protons and may include some multiplication effects at energies above ~300 MeV. The values of neutron yields given are therefore maximal. For all target materials at primary proton energies (E_p) between 50 and 500 MeV, the total neutron yield as shown in Figure 3.21 is roughly proportional to E_p^2; beyond 1,000 MeV the yield is roughly proportional to E_p. The data summarized by Tesch suggest that the ratios of the neutron yields from different target materials are independent of E_p in the range 20 MeV to 1 GeV and are given relative to medium mass number (copper/iron) by:

$$\text{C: Al: Cu-Fe: Sn: Ta-Pb} =$$

$$(0.3 \pm 0.1): (0.6 \pm 0.2): (1.0): (1.5 \pm 0.4): (1.7 \pm 0.2). \quad (4.32)$$

4.8.2 *Proton Energies Below 3 GeV*

In what follows the formalism of Equation 4.9 will be used. The incident neutron spectrum may be divided into several energy groups and the transmission of each group determined. The separate contributions of each of these different neutron energy groups may then be added. However, in practice, the lowest energy group is so rapidly attenuated that its contribution to the total is often neglected. Over a limited range of shield thickness, the approximation of the radiation transmission by an exponential function is satisfactory. For shield thicknesses less than ~100 g cm^{-2}, the value of the effective attenuation length (λ_{eff}) changes with increasing depth in the shield. Nevertheless, in the range of practical interest for proton accelerators, *i.e.*, for shield thicknesses between 200 and 1,200 g cm^{-2}, a single value of λ_{eff} will suffice. In principle, values of the parameter H_θ of Equation 4.9 as a function of both angle and depth are needed for shield design. However, in practice, it is often only necessary to design

shielding in the longitudinal ($\Theta = 0$) and transverse ($\Theta = \pi/2$) directions when only numerical values of the parameters H_0 and $H_{\pi/2}$ are required.

Tesch (1985) has described an empirical approach for estimating the dose equivalent behind concrete shielding using Equation 4.9. He used the available energy spectra of cascade neutrons produced by the interaction of protons with thick targets to calculate the values of $H_{\pi/2}$ as a function of incident proton energy up to 800 MeV. The dose equivalent was obtained by means of the fluence-to-dose conversion factors published by ICRP (1973). These values of $H_{\pi/2}$, normalized for a copper target, are tabulated in Table 4.7.

He also reviewed the available data on the attenuation of the neutron dose equivalent in concrete for this energy range and his summary in terms of the effective attenuation length (λ_{eff}) is shown in Figure 4.26. Using the best fit to the data of Table 4.7 and Figure 4.26, he was able, along with Equation 4.9, to reproduce the original data of Alsmiller *et al.* (1975) and Braid *et al.* (1971) to within a factor of better than three.

A thin target is one in which the energy loss of incident protons in the target is insignificant in affecting the kinetic energy available for neutron production. The yield from a thin target will be proportional to the target thickness. In passing through a thin target, the particles in the beam will be scattered to some degree and some may lie outside the beam acceptance of the accelerator. Such particles may then strike objects (*e.g.*, accelerator or beam-transport components) which will in essence be thick targets. Thus, the impact of a thin target might be thought of as diffusing the apparent location of the beam interaction. The values of λ_{eff} for the neutrons from a thin target are somewhat larger than those for the thick target. This is to be expected because of the slightly softer neutron spectrum emitted from thick targets compared with thin targets.

TABLE 4.7—*Dose equivalent per proton due to neutrons with energies >8 MeV at a distance of 1 m from an unshielded copper target at 90 degrees to the proton beam.*

E_{p} (MeV)	$H_{\pi/2}$ (Sv proton^{-1})
30	1.5×10^{-18}
72	1.8×10^{-17}
230	6.4×10^{-16}
590	8.8×10^{-15}
800	5.8×10^{-15}
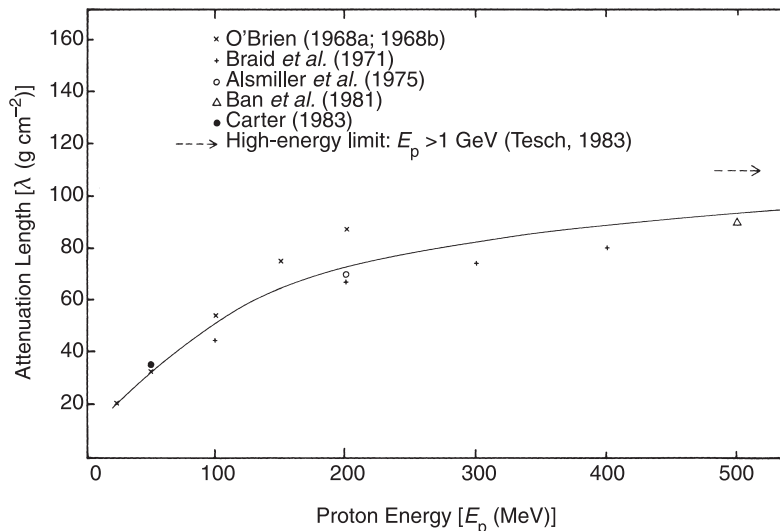
Fig. 4.26. The attenuation lengths for dose equivalent, for concrete, at 90 degrees to the proton beam (Tesch, 1985).

4.8.3 *Proton Energies Above 3 GeV—The Moyer Model*

4.8.3.1 *Introduction.* Design and construction of the first proton accelerators in the giga-electron volt energy region during the 1950s demanded an increased understanding of high-energy particle-accelerator radiation environments (Patterson and Thomas, 1973). Control of the intensity of the radiation field became an urgent task, following experience from the early operation of the originally poorly-shielded Cosmotron and Bevatron (Solon, 1957). The increasing beam intensities produced by weak-focusing synchrotrons in the late 1950s generated a need for efficient shield design, particularly in the transverse direction. This problem was exacerbated by the fact that, at that time, there was no firm theoretical basis for designing accelerator shielding.

Moyer (1961) developed a semi-empirical method and designed a shield for the 6 GeV proton Bevatron to reduce dose-equivalent rates by a factor of 100. Measurements showed that, in practice, the overall effect of the recommended shield was to reduce neutron fluence (proportional to dose equivalent) by a factor between 90 and 100 (Smith, 1965a; Thomas, 1970). This success naturally stimulated an interest in generalizing Moyer's method.

The Moyer model was greatly improved during the mid-1960s as a consequence of the better understanding of accelerator-shielding

calculations which resulted from the design of the proton synchrotrons at FNAL (Batavia, Illinois) and SPS (CERN, Geneva) (Awscholom, 1970; CERN, 1964; Gilbert *et al.*, 1968; LRL, 1965; URA, 1968). These design studies led to a more precise formulation of the Moyer equation, studies of the angular distribution function, determination of values for the parameters of the Moyer equation, and their variation with proton energy.

The following section, which is based on the discussion by Stevenson *et al.* (1982), discusses the generalized formulation of the Moyer model; the derivation of numerical values for the parameters of the model and the variation of these values with proton energy; and, finally, the application of the model to point-source and extended-source calculations.

4.8.3.2 *Generalized Formulation of the Moyer Model.* Early discussions concentrated on neutrons because they make the dominant contribution to dose equivalent outside well-shielded proton accelerators (Perry, 1967). The fact that those neutrons that largely contribute to the dose equivalent (for $E < 50$ MeV) are not those that propagate the hadronic cascade ($E > 150$ MeV) has led to, and still produces, some confusion in the literature.

For an effective point source produced by protons interacting in a thin target and assuming that neutrons are the only secondary particles to be considered, the radiation level on the outside of a shield (Figures 4.27 and 4.28) may be written as:

$$H = \frac{1}{r^2} \int g(E) \mathrm{B}(E,\Theta) \, \mathrm{e}^{-d(\Theta)/\lambda(E)} \, \frac{\mathrm{d}^2 n(E,\Theta)}{\mathrm{d}E \mathrm{d}\Omega} \, \mathrm{d}E, \qquad (4.33)$$

where:

r	=	distance from the source
E	=	neutron energy
g	=	fluence to dose-equivalent conversion coefficient
d	=	shield thickness in the direction Θ
λ	=	effective removal mean free path
B	=	buildup factor
$\dfrac{\mathrm{d}^2 n(E,\Theta)}{\mathrm{d}E \mathrm{d}\Omega}$	=	yield of neutrons per unit solid angle, at angle Θ, per unit energy interval at E

Moyer recognized that, because of the characteristic variation of neutron attenuation lengths as a function of energy, accelerator-radiation fields will effectively be attenuated as a single group and Equation 4.33 will apply. Neutron attenuation lengths diminish rapidly with energy below ~100 MeV, but above 150 MeV are roughly independent of energy (Figure 4.6). Consequently, the greater yields
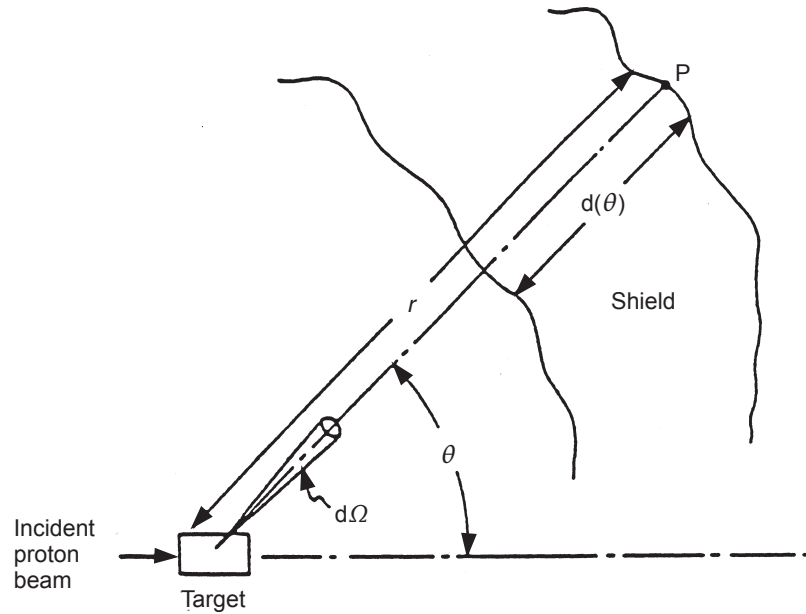
Fig. 4.27. Schematic diagram of shielding geometry for the generalized formulation of the Moyer model.

of low-energy, as compared with high-energy neutrons at the primary interaction will be more than compensated for by the greater attenuation for these neutrons. Thus, the radiation field outside the shield of a high-energy proton accelerator will be determined by neutrons with energy greater than ~150 MeV. Consideration of only the high-energy ($E > 150$ MeV) group of neutrons is not strictly accurate, but allowance is made for lower-energy particles by a buildup factor. Thus, in the Moyer model the approximation is made that:

$$H = r^{-2}\ \Psi(E_{\mathrm{p}})\ \mathrm{e}^{-\beta\theta}\ \mathrm{e}^{-d(\theta)/\lambda}, \tag{4.34}$$

where $\Psi(E_{\mathrm{p}})$ is the source strength parameter (dose equivalent per incident proton) and is a function of incident proton energy (Section 4.8.3.3) and β is the angular-relaxation parameter (Section 4.8.3.3.2). Because the Moyer approximation yields an estimate of the dose equivalent for an equilibrium cascade, the source-strength parameter refers not to a bare source, but to a virtual source derived from the dose equivalent deep in the shield extrapolated to zero shield thickness and unit distance from the source.

Because high-energy pions and protons in the hadronic cascade have very similar cross sections to those of neutrons, it is possible
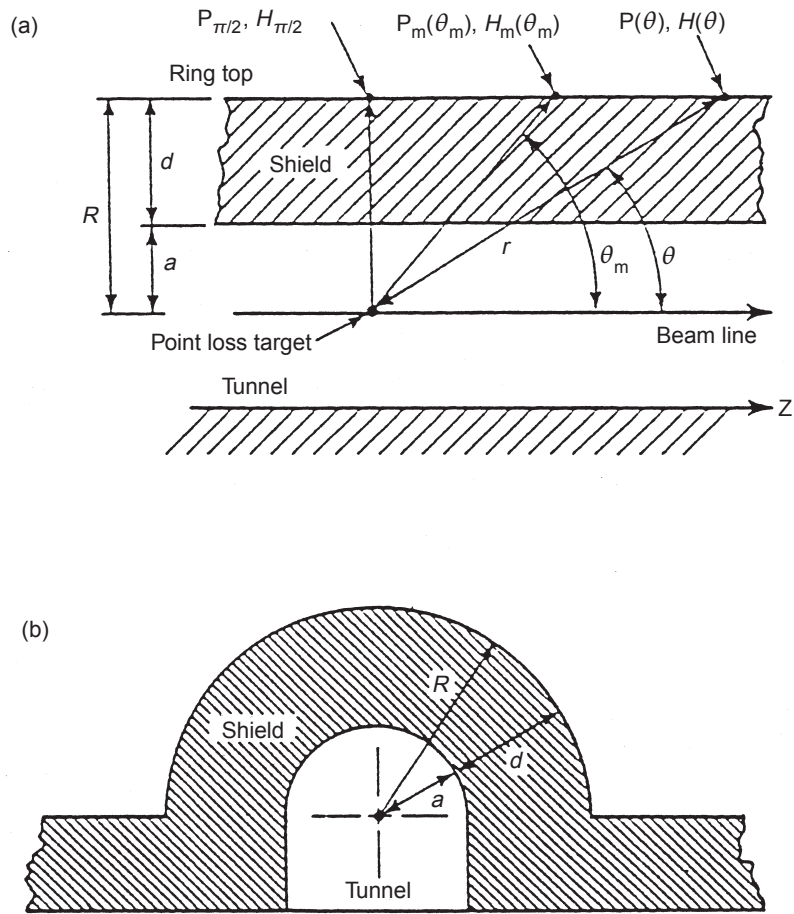
Fig. 4.28. Diagram showing the accelerator shield geometry assumed and defining the symbols in the Moyer model calculations. P(Θ) indicates a point on the outer surface of the shield at angle Θ from the point loss target and $H(\Theta)$ is the corresponding dose equivalent. The subscript m indicates the maximal dose equivalent (H_m) that occurs at point P_m and angle Θ_m. Similarly the corresponding dose equivalent at 90 degrees ($\pi/2$ radians) is designated $H_{\pi/2}$ at point $P_{\pi/2}$ and $\Theta_{\pi/2}$. (a) shows the longitudinal section and (b) the lateral cross section.

to speak of "cascade propagators" rather than just "high-energy neutrons." Deep in the shield these high-energy ($E > 150$ MeV) hadrons are present in relatively small numbers, but they regenerate the cascade. At a shield interface, the radiation field observed consists

of these "propagators," born close to the primary radiation source, accompanied by many lower-energy particles, mainly neutrons, born near the interface.

The essence of the Moyer model, therefore, is that the dose equivalent at any point outside the accelerator shield is largely governed by the simple line-of-sight propagation of the cascade generating particles produced at the first interaction (target) and a multiplication factor used to account for particle buildup. The total neutron fluence rate (and consequently the dose-equivalent rate) will be proportional to the high-energy hadron fluence rate. Because the low-energy components are produced from the high-energy propagators, their intensity decreases with the same attenuation length as that for the propagators.

Several experimental verifications of Moyer's basic assumptions have been reported in the literature. In a series of measurements in concrete irradiated by protons with energy between 2.2 and 6.2 GeV, Smith *et al.* (1964) demonstrated the development of radiation field equilibrium. The radiation attenuation length was independent of the angle to the incident beam direction and of the threshold of the neutron detector used. Smith (1965a) described the excellent agreement between measured radiation levels around the Bevatron and those predicted by Moyer.

4.8.3.3 *Determination of the Moyer Model Parameters*

4.8.3.3.1 *Attenuation parameter.* Gilbert (1969) and Gilbert *et al.* (1968) showed that the neutron fluence rates in the earth shielding of the CERN 25 GeV proton synchrotron could be accounted for with good accuracy using a Moyer-type equation with empirically determined parameters. Typical results over a range of 10^5 in neutron fluence rate and up to a distance of 40 m from the source of radiation, an internal target, were estimated with an accuracy of 20 percent or better. The attenuation length (λ) in earth determined by Gilbert *et al.* was:

$$\rho\lambda = 117 \pm 2 \text{ g cm}^{-2}. \tag{4.35}$$

The attenuation length (λ) appropriate for use in the Moyer model is determined by the neutron inelastic cross section of the constituents of the shield. The inelastic mean free path is related to the inelastic cross section (σ_{inel}) by:

$$\lambda_{inel} = 1/N\sigma_{inel}, \tag{4.36}$$

where N is the number of atoms per unit volume. As a first approximation, one can assume that the inelastic cross section is simply represented by the geometric cross-sectional area of the nucleus. If the nucleon radius is taken as 1.2×10^{-13} m, it then follows that:

$$\rho\lambda_{\text{inel}} = 38\, A^{1/3} \text{ g cm}^{-2}. \qquad (4.37)$$

McCaslin *et al.* (1985b) assumed that the functional dependence of the attenuation length on A is correctly given by Equation 4.37. Using the value for the attenuation length obtained by Gilbert *et al.* (1968), and assuming that the earth in which the measurement was made, consists of 95 percent SiO_2 and 5 percent H_2O (by weight), they obtained the expression:

$$\rho\lambda = 42.8\, A^{1/3} \text{ g cm}^{-2}. \qquad (4.38)$$

4.8.3.3.2 *Angular-relaxation parameter.* The combined effects of the angular distribution and attenuation through shields, in which several interactions have occurred effectively, determines the transverse shielding for proton accelerators in the 1 to 100 GeV range. The apparent angular distribution of the virtual source of neutrons thus controls the transverse shielding rather than the angular distribution close to accelerator targets. Ranft (1967) and Routti and Thomas (1969) showed that the shape of the angular distribution of neutrons greater than 150 MeV produced in primary interactions was nearly independent of primary proton energy in the range $1 < E_p < 300$ GeV. For angles of Θ around $\pi/2$ radians, the angular distribution has a simple exponential form:

$$g(\Theta) = e^{-\beta\theta}. \qquad (4.39)$$

Levine *et al.* (1972) measured the angular distributions around accelerator targets using threshold detectors. Figure 4.29, showing β as a function of detector threshold E_{th}, summarizes these data. The value of β corresponding to $E_{\text{th}} = 150$ MeV is 2.3 ± 0.3 radians^{-1}. The values of β, in the angular range 60 to 120 degrees, were independent of target material (aluminum, copper, tungsten) and did not differ for proton energies of 3.7 and 23 GeV. Experiments at 225 and 400 GeV have confirmed this independence of proton energy (Stevenson *et al.*, 1983).

Stevenson *et al.* (1982) have summarized determinations of β derived from several target and shielding measurements. Assuming invariance of β with primary proton energy, the mean value of β is 2.3 ± 0.1 radian^{-1} in good agreement with the value from Levine *et al.* (1972). This value has also been confirmed with measurements of angular distributions for high-energy neutrons around targets
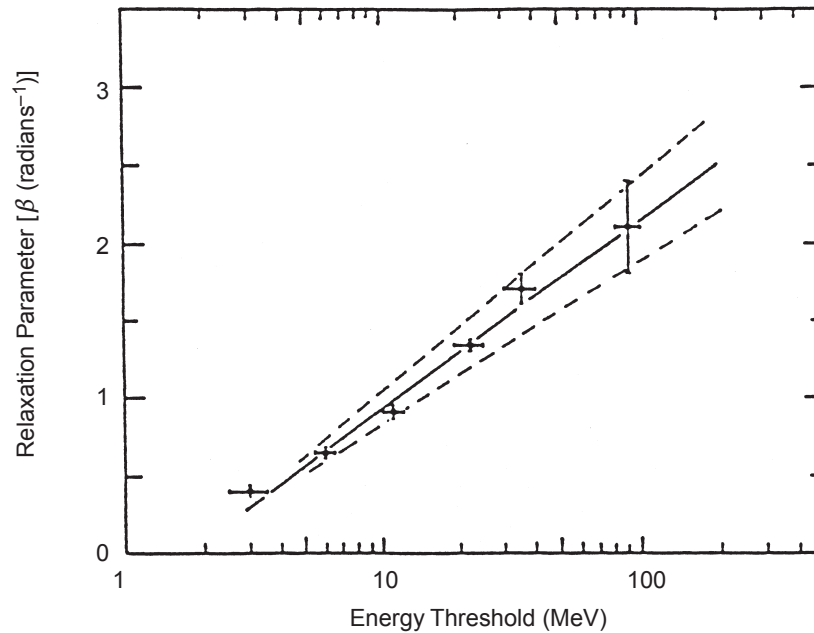
Fig. 4.29.   The angular distribution parameter of the Moyer model as a function of detection energy threshold (Levine *et al.*, 1972).

bombarded with heavy ions of ~500 MeV amu^{-1} (McCaslin *et al.*, 1985a) and for 2.7 GeV protons (Bourgois *et al.*, 1996).

4.8.3.3.3   *Source-strength parameter.*   Because the relaxation parameter is independent of energy and angle, the buildup function can be replaced by a constant for a given target material and primary proton energy (E_p). For an equilibrium cascade, the total dose equivalent is proportional to the fluence of hadrons with energy above 150 MeV.

The best values of the parameters of $\Psi(E_p)$, resulting from statistical analysis of the data in the energy range 7.4 to 350 GeV (Stevenson *et al.*, 1982; Thomas and Thomas, 1984) and shown in Figure 4.30 are:

$$\Psi(E_p) = H_0 \, (E_p/E_0)^m, \tag{4.40}$$

with $E_0 = 1$ GeV, $H_0 = (2.84 \pm 0.14) \times 10^{-13}$ Sv m^2, and m = 0.80 $\pm$ 0.10.

These values have been confirmed by calculation and measurement for proton energies from 200 GeV to 1 TeV by Cossairt *et al.* (1985a), who made a detailed comparison of measured values of absorbed dose with values calculated using the Monte-Carlo simulation code CASIM in both steel and composite absorbers. Gabriel
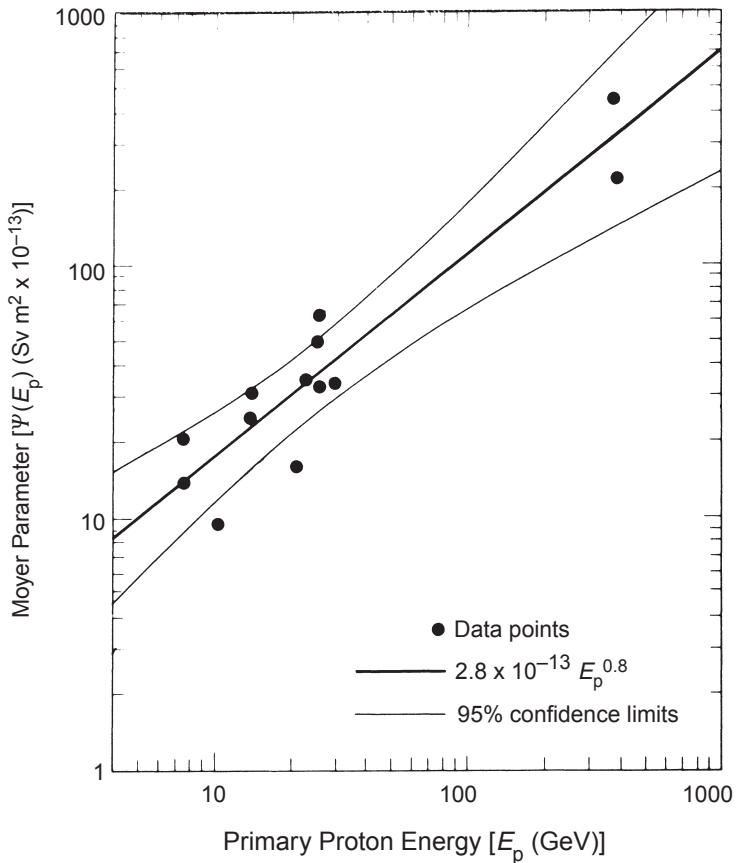
Fig. 4.30. The source strength parameter (Ψ) of the Moyer model as a function of primary proton energy. (Summary of regression analyses of the experimental data.) The regression line $\Psi(E_p) = 2.8 \times 10^{-13} (E_p/E_0)^{0.8}$ is shown as a heavy solid line. Experimental points are shown as a solid circle. The 95 percent confidence limits are shown by light solid lines (Thomas and Thomas, 1984).

et al. (1994) have subsequently shown, from fundamental considerations of the equipartition of energy in hadronic cascades, that a value of m close to 0.8 is to be expected.

Stevenson (1986) has derived values of $H_{\pi/2}$ from cascade calculations in concrete for protons of energy between 400 MeV and 1 TeV that confirm an energy variation of the form $E_p^{0.8}$ as expressed by:

$$H_{\pi/2} = 6.6 \times 10^{-15} (E_p/E_0)^{0.8} \quad \text{Sv m}^2. \tag{4.41}$$

The value of the constant, 6.6×10^{-15} Sv m^2, agrees[29] within 20 percent of the value of H_0 value given above.

In summary, the magnitude and variation with energy of the Moyer model source strength parameter [$\Psi(E_p)$] within the energy range 5 GeV $< E_p <$ 500 GeV, and possibly as high as 1,000 GeV, are best summarized by Equation 4.40. The dose equivalent is given by Equation 4.34 with β = 2.3 radian^{-1} and $\rho\lambda$ = 117 g cm^{-2} in concrete.

4.8.3.4 *Practical Examples*

4.8.3.4.1 *Point source.* Although beam losses at high-energy particle accelerators are usually of an extended nature, often the region of high beam loss will occur over lengths small or comparable with the thickness of the accelerator shields and tunnel radius [the distance (R) in Figure 4.28]. Under such conditions, the assumption of point loss may be used to determine the dose equivalent at the shield surface.

As an example, take the simple, but common, case of side shielding for a target which can be treated as a point source. Suppose that it is required to calculate the dose rate at 5 m from the target, through a steel wall 2.5 m thick capped with 1 m of heavy concrete, when 10^{12} ten giga-electron volts protons per second interact in the target. From Equation 4.40:

$$\Psi(E_p) = H_0 (E_p/E_0)^m$$
$$= 2.84 \times 10^{-13} \times 10^{0.8} \tag{4.42}$$
$$= 1.79 \times 10^{-12} \text{ Sv m}^2.$$

From Equation 4.38, for steel, with A = 55.8 (iron) and density ρ = 7.90 g cm^{-3}:

$$\lambda = 42.8 \, A^{1/3}/\rho = 42.8 \times 3.82/7.90 = 20.7 \text{ cm}. \tag{4.43}$$

For heavy concrete, λ = 163 g cm^{-2} (ρ = 3.6 g cm^{-3}) (Ban *et al.*, 1980) or 0.45 m. Substituting r = 5 m, β = 2.3, and Θ = $\pi/2$ into Equation 4.34 results in:

$$H = \frac{1.79 \times 10^{-12}}{5^2} \, e^{-2.3 \, \pi/2} \, e^{-2.5/0.207} \, e^{-1.0/0.45}$$

$$= 1.2 \times 10^{-21} \text{ Sv/interacting proton.} \tag{4.44}$$

---

[29] $H_{\pi/2}$ is related to H_0 by the equation $H_{\pi/2} = H_0 \, e^{-\beta\pi/2}$. With β = 2.3 radian^{-1}, $H_{\pi/2}$ = 0.027 H_0.

If the same beam dump is not always used, it is conservative to assume $n_{\lambda_{BD}} = 0$ for Steps 5 and 6 of Section 4.7.2, regardless of what is actually installed. Any location where the beam can strike should be shielded in the same manner. Then, for 10^{12} interacting protons per second and 3,600 s h^{-1} the dose-equivalent rate is:

$$\frac{dH}{dt} = 4.3 \ \mu Sv \ h^{-1}. \tag{4.45}$$

It is often incorrectly assumed that the maximal dose equivalent (H_m) occurs directly above or lateral to the point source ($\Theta = \pi/2$ radian), and it is important to estimate the error incurred by making this assumption. Figure 4.31 summarizes the calculation of F(Θ), the ratio of $H(\Theta)$, normalized to the value at $\Theta = \pi/2$, by the relation:

$$F(\Theta) = \frac{H(\Theta)}{H_{\pi/2}} = \frac{e^{-\beta\theta} \ e^{(-d/\lambda)(1-\mathrm{cosec}\ \Theta)}}{\mathrm{cosec}^2\ \Theta \ e^{-\beta\pi/2}}, \tag{4.46}$$

for values of relative shield thickness d/λ between 1 and 20 (McCaslin *et al.*, 1985b). For thin shields, errors of as much as a factor of two can be made with this assumption, but for $d/\lambda > 5$ the errors are less than 40 percent. McCaslin *et al.* (1985b; 1987) have shown that a good approximation for H_m is given by:

$$H_m = 5.9 \times 10^{-2} \ \Psi(E_p) \ N \ e^{-d/\lambda} \ (d/\lambda)^{-0.245}, \tag{4.47}$$

where N is the number of protons lost.

4.8.3.4.2 *Infinite uniform line source.* For an infinite uniform line source of S protons per unit length, Routti and Thomas (1969) showed using the Moyer model expression that the dose equivalent on the shield surface (H_∞) is given by:

$$H_\infty = \frac{\Psi S}{R} \int_0^\pi e^{-\beta\theta} \ e^{(-d/\lambda)\,\mathrm{cosec}\ \theta} \ d\Theta, \tag{4.48}$$

where R is the radial distance to the shield surface. The integral designated by M(β,d/λ), known as a Moyer integral:

$$M(\beta,d/\lambda) = \int_0^\pi e^{-\beta\theta} \ e^{(-d/\lambda)\,\mathrm{cosec}\ \theta} \ d\Theta, \tag{4.49}$$

may be regarded as a generalized form of the sievert integral which is used in the calculation of shielding of extended sources of gamma emitting radioactive materials. Values of Moyer integrals have been tabulated for arguments in the range $0 < \beta < 10$; $0 < d/\lambda < 40$ (Patterson and Thomas, 1973; Routti and Thomas, 1969). Tesch
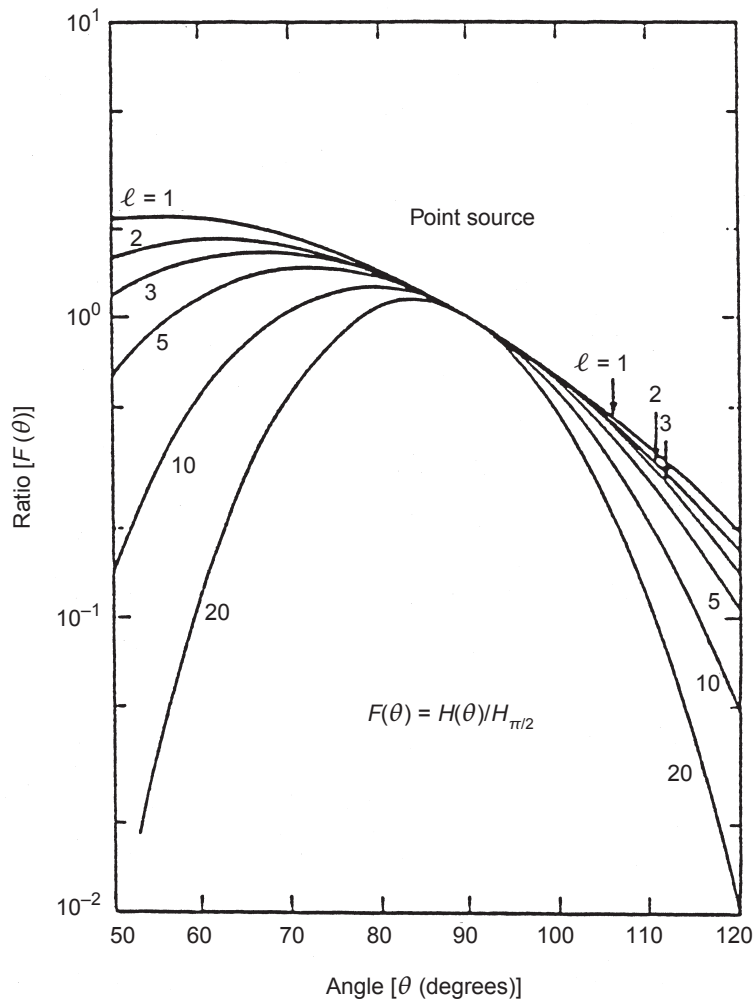
Fig. 4.31. Ratio of dose equivalent on the outer shield surface as a function of angle with respect to beam direction (point source loss) to the same quantity at $\pi/2$ radians (90 degrees). Parameter ℓ is shield thickness in units of the attenuation length (d/λ).

(1983) has shown that M(2.3,d/λ) may be approximated by the expression:

$$M(2.3, d/\lambda) = 0.065 \, e^{-1.09 \, d/\lambda}, \qquad 2 < d/\lambda < 15. \qquad (4.50)$$

4.8.3.4.3 *Finite uniform line source.* Here the more practical case of the dose equivalent produced at a shield surface by a finite, but

uniform, beam loss is considered. Assume that the beam spill strength has a value S protons per unit length over a beam spill length (L) along the beam axis and that beam loss is zero elsewhere. It is convenient to measure distance along the beam axis Z in units of R, placing the origin, Z = 0, at the start of the beam spill, and define a parameter:

$$\eta = L/R, \qquad\qquad (4.51)$$

where R is the perpendicular distance from the beam axis to the shield surface. In shielding calculations, the primary interest lies in the maximal value of the dose equivalent on the shield surface H_L (Z,R). Specimen calculations have been carried out by McCaslin *et al.* (1985b), as shown in Figure 4.32 for $d/\lambda = \ell = 5$. The areas under the curves of Figure 4.32 are proportional to the total beam lost. Because for a constant value of S, the beam spill parameter η is a measure of the total beam loss; these areas are also proportional to η. Inspection of Figure 4.32 shows that for short spill lengths ($\eta < 1$) the source is nearly point-like. Under these conditions, substitution of the appropriate value for N into Equation 4.47 will yield a good estimate of the maximal dose equivalent (H_m). For longer spill lengths ($\eta > 1$), the source behaves more like an infinite uniform line source. In this case, substitution of the appropriate value of S into Equation 4.48 will provide an acceptable estimate of H_m.

For these specimen calculations, McCaslin *et al.* (1985b) summarized their conclusions in Figure 4.33. Values of H_m, for a finite uniform line source, were calculated as a function of beam spill length and are shown as a solid line. The actual value of dose equivalent is bounded by: (1) the assumption of point loss shown as a rising straight line to the left of the diagram, and (2) the assumption of an infinite uniform beam loss shown as a horizontal line in the figure. All other physically possible values of H_m, lie within the approximately triangular cross-hatched area. The shaded area shows the degree of overestimation in H_m, that may be made by assuming the minimum of either point loss or by substituting the value of $S = N/L$ into the infinite uniform loss equation. As shown in Figure 4.33 for $d/\lambda = 5$, the error is greater than 10 percent only between $\eta = 0.6$ and 1.4 and reaches a maximum of about 30 percent.

4.8.3.5 *Conclusions and Limitations of the Moyer Model.*   The Moyer model for high-energy neutron shielding has proved itself a very durable instrument since it was first developed in the early 1960s, and has been utilized in the design of several important high-energy accelerator facilities including a 50 GeV proton synchrotron and the transverse shielding of a 20 TeV collider facility (Chu, 1980;
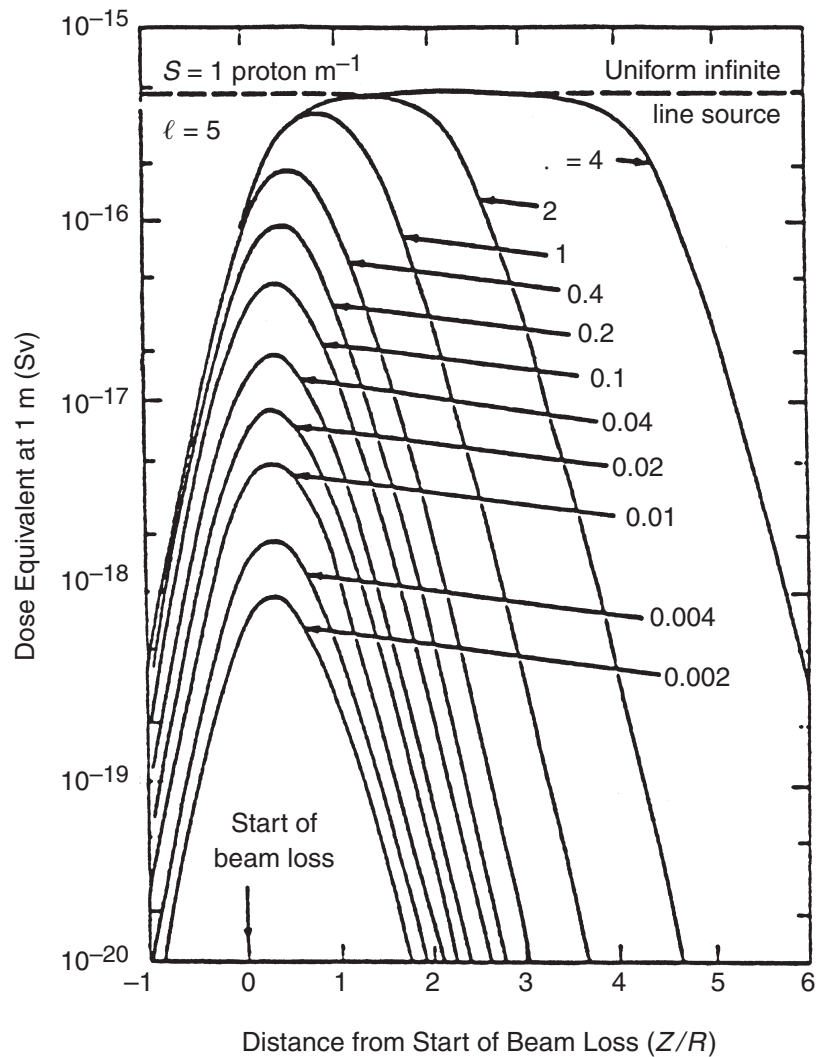
Fig. 4.32. The variation of dose equivalent on the outer shield surface as a function of position along the beam direction for different beam spill lengths $0.0002 < \eta < 4$. The origin of the coordinate system is chosen to be the start of the beam spill. The distance (Z) along the abscissa is indicated in units of the radius (R) (see Figure 4.28). Specimen calculations are shown for a shield thickness $\ell = d/\lambda = 5$, for a uniform beam loss (S) of 1 proton m^{-1}, and for $R = 1$ m and at a proton energy (E) of 10 GeV. Parameter ℓ is shield thickness in units of the attenuation length (d/λ).
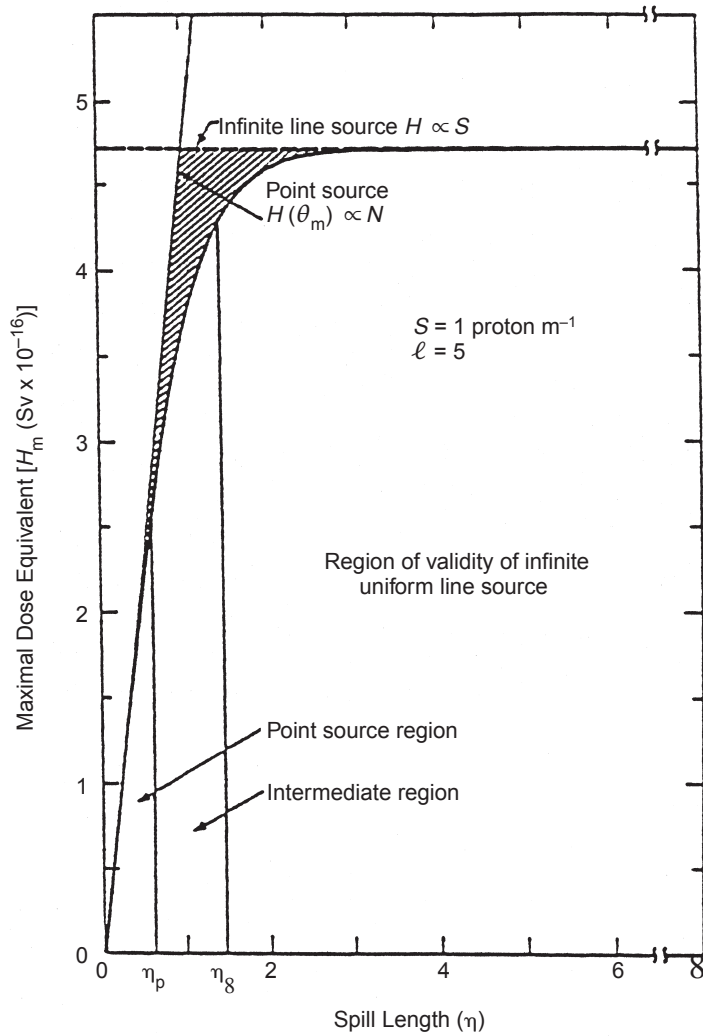
Fig. 4.33. The maximal dose equivalent (H_m) on the shield surface for a finite uniform beam loss as a function of beam spill length parameter (η). Values are calculated using restricted Moyer integrals with the parameters: $S = 1$ proton m^{-1}, $\ell = d/\lambda = 5$, $E = 10$ GeV, $R = 1$ m. The rising straight line to the left is the asymptote obtained if it is assumed that all beam loss occurs at a point. The horizontal line is the limit set by an infinite uniform beam loss. The cross-hatched region shows where intermediate beam losses occur and the error that may arise from incorrect assumptions as to beam loss. Also, this shaded region shows the overestimate that arises by use of the minimum of either the point-source ($N = SL$) or the infinite uniform line-source ($S = N/L$) assumptions.

Cossairt and Elwyn, 1984; Thomas and McCaslin, 1983). Its advantage over sophisticated methods lies in its simplicity; the algorithm contains only three parameters, whose values are well established. The procedure is useful in its own right besides serving as a check on more elaborate, but less transparent, methods of shielding calculation.

However, it is important to understand the limitations of the model. The recommended value of H_0 (2.8×10^{-13} Sv m^2) was determined with small target to shield distances ($a < R$) and directions normal to thick targets ($\Theta = 90$ degrees). Any large departure from these conditions (*i.e.*, in those cases where $\Theta \approx 0$ degrees or $a \approx R$) may result in error.

4.9 Proton Accelerators—Forward Shielding

4.9.1 *Proton Energies Below 3 GeV*

There are surprisingly few published data on the attenuation of neutrons in the forward direction (*i.e.*, along the direction of the proton beam) at energies below 1 GeV. Some early shielding studies for 90 MeV neutrons have been described by Patterson (1957). These suggested that the attenuation length (λ) was approximately given by the value obtained from the inelastic cross section as in Equation 4.36.

Theoretical considerations (Fisher, 1963) suggested that, at least for high energies, the effective attenuation length (λ_{eff}) would in fact be somewhat greater than that predicted by Equation 4.36. Experience of Sychev *et al.* (1966a; 1966b) at Dubna suggested that, in the case of broad beam geometry in the energy range between 350 and 660 MeV, the effective attenuation length was given by:

$$\lambda_{\text{eff}} = (1.3 \pm 0.1) \lambda_{\text{inel}}. \qquad (4.52)$$

4.9.2 *Hadronic Cascade Above 3 GeV*

When considering the specifications of the forward shielding of end stops, two radiation components must be taken into account. The first is that from the hadron cascade itself; this process is always dominant at proton energies less than 10 GeV. The second is that from muons generated by the decay of pions and kaons in the cascade and from the processes of direct production in proton-nucleus interactions. Muons dominate shielding specifications at the higher proton energies (Thomas, 1966), and their attenuation has been considered

in the design studies of several high-energy accelerators (CERN, 1964; LRL, 1965; Theriot *et al.*, 1971; Tigner, 1983; URA, 1968).

The longitudinal development of the hadronic cascade in the forward (incident particle) direction was studied experimentally in an attempt to obtain a definitive value for the effective attenuation length to be used in the shield design (for a bibliography see IAEA, 1988).

The design of beam stops is complicated by the fact that the radiation source is extended and consists not only of the products resulting from the first interaction of the primary beam, but also includes the high-energy forward-moving interaction products from particles that may have undergone many interactions in the shield. As the hadron cascade develops, the average energy of particles decreases and the cone of cascade propagating particles widens with depth in the shield. In the longitudinal direction, the initial buildup and equilibration of the hadron cascade has important consequences for specification of the shield.

Both analytical and Monte-Carlo methods have been used to study the longitudinal and transverse development of the hadron cascade. The simple one-dimensional description of Lindenbaum (1961) provides an instructive analytical treatment of the development of the hadron cascade in a shield, although it is limited in its practical application.

For example, assume that after collision, an incident high-energy primary particle continues in its original direction at a reduced energy but with the same mean free path[30] (λ_{mfp}) while generating a multiplicity (m) of secondary particles also having the same λ_{mfp}, until it has undergone a sufficient number of collisions (n) so as to degrade its energy to the point at which the absorption cross section increases rapidly with decreasing energy ($\sim$150 MeV as may be seen in Figure 4.6), and may be said to be "removed from the cascade." Then, the number of particles in the cascade at depth z can be written as:

$$N_n(z) = N_0 B_n(z/\lambda_{mfp})\, e^{-z/\lambda_{mfp}}. \qquad (4.53)$$

where B_n is a buildup factor for n collisions:

$$n = 1 \qquad B_1 = 1$$
$$n = 2 \qquad B_2 = 1 + (mz/\lambda_{mfp}) \qquad (4.54)$$
$$n = 3 \qquad B_3 = 1 + (mz/\lambda_{mfp}) + (m^2 z^2/2\, \lambda_{mfp}^2),$$

---

[30] Note that the definition of mean free path (λ_{mfp}) is different from the definition of attenuation length (λ).

where m is the number of secondaries generated per collision, assumed constant in this model.

For $n > 1$, the buildup factor does not approach a constant value but is a monotonically increasing function of z. If $mz/\lambda_{mfp} \gg n$, approximately exponential absorption takes place with a mean free path equal to $\lambda_{mfp} + \Delta\lambda_{mfp}$, where $\Delta\lambda_{mfp} = n\lambda_{mfp}/mz$. Figure 4.34 gives the number of particles as a function of depth in the shield for $n = 1$ to 4 and particle multiplicities $m = 1, 2$ and 5. For all cases with $n \geq 2$, the exponential region is not achieved until $z/\lambda \sim 10$. In concrete, this would correspond to a depth of $\sim 1,200$ g cm^{-2}. Figure 4.34 suggests that this simple analysis explains the general shape of the attenuation curve including buildup. However, it is evident that the values of the parameters n and m depend on the particle energy and must be determined from more detailed considerations.

Passow (1962) provided a more complete analytical description of the hadron cascade, which included differentiation between hadrons.
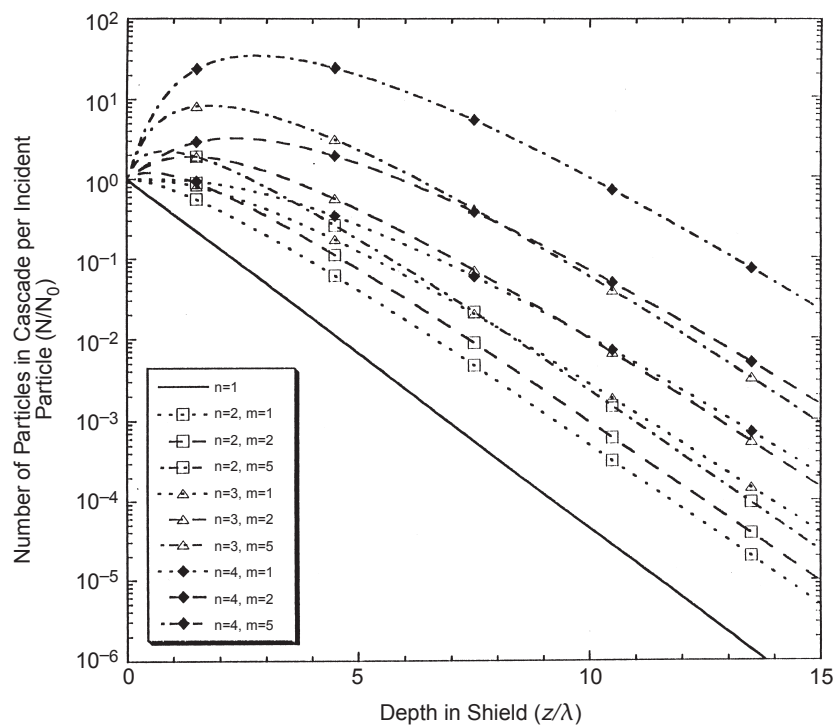
Fig. 4.34. Development of the one-dimensional cascade in the Lindenbaum approximation with $n = 1$ to 4 and $m = 1, 2$ and 5.

In a study by O'Brien (1969), Passow's approximation was reparameterized to force the secondary production spectra to correctly reproduce the partial inelasticities and multiplicities up to energies of 30 GeV or so. The resulting solutions were compared with the experimental data at 19.2 GeV c^{-1} of Citron *et al.* (1965) and with the data of Shen (1964) at 1 and 3 GeV. Figure 4.35 shows reasonable agreement between the experimental data of Citron *et al.* (1965),
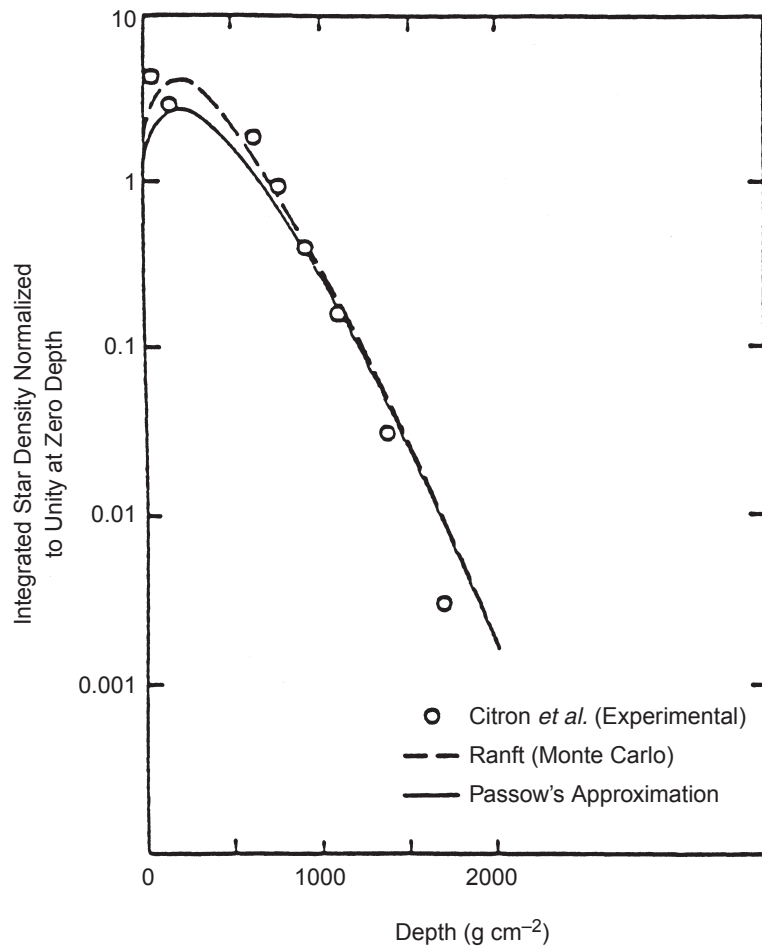
Fig. 4.35. The laterally integrated star density in nuclear emulsions introduced by an 18.3 GeV proton beam incident on an iron slab as a function of depth in the slab. The measurements were made by Citron *et al.* (1965); the Monte-Carlo calculations were performed by Ranft (1967).

Monte-Carlo calculations by Ranft (1967), and calculations using Passow's approximation.

The analytical methods just described require several approximations, including:

- restriction to slab geometry
- neglect of elastic and multiple Coulomb scattering
- assumption that all secondary particle production is in the forward direction
- assumption that particle production is represented by rather simple analytic expressions

Monte-Carlo methods of solving the radiation transport equations formulate the problem as a succession of individual processes, rather than in terms of global physical quantities (Section 4.2.2). The cascade is simulated by making a mathematical "experiment" akin to the real physical situation. Particles in the cascade are tracked from interaction to interaction: these "events" may be, *e.g.*, elastic or Coulomb scattering events, or inelastic nuclear events in which any variety of secondary particle may be produced. The processes and particle production are selected at random from their appropriate probability distributions which are usually expressed either in the form of empirical equations or generated by Monte-Carlo simulation. At any point in the cascade simulation, any required macroscopic physical quantity, such as, *e.g.*, particle fluence, energy fluence, absorbed dose, and density of inelastic interactions may be "scored." That is to say, the individual contribution to the required physical quantity from the particle being followed may be computed and stored. When a sufficient number of particles has been followed and scored, the expectation values of the required global macroscopic quantities may be evaluated to the required statistical accuracy.

None of the restrictions imposed by the analytical solutions apply to the Monte-Carlo solutions. In particular, any three-dimensional geometrical configuration containing many different media may be considered. The main disadvantage of the Monte-Carlo method is that the tracking of a sufficient number of particles to give good statistical accuracy may require considerable time, particularly through thick shields. Limited computational resources may, therefore, lead to data of poor precision.

In any event, the shield designer must never forget that Monte-Carlo methods are inevitably limited by the quality of the theoretical and experimental data used in their encoding. In this respect, they do not differ from other analytical methods or experiments and their results should be evaluated just as critically.

The Monte-Carlo methods may be used to generate the data required for the specification of shielding, even in the most complex geometries. For simple geometries, it is possible to undertake a systematic study of the development of the hadron cascade and summarize a large body of data in the form of simple empirical models.

Such systematic studies of the development of the hadron cascade, in shields of steel and concrete using the CASIM program, have been undertaken by Van Ginneken and Awschalom (1974). The authors give contours of the density of inelastic nuclear interactions ("stars") produced by hadrons above a momentum of 0.3 GeV c^{-1} for incident protons having momenta of 30, 100, 300 and 1,000 GeV c^{-1}. An example of such a contour map taken from that report is given in Figure 4.36 for 30 GeV c^{-1} protons incident upon steel. The data derived from these and similar calculations may be used in the specification of shielding both in the longitudinal and transverse direction by relating the calculated star density to dose equivalent.
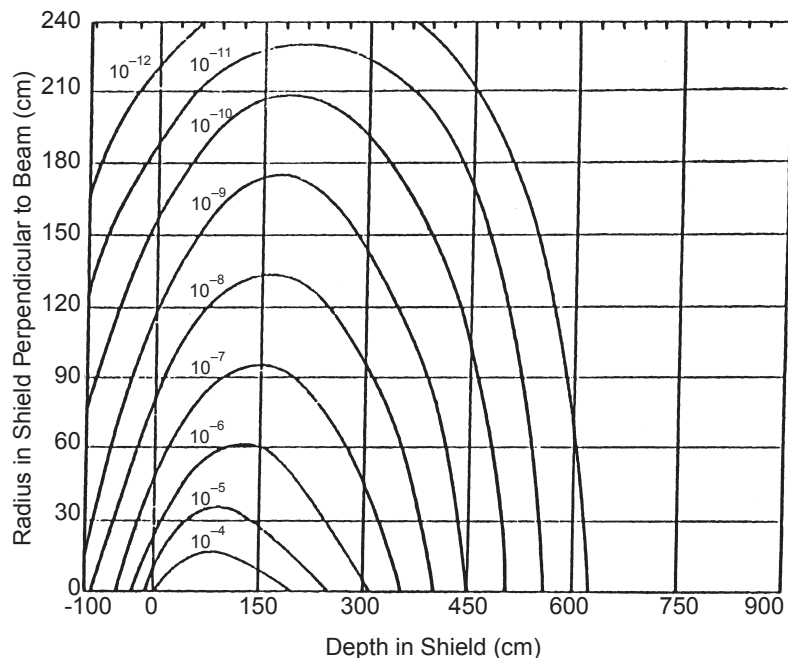
Fig. 4.36. Contours of equal star density (stars cm^{-3}, per incident proton) generated by 30 GeV c^{-1} protons incident on a solid iron cylinder. The beam of 0.3×0.3 cm^2 cross section is centered on the cylinder axis and starts to interact at zero depth. The star density includes only those due to hadrons above 0.3 GeV c^{-1} momentum. Contours of higher star density are not shown for clarity of the plot; those of lower star density are not included due to the statistical uncertainty.

Because of the complex longitudinal development of the cascade, it is not possible as in the case for transverse shielding to specify a virtual source strength that is independent of the thickness of the shield. It is possible, however, to use an empirical formulation:

$$H(z) = S(z)\, e^{-z/\lambda} \tag{4.55}$$

for the dose equivalent at depth z in the shield.

Figures 4.37 and 4.38 show the value of $S(z)$ as a function of depth in steel and concrete, respectively, over the energy range from 3 GeV to 1 TeV. The values of attenuation length (λ) are the same as those determined for the lateral shield case described previously (*viz.*,
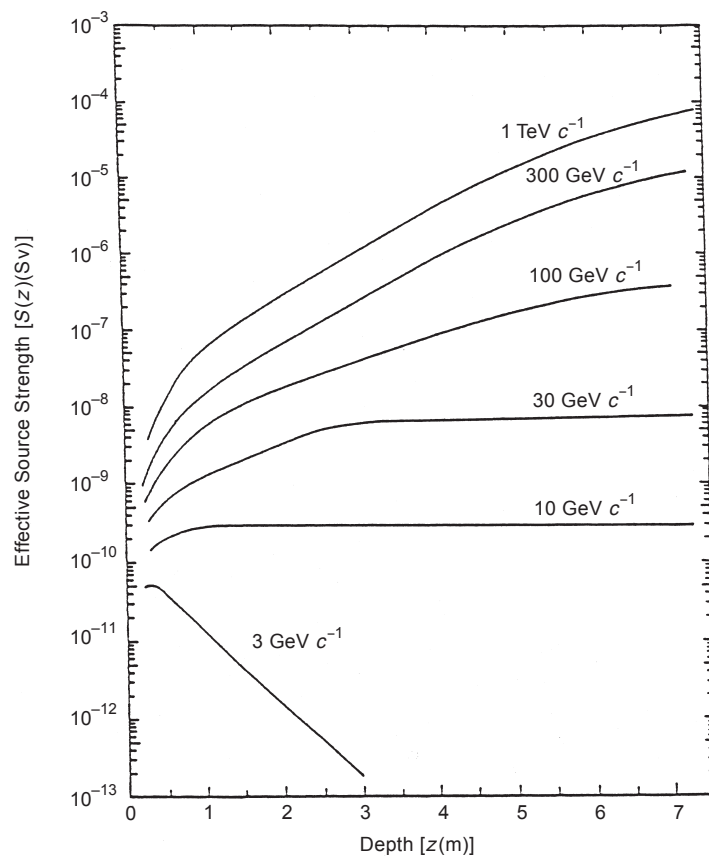
Fig. 4.37. Variation of the effective source strength $[S(z)]$ with depth in a steel shield of density 7.88 g cm^{-3} for cascades initiated by protons of the indicated momenta (IAEA, 1988).
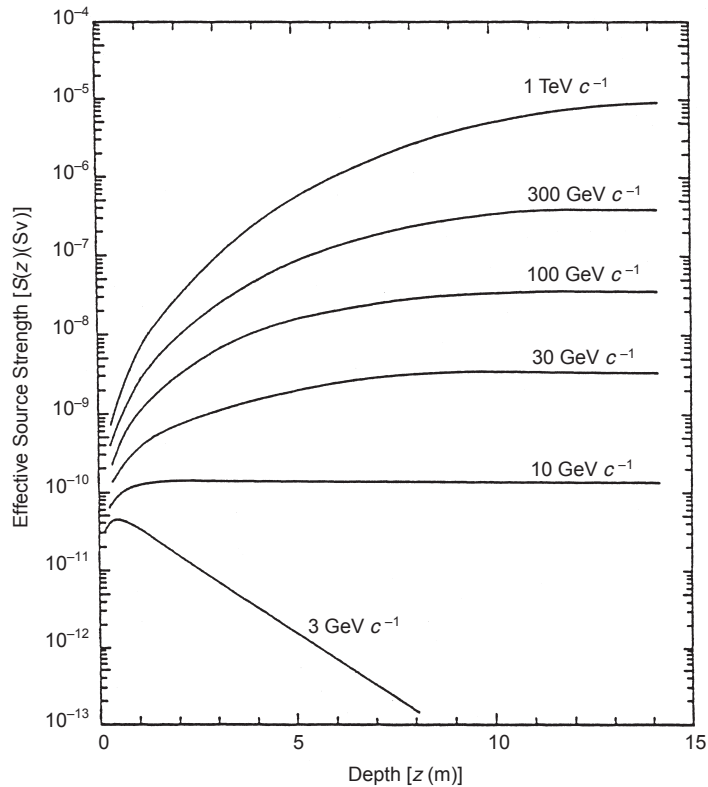
Fig. 4.38.   Variation of the effective source strength [$S(z)$] with depth in a concrete shield of density 2.4 g cm^{-3} for cascades initiated by protons of the indicated momenta (IAEA, 1988).

170 g cm^{-2} for steel and 117 g cm^{-2} for concrete). With the approximation of the complex transmission curve by the simple exponential form of Equation 4.55, the required value of the virtual source strength $S(z)$ approaches plateau values at large depths for the highest proton momenta. The quantity $S(z)$ is nearly constant at momenta around 10 to 30 GeV c^{-1}, and decreases with depth at the lowest proton momentum illustrated, perhaps because the attenuation length is less than the high-energy maximum at these energies.

4.9.3   *Muon Shielding*

Muons are produced by the decay of pions and kaons, either in particle beams or in the cascade induced by high-energy hadrons.

Because muons are weakly interacting particles, they lose energy mainly by ionization, and the principal technique used to shield them is to interpose an ionization range of material in their path. The ionization range of muons in several materials and as a function of energy is shown in Figure 3.39. Consideration of shielding against muons is usually only needed at proton and electron accelerators with energies above 10 GeV. Muons were first identified as a significant problem during the initial operation of the 30 GeV AGS of the Brookhaven National Laboratory (Cowan, 1962) and are commonly observed at the very high-energy accelerators at CERN, Fermilab and Serpukhov (Bertel *et al.*, 1971; Cossairt, 1983; Kang *et al.*, 1972; Nielsen, 1974; Theriot *et al.*, 1971). For completeness, a brief discussion is given here with references to the scientific literature that will enable the interested reader to find further details.

At high-energy physics laboratories, sophisticated radiation transport programs are usually used to specify shielding against muons. Normally, the physical configuration of the accelerator components, beam transport systems, and shielding together with the presence of magnetic fields make the calculation of muon transport complicated. Muon shielding is routinely specified using transport codes based on Monte-Carlo techniques, and particular shielding problems have been solved as needed. There have been only limited attempts to develop simple empirical equations containing a few derived parameters for the specification of muon shielding in simple geometries (Keefe, 1964; LRL, 1965; Thomas, 1964). Nevertheless, an attempt is made here to summarize the muon shielding problem in analytical terms, because it provides a basic understanding of the physical processes involved.

One simple, but usually conservative, approach to shielding muon beams in the beam direction is to place sufficient material in the forward direction so that the muons are completely stopped. This may be done by determining the mean range from Figure 3.39 and adding about 20 percent to allow for straggling (Stevenson, 1976).

An improved technique is to determine the radial width of the muon distribution at different depths in the shield. The spatial and angular distributions of a beam of particles that undergoes multiple scattering in matter are described in a theory developed by Rossi and Greisen (1941) following the treatment of Fermi which was extended by Eyges (1948) to include the slowing down of particles while passing through matter.

The radial distribution of particle fluence at a given depth in the scattering material, independent of angle to the beam axis, is given by:

$$\phi(r) = \frac{N_0}{4\pi A_2} \, e^{-r^2/4A_2} , \tag{4.56}$$

where:

r = radial distance off-axis

N_0 = number of particles incident in the pencil beam

A_2 = an area given by the following integral:

$$A_2 = \int_0^z \chi^2(t) \, (z - t)^2, \tag{4.57}$$

where z is the depth of the plane of interest in the shielding or scattering material and χ^2 is one-quarter of the mean square scattering angle per unit distance. The value of χ^2 depends on the momentum of the particle at depth t. In the Fermi-Eyges theory, all range straggling is ignored and the range-momentum relationship is considered to be monotonic. All scattering is considered to be the sum of many individual small-angle scattering processes. Contours of equal muon fluence may then be determined to guide the shield design. The program TOMCAT was designed to ease the calculation for the cases of real pion, kaon and muon beams (Stevenson, 1981) (see Section 4.2.2.9).

One important parameter in these calculations is the distance (Δ) in air available for decay of pions and kaons into muons. For short distances and high momenta, the decay probability is directly proportional to Δ. For muons created by proton-induced cascades in end stops, Keefe and Noble (1968) showed that an effective length available for decay was 1.8 times the hadron absorption length.

Drugachenok *et al.* (1971) noted, experimentally, that the longitudinal attenuation at energies less than 50 GeV is approximately exponential. Sullivan (1985) was able to theoretically justify the exponential shape. Sullivan showed that the muon fluence at a distance (x) behind the point of interaction of a proton of energy (E) (giga-electron volt) and where pions have a path length in air [Δ(m)] in which to decay is:

$$\phi = 8.5 \times 10^{-2} \frac{E\Delta}{x^2} \, e^{-\alpha t/E}, \tag{4.58}$$

where t is the shield thickness in meters and α is an effective muon energy-loss rate that has a value of 22 GeV m^{-1} in steel and 7.8 GeV m^{-1} in concrete.

It was further shown that the effective muon attenuation mean free path is equivalent to 1/16 of the range of a muon with the energy of the interacting proton. This simple equation gives satisfactory predictions in the energy range 10 to 30 GeV.

4.10 Shielding Materials

If cost and convenience were no criteria, any material in sufficient quantity may be used for shielding against accelerator radiations. However, many practical constraints limit materials generally to those commonly used in construction. Ordinary concrete, steel and earth are most often used for accelerator-facility shielding, but other materials may prove to be more advantageous under certain circumstances.

In selecting a shielding material, the following factors should be evaluated:

- required thickness and weight of material
- possibility of multiple use, *e.g.*, material that serves both shielding and structural purposes
- possibility of use as shielding against both incident neutrons, x rays and gamma rays; thicknesses might differ considerably if any one radiation is to be separately shielded
- uniformity, consistency, homogeneity of shielding
- permanence of shielding, *e.g.*, stability against cracking, flaking, sagging, changing composition (see notes below regarding water content of concrete)
- optical transparency if to be used in windows, resistance to radiation darkening, chemical or biological contamination, internal optical scattering
- cost of the material, including the cost of its installation and maintenance
- architectural appearance; surface characteristics, ease of cleaning or painting
- possibility of inducing radioactivity in the material from continued exposure to radiation (Section 3)

Extensive information on the properties of shielding materials is contained in *Principles of Radiation Shielding* (Chilton *et al.*, 1984); *Engineering Compendium on Radiation Shielding, Volume 2, Shielding Materials* (IAEA, 1975); and IAEA Technical Report 283, *Radiological Safety Aspects of the Operation of Proton Accelerators* (IAEA, 1988). The first two of these references deal largely with neutron shield design, while the last reference deals with proton accelerator-shield design. Much of the material in this Section is derived from this latter reference.

Experience and economic factors have shown that three materials: earth, concrete and steel are principally used in accelerator-shield construction. To a limited extent, other materials such as polyethythene, lead, uranium, water and wood have been used in special

circumstances. In addition, special techniques have been used to reduce the levels of induced activity in concrete by either the selection of aggregates or by the addition of boron components.

The proper selection of materials to be used for the fabrication of targets, collimators, end stops, or heat exchangers is also very important. At electron accelerators, materials having low Z are generally preferred for the construction of these elements so as to reduce secondary-photon production resulting from bombardment by the primary beam. On the other hand at very low-energy proton and heavy-ion accelerators, materials with high Z are preferred for these components because of their reduced neutron yields when compared with lighter materials. However, at ion energies above 5 MeV, neutrons are produced in most materials, so again materials with low Z are preferred.

4.10.1 *Earth*

Earth has many admirable qualities as a shielding material. Table 4.8 gives the elemental composition of representative soils (Chilton *et al.*, 1984). The principal constituent of dry earth is silicon dioxide (S_iO_2) making it an effective shielding material both for photons and

TABLE 4.8—*The elemental composition of representative soils.*[a]

Element	Global Average[b] (Chilton *et al.*, 1984) (percent)	Wilson and Karcher (1966) Average[c] (percent)
Oxygen	43.77	50.2 ± 2.2
Silicon	28.1	26.5 ± 9.2
Aluminum	8.24	6.7 ± 2.9
Iron	5.09	5.5 ± 9.0
Manganese		0.07 ± 0.06
Titanium		0.45 ± 0.43
Calcium	3.65	5.0 ± 6.6
Magnesium	2.11	1.3 ± 1.5
Potassium	2.64	1.4 ± 0.7
Sodium	2.84	0.6 ± 0.5

[a] Based on a dry-weight percentage basis. The total does not add to 100 percent.

[b] This is a mixture approximating the relative abundance of the eight most common elements in Earth's crust.

[c] These are means and standard deviations of compositions of 28 soils selected from throughout the United States.

neutrons. The neutron-attenuating powers of earth are enhanced by its water content. Representative ranges of soil water content (percent of dry weight) are: sand (0 to 10 percent), sandy loam (5 to 20 percent), loam (8 to 25 percent), silty loam (10 to 30 percent), dry loam (14 to 30 percent), and clay (15 to 30 percent). Earth varies in density, depending upon the soil type, water content, and the degree of compaction from ~1.7 g cm^{-3} to as high as 2.2 g cm^{-3}: to be compared with the density of "light" concrete, which is 2.35 g cm^{-3} (Casey *et al.*, 1967; Gilbert *et al.*, 1968). Because of this variation, specific information about the soil characteristics at the accelerator site must be obtained to facilitate effective shielding designs. If earth is to be used as neutron shield, measurements of its water content are required, particularly, if optimum shielding is required and large safety factors may not be used.

One great advantage in the use of earth as a shielding material is that, when the earth is adequately compacted, the shield is free from cracks and voids and neutron "streaming" cannot occur (Section 4.10.2). This property explains why many of the early cyclotrons were constructed inside a concrete vault buried below ground (Livingston, 1952). Earth may be easily put in place, but the opposite side of the coin is that, it may also be easily removed. It is most important to control any movements of earth that might compromise the integrity of the shield.

During the construction of a large accelerator to be sited underground, earth will be readily available and costs can be minimized by placing the accelerator room (or tunnel) at an optimum depth such that the volume of earth excavated equals that required for overhead shielding. Transportation of earth either away from or to the accelerator site will significantly increase construction costs and is to be avoided wherever possible.

4.10.2 *Concrete*

Concrete has advantages as a shielding material in that it may be poured in place, to make permanent shields, or cast into blocks which are movable. Most accelerators are contained within vaults or tunnels which were constructed with reinforced concrete poured into place. In many such cases, the roof of the accelerator vault is designed to support an over-burden of earth shielding.

Concrete blocks are convenient for temporary shielding installations (*e.g.*, experimental equipment) or sometimes for shielding targets, beam stops, etc., so that ready access is possible should the need for maintenance arise. When designing such shielding it is

advisable that, for most efficient assembly, modular blocks be fabricated, *i.e.*, blocks that use a standard dimension and its multiples. The assembly of concrete shields from concrete blocks generally requires the overlapping of the blocks to avoid streaming through the cracks. Interlocking blocks are also available and give more structural integrity, but they are generally harder to maneuver into place. Figure 4.39 shows some typical shielding blocks in use at FNAL. Note the integral multiples in the dimensions and the presence of lifting fixtures.
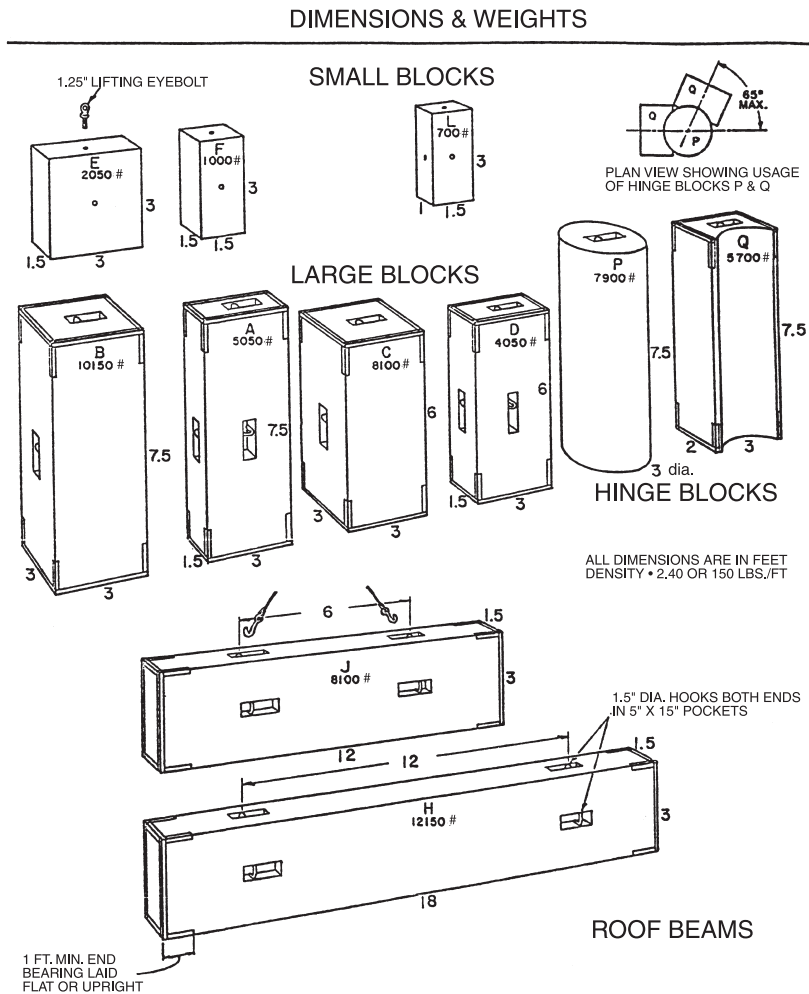
Fig. 4.39. Modular shielding blocks of standard sizes as used at Argonne National Laboratory and FNAL.

It is sometimes efficient to add heavy materials in the concrete aggregate. The resulting increase in density and average Z of the concrete increases its effectiveness for photon shielding. Heavy aggregates, such as barytes (barite) or iron ore, are used to produce concretes of high density (often exceeding 4.5 g cm^{-3}) for special shielding purposes. For photon shielding, those elements in the aggregates with high Z will provide additional absorption, not only because of the increased concrete density, but also because of the Z dependence of the photoelectric and pair-production cross sections. However, such special concretes are expensive and difficult to pour. It is also difficult to ensure uniform composition and density. Where space constraints are severe, and dense shielding is required, the cost-premium of special concretes may often be avoided by specifying a composite shield made of steel and ordinary concrete.

Table 4.9 gives the elemental compositions of various concretes used in shielding calculations (Chilton *et al.*, 1984). The water content of concrete is of great importance in determining its effectiveness for neutron shielding, particularly in the intermediate-energy range. Under some conditions, the water content of concrete may decrease with time; the precise value of its half-value period depends on the ambient temperature of the concrete, but typically it is ~20 y. O'Brien has calculated the magnitude of these effects on accelerator-produced neutron spectra emerging from concrete shields (O'Brien 1968a; 1968b; O'Brien and McLaughlin, 1968).

Sodium-24 produced in the shielding is often a major contributor to ambient radiation levels after the accelerator is turned off. Special, low-sodium aggregates may be used to reduce thermal-neutron-induced radioactivation of concrete and, consequently, the residual radiation levels. The same result may be achieved by the addition of boron compounds such as boron frits or colemanite. Other constituents of shielding such as steel reinforcing bars also can become radioactive. The reader should consult Volume 2 of the IAEA *Engineering Compendium on Radiation Shielding* for further details (IAEA, 1975).

4.10.3 *Other Hydrogenous Materials*

Polyethylene $(CH_2)_n$ is a very effective neutron shield because of its relatively large hydrogen content (approximately five percent by weight) and adequate density (0.92 g cm^{-3}). This material has been widely used to shield neutrons produced by D-D and D-T generators, and electron accelerators. Attenuation data for polyethylene and

TABLE 4.9—*Typical compositions of representative concretes after curing (Chilton et al., 1984).*

Concrete Type	Ordinary	Magnetite[a]	Barytes[b]	Magnetite and Steel	Limonite and Steel[c]	Serpentine[d]
Density (g cm^{-3})	2.35	3.53	3.35	4.64	4.54	2.1
Element	Partial Density (g cm^{-3})					
Hydrogen	0.013	0.011	0.012	0.011	0.031	0.035
Oxygen	1.165	1.168	1.043	0.638	0.708	1.126
Silicon	0.737	0.091	0.035	0.073	0.067	0.460
Calcium	0.194	0.251	0.168	0.258	0.261	0.15
Carbon						0.002
Sodium	0.04					0.009
Magnesium	0.006	0.033	0.004	0.017	0.007	0.297
Aluminum	0.107	0.083	0.014	0.048	0.029	0.042
Sulfur	0.003	0.005	0.361			
Potassium	0.045		0.159		0.004	0.009
Iron	0.029	1.676		3.512	3.421	0.068
Titanium		0.192		0.074		
Chromium		0.006				0.002
Manganese		0.007				
Vanadium		0.011		0.003	0.004	
Barium			1.551			

[a] Magnetite (FeO•Fe$_2$O$_3$) as aggregate.
[b] Barytes, a BaSO$_4$ ore, as aggregate.
[c] Limonite, a hydrated Fe$_2$O$_3$ ore, plus steel punchings, as aggregate.
[d] Serpentine (3MgO•2SiO$_2$•2H$_2$O) as aggregate; a concrete usable at high temperatures with minimal water loss.

for neutrons up to 5 MeV can be found in NCRP Report No. 38 (NCRP, 1971).

Polyethylene is readily machined and may, therefore, be used for shields with complicated geometries. The material has some disadvantages: it is relatively expensive and it is also flammable (but is commercially available with a self-extinguishing additive). In common with all hydrogenous materials, polyethylene presents the difficulty that thermal-neutron capture in hydrogen leads to a buildup of 2.2 MeV photons, and it is possible, therefore, to transform a neutron-shielding problem into a problem of gamma-ray shielding. The addition of a boron compound (such as approximately eight percent B_4C) is valuable in that it produces competition with the thermal neutron capture in hydrogen.[31] The reaction produces an alpha particle, which is stopped locally, and a readily attenuated 0.478 MeV photon. Polyethylene is commercially available with additives of boron (up to 32 percent), lithium (up to 10 percent), and lead (up to 80 percent) in various forms such as sheets, spheres and cylinders. Such materials can be useful to economize on space and to also accomplish shielding of photons and neutrons simultaneously. Furthermore, some of these materials are available in powder form, for molding into a desired shape by the user.

At first sight, water appears to be an attractive material for neutron shielding. Like polyethylene, it is rich in hydrogen and, in addition, it is plentiful and inexpensive. Many of the early neutron generators and cyclotrons were shielded with walls constructed of water-filled cans. More ambitious schemes have used water that could be pumped into or out of spaces sealed off by water-tight doors. Experience has shown, however, that water is not as convenient a shielding material for accelerators as might be thought. The integrity of water-can walls was breached by the rusting of cans and the development of leaks. Maintenance of even such simple shields became inconvenient and expensive. Like polyethylene, water can act as a source of 2.2 MeV photons, but boration is more difficult than for polyethylene. Therefore, it is often necessary to design a composite shield with a high-Z shield material, such as steel or lead, outside the water shield. As a consequence of this experience, water is no longer widely used as a shielding material at particle accelerators.

In the early years of operation of the Bevatron, wood was found to be as effective on a linear basis as concrete for neutron shielding, despite the difference in density of a factor of ~2.5 (Patterson, 1957).

---

[31]Boron has been added to materials other than polyethylene to form effective thermal-neutron shields. These include other plastics, putties, clays and glasses to accomplish specific shielding objectives.

This high efficiency of wood was due to rapid depletion of the intermediate-energy region of the neutron leakage spectrum transmitted through the magnet steel (see Section 4.10.4). Since wood is often considerably cheaper than concrete, it may serve as an economical shielding material. Knowledge of the neutron spectrum is essential before deciding whether wood may effectively replace concrete. One major disadvantage of wood is that it represents a major fire hazard. However, wood can be chemically treated to be fire retardant.

Wood is occasionally used in temporary shields or as plugs and fillers in neutron-shielding barriers. Wood is subject to dimensional changes, occasioned by temperature or humidity changes in the environment. Compressed or reconstituted woods, such as "Masonite" are not as subject to dimensional changes. In either type of material, however, their resistance to radiation damage is quite poor.

Paraffin, plastics and organic oils are hydrogenous materials that are occasionally used for neutron shielding. They all have the great disadvantage that they lack structural stability, unless supported by rigid containers. Great care should be taken in designing shields with these materials because of their flammability. In the past, paraffin, in the form of wax, has been used for neutron shielding, but in recent times its use has been spurned because of the fire hazard. Under some conditions, it can be used if it is packaged in metal containers to reduce this problem. Paraffin treated with fire retardant additives is now commercially available.

Calculations have been made of the attenuation of absorbed dose produced by monoenergetic neutron beams, incident at several angles, on slabs of various materials containing hydrogen (Allen and Futterer, 1963; NCRP, 1971). The materials include Nevada Test Site soil (dry and saturated with water), water, concrete, and polyethylene. The neutron energies range from 0.5 to 5 MeV, and the data give useful comparisons between different shielding materials.

4.10.4   *Steel* [32]

A relatively high density in conjunction with low cost make steel an attractive shielding material. Steel or iron for shielding is generally available in the form of blocks. Occasionally, a large source of scrap steel becomes available, *e.g.*, from decommissioned warships or large

---

[32] Steel is often referred to as an "iron" in the shielding literature. Pure iron is not used for shielding for many reasons, not the least being its cost. It is always an alloy of iron (steel) that is used. The density of 7.9 g cm^{-3} for iron in its purest form is not attained in the bulk quantities of steel necessary for radiation shielding.

accelerators. Such a source of steel is usually economically attractive, but there may be hidden costs, such as cutting the steel into blocks of suitable size, rough machining and transportation from the source that should be included in the cost analysis. In any form, steel poses significant handling difficulties because of its high density. The size of blocks will be limited by the weight capabilities of cranes and other handling facilities. The consequent limitation in volume may result in a large number of lifting operations in the construction or modification of shield walls.

Iron has an important deficiency in shielding neutrons: it contains no hydrogen, and the lowest inelastic energy level of ^{56}Fe is 847 keV. (Natural iron is 91.7 percent ^{56}Fe, 2.2 percent ^{57}Fe, and 0.3 percent ^{58}Fe). Neutrons above 847 keV will be slowed by inelastic scattering, but below this energy they can only lose energy in the dominant isotope, ^{56}Fe, by elastic scattering, a very inefficient process. Consequently, there is a buildup of neutrons below this energy. This deficiency is exacerbated by the fact that the quality factor for neutrons is at a maximum near 700 keV. Natural iron has two regions where the total cross section is very low because of the resonance in ^{56}Fe: at 27.7 keV where the minimum cross section is ~0.5 barn and at 73.9 keV where the minimum cross section is 0.6 barn. The effect is to produce an attenuation length about 50 percent longer than the high-energy attenuation length. This is the major reason why unexpectedly large fluxes of low-energy neutrons are found outside steel shielding. As a shield against high-energy neutrons, natural steel can be quite effective if it is followed by a material made of light elements, such as concrete. The effect of the composite will depend on the total number of geometric collision lengths of the material, as long as the lighter material is thick enough to stop the low-energy neutrons leaking through these anti-resonances.

These facts explain the observation of a very soft neutron radiation field around the Bevatron when it first operated in the 1950s without overhead shielding. Intermediate-energy neutrons streaming through the magnet yoke were an important component of the radiation field (Patterson and Thomas, 1973). Somewhat later, Perry and Shaw observed an increase in the dose-equivalent rate at Nimrod when steel was used to replace an equivalent mass of concrete (Perry, 1967; Perry and Shaw, 1965;). At the same accelerator, Shaw *et al.* (1969) showed that the neutron spectrum outside steel shielding was richer in low-energy neutrons than were the equivalent neutron spectra outside concrete or earth shielding. These earlier reports have been supported by work at FNAL. Figure 4.40 shows two spectra (Elwyn and Cossairt, 1986) obtained using the multisphere technique (Bramblett *et al.*, 1960). The spectra were both measured
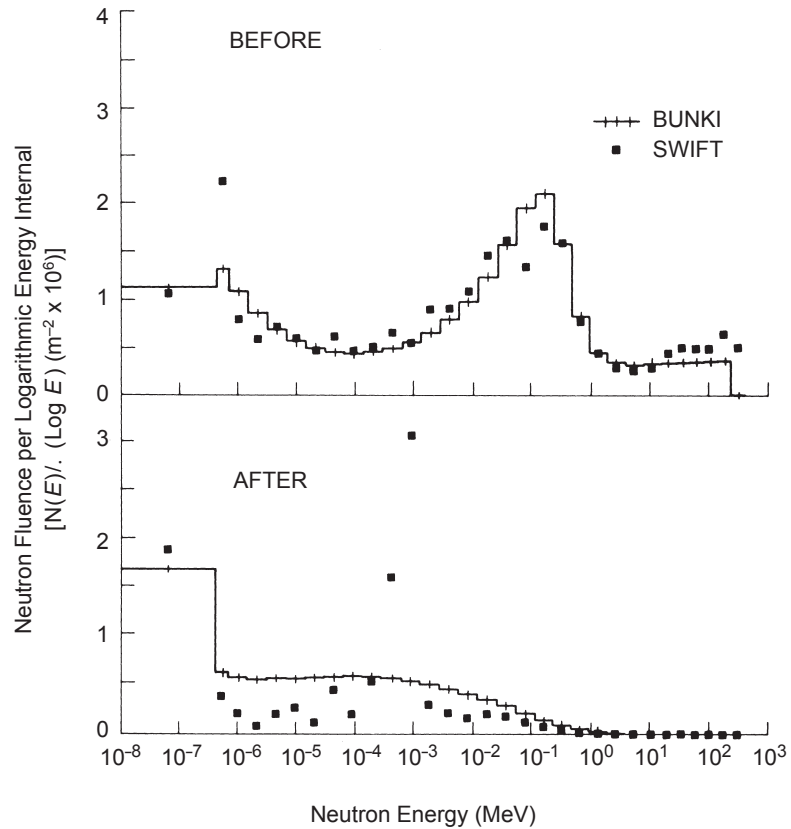
Fig. 4.40.   Neutron energy spectra plotted as neutron fluence per logarithmic energy interval for a beam dump struck by secondary particles from 800 GeV proton interactions in a target far upstream. The spectrum labeled "before" is for a bare-steel shield while the one labeled "after" was obtained after a 91 cm thick layer of concrete was placed over the iron. The histograms and the solid symbols represent results obtained using two different spectrum unfolding computer codes (Elwyn and Cossairt, 1986).

near 90 degrees to a beam dump struck by secondary particles from 800 GeV proton interactions far upstream of the beam dump. One spectrum is for a bare-steel shield while the other was measured after the steel was covered by a 91 cm thick layer of concrete. For the bare-steel shield, the dose-equivalent rate external to the shield was over 40 times that measured after the concrete was installed. This factor is far in excess of the factor of 10 expected from simple attenuation of the equilibrium cascade neutron spectrum. The concrete also reduced the mean quality factor of the neutrons from

5.4 to 2.8. In general, a steel shield "capped" by such a concrete shield will be an efficient use of space. It has been determined that 60 cm of concrete is the most efficient thickness to use for this purpose (Yurista and Cossairt, 1983; Zazula, 1987). Shielding properties of other elements near iron (chiefly copper and nickel) in the periodic table are comparable.

Concrete/steel composite shields are commonly constructed with the steel toward the source side: the intermediate-energy neutrons being removed by a hydrogenous shield (normally concrete) on the outside. McGinley (1992a; 1992b) has published some data for 15 and 18 MV medical accelerators that demonstrate the increase in neutron dose outside the shield as the metal portion (steel or lead) is moved to the outside, and as the metal thickness increases and the concrete thickness decreases. A useful rule of thumb is to ensure that at least one high-energy inelastic interaction mean-free-path thickness of hydrogenous shielding lies on the outside. In practical terms, this translates to ~60 cm of concrete.

Because both steel and concrete blocks will normally be combined in modular shielding, blocks of both materials should stack into the same basic dimensions. In computing shield thicknesses, care must be taken to use the correct density for steel which can vary widely from a low of seven for low-grade cast iron to a high 7.8 g cm^{-3} for some high-quality steels. An important factor, in the choice of a particular iron alloy (steel), will be its elemental composition which can influence the potential level of induced radioactivity. In particular, the use of steels containing cobalt, even at the parts per million level, should be avoided.

4.10.5 *Special Materials*

4.10.5.1 *Materials of High Atomic Number.*   The materials in this category are valuable, particularly, in shielding photons and for minimizing neutron production from ions of energy below ~5 MeV. Thus, *e.g.*, tantalum and platinum are preferred as beam stoppers. Above 5 MeV, light ions produce neutrons when impinging on most materials.

Lead is used for a variety of shielding purposes because the required attenuation may be obtained with thicknesses much less than those for low- or even moderate-Z materials. Lead has a high density (11.3 g cm^{-3}) and, in the form of thin sheets, is widely used to attenuate x rays at the energies used in diagnostic radiology. The thickness advantage for lead is pronounced at x-ray energies below ~0.5 MeV, where photoelectric absorption processes (roughly

proportional to $Z^{4.5}$ per atom) dominate. At photon energies above a few mega-electron volts, the pair-production absorption process (proportional to Z^2 per atom) dominates. Within a photon energy range between ~0.5 MeV and a few mega-electron volts, the weight of lead shielding does not differ much from that of low- or moderate-Z materials for comparable shielding. However, above and below this narrow range lead is better, even on a weight basis, because the absorption processes are proportional to higher powers of Z than is the density.

Pure lead is essentially corrosion-free, but its value as bulk-shielding material is limited because of its poor structural characteristics. Lead sheets or plates tend to flow under their own weight, unless supported against a rigid backing or laminated with structural materials such as wood or steel. Some lead alloys (*e.g.*, with antimony) have improved structural properties, but may lead to the production of undesirable radionuclides, *e.g.*, ^{122}Sb and ^{124}Sb. Lead has been contained in steel boxes to stabilize the material when used in massive shielding.

Lead and lead alloys are available as additives to other materials in order to enhance their capacity for shielding photons. Fabric blankets containing shredded lead can be effectively used to shield radioactive accelerator components to minimize exposures associated with accelerator maintenance activities. However, the chemical toxicity of lead requires care in its fabrication and use so as to properly protect personnel. Lead should always be used for shielding in ways that minimize the production of activation products to avoid possible difficulties with disposal of the material as waste.

Tungsten is an excellent, but relatively expensive, shielding material. Its high density (17 to 18 g cm^{-3})[33] in the machinable sintered form, and high melting temperature (3,410 °C) make it extremely useful as a component in photon shields, as well as in beam collimators and beam dumps, when large quantities of heat must be dissipated. Thus, tungsten is usually placed in front of a depleted uranium back-stop to absorb the peak of the energy dissipation curve and so avoid disruption of the uranium containment.

Uranium is an attractive shielding material. Its high density (19 g cm^{-3}) and relatively high melting point (1,133 °C) make it suitable for efficient shield design when space is at a premium. For example, uranium was used in shielding above the straight sections of the Bevatron. The natural material is available in a depleted form in which ^{235}U is removed from the dominant ^{238}U. Most forms of

---

[33] The density of the pure metal is 19 g cm^{-3} but it is usually machined after sintering, which process reduces the density somewhat.

uranium must be inventoried as "accountable material." Uranium may not be a good material in regions of high neutron fluence because of the relatively high induced radioactivity associated with both neutron- and photo-fission.

In the depleted form, uranium is relatively safe, but if combined with hydrogenous materials, criticality should be considered for the specific depleted uranium available (Borak and Tuyn, 1987), since the degree of "depletion" can apparently vary considerably (de Haas, 1987; Roubaud and Tuyn, 1987). Major drawbacks lie in the properties of the metal. It has a large anisotropic thermal expansion coefficient and also is readily oxidized when exposed to air (especially humid air). The oxide is readily removable and presents a significant internal radiation exposure hazard; uranium compounds are both radioactive and toxic. Prevention of oxidation by sealing the metal with an epoxy resin or paint meets with only limited success due to eventual embrittlement and chipping accelerated by radiation damage. Sealed containers filled with dry air seem to be the best storage solution to limit oxide formation. Small chips of the element are pyrophoric, complicating machining processes by posing yet another safety hazard.

4.10.5.2 *Materials of Low Atomic Number.* Materials with low Z such as aluminum or ordinary concrete are preferred when abating electron fluences to minimize the production of x rays. At some facilities, where no significant hazard can arise from the noxious gases produced and adequate space is available, air may be used to absorb electrons.

4.10.6 *Special Considerations*

There are certain relatively costly-materials whose specialized radiation-attenuation characteristics can be advantageously applied to such purposes as filling apertures in shielding barriers, observation windows, and lining to shielding barriers.

Holes in shielding walls, *e.g.*, for the introduction of piping or ductwork, can be filled by packing them with steel wool (for x rays); with borax, borated paraffin, or borated plaster (for neutrons).

Mortars or plasters containing nuclides with high attenuation characteristics are now commercially available. Such materials have different compositions depending upon whether they are to be used for x-ray or neutron attenuation. They are especially valuable for shielding cast in place around very high intensity sources of radiation. In the same general category of such materials, lead-loaded putties, ceramics, and diatomaceous earths can be utilized.

Linings to shield walls can sometimes reduce overall shielding requirements. For example, a low-*Z* lining (*e.g.*, with plastic materials rich in carbon) to a concrete wall can be used to reduce the intensity of x rays produced by electron impingement on the wall. The basic problem with this approach is to avoid any undue fire hazards resulting from the lining. Similarly, boron-impregnated linings are occasionally used to reduce thermal-neutron fluences, particularly in labyrinths or on outside surfaces of shielding walls in which the neutrons have been attenuated.

Laminates of materials have been used occasionally, with the purpose of reducing shielding thicknesses by taking advantage of the differences in buildup and/or absorption of radiations in selected materials. In general, these laminates provide some economy of space, but at a relatively high cost. Each case must be considered on its own merits.

The natural radioactive background of materials is of concern to designers of accelerator facilities used for low-level radioactivity research. Radiation background is an ever present problem that is aggravated by the importation of masses of material containing naturally-occurring radioactivity. Aside from this specialized application, there is no necessity to take special care in selecting shielding materials for their low intrinsic radioactivity.

Observation windows are generally not used in the types of accelerator facilities that are considered in this Report, but closed-circuit television systems or optical periscopes in labyrinths are often employed. Occasionally, a combination of mirror with window (behind a shielding partition) is utilized. Windows are usually mounted in concrete walls and the thicknesses for equivalent attenuation for the two materials, can differ substantially. The design of the window must, therefore take this difference into consideration, in tapering or compensating the concrete thickness appropriately. Several types of observation windows are commercially available.

4.11 Tunnels, Labyrinths and Ducts

4.11.1 *Introduction*

No practical accelerator shield can be constructed without penetrations for the access of personnel and for the passage of utilities such as control and power cables, cooling-water pipes, heating, ventilation and air-conditioning ducts. Such penetrations compromise the

integrity of the shield and must be designed with great care. Personnel access ways may typically have cross-sectional dimensions of 1×2 m (door sized), while ducts for utilities usually have a smaller area—typically 0.2×0.2 m. Estimation of the transmission of radiation through these penetrations can be difficult, because, *e.g.*, utility ducts are partially filled (*e.g.*, water in pipes, cables) and professional judgment is needed to evaluate the degree of attenuation afforded by these materials.

Ideally, the design goal of any penetration should be to match the designed attenuation provided by the shield wall, but this is usually difficult to match in practice. The radiation source (or potential radiation source for situations of concern such as accidental beam loss) should be evaluated from data given in Section 3. There is no completely satisfactory theoretical basis for the calculation of the attenuation of penetrations, and it is necessary to fall back on experimental data, albedo coefficients, empirical methods, and computer simulations. Computer simulations involve the use of complex Monte-Carlo codes which can be used for both curved and rectilinear labyrinths. This subject has been reviewed in rather extensive detail elsewhere (*e.g.*, IAEA, 1988) and will only be summarized here. In this Section, the results of such work will be presented in order to give the reader useful information in the evaluation of such penetrations.

An overwhelming conclusion of the body of extant data is that the primary particle energy has very little effect on the attenuation of a labyrinth viewing a source of beam loss, other than the increased total yield of neutrons as a function of incident energy and ion type (Section 3). One can estimate the dose, dose equivalent, or neutron fluence at the exit of a labyrinth by using attenuation estimates in conjunction with an estimate of the neutron fluence at the penetration's entrance into the beam enclosure. Thus, results of attenuation measurements obtained at proton accelerators are of general utility.

There are two general rules which should be used in the design of adequate radiation attenuation of penetrations:

- Never place any penetration so that a primary particle or photon beam can point directly towards it or so that it allows an unshielded path for secondary radiations or particles from a significant beam interaction point. (This then limits the design problem to the estimation of the transport of scattered radiation).
- For any adequate labyrinth, the sum of the shield-wall thicknesses between the source of radiation and the exit point of the penetration should be at least equivalent to that which would be required if the labyrinth were not present.

4.11.2 *Design Example for Photons Using Albedos*

A particular application of the reflection coefficients identified in Section 4.3.4 to the design of labyrinths is illustrated here. Figure 4.41 is an example of a labyrinth providing access to a photon source of some known dose equivalent [or dose-equivalent rate (H_0)] at 1 m. In general, some knowledge of the energy spectrum at this location is also needed.

Using the reflection coefficients (α_x) from Figures 4.12 and 4.13, one can use Equation 4.59 to obtain a conservative estimate of the
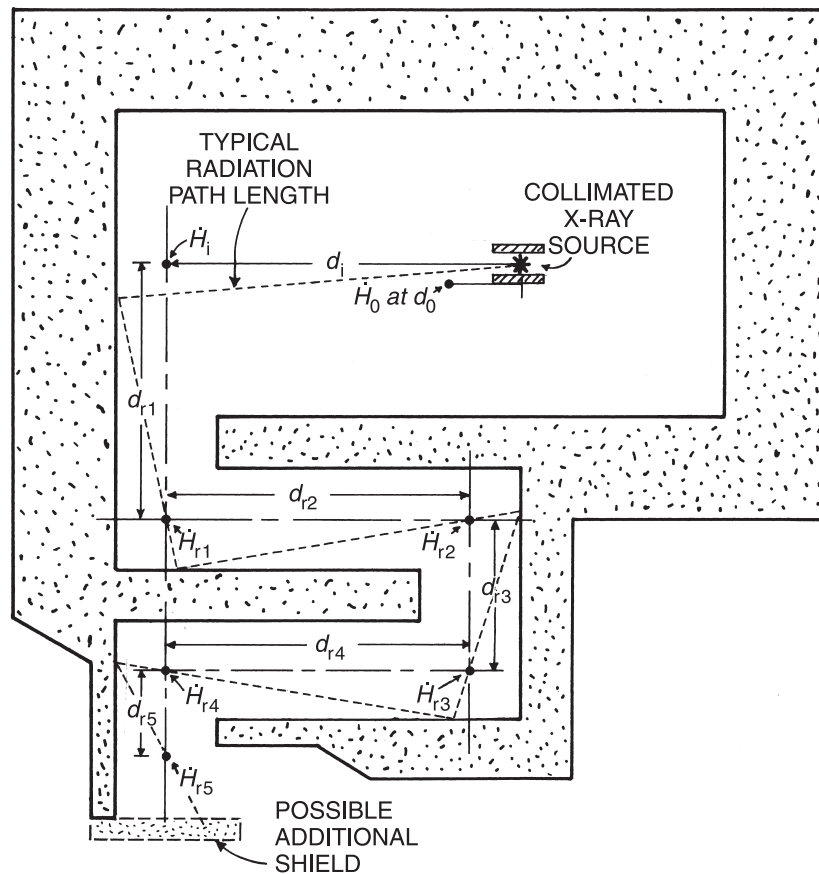
Fig. 4.41. Generalized labyrinth design illustrating successive reflections of photons from a collimated source through the maze. These path lengths can be approximated by a sequence of centerline distances, as shown in the diagram (NCRP, 1977).

dose equivalent [or dose-equivalent rate (H_{r_j})] after j sections of the maze [not counting the initial path to the wall (d_i)]:

$$H_{r_j} = \left(\frac{H_0}{d_i^2}\right) \left(\frac{\alpha_1 A_1}{d_{r_1}^2}\right) \prod_{i=2}^{i=j} \left(\frac{\alpha_i A_i}{d_{r_i}^2}\right).$$ (4.59)

In this formula, the albedo coefficient (α_1) is selected to be representative of the incident photon energy while A_1 estimates the cross-sectional area of the wall struck by the initial beam. A_j is the cross-sectional area of the jth leg of the maze. In the denominator, the distances are those defined in Figure 4.41 and represent the inverse-square law dependence. After the first leg, it is usually a conservative assumption if values for α_j appropriate for 0.5 MeV photons are used. The higher the incident photon energy the more conservative the formula is expected to be. Equation 4.59 is probably most accurate if the ratio $d_{r_j}^2/A_j$ lie between 4 and 40. When the photon energy is above the threshold for photonuclear reactions, neutrons dominate the radiation in labyrinths of length greater than a few meters. The photon fluence in such labyrinths will be composed primarily of gamma rays generated from the capture of neutrons in the walls of the labyrinth (McGinley and Miner, 1995; McGinley *et al.*, 1995). Unfortunately, complications in the transport of neutrons discourage the use of an equation analogous to Equation 4.59 for situations involving neutrons. However, there is an extensive body of empirical neutron information as discussed in the following sections.

4.11.3 *Straight Penetrations—Neutrons and Photons*

The measurements of Gilbert *et al.* (1968) of the transmission of neutrons and photons through a tunnel 2.8 m high, 1.8 m wide, and 100 m long are summarized in Figure 4.42. A 14 GeV proton beam was incident on a target providing a good "point source" at a distance of 3.2 m from the tunnel entrance and at 90 degrees to the proton beam. Activation detectors with different energy thresholds made it possible to obtain limited information on the radiation energy spectrum. The experimental conditions did not allow an absolute normalization to beam loss. Inspection of the figures shows that the lower energy part of the spectrum (thermal and intermediate-energy neutrons) attenuates more rapidly by air and wall scattering than do the higher energy neutrons, and that for short tunnels (<20 m long) the reduction in fast neutron fluence is almost entirely due to the inverse-square law.

Details of the source geometry are very important for a straight penetration. Figure 4.43 shows the transmission of neutrons through
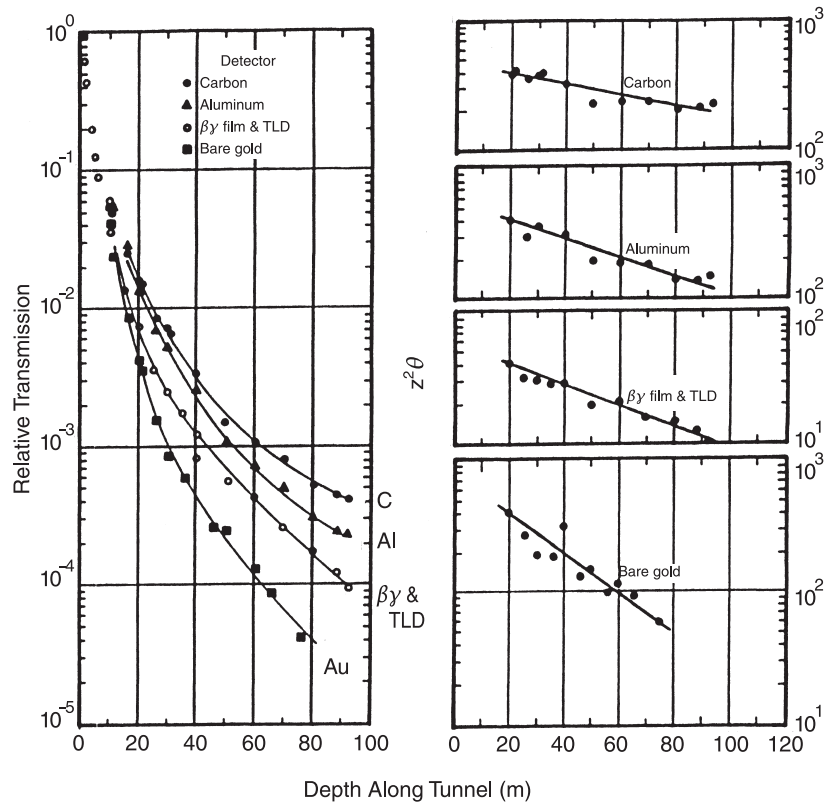
Fig. 4.42. The relative transmission of neutron fluence (Θ) and gamma dose rate along a straight tunnel (left) and the same data ($z^2\Theta$) plotted times the square of the tunnel depth (z) in order to remove the inverse-square law dependence (right) (Gilbert *et al.*, 1968). In the frame to the right, the lines represent fits to determine the approximate attenuation length for the neutrons detected by the different threshold detectors. The thresholds or energy windows of the reactions used as detectors are as follows: ^{12}C(n,2n)^{11}C, 20 MeV; ^{27}Al(n,α)^{24}Na, 6 to 25 MeV; and ^{197}Au(n,γ)^{198}Au, thermal capture.

a straight tunnel for three source geometries: point source, line source, and plane source (or off-axis point source). The data are presented in units of $d/\sqrt{A}$ where d is the distance from the source and A is the cross-sectional area of the tunnel. This scaling is acceptable provided the ratio of the height/width of the penetration lies between the values 0.5 and 2 (IAEA, 1988).

4.11.4 *Transmission of Neutrons Through Labyrinths*

There have been several theoretical, empirical and experimental approaches to estimating the radiation transmission of neutrons
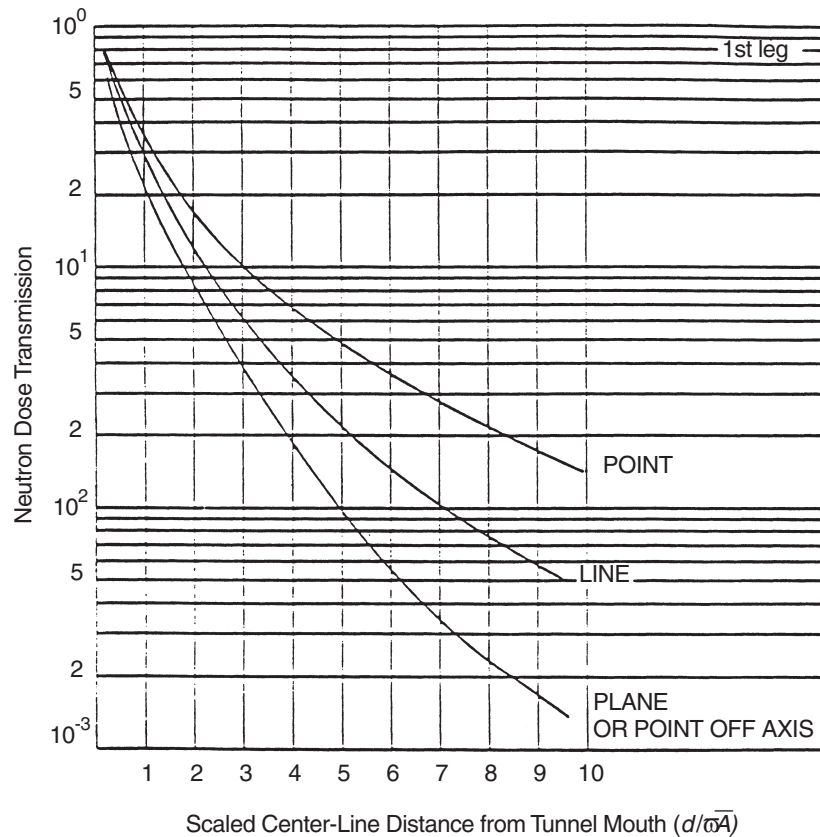
Fig. 4.43. Universal neutron dose transmission curves for the first leg of a labyrinth for different source conditions (taken from IAEA, 1988, original reference is Goebel *et al.*, 1975). d is the distance from the source in the tunnel with a cross-sectional area (A).

through a labyrinth. Labyrinths or mazes may be considered as several connected rectilinear tunnels, usually, but not necessarily with successive legs orthogonal to each other (see Figure 4.41 for an example). The second and successive legs of such "rectilinear" components of the maze change the situation dramatically, principally by modifying the spectrum of the transmitted neutrons.

Figure 4.44 is a "universal curve" for each of the second and succeeding legs due to Goebel *et al.* (1975), who summarized results using the codes SAM-CE (Cohen *et al.*, 1973), AMC (Maerker and Cain, 1967), and ZEUS (d'Hombres *et al.*, 1968). Gollon and Awschalom (1971) have generated similar curves using the ZEUS code for a
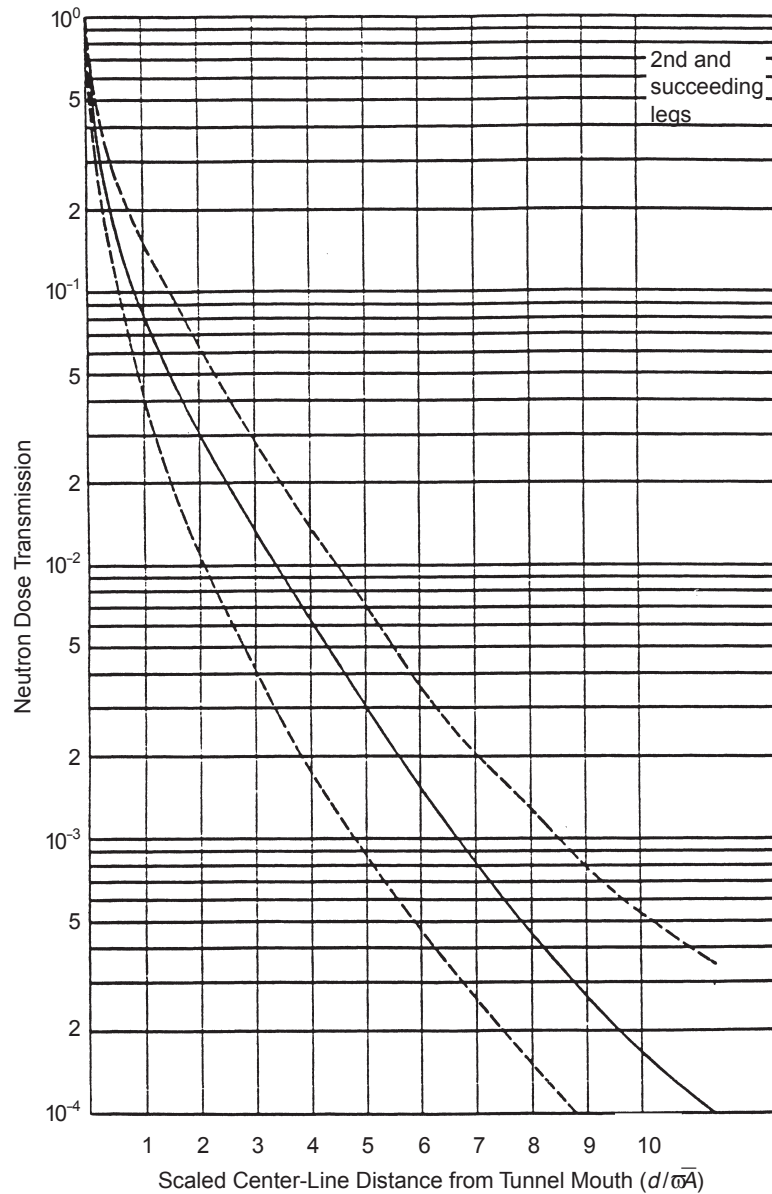
Fig. 4.44. Universal neutron dose transmission curves for each of the second and succeeding legs (taken from IAEA, 1988; original reference is Goebel *et al.*, 1975). The solid curve is an average of the various theoretical results, while the dashed curves represent the extremes found in various individual calculations.

variety of geometries. It will be seen from Figures 4.43 and 4.44 that there is a substantial difference between the transmission of the first and second legs. Subsequent legs have transmissions identical to that of the second leg. The reason for this is that the first leg produces a dramatic change in the radiation spectrum while the spectra of the subsequent legs are similar to one another.

Tesch (1982) has developed an entirely analytic approach to the problem of dose-equivalent rate attenuation by multi-legged labyrinths at proton accelerators. For the first leg (the one directly viewing the point of beam loss), the expression is essentially an inverse-square law dependence with a simple in-scattering factor of two included:

$$H(r_1) \,=\, 2\, H_0(r_0)\, (r_0/r_1)^2 \qquad \text{first leg.} \tag{4.60}$$

The expression for succeeding legs is in the form of the sum of two exponentials:

$$H(r_i) \,=\, \left(\frac{e^{-r_i/0.45} \,+\, 0.022\, A_i^{1.3}\, e^{-r_i/2.35}}{1 \,+\, 0.022\, A_i^{1.3}} \right) H_{oi}, \quad i^{\text{th}} \text{leg (i} > 1), \tag{4.61}$$

where for Equations 4.60 and 4.61:

r_0 = distance from the source to the mouth of the labyrinth in meters
r_1 = distance from the source into the first leg in meters
$H_0(r_0)$ = dose equivalent at the mouth from a point source
A_i = cross-sectional area of the maze (m^2)
H_{oi} = dose equivalent at the entrance to the ith leg
r_i = distance into the ith leg in meters

These formulae do not accommodate the expected scaling with the square root of the tunnel aperture and are best used for personnel labyrinths with cross-sectional areas of ~2 m^2. An advantage of these formulae is that they are simple and may be solved using minimal computational aids.

Few measurements of the transmission of complete labyrinths exist. Stevenson and Squier (1973) have reported measurements made at the 7 GeV Proton Synchrotron NIMROD, and Cossairt *et al.* (1985b) made measurements at the Tevatron at Fermilab.

Figure 4.45 shows the measurement of transmission through the maze shown in Figure 4.46 (Stevenson and Squier, 1973). This two-legged penetration was 2.3 × 2.3 m in cross section and its walls were made of concrete. Four nuclear reactions were used to measure the transmission of neutron fluence. Inspection of this graph shows a large reduction in transmission at the first bend of the labyrinth.
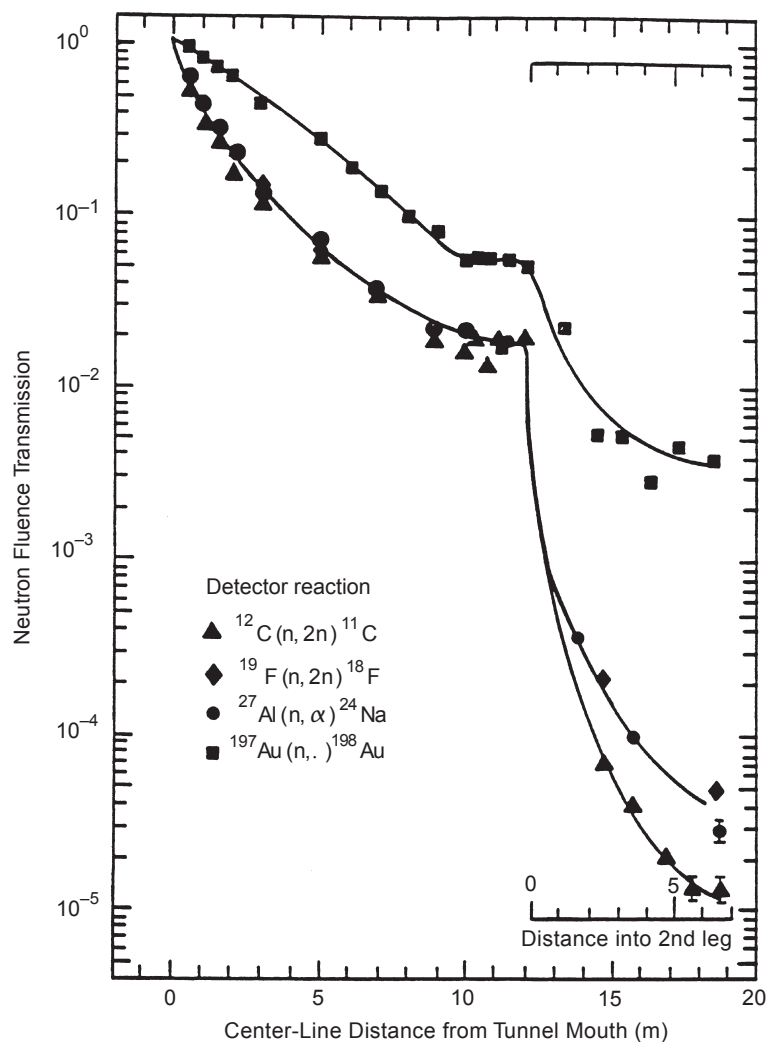
Fig. 4.45. Relative transmission of neutron fluence along the tunnel layout shown in Figure 4.46. The reactions indicated are sensitive to the following regions of neutron energy, E_n: ^{12}C(n,2n)^{11}C, $E_n > 20$ MeV; ^{19}F(n,2n)^{18}F, $11 < E_n < 40$ MeV; ^{27}Al(n,α)^{24}Na, $6 < E_n < 25$ MeV; and ^{197}Au(n,γ)^{198}Au, thermal capture (Stevenson and Squier, 1973).
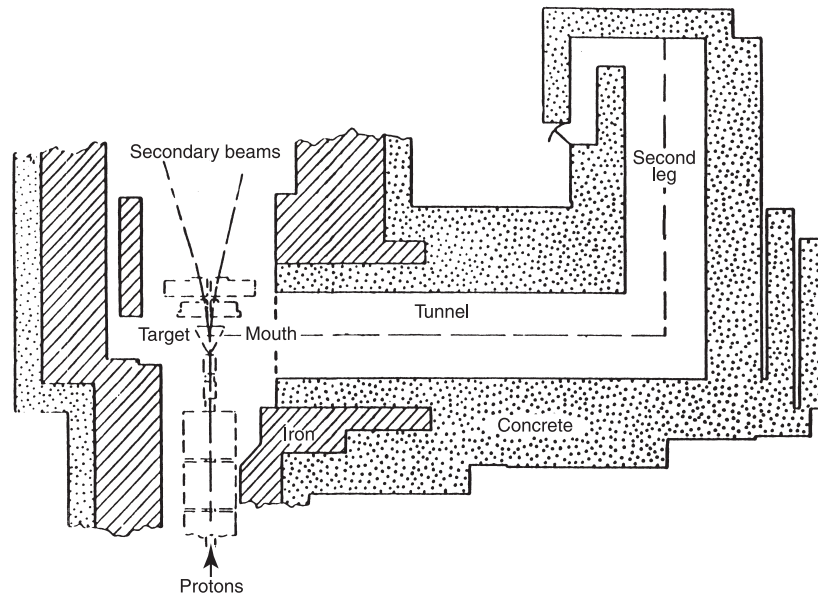
Fig. 4.46. Experimental layout used to study the transmission of neutrons around right-angled bends at a 7 GeV proton synchrotron (Stevenson and Squier, 1973).

Beyond the bend, the transmission of fast neutrons is much lower than that of thermal neutrons.

Figure 4.47 shows the four-legged labyrinth used by Cossairt *et al.* (1985b) for their measurements. The labyrinth gave access to the accelerator tunnel in which 400 GeV protons struck a target. Figure 4.48 shows measurements of absorbed dose along the labyrinth compared with calculations based on the work of Goebel *et al.* (1975), Gollon and Awschalom (1971), and Tesch (1982). The three calculated transmission curves are in fair agreement, even after four legs of the labyrinth. At the deepest penetrations, the measured transmissions agree best with the calculations of Goebel *et al.* The assumption made in these calculations, that after the first bend the transmission of the second, third, fourth and succeeding legs will be identical, is supported by these measurements.

Cossairt *et al.* (1985b) also made measurements of quality factor using a recombination chamber at the end of the first leg and in the middle of the short second leg (Figure 4.47). The results were $Q = 5.5 \pm 0.6$ and $Q = 3.4 \pm 0.1$, respectively. This indicates a softening of the neutron energy spectrum in the second leg which was further verified by a measurement of the neutron energy spectrum

ELEVATION VIEW

SOIL

ALUMINUM TARGET
IN VACUUM BOX

$\vdash$ 3 meters $\dashv$

PLAN VIEW

400 GeV PROTONS

Ⓢ

Ⓡ

r_3

r_2

r_4

r_1

Ⓡ

CONCRETE SHIELDING BLOCKS
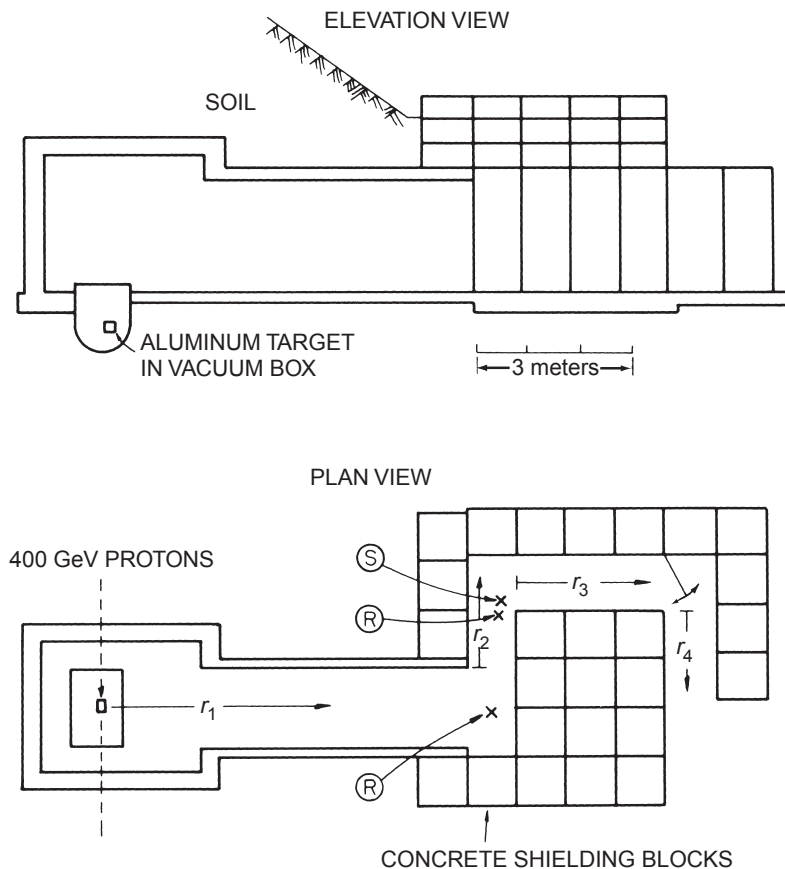
Fig. 4.47. Plan and elevation views of the access labyrinth studied. Coordinates are defined in this figure. Locations of spectrum (S) and recombination chamber (R) measurements are indicated. A beam of 400 GeV protons was incident on a target underneath the floor of this enclosure in the vacuum box (Cossairt *et al.*, 1985b).

that resulted in $Q = 3.1 \pm 0.7$.[34] Such results are consistent with those of Stevenson and Squier (1973).

In summary, the theoretical, empirical and experimental approaches to the estimation of labyrinth transmission give quite good agreement—sufficiently accurate for shield design.

---

[34] These estimates of quality factor were based on the data and recommendations given in ICRP Publications 21 and 26 (ICRP, 1973; 1977).
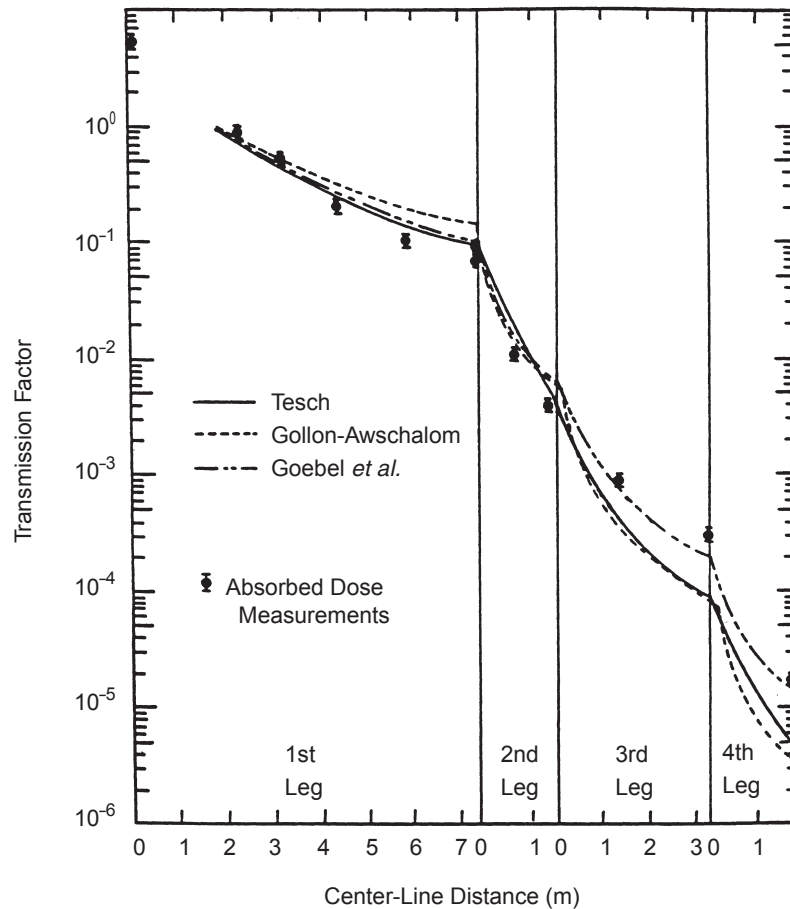
Fig. 4.48. Absorbed dose measurements and predictions of transmission in the entrance tunnel shown in Figure 4.47. All transmission curves are normalized to unity at the tunnel mouth. The measurements are absolute, and are in units of fGy (400 GeV proton)$^{-1}$ incident on the target [measurements by Cossairt *et al.* (1985b); curves from Goebel *et al.* (1975), Gollon and Awschalom (1971), and Tesch (1982)].

4.11.5 *Transmission of Neutrons Through Curved Tunnels*

Curved tunnels are used to provide access to large equipment which cannot negotiate sharp bends. The attenuation of neutrons along such tunnels is effectively an exponential. Patterson and Thomas (1973) suggest that the sparse data available give an attenuation length, $\lambda = 0.7 \sqrt{R}$ where R (meters) is the radius of the tunnel arc.

4.11.6 *Door Design*

Movable shielding doors, rather than labyrinths, may be used to provide access. This is particularly true at some of the smaller accelerators described in this Report. The designer must be aware of several problems that must be addressed in adequate door design. The door must provide the same equivalent radiation attenuation as was achieved by the shield wall. Given the large masses of such doors, their design must be carefully engineered to provide the necessary shielding but, nevertheless, still operate reliably. Safety considerations demand mechanical interlocks that will prevent the accidental crushing of personnel as the door is closed. An escape mechanism must provide for escape from the accelerator vault in the event of equipment or power failures, or fire.

Usually the least expensive construction materials are concrete, steel or lead, and movable doors are often made up as composites of these materials so as to optimize their efficient use of space and/or mass. If lead is used in the construction, it is necessary to design the door so as to prevent its "flowing" under its own weight and to prevent the formation of voids in other ways which would compromise the expected shield attenuation. Cracks or gaps around the perimeter of such doors, which are possible paths for the transmission of scattered radiation, are another possible problem which must be avoided by proper design. (It is poor practice to have a direct beam aim directly at such a crack). Such gaps are usually an inevitable consequence of the need to allow for expansion and possible settling of the building. A conservative solution is to provide an overlap of shielding of at least ten times the width of any gap between the door and the wall or floor. The interface between floor and door can be particularly difficult, given the need to prevent trip hazards, such as can result with a recessed floor. Figure 4.49 illustrates these problems and indicates some possible solutions. Every installation is unique in its layout and this is particularly true of the optimum configurations of its doors. Individual attention must be given to the design of every door.
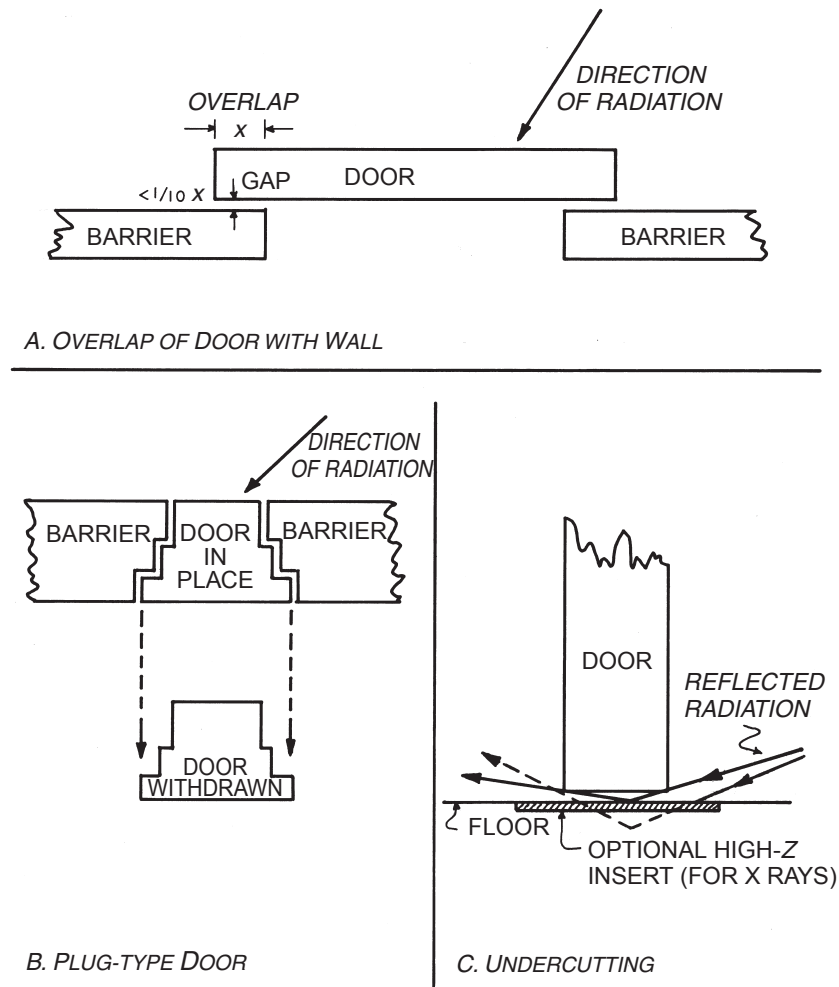
Fig. 4.49. Details of typical shielding doors. For the undercutting case, an optional high-Z insert may reduce the scattering of photons under the door at an electron accelerator. For an ion accelerator, a low-Z insert such as polyethylene or borated polyethylene (to capture thermal neutrons slowed down by the polyethylene) could be beneficial (NCRP, 1977).

5. Techniques of Radiation Measurement at Particle Accelerators

5.1 Introduction to Radiation Dosimetry at Particle Accelerators

The theoretical basis for radiation dosimetry has been extensively discussed by Carlsson (1985). The radiation fields around accelerators are complex, often consisting of many different ionizing radiations extending over a broad range of energies (Baarli, 1969). Several aspects that make radiation dosimetry at particle accelerators sufficiently different from other branches of dosimetry warrant extended discussion. Section 3 shows that the most obvious differences between particle-accelerator-radiation environments and other radiation environments lies in the variety of radiations (and/or particles) to be considered, their energy distributions, and their distributions in time and space. (The additional problems which arise because of pulsed radiation have been discussed in Section 2). In only one other branch of radiation physics—dosimetry during space missions—does the energy of the radiations to be measured extend as wide a range as it does in particle-accelerator environments. Furthermore, it is only at these high energies that the dosimetry of muons, pions, and the rarer nuclear particles is performed.

At particle accelerators, radiation dosimetry is performed for six distinct reasons (McCaslin and Thomas, 1981):

- investigation of radiation accidents
- routine radiological-protection surveys
- individual (personal) monitoring
- environmental monitoring
- beam-intensity measurement
- radiation-field quantification

Of these six topics, the first four are principally concerned with radiological protection, while the last two are of a more general application.

269

Measurements that are made solely for the purposes of radiological protection, *e.g.*, to demonstrate compliance with protection limits, must ultimately be expressed in units of the quantities in which the limits are defined. Two sets of quantities are of importance in radiological protection. Dose limits are expressed in terms of *protection quantities*, and compliance with these limits can be demonstrated by a determination of the appropriate *operational quantity*.

In Publication 60, ICRP (1991) made significant changes in the definitions of the protection quantities and recommended that equivalent dose (D_T) and effective dose (E) be used in radiological protection. These protection quantities are not directly measurable. For exposure of humans by sources of radiation outside the body (external radiations), the convention has been adopted that operational quantities defined by ICRU should be used for practical measurements. The two sets of quantities may be related to radiation field quantities such as particle fluence and, in turn, by sets of conversion coefficients to each other.

The operational quantities now in use, ambient, directional, and personal dose equivalent [$H^*(d)$, $H(d,\Omega)$ and $H_p(d)$, where d is the depth in the medium and Ω is the direction], were originally defined to be compatible with protection quantities defined by ICRP in the seventies and eighties (ICRP, 1977; ICRU, 1985; 1988). However, they remain generally acceptable for the newer protection quantities (ICRP, 1996; ICRU, 1998a).

In Publication 60, ICRP introduced the effective dose as the quantity in which to express protection quantities. The use of dose equivalent was retained for the evaluation of ICRU operational quantities but with a revised $Q(L)$ relationship[35] (ICRP, 1991; 1996; ICRU, 1998a). For protection quantities, radiation quality is taken into account by the use of radiation weighting factors (w_R), which are only indirectly related to LET.

These newer ICRP recommendations present us with an historical discontinuity because the greater part of the body of work presented in this Section was carried out based on recommendations of ICRP in its Publication 26 and its supporting documents (ICRP, 1973; 1977; 1980a; 1980b; 1985; 1988). There has not yet been sufficient time to evaluate this work in terms of the newly-defined quantities.

Measurements made for purposes other than radiological protection—such as, *e.g.*, the design of accelerator shielding, predictions of induced activity or radiation damage—are often more conveniently expressed by physical parameters that specify the radiation field

---

[35]L is used for linear energy transfer (LET).

(energy and spatial distributions of particle fluence) (*e.g.*, Moyer, 1954).

It is natural that, at accelerator laboratories, these physical parameters should be preferred because the necessary instrumentation is available for such measurements and the results of physical measurements of the radiation field may be applied to a variety of tasks, including radiological protection. The converse is not so (Moyer, 1954; Patterson and Thomas, 1973). Furthermore, the physical characterization of the radiation field has a stability not yet achieved by dose-equivalent quantities (Rindi and Thomas, 1973).[36] This is not to denigrate the importance of the necessary task of converting such measurements or calculations of physical quantities into reliable estimates of the quantities related to dose equivalent and effective dose. The argument is given additional emphasis by noting that there has been extended and lively debate on the concept of dose equivalent (Thomas, 1985), the relationship between Q and relative biological effectiveness (Mole, 1979), the relationship between Q and dosimetric quantities (Blohm and Harder, 1985; Rossi, 1977) and, finally, the implications of these quantities for the assignment of Q (Dennis, 1983; Dennis and Dunster, 1985; Sinclair, 1985). In 1986, ICRU published a report entitled *The Quality Factor in Radiation Protection*, in which changes were recommended in both their magnitudes and functional relationships to microdosimetric quantities (ICRU, 1986). These recommendations of ICRU have not been fully adopted by organizations such as NCRP and ICRP in their latest recommendations (ICRP, 1991; NCRP, 1993). The implications of the new recommendations of ICRP in Publication 60 have already been discussed. Doubtless, the introduction of w_R in that document will not end the debate on the appropriate method to be used weighting for radiation quality—a discussion which is likely to continue unabated.

In what follows, this Section will:

- review the special requirements for radiation dosimetry at high-energy particle accelerators
- discuss the radiation fields that exist around particle accelerators and the special instrumentation considerations that arise
- review the practical dosimetric techniques that are available and have been found useful in accelerator-radiation environments

---

[36] Although written more than 20 y ago, the comment on the instability of radiological protection quantifies is still valid. ICRP recommended changes in the protection quantities as recently as 1990 (ICRP, 1991; see also Thomas, 1998).

5.2 Special Consideration of the Techniques of Radiation Dosimetry in Accelerator Environments

The radiation environments at particle accelerators differ from those usually found in radiological protection in that they result from a wide variety of physical phenomena and, therefore, typically consist of several types of ionizing radiation distributed over a broad range of energies and production angles. In addition, the radiation fields have a complex time structure which depends upon the accelerator repetition rate, the details of the RF accelerating system, and the beam-extraction systems.

Several general statements concerning accelerator-radiation fields can be made:

- if muons are produced, neutrons will *always* be present[37]
- high-energy neutrons are *always* accompanied by intermediate-energy, fast and thermal neutrons
- neutron fields, regardless of their origin, are *always* accompanied by photons

Apart from constant beam (direct current) accelerators (*e.g.*, Cockcroft-Walton or Van de Graaff generators), accelerator operation uses a pulse structure that can vary from the picosecond regime to full continuous wave (*i.e.*, 100 percent duty factor) operation. However, even continuous wave operation is not truly continuous because it has "microstructure" features determined by the phase stability requirement of RF acceleration (Section 2). The dosimetry of pulsed radiation is reviewed in Boag (1987) and ICRU Report 34 (ICRU, 1982) where other references to the scientific literature may be found.

As a general rule, the response of active detectors around short-pulse accelerators can be trusted only if the count rate is a very small fraction of the machine pulse rate. This applies to scintillators, gas detectors working in pulsed mode (as opposed to "current" mode) and semiconductors. If T is the accelerator pulse length and f its pulse frequency, $(f^{-1} - T)$ is the inactive time between two pulses. Provided that the detector resolving time (τ) satisfies the condition $T < \tau < (f^{-1} - T)$, the true counting rate (n) can be obtained from the observed rate (m) using the following relationship (Knoll, 1979):

$$n = f \ln\left(\frac{f}{f - m}\right). \tag{5.1}$$

---

[37] Although both muons and neutrons will be produced, they need not necessarily appear at the same location. At Fermilab and CERN, *e.g.*, essentially pure muon beams exist—sometimes several kilometers from the locations of neutron production, because muon production is highly forward-peaked whereas neutron production is quite diffuse and far less directional.

Note that, under these conditions, the value of resolving time (τ) is irrelevant. If the observed count rate is 10 or 20 percent of the machine pulse rate, the corresponding count rate losses due to dead time will be >5 and 10 percent, respectively. This problem is reduced to a certain degree in neutron moderating devices (Section 5.4.3.1).

Because the instruments and techniques discussed here are extensively described in the open literature and in other NCRP reports, they will be outlined only briefly, giving references to the literature, but providing examples of their use at high-energy accelerators and their characteristics in these situations. The volumes by Knoll (1979; 2000) and Tait (1980) are basic references that discuss the principles of a range of modern radiation-detection instruments.

5.3 Application of "Conventional Techniques" to Measurements in Accelerator-Radiation Environments

5.3.1 *Introduction*

The so-called "conventional" instruments include the ionization chamber, the Geiger-Mueller (GM) counter, the proportional counter, and the TLD. All of these are sensitive to the types of radiation produced by accelerators but, as will be shown later in this Section, their measurements must be interpreted with care. Hoefert and Raffnsoe (1980) have published an especially helpful comparison of results obtained with several instrument types discussed later in this Section.

5.3.2 *Ionization Chambers*

The one type of dosimetric instrument of the greatest overall utility at accelerator facilities is the ionization chamber. This instrument in its many forms is well understood, reliable and can give "real-time" indications of absorbed dose. Perhaps the simplest experimental approach to the determination of dose equivalent (H) in accelerator-radiation fields is to measure the absorbed dose (D) with a suitable ionization chamber and multiply the result by an appropriate mean quality factor ($\overline{Q}$):[38]

$$H = \overline{Q}D. \tag{5.2}$$

---

[38] For a discussion of the impact of ICRP Publication 60 on recommended values of quality factors, see Section 5.1.

Many different means of determining absorbed dose by ionization chambers have been developed. The techniques include the use of paired ion chambers, high-pressure argon-filled chambers, and cavity chambers (Boag, 1966; 1987; Burlin, 1968; Goodman and Rossi, 1968; Patterson and Thomas, 1973).

It is important to note that, in accelerator environments, the use of only one chamber to determine dose equivalent is fraught with difficulty because of the variable relative contributions from low-LET radiations (photons and muons) and high-LET radiations (principally neutrons). When neutrons dominate the radiation field—which is usually the case for proton accelerators and also is often the case at high-energy electron accelerators—and a single ionization instrument is used, one should ensure that the materials of the chamber (walls, gas filling) have a reasonable response to neutrons. For this reason, the absorbed dose produced by accelerator-radiation fields is often determined using a tissue-equivalent chamber (Failla and Rossi, 1950; Rossi and Failla, 1956).

The shortcoming of this technique is that it gives only the measurement of D but no information on the mean quality factor ($\overline{Q}$). A conservative approach to the evaluation of dose equivalent is to assume a quality factor of 10, but this can be unreasonably conservative, as experience shows values of $\overline{Q}$ that range between one and six in accelerator environments.[39] Either some detailed knowledge of the radiation environment is required to estimate $\overline{Q}$ or resort must be made to an empirical determination of $\overline{Q}$ using, *e.g.*, recombination chambers (Section 5.5.2). Both methods require additional measurements (Cossairt *et al.*, 1989; Elwyn and Cossairt, 1986). (However, see Section 5.1 on changes introduced in ICRP Publication 60).

Practical problems that arise with the use of ionization chambers in accelerator fields include:

- *RF interference:* Ionization chambers are low-signal, high-gain detectors, sensitive to electromagnetic interference caused by the stray fields from the RF cavities used with particle accelerators. Suitable screening may be necessary.
- *Pulsed-radiation elds*: The electric field strength in the ion chamber may be insufficient to ensure complete charge collection in pulsed-radiation fields of low-duty cycle. Even though the average absorbed dose rates may be low, the rates during pulses

---

[39] ICRP Publication 60 recommended changes in the $Q(L)$ relationship which necessarily changes values of mean quality factor. However, for a variety of reasons the assumption of a value of $\overline{Q} = 10$, in the absence of knowledge of the neutron spectrum, remains conservative in most cases.

may be extremely high. Phase stability of the accelerated beam requires that acceleration takes place only at a limited time interval during each RF (or microwave) cycle. This requirement produces an RF "microstructure" in the beam pulse that may exacerbate the problem of charge collection in the ionization chamber. Boag (1950; 1952; 1987) has discussed the fundamental problems of pulsed-radiation dosimetry, and a review of the literature appears in ICRU Report 34 (ICRU, 1982) (see also *volume recombination* below).

- *Small beam cross sections*: Particle beams, whether primary (direct from the accelerator) or secondary (produced in a target or converter), can have cross-sectional areas that are very small compared to the sizes of the conventional instrument; beam diameters of 1 mm or even smaller are not uncommon. When an instrument is placed in such a beam, two effects must be understood: first, the true in-beam dose will be higher than the nominal instrument reading by a factor given by the ratio of the sensitive volume of the instrument divided by the beam volume within the instrument; and second, the true dose rate within the beam volume may be so high that sizeable corrections are required (*e.g.*, for ion recombination).
- *Volume recombination*: Tesch (1984) has discussed volume recombination effects in typical conditions around accelerators, while measurements of collection efficiencies in accelerator-radiation fields have been made by Oda *et al*. (1982).

5.3.3 *Geiger-Mueller Counters*

GM counters are among the oldest instruments used for the detection of ionizing radiation, and their design, construction and operation is well understood (Emery, 1966). The greatest utility of GM counters in accelerator environments is in the assessment of remnant radioactivity. Their use for this latter purpose is no different from their use with any type of radioactive source, is quite familiar, and will not be discussed further here.

For prompt-radiation fields, the GM counter can be of great help in detecting the presence and location of radiation fields. However, it may be of little use for quantifying the fields, unless the counting rate of the instrument is substantially below the accelerator pulse rate and is also small enough to assure that the counter dead time is insignificant compared with the detection rate of the particles of interest. Otherwise, the problems of counting losses due to dead-time effects severely limit the use of these counters and can lead

to underestimation of the quantities of concern. Furthermore, the response of GM counters is often unknown in the mixed and variable fields near accelerators.

The great advantage of the GM counter lies in its simplicity. It is relatively stable and, when properly operated, does not require very close control of the collector-high-voltage supply. Its chief limitation, when applied to the measurement of accelerator prompt-radiation fields, is that its dead time is of the order of 100 μs, due to the time required for the discharge to be quenched. With suitable techniques, this limitation can be overcome or minimized, thus permitting GM counters to be used in areas of high instantaneous radiation fields, but such methods must be used with care and with complete understanding of the instrument. The GM counter has found wide application in measuring gamma-ray radiation fields at large distances from accelerators where the intensity is low.

5.3.4 *Thermoluminescence Dosimeters*

TLDs have applications at particle accelerators that parallel those in other branches of radiological protection (Tuyn, 1982). TLDs are predominantly used in personal dosimetry as an alternative to photographic film, particularly in the monitoring of exposures from beta particles and photons (Kathren, 1990). The most common use of these devices at accelerators is for the monitoring of dose equivalent to personnel due to work on radioactive material.

A valuable feature of TLDs for application to accelerator environmental radiation monitoring is that they are not adversely affected by pulsed radiation fields or dose-rate dependency.

Because of their small size, TLDs are of particular value in measuring electron and photon exposures to the hands and fingers incurred during such operations, and particularly so when weakly penetrating radiations contribute to the dose equivalent. During maintenance, it is sometimes the case that contact with, and handling of, irradiated accelerator components cannot be avoided. Under these conditions, dose gradients are often very high and the exposure to the hands must be monitored (IAEA, 1988). Sullivan (1982) has shown that the surface absorbed dose resulting from electrons, emitted by accelerator-irradiated metal foils, can be an order of magnitude higher than the absorbed dose from photons.

5.4 Neutron Dosimetry at Particle Accelerators

5.4.1 *Introduction*

Neutron dosimetry is better understood in the energy below 20 MeV than at higher energies. This is because most of the experience

with neutron exposure has been obtained from radioactive neutron sources, nuclear reactors, and low-energy accelerators where the significant dose equivalent is produced by neutrons well below this energy.

For high-energy accelerators, it is often convenient to consider two energy regions which interface at approximately 20 MeV. The choice of 20 MeV roughly corresponds to the upper limit of reliability of moderated thermal-neutron instruments. More importantly, 20 MeV is the threshold of the very convenient activation reaction $^{12}C(n, 2n)^{11}C$, which is in general use at particle accelerators. In consequence, the spectrum of high-energy accelerators is often characterized by the fractions of dose equivalent due to neutrons above and below 20 MeV.

Excellent references that review modern aspects of neutron dosimetry can be found in the work edited by Ing and Piesch (1985). Valuable discussions of neutron dosimetry can also be found in ICRU Report 26 (ICRU, 1976b); NCRP Report No. 38 and No. 79 (NCRP, 1971; 1984); in the texts by IAEA (1979a; 1988) and Patterson and Thomas (1973); and in the proceedings of symposia by Jahr *et al.* (1992) and Menzel *et al.* (1997). This last reference contains many papers dedicated to high-energy neutron fields from cosmic rays and accelerator facilities. Of particular importance are publications related to the CERN reference radiation facility (CERF) (Birattari *et al.*, 1998a; Hoefert and Stevenson, 1994). CERF has been set up at one of the secondary beams from SPS. A positive or negative hadron beam with momentum of either 120 or 205 GeV c^{-1} is stopped in a copper target, 7 cm in diameter and 50 cm in length, which can be installed in two different positions inside an irradiation cave. On top of and alongside these two positions, the secondary particles produced in the target are filtered by shielding consisting of either 80 cm concrete, 160 cm concrete, or 40 cm steel. Several reference exposure locations are available outside the shielding, both on top and on the side. The composition of the CERF field is accurately known with respect to particle type and energy by both other Monte-Carlo calculations and measurements. Since 1993, many types of passive and active neutron detectors have been tested in these reference fields.

5.4.2 *Passive Detectors Used for Neutron Dosimetry*

5.4.2.1 *Thermoluminescence Dosimeters.* Some success has been achieved in using TLDs for individual monitoring of neutrons, particularly in the intermediate-energy region, by variations on the albedo principle (Piesch and Burgkhardt, 1985). TLDs have been used for individual monitoring of neutron exposures, but their application in

the broad neutron spectra typical of high-energy accelerators has been less successful. At SLAC a combination of ^{6}LiF and ^{7}LiF in one badge, with no shielding against external thermal neutrons, was used for many years. The combination works well if the neutron dose equivalent is much smaller than the photon dose equivalent and the ratio of thermal neutron to fast-neutron fluence rates is constant. If these criteria are not met, considerable overestimation of dose equivalent results (Busick *et al*., 1975). Hack (1971) has reported the use of a ^{6}LiF, ^{7}LiF, and nuclear track emulsions (*e.g.*, NTA film; see Section 5.4.2.2) combination to improve the accuracy of neutron personal-dose measurement at a 7 GeV proton synchrotron.

More recently, a similar two-component approach—TLDs combined with track-etch detectors—has gained widespread acceptance. The first component is a properly designed TLD albedo detector, where TLD elements are shielded against external thermal neutrons by cadmium or boron-loaded polyethylene. The second, track-etch component most often consists of CR-39®.[40] This technique has matured to the point where such systems are now used on a large scale by commercial personnel dosimetry services.

Kalef-Ezra and Horowitz (1982) have stressed that there is a great deal of variation in response between individual lithium-fluoride dosimeters, between different batches of dosimeters, and for any particular dosimeter, depending upon its thermal and radiation history. Nevertheless, it is possible, with careful experimental technique to derive an empirical relationship for the response of TLDs as a function of LET of the incident charged particles. This has been done, *e.g.*, in the particular case of ^{7}LiF, and agreement with the predictions of theory has been obtained by Henson and Thomas (1978) and Jahnert (1972) as seen in Figure 5.1. With such an empirical relationship, TLDs may be used for beam dosimetry when the LET of the beam particles is known.

The response of TLDs is known to be a function of the LET of the incident charged particles (*e.g.*, Jahnert, 1972). However, in monoenergetic charged particle beams, as produced by accelerators, this is of no consequence for *relative* absorbed dose measurements. In beams produced by proton accelerators, TLDs have been applied to exploration of the spatial variation of irradiating fields (Smith *et al.*, 1977). At SLAC, TLDs have been used to study the detailed distribution of dose within electromagnetic cascades (Nelson *et al.*, 1966). Further, TLDs have been used as transfer dosimeters from high to low doses

---

[40] Trademark of the PPG Industries, Inc., Pittsburgh, Pennsylvania, from whom the liquid monomer can be obtained. The designation "CR-39" signifies "Columbia Resin, Batch No. 39," a material developed for spectacle lenses.
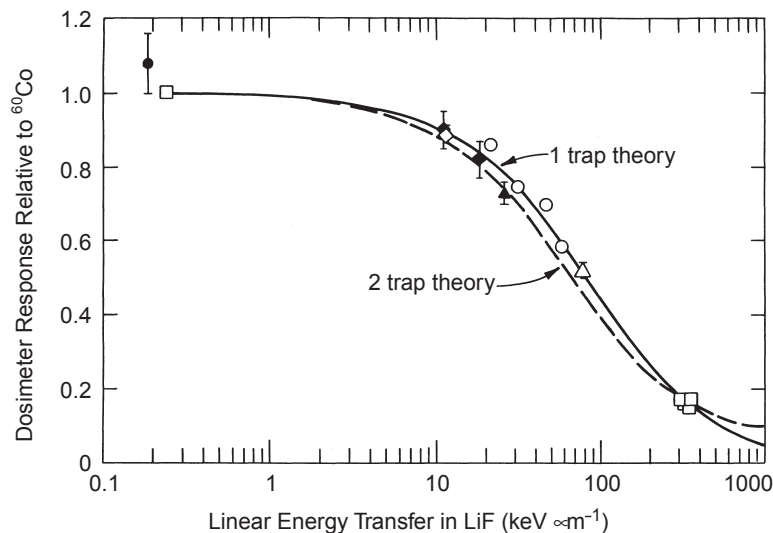
Fig. 5.1. Efficiency of ^{7}Li TLDs as a function of LET. The solid and dashed curves show predictions based on one- and two-trap theory (Jahnert, 1972). Experimental points for protons of several energies and naturally occurring alpha particles due to Jahnert are indicated by open circles and squares, respectively. Experimental points for protons (filled circles), C^{6+} ions (open diamonds), O^{8+} ions (filled diamonds), Ne^{10+} ions (filled triangles), and Ar^{18+} ions (open triangles) are also shown (Thomas and Perez-Mendez, 1980).

to measure activation cross sections (Smith and Thomas, 1976) for absolute dosimetry in radiobiological experiments (Ainsworth *et al.*, 1983; Patrick *et al.*, 1975), and for the determination of W, the average energy required to create an ion pair in gas (Thomas, 1982; Thomas *et al.*, 1980). They have also been employed at accelerators to monitor absorbed doses delivered to electronic equipment that is sensitive to radiation damage, but which must operate in proximity to intense beams.

5.4.2.2 *Nuclear Emulsions.* The use of nuclear emulsions has substantially declined over the last two decades. In personnel dosimetry, they have been mostly replaced by TLDs and track-etch detectors. Furthermore, moderated TLDs supplanted nuclear emulsions as area monitors. However, visualizing proton-recoil tracks and stars, together with their spectroscopic capability, makes nuclear emulsion attractive for special applications. The sensitivity of thin (25 μm) nuclear emulsions that are used for personal dosimetry and known

as Nuclear Track Type A or B (NTA or NTB), is limited to neutrons of energy between approximately 0.5 and 15 MeV. Protons with energies of less than ~0.5 MeV produce tracks too short to observe, whereas, for energies exceeding ~15 MeV, few tracks are observed because the (n,p) reaction cross section decreases with increasing energy. For these reasons, an important preliminary step in the use of nuclear emulsions is a "calibration" for the particular spectrum in which the measurements are to be made. This calibration is ideally done by estimating the true dose equivalent in the field to be monitored by a determination of spectrum, and comparison with the reading from emulsions simultaneously exposed in conjunction with a suitable phantom (*e.g.*, Greenhouse *et al.*, 1987). A valuable tutorial on nuclear-emulsion techniques is available in Patterson and Thomas (1973). Also recommended are the texts by Barkas (1963), Powell *et al.* (1959), and Yagoda (1949).

Nuclear emulsions can be used to record recoil-proton spectra from neutron interactions. This technique is able to give neutron spectrum information in the energy range 2 to 20 MeV. At higher energies, star-prong counting has been utilized to give approximate estimates of the slope of the neutron spectrum (Patterson *et al.*, 1969; Remy, 1965).

5.4.2.3 *Activation Detectors.*   Activation detectors are among the most important types of passive detectors in accelerator-radiation dosimetry. They have the advantage that their response is not influenced by the high duty cycles of some accelerator-radiation beams. Activation detectors may offer good discrimination against radiations other than neutrons [for example, the ^{32}S(n,p)^{32}P reaction]. Use of high-purity materials is essential in avoiding competing reactions. If variation in the accelerator beam is significant within an irradiation time comparable to the half-life of the radionuclide produced, corrections must be made in normalizing the measured activation to the integrated beam current. A correction can be made if an associated beam monitor is available that records beam intensity as a function of time. Alternatively, the correction can be made in an analog fashion by setting the time constant of the beam-current integrator equal to the decay time of the product nuclide, *i.e.*, $RC = t_{decay} = T_{1/2}/\ln 2$, where C is the integrated capacitance, R is a resistance in parallel with C, and $T_{1/2}$ is the half-life (*e.g.*, Knoll, 2000). Barbier (1969) and Swanson and Thomas (1990) give numerous and relevant radionuclide production cross sections for applications of the activation technique at accelerators.

Activation techniques are familiar in the measurement of thermal neutrons, usually by (n,capture) reactions. Holt (1985) has reviewed

the slow-neutron reactions in common use and Table 5.1 summarizes the three thermal neutron reactions most frequently used at activation detectors with higher-energy thresholds.

5.4.2.4 *Threshold Detectors.* A "threshold detector" can be any detector having a specific well-known reaction threshold and, to the extent possible, well-known reaction cross sections. Many activation reactions may also be used as threshold detectors and many of the "real-time" detectors described in Section 5.4.3 must also be considered to be threshold detectors, (*e.g.*, bismuth-fission and thorium-fission). The combination of track-etch detector, such as polycarbonate (Section 5.4.2.6), with a radiator of fissile material (*e.g.*, ^{238}U or bismuth) gives a threshold detector, with reasonable sensitivity and low background. For example, with a bismuth radiator, sensitivities of 600 and 100 μSv may be achieved with 60 and 100 MeV neutrons, respectively. A small number of threshold detectors can be used for crude spectral characterization, or, together with unfolding techniques, for more elaborate spectral studies. Other reactions that are widely used at accelerators to measure high-energy neutrons are given in Table 5.2 together with their thresholds, signature decay products, physical forms as typically used, and production cross sections.

Depending on the production cross section and half-life of the radionuclide produced, some activation detectors, particularly those with high-energy thresholds, are somewhat insensitive. Reactions with high-energy thresholds may, however, be useful for special measurements. For example, the ^{198}Hg(n,spall) ^{149}Tb reaction which has a threshold of approximately 600 MeV has been used with some success, but it involves difficult separation techniques (McCaslin and Stephens, 1967; McCaslin *et al.*, 1966; Shave, 1970). Baker *et al.* (1984; 1991) have measured the cross section of the ^{63,65}Cu(p,spall)^{24}Na reaction using copper foils. This reaction has a threshold of 500 MeV and represents an alternative to the reactions involving the detection of ^{149}Tb. It has been used to measure the fluence of high-energy protons because of its high-threshold energy of 500 MeV along with the relatively long half-life of the reaction product. The latter feature is important when the detector is used in a beam enclosure that is relatively inaccessible. It is believed that the neutron-induced cross section for the Cu(p,spall)^{24}Na is approximately equal to the proton-induced cross section actually measured. Table 5.2 gives important properties of these reactions.

Figure 5.2 shows the excitation functions for the activation reactions most frequently used at accelerators. Of these, the ^{12}C(n,2n)^{11}C reaction has a special place because its threshold at 20 MeV

TABLE 5.1—*Activation reactions commonly used in the determination of thermal neutron fluence rates at particle accelerators.*

Reaction	Decay Products	Half-Life	Detector	Sensitivity[a]
^{115}In(n,γ)^{116}In	β^- γ 0.42 MeV (29%) γ 1.1 MeV (58%) γ 1.3 MeV (84%)	54.2 min	20.3 × 10.2 cm NaI γ spectrometer β^- particle detetcor	Four foils, 6.6 × 15.2 cm, total mass 46 g: sensitivity 300 cpm
^{197}Au(n,γ)^{198}Au	β^- γ 0.42 MeV (95%)	2.7 d	20.3 × 10.2 cm NaI γ spectrometer; β^- particle detector	2.54 cm dia. foil, mass 0.5 g: sensitivity 1.8 cpm 5.08 cm dia. foil, mass 1 g: sensitivity 13.4 cpm
^{23}Na(n,γ)^{24}Na	β^- γ 1.39 MeV (100%) γ 2.75 MeV (100%)	15 h	γ spectrometer	Na$_2$CO$_3$ cylinder 4.5 × 2 cm, mass 12 g Na: sensitivity 3 cpm

[a] Sensitivity at saturation and zero decay time for unit neutron fluence rate ≈ 1 neutron cm^{-2} s^{-1}.

TABLE 5.2—*Important characteristics of various activation-detector techniques.*

Detector	Reaction	Energy Range (MeV)	Half-Life	Typical Detector Size	Cross Section		Detected Particle
					Peak (mb)	High-Energy (mb)	
Sulphur	^{32}S(n,p)^{32}P	>3	14.3 d	2.54 cm dia 4 g disk	500[a]	10[a]	β^-
Aluminum	^{27}Al(n,α)^{24}Na	>6	15 h	16.9 to 6,600 g	11[b]	9[b]	γ
Aluminum	^{27}Al(n,2p4n)^{22}Na	>25	2.6 y	16.9 g	30[b]	10[b]	γ
Plastic scintillator	^{12}C(n,2n)^{11}C	>20	20.4 min	13 to 2,700 g	90[b]	30[b]	β^+,γ
Plastic scintillator	^{12}C(n,spall)^{7}Be	>30	53 d	16.9 g (2.54 cm high)	18[b]	10[b]	γ
Mercury	^{198}Hg(n,spall)^{149}Tb	>600	4.1 h	up to 500 g	2[a]	1[a]	α,γ
Gold foils	^{197}Au(n,spall)^{149}Tb	>600	4.1 h	2.54 cm dia, 0.5 g	1.6[b]	0.7[b]	α,γ
Copper foils	Cu(p,spall)^{24}Na	>600	14.7 h	5.6 cm dia, 9 g	4[c]	3.6[c]	γ

[a] Swanson and Thomas (1990).
[b] Barbier (1969).
[c] Baker *et al.* (1984; 1991).
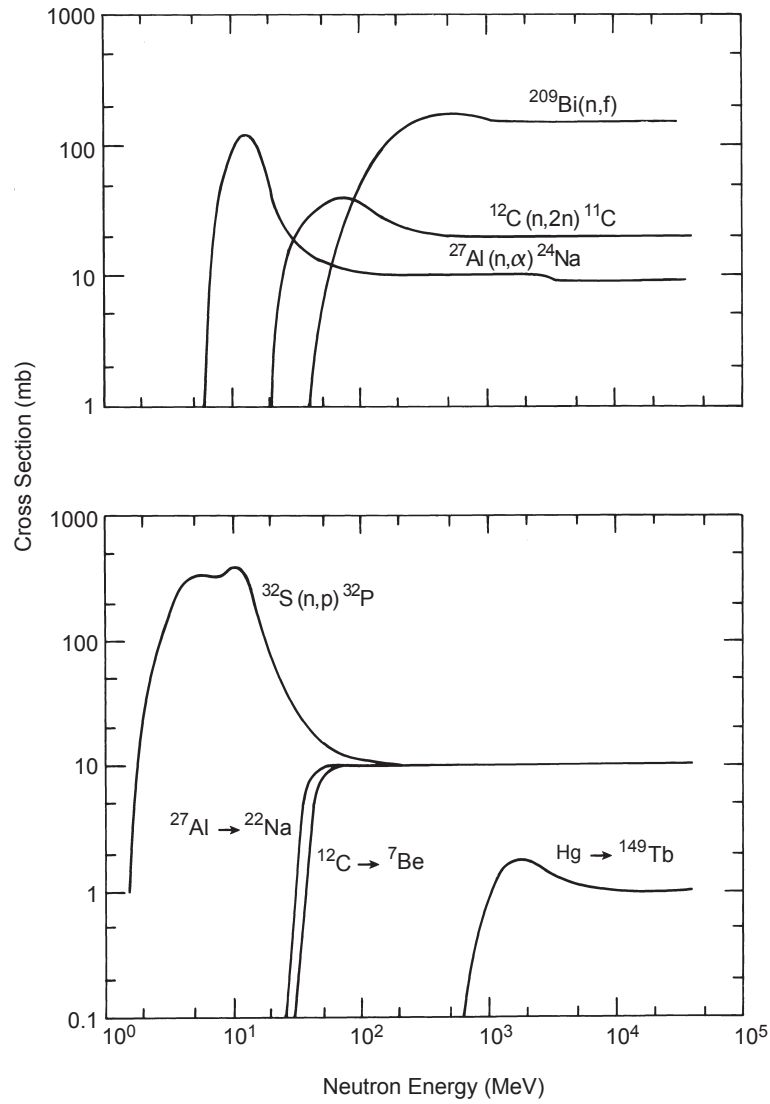
Fig. 5.2. Cross sections for the high-energy neutron detectors used in the 1960s and 1970s by the LBL group [^{27}Al(n,α)^{24}Na; ^{12}C(n,2n)^{11}C; Bi fission, ^{32}S(n,p)^{32}P; ^{27}Al(n,spall)^{22}Na; ^{12}C(n,spall)^{7}Be; Hg$\rightarrow$^{149}Tb] (Gilbert *et al.*, 1968).

represents a convenient boundary between "conventional" neutron dosimetry and the dosimetry of particular interest only at particle accelerators. This reaction was first employed to monitor the intensity of cyclotron beams by Sharpe and Stafford (1951), who also showed that a neutron fluence rate of $\sim$15 n cm^{-2} s^{-1} could be measured using a 4.5 g anthracene crystal. The detection sensitivity for neutrons was improved by the use of a liquid scintillator (Baranov *et al.*, 1957) and solid plastic scintillators (McCaslin, 1960; 1973; Shaw, 1962).

With scintillators of mass 2.7 kg, such as those developed by McCaslin, it was possible to measure a fluence rate of less than 1 n cm^{-2} s^{-1}. The experimental techniques used have been described in detail by McCaslin (1960; 1973) and also by Gilbert *et al.* (1968).

Competing reactions represent an important disadvantage of the method in that ^{11}C is also produced by photons, protons and charged pions as is exhibited in Figure 5.3. Stevenson has investigated the production of ^{11}C in plastic scintillators in radiation fields outside the shielding of a 30 GeV accelerator (Stevenson, 1984). In this work, he was able to use the most recent cross-section data and a consistent definition of dose equivalent. He found that in fields that were in equilibrium (containing a charged-particle component of protons and pions), the calculated fluence to dose-equivalent conversion coefficient was 45 fSv m^2, to be compared with his previous value of 50 fSv m^2 (Stevenson, 1971) and with an early value suggested by Shaw *et al.* (1969) of 60 fSv m^2. This value of 45 fSv m^2 is *inclusive* because it leads one from an instrumentally measured fluence to the *total* dose equivalent *including* that due to the proton and pion component given the approximate equivalency of the fluence-to-dose-equivalent conversion factor for such charged particles.

5.4.2.5 *Moderated Detectors.* The relatively low sensitivity of activation detectors to fast neutrons, with cross sections typically in the millibarn range (Table 5.2), limits their use in radiation protection. However, thermal neutron cross sections in certain elements reach thousands of barns. Using a hydrogenous (typically polyethylene or paraffin) moderator with a thermal detector at its center, fast neutrons are slowed to thermal energies and can be detected with greater efficiency. Spherical, pseudo-spherical, and ortho-cylindrical moderators of various sizes have been used at accelerator facilities. A 9 inch polyethylene sphere has an energy response that approximates the fluence-to-dose-equivalent conversion coefficients. Consequently, its signal does not depend on the shape of the neutron spectrum (see also "rem-meter" in Section 5.4.3.1). Smaller cylindrical moderators, typically 5 or 6 inches in height and diameter, are cheaper and more practical for deployment in great numbers. In this case, however,
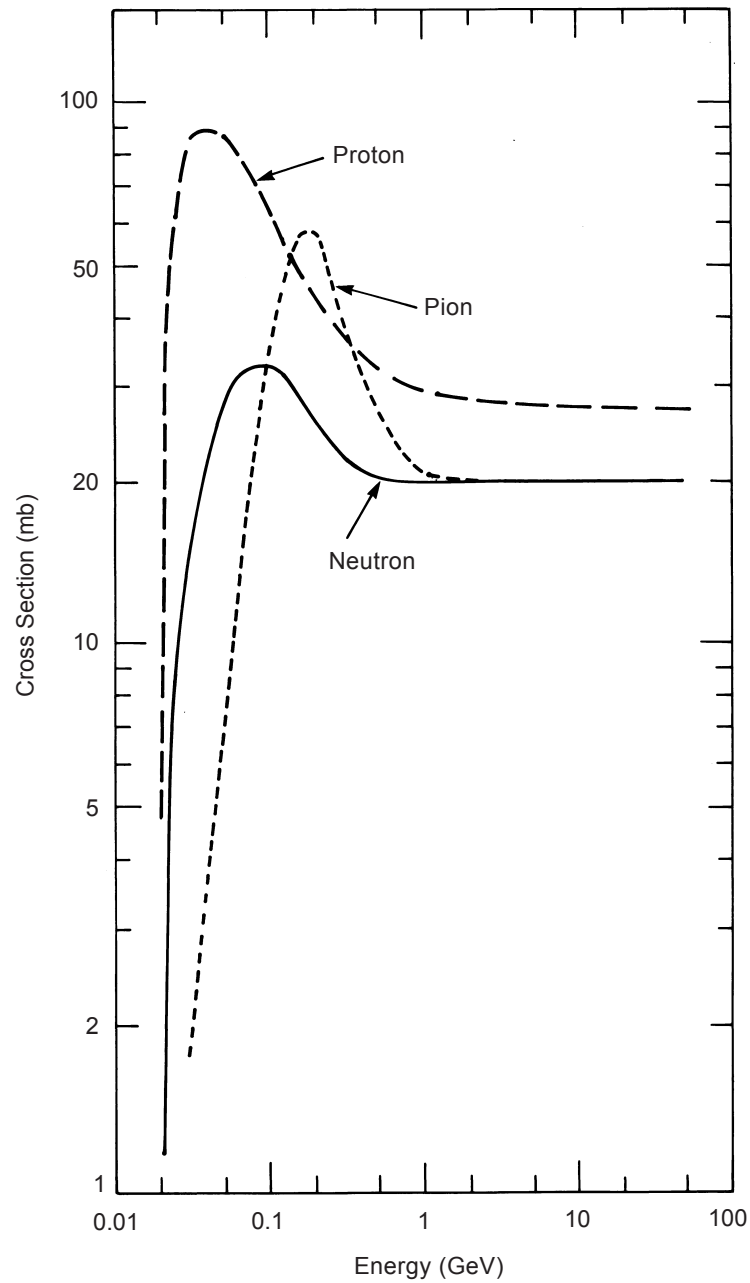
Fig. 5.3. Cross sections for the reaction $^{12}C \rightarrow {}^{11}C$ induced by neutrons, pions and protons. The arithmetic mean of the positive and negative pion cross sections is shown as the pion curve (Stevenson, 1984).

calibrations need to be established based on the knowledge or assumption of the neutron spectrum. Moderated TLDs, *e.g.*, pairs of ^{6}LiF and ^{7}LiF, are widely used as area monitors at accelerator facilities.

Another commonly used arrangement, utilizing a thermal-neutron-sensitive activation detector, is an indium or gold foil placed within a spherical or cylindrical moderator. Many adaptations of the original version by Stephens and Smith (1958) have been reported (Bathow *et al.*, 1967; Carter *et al.*, 1970; Simpson, 1964; Smith, 1958; 1961; 1965b; 1966). The radioactivity induced in the foil, which is placed at the center of the moderator during irradiation, is assayed after irradiation by a suitable radiation detector such as a thin end-window GM counter or a gas-flow proportional counter (better for high count rates). Indium foils of 2.54 cm diameter and 0.014 cm thick (mass 0.5 g) give a counting rate of 5 cpm (counts per minute) at saturation and zero decay time for unit neutron fluence rate when used with a thin-end-window counter. Gold foils of 2.54 cm diameter and 0.020 cm thick (mass 2 g) give about one-third the sensitivity of the indium foils when counted under the same conditions.

5.4.2.6 *Track-Etch Detectors.* Track-etch detectors function by the production of pits or holes in insulators irradiated with neutrons or heavily ionizing charged particles. The material is then etched with a suitable acid or base to enlarge the region thus sensitized. Weaker latent tracks can be developed and a higher sensitivity can be achieved by electro-chemical etching, when an alternating voltage is applied in the etching cell (Hankins *et al.*, 1984; 1985). Early studies of the track-etch technique have been described by Fleischer *et al.* (1963; 1965; 1975) and Price and Walker (1962; 1963). An excellent review is given by Griffith and Tommasino (1990).

Many insulating solids are suitable, and among those investigated are cellulose nitrate, Lexan, and high-grade muscovite mica. Many of these have the advantage that they can be read automatically by use of the spark-through method described, *e.g.*, by Cross and Tommasino (1972). The spark-counting technique depends on having a thin film that has been etched until its tracks have become holes which penetrate, or nearly so, entirely through the film. Electronic equipment permits rapid, automatic counting of tracks in a detector film that might otherwise require hours or days of microscope work. Parameters that affect reproducibility include foil thickness, diameter of etched tracks, voltage applied, atmospheric condition, and length of time between sparks. Improved track resolution and higher maximal hole densities are obtained in a sparking atmosphere of helium. Percentage counting losses are proportional to hole density

up to ~5,000 tracks cm^{-2}. The method has been used mostly experimentally in accelerator-radiation dosimetry. As an alternative to spark-counting, computerized biological colony readers have been successfully used to automate evaluation of track-etch detectors (Griffith *et al.*, 1984; Hankins *et al.*, 1985).

The most successful track-etch material for personal or area monitoring of accelerator-produced neutrons is the CR-39® casting resin (Cross, 1986; Harrison and Tommasino, 1985; Tommasino and Harrison, 1985; Tommasino *et al.*, 1984). It surpasses other track-etch media in its capacity to register recoil protons, its high sensitivity, and wide energy range, up to 15 MeV. When electrochemical etching is applied, the lower limit of the energy range is ~0.1 MeV, which constitutes a substantial improvement over the 0.5 MeV threshold for NTA film.

Some additional characteristics of CR-39® dosimeters that can be used to advantage are:

- Sensitivity is adequate in the range normally encountered in personal dosimetry; in the neutron energy range for which the response is reasonably energy-independent, the sensitivity is ~7 × 10^5 tracks cm^{-2} Sv^{-1}, based on ^{252}Cf calibration. However, the track density per unit dose equivalent is reduced by as much as a factor of two in high-energy spectra (Hoefert *et al.*, 1987).
- Response is linear with dose equivalent up to at least 4 mSv and can be corrected to dose equivalents at least as high as 0.1 Sv. Linearity can be extended to higher dose equivalents by the use of less sensitive track-etch procedures.
- Track fading, such as reported for NTA film, is small or nonexistent.
- Excellent reproducibility is possible; *e.g.*, ±3 percent has been achieved at a dose equivalent of 4 mSv (Hankins *et al.*, 1985).
- As the base material is inexpensive, several individual dosimeters can readily be incorporated into a single dosimeter package. Some can be held in reserve for later development in case problems are suspected with the initial processing.
- The individual dosimeters can be saved to form a permanent record.

Apparent disadvantages of the technique are:

- A strong dependence of response on orientation to the neutron field; the relative sensitivity at grazing incidence decreases to about 15 to 30 percent of that at perpendicular incidence. Special calibrations or corrections must, therefore, be made for fields encountered in practice.

- Background tracks, contributed in part by natural radon and/ or surface defects give a variable background reading which, with good quality CR-39® material, is equivalent to ~80 mSv.
- The number of developed tracks depends strongly on parameters of the etching process and, therefore, must be carefully controlled. There is a strong dependence on the etching temperature and some dependence on the thickness of the material. Details of one such electrochemical development process are outlined by Hankins *et al.* (1984; 1985).
- Labeling of individual films may present some difficulties.

Preliminary evaluations in an accelerator environment have been reported by Greenhouse *et al.* (1987). Fiechtner and Wernli (1999) describe a CR-39® personnel dosimeter that has been in routine use at the Paul Scherrer Institute in Villigen, Switzerland. Sensitivity to high-energy neutrons is enhanced by using a polyethylene radiator. Lithium-loaded polyethylene radiator is used for thermal neutrons. The detection limit in the high-energy equilibrium spectra at the Paul Scherrer Institute is ~0.3 mSv.

5.4.2.7 *Bubble Detectors.* The bubble-damage polymer detector is similar to a bubble chamber, in that a liquid whose normal boiling point is below room temperature is kept under pressure. When pressure is released, bubbles form along the path of a charged particle that has traversed it (Cross and Ing, 1984; Ing, 1986). When operated in this condition, the detector has only momentary sensitive time, but when superheated droplets of a volatile liquid are dispersed in a gelatinous medium the sensitive time is greatly increased (Apfel, 1979). In the detector developed by Ing and Birnboim (1984), superheated droplets of, *e.g.*, one of the freons, are dispersed in a transparent, elastic solid that prevents the droplets from vaporizing and keeps them fixed in location. The solid medium, an acrylamide polymer, also maintains the bubbles at the sites of formation. Due to the nature of the process, the sensitive times can be variable. One should consult the manufacturer of the particular bubble detector being used to determine the degree to which it is appropriate for the intended application.

In his evaluation of the state of personnel dosimetry, Griffith (1987) wrote: "Bubble detectors are an exciting development. The polymer or gel is worn in a clear vial. When a neutron interacts with the medium, a bubble is created that expands to optical dimensions. The detectors are easy to count, very sensitive, have no angular dependence, and the energy response can be tailored to the needs of the dosimetrist. Possible problems include temperature dependence, unit cost, sensitivity to mechanical shock, and potential difficulty in

counting high bubble densities resulting from moderate to high doses. However, many of their characteristics are highly attractive and bubble detector development should be followed closely."

According to Ing (1987), the temperature dependence has been overcome and detectors are produced with constant response over a temperature range of 15 to 35 °C. Recently developed dosimeters can be used as personal or area dosimeters for a four-week period making them suitable for routine use. The material can be tailored to a chosen neutron energy threshold, as low as 10 keV or less. Indeed, dosimeter sets have been produced having arbitrarily chosen thresholds of 0.010, 0.100, 0.500, 1, 3 and 10 MeV. Neutron sensitivity can be adjusted in production to be in the range 0.1 to 3 bubbles μSv^{-1} for a dosimeter volume of 4 mL. Automated readout by means of a video system with pattern recognition has been achieved with the capability of up to 1,000 bubbles 4 mL^{-1} dosimeter. Special bubble detectors have also been developed that can be used for the detection of gamma rays.

In spite of their initial promise, applications of bubble detectors at accelerator facilities remain limited. The advantage of direct reading and high sensitivity is outweighed by their limited life span of approximately three months, with a six month shelf life when stored in a freezer. Considering the additional cost for an automatic reader, bubble detectors are expensive in comparison with other techniques. Lewandowski *et al.* (1993) tested a bubble spectrometry set at SLAC and came to the following conclusions:

- It is difficult and tedious to "manually" count more than a few dozens of bubbles; operator errors are frequent.
- One recommended spectrum stripping method is unusable when low numbers of bubbles (below ~200) are registered. The method starts with the signal from the detector with the highest threshold, *i.e.*, the lowest signal and the largest statistical uncertainty. This uncertainty is then propagated by the unfolding procedure, leading to meaningless results.
- Somewhat better results were obtained when a custom version of the BUNKI unfolding code was used. Nevertheless, high statistical uncertainty on counts that can be read directly by eye often lead to unreliable solutions.

The relatively-narrow dynamic range of bubble detector dose is not compliant with United States external-dosimetry accreditation requirements and their use in a routine dosimetry service would be labor intensive (Romero *et al.*, 1998). However, they remain attractive for short-term special applications, when the need of high sensitivity and direct reading is paramount.

5.4.3 *Active Detectors Used for Neutron Dosimetry*

5.4.3.1 *Moderated Detectors.* As mentioned in Section 5.4.2.5, high sensitivity to fast neutrons can be achieved by combining a thermal neutron detector with a moderator of sufficient size. The three most common active detectors used in such combinations take advantage of the following exo-energetic capture reactions:

- BF_3 proportional counter: $n_{th} + {}^{10}B \rightarrow {}^7Li + \alpha + 2.31$ MeV ($\sigma = 3{,}840$ b)
- ^{3}He proportional counter: $n_{th} + {}^3He \rightarrow {}^3H + p + 0.765$ MeV ($\sigma = 5{,}330$ b)
- ^{6}LiI(Eu) scintillator: $n_{th} + {}^6Li \rightarrow {}^3H + \alpha + 4.78$ MeV ($\sigma = 940$ b)

The cross sections above are given for thermal neutrons and drop as $E_n^{-1/2}$ by about four orders of magnitude at energies near 1 MeV. When used with no moderator, these counters are effectively sensitive only to ambient thermal neutrons (average energy at room temperature, $E_n = 0.025$ eV). The relative merits of the three counters are summarized in Table 5.3. Additional information can be found in the monograph by Knoll (1989).

Thanks to the high *Q*-values of the above reactions, pulses from neutron capture are orders of magnitude larger than those from photon interactions. With a judiciously selected discriminator level photon sensitivity is usually negligible. Photon pulse pile-up is rarely a problem, in particular with the gas detectors. The sensitivity to fast neutrons depends on the moderator arrangement, but is of the

TABLE 5.3—*Comparison of active thermal neutron detectors.*

Type	Advantages	Disadvantages
BF_3	Excellent photon rejection Low cost	Typical filling pressure only 67 to 80 kPa, energy resolution suffers beyond this point
^{3}He	Filling pressure up to 1 MPa More sensitive and more stable than BF_3 Good photon rejection	Expensive
^{6}LiI(Eu)	High sensitivity (solid) Compact size (typically $4 \times 4 \times 1$ mm³) helps to reduce response anisotropy	Photon rejection weaker than gas counters Light-guide and photomultiplier tube partially reduce the advantage of compact size

same order as the sensitivity of the unmoderated counter to thermal neutrons. In terms of dose equivalent, the gamma rejection in BF_3 and ^{3}He counters is typically better than 1 in 10^4. Because the solid ^{6}LiI(Eu) scintillator is relatively more sensitive to photons, its photon discrimination may degrade in strongly dominant photon fields, in particular around pulsed accelerators.

The energy response of a moderated detector is primarily determined by its size and geometrical configuration. The choice of a particular type of thermal neutron detector has more bearing on the absolute sensitivity of the instrument than on the shape of its response function. It is possible to configure a moderated detector so that its response is a good approximation of the fluence-to-dose-equivalent conversion coefficients as a function of energy. Such instruments, called "rem-meters," have the remarkable feature that their signal is proportional to dose equivalent, and this relationship is independent of neutron energy.

The first generation of rem-meters included the following designs:

- 25.4 cm sphere with a 4 $\times$ 4 mm lithium-iodide scintillator (Hankins, 1962)
- 20.2 cm diameter cylinder with BF_3 counter (Andersson and Braun, 1963; 1964)
- hollow paraffin sphere with BF_3 counter (Ladu *et al.*, 1963; 1965)
- 20.8 cm sphere with spherical ^{3}He counter (Leake, 1967; 1968)

Two of these gained widespread use: the Andersson-Braun rem-meter "Snoopy," and the "rem-ball," a 22.9 cm version.

Hankins and Cortez (1975) studied the energy responses of four types of rem-meter instruments. Comparison of their data with the shape of the fluence to dose-equivalent conversion coefficients, as specified in ICRP Publication 26 (ICRP, 1977), shows reasonable agreement up to 7 MeV, after which the response drops rapidly. In a critique of the neutron rem-meter that considered both conceptual and operational aspects of its use, Rogers (1979) has said ". . . rem-meters give adequate indications of the dose-equivalent index only in the range 100 keV to 6 MeV" and indicated that they commonly overestimate the dose equivalent in many typical neutron spectra. These shortcomings arise, in part, from directional properties of the instruments vis-a-vis the directionality of the calibration field. Other problems are related to the "additivity in a mixed field, specification of the dose-equivalent index curve and the instrumental energy-response meters" (Rogers, 1979). Subsequent comparisons were made by Cosack and Lesiecki (1981) of the energy and angular response of eight dose-equivalent survey meters. In this work, the instruments were found to be very similar to each other in their dose-equivalent

energy response and all showed a decreasing response with increasing energy. Large differences were found in the angular response of these instruments. This problem is more pronounced at lower energies and can be substantially reduced by choosing spherical moderators combined with modern spherical ^{3}He or BF$_3$ counters (see, for example, Birattari *et al.*, 1998b).

Until recently, rem-meters emulated the neutron fluence to dose-equivalent conversion coefficients of ICRP Publication 26 (ICRP, 1977). However, those conceived during the last decade attempt to mimic the more recent concept of ambient dose equivalent, H*(10). To minimize over-response in the 10 eV to 100 keV range, rem-meters use a partially perforated layer of boron-loaded rubber or plastic imbedded in the moderator. The decrease in rem-meter sensitivity above ~7 MeV remained a serious limitation in accelerator environments where up to 50 percent of the dose equivalent may be contributed by neutrons with energy above 20 MeV. This problem was overcome when Birattari *et al.* (1990) developed an improved version of the Andersson-Brown design, by adding a 1 cm internal layer of lead. By means of (n,2n), (n,3n), ..., (n, xn) reactions in lead, high-energy neutrons are converted to lower energies and consequently detected with higher efficiency. This rem-meter, called LINUS, has a response function that approximates H*(10) to energies beyond 1 GeV. Calibrations in monoenergetic beams up to 66 MeV and successful tests in high-energy stray radiation fields at the CERN-CEC facility (Birattari *et al.*, 1998a) confirmed the feasibility of this concept. A spherical version of LINUS, using a spherical ^{3}He counter, was later developed (Birattari *et al.*, 1998b) to overcome the anisotropy of its response. Others followed the LINUS concept (*e.g.*, Hsu and Sun, 1995) and several such instruments are now available commercially. In the WENDI rem-meter developed by Olsher *et al.* (2000), lead was replaced by tungsten with the same effect.

Another moderated detector with a very specific function is the "long counter." It consists of a cylindrical paraffin moderator (diameter 20.32 cm, length 35.6 cm) surrounding a 34 cm long BF$_3$ counter along its axis (hence the name "long counter"). This assembly is further protected by a thick, boron-loaded or -lined re-entrant paraffin shield so as to accept neutrons only from the front face of the detector, in the direction along the counter axis. Sensitivity of the original design was found to be independent of energy, to within a factor of two, over an energy range from ~20 keV to 20 MeV (Hanson and McKibben, 1947). Later improved designs by de Pangher and Nichols (1966) and East and Walton (1969), the latter using multiple ^{3}He counters for increased efficiency, achieved a virtually flat

response between 20 keV and 6 MeV. Long counters are mainly used at calibration laboratories as a secondary fluence standard. Designed to measure the fluence in a parallel beam of neutrons, it is often used for fluence measurements from "point" sources, such as isotopic sources or accelerator targets. In this case, the correction for "effective center" of the instrument must be applied (*e.g.*, Mijnheer, 1971).

The mono-directional response and the sheer bulk, ~45 kg, make the long counter impractical for routine use. Stripped of its massive outer shield, the inner part of a long counter, *i.e.*, the long BF_3 counter, surrounded by ~6.3 cm of paraffin or polyethylene moderator, constitutes a very sensitive and more practical instrument. Similar instruments have been used for area and environmental monitoring at LBL (Thomas, 1976), CERN (Rau and Wittekind, 1982a), Fermilab (Cossairt and Coulson, 1985), and SLAC (Liu *et al.*, 1991; Seefred, 2000) (see also Section 6). Dose-equivalent rates comparable with those due to cosmic-ray neutrons, ~60 mSv y^{-1}, are detectable with a system such as this. It remains sensitive to ~20 MeV (Thomas, 1976; Wallace *et al.*, 1961). Whether calibrated in terms of fluence or dose equivalent, its response is anisotropic and no longer independent of energy. Unless this instrument is used only to monitor relative variations of the neutron field with time, specific calibration for the intended environment is required, taking into account counter orientation and directional distribution of the radiation field.

The short-duty cycle encountered at many accelerators is an important consideration for radiation measurements (Section 5.2). Dinter and Tesch (1976) have examined this question for moderated remmeters in pulsed accelerator fields. Because the intrinsic dead time of such instruments (2 to 7 μs) is typically very long compared to the beam pulse length for many accelerator types, it might be expected that instruments of this type would be incapable of registering more than one count per machine pulse. In fact, the diffusion time of thermal neutrons within the moderator introduces a randomly distributed delay between their time of arrival at the instrument and their registration. This delay is not attributable to the slowing down of fast neutrons to thermal energies (which is relatively quick), but is due to the time taken by neutrons, when thermalized, in diffusing inside the moderator before being captured. As stated by Dinter and Tesch (1976), "Although the dose during an accelerator pulse . . . [may] . . . be very high for a given averaged dose rate, the counting losses will be small because the neutrons are 'stored' as thermal neutrons . . . and can reach the detector hundreds of microseconds later." Knowledge of this time distribution permits estimation of the necessary dead-time correction.

The temporal effects of this neutron diffusion and moderation on count rate are shown for four types of instruments studied in Figure 5.4. These were the instruments designed by Leake (1968; 20.8 cm diameter spherical moderator), by Andersson and Braun (1963; 1964; 20.2 cm diameter cylinder), and detectors with spherical moderators of 30 and 45 cm, respectively. The distributions appear to decrease nearly exponentially with time, but changes in the slopes occur when the count rates have declined by a factor of about 10 from the rate at zero delay.
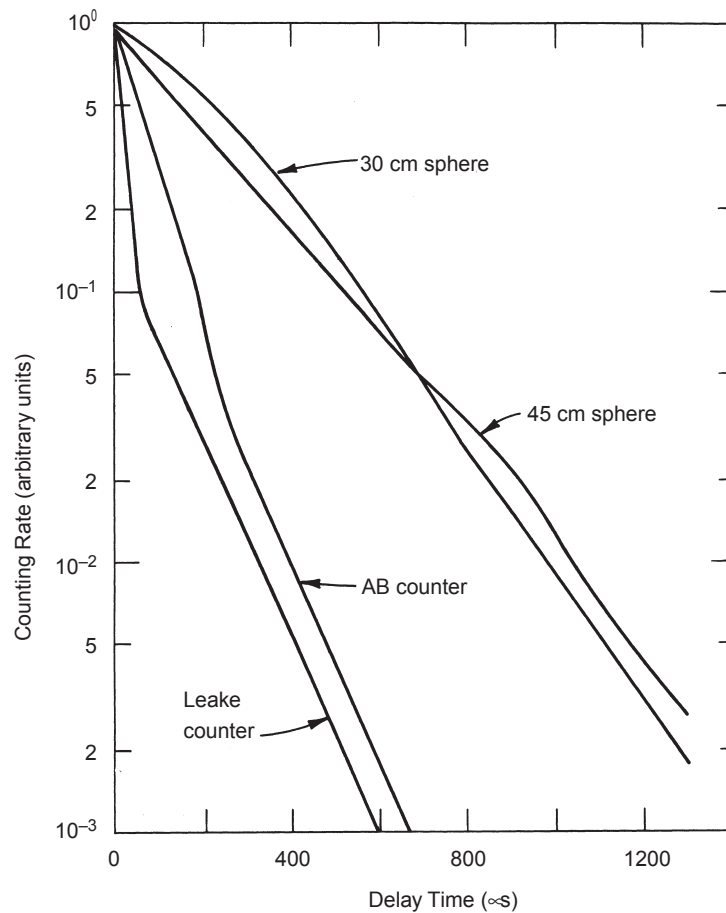
Fig. 5.4. Distribution of the time for neutron moderation in four types of rem counters (Dinter and Tesch, 1976): 30 and 45 cm spheres, ^{6}Li scintillator, AB (Andersson-Braun), and Leake counter.

More recent studies by Arora (1996) and Liu *et al.* (1997) included measurements and computer transport simulations of signal time distributions in moderator spheres of different sizes (2 to 18 inches) and an Andersson-Braun rem-meter. The following additional conclusions can be made about signal time distributions in moderated detectors:

- These distributions are broader in larger moderators, where longer migration paths are possible. This is true for the moderator-induced effect, when the influence of the surrounding environment is excluded (see below).
- They depend on neutron energy because different initial energies lead to different thermal-neutron distributions within the moderator volume and, consequently, different migration times towards the detector. However, this change is less apparent beyond a certain energy limit for a given moderator size. The likely explanation is, that, when the mean-free path of the incoming fast neutrons becomes comparable with the size of the moderator, neutron collision sites are distributed evenly throughout the volume and the thermal neutron distribution no longer changes.
- For lower energies and larger moderators, there is a clear offset between the beam pulse time and the start of the neutron pulses. Because neutrons are slowed down in a short distance from the moderator surface and have a long migration path to the detector, the "first arrivals" are noticeably delayed.
- Neutron moderation also occurs in shielding and structures surrounding the detector. This has a dominant effect on signal time distribution in small moderated devices (~8 cm and smaller), because they are sensitive to low-energy neutrons that emerge from the shielding with some delay. Larger devices are also affected, but to a lesser degree.
- Variations of these distributions with neutron spectra should be less acute behind thick shielding at high-energy accelerator facilities where usual "equilibrium" spectra are expected.
- Even for high-energy spectra, the first neutron signal seems to arrive with a slight delay (several milliseconds) after the beam pulse. The last observation may be useful in coping with interference from intense pulsed-photon fields. A so-called "gamma flash" can be observed around targets at pulsed electron accelerators, when the shielding does not sufficiently absorb photons generated in the electromagnetic shower. Unlike neutrons, these photons appear virtually instantly and simultaneously and pile-up into a single-large pulse that can be mistaken for a neutron

pulse. Vylet *et al.* (1997b) reported such problems with a LiI(Eu) detector used in a set of moderator spheres (see Bonner spheres, Section 5.4.4.1). Taking advantage of the slight delay between the gamma flash and the first neutron pulses, a detection time window was set to block the photons without sacrificing neutron detection efficiency.

5.4.3.2 *Fission Counters.* The fission reactions of ^{235}U, ^{232}Th or ^{237}Np have long been used in the detection of neutrons, particularly, at energies of a few mega-electron volts and below. One of the major advantages of these reactions is that a large amount of energy (~200 MeV) is released in every fission, and this amount of energy does not strongly depend on the energy of the incident neutron. About 80 percent of the energy released is usually shared by two highly charged and therefore heavily ionizing fission fragments. Consequently, these fragments have short ranges in solid materials, but may be detected if the fissionable material is embedded within the detector, as is the case, *e.g.*, in nuclear emulsions, or is adjacent to the detector, as is the case in damage track detectors (Griffith and Tommasino, 1990; Harrison and Tommasino, 1985; Wollenberg and Smith, 1969; 1973), or when the fissile material is plated on electrodes of a gas-filled ionization chamber or pulse counter. Passive detectors previously mentioned, such as ^{238}U and bismuth with polycarbonate etch track material, can be supplemented with on-line pulse-shape discriminators (Tesch, 1970).

Many materials may be used in fission chambers. For example, thorium fission chambers have been applied to a study of the neutron field around a patient treated by heavy-ion radiotherapy (Smith *et al.*, 1981). Natural uranium may also be used in this manner. When using natural uranium, the presence of ^{235}U produces a response of the fission chamber to thermal neutrons, as well as to fast neutrons (Wollenberg and Smith, 1969). At energies of 200 MeV or more, substances not normally thought of as fissionable such as tantalum, gold and bismuth, will fission when bombarded by neutrons or other particles, such as protons or pions. In fact, all heavy materials will fission when bombarded by such energetic particles. Figure 5.5 shows the fission cross sections for several substances as a function of neutron or proton energy.

For the fission of ^{209}Bi by high-energy neutrons or protons, the threshold is ~50 MeV. The fission cross section increases with energy until it becomes constant at ~1 GeV. The fission cross sections for incident neutrons and protons are similar (de Carvalho *et al.*, 1963; Hess *et al.*, 1957; Moyer, 1952). These characteristics make the
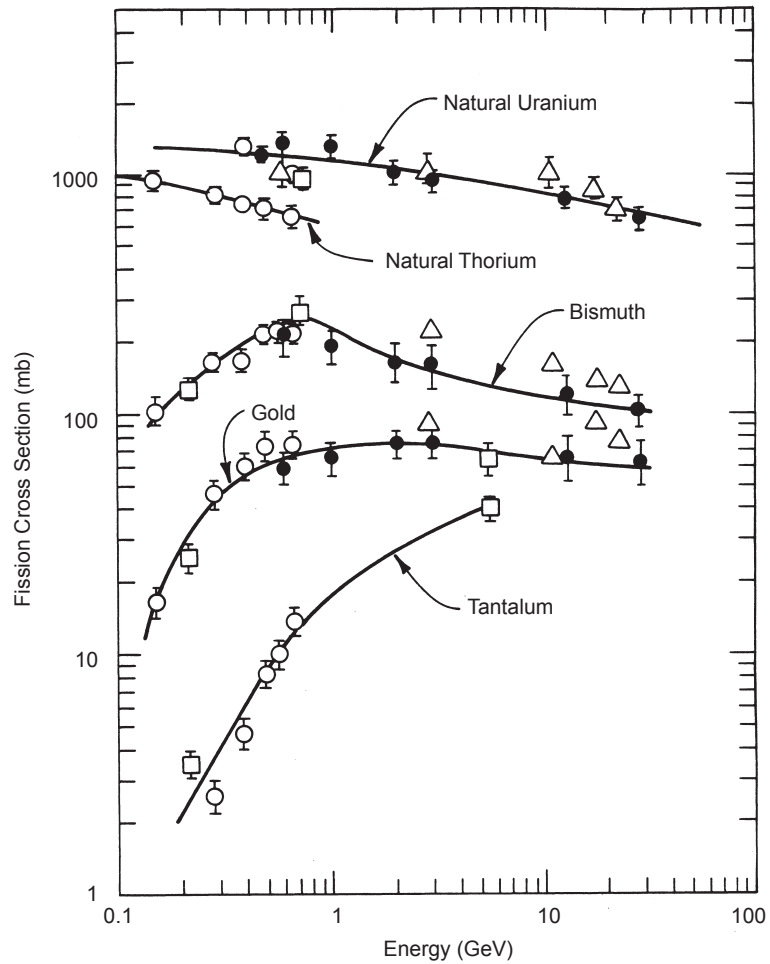
Fig. 5.5. Fission cross sections of natural uranium, natural thorium, bismuth, gold, and tantalum as a function of neutron or proton energy (Patterson and Thomas, 1973). (Solid circles, Hudis and Katcoff, 1969; open circles, Kon'shin *et al.*, 1966; open squares and triangles, Wollenberg and Smith, 1973).

fissioning of bismuth extremely valuable for the detection of neutrons and protons with energies above 50 MeV.

The fact that the fission fragments are highly energetic, but of short range, suggest that they might be detected in a suitably designed ionization chamber. Several papers in the literature describe the features of practical instruments (Beasley, 1959; Hess *et al.*, 1959; Kelly and Wiegand, 1948; McCaslin *et al.*, 1966; Wiegand, 1949).

Small fission chambers have been extremely useful in measuring the intensity of particle beams or monitoring regions close to beams where the radiation intensities are high. However, the limited sensitivity of such small detectors does not permit their application to the measurement of the rather low fluence rates that typically appear outside accelerator shielding. For this latter purpose, larger chambers with a greater amount of fissionable material have been designed in order to achieve greater sensitivity. Operation of the detectors in pulsed mode provides discrimination against photons and low-energy events. The range of fission fragments generated in bismuth is ~4 mg cm^{-2} and, to provide optimum sensitivity for a given amount of bismuth, it is necessary to spread a fissionable material thinly over a large area. The design of such instruments and the means of compensation for their high capacitance have been discussed by de Carvalho *et al.* (1963), Hess *et al.* (1957), McCaslin *et al.* (1966), and Moyer (1952). Although experience at Berkeley has shown the great value of using a detector with a threshold of 50 MeV in determining neutron spectra (Gilbert *et al.*, 1968), bismuth fission chambers have not been widely applied to radiation protection dosimetry at other laboratories.

5.4.4 *Neutron Spectrometry*

5.4.4.1 *Bonner Spheres.* Bonner and his colleagues first described a neutron spectrometer based upon the detection of thermal neutrons at the center of neutron moderators of differing sizes (Bramblett *et al.*, 1960). Polyethylene $(CH_2)_n$ was chosen as the material for the moderator because it is rich in hydrogen, is physically and chemically stable, and can be consistently manufactured to specifications [but see Griffith and Fisher (1976) for a discussion of variations in the density of polyethylene]. In its original form, the thermal neutron detector was a 4 mm diameter $\times$ 4 mm thick ^{6}LiI(Eu) crystal that could be placed at the center of any five spherical polyethylene moderators with diameters ranging between 5.08 and 30.5 cm. An approximately isotropic response was obtained by the choice of a spherical moderator, but the presence of the scintillator and its light pipe

can significantly perturb the angular response, particularly, for the smaller moderators.

The response functions of the Bonner spheres are largely determined by calculations performed using neutron transport codes and, in addition, numerous measured values are published. Bramblett *et al.* (1960) calculated the variation of response with neutron energy for five spheres of various diameters: 5.08, 7.62, 12.7, 20.3 and 30.5 cm. It is not feasible to determine the response functions of the Bonner spheres at all energies by experimental means because of the lack of adequate monoenergetic neutron sources over the energy range of interest. Thermal neutrons are available at graphite moderator assemblies and nuclear reactors, while mono-energetic beams from 8 keV to over 100 MeV are available at a few specialized accelerator facilities. Experimental confirmation of the calculated response functions at these available energies has been reported (Alevra *et al.*, 1988; Aroua *et al.*, 1992; Bramblett *et al.*, 1960; Griffith and Fisher, 1976; Kosako *et al.*, 1985). The measured response functions using time of flight techniques has been reported by Kosako *et al.* (1985) and are in good agreement with the calculated response functions in the regions where comparisons can be made.

Awschalom and Sanna (1985) have summarized both the calculated and the measured response data and Alevra and Siebert (1986) have prepared a critical compilation of published response functions. Only a few sets of calculated response data extend beyond neutron energies of 20 MeV (*e.g.*, Burrus, 1962; McGuire, 1965; O'Brien *et al.*, 1965; Sanna, 1973; Sannikov *et al.*, 1997). These data are valuable in accelerator neutron spectrometry, but only to a limited degree. As can be seen in Figure 5.6., response functions of even the largest spheres fall rapidly beyond 10 to 15 MeV to very low values. Applying the same principle as in the LINUS rem-meter (Section 5.4.3.1), more recent Bonner sphere sets use lead inserts to increase the energy range in the high-energy region (Hsu *et al.*, 1994; Vylet, 2002; Vylet *et al.*, 1997a; 1997b).

Figure 5.6 gives typical response functions derived from the work of Sanna (1973) for polyethylene spherical moderators and a ^{6}LiI scintillator. Sanna also calculated the response functions for water moderators and for gold-foil thermal neutron detectors used with both polyethylene and water moderators. There are often good reasons to use passive instead of active detectors. They might be desirable in pulsed fields and in fields with high charged-particle or photon contamination. Passive detectors that have been used to improve the discrimination in favor of neutrons include activation detectors such as gold, tantalum or cobalt (Smith, 1961; 1965b; 1966); track detectors (Hewitt *et al.*, 1980); and TLDs (Distenfeld, 1975; Weinstein
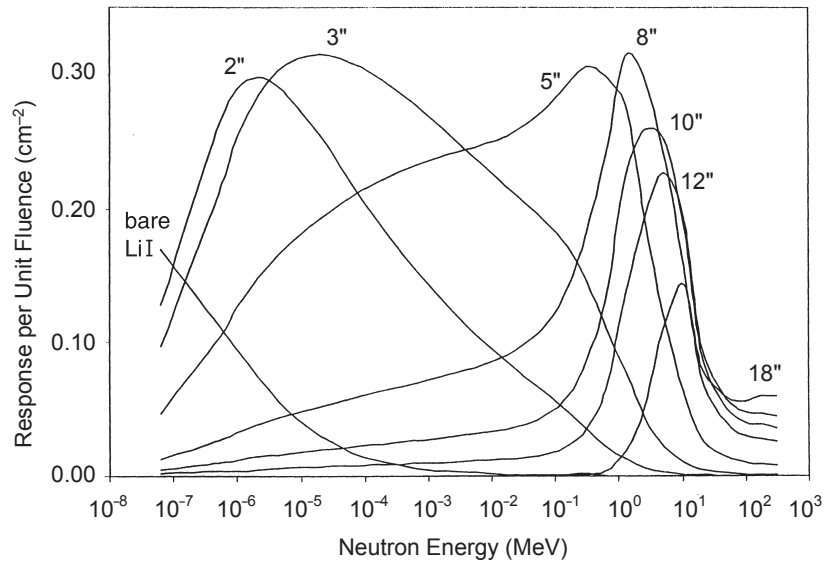
Fig. 5.6.   Response of Bonner sphere detectors as a function of neutron energy for spheres of different diameters (Sanna, 1973).

et al., 1970). Hybrid passive-active systems, suitable for use in pulsed fields, consist of proportional and GM counters used in combination with activation foils (Awschalom and Sanna, 1985). However, when it is necessary to gate out competing radiation sources, active counters such as LiI scintillators, BF_3, or ^{3}He counters must be used, rather than activation counters.

5.4.4.2   *Spectrum-Unfolding Methods.*   Neutron counting rates measured with a set of detectors with differing energy response functions, such as a set of Bonner spheres, are related to the neutron spectrum through the Fredholm equation:

$$C_r = \int_0^\infty N(E)\, R_r(E)\, dE, \tag{5.3}$$

where:
C_r = the counting rate in a detector surrounded by a spherical moderator of radius r
$N(E)$ = the neutron spectrum
$R_r(E)$ = the energy-dependent response function for a sphere of radius r

Given C_r and R_r, $N(E)$ can be obtained by standard unfolding techniques (see, for example, Awshalom and Sanna, 1985; Routti and Sandberg, 1980a; 1980b; 1985.)

In practice, the energy domain is subdivided into n energy groups defined by n + l boundary values E_i. Equation 5.3 is then converted to the discrete form:

$$C_r = \sum_{i=1}^{n} N_i R_{ri} \Delta_i, \qquad (5.4)$$

where:

N_i = the differential neutron fluence in the ith energy group

R_{ri} = the response of the rth sphere to a unit fluence in the ith energy group

$\Delta_i =$
$E_{i+1} - E_i$ = the width of the ith energy group

Detector response functions are obtained by calculations and measurements, as discussed in Section 5.4.4.1, and the set (R_{ri} for r = 1 ... m, i = 1 ... n) is called a "response matrix." The same formalism applies to other detectors such as threshold or activation detectors, used either separately or in combination with the sphere set. Group structures used in popular unfolding codes usually contain between 31 to 640 discrete energy groups, while the number of Bonner spheres used is typically less than 10. Unfolding a neutron spectrum from eight measured count rates using a 40-group structure is thus reduced to solving eight equations for 40 unknowns.

Clearly, Equation 5.4 cannot have a unique solution, and it is well known that there are inherent difficulties due to the underdetermined and sometimes ill-conditioned nature of such a problem. However, by using some *a priori* knowledge and by imposing additional conditions, the user can usually constrain the process to converge towards a solution that is physically realistic. Examples of such constraints are:

- requirement that solutions be positive (essential for fluence)
- coercion towards an expected spectrum shape in a given energy region, such as the "slowing-down," $1/E$, spectrum in the electron volt and kilo-electron volt regions, fission or giant resonance in the mega-electron volts region, or a $1/E^2$ slope beyond 100 MeV
- continuity of the spectrum, *i.e.*, no gaps between contiguous energy regions
- smoothness of the spectrum, limiting the amount of variation allowed between fluence values in adjacent energy groups

The adequacy of a solution can be assessed from the difference between the measured count rates and those calculated using the unfolded spectrum and the response matrix. Many unfolding codes start the unfolding process using a "first-guess" spectrum supplied by the user. An iterative procedure then follows, aimed at minimizing the difference between calculated and measured count rates, using procedures and criteria specific to each program. Popular examples of such codes are BUNKI (Lowry and Johnson, 1984), LOUHI (Routti, 1969; Routti and Sandberg, 1980a), or SAND. A similar approach, with more statistical rigor, is used in STAY'SL (Perey, 1977). Provided that uncertainties on all input parameters, *i.e.*, count rates, response function and first guess, can be specified using covariance matrices (which is rarely the case), the code will in principle find the most likely solution out of all possible physical solutions. The code also calculates a covariance matrix specifying the effect of input parameter uncertainties on the solution spectrum. A radically different approach was adopted in the Monte-Carlo unfolding code, SWIFT (Chambless and Broadway, 1983; O'Brien and Sanna, 1981; 1983; Sanna and O'Brien, 1971). The code uses very few groups (same as the number of detectors). Fluence in each group is generated randomly, the spectrum is then normalized and agreement with measured values is checked. The procedure is repeated $\sim 10^6$ times, and four best solutions are selected. This program does not use a first-guess spectrum nor does it take advantage of any physical insight. A combination of Monte Carlo and the Maximum Entropy method is used in the MIEKE code by Matzke (1988). A more recent code by Reginatto and Goldhagen (1998), MAXED, is also based on the Maximum Entropy method.

From a neutron spectrum derived in this manner that acceptably reproduces the measured counting rates for a given data set, one can determine the neutron fluence, absorbed dose (kerma), and dose equivalent and, thus, assign the quality factor associated with the neutron field to the accuracy generally sufficient for radiation protection. Often, the accuracy is also sufficient to assist in the understanding of radiation damage conditions and also the energies of neutrons which might be present as "background" in a given configuration of experimental apparatus.

Discussions of unfolding procedures in accelerator environments have been published by Birattari and Salomone (1985), Cossairt *et al.* (1985b), Elwyn and Cossairt (1986), McCaslin *et al.* (1986), Nakamura *et al.* (1978), and Thorngate and Griffith (1985). For a complete discussion of neutron spectra, see Cross and Ing (1987).

5.4.4.3 *Proton-Recoil Counters.* Recoil-proton spectra have been measured in real time using bulk plastic scintillation detectors

(Thorngate and Griffith, 1985). Photon background is often eliminated using pulse-shape discrimination (Knoll, 2000). This technique gives neutron spectrum information in the energy range 2 to 20 MeV.

At higher energies, special counter-telescope arrangements (Aleinikov *et al.*, 1974; 1975; 1979; Madey and Waterman, 1973; Penfold and Stevenson, 1968) or spark-chamber arrays (Lim, 1973; Mamont-Ciesla and Rindi, 1974; Rindi, 1969; 1974) are required. Both of these techniques derive directly from high-energy physics detectors and require a complex infrastructure, typically beyond the capabilities of small accelerator laboratories.

The directional nature of some of the stray energetic charged fields observed at accelerators (*e.g.*, from regions of high beam loss such as targets or collimators) suggests that these charged particles may be measured by scintillation-counter telescopes such as are commonly used in nuclear and high-energy physics. The use of counter telescopes is attractive because they may be used to identify the location of "point-like" radiation sources and, when operated in the coincidence mode, they may be calibrated to measure fluence which may, in turn, be readily converted to any desired radiological protection quantity. Counter telescopes were first applied to the detection of protons outside accelerator shielding of Nimrod (a 7 GeV weak-focusing proton synchrotron that operated at the Rutherford Laboratory in the United Kingdom) by Penfold and Stevenson (1968).

5.5 Mixed-Field Dosimetry

5.5.1 *Introduction*

Zielczynski (1971) discussed the uncertainties in mixed-radiation field dosimetry and cites two major difficulties: determination of response functions of detectors and interpretation of measurements and determination of accuracy.

More specifically, dosimetric techniques that span the wide range of accelerator-radiation environments suffer from all or some of the following drawbacks:

- interference from radiations other than those to be measured
- response-rate dependence in intense radiation fields
- complexity
- incomplete instrument response function data
- uncertainties in instrument response interpretation

Many creative and imaginative attempts have been made in the search for a single dosimeter that would permit direct accurate measurement of the entire accelerator-radiation field, including the LET spectrometer of Rossi and Rosenzweig (1955); the modified LET spectrometer of Kuehner *et al.* (Baum *et al.*, 1970a; 1970b; Kuehner and Chester, 1973; Kuehner *et al.*, 1972; 1973); the differential recombination chambers of Zielczynski (1963; 1965), Zielczynski *et al.* (1965), and of Sullivan and Baarli (1963); and the scintillation method of Pszona (1971).

The work preceding the recommendations of ICRP Publication 60 (ICRP, 1991) was largely based upon the recommendations and data contained in ICRP Publication 21 (ICRP, 1973) and its predecessors. The intrinsic theoretical background for most of the work to be described in this Section is to infer a mean quality factor from a measure of LET and by utilizing the relationship between quality factor and LET recommended by ICRP and ICRU. As has been discussed in Section 5.1, the changes recommended in ICRP publications have a profound effect in the interpretation of such measurements.

5.5.2   *Recombination Chambers*

Recalling Equation 5.2, the absorbed dose (D) and the dose equivalent (H) are related by a dimensionless mean quality factor ($\overline{Q}$). For many years, there has been some interest in developing ionization chambers that may determine empirically the value of $\overline{Q}$ in particular radiation fields.

A possible method is based upon the recombination of ions produced in gases. Recombination phenomena have been given considerable study (Boag, 1950; 1952; 1987; Jaffe, 1913; 1929a; 1929b; 1940).

In the irradiated gas of an ionization chamber, the signal (current) from the chamber may be reduced by ion recombination. Jaffe pointed to two distinct types of recombination:

- Inter-columnar recombination or recombination of ions from different tracks before collection. This phenomenon is dose-rate dependent and can be of importance in a pulsed radiation field of short duty cycle (Boag, 1966).
- Intra-columnar recombination occurs between ions within a single track. While generally of little significance when measuring low-LET radiations, this can become important in chambers operated at high gas pressures or when high-LET radiations such as neutrons (recoil protons) are to be measured (Jaffe, 1913; 1929a; 1929b; 1940; Zanstra, 1935).

The phenomenon of intra-columnar recombination may be utilized to determine the average LET of charged particles. This possibility arises because, for an unsaturated ionization chamber, over a considerable range of field strength due to the applied collection potential (V), the collected ionization current (i) is given by the empirical equation:

$$i = kV^n, \tag{5.5}$$

where k is a constant for a given absorbed dose rate and radiation field and n is the "recombination number," which is a function only of unrestricted LET (L_∞). In this equation, "i" can also represent the integrated charge collected over some period of time or normalized to some integral of beam current. Because the mean quality factor ($\overline{Q}$) is defined in terms of L_∞ (ICRP, 1963; 1977), it follows that the recombination number (n) is also a function of $\overline{Q}$, $i.e.$, n = n($\overline{Q}$), a function that may be empirically derived. The empirical nature of the function n($\overline{Q}$) must be stressed because the relationship of $\overline{Q}$ and L is defined by consideration of a wide variety of biological data, and there is no direct theoretical connection between the two functions $\overline{Q}(L_\infty)$ and n($\overline{Q}$).

Work at Brookhaven National Laboratory (Distenfeld and Markoe, 1965), at CERN (Sullivan and Baarli, 1963), and in Warsaw and Dubna (Zielczynski, 1963; 1965; Zielczynski $et\ al.$, 1965), suggested that the quality factor could be estimated to within about 20 percent by recombination chambers. Figure 5.7 shows the response of the chamber constructed at CERN. This was a large-parallel plate chamber, with electric field gradients up to 2,000 V cm^{-1} and operated with tissue-equivalent gas at pressures up to 6 atm.

Cossairt $et\ al.$ (Cossairt and Elwyn, 1987; Cossairt $et\ al.$, 1984; 1985b) at Fermilab, have used the recombination chamber developed by Zielczynski (1963; 1965; 1971; Zielczynski $et\ al.$, 1965), in conjunction with other instruments, to determine the quality factor of radiation fields in which the neutrons were the main component. Consistency was found between the value of $\overline{Q}$ so determined, and the value derived from detailed knowledge of the radiation field, in particular, the neutron spectrum. It was found by Cossairt $et\ al.$ that superior results are obtained in radiation fields where the normalization can be made to some nearby detector such as an ion chamber and, if the index n is obtained from a least squares fit to a log-log plot of i measured as a function of V, suitably normalized over a wide voltage range.

Interest in "$\overline{Q}$ meters" has declined somewhat over the past decade and they are now rarely, if ever, used at accelerator laboratories except for experimental purposes. In addition to the practical
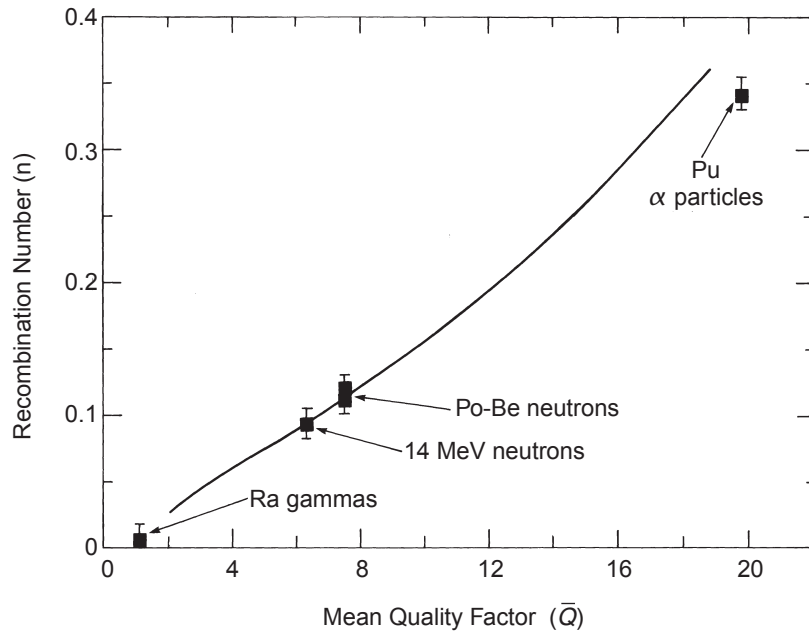
Fig. 5.7. Response of a high-pressure parallel plate recombination chamber as a function of mean quality factor ($\bar{Q}$). The curve shows the response predicted from Jaffe's theory. The experimental points were reported by Sullivan and Baarli (1963).

difficulties previously mentioned, there has been a prolonged theoretical debate on the relationship between Q and linear energy transfer (L). Indeed it has been suggested that lineal energy (y) rather than L be the physical parameter used to specify radiation quality (Dennis and Dunster, 1985; ICRU, 1986). In 1990, ICRP introduced an entirely new scheme for radiation weighting which uses radiation weighting factors (w_R) but retained L, to specify radiation quality (ICRP, 1991).

5.5.3 *Tissue-Equivalent Proportional Counters and Linear Energy Transfer Spectrometry*

In mixed field dosimetry, a promising technique, now available commercially, is that of the tissue-equivalent proportional counter (TEPC), sometimes referred to as the "Rossi counter" after one of its inventors, Rossi and Rosenzweig (1955). These devices have been described in more detail in ICRU Report 36 on *Microdosimetry*

(ICRU, 1983). In such devices, tissue equivalent plastic walls are employed to produce a Bragg-Gray cavity in which a tissue-equivalent gas mixture is maintained at low pressures, typically a few hundred pascals, so that the density of the energy deposited is kept small. Under these conditions, the total energy deposited in the gas will be equal to the LET of the particle multiplied by the path length through the gas. At these low pressures, the gas-filled cavity has the same mass stopping power as a sphere of tissue of diameter ~1 μm; hence, an equivalent diameter of 1 μm. In principle, the determination of absorbed dose from events in such chambers is a straight-forward conversion from a measured pulse-height spectrum (calibrated in energy) to absorbed dose (in tissue) irrespective of the precise physical composition of the radiation field:

$$D(\text{Gy}) = \frac{(1.602 \times 10^{-10})\,\text{C}}{\rho V} \sum_{h_1}^{h_2} hN(h), \qquad (5.6)$$

where the summation in Equation 5.6 is over channels corresponding to the radiation type of interest (see below); V is the sensitive volume (cm^3); ρ is the density (g cm^{-3}); C converts the channel number to energy in mega-electron volts, while h is the channel number, and N(h) is the number of counts in channel number h.

When the pulse height distribution from a TEPC is transformed into an absorbed dose distribution as a function of the lineal energy (y) the transition between photon and neutron induced events can be seen to occur at a pulse height corresponding to approximately 15 keV μm^{-1}. It is possible to determine the mean quality factor ($\overline{Q}$), from a single TEPC measurement. Under the conditions stated above, one can unfold from the pulse-height spectrum the distribution of absorbed dose as a function of LET [$D(L)$] using a formula derived by Rossi (ICRU, 1983). The formula is complicated by the fact that one must average over chord lengths in the spherical TEPC chamber. The assumption is that secondary charged particles generated by neutron interactions in the TEPC wall travel in straight lines and traverse the chamber. The distribution of these chord lengths is then used to calculate the average value of $\overline{Q}$, and hence the dose equivalent. The advent of microcomputers has made portable TEPC-based instruments practical.

Figure 5.8 shows data taken using a typical TEPC in a neutron field with a broad fluence spectrum having energies extending from thermal to approximately 14 MeV. Two measurements were taken first with no additional moderation (Configuration 1) and then with an addition of 20 cm of water (Configuration 2). The TEPC data are plotted as an absorbed dose distribution in lineal energy [yd(y)] using
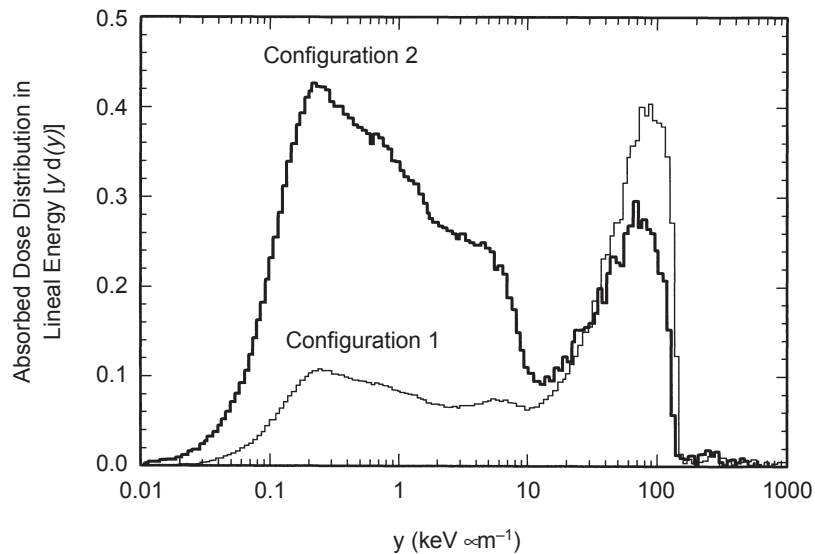
Fig. 5.8. Absorbed dose distribution in lineal energy [y d(y)] measured with a TEPC in two neutron fields labeled "Configuration 1" and "Configuration 2." Configuration 1 uses no additional moderation and in Configuration 2 an additional 20 cm of water was added in front of the TEPC. The additional moderation is responsible for an increased gamma-ray dose observed as an increase in the area under the curve for Configuration 2 in the region from ~0.01 to 15 keV μm^{-1}. The relative fraction of neutron fluence is smaller for Configuration 2 as seen by the decreased area under the curve from ~15 to 150 keV μm^{-1} (adapted from McDonald *et al.*, 1995).

a semi-logarithmic display. This presentation has the advantage of maintaining the area under the curves as proportional to total absorbed dose. The area under the curves in the region of low lineal energy between ~0.01 to 15 keV μm^{-1} results from events produced by photons. The area under the curves between ~15 to 150 keV μm^{-1} results from neutron produced events. Events above 150 keV μm^{-1} result from heavy charged particles, charged nuclei, and nuclear fragments produced from neutron interactions in the wall of the TEPC. For higher energy neutrons, an added complication occurs because there is considerably more overlap between photon and neutron events in the region near 15 keV μm^{-1}. Additional information on applications of TEPCs can be found in ICRU (1983).

5.5.4 *Other Techniques for Direct Assessment of Quality Factor and Dose Equivalent*

The light output from a plastic scintillator may be utilized to obtain an estimate of radiation quality. The method devised by Pszona (1969; 1971) and Pszona and Hoefert (1977) relies on the simultaneous measurement of currents from an ionization chamber and a photomultiplier tube attached to a plastic scintillator. The ratio of the currents is a complex function of LET, but it can be used to give a measure of $\overline{Q}$ in an unknown field, provided the system is properly calibrated.

Another technique, described by Tesch (1970), is to use pulse-shape discrimination on the pulses coming from an organic scintillator to discriminate against photons and to choose a suitable discriminator threshold so that the pulse rate is proportional to dose equivalent.

5.5.5 *Universal Dose-Equivalent Instruments*

All of the techniques discussed above have given satisfactory estimates of quality factor and dose equivalent in near-laboratory conditions of exposure. However, as yet, there is no universal dose-equivalent meter that is sensitive and robust enough to withstand the rigors of measurement in the field, while giving reliable results at occupational radiation levels. This is to be contrasted with the multiple-detector systems described, which have been shown to be reliably consistent for more than 20 y.

This Section has stressed the importance of a sound physical understanding of accelerator environments and so has largely dealt with the causes and characteristics of these fields. When the character of the radiation fields is understood, it is often possible to use instruments and techniques familiar to other fields of radiation dosimetry. This should, however, only be attempted when the response of any instrument in such radiation environments is fully understood.

At particle accelerators, the application of radiation dosimetry goes beyond attempts to quantify individual radiation exposure. Dosimetric data are often needed to determine what changes in accelerator operation or shielding are needed to modify (usually to reduce) radiation environments. It is not surprising therefore, to find that instruments developed for nuclear- and particle-physics

research are often applied to radiation dosimetry at accelerator laboratories. The results of such measurements quantify radiation fields in physical terms—particle type, energy, fluence and angular distributions.

5.6 Environmental Monitoring

5.6.1 *Introduction*

The external dose received from natural sources of ionizing radiation originates from cosmic rays and from gamma-emitting radionuclides in Earth's crust. The United Nations (UNSCEAR, 1982) estimates the external annual effective dose equivalent from all naturally occurring radiation in "normal" parts of the world to be 300 μSv from cosmic sources and 350 μSv from terrestrial radiation (Eisenbud, 1987). This corresponds to a nominal background annual absorbed dose due to gamma rays of approximately 650 μGy that must be subtracted from environmental measurements at the accelerator site. In addition, the fluence rate of cosmic-ray neutrons at sea level at mid-latitudes (41 to 46 °N) is ~65 to 84 m^{-2} s^{-1} (page 868 of Hewitt *et al.*, 1980) corresponding to an annual dose equivalent in the range 60 to 70 μSv (O'Brien, 1975). More current interpretations of external annual effective dose equivalent are 280 μSv for each of the cosmic and terrestrial components for a total of 560 μSv as determined by NCRP (1987a; 1987b). NCRP Report No. 50 is a very useful monograph that summarizes the natural environmental radiation field, as well as measurement procedures (NCRP, 1976b).

Around the world experience at large high-energy particle accelerators has shown that their primary radiological impact on the environment is in the form of prompt radiation. Typically, the magnitudes of population exposure from prompt radiation, radioactive gases and radionuclides in water are in the ratio of 100:10:1. For well shielded, high-power, compact accelerators in the intermediate and low-energy region, releases of radioactive material to the air may make the dominant contribution to the exposure of the public. The primary component of radioactivity released usually consists of the short-lived positron emitters and ^{41}Ar. However, for accelerators that are used primarily for radioisotope production, the highest off-site doses may be due to the release of the more radiologically significant species such as radioiodines. If the accelerator operation involves the bombardment of targets with $Z > 82$ and, hence, the possibility of the production of various radon species, then the radon

progeny, especially long-lived isotopes of polonium, may constitute the most significant contribution to the off-site dose.

Population exposure due to radioactivity induced in materials that are recycled, *e.g.*, magnet iron, copper conductors, and other accelerator components is even smaller (Thomas, 1978a; 1978b; Thomas and Rindi, 1979). Thus, the major consideration is to determine the prompt radiation field by means of environmental monitoring at particle accelerators.

There are three components to the prompt radiation field that are of environmental concern. These are muons, neutrons and photons; and of these three, neutrons are usually most important. In addition, the presence of any induced radioactivity in air and water is monitored at many high-energy installations.

5.6.2 *Neutrons*

5.6.2.1 *Active Moderated Counters.* Use of the moderated long BF_3 counter (a lighter version of the true "long counter") for environmental use at accelerator facilities was discussed in Section 5.4.3.1. These instruments are sensitive enough to measure neutron dose-equivalent rates from cosmic-ray neutrons. When used to record neutron skyshine at LBL, periods of accelerator operation were clearly evident (Thomas, 1976). Devices of the rem-meter type are also used in great numbers for environmental monitoring. Although more costly than the former instrument, commercially produced rem-meters are available with integrated features for data logging and telemetry. Rem-meter energy response is usually adequate for typical skyshine spectra and does not require a specific calibration factor. Instruments with extended energy range (see LINUS in Section 5.4.3.1) may be used when necessary. To achieve high sensitivity needed in environmental applications, high pressure ^{3}He proportional counters might be preferable to BF_3 counters.

5.6.2.2 *Thermoluminescence Dosimeters.* The high-thermal neutron capture cross section of ^{6}Li has led to the application of ^{6}Li phosphors to the detection of neutrons. The response of the ^{6}LiF phosphors to photons may be corrected for by the use of pairs of ^{6}Li-^{7}Li detectors. Neutrons are detected by ^{6}Li after thermalization in a suitable moderator surrounding the detector pair. Such a system has been used at CERN (Bonifas *et al.*, 1974; Tuyn, 1982).

One major disadvantage of this technique is that it is difficult to measure dose-equivalent rates below 100 to 200 μSv y^{-1}. Extreme care must be taken to prevent the dosimeters from being exposed

to thermal neutrons during transport to and from the monitoring site. A successful way of handling the TLD detector pairs is to load them into polyethylene inserts and put the inserts in cadmium cylinders for temporary storage upon reaching the measurement site. The inserts are rapidly removed from the cadmium cylinders. Upon completion of the measurements, the procedure is reversed (Awschalom and Sanna, 1985; Rohloff and Heinzelmann, 1973; Sanna *et al.*, 1980).

5.6.3 *Photons*

5.6.3.1 *Introduction.* Measurements of environmental photons need careful interpretation in order to understand possible interfering sources. The total accelerator-produced radiation level at high-energy accelerator boundaries is in many cases administratively limited to levels as low as 0.1 mSv y^{-1}. Of this, only 10 to 20 percent is likely to be due to photons. The task of identifying 10 μSv y^{-1} due to accelerator operation in a background 50 to 100 times higher is formidable. Variations in the geology with an accelerator site may easily produce local fluctuations of 0.2 mSv y^{-1} or more (Stephens *et al.*, 1975; 1976; Thomas, 1976). Variations in water content in the soil, snow cover, and contributions from radon daughters washed out by rainfall may also significantly perturb the radiation background to an extent much greater than the accelerator operation (Beck *et al.*, 1971; de Planque-Burke, 1975a; 1975b; de Planque-Burke and O'Brien, 1974). Hence, it is necessary that fluctuations in the natural background be understood before the observed detector reading can be interpreted in terms of operation of a nearby accelerator.

5.6.3.2 *Ionization Chambers.* The natural "active" instrument of choice for real-time measurements of environmental photon fields is the ionization chamber. Special chambers have been built having the sensitivity and stability necessary to measure the low-exposure current rates characteristic of environmental gamma radiation in the range of 0.2 to 1.4 pC kg^{-1} s^{-1} of air or an air kerma of 0.024 to 0.17 μGy h^{-1}.

In particular, one type of chamber has received wide acceptance at accelerator laboratories, as well as at nuclear facilities, and has an accuracy of better than ± 1 percent in fields as low as 0.7 pC kg^{-1}s^{-1} of air (10 μR h^{-1}). This instrument was developed by the Environmental Measurements Laboratory of the U.S. Department of Energy (EML, 1997). It is a high-pressure argon-filled ionization chamber of fairly large volume coupled to an electrometer based on a metal oxide

surface field effect transistor. To obtain sufficient sensitivity, the chamber is a stainless-steel spherical shell designed to withstand high gas pressures. Two versions have been used, either 7 or 25 cm in diameter. These chambers are filled with argon gas to 25 atm (with a range of 18 to 25 atm). The center electrode is an aluminum sphere, either 1.9 or 5.1 cm in diameter, held in place with a thinner aluminum rod. The metal oxide surface field effect transistor based electrometer is capable of measuring currents as low as 10^{-15} A (McCaslin, 1964; Negro *et al.*, 1967). Essentially, complete ion collection is obtained with this arrangement at a collection potential of 300 V for dose rates up to several μGy h^{-1}. Thus, the sensitivity is enhanced by the relatively large mass of gas used in conjunction with the high-sensitivity electrometer.

The 25 cm steel-argon ionization chamber pressurized to 25 atm has been found to be nearly optimum because of the following properties:

- a nearly-flat photon energy response over the range from 0.05 to 10 MeV
- nearly complete ionization collection up to 72 pC kg^{-1} s^{-1}
- a currently stated sensitivity of 0.31 A s kg C^{-1}
- calibration can be performed with readily available radionuclide sources
- the metal oxide surface field effect transistor electrometer is rugged enough for field use
- because of its energy response to muon fluxes, it can be used as a muon dosimeter without modification
- the steel shell and argon filling minimize its response to neutron fluxes

5.6.3.3 *Geiger-Mueller Counters.* GM counters are an old, but extremely reliable instrument for determining environmental radiation levels at accelerator laboratories. The detector assembly consists of a thin window GM tube in a stainless-steel cylinder and the associated transistorized circuitry and scalar units. Each dosimeter is packaged in a metal box 15.2 × 15.2 cm with the GM tube assembly, 15.2 × 3.81 cm, mounted on top of the box. The units, while normally operated from an AC line, also contain a rechargeable battery that can run the detector for about six weeks in the event of a power outage. The detector and scaler units provide a sensitivity of ~0.5 nC kg^{-1} of air (2 μR) per register count. Each GM unit was calibrated with a standard 1.35 mg radium source. At the dose rates to be measured, no corrections to dead time effects are necessary.

5.6.3.4 *Thermoluminescence Dosimeters.*   TLDs have been widely used to monitor photon intensities around nuclear power stations and have been successfully adapted for use at particle accelerators (Bonifas *et al.*, 1974; Tuyn, 1982). Lithium fluoride is usually the material of choice due to its nearly tissue-equivalent energy response. The U.S. Department of Energy Environmental Measurements Laboratory has reported extensive studies of the application of lithium fluoride (EML, 1997) to the measurement of external ionizing radiation due to photons and muons. Using ^{7}LiF dosimeters, evaluated monthly, background radiation levels were measured with an accuracy estimated to lie in the range ± 3.5 percent. Variations in the natural background radiation intensity due to changes in the moisture level in the soil were readily observed with these detectors (de Planque-Burke, 1975a; 1975b; de Planque-Burke and O'Brien, 1974).

Calcium fluoride gained popularity thanks to its higher (15 to 30 times) sensitivity compared to earlier LiF(LiF:Mg,Ti) materials (Cameron *et al.*, 1968; Portal, 1981), in spite of its high fading rate. Its use decreased substantially with the appearance of newer sensitive materials, such as Al_2O_3 and the new version of LiF(LiF:Mg,Cu,P) (Saez-Vergara, 1999). These new materials allow accurate reporting at levels on the order of 1 μSv. Aluminum oxide manufactured for Optically Stimulated Luminescence lowers this limit to ~0.4 mSv.

5.6.4   *Muons*

5.6.4.1 *Introduction.*   Muons are commonly observed outside the shielding of accelerators with beam energies greater than 10 GeV (Bertel *et al.*, 1971; Cossairt, 1983; Cowan, 1962; Nelson *et al.*, 1974). In limited regions, muons may be the dominant component of the radiation field at the site boundary, as is the case, *e.g.*, at FNAL (Baker, 1974; Cossairt, 1983; 1987; Elwyn and Freeman, 1984) or the CERN SPS (Nelson *et al.*, 1979; 1983; Rau and Wittekind, 1982b).

5.6.4.2 *Ionization Chambers.*   Muons, like electrons, are leptons, and except for factors dependent on their greater mass, behave very much the same way as electrons when passing through matter. Ionization chambers have been used successfully in measuring the ionization due to cosmic-ray muons (Liboff, 1975; Lowder *et al.*, 1972). However, Hoefert (1984) has reported differences in the determination of the absorbed dose in tissue from muons of up to 30 percent among instruments of different types, but does not attribute a cause. Further work and independent verification are needed.

5.6.4.3 *Counter Telescopes.* As mentioned in Section 5.4.4.3, counter telescopes were first applied to the detection of protons outside accelerator shielding of Nimrod by Penfold and Stevenson (1968). Subsequently, the technique has been applied to the detection of muons by Hoefert and Baarli (1974) at CERN and Cossairt and his colleagues at Fermilab (Cossairt, 1983; Moore and Velen, 1974). Nelson *et al.* (1974) used scintillation paddles for the detection of muons emerging from thick shielding at SLAC.

Cossairt (1983) has described a muon telescope of moderate directional sensitivity, used at FNAL, consisting of two scintillator paddles approximately 20 by 20 cm by 1 cm, separated by 38 cm and operated in coincidence. A 2.5 cm thick aluminum plate is placed between the scintillators to reduce false coincidences due to delta rays. Coincidence data are obtained, both during beam-on and beam-off phases of operation, using gates synchronized with the accelerator duty cycle. The gating is operated by a microwave transmitter, which also provides beam-intensity data. This detector is mobile and has been used to explore the muon fields at Fermilab in some detail (Cossairt, 1983; Cossairt and Elwyn, 1987).

Stevenson has calculated fluence-to-dose-equivalent conversion coefficients for muons and shown them to be only very weakly dependent upon energy over a large portion of the muon energy spectrum of interest at accelerators (Stevenson, 1983). The coefficients range from 330 pSv cm^2 at 500 MeV to 450 pSv cm^2 at 100 GeV. A value of 380 pSv cm^2 will yield the muon dose within ± 20 percent over this energy range (ICRP, 1988).

5.6.4.4 *Other Techniques.* Several other techniques commonly used to detect ionizing radiation have also been used in muon fields. Some examples are:

- *Nuclear emulsions*: Nelson *et al.* (1974) used nuclear emulsions to study the angular distributions of muons emerging from thick shields made of concrete and iron at SLAC.
- *Silicon detectors*: A detector system based on silicon detectors developed by Heijne (1983) was applied to study muon fields through thick-soil shields at CERN (Nelson *et al.*, 1979).
- *Thermoluminescence dosimeters*: TLDs are well-suited as passive detectors of muons. For example, as part of the routine environmental monitoring program at CERN (Goebel, 1985; Rau and Wittekind, 1982b), as many as 90 CaF$_2$:Dy TLDs were suspended in an array at beam height 2 to 5.5 m above ground at the site boundary downstream of the SPS West Experimental Hall. In such applications, the energy response of TLDs to muons must be taken into account. The density effect in the ionization

stopping-power equation predicts that the energy response of TLDs will differ somewhat from the energy response of gases such as air or argon which are commonly used in ionization chambers to monitor accelerator intensity (Lowder and de Planque, 1977; Maiello *et al.*, 1990; O'Brien, 1978).

- *Miscellaneous instruments*: Cossairt and Elwyn (1987) at Fermilab have reported a study of dosimetry in mixed-radiation fields using a variety of instruments. The radiation field was produced by a 400 GeV proton beam and consisted almost totally of muons and neutrons, with the muons contributing 96 percent of the total absorbed dose to the tissues. The detectors used were a recombination ionization chamber, self-reading pocket ion-chamber dosimeters, and ordinary gamma film badges. Plastic scintillator paddles and a Bonner multi-sphere system were used to measure the muon and neutron fluences. It was concluded that simple instrumentation, *viz.*, the pocket dosimeters, and gamma films "provide an adequately accurate record of absorbed dose equivalent in a muon radiation field . . . even when the spectrum is not well known." However, care must be taken in such measurements because a large neutron fluence could effectively mask the muon absorbed-dose equivalent due to the contribution of capture gamma rays.

5.6.5 *Monitoring of Radioactive Emissions in Air*

5.6.5.1 *Radioactive Gas Monitors.* Moy *et al.* (1980) described the radioactive gas and aerosol monitors used at air-extraction points of the CERN accelerators. Air is diverted from the extraction ducts at a rate of 16 $m^3 h^{-1}$, filtered to remove aerosols greater than ~1 μm in size, and passed through a 1 m^3 measuring chamber. Two GM counters are placed inside the measuring chamber to determine the radioactivity of the gas. Because the principal radionuclides emit beta particles, one counter has a thin-wall and responds to both electrons and photons; the second counter is covered by a plexiglass tube with wall thickness of 5 mm and responds to photons only. The difference between the readings of these two counters may be calibrated to give the activity from $\beta^{\pm}$ emitters and also compensates for any fluctuation in the photon background. The system is calibrated by introducing a known amount of ^{85}Kr into the measuring chamber (Ribes *et al.*, 1974; 1976). Two types of GM tubes are used, having calibrated sensitivities of 440 Bq per pulse and 4.3×10^6 Bq per pulse. The less sensitive detectors are placed where the

concentrations of radioactivity in air are usually high during accelerator operation (*e.g.*, at outlets from target stations).

Two digital outputs are provided by the electronics: the instantaneous concentrations of radioactivity and, by multiplying the concentration by the flow rate of air through the ventilation duct, the total activity release. Specifications of the gas monitor are shown in Table 5.4.

Another technique for measuring the activity concentration of radioactive gaseous emissions is discussed in Butala *et al.* (1989). A flow-through ion chamber utilizes a 0.5 μm pore filter, as well as an electrostatic filter to remove particulates and air ions so only air gases reach the ion chambers. The flow rate is set so that sampled air reaches the detector in less than 1 min. Two identical sealed ion chambers continuously monitor the background radiation which is electronically subtracted from the current measured by the air sampling chambers. This allows the unit to be placed in somewhat elevated external penetrating radiation fields. The chamber is calibrated against a known activity of radioactive gas, typically tritiated methane. It can be used for monitoring gaseous emissions of ^{11}C, ^{13}N, and ^{15}O by applying a correction factor to account for the higher average beta-ray energies.

The above method, or its variation, can be used to monitor tritium at accelerators producing tritium or using tritiated targets. Tritium may be present as HT gas and HTO vapor. Because HTO, at equal concentration, is about four orders of magnitude more hazardous than HT, it may be desirable to determine the HT/HTO ratio. This is accomplished using a twin-chamber technique, where the air stream to one chamber passes through a desiccant. A very sensitive HTO detection method consists of bubbling a known volume of air through a bottle containing distilled water or ethylene glycol. Tritium activity in the liquid medium can then be determined by liquid

TABLE 5.4—*Speci cations of the CERN radioactive gas monitors*.[a]

Parameter	Berthold BZ/120A	Phillips 18555
Sensitivity (Bq^{-1} cm^3 s^1 of ^{85}Kr)	1,600	~16
Unshielded background rate (s^{-1})	~7	~0.5
Concentration range (Bq cm^{-3})	0.001 − 1	0.074 − 74
Calibration factor (total release per output pulse) (Bq $pulse^{-1}$)	4.3×10^6	440
Monitor volume (m^3)	~1	~1
Gas flow rate (m^3 h^{-1})	~16	~16

[a] Using two GM detectors in the monitor volume.

scintillation counting. These and other methods, such as passive sampling techniques, are described in NCRP Report No. 47 (NCRP, 1976c) and IAEA Technical Series Report 324 (IAEA, 1991).

5.6.5.2 *Radioactive Aerosols.* The concentration of radioactive aerosols in the released air may be determined by pumping the air through filter systems. At CERN, *e.g.*, air is pumped through a 200 mm diameter filter paper (Schleiter and Schull No. 6) that is clamped in a special cartridge. The total volume of air passing through the filter is measured by a gas counter. A differential manometer connected to the filter indicates whether the filter cartridge is clogged, broken or improperly placed. For ventilation ducts, the air flow through the filters is 16 $m^3 h^{-1}$, but for some routine low-level air sampling, a rate of 30 $m^3 h^{-1}$ is used. Filter cartridges are removed every fortnight and the activity measured in a low-level counting laboratory (Moy *et al.*, 1980).

5.7 Epilogue

It would be inappropriate to end this Section without reminding the reader that there is a general agreement, based upon decades of experience at accelerator laboratories, with the view of Burton Moyer, first enunciated more than 40 y ago, that physical characterization of the accelerator-radiation environment is to be preferred to attempts to reduce its great complexity to a single scalar quantity, such as dose equivalent. Dosimetrists continue their quest for techniques by which a single dosimeter can be applied to an accurate and sufficient specification of the high-energy accelerator-radiation field, but there is good reason for skepticism that such a goal can be achieved. Indeed, the debates concerning the dose-equivalent system recommended in ICRP Publication 26 (ICRP, 1977) that have taken place over the past two decades, may lead one to doubt the permanence of the current system for radiological protection as set forth in ICRP Publication 60 (ICRP, 1991).

6. Environmental Radiological Aspects of Particle Accelerators

6.1 Introduction

In considering environmental impact when particle accelerators are operated, two sources of radiation have to be taken into account. These two radiation sources are prompt radiation and induced radioactivity:

Prompt Radiation: Exists only when the accelerator is operating and ceases when the accelerator is turned off, results both as a consequence of the adventitious loss of part or all of the accelerated beam and normal utilization of the beam. The character of the prompt radiation field close to the accelerator is strongly dependent upon the type and energy of the particle being accelerated. At larger distances, the observed field comprises two components; direct and scattered radiation. In much of the accelerator literature, the term "skyshine" refers to all radiations whether unscattered (direct) or scattered by the ground, air or neighboring buildings (IAEA, 1988).

The precise definition of "skyshine" is not apparent from the literature and is defined here as that radiation observed at a point on the ground surface which arrives at that point having undergone one or more large-angle scatters in the air.

Photon-skyshine was first observed around "hot-cells" which stored large quantities of radioactive material and were built with thick-shield walls, but with no roof (for a review of the early literature, see Clarke, 1968a; 1968b; Leimdorfer, 1968; Price *et al.*, 1957; Woodley, 1970). Neutron skyshine was first observed at particle accelerators with very thin or no overhead shielding: neutrons directed upward were back-scattered to Earth by the air (Lindenbaum, 1957; Moyer, 1957).

Induced Radioactivity: In contrast to the "prompt" external radiation field, radiation from the decay of radioactivity induced in the accelerator structure and its ancillary components by the accelerator

320

beam, or by the prompt radiation that remains after accelerator shutdown.

In addition to presenting an external radiation hazard, the induced radioactivity in the accelerator structure and its ancillary components presents three possible sources of environmental pollution:

- solid materials—maintenance, decommissioning
- radioactive gases—mainly air activation products
- radioactive liquids—mainly cooling water and groundwater

Solid material—because accelerator components can become radioactive, it is important that their movement within and release from the accelerator room be carefully monitored and controlled. Maintenance work on such radioactive components involving machining, soldering or welding may produce radioactive particles or radioactive fumes which can spread contamination and even result in human uptake of radioactivity. When accelerators are decommissioned, care is again necessary in controlling the release or disposal of accelerator shielding and components (Opelka *et al.*, 1979).

Gases and water—induced radioactivity is not limited to solid materials; fluids, including air and water, surrounding the accelerator may also become radioactive. In some ways the activity induced in fluids is more troublesome, not because of its quantity but because radioactive gases and water, including groundwater, are mobile and might transport the radioactivity to locations far from the accelerator. The contribution to the collective dose equivalent to the public by airborne radionuclides from high-energy facilities is, in most cases, lower by at least an order of magnitude than that from prompt radiation. No significant population exposure has been observed, or is expected, from activated solid material and water (Goebel, 1987; Thomas and Rindi, 1979). The radiological impact on the environment of the operation of even the most powerful accelerators is usually very small. However, from the point of view of environmental contamination, considerable thought and analysis must be devoted to the creation of radioactive materials in soil and groundwater.

6.2 Skyshine

6.2.1 *General Considerations*

Particle accelerators of all types can be potent radiation sources and, in some circumstances, their operation may be detected at large

distances by sensitive instruments. For instance, it has been estimated from radiation surveys that 10^9 neutrons s^{-1} leaked from the roof-shield of the Lawrence Berkeley Laboratory Bevatron when it accelerated 10^{12} protons s^{-1} to an energy of 6 GeV. At a distance of ~1 km, a neutron source of this magnitude generates a fluence about the same as that produced by cosmic rays at sea level (Thomas, 1978a; 1978b). Figure 6.1 shows the responses of environmental radiation detectors placed near the 20 GeV electron linac of SLAC (Jenkins, 1974). Neutron and photon detectors were placed ~500 m from the experimental area of the accelerator and their responses are plotted in Figure 6.1 as a function of time. At periods of intense operation the neutron dose-equivalent rate exceeded the neutron background by more than an order of magnitude whereas the photon dose-equivalent rate increased by only 10 to 20 percent of the background rate.

In both examples just cited for high-energy electron and proton accelerators, neutrons dominated the skyshine field. As early as 1965, De Staebler (1965) anticipated this observation and gave the basic reasons for expecting neutrons to make the dominant contribution to the dose equivalent outside the shielding of high-energy, high-intensity accelerators, whether they accelerate electrons or protons. Measurements have amply confirmed that expectation at both proton
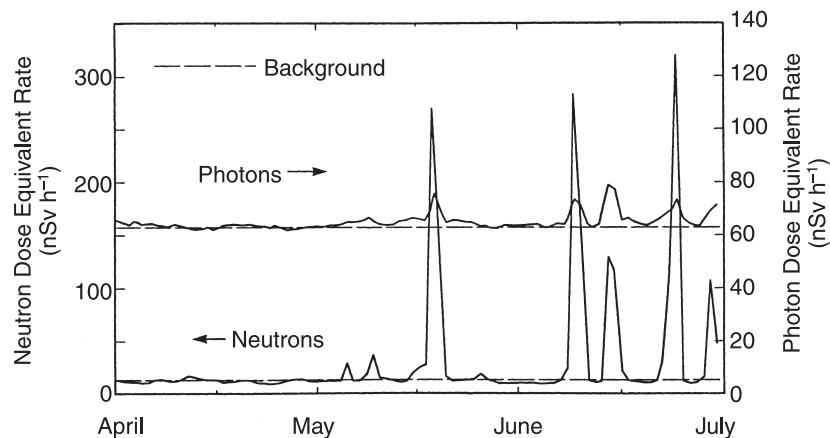
Fig. 6.1. The variation in dose-equivalent rates with time as observed at the boundary of SLAC. The dose-equivalent rates due to both photons and neutrons are indicated by solid lines; natural background due to each component by dashed lines. Periods of intense accelerator operation are evident from the fluctuations in neutron dose-equivalent rate (Jenkins, 1974).

accelerators (IAEA, 1988; Patterson and Thomas, 1973) and electron accelerators (Jenkins, 1974).

Experience has shown that for high-energy accelerators skyshine may make the largest *contribution* to the exposure of the general public as a result of accelerator operation. The *magnitude* of the exposure, which is generally small, depends upon the location of the radiation source and may be important only for those accelerators situated near densely populated areas.

6.2.2 *Neutron Skyshine*

Any accelerator of sufficient energy will produce neutrons in the accelerator enclosure, and the energy of these neutrons will be distributed over a wide range. In passing through the shield, if the shield is sufficiently thick, the primary neutrons, degraded both in energy and intensity, will reach equilibrium with lower-energy neutrons formed by inelastic processes in the shield material. Neutrons are the principal component of radiation transmitted by a thick-roof shield and will emerge into the surrounding air. In those cases where the roof is thin, particle equilibrium may not be achieved and the emerging neutron spectrum will be intermediate between that of the primary source spectrum and the ultimate equilibrium spectrum.

Skyshine results from scattering processes and it is largely lower-energy neutrons that are scattered back to ground. High-energy neutrons, which penetrate the roof, undergo inelastic collisions with air atoms to generate more low-energy neutrons in the air augmenting those which have "leaked" from the roof. In order, therefore, to fully quantify skyshine phenomena, it is necessary to know the intensities and both the energy and angular distributions of neutrons entering the sky above the accelerator.

Lindenbaum made one of the earliest analyses of neutron skyshine at the Brookhaven National Laboratory's Cosmotron (Lindenbaum, 1957), based on existing studies of diffusion theory (Case *et al.*, 1953; Lindenbaum, 1957). The Lindenbaum treatment for evaporation neutrons estimated the neutron fluence around the Cosmotron (a 3 GeV proton synchrotron) to about a factor of two, and was later applied to the estimation of the neutron fluence around a 50 MeV proton linear accelerator with similar success (Simpson and Laws, 1962; Thomas *et al.*, 1962).

Although Lindenbaum's equation was successful in quantifying the radiation of the early Cosmotron it is not of general validity. The absence of overhead shielding at the early Cosmotron resulted

in a radiation field different from that typically found around well-shielded, high-energy accelerators. Lindenbaum's treatment described a situation in which the neutron-leakage spectrum in the air was largely composed of neutrons with energies below a few mega-electron volts produced by the primary proton generated cascade. Leakage from the magnet steel of the Cosmotron provided an intense source of such neutrons and Lindenbaum's use of diffusion theory proved to be adequate to describe the variation of neutron dose equivalent with distance out to ~200 m from the accelerator. However, when an accelerator is well shielded, and the radiation field is consequently controlled by source neutrons of energy greater than 100 MeV, Lindenbaum's treatment is less successful. Moyer (1962) discussed the transport of high-energy neutrons through the atmosphere and showed the magnitude of the physical parameters involved, that the forms of the variation of neutron fluence with distance, both for the diffusion-neutron group and the high-energy neutron group were very similar (Figure 6.2).

The earliest experimental studies of neutron "skyshine" have been reviewed in the literature (IAEA, 1988; Rindi and Thomas, 1975). Only a summary of the general conclusions is given here.

Figure 6.3 summarizes some of the experimental data obtained around several particle accelerators (Rindi and Thomas, 1975). At distances greater than ~200 m from the accelerator, all the observed sets of data could be fitted by equations of the form:

$$\phi(r) = \frac{aQe^{-r/\lambda}}{4\pi r^2} \tag{6.1a}$$

and

$$H(r) = g\phi(r), \tag{6.1b}$$

where:

$\phi(r)$ = neutron fluence[41]

a = source enhancement factor (this dimensionless factor accounts for deviations from the assumed attenuation length of the neutron field close to the source)

---

[41]With few exceptions, time-independent quantities are used throughout this Section in formulating expressions in the text. This is done because dose may be expressed with respect to a variety of time periods, depending on the specific application of the quantity. It is not practicable to give general equations that meet all requirements. The method of presentation here enables the reader to introduce simply the dimensionless factors that generate the particular dose rate required. The exceptions to this general rule are (1) in direct quotations from the literature, (2) when confusion would otherwise result, or (3) in an example calculation that requires dose rate in the answer.
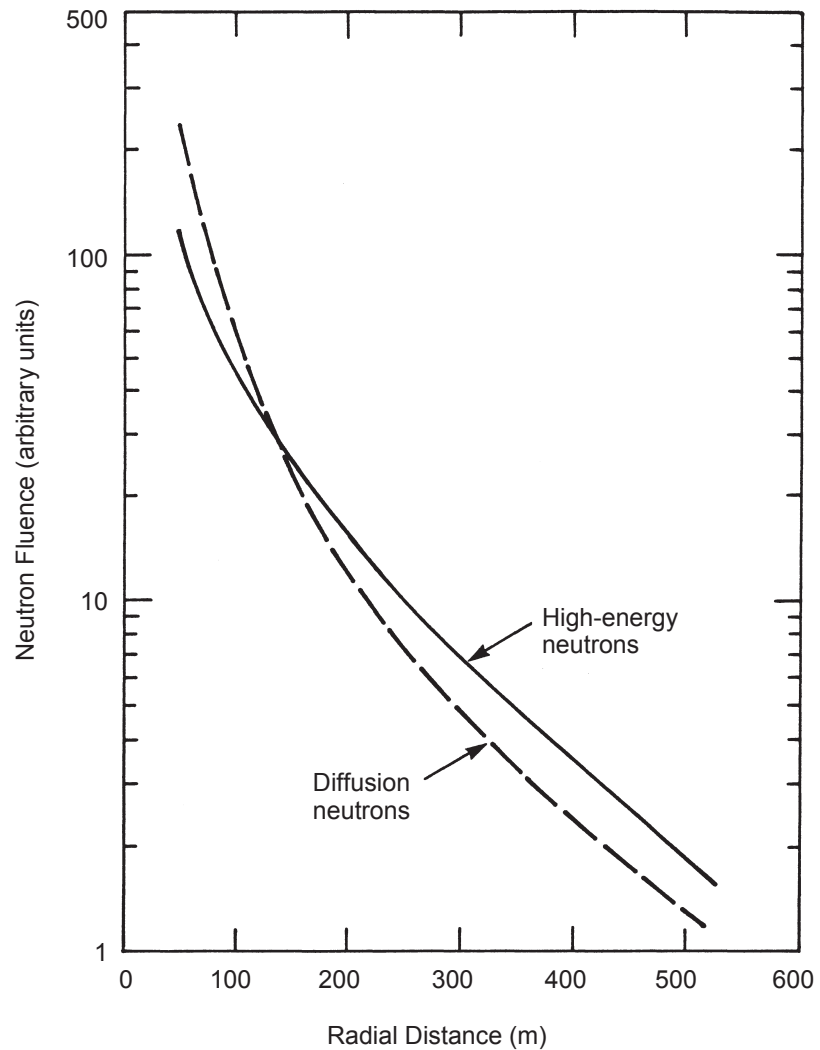
Fig. 6.2. A comparison of the radial variation of the low-energy neutron fluence (by diffusion; dashed line) and that of the high-energy fluence (solid line), at distances out to 500 m from a high-energy accelerator (Moyer, 1962).

Q = the leakage neutron source strength (number of neutrons entering the sky)

r = distance from the accelerator

λ = effective attenuation length of the skyshine neutrons in air

$H(r)$ = dose equivalent

g = fluence-to-dose-equivalent conversion coefficient
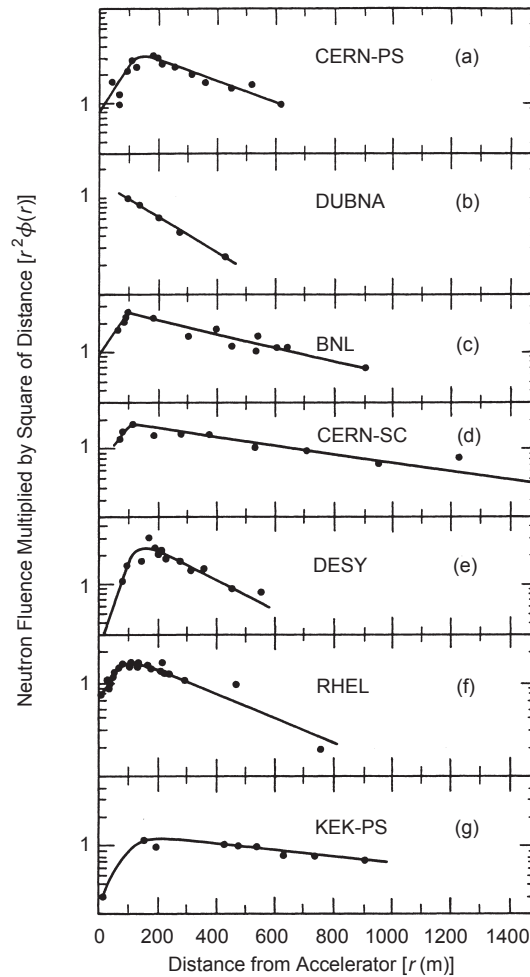
Fig. 6.3. Measurements performed around various accelerators. On the abscissa is the distance from the accelerator in meters; on the ordinate is the product of the measured neutron fluence and the square of the distance. In these conditions, an r^{-2} variation is represented by a horizontal line. (a) Measurements of fast-neutron fluence density performed at the CERN 28 GeV Proton Synchrotron (Ollendorf, 1964). (b) Measurements of fast-neutron fluence density performed at the Dubna 10 GeV Proton Synchrophasotron (Komochkov, 1970; Lebedev *et al.*, 1965). (c) Measurements of dose-equivalent rate performed at the Brookhaven 30 GeV Proton AGS (Distenfeld and Colvett, 1966). (d) Measurements of the fast-neutron fluence density performed at the CERN 600-MeV Proton Synchrocyclotron (Rindi and Baarli, 1963). (e) Fast-neutron fluence density measurements performed at the Deutsches Electronen Synchrotron 7.5 GeV Electron Synchrotron (Bathow *et al.*, 1966). (f) Fast-neutron fluence density measurements performed at the Rutherford Laboratory Proton Linear Accelerator for a proton beam of 50 MeV (Simpson and Laws, 1962; Thomas *et al.*, 1962). (g) Measurements made at the 12 GeV Proton Synchrotron at KEK (IAEA, 1988).

Equations 6.1a and 6.1b give a plausible physical interpretation of observation and require knowledge of four parameters: the leakage source strength (Q), the source enhancement factor (a), the attenuation length (λ), and the conversion coefficient (g) (which is energy-spectrum dependent).

The values of λ observed vary from ~250 m to nearly 1,000 m in air at standard temperature and pressure (Rindi and Thomas, 1975). For conditions where low-energy neutrons dominate, the shield leakage spectra values of λ towards the lower end of the range (*i.e.*, ~250 m) are obtained [*c.f.*, values of λ obtained at large distances from nuclear reactors or D-D and D-T neutron sources (Auxier *et al.*, 1963; French and Mooney, 1971; Haywood *et al.*, 1964; 1965; Stephens and Aceto, 1963)]. Under conditions where high-energy neutrons dominate the leakage spectrum and transport the cascade through the air, the values of λ obtained are close to the value of the high-energy, mean free path in air (100 g cm^{-2} or 800 m at STP).

Formulas of the type given in Equations 6.1a and 6.1b and other expressions derived from experimental data, such as those utilized later in this discussion for the estimation of skyshine from accelerator facilities are acknowledged to be of limited accuracy but they do possess advantages in providing quick and, in many cases, adequate answers. For more accurate representations of particle transport, it is necessary to use computer methods such as those using Monte-Carlo techniques (Nelson and Jenkins, 1980) (see also Section 4.2.2).

There are two distinct aspects of skyshine to which computer calculational techniques may be applied: the determination of the source terms within the accelerator vault and the transmission of these radiations through the shield and air. Of these two calculations, it is the determination of the magnitude of the source term that is most uncertain. Because many accelerators (particularly those used in scientific research) operate under conditions requiring a variety of targets, beam energies, intensities, and differing amounts of local shielding, it is often necessary to derive a source term based on a judgment of average operating conditions. Having estimated the source term, by whatever means, the transport of neutrons through shielding and through the air over ground can then be performed.

The transmission of neutrons through shielding and air can be treated by neutron transport codes (Section 4). Most of the published skyshine studies are limited in scope (for a summary, see IAEA, 1988). To be complete, a numerical treatment of neutron skyshine must address transport for neutrons with energies up to several hundreds of mega-electron volts and also address both source photons and those generated by neutrons in the air, with realistic shielding geometries and with sources simulating accelerator conditions.

Many published calculations are limited to neutrons with energy less than 20 MeV (Kinney, 1962; Ladu *et al.*, 1968). The early calculations of Ladu *et al.* have been summarized by Chilton (1974). Nakamura and his colleagues (Nakamura and Kosako, 1981; Nakamura *et al.*, 1981) used the MORSE computer code to study accelerator skyshine. The calculations of all these authors are in general agreement with the diffusion theory treatment by Lindenbaum and lead one to the view that the transport of low-energy (few mega-electron volts) neutrons produced at an air-ground interface is reasonably well understood. Alsmiller *et al.* (1981b) have made skyshine calculations for monoenergetic neutrons up to 400 MeV and also for photons up to 14 MeV, using the discrete ordinates transport (DOT) code (Rhoades *et al.*, 1979). For selected distances from the skyshine source up to ~1 km, the dose equivalent was calculated as a function of solid angle interval open to the sky for emission. The results are expressed as "importance functions" and tabulated in terms of dose equivalent/source neutron (or photon) for selected energy intervals over the neutron (or photon) spectrum, and are given in Appendix A.

Tables of importance functions can also be obtained as computer readable data files (ORNL, 1990) and are probably the best estimates of skyshine available at the present time. When the magnitude of the source term and the direction and energy of particles entering the sky are known sufficiently well, and provided the geometry corresponds to that shown in Figure 6.4, the dose equivalent at the four distances given in Appendix A may be obtained directly. These four results may then be interpolated to give dose equivalent at intermediate distances.

In making comparisons between the calculations of Ladu *et al.* (1968) or Lindenbaum (1957; 1961) and the importance functions, it is extremely important to be aware that the data of different authors are normalized in different ways. For example, the calculations of Lindenbaum and Ladu assume an isotropic source emitting into all space (4π steradians); the importance functions given in Appendix A assume a source emitting into half space (2π steradians), the hemisphere away from the ground.

The expressions of Chilton (1974), Ladu *et al.* (1968), and Lindenbaum (1957; 1961) deal with the transport of neutrons having energies of a few mega-electron volts and lower. These expressions are of limited utility when the accelerator spectra extend beyond 20 MeV. In order to handle typical accelerator spectra leaking through shielded roofs, it is necessary either to turn to Alsmiller's importance functions or to use more comprehensive empirical formulas.
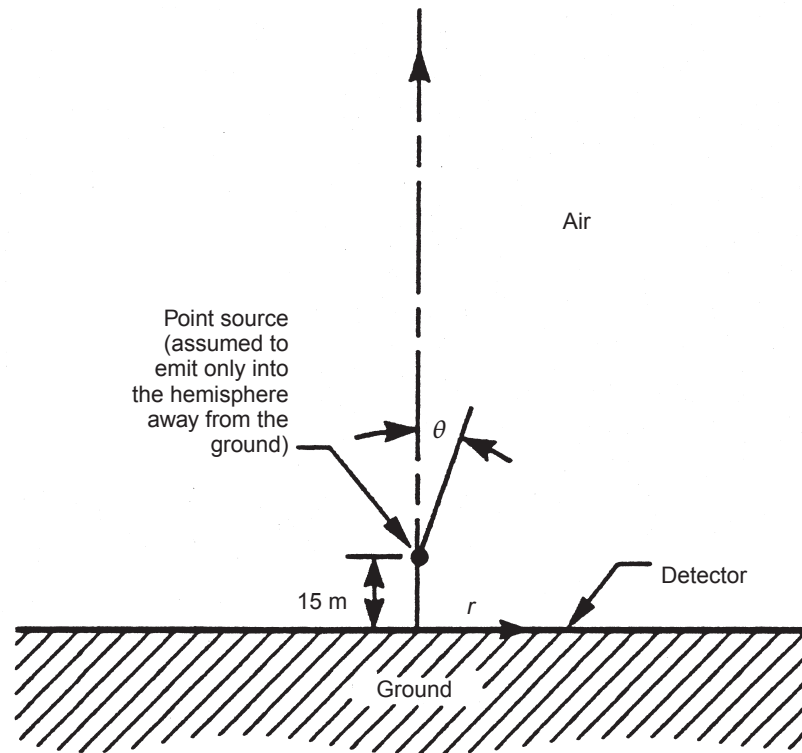
Fig. 6.4. Geometry for which importance functions have been calculated (Alsmiller *et al.*, 1981b).

Stevenson and Thomas (1984) suggested an alternative to using either solely experimental data or solely calculated data by creating an hybrid of both approaches. These authors combined the calculations of importance functions with the experimental data previously discussed. Several simplifying assumptions were made in their treatment, the most important being that the neutron differential energy spectrum had the 1/*E* form. These authors concluded that the neutron dose equivalent per source neutron [*H*(*r*)] could be conservatively expressed as a function of distance by the equation:

$$H(r) = \frac{\kappa}{r^2}\,e^{-r/\lambda}, \tag{6.2}$$

where κ is a constant and has the value 1.5 to 3 $\times$ 10^{-15} Sv m^2 per neutron. The appropriate value of λ is selected from the curve labeled

Stevenson and Thomas shown in Figure 6.5, by assuming that the highest energy of neutrons in the accelerator-produced spectrum (the upper energy cutoff) is the energy of the accelerator beam. Stapleton *et al*. (1994) have reviewed the conclusions reached by Stevenson and Thomas and, in particular, investigated the influence of the angular distribution and energy spectrum on the dose equivalent. They were able to demonstrate that, for distances between ~100 and 1,000 m, the dose equivalent [$H(r)$] is extremely robust against changes in both neutron spectrum and angular distribution. The improvements made by Stapleton *et al*. included:

- using a neutron spectrum that more realistically matches an accelerator-shield-leakage spectrum
- assuming that neutrons are emitted from an accelerator shield with the fluence varying as the cosine of the angle normal to the wall
- assuming that neutrons of energy greater than 400 MeV can be included in the highest energy group of the importance functions, weighted in direct proportion to their energy
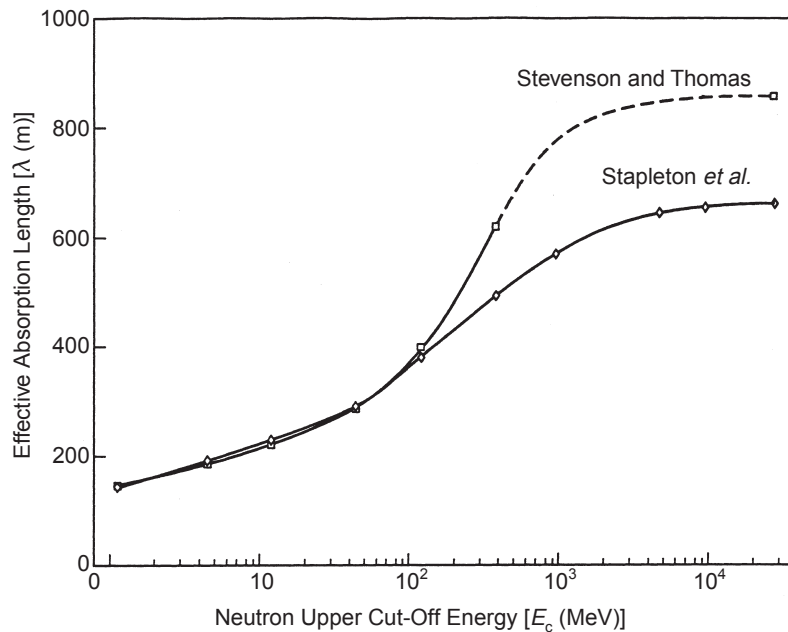
Fig. 6.5. The effective neutron absorption length in air as a function of the upper neutron energy cutoff assuming a l/*E* (Stevenson and Thomas, 1984) and a typical accelerator leakage differential energy spectrum (Stapleton *et al.*, 1994).

- modifying the geometry with an additional parameter h on the assumption that the skyshine source behaves as a virtual source in the sky and, making an approximate correction to Stevenson and Thomas' expression at small values of r (<100 m)

The modified expression derived by Stapleton *et al.* (1994) was:

$$H(r) = \frac{\kappa'}{(h + r)^2}\, e^{-r/\lambda},\tag{6.3}$$

where κ' has the value 2×10^{-15} Sv m^2 per neutron and $h = 40$ m was found to give an improved fit to the importance function data over that previously reported. The value of λ in this case is to be selected from the appropriate curve shown in Figure 6.5.

It must be emphasized that Equation 6.3 is an empirical summary of both theoretical and experimental data and may be used, within some constraints, to facilitate skyshine shield calculations.

6.2.3 *Photon Skyshine*

At high-energy accelerator installations, neutrons generally determine the roof shielding requirements and, thus, usually dominate the radiation environment at large distances from accelerators. However, the photon contribution to the dose equivalent should not be neglected. There are two potential sources of photon skyshine from particle accelerators: the first is prompt radiation, while the second may be from induced radioactivity.

Early observations of photon dose rates around hot cells indicated that overhead scattering of photons could produce higher doses to personnel than could radiation arriving directly through the shield wall. This scattering could, for example, be from overhead viewing mirrors, or from the ceiling of the building or the air above. This problem was analyzed using Compton-scattering theory. An early analysis of scattering from an overhead mirror used for viewing operations over a shield wall provides an excellent illustration of the phenomenon (Price *et al.*, 1957).

Hadrons produced during accelerator operation will always be accompanied by photons, and such gamma enhancement of the dose equivalent is often taken into account by some additional conservatism in the prescribed shielding thicknesses calculated on the basis of neutrons alone. The case of skyshine is no exception. There are a few instances where the prompt-photon skyshine contribution to dose equivalent is significant or even dominant. An example of such a case would be high-intensity electron accelerators with little or no overhead roof shielding.

A potentially important source of photon skyshine arises from photons emitted by decay of radionuclides produced during accelerator operation. Many of these are short-lived (half-lives less than a few hours) and are positron emitters producing a source of 0.511 MeV annihilation photons. In order to reduce this potential source of exposure, it is important to ensure that adequate shielding is placed around accelerator cooling-water systems (pipes, pumps, surge tanks, ion-exchange resin columns), both to reduce local radiation levels to protect plant personnel and also to control photon skyshine at greater distances. Dose-equivalent rates near these installations can be in excess of 1 Sv h^{-1} for beam powers of several hundred kilowatts (Warren *et al.*, 1969).

As is the case for neutrons, the application of the photon spectrum to the photon importance functions will permit the skyshine dose to be determined at given distances. The photon importance functions are tabulated in Appendix A. In addition, there are some instances where analytical approaches, such as that of Price *et al.* (1957), to the estimation of photon skyshine are helpful. An excellent introduction to the theoretical basis for such calculations may be found in Stephenson (1958).

The skyshine generated by a point source situated at the interface of two materials (*e.g.*, air and earth) may be related to the scattered radiation exposure rate produced in an infinite homogeneous medium (S_∞) by an enhancement factor (K_s) (Clarke, 1968a) defined by:

$$K_s = \frac{S_{sky}}{0.5 \, S_\infty}, \qquad (6.4)$$

where S_{sky} is the skyshine intensity and the factor 0.5 is introduced because the source at an earth-air interface can emit only into the upper hemisphere. Clarke has summarized experimental determinations of values of K_s for ^{137}Cs and ^{60}Co photons as function of distance from the source.

Based on the work of Clarke (1968a; 1968b), Chilton (1974), as described in NCRP (1977), developed an empirical relationship for the skyshine from a source of relatively low-energy photons (x rays) at distances between 20 and 250 m from the source:

$$H(r) = \frac{2.5 \times 10^2 H_0 \Omega^{1.3}}{r^2}, \qquad (6.5)$$

where:

    r = source to observer distance in units of meters

    $H(r)$ = dose equivalent per unit fluence from photon skyshine at distance r in units of Sv m^2

Ω = solid angle subtended by the x-ray source and the shielding walls in units of steradians

H_0 = dose equivalent per unit fluence at 1 m from a photon source inside the shielded enclosure in units of Sv m^2

It should be noted that the dose should be reduced to take into account any roof shielding. This will be made clearer in the example discussed later (Section 6.2.4).

A more rigorous analytical approach is given by Stephenson (1958), which, for isotropic scattering, leads to:

$$\phi_s = \frac{\pi N \sigma_{tot} S}{16x} = \frac{\pi \Sigma_{tot} S}{16x}, \qquad (6.6)$$

where:

σ_{tot} and Σ_{tot} = total microscopic and macroscopic scattering cross sections, respectively

S = number of photons per second emitted from the source

N = number of electrons per unit volume of air ($\sim 3.6 \times 10^{20}$ cm^{-3})

x = distance from the source

However, in most practical cases of skyshine, the radiation shining upwards to the sky is limited by the shielding of the building walls to an inverted cone. For the source strength S we now substitute $\omega S/4\pi$ where ω is the solid angle subtended by the hole that is the unshielded roof. Then:

$$\phi_s = \frac{NS\omega}{8\pi x}\left(\frac{\overline{d\sigma}}{d\Omega}\right)(\psi_2 - \psi_1)\left(\pi - \frac{\psi_1}{2} - \frac{\psi_2}{2} - \phi_1\right), \qquad (6.7)$$

where $\overline{d\sigma}/d\Omega$ is the Compton differential-scattering cross section for scattering angles greater than 90 degrees and $(\psi_2 - \psi_1)$ equals the angle subtended by the cone and shield wall and ϕ_1 is the angle from the point of detection to the nearest edge of the source (Stephenson, 1958).

For photons of energy between $\sim$0.05 and 4 MeV, the fluence to dose-equivalent conversion coefficient (ICRP, 1973) is given by:

$$\frac{0.1734}{E(\mu_{en}/\rho)} \quad \text{photons cm}^{-2}\text{ s}^{-1}\text{ }\mu\text{Sv}^{-1}\text{ h}. \qquad (6.8)$$

Taking the value of μ_{en}/ρ (water) to be constant at 3×10^{-3} m^{2}kg^{-1} over the energy range (0.05 to 3 MeV), recasting in units of sieverts and omitting the time dependence, the dose equivalent varies with energy according to the equation:

$$H = 4.806 \times 10^{-11}\ \phi E, \qquad (6.9)$$

where:

H = dose equivalent (sieverts)
ϕ = photon fluence (cm^{-2})
E = photon energy (mega-electron volts)

6.2.4 *Comparisons of Skyshine Calculations*

6.2.4.1 *Neutron Skyshine.* There are four steps in estimating neutron skyshine, three of which are involved in determining the total leakage neutron source strength (Q) from the roof. First, the neutron dose-equivalent rate that might be observed on the roof of an enclosure for a given accelerator operating program is estimated. Second, this dose-equivalent rate is converted to a fluence rate for the appropriate neutron energy spectrum. This may be done by assuming the energy spectrum is similar to that shown in Figure 6.6 and, by using
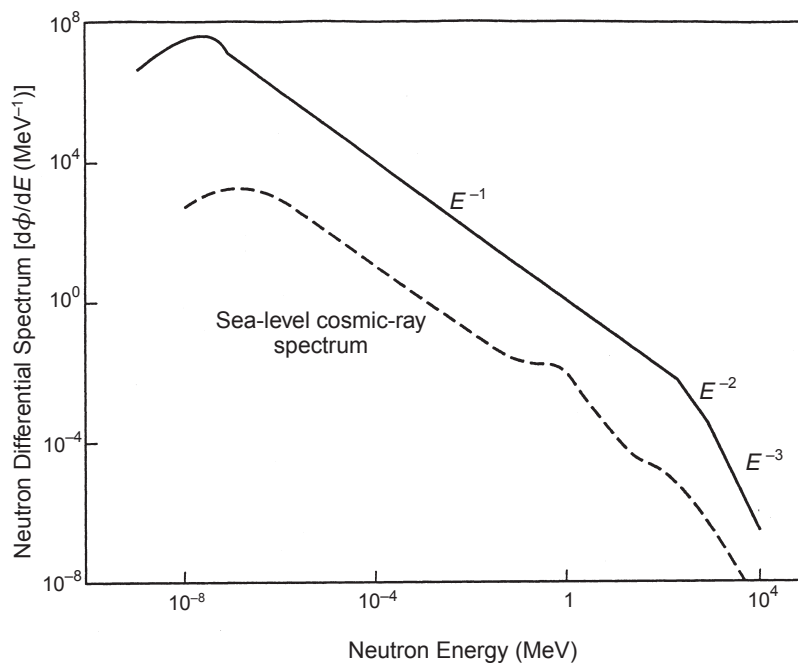
Fig. 6.6. Composite neutron differential spectrum from simple parameterizations to represent lateral shield spectrum (Stapleton *et al.*, 1994). The composite spectrum is compared with the cosmic-ray neutron spectrum at sea level measured by Hess *et al.* (1959).

the dose-to-fluence data for this spectrum given in Table 6.1. Third, the fluences must be summed over the whole roof to calculate the total neutron source strength (Q) from the roof. Finally, $H(r)$ is obtained by multiplying Equation 6.3 by the value of Q so obtained.

A direct comparison using the methods of Stapleton and Chilton is given in Table 6.2, which shows that these methods of calculating neutron dose equivalent due to skyshine show reasonably good agreement out to distances of 1,000 m. These simple recipes must, however, be treated with great caution, particularly so when extrapolated to large and small distances. Beyond 1,000 m, the two methods give increasingly divergent results. The Stapleton method is judged to be the more reliable of the two because the effective attenuation length (λ) in air was obtained by fitting a more appropriate neutron spectrum than was used by Chilton *et al.* (1984).

TABLE 6.1—*Dose equivalent per unit fluence conversion coefficients for the composite neutron spectrum shown in Figure 6.6 as a function of maximal neutron energy (E_{max}) (Stapleton et al., 1994).*

E_{max} (MeV)	Spectrum-Averaged Conversion Coefficient (g) (Equation 6.1b) (fSv m^2)
1.6	4.8
2.5	5.5
4.0	6.3
6.3	7.1
10	7.8
16	8.6
25	9.4
40	10.1
63	10.9
100	11.7
160	12.5
250	13.2
400	13.7
630	14.1
1,000	14.4
1,600	14.5
2,500	14.6
4,000	14.6
6,300	14.7
10,000	

TABLE 6.2—*Neutron skyshine dose equivalent results using two alternative methods of calculation.*

Distance from Source [r (m)]	Stapleton *et al.* (1994) (Sv y^{-1})	Chilton (1974) (Sv y^{-1})
100	1.3×10^{-4}	7.6×10^{-5}
1,000	5.7×10^{-7}	1.9×10^{-6}
10,000	4.3×10^{-15}	4.8×10^{-8}

6.2.4.2 *Photon Skyshine.* As an example of photon-skyshine calculation, a cooling plant for a high-power beam dump is used. Such a beam dump gives rise to considerable radiation from the decay of ^{15}O by positron emission. It is assumed that lateral shielding is provided, but no roof is added.

Table 6.3 summarizes the calculations of photon skyshine by three different methods. In the second column, the result is given for the value of S derived for the example multiplied by the importance function (IF) solution and the fraction of the photon yield entering the sky ($\Omega/4\pi$) (Alsmiller *et al.*, 1981b). The third and fourth columns give the result calculated using Stephenson's (Equation 6.6) and Chilton's (Equation 6.5) methods, respectively. These latter results have been corrected by assuming a 0.2 MeV photon (energy assumed after scattering once), a total attenuation length in air of 67.5 m, and the appropriate buildup factor applied to the distances given in the first column.

6.2.5 *Collective Exposure to the Population*

Prompt radiation frequently dominates the radiation environment of accelerators and is usually the major source of exposure to the

TABLE 6.3—*Photon skyshine results using three alternative methods of calculation.*

Distance from Source [r (m)]	IF $\times$ S $\times$ $\Omega/4\pi$ (Section 6.2.4.2) (Sv y^{-1})	Stephenson (1958) (Sv y^{-1})	Chilton (1974) (Sv y^{-1})
11	5×10^{-4}	7.8×10^{-4}	6.1×10^{-3}
108	5.5×10^{-5}	7.9×10^{-5}	6.2×10^{-5}
495	3×10^{-7}	1.0×10^{-6}	1.7×10^{-7}
1,005	7×10^{-10}	1.5×10^{-9}	1.3×10^{-10}

general population in the vicinity of an accelerator facility. This is particularly so when neutrons are the principal source of dose equivalent.

There is no generally accepted method of calculating population exposure due to neutron skyshine. The model suggested by Stephens *et al.* (1975; 1976) is described here. These authors use the typical variation of dose equivalent with distance (r):

$$H(r) = \frac{A\,\mathrm{e}^{-r/\lambda}}{r^2}\,. \tag{6.10}$$

Assuming roughly a uniform distribution of people of Z_p persons per unit area around the accelerator, then the total population dose equivalent received in the radial interval r_1 to r_2 is given by:

$$M = 2\pi Z_\mathrm{p} A \int_{r_1}^{r_2} \frac{\mathrm{e}^{-r/\lambda}}{r}\,\mathrm{d}r\,, \tag{6.11}$$

where a value for the source term A can be derived from the boundary dose H_0 at distance r_0 from the primary radiation source:

$$A = H_0\,r_0^2\,\mathrm{e}^{-r_0/\lambda}. \tag{6.12}$$

Stephens *et al.* define the parameter $\mu(r_0,\lambda)$:

$$\mu(r_0,\lambda) = \frac{M}{2\pi Z_\mathrm{p} H_0} = r_0^2 \mathrm{e}^{-r_0/\lambda} \int_{r_0}^{r} \frac{\mathrm{e}^{-r/\lambda}}{r}\,\mathrm{d}r. \tag{6.13}$$

The graph of $\mu(r_0,\lambda)$ versus distance in Figure 6.7, with r_0 taken as 200 m for values of r from 200 to 10,000 m, shows that $\mu(r_0,\lambda)$ converges to a constant value. Consequently, it is only necessary to extend the upper limit of the integration to about $(r_0 + 3\,\lambda)$ to obtain a reliable estimate of the total population dose. Figure 6.8 shows the normalized population dose $\mu(r_0,\lambda)$ integrated to the convergence limit as a function of r_0 for various values of λ.

IAEA (1988) suggested the use of the parameter M/H_0 (person dose equivalent per unit dose equivalent measured at the site boundary) as a measure of the environmental radiological impact resulting from penetrating radiation.

6.3 Induced Radioactivity of Environmental Concern Produced by Accelerators

Second only to skyshine, radioactivity produced in the environment presents an important potential for radiation exposure of the
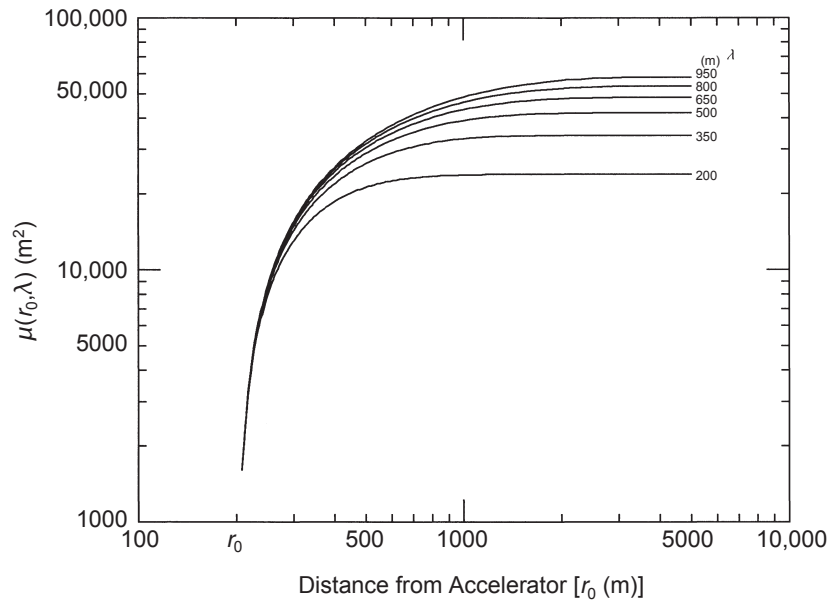
Fig. 6.7. Convergence of the parameter $\mu(r_0,\lambda)$ for $r_0 = 200$ m and various values of absorption length (λ) (Equation 6.13).

general population as a result of accelerator operation. Typically, the magnitude of this exposure is many times smaller than that from "prompt" radiation. In order of importance, the magnitude of exposure from induced activity to the general public is (1) air-activation, (2) groundwater activation, and (3) activated accelerator components.

6.3.1 *Radionuclides Produced in Air*

The principal source of radioactivity in air is the interaction of primary and secondary particles directly with constituent target nuclei of the air. A secondary source of airborne radioactivity is dust, formed by natural erosion and wear, or by work on radioactive accelerator components. The third and final source of airborne radioactivity results from the emission of gaseous radioactivity from liquids irradiated in the accelerator-produced radiation environment.

6.3.1.1 *Radionuclides Produced Directly in Air.* During accelerator operation, radioactive nuclides are produced by the interaction of primary and secondary particles with the air contained in the
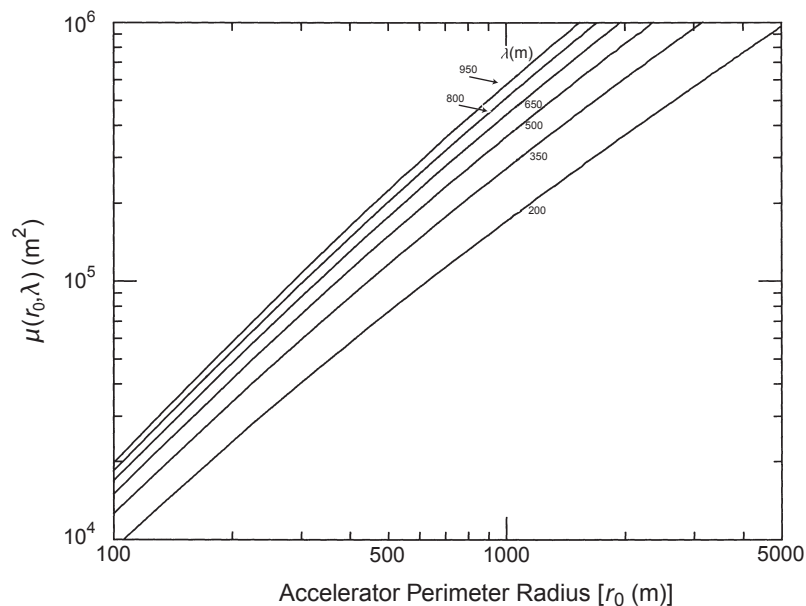
Fig. 6.8. The $\mu(r_0,\lambda)$ integrated to the convergence limit for values of r_0 and various values of absorption length (λ) (Equation 6.13) (Stephens *et al.*, 1975; 1976).

accelerator enclosures. If the air is confined in the accelerator enclosure, there will be no release of radioactivity to the general environment during the operation of the machine. Under these circumstances, a rather high concentration of radioactive gases may accumulate in the accelerator enclosure and it might be necessary to purge the air or allow for decay of radionuclides after periods of accelerator operation before entry is permitted. However, usually air circulation is provided for accelerator enclosures (mainly for purposes of cooling). The residence time of air inside the accelerator enclosures (and, consequently, the irradiation time of the air) is often less than an hour so that the production of high concentrations of radioactive gases with long half-lives is minimal.

The radionuclides generally of significance for environmental contamination are ^3H, ^7Be, ^{11}C, ^{13}N, ^{15}O, and ^{41}Ar. The production of ^3H is limited because of its long half-life, so the environmental impact from this radionuclide is usually small. With the exception of ^3H and ^7Be, the half-lives of most radionuclides produced in air are short, so that there will be some significant decay even during the short

time taken from discharge until they reach inhabited regions near the accelerator.

At proton accelerators, most radionuclides are produced by way of the spallation reaction. A notable exception is, ^{41}Ar, which is produced by the (n,γ) reaction on ^{40}Ar from thermal neutrons. Electron accelerators of sufficient energy to generate photon showers with photon energies above the giant-resonance region can produce radionuclides by the (γ,n) reaction.

There are several tabulations of radionuclides produced in air in the environment of accelerators such as Tables 6.12 and 6.13 of IAEA (1988), Tables 7.4 and 7.5 of Patterson and Thomas (1973), and the tables on pages 128 to 129 of IAEA (1979a), the latter reference dealing with electron accelerators. Further information on radioactive gas production at electron accelerators with energies of 100 MeV or below is given by Kase (1967) and also Brynjolfsson and Martin (1971); for recent information on radioactive gas production at high-energy proton machines, the paper by Butala *et al.* (1989) is of interest.

6.3.1.2 *Photoactivation.*   In the discussion that follows, the familiar nomenclature describing electron interactions will be used (for further details, see IAEA, 1979a; Swanson, 1986). Photoactivation in air occurs when an electron beam strikes a target and generates bremsstrahlung. These photons will have a differential track length $\mathrm{d}\ell/\mathrm{d}k$.

The general expression for photoactivation by an electron beam striking some target material is:

$$S_\mathrm{j} = N_\varepsilon \frac{N_\mathrm{A}}{A_\mathrm{i}} \int \sigma_\mathrm{i}(k) \frac{\mathrm{d}\ell}{\mathrm{d}k} \, \mathrm{d}k, \qquad (6.14)$$

where:

S_j	=	saturated activity of nuclide j
N_ε	=	electron current
N_A	=	Avogadro's number
A_i	=	atomic weight of element i
$\mathrm{d}\ell/\mathrm{d}k$	=	differential photon track length
$\int \sigma_\mathrm{i}(k)\mathrm{d}k$	=	the integrated photoneutron cross section of element i
k	=	photon energy

It should be noted that the activity is contained in the thickness of material traversed by the photon tracks as defined by $\mathrm{d}\ell/\mathrm{d}k$ and is, in effect, the number of photonuclear events occurring for N_ε electrons incident on the target.

For electron beams of energy (E_0) incident on thick targets, provided E_0 is greater than the critical energy of the target material,

the differential photon track length can be estimated using Approximation A of shower theory (Rossi, 1952):

$$\frac{\mathrm{d}\ell}{\mathrm{d}k} = \frac{0.572 X_0 E_0}{k^2} \qquad (6.15)$$

and

$$\sigma_{-2} = \int \frac{\sigma(k)}{k^2} \, \mathrm{d}k, \qquad (6.16)$$

where X_0 is the radiation length in g cm^{-2} and σ_{-2} is the photoproduction cross section integrated over a thick target spectrum in mb MeV^{-1} (10^{-27} cm^2 MeV^{-1}). Therefore:

$$S_j = \frac{2.15 \times 10^{12} P \sigma_{-2} X_0}{A_i} \text{ Bq}, \qquad (6.17)$$

where S_j is in becquerels when the beam power (P) is in kilowatt.

Adopting the proposal by Swanson (1986) for the situation in which a beam strikes a metal component and initiates a shower before entering air, we assume that the shower will develop fully in air in $\sim 5\ X_0$ (at 1 GeV) (Nelson *et al.*, 1966). In this case the activation term, S_j of Equation 6.17, may be scaled downwards by a factor ($X/5\ X_0$), where X is the path length in air expressed in units of radiation length, to obtain the saturated activity in air (S_j^{air}). Rearranging Equation 6.17 slightly, by introducing this scaling factor and converting the units of radiation length to meters of air, we obtain the saturated activity per unit bremsstrahlung path length and per unit electron beam power (S_j^{air}):

$$S_j^{\text{air}} = 5.2 \times 10^{10} \frac{\sigma_{-2} \, f_w^i}{A_i} \quad \text{Bq kW}^{-1}\text{ m}^{-1}, \qquad (6.18)$$

where f_w^i is the weight fraction composition of air of parent nuclide i. The results of this calculation are given in Table 6.4 and for various radionuclides are compared with the published data of IAEA (1979a) in Columns 10 and 11 of Table 6.4.

6.3.1.3 *Thermal-Neutron Capture.* In any assessment of induced radioactivity in air, it is important that thermal neutron capture processes be included. One of the principal activation products observed in air activated by accelerator radiation is ^{41}Ar which is produced from ^{40}Ar.

The activation due to thermal neutrons is given by:

$$S_j = \sigma_{\text{th}} \frac{N_A}{A_i} f_w^i \, \rho \sigma_i \quad \text{Bq cm}^{-3}, \qquad (6.19)$$

TABLE 6.4—*Calculated yields of radionuclides from photoactivated air.*[a]

Radionuclide (j)	Half-Life	Decay	Target Element (i)	Fraction by Weight of Parent	Reaction	Cross Section (σ_{-2}) (mb MeV^{-1})	Equation 6.18 (Bq kW^{-1} m^{-1})	Radionuclide Totals (Bq kW^{-1} m^{-1})	IAEA (1979a) (Bq kW^{-1} m^{-1})
H-3	12.3 y	β^-	N	0.755	(γ,T)	0.002	5.6×10^6	7.1×10^6	5.0×10^6
			O	0.23	(γ,T)	0.002	1.5×10^6		
Be-7	54 d	γ^{EC}	N		(γ,sp)[b]	0.0003	8.4×10^5	1.1×10^6	1.0×10^6
			O		(γ,sp)	0.0003	2.2×10^5		
C-11	20.5 m	β^+	C	0.0001	(γ,n)	0.073	3.9×10^4	1.1×10^7	1.0×10^7
			N		(γ,T)	0.003	8.4×10^6		
			O		(γ,an)[c]	0.003	2.2×10^6		
N-13	10 m	β^+	N		(γ,n)	0.04	1.1×10^8	1.1×10^8	1.0×10^8
O-15	2.1 m	β^+	O		(γ,n)	0.075	5.6×10^7	5.6×10^7	5.6×10^7
Cl-38	37 m	β^-,γ	Ar	0.013	(γ,np)	0.04	6.8×10^5	6.8×10^5	2.2×10^5
Cl-39	55 m	β^-,γ	Ar		(γ,p)	0.5	8.5×10^6	8.5×10^6	1.5×10^6

[a] From Barbier (1969), Berman and Fultz (1975), Dietrich and Berman (1988), and IAEA (1979a).
[b] sp = spallation.
[c] an = annihilation radiation.

where ρ is the density of air and the other symbols were defined earlier.

A simple, but reasonable expression for determining the thermal-neutron fluence inside a concrete vault, ϕ_{th} is that given by Patterson and Wallace (1958):

$$\phi_{th} = \frac{1.25\ Q_F}{S}, \tag{6.20}$$

where:

ϕ_{th} = thermal neutron fluence rate
Q_F = yield of fast neutrons
S = internal surface area of vault

Combining Equation 6.19 and Equation 6.20 and setting Q_F equal to 10^{12} n s^{-1} we obtain:

$$S_j = \frac{7.53 \times 10^8\ f^i_w\ \rho\sigma_i}{SA_i} \quad \text{Bq cm}^{-3}. \tag{6.21}$$

The thermal-neutron production for argon is shown in Table 6.5. It should be noted that the production term is expressed as activity per unit volume and not per meter path length.

6.3.1.4 *Activation by High-Energy Neutrons.* This process, largely due to spallation, occurs by interaction of neutrons with energies in excess of production thresholds of approximately 20 MeV. The expression used to calculate the high-energy yield is:

$$S_j = 100\ Q_{HE}\frac{N_A}{A_i}f^i_w\ \rho\sigma_i. \tag{6.22}$$

Normalizing the high-energy neutron yield (Q_{HE}) to 10^{12} s^{-1}, Equation 6.22 becomes:

$$S_j = 7.28 \times 10^7\frac{f^i_w\ \sigma_i}{A_i}\text{Bq m}^{-1}. \tag{6.23}$$

The factor of 100 shown in Equation 6.22 is used to normalize the production unit path length to 1 m. The production cross sections together with saturated yields for these neutron production processes are given in Table 6.5.

The quantity of radioactivity produced at saturation is calculated by multiplying the saturation yields for the photoproduction and spallation processes by an estimate of air path length and separately determining the concentration for thermal neutron activation. To estimate the actual concentrations, corrections for radioactive buildup and decay must be applied. The buildup and decay of the

TABLE 6.5—*Yields of radionuclides from neutron activation of air.*

Nuclide	Parent Element	Mass Number of Parent	Weight Fraction of Parent Element	Cross Section (mb)	Yield[a] (Bq m^{-1})	Total Yield[a] (Bq m^{-1})
Radionuclides Produced by High-Energy Neutrons[b]						
H-3	Carbon	12	1.2×10^{-4}	10	7.5×10^{3}	1.5×10^{8}
	Nitrogen	14	7.55×10^{-1}	30	1.2×10^{8}	
	Oxygen	16	2.3×10^{-1}	30	3.1×10^{7}	
Be-7	Carbon	12	1.2×10^{-4}	10	7.5×10^{3}	4.5×10^{7}
	Nitrogen	14	7.55×10^{-1}	10	3.9×10^{7}	
	Oxygen	16	2.3×10^{-1}	5	5.2×10^{6}	
C-11	Carbon	12	1.2×10^{-4}	30	2.3×10^{4}	4.5×10^{7}
	Nitrogen	14	7.55×10^{-1}	10	3.9×10^{7}	
	Oxygen	16	2.3×10^{-1}	5	5.2×10^{6}	
N-13	Nitrogen	14	7.55×10^{-1}	10	3.9×10^{7}	4.9×10^{7}
	Oxygen	16	2.3×10^{-1}	9	9.4×10^{6}	
O-15	Oxygen	16	2.3×10^{-1}	40	4.2×10^{7}	4.2×10^{7}
Ar-41 Produced by Thermal Neutrons[a]						
Ar-41	Argon	40	1.3×10^{-2}	610	1.9×10^{5} [c]	1.9×10^{5} [c]

[a] Yield per 10^{12} s^{-1}.
[b] Data from Rindi and Charalambus (1967).
[c] Divide this value by the surface area of the concrete vault enclosure in cm^2 to determine the yield in Bq cm^{-3}.

various radionuclides are controlled by their various decay constants, and the release rate of the radionuclides to the environment is controlled by a constant similar to the decay constant. The basic expression for the production of radioactivity is:

$$S_t = S_{\text{sat}}(1 - e^{-\lambda t}), \tag{6.24}$$

where S_t is the activity after irradiation time (t) and S_{sat} is the saturation activity (long irradiation period with respect to λ).

If air ventilation occurs continuously during irradiation and hence during the growth of radioactivation products, the radioactivity level will be reduced:

$$S_{\text{reduced}} = S_{\text{sat}} \frac{\lambda_{\text{dec}}}{\lambda_{\text{eff}}}, \tag{6.25}$$

where λ_{dec} is the radioactive decay constant and λ_{loss} is the ventilation constant (ventilation rate/enclosure volume) and:

$$\lambda_{\text{eff}} = \lambda_{\text{dec}} + \lambda_{\text{loss}}. \tag{6.26}$$

However, if air is not released during accelerator operation, it is necessary to calculate two quantities, (1) the concentration of radioactivity in the enclosure after a radiation period (t_i) followed by a period when both decay and ventilation loss will occur and (2) the quantity of radioactivity released to the environment from the ventilation loss.

The buildup of radioactivity at the end of an irradiation time (t_i) is given by Equation 6.24. After the beam is turned off and the ventilation turned on, the radioactivity in the enclosure will decrease in concentration by the effective decay constant:

$$S_{t_c} = S_t e^{-\lambda_{\text{eff}} t_c}, \tag{6.27}$$

where t_c is the time after beam is off.

In addition to the radioactivity levels inside the accelerator enclosure, the quantity of radioactivity released during the ventilation cycle (Q) must sometimes be known. This can be calculated from the following expression:

$$Q = S_t R \int_0^T (e^{-t\lambda_{\text{eff}}}) \, dt. \tag{6.28}$$

The solution to Equation 6.28 for the activity released over a period T is given by:

$$Q_T = S_t R \frac{(1 - e^{-\lambda_{\text{eff}} T})}{\lambda_{\text{eff}}} \tag{6.29}$$

and the total activity released, corresponding to $T = \infty$, is:

$$Q_{tot} = \frac{S_t R}{\lambda_{eff}} . \qquad (6.30)$$

This quantity Q_{tot} is required for calculations of dose equivalent to any person who might be environmentally exposed to these releases.

The preceding treatment makes many simplifying assumptions which must be understood. The actual circumstances of beam loss and the resultant radiation coupled with the very often complex geometry of the beam-air path require this treatment to be used with great care. It is unlikely, however, that the use of these formulae will contribute greatly to the overall uncertainties which result mainly from the practical considerations of modeling air activation conditions. Table 6.6 gives an example of the agreement obtained by Peetermans and Baarli (1974) between calculated and measured values of specific activity for four radionuclides at the CERN 600 MeV synchrotron.

6.3.1.5 *Radionuclides Produced in Dust.* Radionuclides in the form of dust or aerosols may be produced by accelerator operations. Direct measurements of removable contamination with beta-particle-sensitive detectors and personal particulate-air samplers generally provide the most direct technique for the identification and quantification of the internal exposure hazards from such dust. Care must be taken to use gamma-sensitive-detectors for those radionuclides which are monitored only by their gamma emissions; *e.g.*, ^{7}Be.

Experience at several large accelerators tends to show that the potential exposure to radioactive dust for maintenance crews working in the accelerator vault is negligible. This problem has been

TABLE 6.6—*A comparison between the measured and calculated values of speci c activity of some long-lived radionuclides produced in air made at the CERN 600 MeV synchrocyclotron "Isolde" area (Peetermans and Baarli, 1974).*

Radionuclide	Half-Life	Measured Concentration (Bq m^{-3})	Calculated Concentration (Bq m^{-3})
H-3	12.26 y	—	0.59
Be-7	53.6 d	10.0	12.0
Na-24	15.0 h	1.3	1.8
P-32	14.5 d	0.22	0.31
P-33	25.0 d	0.074	0.17
Ar-41	1.83 h	—	930.0

discussed at some length by Thomas and Rindi (1979). Busick and Warren (1969) concluded that chemical toxicity and external radiation exposure are the factors that limit the machining of radioactive accelerator components, rather than the inhalation of radioactive dust.

6.3.1.6 *Gaseous Radionuclides Released from Irradiated Water.* In certain circumstances, radionuclides produced in liquids irradiated at accelerators may be released to the environment. For example, tritium produced by spallation reactions in magnet cooling water may be released by the evaporation of water spills and losses during magnet maintenance or replacement. Some unexpected transfer mechanisms may be possible, *e.g.*, Warren *et al.* (1969) studied the production of CO_2, which acts as a carrier for ^{11}C and ^{15}O, in water beam-dumps at SLAC.

6.3.1.7 *Environmental Impact of Airborne Radionuclides.* Calculations and measurements by flow ionization chambers and gamma-spectroscopy on filters confirmed the presence of ^{7}Be, ^{24}Na, ^{28}Mg, ^{31}Si, ^{32}P, and ^{33}P in the ventilation air around an extracted beam at CERN (Peetermans and Baarli, 1974; Rindi, 1972). The measured concentrations were in good agreement with those calculated (Table 6.6). These data suggest that accelerator operation at CERN produces detectable quantities of ^{7}Be close to the high-energy accelerators corresponding to periods of high-intensity operation. On the other hand, at the Lawrence Berkeley Laboratory, where several high-intensity proton and heavy-ion accelerators had operated for many years, a search for possible contamination from ^{7}Be showed that, if it were present, it was at concentrations less than the variation of the natural background of this radionuclide produced by cosmic rays. Nevertheless, measurement of the concentration of ^{7}Be in air or in dust around accelerators may prove to be a valuable indicator of radioactive contamination. Further studies are needed, including measurements of the natural background fluctuation of ^{7}Be in rainwater.

6.3.1.8 *Collective Exposure to the Population from Radioactivity in the Air.* Calculation of the exposure to the general population resulting from the release of radionuclides to the atmosphere requires several steps:

- measurement or calculation of the concentration of all radionuclides released at the ventilation stacks of accelerators. This will include venting characteristics, such as air temperature, release volume, velocity, and stack release height

- studying the path of the radionuclides to points distant from the accelerator laboratory, including topographic and meteorological data
- conversion of the radionuclide concentrations to dose equivalent to an exposed individual, including inputs from all pathways (ingestion, inhalation and immersion)
- summation of the dose equivalent to all exposed individuals, including demographic and agricultural information

The usual analytical treatment is based on the Gaussian-plume-diffusion model, originally proposed by Sutton as early as 1932, and the reader is referred to comprehensive reviews by Gifford (1976) and Slade (1968) for a detailed discussion. More recent publications are IAEA Safety Guide No. 50-SG-3 (IAEA, 1979b) and NCRP Report No. 123 (NCRP, 1996).

At particle accelerators, the dominant means of radiation exposure from radionuclides released to the environment is due to immersion in a cloud of radioactivity. In addition to doses from immersion, doses can also result from exposure to radionuclides deposited on the ground, by immersion in water containing radionuclides, by inhalation of radionuclides in air, and by ingestion of food produced in the area of radionuclide deposition. Typically, these latter sources of exposure at high-energy accelerators are small. They may be more significant for low-energy accelerators used for isotope production.

6.3.2 *Radioactivity Produced in Earth Shielding and Groundwater*

To date, no significant contamination of groundwater systems due to accelerator operations has been observed. Radioactivity induced in the accelerator structure itself, or in the concrete and iron used for shielding is relatively immobile. However, if the shield material is porous to water and is contiguous with the environment (*e.g.*, earth), there exists a potential, which always merits analysis, for the migration of radioactivity and possible entry into groundwater systems used for public water supplies.

An assessment of problems resulting from induced activity in earth shielding falls into several categories:

- identification and estimation of radionuclides present
- evaluation of problems resulting from inhalation of dust during excavation operations or decommissioning
- determination of the continuity of the earth shield with groundwater

- estimation of total yield and specific concentration of radionuclides in the water entrained in the earth shield
- determination of the rate of movement of the radionuclides in the groundwater and estimation of the potential contamination of water supplies

6.3.2.1 *Radionuclides Identiﬁed in Earth and Water.* Several authors have reported the observation of radionuclide production in earth and water, either in laboratory simulations or directly in earth shields. Readers who wish to pursue these studies in detail should consult summaries in standard texts where extensive bibliographies are given (*e.g.*, IAEA, 1988; Patterson and Thomas, 1973). Thomas (1972) gives experimental results for radionuclides produced in earth by the direct interaction of high-energy electrons. Together, these reports give a fairly comprehensive picture of all the major aspects of the production of radionuclides in shielding in accelerator-radiation environments. The radionuclides identified in soils were ^{3}H, ^{7}Be, ^{22}Na, ^{32}P, ^{43}K, ^{45}Ca, ^{47}Ca, ^{46}Sc, ^{47}Sc, ^{51}Cr, ^{54}Mn, ^{55}Fe, ^{59}Fe, ^{58}Co and ^{60}Co. Small concentrations of ^{152}Eu (13 y half-life) have also been identified at some sites where accelerators have operated for many years.

For conditions of accidental beam loss or spills, the accelerator beam would first strike the vacuum chamber wall or some system of collimators. In many cases, sufficient shielding is present so that the only activating particles to reach the earth shield are high-energy neutrons (hadrons), even if the primary beam is high-energy electrons. However, in some beam tunnels, there may be only a thin layer of concrete-like material between the accelerator and the earth.

6.3.2.2 *Magnitude of Radionuclide Concentrations.* Rough estimates of the amount of radioactivity that might be produced in earth shielding are often required. In Sections 3 and 4, there has been substantial discussion of the calculation of neutron fluence rates (ϕ) and star densities outside primary shields. The term star density (stars cm^{-3}) refers to the number of inelastic interaction events per unit volume of the medium through which the interacting particles pass; the star density may be regarded as the product of the particle fluence and an interaction cross section. Spallation reactions, which dominate the radionuclide production, have threshold energies of ~25 MeV.

The total radioactivity produced in the ground (A_a) by Q neutrons entering the earth is given by:

$$A_\text{a} = Q \frac{\Sigma_\text{a}}{\Sigma}, \qquad (6.31)$$

where Σ is the total removal cross section and Σ_a is the total radioactivation cross section. From the known value of the high-energy neutron-removal mean free path in earth of ~100 g cm^{-2} the value of Σ can be calculated to be 0.01 cm^2 g^{-1}. Borak *et al.* (1972) and other workers have reported the total radioactivation cross section (Σ_a) to ~0.0015 cm^2 g^{-1}. From these two cross sections, and Equation 6.31 it may be concluded that about 15 percent of high-energy neutrons give rise to radionuclides of consequence.

The potential for exposure of members of the general public is typically small. This may be understood from a calculation of the total activity produced by a medium-energy, high-power proton accelerator and the consequent concentrations of radionuclides in nearby groundwater. Such an analytical approach is intended to provide an indication of the magnitude of the problem. For a detailed study for regulatory requirements, the reader is referred to a recent comprehensive work on radionuclide production in earth shielding using Monte-Carlo methods and water transport modeling (Dole *et al.*, 1999).

Consider a proton accelerator of 1 GeV in energy, with a beam current of 100 μA, corresponding to a total beam power of 100 kW. To provide the necessary radiation shielding the typical construction of such a facility would place the accelerator inside a concrete tunnel (vault), above which additional shielding is provided by earth. Neutrons produced during accelerator operation will enter the surrounding earth shielding, producing radioactivity in the earth and groundwater.

There are two modes of normal accelerator operation that span the observed range of beam losses. The first case occurs when the full beam intensity interacts with material producing a localized beam loss, for example when the total beam is deliberately "dumped" into a shielded area. The second case occurs during routine operation when a small fraction of the beam is continually lost along the length, or around the circumference, of the accelerator or a beam transport system, producing a spatially extended radiation source.

Case 1. Localized beam loss (beam dump). The following data are used in the calculation:

Beam intensity: 100 μA (6 × 10^{14} proton s^{-1})
High-energy neutrons per 1 GeV proton: 1
High-energy neutron source strength: = 6 × 10^{14} neutrons s^{-1}
Transmission of intrinsic shielding: 10^{-4}

Thus the dumping of 100 μA protons, after allowance is made for the intrinsic shielding of the beam dump and the concrete vault

walls, will produce $\sim 6 \times 10^{10}$ n s^{-1} that enter the earth shield. Substituting the values $Q = 6 \times 10^{10}$ n s^{-1}, $\Sigma = 0.01$ cm^2 g^{-1}, and $\Sigma_a = 0.0015$ cm^2 g^{-1} into Equation 6.31 the total quantity of radioactivity produced in the earth shield (A_a) is then:

$$A_a \approx 10^{10} \text{ Bq.} \tag{6.32}$$

This value of A_a is the total saturated activity in the earth including radionuclides of all half-lives and takes no account of any processes that may change the concentration of these radionuclides.

Case 2. Extended beam loss. The following data are used in the calculation:

Beam intensity: 100 μA $(6 \times 10^{14}$ proton s$^{-1})$
Fraction of beam lost: 10^{-3}
Beam-loss rate: 6×10^{11} proton s^{-1}
High-energy neutrons per 1 GeV proton: 1
High-energy neutron source strength: $= 6 \times 10^{10}$ neutrons s^{-1}
Transmission of intrinsic shielding: 10^{-1}

In addition, for purposes that will become clear, it is also assumed that the accelerator vault is shielded by earth outside of the concrete vault, which has an external radius of 3 m. Extended beam loss is assumed to take place over a length of 300 m along the axis of the accelerator. With these assumptions the total quantity of radioactivity produced in the earth shield (A_a) is also 10^{10} Bq.

However, water quality regulations are not usually based on total activity but rather expressed in terms of the concentration (activity per unit mass or volume) of radioactivity in the earth and groundwater. The concept of an activation zone, which contains essentially all radioactivity produced in the earth by accelerator operation, is helpful in calculating the required concentrations. Although the determination of the volume of this activation zone may be complicated in specific cases, the elements of the calculation may be understood from a simple one-dimensional activation model. For a more rigorous analytical treatment the reader is referred to the work of Bull *et al.* (1997) who discuss the question for a large accelerator site.

An expression similar to Equation 6.31 may be developed for a simple one-dimensional activation model. The neutron fluence at depth r in the earth, $\phi(r)$ is related to the specific activity $[S_a(r)]$ by:

$$S_a(r) = \Sigma_a \phi(r) \quad \text{Bq g}^{-1} \tag{6.33}$$

and the total activity contained within radius r is given by:

$$A_a(r) = Q \Sigma_a \int_0^r e^{-\Sigma r} \, dr = Q \frac{\Sigma_a}{\Sigma} (1 - e^{-\Sigma r}) \quad \text{Bq.} \tag{6.34}$$

It follows that the depth in the shield at which a fraction $(1 - \varepsilon)$ of the total activity is contained (r_ε) is given by:

$$e^{-\Sigma r_\varepsilon} = 1 - \varepsilon. \qquad (6.35)$$

The specific activity declines in an approximately exponential manner with a mean free path λ ($= 1/\Sigma$) of ~100 g cm^{-2} in earth. Thus, in the case considered, the activation zone is defined by a cylindrical annulus extending outwards from the outer surface of the concrete. Because of the exponential character of this decline, it is necessary to define a value of the fraction of the total activity (ε), that satisfactorily places a limit on the outer radius, r_ε of the activation zone. Solution of Equation 6.35 shows that the percentage of the total activity contained within 2.3, 4.6 and 6.9 mean free paths is respectively 90, 99 and 99.9 percent. An acceptable value for ε is usually 0.99 and for earth of density 2 g cm^{-3}, this is equivalent to 2.3 m.

In this case, the activation zone is a cylindrical annulus of inner radius 3 m, thickness 2.3 m, and length 300 m, amounting to a mass of ~4 $\times$ 10^{10} g of earth. The average concentration of accelerator-produced radioactivity in the earth is then 0.25 Bq g^{-1} (~7 pCi g^{-1}) that may be compared with the typical values for the rocks given in Table 6.7. Additionally, it should be remembered that this estimate includes radionuclides of greatly differing decay rates. Also, many of them are unlikely to be transported by groundwater so that only a fraction of this yield might be regarded as significant.

6.3.2.3 *Environmental Impact and Exposure to Members of the Public.* The radionuclides produced in earth shields by accelerator

TABLE 6.7—*Average radium, uranium, thorium. and potassium contents in various rocks (Eisenbud, 1987).*[a]

Type of Rock	Ra-226 (pCi g^{-1})	U-238 (pCi g^{-1})	Th-232 (pCi g^{-1})	K-40 (pCi g^{-1})
Igneous	1.3	1.3	1.3	22
Sandstones	0.71	0.4	0.65	8.8
Shales	1.08	0.4	1.1	22
Limestones	0.42	0.4	0.14	2.2

[a]The values presented in the table are for illustrative purposes for the example in the text. Values of specific activity for each rock type and radionuclide will vary over wide ranges as shown in NCRP Reports No. 93 and No. 94 (NCRP, 1987a; 1987b). For any specific investigation or calculation involving radioactivity in the earth, information for the particular locality should be used.

radiation are, as we have seen, generally of low radiotoxicity and rather short half-life. Nevertheless, their ingestion or inhalation must be considered as a source of exposure to the general public. Ingestion of these materials might occur by the ingestion of food grown in radioactive soils; by drinking contaminated water or by inhalation and swallowing of dusts.

6.3.2.3.1 *Ingestion.* It is unlikely that food will be grown at accelerator sites in contaminated soil. It may certainly be prevented and, therefore, may be disregarded as a source of exposure to the general public.

6.3.2.3.2 *Drinking contaminated water.* The possibility of the transfer of the induced activity into underground water, used for community drinking water supplies, must be considered. This potential is usually small but, if it were not so, the potential could be greatly reduced by the use of water-proof membranes or layers between the activated earth shield and the groundwater system to prevent the transfer of radioactivity. In the discussion which follows, the conservative assumptions are made that the accelerator enclosure is constructed of concrete and that any radiation passing through this concrete can activate the earth shielding surrounding it. Finally, that such an earth shield is contiguous with the outside earth and groundwater.

Only a few of the radionuclides that may be produced by accelerators in earth have been observed in groundwater. This suggests that most of the radionuclides are relatively immobile, and their absence from the groundwater may be attributed to two causes: radioactive decay and absorption in the earth because of the chemical form in which a radionuclide is produced. The radioactive species might not be removable from the system due to either solubility or the physical structure of the soil. For example, if the soil is comprised of coarse sand or rock, any radionuclides born deep inside the grains of sand or rock will remain trapped and will not be available for dissolution in the surrounding groundwater. These aspects of solubility and availability are generally combined and referred to as "wash-out" or "leach-out." Some radionuclides are produced by activation of water directly (*e.g.*, ^{3}H, ^{7}Be, and ^{11}C) and, thus, the total radioactivity in groundwater from these radionuclides is from two sources, direct production and leach-out. In such cases, in order to estimate the contribution from the rock, the activation of the rock alone must be determined and leach-out factors applied to this component of the radioactivity (Baker *et al.*, 1997).

Under normal operating conditions at accelerators, the production of radionuclides in the ground is a continuous process in time,

whereby the amount of radioactivity in the ground at any point converges to an approximately constant value and constant long-term irradiation and groundwater movement conditions may be assumed. However, other conditions are possible where beam losses are accidental so that both the frequency of any significant beam loss and the location at which the loss could occur is uncertain; such conditions could apply, *e.g.*, to the accidental abort of the total charge held in a storage-ring system. Under these conditions, the assumption could be made that the radionuclides are produced in "one-shot" at maximum level and, thereafter, decay and wash away into the groundwater. These two conditions, "equilibrium" or "one-shot," span the range of conditions likely to occur in practice. The analyses of groundwater movement, which follow, can be applied to both production models with very little modification.

Experience shows that ^{3}H and ^{22}Na are the two radionuclides of most concern and it is, therefore, necessary to derive their production cross sections in earth. Their production is generally by high-energy neutron-spallation or a compound-nucleus reactions with thresholds of $\sim$10 to 20 MeV. Cross-section data has been discussed by Barbier (1969) who utilized expressions developed by Rudstam (1966). Additional cross-section data may be obtained from more recent semi-empirical expressions derived by Silberberg and Tsao (1972a; 1972b). More direct data on radionuclide production in earth may be obtained from the work of Borak *et al.* (1972), Bull *et al.* (1997), Dinter and Tesch (1980), Hoyer (1968), and Stapleton and Thomas (1972).

The quantity of water in the soil will influence both the total quantity and the concentration of radionuclides in groundwater after leach-out from the soil. This is especially true for the case of ^{3}H. The leach-out factor for ^{3}H is assumed to be 100 percent. For ^{22}Na, factors of 10 to 20 percent have been observed.

The saturated concentrations of nuclides i in groundwater at distance r in the earth shield are given by:

$$S_i = \frac{\phi(r)\Sigma_i \varepsilon_i \rho}{f_w} \quad \text{Bq cm}^{-3}, \tag{6.36}$$

where:

$\phi(r)$ = neutron fluence at distance r in the ground
Σ_i = cross section for nuclide i
ε_i = leach-out factor
ρ = density of earth
f_w = fraction of water in earth by weight

A similar expression can be written using the star density.

The specific activity is a function of $\phi(r)$ or star density and, therefore, varies with depth in the earth shield. Because the time-scales for the buildup and transport of the radioactivity are usually very

long (many years), the calculation of local specific activities would seem inappropriate. However, there is great concern for safeguarding the quality of groundwater resources, and accelerator designers may be required to apply protection standards for radionuclides in drinking water to regions very close to the site of production (Stapleton and Thomas, 1989).

6.3.2.3.3 *Inhalation.* Dust is created during excavation at accelerator sites and may be inhaled. The magnitude of the inhalation hazard may be estimated, by somewhat, arbitrarily selecting an accelerator-produced radionuclide and comparing its derived air concentration with that typical for dust. For example, the derived air concentration for ^{60}Co (a radionuclide commonly found at many accelerators) is 500 Bq m^{-3}. The limiting concentration of concrete dusts that can be permitted from industrial hygiene considerations is $\sim 5 \times 10^{-3}$ g m^{-3}. Thus, for the radioactivity of the dust to be the controlling hazard, the specific activities of ^{60}Co must exceed 10^5 Bq g^{-1}. This would be an unusually high specific activity for typical accelerator environments. Thus, for example, at the surface of semi-infinite shield walls (thicker than about two or three photon mean free paths) containing a uniform concentration 10^5 Bq g^{-1} of ^{60}Co, the surface dose rate would be more than 70 mSv h^{-1}. Experience suggests this is an unusually high dose rate from shielding around accelerators. Although such high dose rates may commonly be measured at the surface of a beam target or, in exceptional cases, on local target steel shielding, typical levels at the surface of earth or concrete shield are many orders of magnitude lower. These calculations suggest, although they are by no means rigorous, that inhalation and ingestion of accelerator-produced radionuclides, at the levels at which they are commonly observed in the surroundings of accelerators, do not pose any serious potential for exposure.

6.3.3 *Transfer of Radioactivity at Accelerators*

Most radioactive contamination from accelerators is created when the beam activates dispersible materials. The magnitude of the problem is strongly affected by the composition and amount of the material, as well as by how easily it is dispersed. Simple measures, such as good housekeeping to reduce dust and debris within accelerator enclosures, can significantly control contamination. Materials which are both radioactive and toxic present special problems.

At high-energy proton accelerators, materials with higher Z generally have greater potential for contamination because spallation

reactions in these materials produce a wider variety of nuclides, some of which are long-lived.

Some illustrative examples of conditions or operations likely to exacerbate the transfer of radioactivity are as follows:

- Grinding of welds and repair of magnet coils are two examples of activities that produce contamination when magnets are reworked. In the iron or steel magnet yokes of hadron machines, ^{54}Mn is often the primary nuclide of concern. For certain alloys, other nuclides may also need to be considered (*e.g.*, ^{60}Co). In activated copper coils ^{65}Zn, ^{57}Co, ^{58}Co, and ^{60}Co are often present. At electron accelerators, additional nuclides may be present due to photonuclear reactions.
- Magnet coils are often wrapped with fiberglass tape and impregnated with epoxy resins. The remnants of such wrappings (epoxy and fiberglass dust and flakes) can be sources of contamination during repair, as is the residue of sandblasting used to remove old material from the coils. ^{22}Na can often be found in the coil remnants. When heated in ovens to cure or remove the epoxy, ^{3}H can also be driven off.
- Septa which use fine-metal wires are often used to extract beams from high-energy machines. These wires occasionally break and the septa must be repaired. The very fine wires, barely visible to the naked eye, are difficult to see and present a contamination problem since they are quite small and easily transported, *e.g.*, on the sole of a shoe.
- Pumps that are used within accelerator enclosures or that are used outside, but are connected to the enclosures through vacuum lines also can be contaminated, either by direct activation of lubricating oils or by pumping on radioactive material, such as targets. One should be aware that ^{3}H, which is generally not detectable with commonly used survey instruments, can be present in activated pump oil. Care should be used to avoid contamination of personnel or the general area during maintenance of the pumps.
- To prevent surface oxidation, bare metal surfaces are often protected by applying some type of protective coating such as paint, grease or epoxy. For this purpose, materials of low Z generally are preferable. For example, substituting a lithium-based grease for a molybdenum-based lubricant minimizes the number of long-lived nuclides that could be produced.
- At high-energy accelerators, depleted uranium plates are sometimes used in calorimeters. The surface oxide on these plates is a potential contamination source. The degree of oxidation can

vary widely, depending on the surface protection. Uncoated (bare) plates may be located in cryostats, and the cryogenic liquids they contact can become contaminated. Machining operations on uranium plates presents problems because of the production of radioactive waste-chips (which are pyrophoric). Welding operations may result in the emission of contaminated welding fumes.

- Equipment used in areas where activation is, likely, sometimes removed for dismantling and repair elsewhere, *e.g.*, in a machine shop. The contamination can then occur at that location.

Numerous problems can be created by target activation. In addition to the intense residual radiation fields that can be produced by the interaction of the high-energy particles in the target material, physical degradation of the target produced by heating can create significant contamination problems.

6.4 Radiolysis in Water and Air

The production of the nonradioactive toxic gases ozone and oxides of nitrogen is ordinarily discussed in texts on industrial hygiene, but it is considered in this Section because it is an important occupational hazard for some accelerator workers. Furthermore, the treatment of the production and dilution of these gases, rather closely, parallels the production and decay of radioactive air.

The production of both ozone and oxides of nitrogen by radiolysis of air near accelerators have been covered extensively by IAEA (1979a). There are two areas of concern: the health of personnel working in ozone-containing environments and the extremely corrosive nature of the oxides of nitrogen in the presence of water vapor.

At accelerators, corrosion is of particular concern because magnets generally contain large quantities of copper and iron (septum magnets are often made entirely from copper), and it is copper that is most susceptible to corrosion from the products of radiolysis of cooling water. Not only is the copper surface damaged, but the cooling-water purity also is degraded, both effects leading to restriction of the cooling channel openings with consequent loss of cooling efficiency (Hoefert, 1986). Iron components will rapidly rust in air containing moisture and ozone and oxides of nitrogen. The corrosive nature of the irradiated air can be mitigated by ventilation, but also by maintaining a dry environment. Levels of relative humidity at less than 55 percent will greatly assist in reducing corrosion of metals.

It is unlikely that the production of ozone and oxides of nitrogen by accelerator radiation could result in an environmental problem. There is, however, one aspect where radiolysis impinges on environmental concerns and that is the leakage of hydrogen from irradiated beam dump water resulting in loss of activated material to the environment. Studies of the release of hydrogen from water-cooled beam dumps by Walz and Seppi gave rates from air-saturated, high-purity water between 0.26 to 0.44 L MJ^{-1} of beam energy with beam powers ranging from 20 to 170 kW (Walz and Seppi, 1967). Because the release of this gas, in conjunction with radioactive gases such as ^{11}C, resulted in potential exposure to the surroundings, the hydrogen release had to be eliminated by the use of catalytic hydrogen recombiners (Warren *et al.*, 1969).

Hoefert has described the buildup and destruction of ozone during radiation using the following equations (Hoefert, 1986):

$$\mathrm{d}N/\mathrm{d}t = gI - \alpha N - \kappa IN - QN/V, \tag{6.37}$$

where:

$\mathrm{d}N/\mathrm{d}t$ = rate of formation (or decomposition) of ozone per unit volume and unit time (m^{-3} s^{-1})

N = number of ozone molecules per unit volume at time t (m^{-3})

I = energy deposited in air per unit volume and unit time (eV m^{-3} s^{-1})

g = number of ozone molecules formed per unit energy (eV^{-1})

α = rate of decomposition of ozone molecules (s^{-1})

κ = number of ozone molecules destroyed per unit energy and volume (eV^{-1} m^{-3})

Q = ventilation rate of irradiated volume (m^3 s^{-1})

V = irradiated volume (m^3)

The solution of Equation 6.37 is given by:

$$N(t) = \frac{gI}{\alpha + \kappa I + Q/V}\left[1 - e^{-(\alpha + \kappa I + Q/V)t}\right]. \tag{6.38}$$

For long irradiation times, *i.e.*, $t \rightarrow \infty$ the saturation concentrations are given by:

$$N_{\mathrm{sat}} = \frac{gI}{\alpha + \kappa I + Q/V}. \tag{6.39}$$

The usual value of g is 0.074 m^{-3} s^{-1} eV^{-1}, but higher values such as 0.103 m^{-3} s^{-1} eV^{-1} are recommended for high instantaneous dose rates to air within a narrow beam path (IAEA, 1979a). The

decomposition rate (α) has been given by Hoefert as $2.3 \times 10^{-4}\,\text{s}^{-1}$ ($\tau = 72$ min) and κ as $1.4 \times 10^{-16}\,\text{s}^{-1}\,\text{eV}^{-1}$.

If κI is omitted from Equation 6.38, a simplified expression for approximate total yield is obtained:

$$N(t) = \frac{gI}{\alpha + Q/V}\left[1 - \mathrm{e}^{-(\alpha + Q/V)t}\right]. \qquad (6.40)$$

This equation is equivalent to that given by IAEA (1979a) but with different nomenclature.

Table 6.8 sets out g-values for the production of ozone and approximate values for nitrogen dioxide together with some threshold limit values on toxicity; this table is abbreviated from the work by IAEA (1979a), which should be consulted for full details.

TABLE 6.8—*Threshold limit values for radiolysis products in air and their g-values for production (IAEA, 1979a).*

Gas	Symbol	Threshold Limit Values (ppm)	g-Value [molecules (100 eV)$^{-1}$]	
			Low Dose Rate	High Dose Rate
Ozone	O_3	0.1	7.4	10.3
Nitric oxide	NO	25		
Nitrogen dioxide	NO_2	5[a]	(4.8)	(<0.15)

[a] This value is also the ceiling value; maximal concentration allowable at any time.

7. Operational Radiation Safety Program for Accelerators

7.1 Introduction

Fundamentally, operational requirements at accelerator facilities are generally not greatly different from those of other radiological facilities and are discussed in detail in NCRP Report No. 127 (NCRP, 1998). It should be noted, however, that accelerators do not produce the inventory of radionuclides commonly found in the nuclear fuel-cycle industry. Furthermore, accelerators are frequently considered to be "low-hazard" installations on the basis of accident criteria. [Other sources of guidance on this subject are: Casey *et al.* (1988), IAEA (1979a; 1988), and Patterson and Thomas (1973).]

The elements of an operational radiation safety program, as identified in NCRP Report No. 127, are:

- application of ALARA
- organization and administration
- facility design
- orientation and training
- external and internal radiation-exposure control
- control of low-level radioactive waste
- control of exposure to the public
- planning for radiation emergencies

The aspects of these elements of special concern at accelerator facilities are described in the following subsections.

7.2 Program Elements

7.2.1 *Organization*

The key element in any radiological-safety program for an accelerator facility is the appointment to the staff of an adequate number of persons with appropriate accelerator health physics experience.

360

The number of these accelerator health physicists appointed, and their responsibilities, functions and scope, will depend on the size of the accelerator facility and its managerial structure.

At institutions that operate accelerators, the director (or manager) has prime responsibility for safety. This responsibility is normally met by the delegation of duties and functions for safety down through the laboratory's (institution's) administrative structure to managers and supervisors and ultimately (and most importantly) every individual.

To advise and assist the director, staff and other employees on the professional aspects of safety, a number of "safety experts" are employed by the laboratory or, alternatively, are contractually made available. Radiation specialists or accelerator health physicists are among this group of safety experts.

It is a common practice for the safety organization to be placed outside the chain of command of line organizations responsible for operations on the grounds of a potential conflict of interest. The logic for this is not totally clear because "conflicts of interest" inevitably arise at all levels of responsibility and in all aspects of a laboratory's operation. Rather than rely on administrative attempts to prevent such conflicts of interest arising, it is vital to ensure that all staff be sensitive to their possible occurrences, to recognize them, and to ensure open and serious discussion so as to find appropriate solutions to any problems that may arise. The most important influence on the safety culture of a laboratory is for the director and the immediate senior staff to take their responsibilities seriously and professionally. If such is not the case, the professional staff responsible for health and safety at the laboratory are unlikely to function adequately, no matter where they are located in the administrative organization.

In a well-managed facility, the expertise of the radiation-control staff becomes part of the organization's resource for the design and operation of the facility and, consequently, becomes part of the accelerator team as is, for example, any other engineer or physicist. It is important that the radiation control staff be responsible and accountable for the safe operation of those parts of the accelerator that it has actually specified and designed. In this way, the staff members become part of a "problem-solving" style of operation rather than assuming a strict oversight and enforcement role. Thus, the health physicist has a challenge to balance the two aspects of his or her function. It is important both to be a member of the team, accepted as a competent engineer and scientist among other engineers and scientists, and to take responsibility for the radiation safety aspects of design, but also, when necessary, to provide the oversight required to ensure enforcement of safety policies and procedures.

Although many radiation-protection regulations have been promulgated by federal, state or other legal authorities, it is nevertheless necessary to interpret the implementation of these regulations. Such interpretation requires sound judgment on the part of the radiation-protection expert.

Many of the larger laboratories have a safety committee chaired by the director or delegate. This committee's charter is generally to advise the director on all safety matters, to commission and review safety policies and practices, to institute investigations of incidents, and, finally, to make recommendations for the improvement of safety performance and, in the particular case of the radiation-safety program, establish and monitor a program to maintain radiation doses ALARA (ICRP, 1977; NCRP, 1993).

7.2.2 *Facility Design*

The major part of an initial radiation-safety-design effort at an accelerator facility is concerned with the specification of the radiation source terms and the design of adequately protective shielding. The source terms must be defined for commissioning, normal losses during operation, and for any potential accidental loss at full power (see Sections 2 and 3).

In addition to providing passive shielding, facility design must take account of requirements for area and site-boundary radiation monitors, the need for operational programs, access and egress requirements, interlocks and beam-terminating devices, and the need to address a broad spectrum of industrial hazards. Several of these aspects are considered below.

7.2.2.1 *Access and Egress.* Design of emergency escape routes shall comply with applicable building codes and be kept clear of obstructions to ensure easy and rapid egress. Easy access is demanded by the complex industrial nature of an accelerator facility that requires the movement of large equipment. These needs for easy access and egress are in conflict with the design criteria to minimize radiation streaming along access ways (Section 4). Compromises are needed—there are no simple answers to such opposing requirements—but the experienced accelerator health physicist is well aware of these design problems and can be expected to provide reasonable solutions. In so doing, it is most effective for the radiation expert to collaborate directly with the civil construction engineer and/or architect. Such a dialogue is generally effective in avoiding costly work on inappropriate initial designs, and it permits the radiation specialist to

educate the architect in the fundamental requirements of the design for radiation safety.

7.2.2.2 *Radioactivation.* Accelerators can produce radioactive materials that require appropriate administrative controls: firstly, to ensure that staff are not unduly exposed when maintaining accelerator components and secondly to control the dispersion of radioactive materials so that they do not become an environmental hazard when released or removed from the accelerator enclosure. It is important to emphasize that the inventory of radionuclides in such an accelerator-produced radioactive material is quite different from that commonly generated in the nuclear industry based on the nuclear fuel cycle (Section 3). Accelerator-produced radionuclides are generally created through compound nucleus or spallation reactions, with the products usually lying on the neutron-deficient side of the line of stability. Many of these accelerator-produced radionuclides decay by positron emission or electron capture. In some cases, therefore, difficulties may be presented in monitoring with normal hand-held survey instruments because of the inefficiency of such monitors in photon fields where no electrons are present, particularly at low energies.

The choice of accelerator-component materials is one way by which the quantities of accelerator-produced radioactivity may be minimized (Section 3). In selecting materials, some compromise is usually necessary between cost and engineering requirements. The selection of appropriate materials can make maintenance and servicing tasks and ultimate decommissioning much less onerous, reducing both cost and personnel exposures.

At particle accelerators, the radioactivity is generally distributed throughout the irradiated materials—even in rather large or bulky objects such as in magnet yokes and Faraday cups, or any material used to intercept the beam—and not confined to the surface. Measurements of surface dose rates are often adequate to indicate that radioactivity is present, but quantifying the amount of radioactivity is more difficult because of geometrical considerations. The geometry of the irradiated objects and the distribution of the radioactivity make such determinations less amenable to simple measurement. The quantities of surface contamination that must be dealt with are limited because the radioactivity is, in most cases, not readily removable from the irradiated material. However, surface contamination can be present in significant quantities and must not be ignored.

Caution should be taken when handling thin specimens of activated materials (*e.g.*, thin beam targets, stripping foils) because of

the fragility of such objects and the potential for contamination. The potential skin dose from thin targets, because of positron emission, must be evaluated.

Removal of any potentially radioactive material from accelerator rooms should be strictly controlled and radiation monitors provided at all exits.

Engineering design and advanced planning can reduce occupational exposure from radioactive accelerator components. Good design and planning should include:

- local shielding around activated components adjacent to target handling and machine maintenance
- installation of external machine components out of the direct flux of neutrons from bombarded targets
- proper design and use of remote target delivery systems or manual systems with adequate shielding for target transport
- radiation monitoring instrumentation, in good working order, located at the entrance to accelerator vault or shielding to enable personnel to recognize radiation levels prior to entry. Monitor readings should always be supplemented with direct surveys
- extensive surveys conducted and used to establish a profile of post-bombardment radiation levels on key components over time. These data can be used to establish optimal decay times for future reference prior to target handling, maintenance and repair operation
- a preventive maintenance schedule taking into account optimal decay allowance and operational needs to reduce the time spent in areas of elevated dose rates in repair and maintenance situations
- the use of power and tools to reduce time spent in areas of elevated dose rates in repair or maintenance situations
- the use of electronic dosimeters with remote display that can be monitored by personnel who are dedicated for this purpose and not for concurrent repair or maintenance operations
- availability of inactive spare parts for use in maintenance and repair
- use of inactive or "dummy" parts for training operators to work with activated components
- use of leaded gloves when handling activated or contaminated components emitting beta particles or low-energy photons

7.2.2.3 *Ventilation.* Accelerators have the potential to generate both radioactive and chemically-toxic gases, such as ozone, by the interactions of primary or secondary radiations with the constituents of air. In particular, the production of toxic gases is sometimes

associated with various configurations of accelerator operation that may require special containment and handling precautions.

Aerosols containing ^7Be can also be produced in air (see Sections 3 and 6). These particulates generally comprise the major source of surface contamination, often plating down on surfaces in the regions around the accelerator.

It is desirable to minimize ventilation rates to allow decay of radioactive gases before release to the environment, but this often conflicts with the need to maximize ventilation to remove heat from the accelerator room. Also, for reasons of occupational safety, it may be necessary to rapidly exhaust toxic or radioactive gases, to remove particulates by filtration, or to control the effects of the corrosive gases on accelerator equipment. It is important to evaluate these competing needs in order to ensure optimum ventilation designs that, in so far as is possible, satisfy these conflicting requirements.

7.2.2.4 *Facility and Equipment Complexity.* Major accelerator facilities with their wide variety of experimental devices and ancillary support equipment are complex industrial facilities with a broad range of nonradiation hazards. Examples of these hazards include very high voltages, high currents, cryogenics, high temperatures, low pressures, high pressures, ultraviolet, RF, heavy equipment, high-magnetic fields, and lasers. In addition, experiment targets and detectors sometimes use liquid and flammable gases or tritium resulting in further challenges in design for safety. These nonradiation hazards, combined with the unique radiation fields of a high-energy facility, present an unusual mixture of challenges to laboratory management. Both a complete assessment of these potential hazards and adequate controls of those that are present are required prior to operating the accelerator facility.

7.2.3 *Warning and Personnel Security*

The physical size of large accelerator facilities results in access points very remote from the central operations and control facility. The varied ways the accelerator is operated, in terms of different experimental areas, types of experiments and operating conditions (beam current, energy, timing), complicate access requirements. Complexity is added by the need for frequent access to some areas for maintenance or to make experimental set-up changes at times when the accelerator continues to operate with the beam sent to other off-line locations. This complexity of operation places increased demands on the design of engineered protective systems and

administrative control plans, mandating early and continued planning. The intricate operation and control systems of the accelerator, into which this safety system must effectively integrate, require a high level of expertise. NCRP has previously considered this topic in Report No. 88 (NCRP, 1986).

Because of the dispersed character of accelerator facilities, the intense radiation fields produced during machine operation and the constantly changing operating configurations, considerable attention has focused on the need to ensure fail-safe and reliable operating characteristics of the interlock and access control systems. In the past, this has resulted in hard-wired, relay-based systems. Modern evolving technologies, based on solid-state components and programmable logic controllers, are being installed at some facilities. These have the advantages of modularity, capability to expand to very complex systems, good reliability, ready interface to accelerator computer-control systems, self documentation, and record generation and data logging. Care must be taken in setting up the routine testing of the system to ensure that all modes of failure, including non-fail-safe indications and common mode, are tested as thoroughly as possible. Because of the danger that the system logic may be reprogrammed in an unsafe manner, sufficient controls must be established to check and supervise such a system regularly. Independent and redundant systems are normally needed and expected (Casey *et al.*, 1988).

7.2.4 *Monitoring and Control*

7.2.4.1 *Control of Radioactive Material.*   The production of radioactive material when high-energy particles or photons strike accelerator components was mentioned in Section 7.2.2.2 (see also Section 3). This (usually) low-level radioactive material must be carefully controlled, and it is necessary to implement plans for identifying, inventorying, storing and disposing of this material. Adequate personnel to perform these duties and an adequate budget should be provided for this function by laboratory management.

In developing such a plan, it is first necessary to define what the institution considers to be "nonradioactive material." Unfortunately, there is no consistent approach to such a definition. The parameter most commonly used is a reading of the dose rate at the surface of irradiated material. Definitions in current use range from radiation "twice the natural background," 50 to 200 nSv h^{-1} above background. While consensus does not exist, the organization should establish its own practical criteria for its day-to-day operations, which is firmly

founded on reasonable technical arguments supported by statistical data (Lochamy, 1981). Elwyn and Cupps (1993) have written an excellent example of such a technical-basis document for determining whether materials or components removed from accelerator enclosures should be considered radioactive or not from measurements of surface dose rates using survey type instruments. In measuring surface dose rates, care must be taken that the monitoring technique is appropriate for the anticipated activation products; some activation products are not easily detected with routine survey instruments. Wipe tests are recommended to determine whether any activation products are removable. Any plan for control of radioactive materials should include:

- labeling scheme that clearly identifies the hazard level (external dose rate, for example) of an activated object
- designated locations for the storage of materials and equipment. The control of radioactive equipment and hardware is particularly complex at large facilities. An inventory system should be considered
- appropriate procedures for transporting radioactive materials on- and off-site
- program to ensure that material is not removed without proper monitoring and labeling from the place where it might have been irradiated. It is especially important to ensure that radioactive material is not inadvertently introduced into nonradioactive material or equipment stockpiles or waste streams. Particular attention should be paid to materials in environments where they may become radioactive, such as water in closed-loop cooling systems; the earth and concrete shielding surrounding beam enclosures; and magnets, beam pipes, electrostatic septa, or other beam-line components

7.2.4.2 *Radioactive Waste Management.* The health-physics considerations for radioactive waste management at particle accelerators center around two primary aspects, both of which are analogous to those at other radiological facilities. One is the radiation dose that personnel may receive while handling radioactive components of the accelerator. This is addressed as part of the day-to-day operational controls. The second aspect is the potential radiation hazard to the general population. Public exposure might occur from interim, on-site storage of radioactive components or from transport of these materials to other sites, or from improperly-controlled materials which might be released to the public.

An inventory system should be developed to control major components identified for disposal as radioactive waste, and to control

those sealed containers of waste being held for disposal. The inventory system would include the radiological state of each item as of the date it was assessed. All identifiable waste items should be inventoried. Results of radiation surveys should be documented and, as much as possible, be related to the inventory of material and equipment.

Knowledge of the radiation environment, where the waste originated, is an important factor in planning waste-disposal strategies. A certain amount of interim storage (staging) can be included in the plan for disposal. As with the storage areas used during accelerator operation, strict controls should be maintained. Radioactive and non-radioactive materials should be kept segregated, and valuable materials (or "desirable items") which happen to be radioactive should be protected from theft. In some cases, shielded containers, in which highly radioactive components may be stored or shipped, will be necessary.

Contamination problems may arise during dismantling operations, if precautions are not observed or when imprudent original design precludes a desired approach. Examples include torch cutting of activated materials by inexperienced welders or oversized, poured-in-place concrete shielding that has to be demolished. Proper procedures for dealing with such problems are not specific to accelerators, but, in many accelerator facilities, health physics technicians may need to be reminded of potential complications if they have little experience of dealing with loose contamination.

One of the largest health-physics efforts in the waste program, involves its characterization and shipping. A record-keeping system that is consistent with the material-inventory systems is essential, so as to demonstrate an adequate knowledge of the nature of the waste from routine operations and the ability to handle the large volume of data from, *e.g.*, a major decommissioning. As part of the materials-disposition chain, recorded data should, at minimum, identify the material consistent with the inventory system, record radiation readings as items are loaded, identify radioactive constituents, and provide an identifying number of the shipping vehicle. Regulations for shipping radioactive materials are covered in various U.S. Department of Transportation, IAEA, and local rules and regulations. The separate data from the interim inventory, proposed disposition, health-physics radiation surveys, and materials characterization should be combined to form the core of the final-disposition documentation. It should then be possible to determine the final disposition of each identifiable item and what its radiation level was as it left the site.

A more difficult task arises when it is necessary, not only to determine the surface radiation level but to specify, in addition, constituent nuclides and their concentrations in the radioactive material. Various techniques have been employed for such estimates, ranging from "educated guesses" to use of sophisticated radiation-spectrometric instruments or elaborate calculations. The level of effort involved should be consistent with the applicable regulations. For instance, the requirements for waste burial usually necessitate a better estimate of certain nuclides than required for transport. For shipping material and equipment that contains only induced radioactivity, external exposure rate is the most significant parameter, whereas regulations for waste burial should be based on exposure pathways to the general public.

7.2.4.3 *Contamination Control.* Some accelerator-produced nuclides present in activated materials have emission characteristics that create difficulties for routine contamination monitoring (see also Section 7.2.2.2). Notable among these are ^{7}Be, ^{54}Mn, and ^{51}Cr, which do not have a beta emission, x-ray emitters such as ^{55}Fe and ^{59}Ni, and low-energy beta emitters, especially tritium which is a common product of high-energy spallation-type reactions. Monitoring programs designed for mixtures of activation products typically use simple beta detectors. Hence, the health physicist must take care to identify any areas or situations where nuclides which are difficult to detect might dominate, and to monitor the mixture of nuclides routinely encountered in the facility. Circumstances where such nuclides might be a concern are in water systems after substantial decay, *e.g.*, resin beds with ^{7}Be, condensation from air-conditioning units, surface contamination resulting from airborne activation at very high-power facilities, and ^{7}Be concentration in a heating, ventilation and air-conditioning filter media.

7.2.4.4 *Surface Contamination Standards.* The removable contamination limits specified in federal regulations are based, in large part, on the fact that nuclear fission products and activation products lie on the proton-deficient side of the nuclear stability curve and so usually decay by modes that produce beta particles. Field instruments, such as GM detectors, readily detect beta particles. Removable contamination limits have been based on the limit of detectability of these instruments for beta emitters.

The nominal GM-detector field-instrument response function is: 100 cpm over background is equivalent to 1,000 disintegrations per minute (dpm) for ^{60}Co beta particles. This value of 1,000 dpm over 100 cm^2 of surface area serves as the basis for a general limit for

removable surface contamination applied to beta/gamma-emitting radionuclides. Because at accelerator facilities, this restrictive limit results in a problem. The removable contamination limit is not based on the risk of exposure, many radionuclides found at accelerators present a significantly lower risk than fission-product radionuclides.

Radionuclides that do not emit beta particles, such as ^{7}Be, ^{51}Cr, ^{54}Mn, and ^{57}Co, can be identified in removable radioactive material from surfaces at accelerators. In the particular case of ^{7}Be and ^{51}Cr, the combination of photon yield and reduced detector response for the decay photons makes these radionuclides very difficult to detect with a GM detector. To meet current regulatory requirements, accelerator facilities generally evaluate the radionuclides found in their environments and select special field-detection equipment or combinations of equipment that allow them to meet the limit of 1,000 dpm per 100 cm^2. A system based on risk would allow for alternative choices.

Development of a risk-based system for specifying removable surface contamination limits is beyond the scope of this Report. However, a reasonable alternative to the fixed limit of 1,000 dpm per 100 cm^2 for beta/gamma emitters can be developed from a risk-based determination of radioactivity thresholds for determining sealed source accountability. This method was proposed by Shingleton and Lee (1998) and adopted in modified form by the U.S. Department of Energy in its regulation 10 CFR 835 (DOE, 1998). In this method, accountability thresholds are based on the quantity of radionuclide which, if one percent were released, would result in a committed effective dose equivalent or an external effective dose equivalent of 1 mSv to an exposed individual. The accountability threshold determined for ^{60}Co is 3 MBq, while that for ^{7}Be, for example, is 300 MBq. The latter value implies that the permissible limit for removable surface contamination for ^{7}Be might be 10^5 dpm per 100 cm^2 based on relative risk.

When several radionuclides are present, the sum of quotients (each radionuclide divided by its limit) less than unity would represent an acceptable condition. However, application of the ALARA principle would require keeping contamination at a reasonably low level.

If the ratio of radionuclides present is relatively constant and predictable, then one or two (those with the lowest permissible limits) could be selected for the field analysis, and a detector sensitive to those indicator radionuclides could be used. As an example, one could select a conventional 47 mm end-window GM detector, often referred to as a "pancake GM," and a count-rate limit of 100 cpm over background (in a low background area) on a surface or sampling medium under field conditions. A count rate of 100 cpm over background

on the surface or sampling substrate represents approximately 30,000 dpm of ^{7}Be or ^{51}Cr contamination—radionuclides most difficult to detect. This quantity of ^{7}Be is more than three times less than the permissible limit determined above.

Based on the method described, the quantity of radioactivity corresponding to 100 cpm over background determined with field detection equipment represents a reasonable removable-contamination control limit that is easy to implement in practice and does not permit excessive removable radioactivity in the workplace. Other authorities have recommended removable surface-contamination limits for beta/gamma emitters that are higher than 1,000 dpm. For example, the National Health and Medical Research Council of Australia has recommended that 30,000 dpm per 100 cm^2 be used for beta/gamma emitters such as ^{60}Co (NHMRC, 1995). They also recommend contamination-control values for low-radiotoxicity radionuclides as high as ~300,000 dpm per 100 cm^2 based on "facility-specific situations."

7.2.4.5 *Guidance for Clearance.* The American National Standards Institute released *Surface and Volume Radioactivity Standards for Clearance* (ANSI/HPS, 1999), which specifies screening levels for releasing radioactive material from regulatory or other controls. These screening levels may be applicable for determining the disposition of activated or surface contaminated accelerator components. The screening values are based on preventing an individual in the public from receiving an annual radiation dose in excess of 10 μSv from any item or group of items released. All potential exposure pathways are included in the analysis. Some radioactive isotopes produced by accelerator operation, such as ^{7}Be and ^{57}Co, are not included in the table of screening values, but the analysis that is described in the Standard can be applied to any radionuclide to arrive at an appropriate value. Radionuclides are grouped into four categories with screening values ranging from 0.1 to 100 Bq cm^{-2} or Bq g^{-1}. The surface contamination screening values range from 600 to 600,000 dpm per 100 cm^2, which can be compared with the surface contamination standards discussed in the previous section.

7.2.5 *Training*

Radiation safety training at accelerator facilities should follow the guidance contained in NCRP Report No. 127 and No. 134 (NCRP, 1998; 2000). Operators, users, maintenance technicians, and radiation safety personnel shall especially be informed of the potential

for receiving severely damaging or lethal exposures in a short period of time. Details of safety interlock, access control, and warning systems should be emphasized. This should include configuration control procedures for modifications and bypasses. Relevant accident experience at other facilities should be discussed (Busick and Warren, 1979). Associated hazards relative to RF systems, high-voltage and current, magnetic fields, and high-vacuum systems should also be addressed.

Appendix A

Importance Functions for Neutrons and Photons

373

TABLE A.1—*Neutron importance as a function of energy and angle: Mean distance = 11 m (see Section 6.2.1).*

E_{High} (MeV)	E_{Low} (MeV)	Neutron Importance in Sievert for the Cosine Interval				
		0.0–0.2	0.2–0.4	0.4–0.6	0.6–0.8	0.8–1.0
4.00E+02	3.75E+02	5.33E−19	4.94E−19	4.06E−19	3.88E−19	3.52E−19
3.75E+02	3.50E+02	5.16E−19	4.78E−19	3.93E−19	3.78E−19	3.48E−19
3.50E+02	3.25E+02	5.14E−19	4.75E−19	3.92E−19	3.78E−19	3.53E−19
3.25E+02	3.00E+02	5.16E−19	4.78E−19	3.94E−19	3.82E−19	3.59E−19
3.00E+02	2.75E+02	5.26E−19	4.87E−19	4.03E−19	3.92E−19	3.70E−19
2.75E+02	2.50E+02	5.30E−19	4.92E−19	4.09E−19	3.97E−19	3.76E−19
2.50E+02	2.25E+02	5.20E−19	4.83E−19	4.01E−19	3.91E−19	3.71E−19
2.25E+02	2.00E+02	5.08E−19	4.72E−19	3.91E−19	3.82E−19	3.65E−19
2.00E+02	1.75E+02	5.04E−19	4.69E−19	3.89E−19	3.81E−19	3.65E−19
1.75E+02	1.50E+02	5.10E−19	4.75E−19	3.96E−19	3.88E−19	3.73E−19
1.50E+02	1.25E+02	5.27E−19	4.91E−19	4.12E−19	4.04E−19	3.91E−19
1.25E+02	1.00E+02	5.54E−19	5.17E−19	4.36E−19	4.28E−19	4.19E−19
1.00E+02	9.00E+01	5.53E−19	5.18E−19	4.39E−19	4.27E−19	4.09E−19
9.00E+01	8.00E+01	5.56E−19	5.20E−19	4.40E−19	4.28E−19	4.15E−19
8.00E+01	7.00E+01	5.63E−19	5.25E−19	4.46E−19	4.34E−19	4.26E−19
7.00E+01	6.00E+01	5.80E−19	5.41E−19	4.61E−19	4.50E−19	4.49E−19
6.00E+01	5.50E+01	5.68E−19	5.29E−19	4.53E−19	4.37E−19	4.33E−19
5.50E+01	5.00E+01	5.74E−19	5.34E−19	4.57E−19	4.43E−19	4.45E−19
5.00E+01	4.50E+01	5.97E−19	5.55E−19	4.67E−19	4.60E−19	4.88E−19
4.50E+01	4.00E+01	5.65E−19	5.25E−19	4.45E−19	4.38E−19	4.65E−19
4.00E+01	3.50E+01	5.64E−19	5.24E−19	4.45E−19	4.37E−19	4.57E−19

5.02E−19	4.76E−19	4.82E−19	5.69E−19	6.10E−19	3.00E+01	3.50E+01
5.44E−19	5.15E−19	5.22E−19	6.14E−19	6.57E−19	2.75E+01	3.00E+01
5.57E−19	5.31E−19	5.37E−19	6.36E−19	6.80E−19	2.50E+01	2.75E+01
6.06E−19	5.74E−19	5.76E−19	6.81E−19	7.25E−19	2.25E+01	2.50E+01
6.52E−19	6.23E−19	6.24E−19	7.37E−19	7.83E−19	2.00E+01	2.25E+01
6.82E−19	6.70E−19	6.73E−19	7.98E−19	8.46E−19	1.75E+01	2.00E+01
8.53E−19	8.15E−19	8.07E−19	9.36E−19	9.83E−19	1.49E+01	1.75E+01
7.95E−19	8.49E−19	8.48E−19	1.03E−18	1.08E−18	1.35E+01	1.49E+01
7.82E−19	8.55E−19	8.61E−19	1.04E−18	1.10E−18	1.22E+01	1.35E+01
8.76E−19	9.65E−19	9.79E−19	1.15E−18	1.22E−18	1.00E+01	1.22E+01
9.23E−19	1.01E−18	1.03E−18	1.20E−18	1.26E−18	8.19E+00	1.00E+01
9.12E−19	1.11E−18	1.16E−18	1.36E−18	1.44E−18	6.70E+00	8.19E+00
1.31E−18	1.35E−18	1.35E−18	1.52E−18	1.58E−18	5.49E+00	6.70E+00
1.34E−18	1.33E−18	1.32E−18	1.46E−18	1.51E−18	4.49E+00	5.49E+00
2.58E−18	2.46E−18	2.38E−18	2.55E−18	2.58E−18	3.68E+00	4.49E+00
2.39E−18	2.34E−18	2.30E−18	2.48E−18	2.53E−18	3.01E+00	3.68E+00
1.84E−18	1.85E−18	1.83E−18	2.01E−18	2.06E−18	2.47E+00	3.01E+00
1.69E−18	1.79E−18	1.79E−18	2.01E−18	2.08E−18	2.02E+00	2.47E+00
2.22E−18	2.29E−18	2.26E−18	2.52E−18	2.58E−18	1.65E+00	2.02E+00
1.96E−18	2.12E−18	2.11E−18	2.43E−18	2.50E−18	1.35E+00	1.65E+00
2.15E−18	2.25E−18	2.21E−18	2.50E−18	2.56E−18	1.11E+00	1.35E+00
2.68E−18	2.70E−18	2.61E−18	2.83E−18	2.86E−18	9.07E−01	1.11E+00
1.15E−18	1.33E−18	1.35E−18	1.58E−18	1.65E−18	7.43E−01	9.07E−01
1.09E−18	1.25E−18	1.25E−18	1.47E−18	1.52E−18	4.98E−01	7.43E−01
1.45E−18	1.66E−18	1.59E−18	1.81E−18	1.84E−18	3.34E−01	4.98E−01

TABLE A.1—*Neutron importance as a function of energy and angle: Mean distance = 11 m (see Section 6.2.1).* (continued)

E_{High} (MeV)	E_{Low} (MeV)	Neutron Importance in Sievert for the Cosine Interval				
		0.0–0.2	0.2–0.4	0.4–0.6	0.6–0.8	0.8–1.0
3.34E−01	2.24E−01	1.27E−18	1.25E−18	1.11E−18	1.13E−18	9.91E−19
2.24E−01	1.50E−01	9.80E−19	9.60E−19	8.43E−19	8.65E−19	7.44E−19
1.50E−01	8.65E−02	7.33E−19	7.21E−19	6.31E−19	6.52E−19	5.55E−19
8.65E−02	3.18E−02	5.43E−19	5.42E−19	4.82E−19	5.03E−19	4.28E−19
3.18E−02	1.50E−02	4.32E−19	4.37E−19	3.93E−19	4.15E−19	3.52E−19
1.50E−02	7.10E−03	4.30E−19	4.38E−19	3.94E−19	4.21E−19	3.55E−19
7.10E−03	3.35E−03	4.48E−19	4.58E−19	4.11E−19	4.44E−19	3.70E−19
3.35E−03	1.58E−03	4.68E−19	4.80E−19	4.28E−19	4.69E−19	3.85E−19
1.58E−03	4.54E−04	4.91E−19	5.06E−19	4.49E−19	5.01E−19	4.04E−19
4.54E−04	1.01E−04	5.21E−19	5.40E−19	4.74E−19	5.40E−19	4.26E−19
1.01E−04	2.26E−05	5.29E−19	5.49E−19	4.79E−19	5.54E−19	4.29E−19
2.26E−05	1.07E−05	5.20E−19	5.40E−19	4.68E−19	5.46E−19	4.17E−19
1.07E−05	5.04E−06	5.10E−19	5.30E−19	4.57E−19	5.37E−19	4.07E−19
5.04E−06	2.38E−06	4.97E−19	5.16E−19	4.43E−19	5.23E−19	3.92E−19
2.38E−06	1.13E−06	4.76E−19	4.93E−19	4.20E−19	5.01E−19	3.70E−19
1.13E−06	4.14E−07	4.41E−19	4.56E−19	3.83E−19	4.65E−19	3.35E−19
4.14E−07	1.00E−10	3.72E−19	3.88E−19	3.17E−19	4.03E−19	2.74E−19

TABLE A.2—*Neutron importance as a function of energy and angle: Mean distance = 108 m (see Section 6.2.1).*

E_{High} (MeV)	E_{Low} (MeV)	Neutron Importance in Sievert for the Cosine Interval				
		0.0–0.2	0.2–0.4	0.4–0.6	0.6–0.8	0.8–1.0
4.00E + 02	3.75E + 02	3.75E − 19	2.36E − 19	1.58E − 19	1.26E − 19	9.34E − 20
3.75E + 02	3.50E + 02	3.59E − 19	2.27E − 19	1.53E − 19	1.21E − 19	8.96E − 20
3.50E + 02	3.25E + 02	3.50E − 19	2.23E − 19	1.50E − 19	1.20E − 19	8.84E − 20
3.25E + 02	3.00E + 02	3.44E − 19	2.21E − 19	1.49E − 19	1.20E − 19	8.83E − 20
3.00E + 02	2.75E + 02	3.39E − 19	2.19E − 19	1.49E − 19	1.20E − 19	8.92E − 20
2.75E + 02	2.50E + 02	3.33E − 19	2.17E − 19	1.48E − 19	1.20E − 19	8.93E − 20
2.50E + 02	2.25E + 02	3.25E − 19	2.12E − 19	1.45E − 19	1.18E − 19	8.76E − 20
2.25E + 02	2.00E + 02	3.16E − 19	2.07E − 19	1.42E − 19	1.15E − 19	8.55E − 20
2.00E + 02	1.75E + 02	3.09E − 19	2.04E − 19	1.40E − 19	1.14E − 19	8.47E − 20
1.75E + 02	1.50E + 02	3.06E − 19	2.02E − 19	1.40E − 19	1.14E − 19	8.52E − 20
1.50E + 02	1.25E + 02	3.06E − 19	2.04E − 19	1.42E − 19	1.17E − 19	8.72E − 20
1.25E + 02	1.00E + 02	3.12E − 19	2.09E − 19	1.45E − 19	1.20E − 19	9.00E − 20
1.00E + 02	9.00E + 01	3.18E − 19	2.11E − 19	1.46E − 19	1.20E − 19	9.10E − 20
9.00E + 01	8.00E + 01	3.24E − 19	2.14E − 19	1.47E − 19	1.20E − 19	9.08E − 20
8.00E + 01	7.00E + 01	3.34E − 19	2.20E − 19	1.50E − 19	1.21E − 19	9.10E − 20
7.00E + 01	6.00E + 01	3.48E − 19	2.29E − 19	1.54E − 19	1.24E − 19	9.21E − 20
6.00E + 01	5.50E + 01	3.55E − 19	2.30E − 19	1.54E − 19	1.22E − 19	9.07E − 20
5.50E + 01	5.00E + 01	3.62E − 19	2.35E − 19	1.56E − 19	1.23E − 19	9.03E − 20
5.00E + 01	4.50E + 01	4.12E − 19	2.66E − 19	1.72E − 19	1.29E − 19	9.08E − 20
4.50E + 01	4.00E + 01	3.82E − 19	2.47E − 19	1.61E − 19	1.21E − 19	8.62E − 20
4.00E + 01	3.50E + 01	3.69E − 19	2.41E − 19	1.58E − 19	1.20E − 19	8.66E − 20

TABLE A.2—*Neutron importance as a function of energy and angle: Mean distance = 108 m (see Section 6.2.1). (continued)*

E_{High} (MeV)	E_{Low} (MeV)	Neutron Importance in Sievert for the Cosine Interval				
		0.0–0.2	0.2–0.4	0.4–0.6	0.6–0.8	0.8–1.0
3.50E+01	3.00E+01	3.87E−19	2.55E−19	1.67E−19	1.28E−19	9.19E−20
3.00E+01	2.75E+01	4.09E−19	2.70E−19	1.77E−19	1.35E−19	9.74E−20
2.75E+01	2.50E+01	4.14E−19	2.75E−19	1.81E−19	1.38E−19	1.00E−19
2.50E+01	2.25E+01	4.20E−19	2.82E−19	1.88E−19	1.44E−19	1.05E−19
2.25E+01	2.00E+01	4.24E−19	2.89E−19	1.95E−19	1.51E−19	1.12E−19
2.00E+01	1.75E+01	4.28E−19	2.95E−19	2.02E−19	1.59E−19	1.20E−19
1.75E+01	1.49E+01	4.32E−19	3.05E−19	2.12E−19	1.70E−19	1.30E−19
1.49E+01	1.35E+01	3.77E−19	2.77E−19	2.03E−19	1.73E−19	1.39E−19
1.35E+01	1.22E+01	3.78E−19	2.78E−19	2.05E−19	1.76E−19	1.42E−19
1.22E+01	1.00E+01	3.77E−19	2.82E−19	2.12E−19	1.87E−19	1.55E−19
1.00E+01	8.19E+00	3.77E−19	2.85E−19	2.17E−19	1.96E−19	1.63E−19
8.19E+00	6.70E+00	4.04E−19	3.04E−19	2.36E−19	2.18E−19	1.87E−19
6.70E+00	5.49E+00	4.23E−19	3.19E−19	2.38E−19	2.13E−19	1.76E−19
5.49E+00	4.49E+00	3.89E−19	2.92E−19	2.16E−19	1.89E−19	1.54E−19
4.49E+00	3.68E+00	5.10E−19	4.12E−19	3.09E−19	2.70E−19	2.26E−19
3.68E+00	3.01E+00	5.17E−19	4.22E−19	3.21E−19	2.88E−19	2.47E−19
3.01E+00	2.47E+00	4.68E−19	3.78E−19	2.95E−19	2.72E−19	2.33E−19
2.47E+00	2.02E+00	4.91E−19	3.92E−19	3.10E−19	2.84E−19	2.45E−19
2.02E+00	1.65E+00	5.46E−19	4.44E−19	3.52E−19	3.14E−19	2.75E−19
1.65E+00	1.35E+00	5.40E−19	4.39E−19	3.50E−19	3.06E−19	2.74E−19
1.35E+00	1.11E+00	5.23E−19	4.24E−19	3.34E−19	2.88E−19	2.53E−19
1.11E+00	9.07E−01	4.86E−19	4.09E−19	3.23E−19	2.82E−19	2.53E−19
9.07E−01	7.43E−01	3.60E−19	2.85E−19	2.27E−19	2.02E−19	1.79E−19
7.43E−01	4.98E−01	2.93E−19	2.36E−19	1.89E−19	1.64E−19	1.48E−19
4.98E−01	3.34E−01	2.30E−19	2.00E−19	1.68E−19	1.42E−19	1.38E−19

3.34E − 01	2.24E − 01	1.59E − 19	1.38E − 19	1.16E − 19	1.01E − 19	9.77E − 20
2.24E − 01	1.50E − 01	1.18E − 19	1.03E − 19	8.78E − 20	7.56E − 20	7.44E − 20
1.50E − 01	8.65E − 02	8.55E − 20	7.66E − 20	6.70E − 20	5.76E − 20	5.81E − 20
8.65E − 02	3.18E − 02	5.82E − 20	5.54E − 20	5.10E − 20	4.39E − 20	4.64E − 20
3.18E − 02	1.50E − 02	4.44E − 20	4.41E − 20	4.23E − 20	3.64E − 20	3.97E − 20
1.50E − 02	7.10E − 03	4.17E − 20	4.21E − 20	4.08E − 20	3.52E − 20	3.86E − 20
7.10E − 03	3.35E − 03	4.06E − 20	4.11E − 20	4.01E − 20	3.45E − 20	3.79E − 20
3.35E − 03	1.58E − 03	3.93E − 20	3.99E − 20	3.91E − 20	3.37E − 20	3.69E − 20
1.58E − 03	4.54E − 04	3.76E − 20	3.85E − 20	3.78E − 20	3.28E − 20	3.58E − 20
4.54E − 04	1.01E − 04	3.51E − 20	3.60E − 20	3.55E − 20	3.08E − 20	3.34E − 20
1.01E − 04	2.26E − 05	3.16E − 20	3.24E − 20	3.17E − 20	2.76E − 20	2.97E − 20
2.26E − 05	1.07E − 05	2.77E − 20	2.81E − 20	2.74E − 20	2.36E − 20	2.52E − 20
1.07E − 05	5.04E − 06	2.53E − 20	2.55E − 20	2.46E − 20	2.12E − 20	2.24E − 20
5.04E − 06	2.38E − 06	2.25E − 20	2.25E − 20	2.15E − 20	1.84E − 20	1.93E − 20
2.38E − 06	1.13E − 06	1.93E − 20	1.91E − 20	1.80E − 20	1.54E − 20	1.59E − 20
1.13E − 06	4.14E − 07	1.58E − 20	1.53E − 20	1.42E − 20	1.21E − 20	1.23E − 20
4.14E − 07	1.00E − 10	1.02E − 20	9.86E − 21	9.04E − 21	7.89E − 21	7.67E − 21

TABLE A.3—*Neutron importance as a function of energy and angle: Mean distance = 495 m (see Section 6.2.1).*

E_{High} (MeV)	E_{Low} (MeV)	Neutron Importance in Sievert for the Cosine Interval				
		0.0–0.2	0.2–0.4	0.4–0.6	0.6–0.8	0.8–1.0
4.00E+02	3.75E+02	6.04E−20	3.72E−20	2.39E−20	1.71E−20	9.01E−21
3.75E+02	3.50E+02	5.80E−20	3.57E−20	2.29E−20	1.63E−20	8.53E−21
3.50E+02	3.25E+02	5.62E−20	3.46E−20	2.23E−20	1.59E−20	8.28E−21
3.25E+02	3.00E+02	5.47E−20	3.37E−20	2.17E−20	1.55E−20	8.14E−21
3.00E+02	2.75E+02	5.32E−20	3.28E−20	2.12E−20	1.51E−20	7.97E−21
2.75E+02	2.50E+02	5.17E−20	3.18E−20	2.05E−20	1.46E−20	7.74E−21
2.50E+02	2.25E+02	5.00E−20	3.07E−20	1.98E−20	1.41E−20	7.46E−21
2.25E+02	2.00E+02	4.83E−20	2.95E−20	1.90E−20	1.35E−20	7.15E−21
2.00E+02	1.75E+02	4.67E−20	2.85E−20	1.83E−20	1.30E−20	6.90E−21
1.75E+02	1.50E+02	4.52E−20	2.76E−20	1.77E−20	1.25E−20	6.71E−21
1.50E+02	1.25E+02	4.39E−20	2.67E−20	1.72E−20	1.21E−20	6.53E−21
1.25E+02	1.00E+02	4.24E−20	2.58E−20	1.66E−20	1.17E−20	6.33E−21
1.00E+02	9.00E+01	4.12E−20	2.51E−20	1.61E−20	1.13E−20	6.20E−21
9.00E+01	8.00E+01	4.04E−20	2.47E−20	1.59E−20	1.12E−20	6.07E−21
8.00E+01	7.00E+01	3.94E−20	2.43E−20	1.57E−20	1.11E−20	5.96E−21
7.00E+01	6.00E+01	3.83E−20	2.39E−20	1.56E−20	1.11E−20	5.89E−21
6.00E+01	5.50E+01	3.70E−20	2.34E−20	1.52E−20	1.09E−20	5.77E−21
5.50E+01	5.00E+01	3.57E−20	2.29E−20	1.51E−20	1.09E−20	5.79E−21
5.00E+01	4.50E+01	3.37E−20	2.31E−20	1.59E−20	1.19E−20	6.54E−21
4.50E+01	4.00E+01	3.16E−20	2.13E−20	1.45E−20	1.08E−20	5.86E−21
4.00E+01	3.50E+01	2.99E−20	2.00E−20	1.36E−20	1.02E−20	5.62E−21

3.50E+01	3.00E+01	2.79E−20	1.92E−20	1.34E−20	1.03E−20	5.89E−21
3.00E+01	2.75E+01	2.57E−20	1.83E−20	1.31E−20	1.03E−20	6.12E−21
2.75E+01	2.50E+01	2.41E−20	1.75E−20	1.27E−20	1.01E−20	6.19E−21
2.50E+01	2.25E+01	2.26E−20	1.66E−20	1.22E−20	9.97E−21	6.25E−21
2.25E+01	2.00E+01	2.12E−20	1.58E−20	1.18E−20	9.77E−21	6.29E−21
2.00E+01	1.75E+01	1.97E−20	1.49E−20	1.12E−20	9.48E−21	6.28E−21
1.75E+01	1.49E+01	1.77E−20	1.35E−20	1.03E−20	8.86E−21	6.00E−21
1.49E+01	1.35E+01	1.28E−20	1.02E−20	8.24E−21	7.63E−21	5.65E−21
1.35E+01	1.22E+01	1.27E−20	1.01E−20	8.21E−21	7.64E−21	5.71E−21
1.22E+01	1.00E+01	1.29E−20	1.03E−20	8.37E−21	7.89E−21	6.00E−21
1.00E+01	8.19E+00	1.46E−20	1.13E−20	9.10E−21	8.45E−21	6.36E−21
8.19E+00	6.70E+00	1.38E−20	1.10E−20	8.98E−21	8.57E−21	6.72E−21
6.70E+00	5.49E+00	1.42E−20	1.09E−20	8.75E−21	8.10E−21	6.09E−21
5.49E+00	4.49E+00	1.28E−20	9.56E−21	7.42E−21	6.59E−21	4.78E−21
4.49E+00	3.68E+00	9.02E−21	8.00E−21	6.95E−21	6.80E−21	5.55E−21
3.68E+00	3.01E+00	9.63E−21	8.64E−21	7.61E−21	7.62E−21	6.32E−21
3.01E+00	2.47E+00	1.25E−20	1.04E−20	8.76E−21	8.41E−21	6.65E−21
2.47E+00	2.02E+00	1.27E−20	1.05E−20	8.63E−21	8.05E−21	6.27E−21
2.02E+00	1.65E+00	9.05E−21	8.09E−21	6.98E−21	6.69E−21	5.47E−21
1.65E+00	1.35E+00	6.93E−21	6.51E−21	5.79E−21	5.66E−21	4.80E−21
1.35E+00	1.11E+00	6.20E−21	5.72E−21	5.01E−21	4.80E−21	4.00E−21
1.11E+00	9.07E−01	4.14E−21	3.99E−21	3.62E−21	3.61E−21	3.16E−21
9.07E−01	7.43E−01	4.63E−21	3.98E−21	3.34E−21	3.14E−21	2.50E−21
7.43E−01	4.98E−01	2.31E−21	2.06E−21	1.76E−21	1.67E−21	1.37E−21
4.98E−01	3.34E−01	7.41E−22	7.71E−22	7.36E−22	7.11E−22	6.89E−22

TABLE A.3—*Neutron importance as a function of energy and angle: Mean distance = 495 m (see Section 6.2.1).* (continued)

E_{High} (MeV)	E_{Low} (MeV)	Neutron Importance in Sievert for the Cosine Interval				
		0.0–0.2	0.2–0.4	0.4–0.6	0.6–0.8	0.8–1.0
3.34E − 01	2.24E − 01	5.95E − 22	6.01E − 22	5.61E − 22	5.47E − 22	5.07E − 22
2.24E − 01	1.50E − 01	3.96E − 22	4.11E − 22	3.92E − 22	3.82E − 22	3.65E − 22
1.50E − 01	8.65E − 02	2.72E − 22	2.91E − 22	2.84E − 22	2.77E − 22	2.74E − 22
8.65E − 02	3.18E − 02	1.79E − 22	1.97E − 22	1.98E − 22	1.89E − 22	1.99E − 22
3.18E − 02	1.50E − 02	1.13E − 22	1.25E − 22	1.28E − 22	1.20E − 22	1.31E − 22
1.50E − 02	7.10E − 03	8.68E − 23	9.62E − 23	9.91E − 23	9.16E − 23	1.01E − 22
7.10E − 03	3.35E − 03	6.85E − 23	7.59E − 23	7.83E − 23	7.20E − 23	8.01E − 23
3.35E − 03	1.58E − 03	5.45E − 23	6.03E − 23	6.23E − 23	5.71E − 23	6.38E − 23
1.58E − 03	4.54E − 04	4.37E − 23	4.84E − 23	5.02E − 23	4.59E − 23	5.15E − 23
4.54E − 04	1.01E − 04	3.15E − 23	3.48E − 23	3.61E − 23	3.30E − 23	3.70E − 23
1.01E − 04	2.26E − 05	2.28E − 23	2.50E − 23	2.60E − 23	2.38E − 23	2.66E − 23
2.26E − 05	1.07E − 05	1.77E − 23	1.94E − 23	2.02E − 23	1.86E − 23	2.09E − 23
1.07E − 05	5.04E − 06	1.62E − 23	1.78E − 23	1.85E − 23	1.72E − 23	1.93E − 23
5.04E − 06	2.38E − 06	1.50E − 23	1.65E − 23	1.72E − 23	1.61E − 23	1.82E − 23
2.38E − 06	1.13E − 06	1.39E − 23	1.53E − 23	1.61E − 23	1.52E − 23	1.72E − 23
1.13E − 06	4.14E − 07	1.25E − 23	1.38E − 23	1.47E − 23	1.41E − 23	1.61E − 23
4.14E − 07	1.00E − 10	9.83E − 24	1.09E − 23	1.17E − 23	1.18E − 23	1.36E − 23

TABLE A.4—*Neutron importance as a function of energy and angle: Mean distance = 1,005 m (see Section 6.2.1).*

E_{High} (MeV)	E_{Low} (MeV)	Neutron Importance in Sievert for the Cosine Interval				
		0.0–0.2	0.2–0.4	0.4–0.6	0.6–0.8	0.8–1.0
4.00E+02	3.75E+02	1.64E−20	1.01E−20	5.70E−21	3.11E−21	1.21E−21
3.75E+02	3.50E+02	1.58E−20	9.68E−21	5.42E−21	2.94E−21	1.14E−21
3.50E+02	3.25E+02	1.52E−20	9.27E−21	5.17E−21	2.79E−21	1.08E−21
3.25E+02	3.00E+02	1.47E−20	8.87E−21	4.92E−21	2.65E−21	1.03E−21
3.00E+02	2.75E+02	1.41E−20	8.43E−21	4.65E−21	2.49E−21	9.60E−22
2.75E+02	2.50E+02	1.35E−20	7.98E−21	4.36E−21	2.31E−21	8.87E−22
2.50E+02	2.25E+02	1.29E−20	7.55E−21	4.08E−21	2.15E−21	8.15E−22
2.25E+02	2.00E+02	1.23E−20	7.08E−21	3.79E−21	1.97E−21	7.42E−22
2.00E+02	1.75E+02	1.17E−20	6.63E−21	3.51E−21	1.81E−21	6.77E−22
1.75E+02	1.50E+02	1.10E−20	6.14E−21	3.22E−21	1.65E−21	6.13E−22
1.50E+02	1.25E+02	1.02E−20	5.60E−21	2.90E−21	1.47E−21	5.45E−22
1.25E+02	1.00E+02	9.09E−21	4.98E−21	2.58E−21	1.31E−21	4.79E−22
1.00E+02	9.00E+01	8.16E−21	4.51E−21	2.33E−21	1.17E−21	4.18E−22
9.00E+01	8.00E+01	7.51E−21	4.22E−21	2.22E−21	1.14E−21	4.06E−22
8.00E+01	7.00E+01	6.76E−21	3.91E−21	2.11E−21	1.11E−21	4.05E−22
7.00E+01	6.00E+01	5.92E−21	3.55E−21	1.98E−21	1.08E−21	4.07E−22
6.00E+01	5.50E+01	5.22E−21	3.25E−21	1.86E−21	1.04E−21	4.00E−22
5.50E+01	5.00E+01	4.64E−21	2.97E−21	1.76E−21	1.02E−21	4.19E−22
5.00E+01	4.50E+01	3.44E−21	2.56E−21	1.70E−21	1.12E−21	5.42E−22
4.50E+01	4.00E+01	3.23E−21	2.29E−21	1.47E−21	9.38E−22	4.35E−22
4.00E+01	3.50E+01	2.91E−21	2.02E−21	1.28E−21	8.08E−22	3.77E−22

TABLE A.4—*Neutron importance as a function of energy and angle: Mean distance = 1,005 m (see Section 6.2.1).* (continued)

E_{High} (MeV)	E_{Low} (MeV)	Neutron Importance in Sievert for the Cosine Interval				
		0.0–0.2	0.2–0.4	0.4–0.6	0.6–0.8	0.8–1.0
3.50E+01	3.00E+01	2.31E−21	1.68E−21	1.11E−21	7.32E−22	3.69E−22
3.00E+01	2.75E+01	1.77E−21	1.36E−21	9.42E−22	6.55E−22	3.53E−22
2.75E+01	2.50E+01	1.51E−21	1.19E−21	8.39E−22	5.99E−22	3.37E−22
2.50E+01	2.25E+01	1.28E−21	1.03E−21	7.39E−22	5.42E−22	3.18E−22
2.25E+01	2.00E+01	1.09E−21	8.87E−22	6.48E−22	4.82E−22	2.94E−22
2.00E+01	1.75E+01	9.14E−22	7.51E−22	5.56E−22	4.24E−22	2.67E−22
1.75E+01	1.49E+01	7.29E−22	6.03E−22	4.52E−22	3.52E−22	2.28E−22
1.49E+01	1.35E+01	4.61E−22	3.98E−22	3.19E−22	2.73E−22	2.03E−22
1.35E+01	1.22E+01	4.48E−22	3.90E−22	3.15E−22	2.71E−22	2.03E−22
1.22E+01	1.00E+01	4.80E−22	4.08E−22	3.27E−22	2.82E−22	2.15E−22
1.00E+01	8.19E+00	6.22E−22	4.95E−22	3.79E−22	3.12E−22	2.30E−22
8.19E+00	6.70E+00	5.21E−22	4.31E−22	3.42E−22	2.96E−22	2.30E−22
6.70E+00	5.49E+00	5.31E−22	4.32E−22	3.34E−22	2.78E−22	2.05E−22
5.49E+00	4.49E+00	4.44E−22	3.48E−22	2.60E−22	2.07E−22	1.43E−22
4.49E+00	3.68E+00	1.85E−22	1.84E−22	1.66E−22	1.59E−22	1.31E−22
3.68E+00	3.01E+00	2.01E−22	1.98E−22	1.78E−22	1.71E−22	1.43E−22
3.01E+00	2.47E+00	3.22E−22	2.76E−22	2.21E−22	1.90E−22	1.45E−22
2.47E+00	2.02E+00	2.78E−22	2.34E−22	1.82E−22	1.52E−22	1.10E−22
2.02E+00	1.65E+00	1.18E−22	1.15E−22	9.94E−23	9.13E−23	7.26E−23
1.65E+00	1.35E+00	7.10E−23	7.30E−23	6.68E−23	6.45E−23	5.43E−23
1.35E+00	1.11E+00	5.71E−23	5.79E−23	5.22E−23	4.95E−23	4.08E−23
1.11E+00	9.07E−01	3.22E−23	3.35E−23	3.14E−23	3.10E−23	2.74E−23
9.07E−01	7.43E−01	4.20E−23	3.85E−23	3.20E−23	2.83E−23	2.18E−23
7.43E−01	4.98E−01	1.12E−23	1.09E−23	9.51E−24	8.77E−24	7.15E−24
4.98E−01	3.34E−01	2.27E−24	2.45E−24	2.42E−24	2.39E−24	2.37E−24

3.34E − 01	2.24E − 01	1.84E − 24	1.97E − 24	1.91E − 24	1.91E − 24	1.83E − 24
2.24E − 01	1.50E − 01	1.32E − 24	1.43E − 24	1.41E − 24	1.41E − 24	1.41E − 24
1.50E − 01	8.65E − 02	1.04E − 24	1.13E − 24	1.14E − 24	1.14E − 24	1.19E − 24
8.65E − 02	3.18E − 02	8.64E − 25	9.44E − 25	9.67E − 25	9.37E − 25	1.03E − 24
3.18E − 02	1.50E − 02	7.58E − 25	8.30E − 25	8.62E − 25	8.15E − 25	9.25E − 25
1.50E − 02	7.10E − 03	7.25E − 25	7.95E − 25	8.30E − 25	7.79E − 25	8.92E − 25
7.10E − 03	3.35E − 03	7.01E − 25	7.70E − 25	8.07E − 25	7.55E − 25	8.68E − 25
3.35E − 03	1.58E − 03	6.80E − 25	7.48E − 25	7.86E − 25	7.35E − 25	8.47E − 25
1.58E − 03	4.54E − 04	6.58E − 25	7.25E − 25	7.65E − 25	7.15E − 25	8.24E − 25
4.54E − 04	1.01E − 04	6.27E − 25	6.93E − 25	7.32E − 25	6.86E − 25	7.90E − 25
1.01E − 04	2.26E − 05	5.91E − 25	6.53E − 25	6.91E − 25	6.51E − 25	7.49E − 25
2.26E − 05	1.07E − 05	5.50E − 25	6.07E − 25	6.43E − 25	6.08E − 25	6.99E − 25
1.07E − 05	5.04E − 06	5.21E − 25	5.75E − 25	6.07E − 25	5.76E − 25	6.63E − 25
5.04E − 06	2.38E − 06	4.89E − 25	5.37E − 25	5.66E − 25	5.39E − 25	6.19E − 25
2.38E − 06	1.13E − 06	4.52E − 25	4.94E − 25	5.19E − 25	4.96E − 25	5.67E − 25
1.13E − 06	4.14E − 07	4.11E − 25	4.46E − 25	4.65E − 25	4.47E − 25	5.06E − 25
4.14E − 07	1.00E − 10	3.50E − 25	3.76E − 25	3.86E − 25	3.75E − 25	4.11E − 25

TABLE A.5—*Photon importance as a function of energy and angle: Mean distance = 11 m (see Section 6.2.3).*

E_{High} (MeV)	E_{Low} (MeV)	Neutron Importance in Sievert for the Cosine Interval				
		0.0–0.2	0.2–0.4	0.4–0.6	0.6–0.8	0.8–1.0
1.40E+01	1.20E+01	4.76E−21	3.48E−21	3.61E−21	2.34E−21	8.79E−22
1.20E+01	1.00E+01	4.52E−21	3.32E−21	3.40E−21	2.21E−21	8.29E−22
1.00E+01	8.00E+00	4.21E−21	3.10E−21	3.12E−21	2.03E−21	7.65E−22
8.00E+00	7.50E+00	4.00E−21	2.88E−21	3.00E−21	1.82E−21	6.47E−22
7.50E+00	7.00E+00	3.91E−21	2.83E−21	2.93E−21	1.78E−21	6.30E−22
7.00E+00	6.50E+00	3.86E−21	2.79E−21	2.87E−21	1.74E−21	6.17E−22
6.50E+00	6.00E+00	3.81E−21	2.76E−21	2.81E−21	1.71E−21	6.07E−22
6.00E+00	5.50E+00	3.77E−21	2.74E−21	2.75E−21	1.69E−21	6.02E−22
5.50E+00	5.00E+00	3.75E−21	2.82E−21	2.71E−21	1.69E−21	6.04E−22
5.00E+00	4.50E+00	3.82E−21	2.82E−21	2.65E−21	1.54E−21	6.07E−22
4.50E+00	4.00E+00	3.80E−21	2.82E−21	2.59E−21	1.54E−21	6.14E−22
4.00E+00	3.50E+00	3.80E−21	2.75E−21	2.62E−21	1.71E−21	6.53E−22
3.50E+00	3.00E+00	3.89E−21	2.96E−21	2.65E−21	1.78E−21	7.90E−22
3.00E+00	2.50E+00	4.01E−21	3.26E−21	2.78E−21	2.05E−21	1.00E−21
2.50E+00	2.00E+00	4.27E−21	3.74E−21	3.03E−21	2.54E−21	1.61E−21
2.00E+00	1.50E+00	4.91E−21	4.52E−21	3.55E−21	3.40E−21	2.92E−21
1.50E+00	1.00E+00	6.09E−21	5.73E−21	4.42E−21	4.72E−21	4.84E−21
1.00E+00	4.00E−01	7.01E−21	6.62E−21	6.18E−21	5.39E−21	5.08E−21
4.00E−01	2.00E−01	7.09E−21	6.78E−21	5.59E−21	5.84E−21	5.29E−21
2.00E−01	1.00E−01	5.86E−21	5.62E−21	4.64E−21	5.05E−21	4.14E−21
1.00E−01	1.00E−02	2.59E−21	2.65E−21	2.10E−21	3.03E−21	1.90E−21

TABLE A.6—*Photon importance as a function of energy and angle: Mean distance = 108 m (see Section 6.2.3).*

E_{High} (MeV)	E_{Low} (MeV)	Neutron Importance in Sievert for the Cosine Interval				
		0.0–0.2	0.2–0.4	0.4–0.6	0.6–0.8	0.8–1.0
1.40E+01	1.20E+01	3.46E−21	1.42E−21	8.42E−22	6.86E−22	6.61E−22
1.20E+01	1.00E+01	3.40E−21	1.42E−21	8.32E−22	6.62E−22	6.31E−22
1.00E+01	8.00E+00	3.31E−21	1.42E−21	8.19E−22	6.32E−22	5.64E−22
8.00E+00	7.50E+00	3.49E−21	1.42E−21	7.95E−22	6.08E−22	5.75E−22
7.50E+00	7.00E+00	3.48E−21	1.42E−21	7.95E−22	6.02E−22	5.63E−22
7.00E+00	6.50E+00	3.47E−21	1.43E−21	7.97E−22	5.98E−22	5.51E−22
6.50E+00	6.00E+00	3.46E−21	1.44E−21	8.02E−22	5.95E−22	5.39E−22
6.00E+00	5.50E+00	3.44E−21	1.46E−21	8.11E−22	5.95E−22	5.21E−22
5.50E+00	5.00E+00	3.43E−21	1.48E−21	8.23E−22	5.97E−22	5.20E−22
5.00E+00	4.50E+00	3.40E−21	1.50E−21	8.36E−22	6.00E−22	5.39E−22
4.50E+00	4.00E+00	3.37E−21	1.52E−21	8.52E−22	6.04E−22	5.25E−22
4.00E+00	3.50E+00	3.32E−21	1.55E−21	8.72E−22	6.12E−22	5.12E−22
3.50E+00	3.00E+00	3.26E−21	1.58E−21	9.01E−22	6.27E−22	5.14E−22
3.00E+00	2.50E+00	3.18E−21	1.62E−21	9.40E−22	6.50E−22	5.06E−22
2.50E+00	2.00E+00	3.07E−21	1.67E−21	9.94E−22	6.88E−22	5.07E−22
2.00E+00	1.50E+00	2.92E−21	1.73E−21	1.07E−21	7.44E−22	5.18E−22
1.50E+00	1.00E+00	2.69E−21	1.79E−21	1.16E−21	8.20E−22	5.46E−22
1.00E+00	4.00E−01	2.60E−21	1.75E−21	1.16E−21	8.43E−22	6.06E−22
4.00E−01	2.00E−01	1.69E−21	1.21E−21	8.52E−22	6.43E−22	5.13E−22
2.00E−01	1.00E−01	8.83E−22	6.58E−22	4.89E−22	3.81E−22	3.28E−22
1.00E−01	1.00E−02	4.34E−23	3.28E−23	2.33E−23	1.96E−23	1.47E−23

TABLE A.7—*Photon importance as a function of energy and angle: Mean distance = 495 m (see Section 6.2.3).*

E_{High} (MeV)	E_{Low} (MeV)	Neutron Importance in Sievert for the Cosine Interval				
		0.0–0.2	0.2–0.4	0.4–0.6	0.6–0.8	0.8–1.0
1.40E+01	1.20E+01	3.45E−22	1.32E−22	4.68E−23	1.62E−23	1.77E−23
1.20E+01	1.00E+01	3.27E−22	1.27E−22	4.58E−23	1.56E−23	1.60E−23
1.00E+01	8.00E+00	3.04E−22	1.20E−22	4.49E−23	1.54E−23	1.36E−23
8.00E+00	7.50E+00	3.11E−22	1.24E−22	4.50E−23	1.42E−23	1.36E−23
7.50E+00	7.00E+00	3.02E−22	1.21E−22	4.42E−23	1.37E−23	1.29E−23
7.00E+00	6.50E+00	2.93E−22	1.18E−22	4.45E−23	1.43E−23	1.22E−23
6.50E+00	6.00E+00	2.83E−22	1.15E−22	4.55E−23	1.41E−23	1.14E−23
6.00E+00	5.50E+00	2.71E−22	1.12E−22	4.47E−23	1.51E−23	1.08E−23
5.50E+00	5.00E+00	2.58E−22	1.08E−22	4.40E−23	1.61E−23	1.03E−23
5.00E+00	4.50E+00	2.43E−22	1.03E−22	4.33E−23	1.60E−23	9.65E−24
4.50E+00	4.00E+00	2.26E−22	9.82E−23	4.23E−23	1.55E−23	9.56E−24
4.00E+00	3.50E+00	2.07E−22	9.21E−23	4.11E−23	1.78E−23	8.87E−24
3.50E+00	3.00E+00	1.85E−22	8.48E−23	3.95E−23	1.90E−23	8.21E−24
3.00E+00	2.50E+00	1.60E−22	7.61E−23	3.73E−23	1.94E−23	7.60E−24
2.50E+00	2.00E+00	1.32E−22	6.56E−23	3.43E−23	1.98E−23	8.60E−24
2.00E+00	1.50E+00	1.00E−22	5.30E−23	3.00E−23	1.93E−23	8.73E−24
1.50E+00	1.00E+00	6.64E−23	3.85E−23	2.42E−23	1.75E−23	8.67E−24
1.00E+00	4.00E−01	3.48E−23	2.33E−23	1.57E−23	1.20E−23	6.54E−24
4.00E−01	2.00E−01	7.50E−24	5.88E−24	4.45E−24	3.71E−24	2.55E−24
2.00E−01	1.00E−01	1.67E−24	1.45E−24	1.20E−24	1.08E−24	8.65E−25
1.00E−01	1.00E−02	1.32E−29	1.03E−29	6.95E−30	4.91E−30	3.79E−30

TABLE A.8—*Photon importance as a function of energy and angle: Mean distance = 1,005 m (see Section 6.2.3).*

E_{High} (MeV)	E_{Low} (MeV)	Neutron Importance in Sievert for the Cosine Interval				
		0.0–0.2	0.2–0.4	0.4–0.6	0.6–0.8	0.8–1.0
1.40E+01	1.20E+01	5.00E−23	1.70E−23	3.62E−24	3.90E−25	5.10E−26
1.20E+01	1.00E+01	4.50E−23	1.53E−23	3.58E−24	3.94E−25	4.90E−26
1.00E+01	8.00E+00	3.88E−23	1.34E−23	3.32E−24	4.70E−25	4.43E−26
8.00E+00	7.50E+00	3.68E−23	1.34E−23	3.35E−24	4.79E−25	4.40E−26
7.50E+00	7.00E+00	3.46E−23	1.26E−23	3.21E−24	4.93E−25	4.44E−26
7.00E+00	6.50E+00	3.23E−23	1.19E−23	3.09E−24	4.79E−25	4.21E−26
6.50E+00	6.00E+00	2.97E−23	1.10E−23	2.92E−24	4.63E−25	4.15E−26
6.00E+00	5.50E+00	2.70E−23	1.01E−23	2.89E−24	4.43E−25	3.78E−26
5.50E+00	5.00E+00	2.41E−23	9.13E−24	2.69E−24	4.18E−25	3.72E−26
5.00E+00	4.50E+00	2.11E−23	8.12E−24	2.50E−24	4.04E−25	3.66E−26
4.50E+00	4.00E+00	1.81E−23	7.08E−24	2.29E−24	3.92E−25	3.34E−26
4.00E+00	3.50E+00	1.50E−23	5.97E−24	2.01E−24	4.18E−25	3.10E−26
3.50E+00	3.00E+00	1.18E−23	4.83E−24	1.72E−24	4.33E−25	4.28E−26
3.00E+00	2.50E+00	8.70E−24	3.68E−24	1.40E−24	4.35E−25	5.40E−26
2.50E+00	2.00E+00	5.82E−24	2.55E−24	1.06E−24	4.04E−25	7.67E−26
2.00E+00	1.50E+00	3.33E−24	1.54E−24	7.11E−25	3.34E−25	1.12E−25
1.50E+00	1.00E+00	1.48E−24	7.41E−25	3.96E−25	2.31E−25	1.09E−25
1.00E+00	4.00E−01	3.56E−25	2.51E−25	1.65E−25	1.12E−25	5.97E−26
4.00E−01	2.00E−01	1.76E−26	1.54E−26	1.19E−26	9.54E−27	6.48E−27
2.00E−01	1.00E−01	1.68E−27	1.66E−27	1.45E−27	1.32E−27	1.08E−27
1.00E−01	1.00E−02	2.28E−38	1.57E−38	1.05E−38	6.94E−39	5.84E−39

Appendix B

Kinematic Relations

At particle accelerators, special relativity becomes an important consideration in calculating the orbits of particles, their momenta, transit times, and other quantities which sometimes need to be understood by the health physicist. In this Appendix, the important facts of special relativity are presented along with tabulations of representative values for various species of charged particles which might be encountered at accelerators.

According to special relativity, the total energy (E) is related to the kinetic energy (T) and the rest energy m_0c^2 through the following equations:

$$E = T + m_0c^2 \text{ and } E = \gamma m_0c^2, \tag{B.1}$$

with the quantity γ related to the velocity of the particle by:

$$\gamma = \frac{1}{\sqrt{1 - \beta^2}}, \quad \text{where } \beta = v/c. \tag{B.2}$$

In the above, v is the particle velocity in the reference frame at rest in the laboratory and c is the speed of light. Thus, γ is related to T by:

$$\gamma = 1 + \frac{T}{m_0c^2}, \tag{B.3}$$

where T and the rest energy are in consistent units, usually chosen for convenience to be mega-electron volts (MeV) or multiples thereof [giga-electron volt (GeV), tera-electron volt (TeV), etc.]. Obviously, β is given by:

$$\beta = \frac{\sqrt{\gamma^2 - 1}}{\gamma}. \tag{B.4}$$

To obtain momentum (p) as a function of kinetic energy, one must use the equation:

390

$$E^2 = p^2c^2 + (m_0c^2)^2, \tag{B.5}$$

and along with Equation B.1 to get:

$$pc = (T^2 + 2\ Tm_0c^2)^{1/2}. \tag{B.6}$$

For convenience, the following Tables B.1 through B.13 give values of momentum (p) in MeV c^{-1} and gamma and beta as functions of kinetic energy in mega-electron volts for protons, ions (deuterons to ^{238}U), pions, kaons, electrons, and muons. The kinetic energy per nucleon (T/A) is also given for the nuclear ions. In each table, the rest-mass energy of the particle is given explicitly in the heading.

TABLE B.1—*Protons*.

Rest Mass (MeV)	T/A (MeV A⁻¹)	T (MeV)	Momentum (MeV c⁻¹)	Beta (v c⁻¹)	Gamma (1 − β²)⁻¹ᐟ²
938.2723	1.00E+00	1.00E+00	4.3330643E+01	0.0461321416	1.0010658E+00
938.2723	2.00E+00	2.00E+00	6.1295099E+01	0.0651886686	1.0021316E+00
938.2723	5.00E+00	5.00E+00	9.6993417E+01	0.1028265298	1.0053289E+00
938.2723	1.00E+01	1.00E+01	1.3735154E+02	0.1448439880	1.0106579E+00
938.2723	2.00E+01	2.00E+01	1.9475855E+02	0.2032392546	1.0213158E+00
938.2723	5.00E+01	5.00E+01	3.1036628E+02	0.3140493603	1.0532894E+00
938.2723	1.00E+02	1.00E+02	4.4458347E+02	0.4281954435	1.1065789E+00
938.2723	2.00E+02	2.00E+02	6.4444466E+02	0.5661603644	1.2131577E+00
938.2723	5.00E+02	5.00E+02	1.0900790E+03	0.7579086615	1.5328943E+00
938.2723	1.00E+03	1.00E+03	1.6960379E+03	0.8750256155	2.0657887E+00
938.2723	2.00E+03	2.00E+03	2.7844370E+03	0.9476442884	3.1315774E+00
938.2723	5.00E+03	5.00E+03	5.8636783E+03	0.9874384309	6.3289434E+00
938.2723	1.00E+04	1.00E+04	1.0897956E+04	0.9963142028	1.1657887E+01
938.2723	2.00E+04	2.00E+04	2.0917239E+04	0.9989954668	2.2315774E+01
938.2723	5.00E+04	5.00E+04	5.0929630E+04	0.9998303413	5.4289434E+01
938.2723	1.00E+05	1.00E+05	1.0093391E+05	0.9999567959	1.0757887E+02
938.2723	2.00E+05	2.00E+05	2.0093608E+05	0.9999890980	2.1415774E+02
938.2723	5.00E+05	5.00E+05	5.0093739E+05	0.9999982459	5.3389434E+02
938.2723	1.00E+06	1.00E+06	1.0009378E+06	0.9999995606	1.0667887E+03
938.2723	2.00E+06	2.00E+06	2.0009381E+06	0.9999998901	2.1325774E+03
938.2723	5.00E+06	5.00E+06	5.0009382E+06	0.9999999824	5.3294434E+03
938.2723	1.00E+07	1.00E+07	1.0000938E+07	0.9999999956	1.0658887E+04
938.2723	2.00E+07	2.00E+07	2.0000938E+07	0.9999999989	2.1316774E+04

TABLE B.2—*Deuterons*.

Rest Mass (MeV)	T/A (MeV A^{-1})	T (MeV)	Momentum (MeV c^{-1})	Beta (v c^{-1})	Gamma (1 − β^2)$^{-1/2}$
1875.613	1.00E+00	2.00E+00	8.6639783E+01	0.0461435786	1.0010663E+00
1875.613	2.00E+00	4.00E+00	1.2255980E+02	0.0652048042	1.0021326E+00
1875.613	5.00E+00	1.00E+01	1.9393880E+02	0.1028518603	1.0053316E+00
1875.613	1.00E+01	2.00E+01	2.7463525E+02	0.1448793868	1.0106632E+00
1875.613	2.00E+01	4.00E+01	3.8942142E+02	0.2032881469	1.0213264E+00
1875.613	5.00E+01	1.00E+02	6.2058247E+02	0.3141214744	1.0533159E+00
1875.613	1.00E+02	2.00E+02	8.8895737E+02	0.4282866637	1.1066318E+00
1875.613	2.00E+02	4.00E+02	1.2886002E+03	0.5662650770	1.2132636E+00
1875.613	5.00E+02	1.00E+03	2.1797307E+03	0.7580055860	1.5331590E+00
1875.613	1.00E+03	2.00E+03	3.3915265E+03	0.8750942109	2.0663181E+00
1875.613	2.00E+03	4.00E+03	5.5682047E+03	0.9476806484	3.1326361E+00
1875.613	5.00E+03	1.00E+04	1.1726562E+04	0.9874489979	6.3315903E+00
1875.613	1.00E+04	2.00E+04	2.1795057E+04	0.9963175541	1.1663181E+01
1875.613	2.00E+04	4.00E+04	4.1833587E+04	0.9989964198	2.2326361E+01
1875.613	5.00E+04	1.00E+05	1.0185835E+05	0.9998305066	5.4315903E+01
1875.613	1.00E+05	2.00E+05	2.0186690E+05	0.9999568383	1.0763181E+02
1875.613	2.00E+05	4.00E+05	4.0187124E+05	0.9999891088	2.1426361E+02
1875.613	5.00E+05	1.00E+06	1.0018739E+06	0.9999982476	5.3415903E+02

TABLE B.3—*Helium-3.*

Rest Mass (MeV)	T/A (MeV A^{-1})	T (MeV)	Momentum (MeV c^{-1})	Beta (v c^{-1})	Gamma (1 − β^2)$^{-1/2}$
2809.436	5.00E+00	1.50E+01	2.9070273E+02	0.1029241713	1.0053391E+00
2809.436	1.00E+01	3.00E+01	4.1166268E+02	0.1449804389	1.0106783E+00
2809.436	2.00E+01	6.00E+01	5.8372281E+02	0.2034277157	1.0213566E+00
2809.436	5.00E+01	1.50E+02	9.3023158E+02	0.3143273191	1.0533915E+00
2809.436	1.00E+02	3.00E+02	1.3325395E+03	0.4285470196	1.1067830E+00
2809.436	2.00E+02	6.00E+02	1.9316633E+03	0.5665638905	1.2135660E+00
2809.436	5.00E+02	1.50E+03	3.2677680E+03	0.7582820688	1.5339150E+00
2809.436	1.00E+03	3.00E+03	5.0849401E+03	0.8752898074	2.0678300E+00
2809.436	2.00E+03	6.00E+03	8.3494450E+03	0.9477842862	3.1356600E+00
2809.436	5.00E+03	1.50E+04	1.7586446E+04	0.9874791047	6.3391499E+00
2809.436	1.00E+04	3.00E+04	3.2688930E+04	0.9963271004	1.1678300E+01
2809.436	2.00E+04	6.00E+04	6.2746572E+04	0.9989991341	2.2356600E+01
2809.436	5.00E+04	1.50E+05	1.5278361E+05	0.9998309775	5.4391499E+01
2809.436	1.00E+05	3.00E+05	3.0279640E+05	0.9999569593	1.0778300E+02
2809.436	2.00E+05	6.00E+05	6.0280289E+05	0.9999891395	2.1456600E+02
2809.436	5.00E+05	1.50E+06	1.5028068E+06	0.9999982526	5.3491499E+02

TABLE B.4—*Helium-4.*

Rest Mass (MeV)	T/A (MeV A^{-1})	T (MeV)	Momentum (MeV c^{-1})	Beta ($v\,c^{-1}$)	Gamma $(1 - \beta^2)^{-1/2}$
3728.431	1.00E+00	4.00E+00	1.7275256E+02	0.0462841947	1.0010728E+00
3728.431	2.00E+00	8.00E+00	2.4437450E+02	0.0654031881	1.0021457E+00
3728.431	5.00E+00	2.00E+01	3.8670045E+02	0.1031632842	1.0053642E+00
3728.431	1.00E+01	4.00E+01	5.4760796E+02	0.1453145784	1.0107284E+00
3728.431	2.00E+01	8.00E+01	7.7649788E+02	0.2038891821	1.0214567E+00
3728.431	5.00E+01	2.00E+02	1.2374863E+03	0.3150077787	1.0536419E+00
3728.431	1.00E+02	4.00E+02	1.7727788E+03	0.4294074033	1.1072837E+00
3728.431	2.00E+02	8.00E+02	2.5701147E+03	0.5675508152	1.2145675E+00
3728.431	5.00E+02	2.00E+03	4.3489911E+03	0.7591941227	1.5364187E+00
3728.431	1.00E+03	4.00E+03	6.7695973E+03	0.8759342393	2.0728373E+00
3728.431	2.00E+03	8.00E+03	1.1120022E+04	0.9481253121	3.1456747E+00
3728.431	5.00E+03	2.00E+04	2.3433677E+04	0.9875780440	6.3641867E+00
3728.431	1.00E+04	4.00E+04	4.3569192E+04	0.9963584531	1.1728373E+01
3728.431	2.00E+04	8.00E+04	8.3645376E+04	0.9990080455	2.2456747E+01
3728.431	5.00E+04	2.00E+05	2.0369431E+05	0.9998325229	5.4641867E+01
3728.431	1.00E+05	4.00E+05	4.0371121E+05	0.9999573565	1.0828373E+02
3728.431	2.00E+05	8.00E+05	8.0371978E+05	0.9999892402	2.1556747E+02
3728.431	5.00E+05	2.00E+06	2.0037250E+06	0.9999982688	5.3741867E+02

TABLE B.5—*Lithium-6.*

Rest Mass (MeV)	T/A (MeV A^{-1})	T (MeV)	Momentum (MeV c^{-1})	Beta ($v\,c^{-1}$)	Gamma $(1 - \beta^2)^{-1/2}$
5603.096	1.00E + 00	6.00E + 00	2.5937068E + 02	0.0462410849	1.0010708E + 00
5603.096	2.00E + 00	1.20E + 01	3.6690367E + 02	0.0653423684	1.0021417E + 00
5603.096	5.00E + 00	3.00E + 01	5.8059087E + 02	0.1030678106	1.0053542E + 00
5603.096	1.00E + 01	6.00E + 01	8.2217487E + 02	0.1451811645	1.0107084E + 00
5603.096	2.00E + 01	1.20E + 02	1.1658229E + 03	0.2037049357	1.0214167E + 00
5603.096	5.00E + 01	3.00E + 02	1.8579175E + 03	0.3147361222	1.0535418E + 00
5603.096	1.00E + 02	6.00E + 02	2.6615250E + 03	0.4296639668	1.1070837E + 00
5603.096	2.00E + 02	1.20E + 03	3.8584233E + 03	0.5671569687	1.2141673E + 00
5603.096	5.00E + 02	3.00E + 03	6.5282904E + 03	0.7588303600	1.5354183E + 00
5603.096	1.00E + 03	6.00E + 03	1.0160568E + 04	0.8756773613	2.0708366E + 00
5603.096	2.00E + 03	1.20E + 04	1.6687549E + 04	0.9479894543	3.1416731E + 00
5603.096	5.00E + 03	3.00E + 04	3.5159433E + 04	0.9875386523	6.3541828E + 00
5603.096	1.00E + 04	6.00E + 04	6.5363381E + 04	0.9963459739	1.1708366E + 01
5603.096	2.00E + 04	1.20E + 05	1.2547806E + 05	0.9990044991	2.2416731E + 01
5603.096	5.00E + 04	3.00E + 05	3.0555173E + 05	0.9998319080	5.4541828E + 01
5603.096	1.00E + 05	6.00E + 05	6.0557718E + 05	0.9999571985	1.0808366E + 02
5603.096	2.00E + 05	1.20E + 06	1.2055901E + 06	0.9999892001	2.1516731E + 02
5603.096	5.00E + 05	3.00E + 06	3.0055979E + 06	0.9999982623	5.3641828E + 02

TABLE B.6—*Carbon-12*.

Rest Mass (MeV)	T/A (MeV A^{-1})	T (MeV)	Momentum (MeV c^{-1})	Beta ($v\,c^{-1}$)	Gamma $(1 - \beta^2)^{-1/2}$
11178.02	1.00E+00	1.20E+01	5.1808926E+02	0.0462992254	1.0010735E+00
11178.02	2.00E+00	2.40E+01	7.3285537E+02	0.0654243937	1.0021471E+00
11178.02	5.00E+00	6.00E+01	1.1597251E+03	0.1031965720	1.0053677E+00
11178.02	1.00E+01	1.20E+02	1.6422925E+03	0.1453610937	1.0107354E+00
11178.02	2.00E+01	2.40E+02	2.3287442E+03	0.2039534185	1.0214707E+00
11178.02	5.00E+01	6.00E+02	3.7112833E+03	0.3151024821	1.0536768E+00
11178.02	1.00E+02	1.20E+03	5.3166952E+03	0.4295271145	1.1073535E+00
11178.02	2.00E+02	2.40E+03	7.7080799E+03	0.5676880662	1.2147071E+00
11178.02	5.00E+02	6.00E+03	1.3043628E+04	0.7593208257	1.5367677E+00
11178.02	1.00E+03	1.20E+04	2.0304494E+04	0.8760236674	2.0735354E+00
11178.02	2.00E+03	2.40E+04	3.3354834E+04	0.9481725843	3.1470708E+00
11178.02	5.00E+03	6.00E+04	7.0294825E+04	0.9875917431	6.3676769E+00
11178.02	1.00E+04	1.20E+05	1.3070090E+05	0.9963627919	1.1735354E+01
11178.02	2.00E+04	2.40E+05	2.5092917E+05	0.9990092783	2.2470708E+01
11178.02	5.00E+04	6.00E+05	6.1107579E+05	0.9998327367	5.4676769E+01
11178.02	1.00E+05	1.20E+06	1.2111264E+06	0.9999574114	1.0835354E+02
11178.02	2.00E+05	2.40E+06	2.4111521E+06	0.9999892541	2.1570708E+02
11178.02	5.00E+05	6.00E+06	6.0111676E+06	0.9999982711	5.3776769E+02

TABLE B.7—*Iron-56.*

Rest Mass (MeV)	T/A (MeV A^{-1})	T (MeV)	Momentum (MeV c^{-1})	Beta (v c^{-1})	Gamma (1 − β^2)$^{-1/2}$
52103.49	1.00E + 00	5.60E + 01	2.4163458E + 03	0.0463261004	1.0010748E + 00
52103.49	2.00E + 00	1.12E + 02	3.4181465E + 03	0.0654623090	1.0021496E + 00
52103.49	5.00E + 00	2.80E + 02	5.4089143E + 03	0.1032560898	1.0053739E + 00
52103.49	1.00E + 01	5.60E + 02	7.6596024E + 03	0.1454442611	1.0107478E + 00
52103.49	2.00E + 01	1.12E + 03	1.0861225E + 04	0.2040682680	1.0214957E + 00
52103.49	5.00E + 01	2.80E + 03	1.7309522E + 04	0.3152717937	1.0537392E + 00
52103.49	1.00E + 02	5.60E + 03	2.4797562E + 04	0.4297411151	1.1074784E + 00
52103.49	2.00E + 02	1.12E + 04	3.5952165E + 04	0.5679333811	1.2149568E + 00
52103.49	5.00E + 02	2.80E + 04	6.0842382E + 04	0.7595472050	1.5373920E + 00
52103.49	1.00E + 03	5.60E + 04	9.4718482E + 04	0.8761833892	2.0747840E + 00
52103.49	2.00E + 03	1.12E + 05	1.5561228E + 05	0.9482569824	3.1495681E + 00
52103.49	5.00E + 03	2.80E + 05	3.2799078E + 05	0.9876161916	6.3739202E + 00
52103.49	1.00E + 04	5.60E + 05	6.0988188E + 05	0.9963705337	1.1747840E + 01
52103.49	2.00E + 04	1.12E + 06	1.1709448E + 06	0.9990114778	2.2495681E + 01
52103.49	5.00E + 04	2.80E + 06	2.8516275E + 06	0.9998331181	5.4739202E + 01
52103.49	1.00E + 05	5.60E + 06	5.6518633E + 06	0.9999575094	1.0847840E + 02
52103.49	2.00E + 05	1.12E + 07	1.1251983E + 07	0.9999892789	2.1595681E + 02
52103.49	5.00E + 05	2.80E + 07	2.8052055E + 07	0.9999982751	5.3839202E + 02

TABLE B.8—*Lead-208*.

Rest Mass (MeV)	T/A (MeV A^{-1})	T (MeV)	Momentum (MeV c^{-1})	Beta ($v\,c^{-1}$)	Gamma $(1 - \beta^2)^{-1/2}$
193730.6	1.00E + 00	2.08E + 02	8.9797101E + 03	0.0463018198	1.0010737E + 00
193730.6	2.00E + 00	4.16E + 02	1.2702634E + 04	0.0654280538	1.0021473E + 00
193730.6	5.00E + 00	1.04E + 03	2.0100777E + 04	0.1032023175	1.0053683E + 00
193730.6	1.00E + 01	2.08E + 03	2.8464815E + 04	0.1453691223	1.0107366E + 00
193730.6	2.00E + 01	4.16E + 03	4.0362658E + 04	0.2039645056	1.0214731E + 00
193730.6	5.00E + 01	1.04E + 04	6.4325395E + 04	0.3151188273	1.0536828E + 00
193730.6	1.00E + 02	2.08E + 04	9.2151142E + 04	0.4295477752	1.1073656E + 00
193730.6	2.00E + 02	4.16E + 04	1.3359995E + 05	0.5677117523	1.2147312E + 00
193730.6	5.00E + 02	1.04E + 05	2.2607955E + 05	0.7593426881	1.5368279E + 00
193730.6	1.00E + 03	2.08E + 05	3.5193171E + 05	0.8760390957	2.0736559E + 00
193730.6	2.00E + 03	4.16E + 05	5.7813481E + 05	0.9481807385	3.1473118E + 00
193730.6	5.00E + 03	1.04E + 06	1.2184251E + 06	0.9875941058	6.3682795E + 00
193730.6	1.00E + 04	2.08E + 06	2.2654623E + 06	0.9963635401	1.1736559E + 01
193730.6	2.00E + 04	4.16E + 06	4.3494182E + 06	0.9990094909	2.2473118E + 01
193730.6	5.00E + 04	1.04E + 07	1.0591959E + 07	0.9998327736	5.4682795E + 01
193730.6	1.00E + 05	2.08E + 07	2.0992837E + 07	0.9999574209	1.0836559E + 02
193730.6	2.00E + 05	4.16E + 07	4.1793282E + 07	0.9999892565	2.1573118E + 02
193730.6	5.00E + 05	1.04E + 08	1.0419355E + 08	0.9999982714	5.3782795E + 02

TABLE B.9—*Uranium-238*.

Rest Mass (MeV)	T/A (MeV A^{-1})	T (MeV)	Momentum (MeV c^{-1})	Beta ($v\,c^{-1}$)	Gamma $(1 - \beta^2)^{-1/2}$
221744.7	1.00E + 00	2.38E + 02	1.0276533E + 04	0.0462942948	1.0010733E + 00
221744.7	2.00E + 00	4.76E + 02	1.4537109E + 04	0.0654174374	1.0021466E + 00
221744.7	5.00E + 00	1.19E + 03	2.3003662E + 04	0.1031856523	1.0053665E + 00
221744.7	1.00E + 01	2.38E + 03	3.2575592E + 04	0.1453458350	1.0107331E + 00
221744.7	2.00E + 01	4.76E + 03	4.6191635E + 04	0.2039323467	1.0214661E + 00
221744.7	5.00E + 01	1.19E + 04	7.3614767E + 04	0.3150714165	1.0536653E + 00
221744.7	1.00E + 02	2.38E + 04	1.0545846E + 05	0.4294878465	1.1073306E + 00
221744.7	2.00E + 02	4.76E + 04	1.5289165E + 05	0.5676430465	1.2146613E + 00
221744.7	5.00E + 02	1.19E + 05	2.5872039E + 05	0.7592792695	1.5366532E + 00
221744.7	1.00E + 03	2.38E + 05	4.0273375E + 05	0.8759943393	2.0733064E + 00
221744.7	2.00E + 03	4.76E + 05	6.6157158E + 05	0.9481570827	3.1466127E + 00
221744.7	5.00E + 03	1.19E + 06	1.3942211E + 06	0.9875872513	6.3665319E + 00
221744.7	1.00E + 04	2.38E + 06	2.5922779E + 06	0.9963613693	1.1733064E + 01
221744.7	2.00E + 04	4.76E + 06	4.9768072E + 06	0.9990088741	2.2466127E + 01
221744.7	5.00E + 04	1.19E + 07	1.2119716E + 07	0.9998326666	5.4665319E + 01
221744.7	1.00E + 05	2.38E + 07	2.4020721E + 07	0.9999573934	1.0833064E + 02
221744.7	2.00E + 05	4.76E + 07	4.7821231E + 07	0.9999892495	2.1566127E + 02
221744.7	5.00E + 05	1.19E + 08	1.1922154E + 08	0.9999982703	5.3765319E + 02

Table B.10—*Pions.*

Rest Mass (MeV)	T/A (MeV A^{-1})	T (MeV)	Momentum (MeV c^{-1})	Beta ($v\,c^{-1}$)	Gamma $(1-\beta^2)^{-1/2}$
139.5676	1.00E + 00	1.00E + 00	1.6737240E + 01	0.1190689740	1.0071650E + 00
139.5676	2.00E + 00	2.00E + 00	2.3712242E + 01	0.1674976588	1.0143300E + 00
139.5676	5.00E + 00	5.00E + 00	3.7691856E + 01	0.2607213226	1.0358249E + 00
139.5676	1.00E + 01	1.00E + 01	5.3771293E + 01	0.3595116419	1.0716499E + 00
139.5676	2.00E + 01	2.00E + 01	7.7347941E + 01	0.4847346275	1.1432997E + 00
139.5676	5.00E + 01	5.00E + 01	1.2828390E + 02	0.6767185104	1.3582493E + 00
139.5676	1.00E + 02	1.00E + 02	1.9471394E + 02	0.8127724452	1.7164987E + 00
139.5676	2.00E + 02	2.00E + 02	3.0955943E + 02	0.9116282851	2.4329973E + 00
139.5676	5.00E + 02	5.00E + 02	6.2415351E + 02	0.9758991962	4.5824934E + 00
139.5676	1.00E + 03	1.00E + 03	1.1309886E + 03	0.9924717008	8.1649867E + 00
139.5676	2.00E + 03	2.00E + 03	2.1350106E + 03	0.9978701455	1.5329973E + 01
139.5676	5.00E + 03	5.00E + 03	5.1376722E + 03	0.9996312210	3.6824934E + 01
139.5676	1.00E + 04	1.00E + 04	1.0138607E + 04	0.9999052627	7.2649867E + 01
139.5676	2.00E + 04	2.00E + 04	2.0139084E + 04	0.9999759871	1.4429973E + 02
139.5676	5.00E + 04	5.00E + 04	5.0139373E + 04	0.9999961258	3.5924934E + 02
139.5676	1.00E + 05	1.00E + 05	1.0013947E + 05	0.9999990288	7.1749867E + 02
139.5676	2.00E + 05	2.00E + 05	2.0013952E + 05	0.9999997569	1.4339973E + 03
139.5676	5.00E + 05	5.00E + 05	5.0013955E + 05	0.9999999611	3.5834934E + 03
139.5676	1.00E + 06	1.00E + 06	1.0001396E + 06	0.9999999903	7.1659867E + 03
139.5676	2.00E + 06	2.00E + 06	2.0001396E + 06	0.9999999976	1.4330973E + 04
139.5676	5.00E + 06	5.00E + 06	5.0001396E + 06	0.9999999996	3.5825934E + 04
139.5676	1.00E + 07	1.00E + 07	1.0000140E + 07	0.9999999999	7.1650867E + 04
139.5676	2.00E + 07	2.00E + 07	2.0000140E + 07	1.0000000000	1.4330073E + 05

TABLE B.11—*Kaons.*

Rest Mass (MeV)	T/A (MeV A^{-1})	T (MeV)	Momentum (MeV c^{-1})	Beta ($v\,c^{-1}$)	Gamma $(1-\beta^2)^{-1/2}$
493.646	1.00E + 00	1.00E + 00	3.1437112E + 01	0.0635547681	1.0020257E + 00
493.646	2.00E + 00	2.00E + 00	4.4481277E + 01	0.0897440451	1.0040515E + 00
493.646	5.00E + 00	5.00E + 00	7.0437632E + 01	0.1412577901	1.0101287E + 00
493.646	1.00E + 01	1.00E + 01	9.9864508E + 01	0.1982831358	1.0202574E + 00
493.646	2.00E + 01	2.00E + 01	1.4193604E + 02	0.2763304726	1.0405149E + 00
493.646	5.00E + 01	5.00E + 01	2.2773801E + 02	0.4189086416	1.1012872E + 00
493.646	1.00E + 02	1.00E + 02	3.2974111E + 02	0.5554507410	1.2025743E + 00
493.646	2.00E + 02	2.00E + 02	4.8729703E + 02	0.7025154541	1.4051486E + 00
493.646	5.00E + 02	5.00E + 02	8.6234912E + 02	0.8678635221	2.0128716E + 00
493.646	1.00E + 03	1.00E + 03	1.4097134E + 03	0.9438069302	3.0257431E + 00
493.646	2.00E + 03	2.00E + 03	2.4442962E + 03	0.9802097883	5.0514863E + 00
493.646	5.00E + 03	5.00E + 03	5.4714221E + 03	0.9959546208	1.1128716E + 01
493.646	1.00E + 04	1.00E + 04	1.0482028E + 04	0.9988928948	2.1257431E + 01
493.646	2.00E + 04	2.00E + 04	2.0487700E + 04	0.9997098478	4.1514863E + 01
493.646	5.00E + 04	5.00E + 04	5.0491233E + 04	0.9999522099	1.0228716E + 02
493.646	1.00E + 05	1.00E + 05	1.0049243E + 05	0.9999879350	2.0357431E + 02
493.646	2.00E + 05	2.00E + 05	2.0049304E + 05	0.9999969689	4.0614863E + 02
493.646	5.00E + 05	5.00E + 05	5.0049340E + 05	0.9999995136	1.0138716E + 03
493.646	1.00E + 06	1.00E + 06	1.0004935E + 06	0.9999998783	2.0267431E + 03
493.646	2.00E + 06	2.00E + 06	2.0004936E + 06	0.9999999696	4.0524863E + 03
493.646	5.00E + 06	5.00E + 06	5.0004936E + 06	0.9999999951	1.0129716E + 04
493.646	1.00E + 07	1.00E + 07	1.0000494E + 07	0.9999999988	2.0258431E + 04
493.646	2.00E + 07	2.00E + 07	2.0000494E + 07	0.9999999997	4.0515863E + 04

TABLE B.12—*Electrons.*

Rest Mass (MeV)	T/A (MeV A⁻¹)	T (MeV)	Momentum (MeV c^{-1})	Beta ($v\,c^{-1}$)	Gamma $(1 - \beta^2)^{-1/2}$
0.51099906	1.00E+00	1.00E+00	1.4219698E+00	0.9410792107	2.9569508E+00
0.51099906	2.00E+00	2.00E+00	2.4584540E+00	0.9790740561	4.9139015E+00
0.51099906	5.00E+00	5.00E+00	5.4872571E+00	0.9956918974	1.0784754E+01
0.51099906	1.00E+01	1.00E+01	1.0498570E+01	0.9988175602	2.0569508E+01
0.51099906	2.00E+01	2.00E+01	2.0504633E+01	0.9996896127	4.0139015E+01
0.51099906	5.00E+01	5.00E+01	5.0508414E+01	0.9999488260	9.8847538E+01
0.51099906	1.00E+02	1.00E+02	1.0050970E+02	0.9999870763	1.9669508E+02
0.51099906	2.00E+02	2.00E+02	2.0051035E+02	0.9999967526	3.9239015E+02
0.51099906	5.00E+02	5.00E+02	5.0051074E+02	0.9999994788	9.7947538E+02
0.51099906	1.00E+03	1.00E+03	1.0005109E+03	0.9999998696	1.9579508E+03
0.51099906	2.00E+03	2.00E+03	2.0005109E+03	0.9999999674	3.9149015E+03
0.51099906	5.00E+03	5.00E+03	5.0005110E+03	0.9999999948	9.7857538E+03
0.51099906	1.00E+04	1.00E+04	1.0000511E+04	0.9999999987	1.9570508E+04
0.51099906	2.00E+04	2.00E+04	2.0000511E+04	0.9999999997	3.9140015E+04
0.51099906	5.00E+04	5.00E+04	5.0000511E+04	0.9999999999	9.7848538E+04
0.51099906	1.00E+05	1.00E+05	1.0000051E+05	1.0000000000	1.9569608E+05
0.51099906	2.00E+05	2.00E+05	2.0000051E+05	1.0000000000	3.9139115E+05
0.51099906	5.00E+05	5.00E+05	5.0000051E+05	1.0000000000	9.7847638E+05
0.51099906	1.00E+06	1.00E+06	1.0000005E+06	1.0000000000	1.9569518E+06
0.51099906	2.00E+06	2.00E+06	2.0000005E+06	1.0000000000	3.9139025E+06
0.51099906	5.00E+06	5.00E+06	5.0000005E+06	1.0000000000	9.7847548E+06
0.51099906	1.00E+07	1.00E+07	1.0000001E+07	1.0000000000	1.9569509E+07
0.51099906	2.00E+07	2.00E+07	2.0000001E+07	1.0000000000	3.9139016E+07

TABLE B.13—*Muons*.

Rest Mass (MeV)	T/A (MeV A^{-1})	T (MeV)	Momentum (MeV c^{-1})	Beta (v c^{-1})	Gamma $(1 - \beta^2)^{-1/2}$
105.658387	1.00E + 00	1.00E + 00	1.4571094E + 01	0.1366146085	1.0094645E + 00
105.658387	2.00E + 00	2.00E + 00	2.0655109E + 01	0.1918578762	1.0189289E + 00
105.658387	5.00E + 00	5.00E + 00	3.2887442E + 01	0.2971979199	1.0473223E + 00
105.658387	1.00E + 01	1.00E + 01	4.7044317E + 01	0.4067523159	1.0946446E + 00
105.658387	2.00E + 01	2.00E + 01	6.8017170E + 01	0.5412863566	1.1892893E + 00
105.658387	5.00E + 01	5.00E + 01	1.1430590E + 02	0.7343381997	1.4732232E + 00
105.658387	1.00E + 02	1.00E + 02	1.7644171E + 02	0.8579358889	1.9464464E + 00
105.658387	2.00E + 02	2.00E + 02	2.8681589E + 02	0.9383543926	2.8928928E + 00
105.658387	5.00E + 02	5.00E + 02	5.9637101E + 02	0.9846656587	5.7322320E + 00
105.658387	1.00E + 03	1.00E + 03	1.1005984E + 03	0.9954235267	1.0464464E + 01
105.658387	2.00E + 03	2.00E + 03	2.1030058E + 03	0.9987402750	1.9928928E + 01
105.658387	5.00E + 03	5.00E + 03	5.1045650E + 03	0.9997858486	4.8322320E + 01
105.658387	1.00E + 04	1.00E + 04	1.0105106E + 04	0.9999453411	9.5644640E + 01
105.658387	2.00E + 04	2.00E + 04	2.0105381E + 04	0.9999861916	1.9028928E + 02
105.658387	5.00E + 04	5.00E + 04	5.0105547E + 04	0.9999977767	4.7422320E + 02
105.658387	1.00E + 05	1.00E + 05	1.0010560E + 05	0.9999994430	9.4744640E + 02
105.658387	2.00E + 05	2.00E + 05	2.0010563E + 05	0.9999998606	1.8938928E + 03
105.658387	5.00E + 05	5.00E + 05	5.0010565E + 05	0.9999999777	4.7332320E + 03
105.658387	1.00E + 06	1.00E + 06	1.0001057E + 06	0.9999999944	9.4654640E + 03
105.658387	2.00E + 06	2.00E + 06	2.0001057E + 06	0.9999999986	1.8929928E + 04
105.658387	5.00E + 06	5.00E + 06	5.0001057E + 06	0.9999999998	4.7323320E + 04
105.658387	1.00E + 07	1.00E + 07	1.0000106E + 07	0.9999999999	9.4645640E + 04
105.658387	2.00E + 07	2.00E + 07	2.0000106E + 07	1.0000000000	1.8929028E + 05

Glossary

The following definitions are given to clarify the contents of this Report. The recommended quantities of NCRP, ICRP and ICRU are continually being reviewed. It is recommended that the reader consult current recommendations of these bodies for further details.

absorbed dose (*D*): The quotient of $d\bar{\epsilon}$ by dm where $d\bar{\epsilon}$ is the mean energy imparted by ionizing radiation to matter of mass dm, thus $D = d\bar{\epsilon}/dm$. The special name for the unit of absorbed dose is the gray (Gy).

absorption: A phenomenon in which some or all of the energy in a beam of radiation is transferred to the matter which it traverses.

accelerator: A device for imparting kinetic energy to charged particles (see also neutron generator, x-ray generator).

activation: The process of inducing radioactivity by irradiation—more accurately radioactivation.

activity: The number of spontaneous nuclear transformations which occur in a quantity of a radioactive nuclide per unit time. The special unit of activity is the becquerel (Bq) in the International System of Units (SI) and the curie (Ci) in the cgs system of units.

albedo: [see reflected (scattered) radiation].

ambient dose equivalent [*H**(*d*)]: The ambient dose equivalent [$H^*(d)$] at a point in a radiation field, is the dose equivalent that would be produced by the corresponding expanded and aligned field, in ICRU sphere at a depth (*d*) on the radius opposing the direction of the aligned field. The unit of ambient dose equivalent in the SI system of units is joule per kilogram (J kg^{-1}) and its special name is the sievert (Sv).

anisotropic: Not isotropic; having different properties in different directions (see also isotropic).

annihilation radiation: The electromagnetic radiation emitted as a result of the combination and disappearance of an electron and a positron. Two gamma rays of 0.511 MeV energy each are emitted in most cases.

area: (see controlled, occupiable, radioactivity areas).

area occupancy factor (T): Used for shielding calculations. A factor (usually ≤1) by which the dose-equivalent rate or neutron fluence rate should be multiplied to correct for the degree of occupancy, relative to a work week (nominally of 40 h), of the area in question while the radiation source is "on" and the barrier protecting the point of interest is being irradiated.

attenuation: The reduction of dose equivalent or other physical properties of a radiation field upon the passage of radiation through matter. This Report is often concerned with broad-beam attenuation that occurs when

405

the area of the radiation field is large at the barrier or shield-face (in contrast to a small diameter beam).

attenuation length (λ): The penetration distance in which the intensity of a radiation beam is attenuated by a factor of e (see tenth-value layer).

back (scattering) reflection: The reflection of radiation in a direction generally greater than 90 degrees to that of the incident radiation.

beam: A flow of electromagnetic or particulate radiation that is either (1) collimated and generally unidirectional or (2) divergent from a small source but restricted to a small-solid angle (charged-particle beam, radiation beam).

becquerel (Bq): The special name for the unit of activity in the SI system of units. 1 Bq = one nuclear transformation per second.

bremsstrahlung: The electromagnetic radiation associated with the acceleration or deceleration of charged particles, particularly in the vicinity of the Coulomb fields of nuclei (see also x ray).

broad-beam conditions: Conditions of a radiation-shielding situation, in which the beam impinging on the shield surface, includes scattered radiation and is laterally extensive.

buildup (of radiation in material): That part of the total value of a specified radiation quantity at any point due to radiation that has undergone interactions in the material or that results from such interactions.

capture gamma ray: A photon emitted as an immediate result of the neutron-capture process.

cgs system: The system of units using centimeters, grams and seconds.

charged particle: An atomic or subatomic quantity of matter (*e.g.*, electron, proton, alpha particle, ionized atom) having a net positive or negative electrical charge of one or more elementary units of charge.

collimate: To reduce the cross-sectional area of a beam of photons or particles.

collimator: Any arrangement of slits or apertures that limits a stream of particles or photons to a beam in which all particles or photons move in the same (or nearly the same) direction.

Compton scattering: The inelastic scattering of a photon by an essentially unbound electron.

concrete (ordinary): Concrete whose constituents are those usually utilized in construction. Thus, ordinary concrete excludes those mixtures where special materials (iron, etc.) have been added to enhance the radiation-shielding properties. For example, the term excludes "heavy concrete."

controlled area: An area, outside a restricted area but inside the site boundary, to which access may be limited for any reason.

conversion coefficient: The quotient of the dose equivalent under specified conditions and the associated field quantity (air kerma or fluence). Conversion coefficients, when given for a range of beam energies (and possibly beam directions), define a conversion function.

curie (Ci): The special unit of activity in the cgs system of units. One curie is exactly 3.7×10^{10} nuclear transformations per second (s^{-1}). Also, the quantity of any radioactive material having an activity of one curie (see also becquerel.)

diaphragm: A device with a central aperture designed to restrict the beam to an appropriate area at the point of interest.

direct radiation: Radiation emitted from the target or source (see also primary radiation).

directional dose equivalent: The directional dose equivalent $[H'(d, \Omega)]$ at a point in a radiation field, is the dose equivalent that would be produced by the corresponding expanded field, in ICRU sphere at depth (d) on a radius in a specified direction (Ω). The unit of directional dose equivalent in the SI system of units is joule per kilogram $(J\,kg^{-1})$ and its special name is the sievert (Sv).

directly ionizing radiation: Charged particles (electrons, protons, alpha particles, etc.) having sufficient kinetic energy to produce ionization by collision.

dose: A colloquial term. For precision, it should be appropriately qualified (see absorbed dose, dose equivalent, dose-equivalent index, effective dose, and equivalent dose).

dose equivalent: The dose equivalent (H) is the product of Q and D at a point in tissue, where D is the absorbed dose and Q is the quality factor at that point, thus $H = QD$. The unit of dose equivalent in the SI system of units is joule per kilogram $(J\,kg^{-1})$ and its special name is the sievert (Sv).

dose-equivalent index (H_I):[42] The maximal dose equivalent within a 30 cm diameter sphere centered at the point of interest and consisting of material equivalent to soft tissue with a density of 1 g cm^{-3}. The outer 0.07 mm-thick shell is ignored. In general, the maximal values of the quality factor (Q) and the absorbed dose (D) occur at different locations in the sphere. However, $Q_{max}D_{max}$ is a conservative estimate for H_I.

duty cycle: The fraction of the operation cycle of an accelerator during which radiation is produced; the product of the pulse duration and the pulse-repetition frequency.

effective dose (ICRP Publication 60): The sum of the weighted equivalent doses in all the tissues and organs of the body. It is given by the expression:

$$E = \sum_T w_T H_T, \tag{G.1}$$

where H_T is the equivalent dose in tissue (T) and ω_T is the weighting factor for tissue (T) (see Table G.3 under tissue weighting factors). The effective dose can also be expressed as the sum of the doubly weighted absorbed dose in all the tissues and organs of the body (paragraph 28 of ICRP, 1991).

effective dose equivalent (ICRP Publication 26):[42] The effective dose equivalent (H_E) is the weighted average of the dose equivalents in tissues or organs (H_T), each weighted by a weighting factor (w_T), thus: $H_E = \Sigma\, w_T H_T$ where H_T is the dose equivalent in tissue (T) and w_T is the tissue weighting factor for tissue (T) recommended in ICRP Publication 26 (see Table G.4 under tissue weighting factor).

---

[42] Obsolete quantity included for completeness.

effective dose limits: Recommended limit of the effective dose.

efficiency (of x-ray production): The fraction of electron power incident on a target that is converted to x-ray power.

endoergic; endothermal: Characterized by the absorption of energy or heat. Endoergic reactions absorb energy as they progress. Endothermal reactions absorb heat as they progress.

energy imparted: The energy imparted (ε) by ionizing radiation to matter in a volume, is: $\varepsilon = R_{\text{in}} - R_{\text{out}} + \Sigma Q$ where R_{in} is the radiant energy incident on the volume, *i.e.*, the sum of the energies (excluding rest energies) of all those charged and uncharged ionizing particles which enter the volume, R_{out} is the radiant energy emerging from the volume, *i.e.*, the sum of the energies (excluding rest energies) of all those charged and uncharged ionizing particles which leave the volume, and ΣQ is the sum of all changes of the rest mass energy of nuclei and elementary particles in any interactions which occur in the volume. (In the sum, decreases are denoted by a + sign and increases are denoted by a − sign). The expectation value of ε, termed the *mean energy imparted, $\bar{\varepsilon}$, is closely related to the de nition of absorbed dose.*

equilibrium tenth-value layer (TVL) [or half-value layer (HVL)]: The thickness of a specific material that attenuates a specified radiation by a factor of 10 (or 2), under broad-beam conditions, in that penetration region where the radiation directional and spectral distributions are practically independent of thickness, so that a single value of the TVL (or HVL) is valid. The attenuation length (λ), tenth-value layer (λ_{10}), and the half-value layer (λ_2) are related by the equations:

$$\lambda_{10} = \lambda \ln 10 = 2.3026\,\lambda \text{ and } \lambda_2 = \lambda \ln 2 = 0.6931\,\lambda. \qquad \text{(G.2)}$$

equivalent dose (ICRP Publication 60): A quantity used for radiation-protection purposes that takes into account the different probability of effects which occur with the same absorbed dose delivered by radiations with different radiation weighting factor (w_{R}) values. It is defined as the product of the averaged absorbed dose in a specified organ or tissue (D_{T}) and w_{R}. The unit of equivalent dose in the SI system of units is joules per kilogram (J kg^{-1}) and its special name is the sievert (Sv). Values of radiation weighting factors recommended by ICRP are given in Table G.2 under the definition of radiation weighting factors.

expanded and aligned field: A uniform, unidirectional radiation field with fluence and its energy distribution equal to that of the actual field at the point of reference.

expanded field: Hypothetical radiation field in which the fluence and its angular and energy distributions are the same throughout the volume of interest as in the actual field at the point of reference.

exposure (X): A measure of x- or gamma-ray radiation based upon the ionization produced in air by x rays or gamma rays. The special unit of exposure in the cgs system of units is the roentgen (R). In SI, exposure is measured in units of C kg^{-1}.

extended source (of radiation): A source of particles or photons which cannot be considered a point source, *e.g.*, whose linear dimensions are greater than one-tenth the distance between source and observation point.

face, exit: The surface of the shielding barrier from which attenuated radiation leaves the shielding material.

fail-safe (relating to circuit or system): Having the property that any failure causes a sequence of actions which *always* results in a safe situation.

fast neutrons: Neutrons of energies above a few hundred kilo-electron volts.

fluence, particle (ϕ): The quotient of dN by da, where dN is the number of particles incident on a sphere of cross-sectional area da, thus: $\phi = $ dN/da. Fluence is usually expressed in cm^{-2}.

fluence rate, particle; flux density ($\dot{\phi}$): The quotient of dϕ by dt, where dϕ is the increment of particle fluence in the time interval dt. $\dot{\phi}$ is usually expressed in cm^{-2} s^{-1}.

gamma ray: Electromagnetic radiation emitted in the process of nuclear transition or radioactive decay.

general public: In the context of this Report, the general mass of the populace not regarded as radiation workers.

gray (Gy): The special unit of absorbed dose is the gray. 1 Gy $= $ 1 J kg^{-1}.

half-life, radioactive: The time for the activity of any particular radioactive nuclide to be reduced to one-half its initial value.

half-value layer (HVL) (or thickness): The thickness of a specified substance which, when introduced into the path of a given beam of radiation, reduces the magnitude of the absorbed dose, dose equivalent, or effective dose quantities by a factor of two. The values of the half-value layer for the particular absorbed dose, dose equivalent, or effective dose quantities of interest may not necessarily be the same (see also equilibrium tenth-value layer).

ICRU sphere: A tissue-equivalent sphere prescribed in ICRU Report 33 (ICRU, 1980) as having a diameter of 30 cm, a composition by mass of 76.2 percent oxygen, 10.1 percent hydrogen, 11.1 percent carbon, and 2.6 percent nitrogen, and density of 1 g cm^{-3}.

individual monitoring: The performance and interpretation of measurements by devices worn by individuals, where such measurements are intended to provide an estimate of the dose equivalent to tissues of the body. The results of individual monitoring are mainly used to confirm the safety of working conditions, to identify unexpected exposures, and to keep records.

interference (in shielding barrier): Discontinuity or void in a shielding barrier, *e.g.*, aperture, piping, ductwork, maze, which tends to reduce the effective thickness of the barrier.

interlock: Device which automatically shuts off or reduces the radiation emission rate from an accelerator to acceptable levels, *e.g.*, when opening the door into a radiation area. In certain applications, an interlock can be used to prevent entry into a radiation area.

ionizing radiation: Any radiation consisting of directly or indirectly ionizing particles or photons or a mixture of both.

irradiation: Exposure to ionizing radiation.

isotropic: A condition in which properties are the same in whatever direction they are measured. With reference to radiation emission, this term

indicates equal emission in all directions from a point source or each differential-size element of any extended source (see also anisotropic).

kerma (K): The quotient of dE_{tr} by dm, where dE_{tr} is the sum of the initial kinetic energies of all the charged ionizing particles liberated by uncharged ionizing particles in a material of mass dm: $K = dE_{tr}/dm$. The unit of kerma in the SI system of units is joule per kilogram (J kg^{-1}) and its special name is the gray (Gy). 1 Gy = 1 J kg^{-1}.

leakage radiation: All radiation, except the useful beam, coming from within the accelerator components, *e.g.*, that radiation that is attenuated by a collimator, diaphragm, or source shielding.

linear energy transfer [LET (L)]: The average energy lost by a directly ionizing particle per unit distance of its travel in a medium.

mean free path (for a given type of interaction, *e.g.*, scattering or absorption): The average distance that particles of a specified type travel before a specified type of interaction takes place in a given medium. If the term *mean free path* is used without specifying the interaction, the term means the average distance a particle will travel before having an interaction of any sort.

monitor, radiation: A radiation-measuring assembly provided with devices intended to draw attention to an event or situation which might result in overexposure to the radiation. The assembly may include indicating and/or recording instruments.

monoenergetic: Possessing a single energy. This term is sometimes used to characterize a radiation field in which the particles or photons have various energies within a narrowly-limited band.

narrow-beam conditions: Conditions of a radiation-shielding situation in which the beam impinging on the shield surface excludes scattered radiation and is laterally restricted.

neutron capture: A process in which a neutron becomes part of the nucleus with which it collides without release of another heavy particle.

neutron generator: A type of accelerator in which the ion beam or the x-ray beam is used mainly for the production of neutrons; *e.g.*, low-voltage deuteron accelerators.

nuclear reaction: An interaction between a photon, particle or nucleus, and a target nucleus, leading to the emission of one or more particles and/or photons.

nuclide: A species of atom having specified numbers of neutrons and protons in its nucleus.

occupational exposure: Exposure of an individual to ionizing radiation in a controlled area or in the course of employment in which the individual's normal duties or authorized activities necessarily involve the likelihood of exposure to ionizing radiation.

occupiable area: Any room or other space, indoors or outdoors, that is likely to be occupied during an irradiation, by any person, either regularly or periodically during the course of the individual's work, habitation or recreation.

operational quantity: A quantity with which, by means of its measurement, compliance with dose limits may be demonstrated. Examples of

operational quantities are ambient dose equivalent, directional dose equivalent, and personal dose equivalent.

organ dose: The mean absorbed dose ($\overline{D}_T$) in a specified tissue or organ of the human body (T) given by $\overline{D}_T = \frac{1}{M_T} \int_{M_T} D\, dm$ where M_T is the mass of tissue or organ, and D is the absorbed dose in the mass element dm.

pair production: The simultaneous production of an electron and a positron by an interaction of a photon or a fast charged particle with the electronic field of a nucleus or other particle.

path length: Total length of the path of a particle moving through a medium, measured along the actual path, whether or not rectilinear.

personal dose equivalent: The personal dose equivalent [$H_p(d)$] is the dose equivalent in soft tissue, at an appropriate depth (d) below a specified point on the body. The unit of personal dose equivalent in the SI system of units is joule per kilogram (J kg^{-1}) and its special name is the sievert (Sv).

photoneutron: A neutron released from a nucleus by a photonuclear reaction.

photodisintegration: Any transformation of a nucleus induced by photons.

photonuclear: Pertaining to the interaction of a photon with a nucleus.

photofission: Fission of a nucleus induced by a photon.

photoelectric effect: The interaction of a photon with an atom, resulting in the absorption of the incident photon and the release of a bound electron from that atom with energy equal to the photon energy less the electron binding energy.

photon: An energy quantum of electromagnetic radiation. In this Report, an x ray or gamma ray.

point source (of radiation): Any radiation source measured from a distance that is much greater than the linear size of the source. In this Report, a source whose linear dimensions are less than 10 percent of the measurement distance may be considered a point source for shielding purposes.

primary radiation: The radiation of earliest origin in the context of the situation considered. For example, electron radiation impinging on a shielding wall may be considered as "primary," from the standpoint of shielding against electrons. The x rays produced from this impingement may be considered as "primary" from the standpoint of shielding against x rays.

protection quantity: A quantity in terms of which dose limits are expressed. Examples of protection quantities are effective dose and organ equivalent dose.

qualified expert on radiation shielding: A person having the knowledge and training to undertake the analysis and design of a radiation-shielding system.

quality factor (Q): A dimensionless quantity used to weight absorbed doses for the biological effectiveness of the charged particles producing the absorbed dose. Quality factor is expressed as a function of linear energy transfer (L) in water. The values of $Q(L)$ as a function of L in ICRP Publication 60 are given by the following relations:

$$Q(L) = 1 \qquad\qquad\qquad L < 10$$
$$Q(L) = 0.32\,L - 2.2 \qquad\quad 10 \leq L \leq 100$$
$$Q(L) = 300\sqrt{L} \qquad\qquad\quad L > 100$$

where L is expressed in keV $\mu\mathrm{m}^{-1}$.

The mean quality factor $(\overline{Q}_T)$ in a specified tissue or organ (T), is given by:

$$\overline{Q}_T = \frac{1}{M_T \overline{D}_T} \int_{M_T} QD \; \mathrm{d}m \qquad\qquad (G.3)$$

where $\overline{D}_T$ is the mean absorbed dose to the tissue or organ, M_T is its mass, and Q and D are the quality factors and the absorbed dose in the mass element $\mathrm{d}m$, respectively. Because $D = \mathrm{d}\overline{\varepsilon}/\mathrm{d}m$, we may write:

$$\overline{Q}_T = \frac{1}{M_T \overline{D}_T} \int_{M_T} Q\left(\frac{\mathrm{d}\overline{\varepsilon}}{\mathrm{d}m}\right) \mathrm{d}m. \qquad\qquad (G.4)$$

Prior to ICRP Publication 60, the recommended values of quality factor (ICRP, 1977) were as shown in Table G.1.

rad: The special unit of absorbed dose in the cgs system of units (1 rad = 100 erg g^{-1}; 10^{-2} joules kg^{-1}).

radiation: Propagation of energy through space. In the context of this Report, electromagnetic radiation (x or gamma rays), or corpuscular radiation (electrons, protons, atomic ions, neutrons, heavy particles), capable of producing ionization, directly or through the production of secondary charged particles.

radiation length: The mean path length required to reduce the energy of a relativistic charged particle by a factor of e, usually denoted by the symbol X_0.

radiation level: The dose-equivalent rate of the radiation field at the point in question.

radiation protection (safety) officer: The person directly responsible for radiation protection.

radiation (protection) survey: An evaluation of the radiation safety in and around an installation.

TABLE G.1—*Recommended values of quality factor in ICRP Publication 26 (ICRP, 1977).*

L in water (keV μm^{-1})	Recommended Value of Quality Factor (Q)
3.5 (and less)	1
7	2
23	5
53	10
175 (and above)	20

radiation weighting factor (w_R): A factor by which the tissue or organ absorbed dose is multiplied to account for the relative health hazard of different types of radiation. Table G.2 gives the values of radiation weighting factor recommended for radiological protection purposes. When calculation of the radiation weighting factors for neutrons requires a continuous function, the following approximation can be used: $w_R = 5 + 17 \exp\{-[\ln(2E)]^2/6\}$, where E is the neutron energy in mega-electron volts. For radiation types and energies not included in Table G.2, w_R can be taken to be equal to $\overline{Q}$ at 10 mm depth in the ICRU sphere and can be obtained from $\overline{Q} = \dfrac{1}{D}\int_L Q(L)D(L)\mathrm{d}L$, where D is the absorbed dose, $Q(L)$ is the quality factor in terms of the unrestricted linear energy transfer (L) in water, specified in ICRP Publication 60, and $\mathrm{d}D/\mathrm{d}L$ is the distribution of D in L.

radioactive contamination: At particle accelerators, it is important to understand that radioactive contamination is substantially different in form than that found in many laboratories that use radioactive materials. At accelerator laboratories, contamination is defined as: a radioactive substance in the form of acquired material, rather than that produced directly by irradiation of an article or substance. In the case of solids, it takes the form of a surface layer, which may, or may not, be readily removed in a process of decontamination.

radioactivity, induced: Radioactivity in nuclides produced by nuclear reactions.

radioactivity area: Any area in which radioactive materials are present.

redundancy (in interlock systems): Repetition; a situation in which two or more systems are designed to perform the same or approximately the same function, thus providing a safety factor in the instance of the failure of one of the systems.

TABLE G.2—*Recommended values for radiation weighting factors in ICRP Publication 60 (ICRP, 1991).*

Radiation	Energy Range	Radiation Weighting Factor (w_R)
Photons	All energies	1
Electrons and muons	All energies[a]	1
Neutrons	<10 keV	5
Neutrons	10 to 100 keV	10
Neutrons	100 keV to 2 MeV	20
Neutrons	2 to 20 MeV	10
Neutrons	>20 MeV	5
Protons, other than recoil protons	>2 MeV	5
Alpha particles, fission fragments, heavy nuclei	All energies	20

[a] Excluding Auger electrons emitted from nuclei to deoxyribonucleic acid (DNA), for which special microdosimetric considerations are needed.

reflected (scattered) radiation: Radiation that, during passage through matter, has been deviated in direction. It may have been modified also by a change, usually a decrease, in energy. Scattering in 180 degree direction is back scattering.

reflection coefficient: The fraction of radiation (fluence, energy, absorbed dose, etc.) expressed by the ratio of the amount back scattered to that incident.

relative biological effectiveness: Biological potency of one radiation as compared with another, in terms of the inverse ratio of the respective absorbed doses that produce the same biological effect. The use of this term is to be restricted to radiobiology, and it should be distinguished from the quality factor (Q) which is employed in radiation protection.

rem: The special unit of dose equivalent in the cgs system of units.

roentgen (R): The special unit of exposure for photons in air in the cgs system of units; equal to 2.58×10^{-4} C kg^{-1} (exactly).

scattered radiation: [see reflected (scattered) radiation].

secondary electrons: Electrons, such as delta rays, ejected along the path of a charged particle or a photon.

secondary radiation: Particles or photons produced by the interaction with matter of a type of radiation regarded as "primary."

self-shielding: In accelerator practice, characteristic of a radiation-source design in which sufficient shielding material is incorporated adjacent to the source to reduce external dose rates below dose limits.

shall: Indicative of a recommendation that is necessary to meet the currently accepted standards of radiation protection.

shielding, local: Shielding material installed adjacent to, or close by, a radiation source, *e.g.*, diaphragm and collimator around x-ray producing target.

should: Indicative of a recommendation that is to be applied when practicable.

sievert (Sv): The special name for the unit of effective dose and equivalent dose in the SI system of units, 1 Sv = 1 J kg^{-1}.

skyshine: Radiation reflected back to Earth by the atmosphere above a radiation-producing facility.

slowing down (of neutrons): Decrease in energy of a neutron, usually due to repetitive collisions of the neutrons with the matter through which they traverse.

spatially isotropic (or isotropic) field: Uniform directional distribution of the particle fluence (or fluence rate) in space.

stopping power (of electrons or ions): A measure of the average energy loss of a charged particle passing through a material. Linear stopping power is specified as energy loss per unit distance traveled. Mass stopping power is specified as energy lost per unit distance traveled, divided by the density of the material.

straggling (of electrons or ions): The random variation or fluctuation of a property associated with charged particles in passing through matter. It is applied especially to range or penetration distance.

target: Any object or surface of an object bombarded by particles or photons.

tenth-value layer (TVL) (or thickness) [or half-value layer (HVL)]: The thickness of a specified substance which, when introduced into the path of a given beam of radiation, reduces the absorbed dose, dose equivalent or other physical quantities of the radiation field to one-tenth or one-half, respectively. The magnitude of the tenth- or half-value layers may be different for the different physical quantities (see equilibrium tenth-value layer and also half-value layer).

thermal neutrons: Neutrons in thermal equilibrium with their surroundings.

thick shield: Shield which effects a substantial reduction of a radiation field as a result of its presence.

thick target: Target whose dimension in the direction of incident particulate radiation is equal to or greater than the range of the incident particles.

threshold, nuclear-reaction: The minimum, particle or photon energy required to initiate a specific endothermal (endoergic) nuclear reaction.

threshold, radiation-effect (or radiation-damage): The minimum absorbed dose (or dose equivalent) of radiation that will produce a specified effect or a specified type of damage to the irradiated material.

tissue weighting factor (w_T): A factor by which the equivalent dose to an organ or tissue is multiplied in order to account for the relative stochastic detriment resulting from the exposure of different organs and tissues (see Tables G.3 and G.4 for the tissue weighting factors used for radiation protection purposes as specified in ICRP Publications 60 and 26, respectively).

TABLE G.3—*Tissue weighting factors recommended in ICRP Publication 60 (ICRP, 1991).*

Tissue or Organ	Tissue Weighting Factor (w_T)
Gonads	0.20
Bone marrow (red)	0.12
Colon	0.12
Lung	0.12
Stomach	0.12
Bladder	0.05
Breast	0.05
Liver	0.05
Oesophagus	0.05
Thyroid	0.05
Skin	0.01
Bone surface	0.01
Remainder[a]	0.05

[a] For the purposes of calculation, the remainder is composed of adrenal glands, brain, upper large intestine, small intestine, kidney, muscle, pancreas, spleen, thymus, and uterus. In those exceptional cases in which a single one of the remainder tissues or organs receives an equivalent dose in excess of the highest dose in any of the 12 tissues or for which a weighting factor is specified, a weighting factor of 0.025 shall be applied to that tissue or organ and a weighting factor of 0.025 to the average dose in the rest of the remainder as defined above.

TABLE G.4—*Tissue weighting factors recommended in ICRP Publication 26 (ICRP, 1977).*

Tissue or Organ	Tissue Weighting Factor (w_T)
Gonads	0.25
Bone marrow (red)	0.12
Lung	0.12
Breast	0.15
Thyroid	0.03
Bone surface	0.03
Remainder	0.03

undercutting: Penetration of radiation through cracks of shielding barriers or through thin sections of such barriers (*e.g.*, edges of structures), resulting in a greater dose-equivalent rate than that resulting from passage of radiation through the bulk of the shielding barrier.

useful beam (or radiation): That part of the radiation from a target which emerges from the source and its housing through an aperture, diaphragm or collimator.

week, work: Any combination of time intervals adding up to 40 h within seven consecutive days.

x ray: Electromagnetic radiation of energy usually above 1 keV. X rays are produced by impingement of charged particles (usually electrons) on materials (see bremsstrahlung and characteristic x rays).

x-ray converter: Material in which electron energy is converted to x-ray energy, *e.g.*, a thick target of high-Z material. In this Report, the term is usually applied to a target in which electron power is converted with a high degree of efficiency into x-ray power.

x-ray generator: A type of electron accelerator in which the electron beam is used mainly for the production of x rays.

yield (*Y*): The total radiation emitted per unit time from an accelerator target as measured over a particular solid angle divided by the beam current incident on the target.

Z; low Z, high Z: The symbol for the atomic number of a nucleus, *i.e.*, the number of protons contained in the nucleus. Low Z describes nuclei with $Z \leq 26$. High Z describes nuclei with $Z > 26$. Very high Z describes nuclei with $Z > 73$.

References

AAPM (1986a). American Association of Physicists in Medicine. *Protocol for Heavy Charged-Particle Therapy Beam Dosimetry*, Radiation Therapy Committee Task Group, Report No. 16 (Medical Physics Publishing, Madison, Wisconsin).

AAPM (1986b). American Association of Physicists in Medicine. *Neutron Measurements Around High-Energy X-Ray Radiotherapy Machines*, Radiation Therapy Committee Task Group, Report No. 19 (Medical Physics Publishing, Madison, Wisconsin).

AGOSTEO, S. and FROGLIO PARA, A. (1994). "Energy and spatial dependence of neutron fluxes in radiotherapy rooms for a simple dose estimate method," Nucl. Instrum. Methods **B93**, 362–369.

AINSWORTH, E.J., KELLY, L.S., MAHLMANN, L.J., SCHOOLEY, J.C., THOMAS, R.H., HOWARD, J. and ALPEN, E.L. (1983). "Response of colony-forming units—Spleen to heavy charged particles," Radiat. Res. **96**, 180–197.

ALEINIKOV, V.E., GERDT, V.P. and KOMOCHKOV, M.M. (1974). *Neutron Spectra Outside the Shielding of High Energy Proton Accelerators*, JINR-P16-8176 (Joint Institute for Nuclear Research, Dubna, Russia).

ALEINIKOV, V.E., GERDT, V.P. and TIMOSHENKO, G.N. (1975). *Measurement of Spectra of High-Energy Protons Generated in the Shielding of 680 MeV Synchrocyclotron*," JNIR-P16-9400 (Joint Institute for Nuclear Research, Dubna, Russia).

ALEINIKOV, V.E., KOMOCHKOV, M.M., KRILOV, A.R., TIMOSHENKO, G.H. and HAHN, G. (1979). *The Energy-Angle Distributions of the Proton Component of the Radiation Field Behind the 660 MeV Synchrotron Shielding*, JINR-P-16-12732 (Joint Institute for Nuclear Research, Dubna, Russia).

ALEINIKOV, V.E., CHEREVATENKO, A.P., CLAPIER, F.B. and TSOVBUN, V.I. (1985). "Neutron radiation field due to 6.6 MeV/amu ^{58}Ni ions bombarding a thick Cu target," Radiat. Prot. Dosim. **11**(4), 245–248.

ALEVRA, A.V. and SIEBERT, B.R.L. (1986). *In uence of Neutron Spectra and Fluence Response Data on the Determination of Dose Equivalent with Bonner Spheres*, CERN-PTB-ND-28 (European Organisation for Nuclear Research, Geneva).

ALEVRA, A.V., COSACK, M., HUNT, J.B., THOMAS, D.J. and SCHRAUBE, H. (1988). "Experimental determination of the response of four Bonner sphere sets to monoenergetic neutrons," Radiat. Prot. Dosim. **23**(1–4), 293–296.

ALLEN, F.J. and FUTTERER, A.T. (1963). "Neutron transmission data," Nucleonics **21,** 120–121.

417

ALSMILLER, R.G., JR. and BARISH, J. (1969). "High-energy (<18 GeV) muon transport calculations and comparison with experiment," Nucl. Instrum. Methods **71**, 121–124.

ALSMILLER, R.G., JR. and BARISH, J. (1973). "Shielding against the neutrons produced when 400-MeV electrons are incident on a thick copper target," Part. Accel. **5**, 155–159.

ALSMILLER, R.G., JR. and MORAN, H.S. (1966). *Electron-Photon Cascade Calculations and Neutron Yields from Electrons in Thick Targets*, ORNL-TM-1502 (Oak Ridge National Laboratory, Oak Ridge, Tennessee).

ALSMILLER, R.G., JR. and MORAN, J.S. (1967). "Electron-photon cascade calculations and neutron yields from electrons in thick targets," Nucl. Instrum. Methods **48,** 109–116.

ALSMILLER. R.G., JR. and MORAN, H.S. (1968). *The Electron-Photon Cascade Induced in Lead by Photons in the Energy Range 15 to 100 MeV*, ORNL-4192 (Oak Ridge National Laboratory, Oak Ridge, Tennessee).

ALSMILLER, R.G., JR. and MORAN, H.S. (1970a). "Calculation of the energy deposited in thick targets by high-energy (1 GeV) electron-photon cascades and comparison with experiment-II," Nucl. Sci. Eng. **40**, 483–485.

ALSMILLER, R.G., JR. and MORAN, H.S. (1970b). *Energy Deposition by 45-GeV Photons in Be and Al*, ORNL-4631 (Oak Ridge National Laboratory, Oak Ridge, Tennessee).

ALSMILLER, R.G., JR., LEIMDORFER, M. and BARISH, J. (1967). *Analytical Representation of Nonelastic Cross Sections and Particle-Emission Spectra from Nucleon—Nucleus Collisions in the Energy Range 25 to 400 MeV*, ORNL-4046 (Oak Ridge National Laboratory, Oak Ridge, Tennessee).

ALSMILLER, R.G., JR., MYNATT, R.G., BARISH, J. and ENGLE, W.W., JR. (1969a). "High energy (<400 MeV) neutron transport using the method of discrete ordinates," Nucl. Sci. Eng. **36,** 251.

ALSMILLER, R.G., JR., MYNATT, F.R., BARISH, J. and ENGLE, W.W., JR. (1969b). "Shielding against neutrons in the energy range 50 to 400 MeV," Nucl. Instrum. Methods **72**, 213–216.

ALSMILLER, R.G., JR., BARISH, J. and DODGE, S.R. (1974). *Energy Deposition by High-Energy Electrons (50 to 200 MeV) in Water*, ORNL-TM-4419 (Oak Ridge National Laboratory, Oak Ridge, Tennessee).

ALSMILLER, R.G., JR., SANTORO, R.T. and BARISH, J. (1975). "Shielding calculations for a 200-MeV proton accelerator and comparisons with experimental data," Part. Accel. **7**, 1–7.

ALSMILLER, R.G., JR., BARISH, J., BARNES, J.M. and SANTORO, R.T. (1981a). "Calculated neutron production by 190- to 268-MeV protons in a water-cooled tantalum target," Nucl. Sci. Eng. **80**, 452–455.

ALSMILLER, R.G., JR., BARISH, J. and CHILD, R.L. (1981b). "Skyshine at neutron energies ≤400 MeV," Part. Accel. **11**, 131–141.

ANDERSSON, I.O. and BRAUN, J. (1963). "A neutron rem counter with uniform sensitivity from 0.025 MeV to 10 MeV," pages 87 to 95 in *Neutron Dosimetry*, Vol. 2, STI/PUB/69 (International Atomic Energy Agency, Vienna).

ANDERSSON, I.O. and BRAUN, J. (1964). "A neutron rem counter," Nukleonik **6**, 237–241.

ANSI/HPS (1999). American National Standards Institute/Health Physics Society. *Surface and Volume Radioactivity Standards for Clearance*, ANSI/HPS N13.12 (Health Physics Society, McLean, Virginia).

ANTIPOV, A.V., BAJSHEV, I.S., GOLOVACHIK, V.T., KRUPNYJI, G.I., KUSTAREV, V.M., LEBEDEV, V.N. and HOEFERT, M. (1978). *Comparison of Dose Equivalent Measurements Behind the IHEP Accelerator Shielding Using Different Methods*, IFVEORI 78-15 (Institute of High Energy Physics, Serpukhov, Russia).

APFEL, R.E. (1979). "The superheated drop detector," Nucl. Instrum. Methods **162**, 603–608.

ARMSTRONG, T.W. (1978). "The HETC Hadronic Cascade Code," Lecture 23 in *Computer Techniques in Radiation Transport and Dosimetry*, Nelson, W.R. and Jenkins, T.M., Eds. (Plenum Press, New York).

ARMSTRONG, T.W. and ALSMILLER, JR., R.G. (1969). "Calculation of the residual photon dose rate around high-energy proton accelerators," Nucl. Sci. Eng. **38**, 53–62.

ARMSTRONG, T.W. and BARISH, J. (1970). "Calculation of the residual photon dose rate due to the activation of concrete by neutrons from a 3-GeV proton beam in iron," pages 70 to 91 in *Proceedings of the Second International Conference on Accelerator Dosimetry and Experience*, Stanford Linear Accelerator Center, CONF-691101 (National Technical Information Service, Springfield, Virginia).

ARORA, R. (1996). *Calculations of the Neutron Arrival Time Distributions for Moderator-Type Detectors*, MS Thesis (San Jose State University, San Jose, California).

AROUA, A., GRECESCU, M., LERCH, P., PRETRE, S., VALLEY, J.F. and VYLET, V. (1992). "Evaluation and test of the response matrix of a multi-sphere neutron spectrometer in a wide energy range. Part I. Calibration," Nucl. Instrum. Methods **A321**, 298–304.

ASANO, Y. and SASAMOTO, N. (1994). "Development of shielding design code for synchrotron radiation beam line," Radiat. Phys. Chem. **44**, 133–137.

ASHTON, F. and COATS, R.B. (1968). "The energy spectrum of cosmic-ray neutrons at sea level in the range 20 − 4000 GeV," J. Phys. A: Gen. Phys. **1**, 169–171.

AUXIER, J.A., HAYWOOD, F.F. and GILLEY, L.W. (1963). *General Correlative Studies — Operation BREN*, CEX 62.03 (Oak Ridge National Laboratory, Oak Ridge, Tennessee).

AWSCHALOM, M. (1970). *Lateral Shielding for the 8-GeV and 200-GeV Synchrotrons*, FERMILAB-TM-241 (Fermi National Accelerator Laboratory, Batavia, Illinois).

AWSCHALOM, M. and SANNA, R.S. (1985). "Applications of Bonner sphere detectors in neutron field dosimetry," Radiat. Prot. Dosim. **10**(1–4), 89–101.

BAARLI, J. (1969). "Dosimetry of very high energy radiation," pages 291 to 320 in *Health Physics*, Duhamel, A.M.F., Ed. (Pergamon Press, New York).

BAARLI, J. and SULLIVAN, A.H. (1965a). "Radiation dosimetry for protection purposes near high-energy particle accelerators," Health Phys. **11**, 353–361.

BAARLI, J. and SULLIVAN, A.H. (1965b). "Health physics survey methods for the measurement of stray radiation around the CERN high-energy accelerators," pages 103 to 116 in *Proceedings of the Symposium on Accelerator Radiation Dosimetry Experiment*, CONF-651109 (National Technical Information Service, Springfield, Virginia).

BAIR, J.K. and DEL CAMPO, J.G. (1979). "Neutron yields from alpha-particle bombardment," Nucl. Sci. Eng. **71**, 18–28.

BAKER, S.I. (1974). "Fermi National Accelerator Laboratory environmental monitoring report," pages 561 to 594 in *Environmental Monitoring at Major U.S. Energy Research and Development Administration Contractor Sites—Calendar Year 1974*, ERDA-54 (National Technical Information Service, Springfield, Virginia).

BAKER, S.I., KERNS, C.R., PORDES, S.H., CUMMING, J.B., SOUKAS, A., AGORITSAS, V. and STEVENSON, G.R. (1984). "Absolute cross section for the production of ^{24}Na in Cu by 400 GeV protons," Nucl. Instrum. Methods **A222**, 467–473.

BAKER, S.I., ALLEN, R.A., YURISTA, P., AGORITSAS, V.V. and CUMMING, J.B. (1991). "Cu(p,x)^{24}Na cross section from 30 to 800 GeV," Phys. Rev. **C43**, 2862–2865.

BAKER, S.I., BULL, J.S. and GOSS, D.L. (1997). "Leaching of accelerator-produced radionuclides," Health Phys. **73**, 912–918.

BAN, S., HIRAYAMA, H., KONDO, K., MIURA, S., HOZUMI, K., TAINO, M., YAMAMOTO, A., HIRABAYASHI, H. and KATOH, K. (1980). "Measurement of transverse attenuation lengths for paraffin, heavy concrete and iron around an external target for 12 GeV protons," Nucl. Instrum. Methods **174**, 271–276.

BAN, S., HIRAYAMA, H. and KATOH, K. (1981). "Measurement of secondary neutron fluxes around beam stop for 500 MeV protons," Nucl. Instrum. Methods **184**, 409–412.

BARANOV, P.S., GOLDANSKII, V.I. and ROGANOV, V.S. (1957). "Dosimeter for high energy neutrons," Rev. Sci. Instrum. **28**, 1029–1032.

BARBALAT, O. (1991). "From fundamentals to waste disposal," Phys. World **4**, 31–37.

BARBIER, M. (1969). *Induced Radioactivity* (Elsevier Science, New York).

BARKAS, W.H. (1963). *Nuclear Research Emulsions, Volume 1: Techniques and Theory; Volume 2: Particle Behavior and Emulsion Applications* (Academic Press, New York).

BARKAS, W.H. and BERGER, M.J. (1964). *Tables of Energy Losses and Ranges of Heavy Charged Particles*, NASA SP-3013 (National Technical Information Service, Springfield, Virginia).

BATHOW, G., FREYTAG, E. and TESCH, K. (1967). "Measurements on 6.3 GeV electromagnetic cascades and cascade-produced neutrons," Nucl. Phys. **B2**, 669–689.

BATHOW, G., CLAUSEN, U., FREYTAG, E. and TESCH, K. (1966). *Skyshine Measurement and its Comparison with Estimates from Diffusion*

Theory, DESY-66/3 (National Technical Information Service, Springfield, Virginia).

BATHOW, G., FREYTAG, E., TESCH, K., KAJIKAWA, R. and KOEBBERLING, M. (1969). "Measurements of the longitudinal and lateral development of electromagnetic cascades in lead, copper and aluminum at 6 GeV," pages 222 to 242 in *Proceedings of the Second International Conference on Accelerator Dosimetry and Experience*, CONF-69110 (National Technical Information Service, Springfield, Virginia).

BATHOW, G., FREYTAG, E., KOBBERLING, M., TESCH, K. and KAJIKAWA, R. (1970). "Measurements of the longitudinal and lateral development of electromagnetic cascades in lead, copper and aluminum at 6 GeV," Nucl. Phys. **B20**, 592–602.

BAUM, J.W., WOODCOCK, R.C. and KUEHNER, A.V. (1970a). "Factors affecting pulse size in sealed tissue-equivalent counter" pages 648 to 659 in *Proceedings of the Second International Conference on Accelerator Dosimetry and Experience*, CONF-691101 (National Technical Information Service, Springfield, Virginia).

BAUM, J.W., KUEHNER, A.V. and CHASE, R.L. (1970b). "Dose equivalent meter designs based on tissue equivalent proportional counters," Health Phys. **19**, 813–824.

BAUR, A., BOURDET, L., DEJONGHE, G., GONNORD, J., MONNIER, A., NIMAL, J.C. and VERGNAUD, T. (1980). *TRIPOLI 2: Three-Dimensional Polyenergetic Monte Carlo Radiation Transport Program*, Vols. I and II, OLS-80-110; Vol. III, OLS-80-165 (Commissariat a l'Energie Atomique, Fontenay-aux-Roses, France).

BEASLEY, J.W. (1959). *The Mean Fission-Fragment Range in Bismuth as Applied to Pulse-Type Ion Chambers*, UCRL-8760 (National Technical Information Service, Springfield, Virginia).

BECK, H.L. (1970a). "A new calculation of dose rates from high energy electrons and photons incident on 30 cm water slabs," Nucl. Instrum. Methods **78**, 333–334.

BECK, H.L. (1970b). "The influence of the density effect on electron-induces cascade showers in water and aluminum," Nucl. Sci. Eng. **39**, 120–121.

BECK, H.L. (1971). "Monte Carlo calculations of electromagnetic shower transition effects," Nucl. Instrum. Methods **91**, 525–531.

BECK, H.L., LOWDER, W.M. and MCLAUGHLIN, J.E. (1971). "*In situ* external environmental gamma-ray measurements utilizing Ge(Li) and NaI(Tl) spectrometry and pressurized ionization chambers," pages 499 to 513 in *Rapid Methods for Measuring Radioactivity in the Environment*, STI/PUB/289 (International Atomic Energy Agency, Vienna).

BERGER, M.J. (1963). "Monte Carlo calculation of the penetration and diffusion of fast charged particles," pages 135 to 215 in *Methods in Computational Physics*, Vol. 1, Alder B., French, S. and Rothenberg, M., Eds. (Academic Press, New York).

BERGER, M.J. and SELTZER, S.M. (1964). *Tables of Energy Losses and Ranges of Electrons and Positrons*, NASA-SP-3012 (National Aeronautics and Space Administration, Washington).

BERGER, M.J. and SELTZER, S.M. (1966). *Additional Stopping Power and Range Tables for Protons, Mesons, and Electrons*, NASA-SP-3036 (National Aeronautics and Space Administration, Washington).

BERGER, M.J. and SELTZER, S.M. (1968). *ETRAN Monte Carlo Code System for Electron and Photon Transport Through Extended Media*, Radiation Safety Information Computational Center Report CCC-107 (Oak Ridge National Laboratory, Oak Ridge, Tennessee).

BERGER, M.J. and SELTZER, S.M. (1970). "Bremsstrahlung and photoneutrons from thick tungsten and tantalum targets," Phys. Rev. **C2**, 621–631.

BERGER, M.J. and SELTZER, S.M. (1982). *Stopping Powers and Ranges of Electrons and Positrons*, NBSIR 82-2550 (National Technical Information Service, Springfield, Virginia).

BERMAN, B.L. and FULTZ, S.C. (1975). "Measurements of the giant dipole resonance with monoenergetic photons," Rev. Mod. Phys. **47**, 713–761.

BERTEL, E., DE SEREVILLE, B., FREYTAG, E. and WACHSMUTH, H. (1971). "Shielding against muons," pages 79 to 90 in *Radiation Problems Encountered in the Design of Multi-GeV Facilities,* Goebel, K., Ed., CERN-71-21 (European Organisation for Nuclear Research, Geneva).

BERTINI, H.W. (1963). "Low-energy intranuclear cascade calculation," Phys. Rev. **131,** 1801–1821.

BERTINI, H.W., HARP, G.D. and BERTRAND, F.E. (1974). "Comparisons of predictions from two intranuclear-cascade models with measured secondary proton spectra at several angles from 62- and 39-MeV protons on various elements," Phys. Rev. **C10**, 2472.

BERTINI, H.W., SANTORO, R.T. and HERMAN, O.W. (1976). "Calculated nucleon spectra at several angles from 192-, 500-, 700-, and 900-MeV carbon-12 on iron-56," Phys. Rev. **C14**, 590–595.

BIRATTARI, C. and SALOMONE, A. (1985). "Neutron spectrum measurements at a 40-MeV proton cyclotron," Health Phys. **49**, 919–936.

BIRATTARI, C., FERRARI, A., NUCCETELLI, C., PELLICCIONI, M. and SILARI, M. (1990). "An extended range neutron rem counter," Nucl. Instrum. Methods **A297**, 250–257.

BIRATTARI, C., FERRARI, A., HOEFERT, M., OTTO, T., RANCATI, T. and SILARI, M. (1998a). "Recent results at the CERN-EC high energy reference field facility," pages 219 to 234 in *Proceedings of the Third Specialists Meeting on Shielding Aspects of Accelerators, Targets and Irradiation Facilities (SATIF3)* (Organisation for Economic Cooperation and Development/Nuclear Energy Agency, Paris).

BIRATTARI, C., ESPOSITO, A., FERRARI, A., PELLICCIONI, M., RANCATI, T. and SILARI, M. (1998b). "The extended range neutron rem counter LINUS: Overview and latest developments," Radiat. Prot. Dosim. **76**(3), 135–148.

BLIZARD, E.P. and ABBOTT, L.S., Eds. (1962). *Reactor Handbook, Volume III, Part B, Shielding,* 2nd ed. (Interscience, New York).

BLOHM, R. and HARDER, D. (1985). "Restricted LET: Still a good parameter of radiation quality for electrons and photons," Radiat. Prot. Dosim. **13**(1-4), 377–381.

BLUMBERG, L. and SCHLESINGER, S.I. (1956). *Relativistic Tables of Energy and Angle Relationships for the T(p,n)He, D(d,n)He Reactions*, AECU-3118 (National Technical Information Service, Springfield, Virginia).

BLY, J.H. and BURRILL, E.A. (1959). "High-energy radiography in the 6 to 40 MeV range," in *Symposium on Nondestructive Testing in the Missile Industry*, Special Technical Publication 278 (American Society for Testing Materials International, West Conshohocken, Pennsylvania).

BOAG, J.W. (1950). "Ionization measurements at very high intensities. I. Pulsed radiation beams," Brit. J. Radiol. **23**, 601–611.

BOAG, J.W. (1952). "The saturation curve for ionization measurements in pulsed radiation beams," Brit. J. Radiol. **25**, 649–650.

BOAG, J.W. (1966). "Ionization chambers," pages 2 to 72 in *Radiation Dosimetry, Volume 2. Instrumentation*, Attix, F.H. and Roesch, W.C., Eds. (Academic Press, New York).

BOAG, J.W. (1987). "Ionization dosimetry," pages 169 to 243 in *The Dosimetry of Ionizing Radiation*, Vol. II, Kase, K.R., Bjarngard, B.E. and Attix, F.H., Eds. (Academic Press, New York).

BONIFAS, A., GEROUDET, J.M., MARCHAL, H. and TUYN, J.W.N. (1974). *On the Use of Thermoluminescence Dosimetry for Stray Radiation Monitoring on the CERN Site*, CERN-HP-74-138 (European Organisation for Nuclear Research, Geneva).

BORAK, T.B., AWSCHALOM, M., FAIRMAN, W., IWANI, F. and SEDLET, J. (1972). "The underground migration of radionuclides produced in soil near high energy proton accelerators," Health Phys. **23**, 679–687.

BORAK, T.B. and TUYN, J.W.N. (1987). *Can Uranium Calorimeters Become Critical?* CERN-TIS-RP-194 (European Organisation for Nuclear Research, Geneva).

BOURGOIS, L., DELACROIX, D., FERREUX, L. and MASSON, L. (1996). "Dose equivalent measurements at a 2.7 GeV proton accelerator and comparison with the Moyer model," Health Phys. **70,** 36–40**.**

BRAID, T.H., RAPIDS, R.F., SIEMSSEN, R.H., TIPPIE, J.W. and O'BRIEN, K. (1971). "Calculations of shielding for large cyclotrons," IEEE Trans. Nucl. Sci. **NS-18**, 824–827.

BRAMBLETT, R.L., EWING, R.I. and BONNER, T.W. (1960). "A new type of neutron spectrometer," Nucl. Instrum. Methods **9**, 1–12.

BRAUER, E. and THOMLINSON, W. (1988). "Experimental verification of PHOTON: A program for use in x-ray shielding calculations," Nucl. Instrum. Methods **A266**, 195–198.

BRIANTI, G. and HUBNER, K. (1984). "Large Hadron Collider in the LEP tunnel: A feasibility study of possible options," pages 207 to 225 in *ICFA Seminar on Future Perspectives in High-Energy Physics*, CERN-DIR-TECH-84-01 (European Organisation for Nuclear Research, Geneva).

BRIESMEISTER, J.F., Ed. (2000) *MCNP: A General Monte Carlo N-Particle Transport Code*, LA-13709-M (Los Alamos National Laboratory, Los Alamos, New Mexico).

BROCKMANN, R., KEIL, P., KNOP, G. and WUCHERER, P. (1971). "Elektron-photon-kaskaden in blei bei primaenergien von 100, 200 und 400 MeV," Z. Physik **243**, 464–479.

BROOKE, G. and WOLFENDALE, A.W. (1964). "The momentum spectrum of cosmic ray protons near sea level in the momentum range 0.6 to 150 GeV/c," Proc. Phys. Soc. **83**, 843–851.

BROOKE, G., MEYER, M.A. and WOLFENDALE, A.W. (1964). "The energy spectrum of cosmic ray pions near sea level in the range 0.7 to 150 GeV," Proc. Phys. Soc. **83**, 871–877.

BROOME, T.A., PERRY, D.R., STAPLETON, G.B. and DUC, D. (1983). "Particle distribution around a copper beam stop for 72 MeV protons," Health Phys. **44**, 487–499.

BROWN, G.S. and MONCTON, D.E. (1991). *Handbook on Synchrotron Radiation*, Vol. 3 (Elsevier Science, New York).

BRYNJOLFSSON, A. and MARTIN, T.G., III (1971). "Bremsstrahlung production and shielding of static and linear electron accelerators below 50 MeV. Toxic gas production, required exhaust rates, and radiation instrumentation," Int. J. Appl. Radiat. Isot. **22**, 29–40.

BUECHNER, W.W., VAN DE GRAAFF, R.J., BURRILL, E.A. and SPERDUTO, A. (1948). "Thick-target x-ray production in the range from 1250 to 2350 kilovolts," Phys. Rev. **74**, 1348–1352.

BULL, J.S., ROMERO, V.D., BAKER, S.I., STAPLETON, G.B., GOSS, D.L. and COULSON, L.V. (1997). "Groundwater activation at the Superconducting Supercollider: A new design model," Health Phys. **73**, 800–807.

BURFEINDT, H. (1967). *Monte-Carlo-Rechnung fur 3-GeV-Schauer in Blei*, DESY-67/24 (Deutsches Elektronen-Synchrotron, Hamburg).

BURLIN, T.E. (1968). "Cavity chamber theory," pages 331 to 392 in *Radiation Dosimetry*, Vol. 1, Attix, F.H. and Roesch, W.C. Eds. (Academic Press, New York).

BURRILL, E.A. (1968). "The shielding problem with low-energy particle accelerators," Nucl. Saf. **96**, 457–466.

BURRUS, W.A. (1962). "Bonner spheres and threshold detectors for neutron spectroscopy," pages 296 to 302 in *Oak Ridge National Laboratory Neutron Physics Division Annual Report,* ORNL-3360 (Oak Ridge National Laboratory, Oak Ridge, Tennessee).

BUSICK, D.D. and WARREN, G.J. (1969). "Operational health physics associated with induced radioactivity at the Stanford Linear Accelerator Center," page 139 in *Proceedings of the Second International Conference on Accelerator Dosimetry and Experience*, CONF-691101 (National Technical Informative Service, Springfield, Virginia).

BUSICK, D.D. and WARREN, G.J. (1979). *Unique Safety Manual for Experimental Personnel*, SLAC-PUB-2384 (National Technical Information Service, Springfield, Virginia).

BUSICK, D.D., JENKINS, T.M. and SWANSON, W.P. (1975). *Personnel Neutron Dosimetry at SLAC*, SLAC-PUB-3153 (National Technical Information Service, Springfield, Virginia).

BUTALA, S.W., BAKER, S.I. and YURISTA, P.M. (1989). "Measurements of radioactive gaseous releases to air from target halls at a high-energy proton accelerator," Health Phys. **57**, 909–916.

CAMERON, J.R, SUNTHARALINGAM, N. and KENNEY, G.N. (1968). *Thermoluminescent Dosimetry* (University of Wisconsin Press, Madison, Wisconsin).

CAPONE, T., BAARLI, J., CHARALAMBUS, S., DUTRANNOIS, J.Y., FREEMAN, J.Y., GOEBEL, K., MIDDELKOOP, W.C., OVERTON, T.R., RINDI, A. and SULLIVAN, A.H. (1965). *A Radiation Survey Inside and Outside the CPS Tunnel to Estimate the Effectiveness of Roof Shielding*, CERN-DI-HP-71 (European Organisation for Nuclear Research, Geneva).

CAA (1963). Clean Air Act. Public Law 88-206, 77 Stat. 392, as amended (December 17) (U.S. Government Printing Office, Washington).

CARLSSON, G.A. (1985). "Theoretical basis for dosimetry," pages 1 to 75 in *The Dosimetry of Ionizing Radiation*, Vol. 1, Kase, K.R., Bjarngard, B. and Attix, F.H., Eds. (Academic Press, New York).

CARTER, L.L. (1983). "Bulk shield design for neutron energies below 50 MeV," Nucl. Tech. **3**, 165.

CARTER, L.L. and CASHWELL, E.D. (1975). *Particle-Transport Simulation with the Monte Carlo Method*, TID 26607 (National Technical Information Center, Springfield, Virginia).

CARTER, T.M., CHAKALIAN, V.M. and THOMAS, R.H. (1970). "Stanford Mark I moderator calibration using tantalum," in *Stanford University Health Physics Department Internal Report* TN/70-2 (Leland Stanford University Junior University, Stanford, California).

CASE, K.M., DE HOFFMANN, F. and PLACZEK, G. (1953). *Introduction to the Theory of Neutron Diffusion*, Vol. 1 (Los Alamos National Laboratory, Los Alamos, New Mexico).

CASEY, W.R., DISTENFELD, C.H., LEVINE, G.S., MOORE, W.H. and SMITH, L.W. (1967). "Sand as a side shield for 30 GeV protons stopping in the Brookhaven AGS," Nucl. Instrum. Methods **55**, 253–268.

CASEY, W.R., MILLER, A.J., MCCASLIN, J.B. and COULSON, L.V. (1988). *Health Physics Manual of Good Practices for Accelerator Facilities*, SLAC-327 (National Technical Information Service, Springfield, Virginia).

CEBAF (1986). Continuous Electron Beam Accelerator Facility. *CEBAF Conceptual Design Report* (Thomas Jefferson National Accelerator Facility, Newport News, Virginia).

CEBAF (1987). Continuous Electron Beam Accelerator Facility. *Radiation Control Review*, TN87-061 (Thomas Jefferson National Accelerator Facility, Newport News, Virginia).

CERN (1964). European Organisation for Nuclear Research. *Report on the Design Study of a 300 GeV Proton Synchrotron*, Study Group on New Accelerators, CERN-563 (European Organisation for Nuclear Research, Geneva).

CERN (1971). European Organisation for Nuclear Research. *Proceedings of the 8th International Conference on High Energy Accelerators CERN 1971*, Blewett, M.H. and Vogt-Nilsen, N., Eds. (European Organisation for Nuclear Research, Geneva).

CERN (1977). European Organisation for Nuclear Research. "Theoretical aspects of the behavior of beams in accelerators and storage rings," in *Proceedings First Course of the International School of Particle Accelerators of the Ettore-Majorana Centre for Scienti c Culture*, Blewett, M.H., Ed., CERN-77-113 (European Organisation for Nuclear Research, Geneva).

CERN (1985). European Organisation for Nuclear Research. *Proceedings of the CERN Accelerator School*, *Gif-sur-Yvette*, *France*, Bryant, P. and Turner, S., Eds, CERN-85-19 (European Organisation for Nuclear Research, Geneva).

CHAMBLESS, D.A. and BROADWAY, J.A. (1983). "Letter: Comments on neutron spectral unfolding using the Monte Carlo method," Nucl. Instrum. Methods **214,** 543–545.

CHAPMAN, D. (1988). *PHOTON: A User's Manual*, BNL 40822 (Brookhaven National Laboratory, Upton, New York).

CHAPMAN, G.T. and STORRS, C.L. (1955). *Effective Neutron Removal Cross Sections for Shielding*, AECD-3978 (Oak Ridge National Laboratory, Oak Ridge, Tennessee).

CHAPMAN, D., GMUR, N., LAZARZ, N. and THOMLINSON, W. (1988). "PHOTON: A program for synchrotron radiation dose calculations," Nucl. Instrum. Methods **A266**, 191–194.

CHILTON, A.B. (1965). "Backscattering of gamma rays from point sources by an infinite-plane concrete surface," Nucl. Sci. Eng. **21**, 194–200.

CHILTON, A.B. (1974). *Working Paper on Neutron Skyshine for Accelerator Sources*, informal report (Department of Nuclear Engineering, University of Illinois, Urbana).

CHILTON, A.B. and HUDDLESTON, C.M. (1963). "A semiempirical formula for differential dose albedo for gamma rays on concrete," Trans. Am. Nucl. Soc. **5**, 220.

CHILTON, A.B., DAVISSON, C.M. and BEACH, L.A. (1965). "Parameters for C-H albedo formula for gamma rays reflected from water, concrete, iron and lead," Trans. Am. Nucl. Soc. **8**, 656–657.

CHILTON, A.B., SHULTIS, J.K. and FAW, R.E. (1984). *Principles of Radiation Shielding* (Prentice Hall, Englewood Cliffs, New Jersey).

CHU, Y.C. (1980). *The Estimation of Transverse Shielding Thickness for the BPS*, CERN-HS-RP-TM-80-14 (European Organisation for Nuclear Research, Geneva).

CIONI, G. and TREVES, A. (1969). "A simplified method of simulating electromagnetic showers," Nuovo Cimento **62B**, 371–378.

CITRON, A., HOFFMANN, L., PASSOW, C., NELSON, W.R. and WHITEHEAD, M. (1965). "A study of the nuclear cascade in steel initiated by 19.2 GeV/c protons," Nucl. Instrum. Methods **32**, 53–56.

CLAPIER, F. and ZAIDINS, C.S. (1983). "Neutron dose equivalent rates due to heavy ion beams," Nucl. Instrum. Methods **217**, 489–494.

CLARKE, E.T. (1968a). "Photon fields near earth-air interface," pages 255 to 256 in *Engineering Compendium on Radiation Shielding, Volume 1, Shielding Fundamentals and Methods*, Jaeger, R.G., Blizard, E.P., Chilton, A.B., Grotenhuis, M., Hoenig, A., Jaeger, T.A. and Eiseniohr, H.H., Ed. (Springer-Verlag, New York).

CLARKE, E.T. (1968b). "Skyshine," page 257 in *Engineering Compendium on Radiation Shielding, Volume 1, Shielding Fundamentals and Methods*, Jaeger, R.G., Blizard, E.P., Chilton, A.B., Grotenhuis, M., Hoenig, A., Jaeger, T.A. and Eiseniohr, H.H., Ed. (Springer-Verlag, New York).

CLEMENT, G. and KESSLER, P. (1965). "Electroproduction de muons de tres haute energie," Nuovo Cimento **37**, 876–887.

CLOTH, P., FILGES, D., NEEF, R.D., STERZENBACH, G., REUL, C., ARMSTRONG, T., COLEBORN, B.L., ANDERS, B. and BRUCKMANN, H. (1988). *HERMES: A Monte Carlo Program System for Beam-Materials Interaction Studies*, JUEL 2203 (Forschungszentrum, Julich, Germany).

COCKCROFT, J.D. and WALTON, E.T.S. (1932a). "Experiments with high velocity positive ions. I: Further developments in the method of obtaining high velocity positive ions," Proc. Roy. Soc. (London) **A136,** 619–630.

COCKCROFT, J.D. and WALTON, E.T.S. (1932b). "Experiments with high velocity positive ions. II: The disintegration of elements by high velocity protons," Proc. Roy. Soc. (London) **A137**, 229–242.

COCKCROFT, J.D. and WALTON, E.T.S. (1934). "Experiments with high velocity positive ions. III: The disintegration of lithium, boron and carbon by heavy hydrogen ions," Proc. Roy. Soc. (London) **A144**, 704–720.

COHEN, B.L. (1978). "Nuclear cross sections," pages 91 to 212 in *CRC Handbook of Radiation Measurement and Protection, Section A: Volume I. Physical Science and Engineering Data*, Brodsky, A., Ed. (CRC Press, Inc., Boca Raton, Florida).

COHEN, M.O., GUBER, W., TROUBETZKOY, E.S., LICHTENSTEIN, H. and STEINBERG, H.A. (1973). *SAM-CE: A Three-Dimensional Monte Carlo Code for Solution of the Forward Neutron and Forward and Adjoint Gamma-Ray Transport Equations*, DNA-2830-F, Rev. B (National Technical Information Service, Springfield, Virginia).

COLEMAN, F.J. (1975). *A Review of Shielding Data for the SL75-20 Linear Accelerator*, M.E.L. Equipment Co., Publication No. 1013-10-75 (Manor Royal, Crawley, Sussex).

COLEMAN, W.A. and ARMSTRONG, T.W. (1970). *The Nucleon-Meson Transport Code NMTC*, ORNL-4606 (Oak Ridge National Laboratory, Oak Ridge, Tennessee).

COSACK, M. and LESIECKI, H. (1981). "Dependence of the response of eight neutron dose equivalent survey meters with regard to the energy and direction of incident neutrons," pages 407 to 420 in *Proceedings of the Fourth Symposium on Neutron Dosimetry*, EUR-7448 (Commission of the European Communities, Luxembourg).

COSSAIRT, J.D. (1983). "Recent muon fluence measurements at Fermilab," Health Phys. **45**, 651–658.

COSSAIRT, J.D. (1987). "Shielding design at Fermilab: Calculations and measurements," pages 642 to 658 in *Proceedings of the Twentieth Midyear Topical Symposium of the Health Physics Society, Health Physics of Radiation-Producing Machines*, Busick, D.D. and Swanson, W.P., Eds., CONF-8702106 (National Technical Information Service, Springfield, Virginia).

COSSAIRT, J.D. (1996). "On residual dose rate within particle accelerator enclosures," Health Phys. **71**, 315–319.

COSSAIRT, J.D. and COULSON, L.V. (1985). "Neutron skyshine measurements at Fermilab," Health Phys. **48**, 175–181.

COSSAIRT, J.D. and ELWYN, A.J. (1984). "Shielding considerations for fixed target usage of the SSC," pages 19 to 23 in *Proceedings of the SSC*

Fixed Target Workshop' FERMILAB-FN-404 (Fermi National Accelerator Laboratory, Batavia, Illinois).

COSSAIRT, J.D. and ELWYN, A.J. (1987). "Personal dosimetry in a mixed field of high-energy muons and neutrons," Health Phys. **52**, 813–818.

COSSAIRT, J.D., GROBE, D.W. and GERARDI, M.A. (1984). *Measurements of Radiation Quality Factors Using a Recombination Chamber*, FERMI-LAB-TM-1248 (Fermi National Accelerator Laboratory, Batavia, Illinois).

COSSAIRT, J.D., BUTALA, S.W. and GERARDI, M.A. (1985a). "Absorbed dose measurements at an 800 GeV proton accelerator; comparison with Monte Carlo calculations," Nucl. Instrum. Methods **A238,** 504–508.

COSSAIRT, J.D., COUCH, J.G., ELWYN, A.L. and FREEMAN, W.S. (1985b). "Radiation measurements in a labyrinth penetration at a high-energy proton accelerator," Health Phys. **49**, 907–917.

COSSAIRT, J.D., ELWYN, A.J., FREEMAN, W.S. and BUTALA, S.W. (1988). "A study of the transport of high energy muons through a soil shield at the Tevatron," Nucl. Instrum. Methods **A276**, 78–85.

COSSAIRT, J.D., ELWYN, A.J., FREEMAN, W.S., SALSBURY, W.C. and YURISTA, P.M. (1989). "Measurements of neutrons in enclosures and outside of shielding at the Tevatron," pages 190 to 199 in *Proceedings of the Twenty-Second Midyear Topical Meeting of the Health Physics Society on Instrumentation*, FERMILAB-CONF-88-106 (Fermi National Accelerator Laboratory, Batavia, Illinois).

COWAN, F.P. (1962). "A preliminary report on health physics problems at the Brookhaven Alternating Gradient Synchrotron," pages 143 to 146 in *Proceedings Premier Colloque International sur la Protection aupres des Grands Accildrateurs*, Bonet-Maury, P., Duhamel, M. and Perrin, F., Eds. (Presses Universitaires de France, Paris).

CRCPD (1991). Conference of Radiation Control Program Directors. *Suggested State Regulations for Control of Radiation, Volume 1 (Ionizing)* and *Volume II (Nonionizing)* (Conference of Radiation Control Program Directors, Frankfort, Kentucky).

CROSS, W.G. (1986). "Characteristics of track detectors for personnel neutron dosimetry," pages 533 to 542 in *Proceedings of the 13th International Conference on Solid State Nuclear Track Detectors*, Tommasino, L., Baroni, G. and Campos-Venuti, G., Eds., Nucl. Tracks Radiat. Meas. **12**, 533–542.

CROSS, W.G. and ING, H. (1984). "Overview of neutron dosimetry in Canada," pages 13 to 28 in *Tenth DOE Workshop on Personnel Neutron Dosimetry*, CONF-8308140 (National Technical Information Service, Springfield, Virginia).

CROSS, W.G. and ING, H. (1987). "Neutron spectra," pages 91 to 167 in *The Dosimetry of Ionizing Radiation*, Vol. II, Kase, K.R., Bjarngard, B.E. and Attix, F.H., Eds. (Academic Press, New York).

CROSS, W.G. and TOMMASINO, L. (1972). "Improvements in the spark counting technique for damage track neutron dosimeters," pages 283 to 301 in *Proceedings of the First Symposium on Neutron Dosimetry in Biology and Medicine*, Burger, G., Schraube, H. and Ebert, H.G., Eds., EUR:A896 (Commission of the European Communities, Luxembourg).

DAVISON, B. (1957). *Neutron Transport Theory* (Clarendon Press, Oxford, United Kingdom).

DE CARVALHO, H.G., CORTINI, G., MUCHNIK, M., POTENZA, G., RIN-ZIVILLO, R. and LOCK, W.O. (1963). "Fission of uranium, thorium and bismuth by 20-GeV protons," Nuovo Cimento **27**, 468–474.

DE HAAS, J.B.M. (1987). *Criticality Calculations for the UA-1 Calorimeter at CERN*, ECN-87-042 (Stichting, Energieonderzoek Centrum, Netherlands).

DEJUS, R.J., KHOUNSARY, A.M., BROWN, D.A. and VICCARO, P.J. (1992). "Calculation of wiggler spectrum and its absorption in media," Nucl. Instrum. Methods **A319**, 207–212.

DE LUCA, P.M., JR., OTTE, R.A., SWANSON, W.P., SCHILTHELM, S.W. and ROGERS, G. (1987). "Radiation measurements at Aladdin, a 1-GeV electron storage ring," pages 486 to 494 in *Proceedings of the Twentieth Midyear Topical Symposium of the Health Physics Society, Health Physics of Radiation-Producing Machines*, Busick, D.D. and Swanson, W.P., Eds., CONF-8602106 (National Technical Information Service, Springfield, Virginia).

DEMARCO, J.J., SOLBERG, T.D., WALLACE, R.E. and SMATHERS, J.B. (1995). "A verification of the Monte Carlo code MCNP for thick target bremsstrahlung calculations," Med. Phys. **22**, 11–16.

DENNIS, J.A. (1983). "Biological effects of neutron radiation and their implications for the nuclear power industry," Nucl. Energy **22**, 87–93.

DENNIS, J.A. and DUNSTER, H.J. (1985). "Radiation quality and radiation protection: Implications of changes in quality factors," Radiat. Prot. Dosim. **13**(1–4), 327–334.

DE PANGHER, J. and NICHOLS, L.L. (1966). *A Precision Long Counter for Measuring Fast Neutron Flux Density*, BNWL-260 (National Technical Information Service, Springfield, Virginia).

DE PLANQUE-BURKE, G. (1975a). "Thermoluminescent dosimeter measurements of perturbations of the natural radiation environment," pages 305 to 315 in *Proceedings of the Second Conference on Natural Radiation Environment*, Vol. II, CONF-720805 (National Technical Information Service, Springfield, Virginia).

DE PLANQUE-BURKE, G. (1975b). *Operating Manual for GRANIA, a Code for the Analysis of Climatic Effects on Natural Environmental Gamma Ray Exposure Rates,* HASL-289 (National Technical Information Service, Springfield, Virginia).

DE PLANQUE-BURKE, G. and O'BRIEN, K. (1974). *Operating Manual for GRANIA, a Code for the Analysis of Climatic Effects on Natural Environmental Gamma Ray Exposure Rates*, HASL-283 (National Technical Information Service, Springfield, Virginia).

DE STAEBLER, H., JR. (1965). *Transverse Shielding for the Stanford Two-Mile Accelerator*, SLAC-9 (Stanford Linear Accelerator Center, Menlo Park, California).

DE STAEBLER, H., JENKINS, T.M. and NELSON, W.R. (1968). "Shielding and radiation," pages 1029 to 1067 in *The Stanford Two-Mile Accelerator*, Neal, R.B., Ed. (Benjamin, New York).

D'HOMBRES, M.M., DEVILLERS, C., GERVAISE, F., DE SEREVILLE, B. and TARDY-JOUBERT, P. (1968). *Propagation des Neutrons dans les Tunnels d'Acess à un Accelerateur de Haute Energie à Protons*, R-3491 (Centre d'Etudes Nucleaires de Saclay, Saclay, France).

DICKINSON, W.C. and LENT, E.M. (1968). *Calculation of Forward Bremsstrahlung Spectra from Thick Targets*, UCRL-50442 (Lawrence Livermore National Laboratory, Livermore, California).

DIETRICH, S.S. and BERMAN, B.L. (1988). "Atlas of photoneutron cross sections obtained with monoenergetic photons," At. Data Nucl. Data Tables **38**, 199–338.

DIN (1975). Deutsche Industrie Norm. *Medizinische Elektronenbeschleuniger-Anlagen, Teil 2: Strahlenschutzregeln fur die Errichtung* [Medical Electron Accelerator Facilities, Part 2: Radiation Protection Rules for Installation], Draft Report No. DIN-6847 (Beuth-Vertrieb, Berlin).

DINTER, H. and TESCH, K. (1976). *Moderated Rem Meters in Pulsed Neutron Fields,* DESY-76/08 (Deutsches Elektronen-Synchrotron, Hamburg).

DINTER, H. and TESCH, K. (1977). "Dose and shielding parameters of electron-photon stray radiation from a high-energy electron beam," Nucl. Instrum. Methods **143**, 349–355.

DINTER, H. and TESCH, K. (1980). *Investigation of the Protection of the Environment Against Radiation at the Storage Ring HERA*, DESY/HERA 80/04 (Deutsches Elektronen-Synchrotron, Hamburg).

DINTER, H. and TESCH, K. (1992). "Determination of neutron spectra behind lateral shielding of high energy proton accelerators," Radiat. Prot. Dosim. **42**(1), 5–10.

DINTER, H., PANG, J. and TESCH, K. (1988). *Calculations of Doses Due to Electron-Photon Stray Radiation from a High-Energy Electron Beam Behind Lateral Shielding*, DESY-88-117 (Deutches Elektronen-Synchrotron, Hamburg).

DISTENFELD, C. (1975). *Improvements and Tests of the Bonner Sphere Multisphere Spectrometer*, BNL-21293 (National Technical Information Service, Springfield, Virginia).

DISTENFELD, C.H. and COLVETT, R.D. (1966). "Skyshine considerations for accelerator shielding design," Nucl. Sci. Eng. **26**, 117–121.

DISTENFELD, C.H. and MARKOE, A.M. (1965). "Determination of quality factor through the utilization of a balanced tissue-equivalent ionization chamber," pages 181 to 198 in *Proceedings of the USAEC First Symposium on Accelerator Radiation Dosimetry and Experience*, CONF-651109 (National Technical Information Service, Springfield, Virginia).

DOE (1984). U.S. Department of Energy. *Superconducting Super Collider: Report of the Reference Design Group*, DOE-SF-00098-T3 (National Technical Information Service, Springfield, Virginia).

DOE (1992). U.S. Department of Energy. *Safety of Accelerator Facilities* (U.S. Department of Energy, Washington).

DOE (1993). U.S. Department of Energy. *Guidance for an Accelerator Facility Safety Program*, No. 6 (U.S. Department of Energy, Washington).

DOE (1994). U.S. Department of Energy. *Background [Bases and Rationale] for Guidance for an Accelerator Facility Safety Program* (U.S. Department of Energy, Washington).

DOE (1998). U.S. Department of Energy. *Occupational Radiation Protection*, 10 CFR 835, (November 4) (U.S. Government Printing Office, Washington).

DOLE, R.L., JOHNSON, J.O., HETRICK, D.M., WATSON, D.B., HUFF, D.D., DE VORE, J.R., MCNEALY, G.S. and BARNES, J.M. (1999). *Migration of Activation Products from the Oak Ridge Spallation Neutron Source Facility Shield Berm on Chestnut Ridge on the Oak Ridge Reservation*, ORNL/TM-1999/290 (National Technical Information Service, Springfield, Virginia).

DRUGACHENOK, S.A., KIMEL, L.R., KRUPNYI, G.I., LEBEDEV, V.N. and SIDORIN, V.P. (1971). *Passing of High-Energy Muons through Steel Shielding*, IFVE-ORE-71-25 (National Technical Information Service, Springfield, Virginia).

DUDZIAK, D.J. (1968). *Attenuation of Fast Neutron Biological Dose in Non-hydrogenous Shields Followed by Thin Hydrogenous Shields*, LA-DC-9418 (Los Alamos National Laboratory, Los Alamos, New Mexico).

DUDZIAK, D.J. and SCHMUCKER, J.E. (1968). *Hydrogenous-Material-Dependent Removal Cross Section of Lead for Fast Neutron Biological Dose*, WAPD-TM-662 (Bettis Atomic Power Laboratory, Pittsburgh, Pennsylvania).

EAST, L.V. and WALTON, R.B. (1969). "Polyethylene moderated ^{3}He neutron detectors," Nucl. Instrum. Methods **72**, 161–166.

EDWARDS, H.T. (1985). "The Tevatron energy doubler: A superconducting accelerator," Ann. Rev. Nucl. Part. Sci. **35**, 605–660.

EISENBUD, M. (1987). *Environmental Radioactivity: From Natural, Industrial, and Military Sources*, 3rd ed. (Academic Press, New York).

EISENHAUER, C.M., SCHWARTZ, R.B. and JOHNSON, T. (1982). "Measurement of neutrons reflected from the surface of a calibration room," Health Phys. **42**, 489–495.

ELWYN, A.J. and COSSAIRT, J.D. (1986). "A study of neutron leakage through an Fe shield at an accelerator," Health Phys. **51**, 723–735.

ELWYN, A.J. and COSSAIRT, J.D. (1987). "Neutron leakage through an iron shield at a high-energy accelerator," pages 424 to 431 in *Proceedings of the Twentieth Midyear Topical Symposium of the Health Physics Society, Health Physics of Radiation-Producing Machines*, Busick, D.D. and Swanson, W.P., Eds., CONF-8602106 (National Technical Information Service, Springfield, Virginia).

ELWYN, A.J. and CUPPS, V. (1993). *Fermi National Accelerator Laboratory Radioactivity Release Criteria for Materials, Equipment and Waste*, Fermilab Radiation Physics Note 109, Fermilab ES&H Section (Fermi National Accelerator Laboratory, Batavia, Illinois).

ELWYN, A.J. and FREEMAN, W.S. (1984). *Muon Fluence Measurements at 800-GeV*, FERMILAB-TM-1288 (Fermi National Accelerator Laboratory, Batavia, Illinois).

EMERY, E.W. (1966). "Geiger-Mueller and proportional counters," pages 73 to 122 in *Radiation Dosimetry*, Vol. II, Attix, F.H. and Roesch, W.C., Eds. (Academic Press, New York).

EML (1997). Environmental Measurements Laboratory. *EML Procedures Manual*, 28th Edition, HASL-300 (U.S. Department of Energy, New York).

EMMETT, M.B. (1985). *MORSE-CGA, A Monte Carlo Radiation Transport Code with Array Geometry Capability*, ORNL-6174 (National Technical Information Service, Springfield, Virginia).

ENGE, H.A. (1966). *Introduction to Nuclear Physics* (Addison-Wesley Publishing Company, Reading, Massachusetts).

EPA (1976). U.S. Environmental Protection Agency. *National Interim Primary Drinking Water Regulations,* PB-267 630 (National Technical Information Services, Springfield, Virginia).

EPA (1987a). U.S. Environmental Protection Agency. *Protection of the Environment*, 40 CFR 61, Subparts A & H (July 1) (U.S. Government Printing Office, Washington).

EPA (1987b). U.S. Environmental Protection Agency. *Protection of the Environment*, 40 CFR 131.12 (July 1) (U.S. Government Printing Office, Washington).

EPA (1987c). U.S. Environmental Protection Agency. *Protection of the Environment*, 40 CFR 141.16 (July 1) (U.S. Government Printing Office, Washington).

EPA (1989a). U.S. Environmental Protection Agency. *Risk Assessment Methodology: Environmental Impact Statement for NESHAPS Radionuclides, Background Information Document*, Vol. 1, EPA 520/1-89-0005 (U.S. Environmental Protection Agency, Washington).

EPA (1989b). U.S. Environmental Protection Agency. *User's Guide for AIRDOS-PC*, EPA 520/6-89-035 (U.S. Government Printing Office, Washington).

ESPOSITO, A. and PELLICCIONI, M. (1982). "Radiation protection problems at a synchrotron radiation facility," Health Phys. **42**, 703–711.

ESPOSITO, A. and PELLICCIONI, M. (1986). *Gas Bremsstrahlung Production in the ADONE Storage Ring*, LNF-86/23(NT) (Nucleare Laboratori Nazionali di Frascati, Frascati, Italy).

ESPOSITO, A., PELLICCIONI, M. and RINDI, A. (1978). *Radiation Doses at an Electron and Positron Linac and Storage Ring*, LNF-78/39(R) (Nucleare Laboratori Nazionali di Frascati, Frascati, Italy).

EYGES, L. (1948). "Multiple scattering with energy loss," Phys. Rev. **74,** 1534–1535.

FADDEGON, B.A., ROSS, C.K. and ROGERS, D.W.O. (1990). "Forward-directed bremsstrahlung of 10- to 30-MeV electrons incident on thick targets of Al and Pb," Med. Phys. **17**, 773–785.

FADDEGON, B.A., ROSS, C.K. and ROGERS, D.W.O. (1991). "Angular distribution of bremsstrahlung from 15-MeV electrons incident on thick targets of Be, Al and Pb," Med. Phys. **18**, 727–739.

FAILLA, G. and ROSSI, H.H. (1950). "Dosimetry of ionizing particles," Am. J. Roentgenol. Radium. Ther. **64**, 489–491.

FASSO, A. and HOEFERT, M. (1976). "Distributions of secondary particles around various targets exposed to 50 MeV protons," Nucl. Instrum. Methods **133**, 213–218.

FASSO, A., GOEBEL, K., HOEFERT, M., RAU, G., SCHONBACHER, H., STEVENSON, G.R., SULLIVAN, A.H., SWANSON, W.P. and TUYN, J.W.N. (1984a). *Radiation Problems in the Design of the Large Electron-Positron Collider (LEP)*, CERN-84-02 (European Organisation for Nuclear Research, Geneva).

FASSO, A., GOEBEL, K., HOEFERT, M., SCHONBACHER, H. and STEVENSON, G. (1984b). *Radiation Protection for a Large Hadron Collider*, Technical Inspection and Safety Commission, CERN-TIS-RP-IR-84-20 (European Organisation for Nuclear Research, Geneva).

FASSO, A., GOEBEL, K., HOEFERT, M., RANFT, J. and STEVENSON, G. (1990). "Muon transport," Chapter 4 in *Landolt-Bornstein: Numerical Data and Functional Relationships in Science and Technology, Volume 11, Shielding Against High Energy Radiation*, Schopper, H., Ed. (Springer-Verlag, New York).

FASSO, A., FERRARI, A., RANFT, J. and SALA, P.R. (2001). "FLUKA: Status and prospective for hadronic applications," pages 955 in 960 in *Electron-Photon Transport in Fluka: Proceedings of the Monte Carlo 2000 Conference*, Kling, A., Barao, F., Nakagawa, M., Tavora, L. and Paz, P., Eds. (Springer-Verlag, New York).

FERRARI, A., PELLICCIONI, M. and SALA, P.R. (1993). "Bremsstrahlung source terms for intermediate energy electron accelerators," Nucl. Instrum. Methods **B82**, 32–38.

FERRARI, A., RANFT, J. and SALA, P.R. (2001). "The FLUKA radiation transport code and its use for space problems," Physica Medica **17**, 72–80.

FIECHTNER, A. and WERNLI, C. (1999). "Individual neutron monitoring with CR-39 detectors at an accelerator centre," Radiat. Prot. Dosim. **85**(1–4), 35–38.

FISHER, C.M. (1963). "Note on the nuclear cascade in shielding materials," pages 25 to 37 in *Report of the Shielding Conference Held at the Rutherford Laboratory*, NIRL/R/40, Thomas R.H., Ed. (Rutherford Appleton Laboratory, Oxfordshire, United Kingdom).

FLEISCHER, R.L., PRICE, P.B. and WALKER, R.M. (1963). "Method of forming fine holes of near atomic dimensions," Rev. Sci. Instrum. **34**, 510–512.

FLEISCHER, R.L., PRICE, P.B. and WALKER, R.M. (1965). "Tracks of charged particles in solids," Science **149**, 383–393.

FLEISCHER, R.L., PRICE, P.B. and WALKER, R.M. (1975). *Nuclear Tracks in Solids: Principles and Applications* (University of California Press, Berkeley, California).

FLUGGE, S., Ed. (1959). *Handbuch der Physik, Volume XLIV: Nuclear Instrumentation I* (Springer-Verlag, New York).

FNAL (1982). Fermi National Accelerator Laboratory. *Physics of High Energy Particle Accelerators*, Carrigan, R.A., Huson, F.R. and Month, M. Eds., AIP Conference Proceedings No. 87 (American Institute of Physics, New York).

FNAL (1983a). Fermi National Accelerator Laboratory. *Proceedings of the 12th International Conference on High-Energy Accelerators*, Cole, F.T. and

Donaldson, R., Eds. (Fermi National Accelerator Laboratory, Batavia, Illinois).

FNAL (1983b). Fermi National Accelerator Laboratory. *Physics of High Energy Particle Accelerators*, Month, M. Ed., AIP Conference Proceedings No. 105 (American Institute of Physics, New York).

FNAL (1985). Fermi National Accelerator Laboratory. *Physics of High Energy Particle Accelerators*, Month, M., Dahl, P.F. and Dienes, M., Eds., AIP Conference Proceedings No. 127 (American Institute of Physics, New York).

FORD, R.L. and NELSON, W.R. (1978). *The EGS Code System: Computer Programmes for the Monte Carlo Simulation of Electromagnetic Cascades Showers*, SLAC-210, Version 3 (Stanford Linear Accelerator Center, Menlo Park, California).

FOURNIE, E.M. and CHILTON, A.B. (1980), "Gamma-ray buildup factors for concrete slab shields under slant incidence conditions," Nucl. Sci. Eng. **76**, 66–69.

FRENCH, R.L. and MOONEY, L.G. (1971). "Differential measurements of fast-neutron air-ground interface effects," Nucl. Sci. Eng. **43**, 273–280.

FREYTAG, E. and RANFT, J. (1971). "Hadronic and electromagnetic cascades," Chapter 3 in *Radiation Problems Encountered in the Design of Multi-GeV Research Facilities* Goebel, K., Ed., CERN-71-21 (European Organisation for Nuclear Research, Geneva).

GABRIEL, T.A. (1985). *The High-Energy Transport Code HETC*, ORNL-TM-9727 (National Technical Information Service, Springfield, Virginia).

GABRIEL, T.A. and ALSMILLER, R.G., JR. (1969). *Photonucleon and Photopion Production from High-Energy (50-400 MeV) Electrons in Thick Copper Targets*, ORNL-4443 (Oak Ridge National Laboratory, Oak Ridge, Tennessee).

GABRIEL, T.A. and SANTORO, R.T. (1971). "Calculation of the long-lived activity in soil produced by 500-GeV protons," Nucl. Instrum. Methods **95**, 275–283.

GABRIEL, T.A., BISHOP, B.L., ALSMILLER, F.S., ALSMILLER, JR., R.G. and JOHNSON, J.O. (1989). *CALOR89: A Monte Carlo Program Package for the Design and Analysis of Calorimeter Systems*, ORNL-TM-11185 (Oak Ridge National Laboratory, Oak Ridge, Tennessee).

GABRIEL, T.A., GROOM, D.E., JOB, P.K., MOKHOV, N.V. and STEVENSON, G.R. (1994). "Energy dependence of hadronic activity," Nucl. Instrum. Methods **A338,** 336–347.

GIBBONS, J.H. (1956). "Neutron resonances in the keV region," Phys. Rev. **102**, 1574–1579.

GIBBONS, J.H. and MACKLIN, R.L. (1958). "Total cross section for $T(p,n)^3He$," Bull. Am. Phys. Soc. **3**, 365.

GIBBONS, J.H. and MACKLIN, R.L. (1959). "Total neutron yields from light elements under proton and alpha bombardment," Phys. Rev. **114**, 571–580.

GIBBONS, J.H. and NEWSON, H.W. (1960). "The $^7Li(p,n)^7Be$ reaction" in *Fast Neutron Physics*, Marion, J.B. and Fowler, J.L., Eds. (Interscience, New York).

GIFFORD, F.A., JR. (1976). "Turbulent diffusion-typing schemes: A review," Nucl. Saf. **17**, 68–86.

GILBERT, W.S. (1969). "Shielding measurements at the CERN 25 GeV proton synchrotron," pages 323 to 340 in *Proceedings of the Second International Conference on Accelerator Dosimetry and Experience*, CONF-691101 (National Technical Information Service, Springfield, Virginia).

GILBERT, W.S., KEEFE, D., MCCASLIN, J.B., PATTERSON, H.W., SMITH, A.R., STEPHENS, L.D., SHAW, K.B., STEVENSON, G.R., THOMAS, R.H., FORTUNE and GOEBEL, K. (1968). *1966 CERN-LRL-RHEL Shielding Experiment at the CERN Proton Synchrotron*, UCRL-17941 (Lawrence Radiation Laboratory, University of California, Berkeley, California).

GOEBEL, K., Ed. (1985). *Radiation Protection Group Annual Report (1984)*, CERN-TIS-RP-146 (European Organisation for Nuclear Research, Geneva).

GOEBEL, K. (1987). "Radiation protection for the CERN large electron project LEP," pages 584 to 595 in *Proceedings of the Twentieth Midyear Topical Symposium of the Health Physics Society, Health Physics of Radiation-Producing Machines*, Busick, D.D. and Swanson, W.P., Eds., CONF-8602106 (National Technical Information Service, Springfield, Virginia).

GOEBEL, K., STEVENSON, G.R., ROUTTI, J.T. and VOGT, H.G. (1975). *Evaluating Dose Rates Due to Neutron Leakage Through the Access Tunnels of the SPS*, CERN-LABII-RA-Note-75-10 (European Organisation for Nuclear Research, Geneva).

GOLDIE, C.H., WRIGHT, K.A., ANSON, J.H., CLOUD, R.W. and TRUMP, J.G. (1954). "Radiographic properties of x-rays in the two-to-six million volt range," ASTM Bull. **49**, 201.

GOLLON, P.J. (1976). "Production of radioactivity by particle accelerators," IEEE Trans. Nucl. Sci. **NS-23**, 1395–1399.

GOLLON, P.J. (1978). *Soil Activation Calculations for the Anti-Proton Target Area*, FERMILAB-TM-816 (Fermi National Accelerator Laboratory, Batavia, Illinois).

GOLLON, P.J. and AWSCHALOM, M. (1971). *Design of Penetrations in Hadron Shields*, Vol. 2, CERN-71-16 (European Organisation for Nuclear Research, Geneva).

GOODMAN, L.J. and ROSSI, H.H. (1968). "The measurement of dose equivalent using paired ionization chambers," Health Phys. **14**, 168–170.

GOUDSMIT, S.A. and SAUNDERSON, J.L. (1940). "Multiple scattering of electrons," Phys. Rev. **57**, 24.

GREENHOUSE, N.A., DE CASTRO, T.M., MCCASLIN, J.B., SMITH, A.R., SUN, R.K. and HANKINS, D.E. (1987). "An evaluation of NTA film in an accelerator environment and comparisons with CR-39," Radiat. Prot. Dosim. **20**(3), 143–147.

GRIFFITH, R.V. (1987). "Personnel dosimetry developments," in *Summary and Minutes of DOE Accelerator Contractor's Planning Meeting on Accelerator Health Physics Research Needs*, Coulson, L., Ed. (Fermi National Accelerator Laboratory, Batavia, Illinois).

GRIFFITH, R.V. and FISHER, J.C. (1976). *Measurement of the Responses of Multisphere Detectors with Monoenergetic Neutrons, 0.1 to 18.5 MeV,* Hazards Control Department Report No. 55, UCRL-50007-75-2 (Lawrence Livermore National Laboratory, Livermore, California).

GRIFFITH, R.V. and TOMMASINO, L. (1990). "Etch track detectors," pages 323 to 426 in *Dosimetry of Ionizing Radiation*, Vol. III, Kase, K.R., Bjarngard, B.E. and Attix, F.H., Eds. (Academic Press, New York).

GRIFFITH, R.V., MCMAHON, T.A. and ESPINOSA, G. (1984). "A commercial bacterial colony counter for semiautomatic track counting," Nucl. Tracks Radiat. Meas. **8**, 215–218.

HACK, R.C. (1971). *Personal Fast Neutron Dosimetry Around Nimrod*, RHEL/M-R8 (Rutherford Appleton Laboratory, Oxfordshire, United Kingdom).

HAGAN, W.K., COLBURN, B.L., ARMSTRONG, T.W. and ALLEN, M. (1988). "Radiation shielding calculations for a 70- to 250-MeV proton therapy facility," Nucl. Sci. Eng. **98**, 272–278.

HALBLEIB, J.A., KENSEK, R.P., MEHLHORN, T.A., VALDEZ, G.D., SELTZER, S.M. and BERGER, M.J. (1992). *ITS Version 3.0: The Integrated TIGER Series of Coupled Electron/Photon Monte Carlo Transport Codes*, SAND-91-1634 (Sandia National Laboratories, Albuquerque, New Mexico).

HANKINS, D.E. (1962). *Neutron Monitoring Instrument Having a Response Approximately Proportional to the Dose Rate from Thermal to 7.0 MeV*, LA-2717 (Los Alamos National Laboratory, Los Alamos, New Mexico).

HANKINS, D.E. and CORTEZ, J.R. (1975). "Energy dependence of four neutron remmeter instruments," Health Phys. **28**, 305–307.

HANKINS, D.E., HOMANN, S.G. and DAVIS, J. (1984). "Use of CR-39 foils for personnel neutron dosimetry: New electrochemical etching chambers and procedures," pages 11 to 19 in *Annual Technology Review 1984*, Griffith, R.V. and Anderson, K.J., Eds., UCRL 50007-84 (Lawrence Livermore National Laboratory, Livermore, California).

HANKINS, D.E., HOMANN, S.G. and WESTERMARK, J. (1985). "Use of CR-39 foils for personnel neutron dosimetry: Improved electrochemical etching chambers and procedures" pages 79 to 87 in *Annual Technology Review 1985*, Griffith, R.V. and Anderson, K.J. Eds., UCRL 50007-85 (Lawrence Livermore National Laboratory, Livermore, California).

HANNA, R.C. (1955). "Disintegration of ^{7}Be by slow neutrons," Phil. Mag. **46**, 381–392.

HANSON, A.O. and MCKIBBEN, J.L. (1947). "A neutron detector having uniform sensitivity from 10 keV to 3 MeV," Phys. Rev. **72**, 673–677.

HARRISON, K.G. and TOMMASINO, L. (1985). "Damage track detectors for neutron dosimetry: II. Characteristics of different detection systems," Radiat. Prot. Dosim. **10**(1–4), 219–235.

HAYWOOD, F.F., AUXIER, J.A. and LOY, E.T. (1964). *An Experimental Investigation of the Spatial Distribution of Dose in an Air-Over-Ground Geometry*, CEX, 62-14 (Oak Ridge National Laboratory, Oak Ridge, Tennessee).

HAYWOOD, F.F., PROVENZANO, T.G. and AUXIER, J.A., Eds. (1965). *Operations Plan-Operation HENRE*, CEX, 65-03 (National Technical Information Service, Springfield, Virginia).

HEIJNE, E.H.M. (1983). *Muon Flux Measurement with Silicon Detectors in the CERN Neutrino Beams*, CERN-83-06 (European Organisation for Nuclear Research, Geneva).

HEITLER, W. (1954). *The Quantum Theory of Radiation*, 3rd ed. (Clarendon Press, Oxford, United Kingdom).

HENSON, A.M. and THOMAS, R.H. (1978). "Measurement of the efficiency of ^{7}LiF thermoluminescent dosimeters of heavy ions," Health Phys. **34**, 389–390.

HERMINGHAUS, H. (1984). "Survey on CW electron accelerators," in *Proceedings of the 1984 Linear Accelerator Conference*, Angert, N., Ed., FRG Report GS18471 (Gessellshaft fur Schwerionenforschung, Darmstadt).

HESS, W.N., PATTERSON, H.W. and WALLACE, R. (1957). "Delay-line chamber has large area, low capacitance," Nucleonics **15**, 74–79.

HESS, W.N., PATTERSON, H.W., WALLACE, R. and CHUPP, E.L. (1959). "Cosmic-ray neutron energy spectrum," Phys. Rev. **116,** 445–457.

HEWITT, J.E., HUGHES, L., MCCASLIN, J.B., SMITH, A.R., STEPHENS, L.D., SYVERTSON, C.A., THOMAS, R.H. and TUCKER, A.B. (1980). "Exposure to cosmic-ray neutrons at commercial jet aircraft altitudes," pages 855 to 881 in *Natural Radiation Environment III*, Vol. 2, Gesell, T.F. and Lowder, W.M., Eds., CONF-780422 (National Technical Information Services, Springfield, Virginia).

HIRAYAMA, H., BAN, S. and MIURA, S. (1987). "Investigations of electromagnetic cascades produced in lead by 2.5-GeV bremsstrahlung," Nucl. Sci. Eng. **96**, 66–72.

HOEFERT, M. (1984). *Muons and Exposure Dose*, CERN-TIS-RP-IR-84-23 (European Organisation for Nuclear Research, Geneva).

HOEFERT, M. (1986). *Experience at CERN in Various Fields of Radiation Protection*, CERN-TIS-RP-175-CF (European Organisation for Nuclear Research, Geneva).

HOEFERT, M. and BAARLI, J. (1974). "Some preliminary investigations on the contribution of muons to the stray radiation level around the CERN 28 GeV Proton Synchrotron," pages 841 to 845 in *Proceedings of the Third International Congress of IRPA*, Snyder, W.S., Ed., CONF-730907-P1 (National Technical Information Service, Springfield, Virginia).

HOEFERT, M. and RAFFNSOE, C. (1980). "Measurement of absolute absorbed dose and dose-equivalent response for instruments used around high-energy proton accelerators," Nucl. Instrum. Methods **176**, 443–448.

HOEFERT, M. and STEVENSON, G. R. (1994). "The CERN-CEC high-energy reference field facility," pages 635 to 642 in *Proceedings of the Eighth International Conference on Radiation Shielding* (American Nuclear Society, LaGrange Park, Illinois).

HOEFERT, M. BARTLETT, D.T. and PIESCH, E. (1987). "Personnel neutron monitoring around high energy accelerators," Radiat. Prot. Dos. **20**(1–2), 103–108.

HOLT, P.D. (1985). "Passive detectors for neutron fluence measurement," Radiat Prot. Dosim. **10**(1–4), 251–264.

HOYER, F.E. (1968). *Induced Radioactivity in Earth Shielding on Top of High-Energy Particle Accelerators*, CERN-68-42 (European Organisation for Nuclear Research, Geneva).

HSU, H.H. and SUN, R.K. (1995). "Monte Carlo calculations of high energy neutron responses for improved Andersson-Braun rem meters," Radiat. Prot. Dosim. **61**(1–3), 167–170.

HSU, H.H., ALVAR, K.R. and VASILIK, D.G. (1994). "A new Bonner-sphere set for high energy neutron measurements: Monte Carlo simulation," IEEE Trans. Nucl. Sci. **41**, 938–940.

HUBBARD, E.L., MAIN, R.M. and PYLE, R.V. (1960). "Neutron production by heavy-ion bombardment," Phys. Rev. **118**, 507–514.

HUBBELL, J.H. (1969). *Photon Cross Sections, Attenuation Coef cients, and Energy Absorption Coef cients from 10 keV to 100 GeV*, Publication No. NSRDS-NBS 29 (U.S. Government Printing Office, Washington).

HUBBELL, J.H. (1977). "Photon mass attenuation and mass energy-absorption coefficients for H, C, N, O, Ar and seven mixtures form 0.1 keV to 20 MeV," Radiat. Res. **70**, 58–81.

HUBBELL, J.H. (1982). "Photon mass attenuation and energy-absorption coefficients," Int. J. Appl. Radiat. Isot. **33**, 1269–1290.

HUBBELL, J.H., GIMM, H.A. and OVERBO, I. (1980). "Pair, triplet and total atomic cross sections (and mass attenuation coefficients) for 1 MeV-100 GeV photons in elements Z = 1 to 100," J. Phys. Chem. Ref. Data **9**, 1023–1147.

HUDIS, J. and KATCOFF, S. (1969). "High-energy proton fission cross sections of U, Bi, Au, and Ag measured with mica track detectors," Phys. Rev. **180**, 1122–1130.

HUMPHRIES, S., JR. (1986). *Principles of Charged Particle Acceleration* (John Wiley and Sons, New York).

IAEA (1968). International Atomic Energy Agency. *Engineering Compendium on Radiation Shielding, Volume 1, Shielding Fundamentals and Methods*, Jaeger, R.G., Blizard, E.P., Chilton, A.B., Grotenhuis, M., Honig, A., Jaeger, T.A. and Eisenlohr, H.H., Eds. (Springer-Verlag, New York).

IAEA (1970). International Atomic Energy Agency. *Engineering Compendium on Radiation Shielding, Volume 3, Shield Design and Engineering*, Jaeger, R.G., Blizard, E.P., Chilton, A.B., Grotenhuis, M., Hoenig, A., Jaeger, T.A. and Eisenlohr, H.H., Eds. (Springer-Verlag, New York).

IAEA (1975). International Atomic Energy Agency. *Engineering Compendium on Radiation Shielding, Volume 2, Shielding Materials*, Jaeger, R.G., Blizard, E.P., Chilton, A.B., Grotenhuis, M., Hoenig, A., Jaeger, T.A. and Eisenlohr, H.H., Eds. (Springer-Verlag, New York).

IAEA (1976). International Atomic Energy Agency. *Radiological Safety Aspects of the Operation of Neutron Generators*, Safety Series No. 42, STI/PUB/427 (International Atomic Energy Agency, Vienna).

IAEA (1979a). International Atomic Energy Agency. *Radiological Safety Aspects of the Operation of Electron Linear Accelerators*, Technical Report

Series No. 188, STI/DOC/010/188 (International Atomic Energy Agency, Vienna).

IAEA (1979b). International Atomic Energy Agency. *Operational Limits and Conditions for Nuclear Power Plants*, Safety Guide 50-SG-3 (International Atomic Energy Agency, Vienna).

IAEA (1988). International Atomic Energy Agency. *Radiological Safety Aspects of the Operation of Proton Accelerators*, Technical Report Series No. 283, STI/DOC/010/283 (International Atomic Energy Agency, Vienna).

IAEA (1991). International Atomic Energy Agency. *Safe Handling of Tritium: Review of Data and Experience*, Technical Report Series No. 324, STI/DOC/010/324 (International Atomic Energy Agency, Vienna).

ICRP (1963). International Commission on Radiological Protection. "Report of the RBE Committee to the International Commissions on Radiological Protection and on Radiological Units and Measurements," Health Phys. **9**, 357–384.

ICRP (1973). International Commission on Radiological Protection. *Data for Protection Against Ionizing Radiation from External Sources: Supplement to ICRP Publication 15*, ICRP Publication 21 (Elsevier Science, New York).

ICRP (1977). International Commission on Radiological Protection. *Recommendations of the International Commission on Radiological Protection*, ICRP Publication 26, Annals of ICRP **1** (Elsevier Science, New York).

ICRP (1980a). International Commission on Radiological Protection. *Statement and Recommendations of the International Commission on Radiological Protection from its 1980 Stockholm Meeting*, ICRP Publication 30, Part 2, Annals of ICRP **4** (3/4) (Elsevier Science, New York).

ICRP (1980b). International Commission on Radiological Protection. *Statement and Recommendations of the 1980 Brighton Meeting of the ICRP: Limits of Intakes of Radionuclides by Workers*, ICRP Publication 30, Part 2, Annals of ICRP **4** (Elsevier Science, New York).

ICRP (1984). International Commission on Radiological Protection. *A Compilation of the Major Concepts and Quantities in Use by ICRP*, ICRP Publication 42, Annals of ICRP **14** (Elsevier Science, New York).

ICRP (1985). International Commission on Radiological Protection. *Statement from the 1985 Paris Meeting of the ICRP: Quantitative Bases for Developing a Uni ed Index of Harm*, ICRP Publication 45, Annals of ICRP **15** (Elsevier Science, New York).

ICRP (1988). International Commission on Radiological Protection. *Data for Use in Protection Against External Radiation*, ICRP Publication 51, Annals of ICRP **17** (Elsevier Science, New York).

ICRP (1991). International Commission on Radiological Protection. *1990 Recommendations of the International Commission on Radiological Protection*, ICRP Publication 60, Annals of ICRP **21** (Elsevier Science, New York).

ICRP (1996). International Commission on Radiological Protection. *Conversion Coef cients for Use in Radiological Protection Against External Radiation*, ICRP Publication 74, Annals of ICRP **26** (Elsevier Science, New York).

ICRP (1997a). International Commission on Radiological Protection. *General Principles for the Radiation Protection of Workers*, ICRP Publication 75, Annals of ICRP **27** (Elsevier Science, New York).

ICRP (1997b). International Commission on Radiological Protection. *Protection from Potential Exposures: Application to Selected Radiation Sources*, ICRP Publication 76, Annals of ICRP **27** (Elsevier Science, New York).

ICRU (1976a). International Commission on Radiation Units and Measurements. *Conceptual Basis for the Determination of Dose Equivalent*, ICRU Report 25 (International Commission on Radiation Units and Measurements, Bethesda, Maryland).

ICRU (1976b). International Commission on Radiation Units and Measurements. *Neutron Dosimetry for Biology and Medicine*, ICRU Report 26 (International Commission on Radiation Units and Measurements, Bethesda, Maryland).

ICRU (1978). International Commission on Radiation Units and Measurements. *Basic Aspects of High Energy Particle Interactions and Radiation Dosimetry*, ICRU Report 28 (International Commission on Radiation Units and Measurements, Bethesda, Maryland).

ICRU (1980). International Commission on Radiation Units and Measurements. *Radiation Quantities and Units*, ICRU Report 33 (International Commission on Radiation Units and Measurements, Bethesda, Maryland).

ICRU (1982). International Commission on Radiation Units and Measurements. *The Dosimetry of Pulsed Radiation*, ICRU Report 34 (International Commission on Radiation Units and Measurements, Bethesda, Maryland).

ICRU (1983). International Commission on Radiation Units and Measurements. *Microdosimetry*, ICRU Report 36 (International Commission on Radiation Units and Measurements, Bethesda, Maryland).

ICRU (1984). International Commission on Radiation Units and Measurements. *Stopping Powers for Electrons and Positrons*, ICRU Report 37 (International Commission on Radiation Units and Measurements, Bethesda, Maryland).

ICRU (1985). International Commission on Radiation Units and Measurements. *Determination of Dose Equivalents Resulting from External Radiation Sources*, ICRU Report 39 (International Commission on Radiation Units and Measurements, Bethesda, Maryland).

ICRU (1986). International Commission on Radiation Units and Measurements. *The Quality Factor in Radiation Protection*, ICRU Report 40 (International Commission on Radiation Units and Measurements, Bethesda, Maryland).

ICRU (1988). International Commission on Radiation Units and Measurements. *Determination of Dose Equivalents from External Radiation Sources—Part 2*, ICRU Report 43 (International Commission on Radiation Units and Measurements, Bethesda, Maryland).

ICRU (1992a). International Commission on Radiation Units and Measurements. *Photon, Electron, Proton and Neutron Interaction Data for Body*

Tissues, ICRU Report 46 (International Commission on Radiation Units and Measurements, Bethesda, Maryland).

ICRU (1992b). International Commission on Radiation Units and Measurements. *Measurement of Dose Equivalents from External Photon and Electron Radiations*, ICRU Report 47 (International Commission on Radiation Units and Measurements, Bethesda, Maryland).

ICRU (1993a). International Commission on Radiation Units and Measurements. *Quantities and Units in Radiation Protection Dosimetry*, ICRU Report 51 (International Commission on Radiation Units and Measurements, Bethesda, Maryland).

ICRU (1993b). International Commission on Radiation Units and Measurements. *Stopping Powers and Ranges for Protons and Alpha Particles*, ICRU Report 49 (International Commission on Radiation Units and Measurements, Bethesda, Maryland).

ICRU (1998a). International Commission on Radiation Units and Measurements. *Conversion Coef cients for Use in Radiological Protection Against External Radiation*, ICRU Report 57 (International Commission on Radiation Units and Measurements, Bethesda, Maryland).

ICRU (1998b). International Commission on Radiation Units and Measurements. *Fundamental Quantities and Units for Ionizing Radiation*, ICRU Report 60 (International Commission on Radiation Units and Measurements, Bethesda, Maryland).

IEEE (1975). Institute of Electrical and Electronics Engineers. *1975 Particle Accelerator Conference, Accelerator Engineering and Technology,* IEEE Trans. Nucl. Sci. **NS-22**.

IEEE (1977). Institute of Electrical and Electronics Engineers. *1977 Particle Accelerator Conference, Accelerator Engineering and Technology,* IEEE Trans. Nucl. Sci. **NS-24**.

IEEE (1979). Institute of Electrical and Electronics Engineers. *1979 Particle Accelerator Conference, Accelerator Engineering and Technology,* IEEE Trans. Nucl. Sci. **NS-26**.

IEEE (1981). Institute of Electrical and Electronics Engineers. *1981 Particle Accelerator Conference, Accelerator Engineering and Technology*, IEEE Trans. Nucl. Sci. **NS 28**.

IEEE (1983). Institute of Electrical and Electronics Engineers. *1983 Particle Accelerator Conference, Accelerator Engineering and Technology,* IEEE Trans. Nucl. Sci. **NS-30**.

IEEE (1985). Institute of Electrical and Electronics Engineers. *1985 Particle Accelerator Conference, Accelerator Engineering and Technology*, IEEE Trans. Nucl. Sci. **NS-32**.

ING, H. (1986). "The status of the bubble damage polymer detector," Nucl. Tracks Radiat. Meas. **12**, 49–54.

ING, H. (1987). "A new bubble detector for the detection of gamma rays," (abstract) Health Phys. **52**, S67.

ING, H. and BIRNBOIM, H.C. (1984). "A bubble-damage polymer detector for neutrons," Nucl. Tracks Radiat. Meas. **8**, 285–288.

ING, H. and PIESCH, E., Eds. (1985). "Neutron dosimetry in radiation protection: Special issue," Radiat. Prot. Dosim. **10**(1–4).

JAFFE, G. (1913). " Zur Theorie der Ionisation in Kolonnen: I," Ann. Physik. **42**, 303–344.

JAFFE, G. (1929a). "Zur Theorie der Ionisation in Kolonnen: II," Ann. Physik. **1**, 977–1008.

JAFFE, G. (1929b). "Kolonnenionisation in Gasen bei erhohtem Druk," Phyik. Z. **30**, 849–856.

JAFFE, G. (1940). "On the theory of recombination," Phys Rev. **58**, 968–976.

JAHNERT, B. (1972). "The response of TLD-700 thermoluminescent dosimeters to protons and alpha-particles," Health Phys. **23**, 112–114.

JAHR, R., ALBERTS, W.G., MENZEL, H. and SCHRAUBE, H., Eds. (1992). *Proceedings of the Seventh Symposium on Neutron Dosimetry*, Radiat. Prot. Dosim. **44**(1–4).

JAKEWAYS, R. and CALDER, I.R. (1970). "An experimental study of the longitudinal development of electron initiated cascades in lead in the energy range 0.5 to 4.0 GeV," Nucl. Instrum. Methods **84**, 79–82.

JANNI, J.F. (1982). "Calculations of energy loss, range, and probability of inelastic nuclear collisions for 0.1- to 1000-MeV protons," At. Data Nucl. Data Tables **27,** 147.

JAUCH, J.M. and ROHRLICH, F. (1976). *The Theory of Photons and Electrons*, 2nd ed. (Springer-Verlag, New York).

JENKINS, T.M. (1974). "Accelerator boundary doses and skyline," Health Phys. **27**, 251–257.

JENKINS, T.M. (1979). "Neutron and photon measurements through concrete from a 15 GeV electron beam on a target—comparison with models and calculations," Nucl. Instrum. Methods **159**, 265–288.

KALEF-EZRA, J. and HOROWITZ, Y.S. (1982). "Heavy charged particle thermoluminescence dosimetry: Track structure theory and experiments," Int. J. Appl. Radiat. Isot. **33**, 1085–1100.

KANG, Y., LEE, K., ROBERTS, A., SNOWDON, S.C., THERIOT, D. and MEYER, S.L. (1972). "Design of a magnetized iron muon shield for a high-energy neutrino laboratory," Part. Accel. **4**, 31–41.

KARZMARK, C.J. and CAPONE, T. (1968). "Measurements of 6 MV x-rays, I. Primary radiation absorption in lead, steel and concrete," Br. J. Radiol. **41**, 33–39.

KARZMARK, C.J., NUNAN, C.S. and TANABE, E. (1993). *Medical Electron Accelerators* (McGraw-Hill, Inc., New York).

KASE, K.R. (1967). "Radioactive gas production at a 100-MeV electron Linac facility," Health Phys. **13**, 869–876.

KASE, K.R., BJARNGARD, B. and ATTIX, F.H. (1990). *Dosimetry of Ionizing Radiation, Volume III* (Academic Press, New York).

KASE, K.R., MAO, X.S., NELSON, W.R., LIU, J.C., KLECK, J.H. and ELSALIM, M. (1998). "Neutron fluence and energy spectra around the Varian Clinac 2100C/2300C medical accelerator," Health Phys. **74**, 38–47.

KATHREN, R.L. (1990). "External beta-photon dosimetry for radiation protection," pages 321 to 370 in *Dosimetry of Ionizing Radiation, III*, Kase, K.R., Bjarngard, B. and Attix, F.H., Eds. (Academic Press, New York).

KEEFE, D. (1964). *Mu-Meson Shielding Problems at 200 GeV: Approximate Calculations*, UCID-10018 (Lawrence Berkeley Laboratories, Berkeley, California).

KEEFE, D. and NOBLE, C.M. (1968). "Radiation shielding for high energy muons: The case of a cylindrically symmetrical shield and no magnetic fields," Nucl. Instrum. Methods **64**, 173–180.

KELLER, L.P. (1991). *Calculation of Muon Background in a 0.5 TeV Linear Collider*, SLAC-PUB-5533 (Stanford Linear Accelerator Center, Menlo Park, California).

KELLER, L.P. (1993). *Muon Background in a 1.0-TeV Linear Collider*, SLAC-PUB-6385. (Stanford Linear Accelerator Center, Menlo Park, California).

KELLER, K.A., LANGE, J. and MUENZEL, H. (1974). *Landolt-Bornstein: Numerical Data and Functional Relationships in Science and Technology, Group 1, Volume 5, Part C*, Shopper, H., Ed. (Springer-Verlag, New York).

KELLY, E.L. and WIEGAND, C. (1948). "Fission of elements from Pt to Bi by high energy neutrons," Phys. Rev. **73**, 1135–1139.

KIMURA, K., ISHIKAWA, T., KINNO, M., YAMADERA, A. and NAKA-MURA, T. (1994). "Residual long-lived radioactivity distribution in the inner concrete wall of a cyclotron vault," Health Phys. **67**, 621–631.

KINNEY, W.E. (1962). *A Monte Carlo Calculation of Scattered Neutron Fluxes at an Air-Ground Interface Due to Point Isotropic Sources on the Interface*, ORNL-3287 (Oak Ridge National Laboratory, Oak Ridge, Tennessee).

KIRALY, P. and WOLFENDALE, A.W. (1970). "Rate of energy loss and sea-level spectrum of muons above 1000 GeV," Phys. Letters **32B**, 510–512.

KIRN, F.S. and KENNEDY, R.J. (1954). "Betatron x-rays: How much concrete for shielding?" Nucleonics **12,** 44–48.

KLEIN, O. and NISHINA, Y. (1929). "Uber die streuung von strahlung durah freie elektronen nach der neuen relativistis-chen quantendynamik von dirac," Z. Physik **52**, 853–868.

KNASEL, T.M. (1970). "Accurate calculation of radiation lengths," Nucl. Instrum. Methods **83**, 217–220.

KNOLL, G.F. (1979). *Radiation Detection and Measurement* (Wiley and Sons, New York).

KNOLL, G.F. (1989). *Radiation Detection and Measurement*, 2nd ed. (Wiley and Sons, New York).

KNOLL, G.F. (2000). *Radiation Detection and Measurement*, 3rd ed. (Wiley and Sons, New York).

KOCH, E.E., Ed. (1983). *Handbook on Synchrotron Radiation*, Vol. 1 (Elsevier Science, New York).

KOCH, H.W. and MOTZ, J.W. (1959). "Bremsstrahlung cross section formulas and related data," Rev. Mod. Phys. **31**, 920–955.

KOHAUPT, R.D. and VOSS, G.A. (1983). "Progress and problems in the performance of e^+e^- storage rings," Ann. Rev. Nucl. Part. Sci. **33**, 67–104.

KOMOCHKOV, M.M. (1970). "The Dubna Synchrophasotron," pages 171 to 174 in *Engineering Compendium on Radiation Shielding, Volume 3, Shield Design and Engineering*, Jaeger, R.G., Blizard, E.P., Chilton, A.B., Grotenhuis, M., Hoenig, A., Jaeger, T.A. and Eisenlohr, H.H., Eds. (Springer-Verlag, New York).

KONSHIN, V.A., MATUSEVICH, E.S. and REGUSHEVSKII, V.I. (1966). "Cross sections for the fission of ^{181}Ta, Re, Pt, ^{197}Au, Pb, ^{209}Bi, ^{235}Th, ^{235}U and ^{238}U by protons with energies 150 to 660 MeV," Sov. J. Nucl. Phys. **2,** 489–492.

KOSAKO, T., NAKAMURA, T. and IWAI, S. (1985). "Estimation of response functions of moderating type neutron detectors by the time-of-flight method combined with a large lead pile," Nucl. Instrum. Methods **A235**, 103–122.

KRUGLOV, S.P. and LOPATIN, I.V. (1960). "A study of the dispersion of the energy of an impact radiation beam from an absorption calorimeter," Zh. Tekh. Fiz. **30**, 424.

KUEHNER, A.V. and CHESTER, J.D. (1973). *Dose Equivalent Meter Operating Instructions*, Internal report, Health and Safety Division (Brookhaven National Laboratory, Upton, New York).

KUEHNER, A.V., CHESTER, J.D. and BAUM, J.W. (1972). *Portable Mixed Radiation Dose Equivalent Meter*, BNL-17298 (National Technical Information Service, Springfield, Virginia).

KUEHNER, A.V., CHESTER, J.D. and BAUM, J.W. (1973). "Portable mixed radiation dose-equivalent meter for protection monitoring," pages 233 to 246 in *Neutron Monitoring for Radiation Protection Purposes*, Vol. 1, STI/PUB/318 (International Atomic Energy Agency, Vienna).

LADU, M., PELLICCIONI, M. and ROTONDI, E. (1963). "On the response to fast neutrons of a BF_3 counter in a paraffin spherical-hollow moderator," Nucl. Instrum. Methods **23**, 173–174.

LADU, M., PELLICCIONI, M. and ROTONDI, E. (1965). "Flat response to neutrons between 20 keV and 14 MeV of a BF_3 counter in a spherical hollow moderator," Nucl. Instrum. Methods **32**, 175–176.

LADU, M., PELLICCIONI, M., PICCHI, P. and VERRI, G. (1968). "A contribution to the skyshine study," Nucl. Instrum. Methods **62**, 51–56.

LAHTI, G.P. (1986). "Approximate techniques for calculating gamma ray dose rates in nuclear power plants," pages 15 to 41 in *Approximate Calculational Techniques for Radiation Protection Applications,* Rice, A.F. and Roussin, R.W., Eds. ORNL/RSIC-48, ANS/SD-86/17 (National Technical Information Service, Springfield, Virginia).

LAMPLEY, C.M., ANDREW, M.C. and WELLS, M.B. (1988). *The SKYSHINE-III Procedure: Calculation of the Effects of a Structure Design on Neutron, Primary Gamma Ray and Secondary Gamma Ray Dose Rates in Air*, RRA-T8209A (Radiation Research Associates, Ft. Worth, Texas).

LANDRY D.J. and ANDERSON, D.W. (1991). "Measurement of accelerator bremsstrahlung spectra with a high-efficiency Ge detector," Med. Phys. **18**, 527–532.

LAPOSTOLLE, P.M. and SEPTIER, A.L., Eds. (1970). *Linear Accelerators* (Elsevier Science, New York).

LARIVIERE, P.D. (1984). "Transmission in concrete of primary and leakage x rays from a 24-MV medical linear accelerator," Health Phys. **47**, 819–827.

LAWRENCE, E.O. and LIVINGSTON, M.S. (1932). "The production of high speed light ions without the use of high voltages," Phys. Rev. **40**, 19–35.

LAWRENCE, E.O., LIVINGSTON, M.S. and WHITE, M.G. (1932). "The disintegration of lithium by swiftly-moving protons," Phys. Rev. **42**, 150–151.

LAWSON, J.D. and TIGNER, M. (1984). "The physics of particle accelerators," Ann. Rev. Nucl. Part. Sci. **34**, 99–123

LEAKE, J.W. (1967). "Portable instruments for the measurement of neutron dose-equivalent rate in steady-state and pulsed neutron fields," pages 313 to 326 in *Neutron Monitoring*, STI/PUB/136 (International Atomic Energy Agency, Vienna).

LEAKE, J.W. (1968). "An improved spherical dose equivalent neutron detector," Nucl. Instrum. Methods **63**, 329–332.

LEBEDEV, V.N., ZOLIN, L.S. and SALATSKAYA, M.I. (1965). *A Distribution of the Penetrating Radiation Field over the Protective Zone of the 10 GeV Synchrophasotron*, JNIR-P-2177 (Joint Institute for Nuclear Research, Dubna, Russia).

LEIMDORFER, M. (1968). "The backscattering of photons," pages 233 to 245 in *Engineering Compendium on Radiation Shielding, Volume 1, Shielding Fundamentals and Methods*, Jaeger, R.G., Blizard, E.P., Chilton, A.B., Grotenhuis, M., Honig, A., Jaeger, T.A. and Eisenlohr, H.H., Eds. (Springer-Verlag, New York).

LEVINE, G.S., SQUIER, D.M., STAPLETON, G.B., STEVENSON, G.R., GOEBEL, K. and RANFT, J. (1972). "The angular dependence of dose and hadron yields from targets in 8 GeV/c and 24 GeV/c extracted proton beams," Part. Accel. **3**, 91–101.

LEWANDOWSKI, M.A., IPE, N.E. and VYLET. V. (1993). "Measurement of neutron dose equivalent and spectra at the Stanford Linear Accelerator Center," Health Phys. **64**, S13.

LIBOFF, A.R. (1975). "Cosmic radiation in the lower atmosphere," pages 55 to 67 in *Natural Radiation Environment II*, Adams, J.S.A., Lowder, W.M. and Gesell, T.F., Eds., CONF-720805-Pl (National Technical Information Service, Springfield, Virginia).

LIM, C.E. (1973). *The Development of a Neutron Spectrometer Using Multi-Wire Spark Chambers for the Measurement of the Spectra of Stray Neutrons in the Vicinity of High Energy Accelerators*, Ph.D. Thesis, LBL 1719 (University of California, Lawrence Berkeley Laboratory, Berkeley, California).

LINDENBAUM, S.J. (1957). "Brookhaven National Laboratory proton synchrotron," pages 28 to 37 in *Conference on Shielding of High Energy Accelerators,* TID-7545 (Technical Information Service Extension, Oak Ridge, Tennessee).

LINDENBAUM, S.J. (1961). "The shielding of high-energy accelerators," Ann. Rev. Nucl. Sci. **11,** 213.

LIU, J.C., JENKINS, T.M., MCCALL, R.C. and IPE, N.E. (1991). "Neutron dosimetry at SLAC: Neutron sources and instrumentation," SLAC-TN-91-3 (Stanford Linear Accelerator Center, Menlo Park, California).

LIU, J.C., ROKNI, S., VYLET, V., ARORA, R., SEMONES, S. and JUSTUS, A. (1997). "Neutron detection time distributions of multisphere LiI

detectors and AB rem meter at a 20-MeV electron linac," Radiat. Prot. Dosim. **71**(4), 251–259.

LIVESEY, D.L. (1966). *Atomic and Nuclear Physics* (Blaisdell Publishing Company, Walthan, Massachusetts).

LIVINGOOD, J.J. (1961). *Principles of Cyclic Particle Accelerators* (Van Nostrand, New York).

LIVINGSTON, M.S. (1952). "High-energy accelerators; standard cyclotron," "High-energy accelerators; synchrocyclotron," and "High-energy accelerators; proton synchrotron," Ann. Rev. Nucl. Sci. **1**, 157–162, 163–168.

LIVINGSTON, M.S., Ed. (1966). *The Development of High-Energy Accelerators* (Dover Publications, New York).

LIVINGSTON, M.S. and BLEWETT, J.P. (1962). *Particle Accelerators* (McGraw Hill, New York).

LOCHAMY, J.C. (1981). *The Minimum Detectable Activity Content*, PSD No. 17 (EG&G ORTEC, Oak Ridge, Tennessee).

LOKAN, K.H., SHERMAN, N.K., GELLIE, R.W., HENRY, W.H., LEVESQUE, R., NOWAK, A., TEATHER, G.G. and LUNDQUIST, J.R. (1972). "Bremsstrahlung attenuation measurements in ilmenite loaded concretes," Health Phys. **23**, 193–199.

LOWDER, W.M. and DE PLANQUE, G. (1977). *The Response of LiF Dosimeters to Natural Environmental Radiation*, HASL-313 (National Technical Information Service, Springfield, Virginia).

LOWDER, W.M., RAFT, P.D. and BECK, H.L. (1972). "Experimental determination of cosmic-ray charged-particle intensity profiles in the atmosphere," pages 908 to 912 in *Proceedings of the National Symposium on Natural and Manmade Radiation in Space*, Warman, E.A., Ed., NASA TM-X-2440 (National Technical Information Service, Springfield, Virginia).

LOWRY, K.A. and JOHNSON, T.L. (1984). "Modification to iterative recursion unfolding algorithms and computer codes to find more appropriate neutron spectra," Health Phys. **47**, 587–593.

LRL (1965). Lawrence Radiation Laboratory. *200 BeV Design Study*, UCRL-1600 (Lawrence Radiation Laboratory, Berkeley, California).

LUX, I. and KOBLINGER, L. (1991). *Monte Carlo Particle Transport Methods: Neutron and Photon Calculations* (CRC Press, Boca Raton, Florida).

MACKLIN R.L. and GIBBONS, J.H. (1958a). "(p,n) reactions in light nuclei," Bull. Am. Phys. Soc. **3**, 26.

MACKLIN R.L. and GIBBONS, J.H. (1958b). "Study of the $T(p,n)^3$He and $^7Li(p,n)^7$Be reactions," Phys. Rev. **109**, 105.

MADEY, R. (1968). "Nuclear accelerators in general," pages 49 to 56 in *Engineering Compendium on Radiation Shielding, Volume 1, Shielding Fundamentals and Methods*, Jaeger, R.G., Blizard, E.P., Chilton, A.B., Grotenhuis, M., Honig, A., Jaeger, T.A. and Eisenlohr, H.H., Eds. (Springer-Verlag, New York).

MADEY, R. and WATERMAN, F.M. (1973). "Neutron spectorscopy from 1 MeV to 1 GeV," pages 113 to 121 in *Neutron Monitoring for Radiation Protection Purposes*, Vol. 1, STI/PUB/318 (International Atomic Energy, Vienna).

MAERKER, R.E. and CAIN, V.R. (1967). *AMC: A Monte Carlo Code Utilizing the Albedo Approach for Calculating Neutron and Capture Gamma-Ray Distributions in Rectangular Concrete Ducts*, ORNL-3964 (Oak Ridge National Laboratory, Oak Ridge, Tennessee).

MAIELLO, M.L., GULBIN, J.F., DE PLANQUE, G. and GESELL, T.F. (1990). "8th international intercomparison of environmental dosimeters," Radiat. Prot. Dosim. **32**(2), 91–98.

MAMONT-CIESLA, K. and RINDI, A. (1974). *Spark Chamber Neutron and Spectrometer: First Report on Performances,* LBL-3343 (Lawrence Berkeley Laboratory, Berkeley, California).

MAO, X.S., KASE, K.R. and NELSON, W.R. (1996). "Giant dipole resonance neutron yields produced by electrons as a function of target material and thickness," Health Phys. **70**, 207–214.

MAO, X., KASE, K.R., LIU, J.C., NELSON, W.R., KLECK, J.H. and JOHNSON, S. (1997). "Neutron sources in the Varian Clinac 2100C/2300C medical accelerator calculated by EGS4 code," Health Phys. **72**, 524–529.

MAO, X.S., FASSO, A., LIU, J.C., NELSON, W.R. and ROKNI, S. (2000). *90° bremsstrahlung source term produced in thick targets by 50-MeV to 10-GeV electrons*, SLAC-PUB-7722 (Stanford Linear Accelerator Center, Menlo Park, California).

MARGENAU, H. and MURPHY, G.M. (1943). *The Mathematics of Physics and Chemistry* (Van Nostrand, New York).

MARUYAMA, T., KUMAMOTO. Y., KATO, Y., HASHIZUME, T. and YAMAMOTO, M. (1971). "Attenuation of 4-32 MV x-rays in ordinary concrete, heavy concrete, iron and lead," Health Phys. **20**, 277–284.

MASLOV, M.A., MOKHOV, N.V. and UZUNIAN, A.V. (1983). "Calculation of muonic fields around large high energy proton accelerators," Nucl. Instrum. Methods **217**, 419–424.

MATZKE, M. (1988). "Estimation of dose equivalent from reaction rates of Bonner spheres without using *a priori* fluence information," Radiat. Prot. Dosim. **23**(1–4), 297–300.

MCCALL, R.C., JENKINS, T.M. and SHORE, R.A. (1979). "Transport of accelerator produced neutrons in a concrete room," IEEE Trans. Nucl. Sci. **NS-26**, 1593–1602.

MCCASLIN, J.B. (1960). "A high-energy neutron-flux detector," Health Phys. **2**, 399–407.

MCCASLIN, J.B. (1964). "Electrometer for ionization chambers using metal-oxide-semiconductor field-effect transistors," Rev. Sci. Instrum. **35**, 1587–1591.

MCCASLIN, J.B. (1973). "Detection of neutrons greater than 20 MeV from the production of ^{11}C," pages 621 to 626 in *Accelerator Health Physics,* Patterson, H.W. and Thomas, R.H., Eds. (Academic Press, New York).

MCCASLIN, J.B. and STEPHENS, L.D. (1967). *High-Sensitivity Neutron and Proton Flux Detector with a Practical Threshold Near 600 MeV, Using Hg (spallation) [149]Tb,* UCRL-17505 (Lawrence Radiation Laboratory, Berkeley, California).

MCCASLIN, J.B. and STEPHENS, L.D. (1976). *Effect of Neutron Scattering on the Calibration of Moderated BF_3 Detectors*, Internal Note HPN-57 (Lawrence Berkeley Laboratory, Berkeley, California).

MCCASLIN, J.B. and THOMAS, R.H. (1981). "Practical neutron dosimetry at high energies," pages 137 to 175 in *Proceedings of the European Seminar on Radiation Protection Quantities for External Exposure*, CONF-8010168 (National Technical Information Service, Springfield, Virginia).

MCCASLIN, J.B., PATTERSON, H.W., SMITH, A.R. and STEPHENS, L.D. (1966). "Some recent developments in techniques for monitoring high-energy accelerator radiation," pages 1131 to 1137 in *Proceedings of the First International Congress of Radiation Protection*, CONF-660920 (National Technical Information Service, Springfield, Virginia).

MCCASLIN, J.B., STEPHENS, L.D. and THOMAS, R.H. (1983). "Ground scattering contribution in neutron calibrations," Health Phys. **44**, 437–439.

MCCASLIN, J.B., LA PLANT, P.R., SMITH, A.R., SWANSON, W.P. and THOMAS, R.H. (1985a). "Neutron production by Ne and Si ions on a thick Cu target at 670 MeV with application to radiation protection," IEEE Trans. Nucl Sci. **NS-32**, 3104–3106.

MCCASLIN, J.B., SWANSON, W.P. and THOMAS, R.H. (1985b). *Moyer Model Approximations for Point and Extended Beam Losses*, LBL-14699 (Lawrence Berkeley Laboratory, Berkeley, California).

MCCASLIN, J.B., SUN, R.K.S., SWANSON, W.P., ELWYN, A.J., FREE-MAN, W. S. and YURISTA, P.M. (1986). *Measurement of Neutron Spectra and Doses in the Tevatron Tunnel for 800 GeV Circulating Proton Beams*, SSC-58 (National Technical Information Service, Springfield, Virginia).

MCCASLIN, J.B., SWANSON, W.P. and THOMAS, R.H. (1987). "Moyer model approximations for point and extended beam losses," Nucl. Instrum. Methods **A256**, 418–426.

MCCASLIN, J.B., SUN, R.K.S., SWANSON, W.P., COSSAIRT, J.D., ELWYN, A.J., FREEMAN, W.S., JOESTLEIN, H., MOORE, C.D., YURISTA, P.M. and GROOM, D. E. (1988). "Radiation environment in the tunnel of a high-energy proton accelerator at energies near 1 TeV," pages 137 to 140 in *Proceedings of the International Congress of the International Radiation Protection Association*, CONF-880404-18 (National Technical Information Service, Springfield, Virginia).

MCDONALD, J.C., POSNY, F., GERDUNG-LIST, S., CHARTIER, J.L. and KURKDJIAN, J. (1995). "Dosimetric measurements in simulated practical neutron fields using several dosemeter systems," Radiat. Prot. Dosim. **62**(4), 197–202.

MCGINLEY, P.H. (1992a). "Photoneutron production in the primary barrier of medical accelerator rooms," Health Phys. **62**, 359–362 (also see *Errata*, Health Phys. **63**, 366.)

MCGINLEY, P.H. (1992b). "Photoneutron fields in medical accelerator rooms with primary barriers constructed of concrete and metals," Health Phys. **63**, 698–701.

MCGINLEY, P.H. and MINER, M.S. (1995). "A method of eliminating the maze door of medical accelerator rooms," Radiat. Prot. Manage. **12**, 29–37.

MCGINLEY, P.H., MINER, M. and MITCHUM, M.L. (1995). "A method for calculating the dose due to capture gamma rays in accelerator mazes," Phys. Med. Biol. **40**, 1467–1473.

MCGUIRE, S.A. (1965). *A Dose Monitoring Instrument for Neutrons from Thermal to 100 MeV*, LA-3435 (Los Alamos National Laboratory, Los Alamos, New Mexico).

MENZEL, H.G., CHARTIER, J.L., JAHR, R. and RANNOU, A., Eds. (1997). *Proceedings of the Eighth Symposium on Neutron Dosimetry*, Radiat. Prot. Dosim. **70**(1–4).

MESSEL, H. and CRAWFORD, D.F. (1970). *Electron-Photon Shower Distribution Function; Tables for Lead, Copper, and Air Absorbers* (Elsevier Science, New York).

METROPOLIS, N., BIVINS, R, STORM, M., MILLER, J.M., FRIEDLANDER, G. and TURKEVICH, A. (1958a). "Monte Carlo calculations of intranuclear cascades. I. Low-energy studies," Phys. Rev. **110**, 185–203.

METROPOLIS, N., BIVINS, R., STORM, M., MILLER, J.M., FRIEDLANDER, G. and TURKEVICH, A. (1958b). "Monte Carlo calculations of intranuclear cascades. II. High-energy studies and pion processes," Phys. Rev. **110**, 204–219.

MIJNHEER, B.J. (1971). *Standard Fluxes and Standard Moderating Counters for Neutron Fluence Measurements*, Thesis (University of Amsterdam, Netherlands).

MILLER, W. and KENNEDY, R.J. (1956). "Attenuation of 86- and 176-MeV synchrotron x-rays in concrete and lead," Radiat. Res. **4**, 360–366.

MOE, H.J. (1991). *Advanced Photon Source: Radiological Design Consideration*, APS-LS-141-Rev. (Argonne National Laboratory, Argonne, Illinois).

MOHAN, R., CHUI, C. and LIDOFSKY, L. (1985). "Energy and angular distributions of photons from medical linear accelerators," Med. Phys. **12**, 592–597.

MOKHOV, N.V. (1995). *The MARS Code System User's Guide, Version 13(95)*, FERMILAB-FN-628 (Fermi National Accelerator Laboratory, Batavia, Illinois).

MOLE, R.H. (1979). "RBE for carcinogenesis by fission neutrons," Health Phys. **36**, 463–465.

MOLIERE, G. (1948). "Theorie der Streuung schneller geladener Teilchen II. Mehrfach- und Vielfachstreuung," Z. Naturforschg. **3a**, 78–97.

MOORE, C. and VELEN, S. (1974). *Muon Beam Halo Studies*, FERMILAB-TM-497 (Fermi National Accelerator Laboratory, Batavia, Illinois).

MORITZ, L.E., SUZUKI, T., NOGUCHI, M., OKI, Y., MIURA, T., MIURA, S., TAWARA, H., BAN, S., HIRAYAMA, H. and KONDO, K. (1990). "Characteristics of the neutron field in the KEK counter wall," Health Phys. **58**, 487–492.

MOY, B., RAU, G. and SCHWENKE, D. (1980). *The Instrumentation for Monitoring the Environment Around CERN*, CERN-HS-RP-050 (European Organisation for Nuclear Research, Geneva).

MOYER, B.J. (1952). "Survey methods for fast- and high-energy neutrons," Nucleonics **10**, 14–19.

MOYER, B.J. (1954). "Neutron physics of concern to the biologist," Radiat. Res. **1**, 10–22.

MOYER, B.J. (1957). "Build-up factors," pages 96 to 100 in *Conference on Shielding of High Energy Accelerators*, Solon, L., Ed., TID-7545 (National Technical Information Service, Springfield, Virginia).

MOYER, B.J. (1961). *Evaluation of Shielding Required for the Improved Bevatron*, UCRL-9769 (Lawrence Berkeley Laboratory, Berkeley, California).

MOYER, B.J. (1962). "Method of calculating the shielding enclosure for the Berkeley Bevatron," pages 65 to 70 in *Premier Colloque International sur la Protection aupres des grands Acceleratuers* (University of France Presses, Paris).

MUELLER, D. (1972). "Electron showers of high primary energy in lead," Phys. Rev. **D5**, 2677–2683.

NAGEL, H. (1956). "Electron-photon cascades in lead and Monte Carlo calculation for primary electron energies between 100 and 1000 MeV," Z. Physik **186**, 319.

NAKAMURA, T. and KOSAKO, T. (1981). "A systematic study on the neutron skyshine from nuclear facilities, Part I: Monte Carlo analysis of neutron propagation in air over ground environment from a monoenergetic source," Nucl. Sci. Eng. **77**, 168.

NAKAMURA, T., YOSHIDA, M. and SHIN, K. (1978). "Spectra measurements of neutrons and photons from thick targets of C, Fe, Cu, and Pb by 52 MeV protons," Nucl. Instrum. Methods **151**, 493–503.

NAKAMURA, T., KOSAKO, T., HAYASHI, K., BAN, S. and KATOH, K. (1981). "A systematic study on the neutron skyshine from nuclear facilities, part II: Experimental approach to the behavior of environmental neutrons around an electron synchrotron," Nucl. Sci. Eng. **77**, 182–191.

NAKAMURA, T., FUJII, M. and SHIN, K. (1983). "Neutron production from thick targets of carbon, iron, copper and lead by 30- and 52-MeV protons," Nucl. Sci. Eng. **83**, 444–458.

NAKAMURA, T., OHKUBO, T. and UWAMINO, Y. (1987). "Spatial distribution of radionuclides produced in copper by photonuclear spallation reactions," Nucl. Instrum. Methods **A256**, 505–512.

NBS (1954). National Bureau of Standards. *Protection Against Betatron-Synchrotron Radiations Up to 100 Million Electron Volts*, NBS Handbook No. 55 (U.S. Government Printing Office, Washington).

NBS (1964a). National Bureau of Standards. *Physical Aspects of Irradiation*, NBS Handbook No. 85 (U.S. Government Printing Office, Washington).

NBS (1964b). National Bureau of Standards. *Shielding for High-Energy Electron Accelerator Installations*, NBS Handbook No. 97 (U.S. Government Printing Office, Washington).

NCRP (1970). National Council on Radiation Protection and Measurements. *Medical X-Ray and Gamma-Ray Protection for Energies Up to 10 MeV—Structural Shielding Design and Evaluation Handbook*, NCRP Report No. 34 (National Council on Radiation Protection and Measurements, Bethesda, Maryland).

NCRP (1971). National Council on Radiation Protection and Measurements. *Protection Against Neutron Radiation*, NCRP Report No. 38 (National Council on Radiation Protection and Measurements Bethesda, Maryland).

NCRP (1976a). National Council on Radiation Protection and Measurements. *Structural Shielding Design and Evaluation for Medical Use of X Rays and Gamma Rays of Energies Up to 10 MeV*, NCRP Report

No. 49 (National Council on Radiation Protection and Measurements, Bethesda, Maryland).

NCRP (1976b). National Council on Radiation Protection and Measurements. *Environmental Radiation Measurements*, NCRP Report No. 50 (National Council on Radiation Protection and Measurements, Bethesda, Maryland).

NCRP (1976c). National Council on Radiation Protection and Measurements. *Tritium Measurement Techniques*, NCRP Report No. 47 (National Council on Radiation Protection and Measurements, Bethesda, Maryland).

NCRP (1977). National Council on Radiation Protection and Measurements. *Radiation Protection Design Guidelines for 0.1 – 100 MeV Particle Accelerator Facilities*, NCRP Report No. 51 (National Council on Radiation Protection and Measurements, Bethesda, Maryland).

NCRP (1978). National Council on Radiation Protection and Measurements. *Operational Radiation Safety Program*, NCRP Report No. 59 (National Council on Radiation Protection and Measurements, Bethesda, Maryland).

NCRP (1983). National Council on Radiation Protection and Measurements. *Radiation Protection and Measurements for Low Voltage Neutron Generators*, NCRP Report No. 72 (National Council on Radiation Protection and Measurements, Bethesda, Maryland).

NCRP (1984). National Council on Radiation Protection and Measurements. *Neutron Contamination from Medical Electron Accelerators,* NCRP Report No. 79 (National Council on Radiation Protection and Measurements, Bethesda, Maryland).

NCRP (1986). National Council on Radiation Protection and Measurements. *Radiation Alarms and Access Control Systems*, NCRP Report No. 88 (National Council on Radiation Protection and Measurements, Bethesda, Maryland).

NCRP (1987a). National Council on Radiation Protection and Measurements. *Ionizing Radiation Exposure of the Population of the United States*, NCRP Report No. 93 (National Council on Radiation Protection and Measurements, Bethesda, Maryland).

NCRP (1987b). National Council on Radiation Protection and Measurements. *Exposure of the Population in the United States and Canada from Natural Background Radiation*, NCRP Report No. 94 (National Council on Radiation Protection and Measurements, Bethesda, Maryland).

NCRP (1989). National Council on Radiation Protection and Measurements. *Medical X-Ray, Electron Beam and Gamma-Ray Protection for Energies Up to 50 MeV (Equipment Design, Performance and Use)*, NCRP Report No. 102 (National Council on Radiation Protection and Measurements, Bethesda, Maryland).

NCRP (1993). National Council on Radiation Protection and Measurements. *Limitation of Exposure to Ionizing Radiation*, NCRP Report No. 116 (National Council on Radiation Protection and Measurements, Bethesda, Maryland).

NCRP (1996). National Council on Radiation Protection and Measurements. *Screening Models for Releases of Radionuclides to Atmosphere, Surface Water, and Ground*, NCRP Report No. 123 (National Council on Radiation Protection and Measurements, Bethesda, Maryland).

NCRP (1998). National Council on Radiation Protection and Measurements. *Operational Radiation Safety Program*, NCRP Report No. 127 (National Council on Radiation Protection and Measurements, Bethesda, Maryland).

NCRP (2000). National Council on Radiation Protection and Measurements. *Operational Radiation Safety Training*, NCRP Report No. 134 (National Council on Radiation Protection and Measurements, Bethesda, Maryland).

NEET, D.A.G. (1965). *Radiation Exposure in the Switchyard*, SLAC-TN-65-9 (Stanford Linear Accelerator Center, Stanford, California).

NEGRO, V.C., CASSIDY, M.E. and GRAVESON, R.T. (1967). "A guarded insulated gate field effect electrometer," IEEE Trans. Nucl. Sci. **NS-14**, 135–142.

NELSON, W.R. (1968). "The shielding of muons around high-energy electron accelerators: Theory and measurement," Nucl. Instrum. Methods **66**, 293–303.

NELSON, W.R. and JENKINS, T.M., Eds. (1980). *Computer Techniques in Radiation Transport and Dosimetry* (Plenum Press, New York).

NELSON, W.R. and KASE, K.R. (1974). "Muon shielding around high-energy electron accelerators. Part I. Theory," Nucl. Instrum. Methods **120**, 401–411.

NELSON, W.R. and LARIVIERE, P.D. (1984). "Primary and leakage radiation calculations at 6, 10 and 25 MeV," Health Phys. **47**, 811–818.

NELSON, W.R., JENKINS, T.M., MCCALL, R.C. and COBB, J.K. (1966). "Electron-induced cascade showers in copper and lead at 1 GeV," Phys, Rev. **149**, 201–208.

NELSON, W.R., KASE, K.R. and SVENSSON, G.K. (1974). "Muon shielding around high-energy electron accelerators. Part II. Experimental investigation," Nucl. Instrum. Methods **120**, 414–429.

NELSON, W.R., STEVENSON, G.R., HEIJNE, E.H.M., JARRON, P., LIU, K.L. and NEILSEN, M. (1979). *Preliminary Profile Measurements of High-Energy Muon Beams in a Soil Shield*, CERN-HS-RP-042 (European Organisation for Nuclear Research, Geneva).

NELSON, W.R., JENKINS, T.M., STEVENSON, G.R., NIELSEN, M., HEIJNE, E.H.M., JARRON, P., LORD, J. and ANDERSON, S. (1983). "Transport of high energy muons in a soil shield," Nucl. Instrum. Methods **215**, 385–396.

NELSON, W.R., HIRAYAMA, H. and ROGERS, D.W.O. (1985). *The EGS4 Code-System*, SLAC 265 (Stanford Linear Accelerator Center, Menlo Park, California).

NEPA (1969). National Environmental Policy Act. Public Law 91-190, 83 Stat. 852, as amended (January 1, 1970) (U.S. Government Printing Office, Washington).

NHMRC (1995). National Health and Medical Research Council of Australia. *Recommended Limits on Radioactive Contamination on Surfaces in Laboratories*, Radiation Health Series No. 38 (Australian Radiation Protection and Nuclear Safety Agency, Yallambie, Victoria, Australia).

NIELSEN, B. (1974). *Muon Measurements for Radiation Protection*, CERN-HP-74-135 (European Organisation for Nuclear Research, Geneva).

NORTHCLIFFE, L.C. and SCHILLING, R.F. (1970). "Range and stopping-power tables for heavy ions," Nucl. Data Tables **A7**, 233–463.

O'BRIEN, K. (1968a). *Transverse Shielding Calculations for Components of a 1/2-TeV Proton Synchrotron*, HASL-199 (National Technical Information Service, Springfield, Virginia).

O'BRIEN, K. (1968b). *Tables for the Determination of the Lateral Shielding Requirements of High-Energy Accelerators*, HASL-203 (National Technical Information Service, Springfield, Virginia).

O'BRIEN, K. (1969). "Extra-nuclear hadron cascade calculations using Passow's approximation," Nucl. Instrum. Methods **72,** 93–98.

O'BRIEN, K. (1970). *Shielding Calculations for Broad Neutron Beams Normally Incident on Slabs of Concrete*, HASL-221 (National Technical Information Service, Springfield, Virginia).

O'BRIEN, K. (1971a). *Neutron Spectra in the Side-Shielding of a Large Particle Accelerator*, HASL 240 (National Technical Information Service, Springfield, Virginia).

O'BRIEN, K. (1971b). "Cosmic-ray propagation in the atmosphere," Nuovo Cimento **3A**, 521–547.

O'BRIEN, K. (1972). "Propagation of muons underground and the primary cosmic-ray spectrum below 40 TeV," Phys. Rev. **D5**, 597–605.

O'BRIEN, K. (1975). "The cosmic-ray field at ground level," pages 15 to 54 in *The Natural Radiation Environment II, Part 1, Proceedings of the Second International Symposium on the Natural Radiation Environment*, Adams, A.S., Lowder, W.M. and Gesell, T.F., Eds., CONF-720805 (National Technical Information Service, Springfield, Virginia).

O'BRIEN, K. (1978). "The response of LiF thermoluminescence dosimeters to the ground-level cosmic-ray background," Int. J. Appl. Radiat. Isot. **29**, 735–739.

O'BRIEN, K. (1980). "The physics of radiation transport," in *Computer Techniques in Radiation Transport and Dosimetry*, Nelson, W.R. and Jenkins, T.M., Eds. (Plenum Press, New York).

O'BRIEN, K. and MCLAUGHLIN, J.E. (1968). "The propagation of the neutron component of the nucleonic cascade at energies less than 500 MeV: Theory and a solution to the accelerator transverse shielding problem," Nucl. Instrum. Methods **60,** 129–140.

O'BRIEN, K. and SANNA, R. (1981). "Neutron spectrum unfolding using the Monte Carlo method," Nucl. Instrum. Methods **185**, 277–286.

O'BRIEN, K. and SANNA, R. (1983). "Reply to Chambless and Broadway," Nucl. Instrum. Methods **214**, 547–549.

O'BRIEN, K., SANNA, R.S. and MCLAUGHLIN, J.E. (1965). "Inference of accelerator stray neutron spectra from various measurements," pages 286 to 305 in *Proceedings of the USAEC First Symposium on Accelerator*

Radiation Dosimetry and Experience, CONF-651109 (National Technical Information Service, Springfield, Virginia).

O'BRIEN, K., SANDMEIR, H.A., HANSEN, G.E. and CAMPBELL, G.A. (1978). "Cosmic-ray induced neutron background sources and fluxes for geometries of air over water, ground, iron and aluminum," J. Geophys. Res. **83**, 114–120.

O'CONNOR, D.T., CRISCUOLO, E.L. and PACE, A.L. (1949). "10 MeV x-ray technique, papers on radiography," Am. Soc. Test. Mater. Spec. Tech. Publ. **96**.

ODA, K., KOBAYASHI, H., YAMAMOTO, T. and KAWANISUI, M. (1982). "Experimental determination of collection efficiency of ionization chamber infield of pulsed x-rays," J. Nucl. Sci. Technol. (Japan) **19**, 89–95.

O'DELL, A.A., JR., SANDIFER, C.W., KNOWLEN, R.B. and GEORGE, W.D. (1968). "Measurements of absolute thick-target bremsstrahlung spectra," Nucl. Instrum. Methods **61**, 340–346.

OHNESORGE, W.F., BUTLER, H.M., FULMER, C.B. and MOSKO, S.W. (1980). "Heavy ion target area fast neutron dose equivalent rates," Health Phys. **39**, 633–636.

OLLENDORF, W. (1964). *A Study of Radiation Levels at the CERN Site*, CERN-DI-HP-66 (European Organisation for Nuclear Research, Geneva).

OLSHER, R.H., HSU, H.H., BEVERDING, A., KLECK, J.H., CASSON, W.H., VASILIK, D.G. and DEVINE, R.T. (2000). "WENDI: An improved neutron rem meter," Health Phys. **79**, 170–181.

OPELKA, J.H., MUNDIS, R.L., MARMER, G.J., PETERSON, J.M., SISKIND, B. and KIKTA, M.J. (1979). *Particle-Accelerator Decommissioning*, ANL/ES-82 (Argonne National Laboratory, Argonne, Illinois).

ORNL (1990). Oak Ridge National Laboratory. *RSIC Computer Code and Data Collections*, DCL-93/Skyport, Radiation Shielding Information Center (Oak Ridge National Laboratory, Oak Ridge, Tennessee).

OSBORNE, J.L., WOLFENDALE, A.W. and PALMER, N.S. (1964). "The spectrum of high-energy cosmic ray muons," Proc. Phys. Soc. (London) **84**, 911–913.

OTTE, R.A., SWANSON, W.P., ROWE, E.M. and DELUCA, P.M., JR. (1987). "Aladdin, a 1-GeV electron storage ring: An opportunity to understand its radiation patterns," pages 479 to 485 in *Proceedings of the Twentieth Midyear Topical Symposium of the Health Physics Society, Health Physics of Radiation-Producing Machines*, Busick, D.D. and Swanson, W.P., Eds., CONF-8602106 (National Technical Information Service, Springfield, Virginia).

PAGES, K., BERTEL, E., JOFFRE, H. and SKLAVENITIS, L. (1972). "Energy loss, range, and bremsstrahlung yield for 10-keV to 100-MeV electrons in various elements and chemical compounds," At. Data Nucl. Data Tables **4**, 1–127.

PANOFSKY, W.K.H. (1980). "Needs versus means in high-energy physics," Phys. Today **33**, 24–33.

PASSOW, C. (1962). *Phenomenologische Theorie zur Berechnung einer Kaskade aus Schweren Teilchen (Nukleonenkaskade) in der Materie*, DESY-Notiz A 2.85 (Deutsches Elektronen-Synchrotron, Hamburg).

PATRICK, J.W., STEPHENS, L.D., THOMAS, R.H. and KELLY, L.S. (1975). "The design of an experiment to study leukemogenesis in mice irradiated by energetic heavy ions," Radiat. Res. **64**, 492–508.

PATTERSON, H.W. (1957). *The University of California Radiation Laboratory Synchrocyclotron* (Lawrence Berkeley Laboratory, Berkeley, California).

PATTERSON, H.W. and THOMAS, R.H. (1973). *Accelerator Health Physics* (Academic Press, New York).

PATTERSON, H.W. and WALLACE, R.W. (1958). *A Method of Calibrating Slow Neutron Detectors,* UCRL-8359 (Lawrence Radiation Laboratory, Berkeley, California).

PATTERSON, H.W., HECKMAN, H.H. and ROUTTI, J.T. (1969). "New measurements of star production in nuclear emulsions and applications to high-energy neutron spectroscopy," pages 750 to 763 in *Proceedings of the Second International Conference on Accelerator Dosimetry and Experience*, CONF-691101 (National Technical Information Service, Springfield, Virginia).

PEETERMANS, A. and BAARLI, J. (1974). "Radioactive gas and aerosol production by the CERN high-energy accelerators and evaluation of their influences on environmental problems," in *Environmental Surveillance Around Nuclear Installations*, STI/PUB/353 (International Atomic Energy Agency, Vienna).

PELLICCIONI, M. and ESPOSITO, A.S. (1987). "Measurements of gas bremsstrahlung in the Adone storage ring," pages 495 to 501 in *Proceedings of the Twentieth Midyear Topical Symposium of the Health Physics Society, Health Physics of Radiation-Producing Machines*, Busick D.D. and Swanson, W.P., Eds., CONF-8602106 (National Technical Information Service, Springfield, Virginia).

PENFOLD, J. and STEVENSON, G.R. (1968). *Preliminary Measurements of the Angular Distribution of the Stray Radiation Field,* RP/PN/29 (Rutherford Appleton Laboratory, Oxfordshire, United Kingdom).

PEREY, F.G. (1977). *Least-Squares Dosimetry Unfolding: The Program STAY'SL*, ORNL/TM-6062, ENDF-254 (Oak Ridge National Laboratory, Oak Ridge, Tennessee).

PERKINS, D.H. (1963). "Results from cosmic ray experiments," in *High-Energy Physics Study*, UCRL-10022 (Lawrence Berkeley Laboratory, Berkeley, California).

PERRY, D.R. (1967). "Neutron dosimetry methods and experience in the 7 GeV proton synchrotron, Nimrod," pages 355 to 374 in *Neutron Monitoring*, STI/PUB/136 (International Atomic Energy Agency, Vienna).

PERRY, D.R. and SHAW, K.B. (1965). "Radiation levels in and around Nimrod," pages 20 to 33 in *Proceedings of the First Symposium on Accelerator Radiation Dosimetry and Experience*, CONF-651109 (National Technical Information Service, Springfield, Virginia).

PERSICO, E., FERRARI, E. and SEGRE, S.E. (1968). *Principles of Particle Accelerators* (W.A. Benjamin, New York).

PIESCH, E. and BURGKHARDT, B. (1985). "Albedo neutron dosimetry," Radiat. Prot. Dosim. **10**(1–4), 175–188.

PLECHATY, E.F., CULLEN, D.E. and HOWERTON, R.J. (1975). *Tables and Graphs of Photon-Interaction Cross Sections from 1.0 keV to 100 MeV Derived from the LLL Evaluated Nuclear Data Library*, UCRL-50400 (Lawrence Livermore National Laboratory, Livermore, California).

POLLOCK, R. (1981). "Tritium contamination in accelerator cryogenic facilities," Health Phys. **40**, 565.

PORTAL, G. (1981). "Preparation and properties of principal TL products," in *Applied Thermoluminescence Dosimetry*, Oberhofer, M. and Scharmann, A., Eds. (A. Hilger, Boston).

POWELL, C.F., FOWLER, P.H. and PERKINS, D.H. (1959). *The Study of Elementary Particles by the Photographic Method* (Elsevier Science, New York).

PRAEL, R.E. and LICHTENSTEIN, H. (1989). *User Guide to LCS: The LAHET Code System*, LA-UR-89-3014 (Los Alamos National Laboratory, Los Alamos, New Mexico).

PRICE, P.B. and WALKER, R.M. (1962). "Observations of charged-particle tracks in solids," J. Appl. Phys. **33**, 3400–3406.

PRICE, P.B. and WALKER, R.M. (1963). "A simple method of measuring low uranium concentrations in natural crystals," Appl. Phys. Letters **2**, 23–25.

PRICE, B.T., HORTON, C.C. and SPINNEY, K.T. (1957). *Radiation Shielding* (Elsevier Science, New York).

PRICE, J.H., COLLINS, D.G. and WELLS, M.B. (1976). *Utilization Instructions for SKYSHINE*, RRA-N7608 (Radiation Research Associates, Ft. Worth, Texas).

PRUITT, J.S. (1964). "High energy x-ray photon albedo," Nucl. Instrum. Methods **27** 23–28.

PSZONA, S. (1969). "A new approach for determining quality factor and dose equivalent in mixed radiation fields," Health Phys. **16**, 9–11.

PSZONA, S. (1971). "The NE-102A organic scintillation detector as an acceptable LET dependent detector for quality factor and dose equivalent determination in mixed radiation fields," pages 388 to 402 in *Proceedings of the International Congress on Protection Against Accelerator and Space Radiation*, CERN-71-16 (European Organisation for Nuclear Research, Geneva).

PSZONA, S. and HOEFERT, M. (1977). "A rapid method for the determination of dose equivalent in mixed radiation fields," Nucl. Instrum. Methods **146**, 509–512.

RANFT, J. (1967). "Improved Monte Carlo calculation of the nucleon-meson cascade in shielding material, I. Description of the method of calculation," and "II. Comparison of the result for incident proton bemas with momenta of 10 and 20 GeV/c with experimental data," Nucl. Instrum. Methods **48**, 133–140, 261–276.

RANFT, J. and ROUTTI, J.T. (1972). "Hadronic cascade calculations of angular distributions of integrated secondary particle fluxes from external targets and new empirical formulae describing particle production in proton-nucleus collisions," Part. Accel. **4,** 101–110.

RAU, G. and WITTEKIND, D. (1982a). *Proposal for Measuring the Natural Radiation Around the Future LEP*, CERN-HS-RP-TM-82-28 (European Organisation for Nuclear Research, Geneva).

RAU, G. and WITTEKIND, D. (1982b). *Environmental Radiation Monitoring on the CERN Sites During 1981*, CERN-HS-RP-IR-82-13 (European Organisation for Nuclear Research, Geneva).

RCHSA (1968). Radiation Control for Health and Safety Act. Public Law 90-602 (U.S. Government Printing Office, Washington).

REGINATTO, M. and GOLDHAGEN, P. (1998). *MAXED: A Computer Code for the Deconvolution of Multisphere Neutron Spectrometer Data Using the Maximum Entropy Method*, EML-595 (National Technical Information Service, Springfield, Virginia).

REMY, R. (1965). *Neutron Spectroscopy by the Use of Nuclear Stars from 20 to 300 MeV*, M.S. Thesis, UCRL-16325 (National Technical Information Service, Springfield, Virginia).

RHOADES, W.A., SIMPSON, D.B., CHILDS, R.L. and ENGLE, W.W., JR. (1979). *DOT-IV Two-Dimensional Discrete Ordinates Transport Code With Space-Dependent Mesh and Quadrature*, ORNL/TM-6529 (Oak Ridge National Laboratory, Oak Ridge, Tennessee).

RIBES, J.B., MOY, B. and RAU, G. (1974). *Systeme de Mesure de la Radioactivite de l' Air*, CERN-LABII RA-Note-74-6 (European Organisation for Nuclear Research, Geneva).

RIBES, J.B., MOY, B. and RAU, G. (1976). *Etalonnage du Systeme de Ventilation*, CERN-SPS-RA-SM-76-18 (European Organisation for Nuclear Research, Geneva).

RINDI, A. (1969). "Present and projected uses of multiwire spark chambers in health physics," pages 660 to 671 in *Proceedings of the Second International Conference on Accelerator Dosimetry and Experience*, CONF-691101 (National Technical Information Service, Springfield, Virginia).

RINDI, A. (1972). *La Radioactivite Induite dans l'Air de l'Accelerateur de Protons de 300 GeV du CERN*, CERN-LABII-RA-72-5 (European Organisation for Nuclear Research, Geneva).

RINDI, A. (1974). "A spectrometer for measuring charged particles and neutrons," Nucl. Instrum. Methods **116,** 471–475.

RINDI, A. (1982). "Gas bremsstrahlung from electron storage rings," Health Phys. **42**, 187–193.

RINDI, A. and BAARLI, J. (1963). *Scattered Radiation at Large Distance from the CERN 600 MeV Synchrocyclotron*, CERN-DI-HP-19 (European Organisation for Nuclear Research, Geneva).

RINDI, A. and CHARALAMBUS, S. (1967). "Airborne radioactivity produced at high-energy accelerators," Nucl. Instrum. Methods **47**, 227–232.

RINDI, A. and THOMAS, R.H. (1973). "The radiation environment of high-energy accelerators," Ann. Rev. Nucl. Sci. **23**, 315–346.

RINDI, A. and THOMAS, R.H. (1975). "Skyshine—A paper tiger?" Part. Accel. **7**, 23–29.

ROENTGEN, W.C. (1895). "Ueber eine neue art von strahlen. Erste mitt," Sitzungsberichte der Wuerzburger Physik. Medic. Gesellschaft, **137**.

ROGERS, D.W.O. (1979). "Why not to trust a neutron rem-meter," Health Phys. **37**, 735–742.

ROHLOFF, F. and HEINZELMANN, M. (1973). "Influence of detector types and equipment on the sensitivity of Bonner spheres," pages 269 to 277

in *Neutron Monitoring for Radiation Protection Purposes*, Vol. 1, STI/PUB/318 (International Atomic Energy Agency, Vienna).

ROKNI, S.H., KELLER , L.P. and NELSON, W.R. (1996). *Calculation of Muon Background in Electron Accelerators Using the Monte Carlo Computer Program MUCARLO*, SLAC-PUB-7054 (Stanford Linear Accelerator Center, Menlo Park, California).

ROMERO, L.L., HOFFMAN, J.M., FOLTYN, E.M. and BUHL, T.E. (1998). *Operational Comparison of Bubble (Super Heated Drop) Dosimetry with Routine Albedo TLD for a Selected Group of Pu-238 Workers at Los Alamos National Laboratory*, LAUR-98-1055 (Los Alamos National Laboratory, Los Alamos, New Mexico).

ROSSI, B. (1952). *High-Energy Particles* (Prentice Hall, Upper Saddle River, New Jersey).

ROSSI, H.H. (1977). "A proposal for revision of the quality factor," Radiat. Environ. Biophys. **14**, 275–283.

ROSSI, H.H. and FAILLA, G. (1956). "Tissue equivalent ionization chamber," Nucleonics **14**, 32–37.

ROSSI, B. and GREISEN, K. (1941). "Cosmic-ray theory," Rev. Mod. Phys. **13**, 240–309.

ROSSI, H.H. and ROSENZWEIG, W. (1955). "A device for the measurement of dose as a function of specific ionization," Radiology **64**, 404–411.

ROUBAUD, G. and TUYN, J.W.N. (1987). *Determination of the Uranium-235 Content in Uranium Plates Used for CERN Calorimeters*, CERN-TIS-RP-TM-87-28 (European Organisation for Nuclear Research, Geneva).

ROUSSIN, R.W. and SCHMIDT, F.A.R. (1971). "Adjoint Sn calculations of coupled neutron and gamma-ray transport through concrete slabs," Nucl. Eng. Des. **15,** 319–343.

ROUSSIN, R.W., ALSMILLER, R.G., JR. and BARISH, J. (1973). "Calculations of the transport of neutrons and secondary gamma rays through concrete for incident neutrons in the energy range 15 to 75 MeV," Nucl. Eng. Des. **24,** 2.

ROUTTI, J.T. (1969). *High-Energy Neutron Spectroscopy with Activation Detectors, Incorporating New Methods for the Analysis of Ge(Li) Gamma-Ray Spectra and the Solution of Fredholm Integral Equations*, Ph.D. Thesis, UCRL-18514 (Lawrence Berkeley Laboratory, Berkeley, California).

ROUTTI, J.T. and SANDBERG, J.V. (1980a). "General purpose unfolding program LOUI 78 with linear and nonlinear regularizations," Compt. Phys. Comun. **21**, 119–144.

ROUTTI, J.T. and SANDBERG, J.V. (1980b). "Unfolding techniques for activation detector analysis," pages 389 to 407 in *Computer Techniques in Radiation Transport and Dosimetry*, Nelson, W.R. and Jenkins, T.M., Eds. (Plenum Press, New York).

ROUTTI, J.T. and SANDBERG, J.V. (1985). "Unfolding activation and multisphere detector data," Radiat. Prot. Dosim. **10**(1–4), 103–110.

ROUTTI, J.T. and THOMAS, R.H. (1969). "Moyer integrals for estimating shielding of high-energy accelerators," Nucl. Instrum. Methods **76**, 157–163.

RUDSTAM, G. (1966). "Systematics of spallation yields," Z. Naturforsch **21a**, 1027–1041.

SAEZ-VERGARA, J.C. (1999). "Practical aspects on the implementation of LiF:Mg,Cu,P in routine environmental monitoring programmes," Radiat. Prot. Dosim. **85**(1–4), 237–244.

SANNA, R.S. (1973). *Thirty-One Group Response Matrices for the Multi-sphere Neutron Spectrometer Over the Energy Range Thermal to 400 MeV*, HASL-267 (National Technical Information Service, Springfield, Virginia).

SANNA, R. and O'BRIEN, K. (1971). "Monte-Carlo unfolding of neutron spectra," Nucl. Instrum. Methods **91,** 573-576.

SANNA, R.S., HAJNAL, F., MCLAUGHLIN, J.E., GULBIN, J.G. and RYAN, R.M. (1980). *Neutron Measurements Inside PWR Containments*, EML-379 (National Technical Information Service, Springfield, Virginia).

SANNIKOV, A.V., MARES, V. and SCHRAUBE, H. (1997). "High energy response functions of Bonner spectrometers," Radiat. Prot. Dosim. **70**(1–4), 291–294.

SCAG, D.A. (1954). "Discussion of radiographic characteristics of high energy x-rays," Nondestr. Test. **12,** 47.

SCHAEFFER, N.M., Ed. (1973). *Reactor Shielding for Nuclear Engineers*, TID-25921 (National Technical Information Service, Springfield, Virginia).

SCHARF, W. (1986). *Particle Accelerators and Their Uses* (Harwood Academic Publishers, New York).

SCHILTHELM, S.W., DELUCA, P.M., JR., SWANSON, W.P., OTTE, R.A. and PEDLEY, R.T. (1985). *Steady State Radiation Survey Measurements at Aladdin Synchrotron Light Source*, Technical Note SRC-32 (Synchrotron Radiation Center, University of Wisconsin, Stoughton, Wisconsin).

SCHOPPER, H., FASSO, E., GOEBEL, K., HOEFERT, M., RANFT, J. and STEVENSON, G., Eds. (1990). *Landolt-Bornstein: Numerical Data and Functional Relationships in Science and Technology, New Series; Group I, Nuclear and Particle Physics Volume II: Shielding Against High Energy Radiation* (Springer-Verlag, New York).

SDWA (1974). Safe Drinking Water Act. Public Law 93-523, 88 Stat. 1660, as amended (December 16) (U.S. Government Printing Office, Washington).

SEEFRED, R.H. (2000). "A real time neutron monitor for testing the integrity of shielding," pages 267 to 268 in *Proceedings of the 33rd Midyear Topical Meeting of the Health Physics Society* (Health Physics Society, McLean, Virginia).

SELTZER, S.M. and BERGER, M.J. (1982a). "Evaluation of the collision stopping power of elements and compounds for electrons and positrons," Int. J. Appl. Radiat. Isot. **33**, 1189–1218.

SELTZER, S.M. and BERGER, M.J. (1982b). "Procedure for calculating the radiation stopping power for electrons," Int. J. Appl. Radiat. Isot. **33**, 1219–1226.

SELTZER, S.M. and BERGER, M.J. (1985). "Bremsstrahlung spectra from electron interactions with screened atomic nuclei and orbital electron," Nucl. Instrum. Methods **B12**, 95–134.

SESSLER, A.M. (1988). "New particle acceleration techniques," Phys. Today **41**, 26–34.

SHARPE, I. and STAFFORD, G.H. (1951). "The ^{12}C (n, 2n)^{11}C reaction in an anthracene crystal," Proc. Phys. Soc. (London) **A64**, 211–212.

SHAVE, A.J. (1970). *The Extraction of Terbium from Mercury by a Chemical Method,* RP/PN/43 (Rutherford Appleton Laboratory, Oxfordshire, United Kingdom).

SHAW, K.B. (1962). *High Energy Flux Measurements Using Plastic Scintillators*, CERN-DI-HP-6 (European Organisation for Nuclear Research, Geneva).

SHAW, K.B., STEVENSON, G.R. and THOMAS, R.H. (1969). "Evaluation of dose equivalent from neutron energy spectra," Health Phys. **17**, 459–469.

SHEN, S.P. (1964). *Passage of High-Energy Particles in Matter: Nuclear Cascades Induced in Dense Media by 1 and 3 GeV Protons*, BNL-8721 (Brookhaven National Laboratory, Upton, New York).

SHINGLETON, K.L. and LEE, D.W. (1998). "Radioactive sealed source accountability: A risk-based approach," Health Phys. **74**, 435–441.

SHULTIS, J.K. and FAW, R.E. (1996). *Radiation Shielding* (Prentice Hall, Upper Saddle River, New Jersey).

SHULTIS, J.K., FAW, R.E. and KHAN, F.A. (1997a). *SKYNEUT: A Code for Neutron Skyshine Calculations Using the Integral Line-Beam Method*, KSU 9503 (Kansas State University, Manhattan, Kansas).

SHULTIS, J.K., FAW, R.E. and STEDRY, M.H. (1997b). *McSKY: A Hybrid Monte-Carlo Line-Beam Code for Shielded Gamma Skyshine Calculations*, KSU 9501 (Kansas State University, Manhattan, Kansas).

SHULTIS, J.K., FAW , R.E. and BROCKHOFF, C. (1998). *SKYDOSE: A Code for Gamma Skyshine Calculations Using the Integral Line-Beam Method*, KSU 9502 (Kansas State University, Manhattan, Kansas).

SHURE, K., O'BRIEN, J.A. and ROTHENBERG, D.M. (1969). "Neutron dose rate attenuation by iron and lead," Nucl. Sci. Eng. **35**, 371–375.

SILBERBERG, R. and TSAO, C.H. (1972a). "Partial cross sections in high-energy nuclear reactions, and astrophysical applications. I. Targets with Z ≤ 28," Astrophys. J. **25**, 315–333.

SILBERBERG, R. and TSAO, C.H. (1972b). "Partial cross-sections in high energy nuclear reactions, and astrophysical applications. II. Targets heavier than metal," Astrophys J. **25**, 335–368.

SIMPSON, P.W. (1964). *The Measurement of Accelerator Produced Neutron Flux by Activation of Indium, Gold and Cobalt,* NIRL/M/70 (Rutherford Appleton Laboratory, Oxfordshire, United Kingdom).

SIMPSON, P.W. and LAWS, D. (1962). "Addendum" to *Neutron Surveys Around the Rutherford Laboratory 50 MeV Proton Linear Accelerator* (Rutherford Appleton Laboratory, Oxfordshire, United Kingdom).

SINCLAIR, W.K. (1985). "Experimental RBE values of high LET radiations of low doses and the implications for quality factor assignment," Radiat. Prot. Dosim. **13**(1-4), 319–326.

SLADE, D.H., Ed. (1968). *Meteorology and Atomic Energy* (National Technical Information Service, Springfield, Virginia).

SMITH, A.R. (1958). *The Stray Radiation Field of the Bevatron*, UCRL-8377 (Lawrence Berkeley Laboratory, Berkeley, California).

SMITH, A.R. (1961). "A cobalt neutron-flux integrator," Health Phys. **7**, 40–47.

SMITH, A.R. (1965a). *Some Experimental Shielding Studies at the 6.2 BeV Berkeley Bevatron*, CONF-651109 (National Technical Information Service, Springfield, Virginia).

SMITH, A.R. (1965b). "Threshold detector applications to neutron spectroscopy at the Berkeley accelerators," pages 224 to 273 in *Proceedings of First Symposium on Accelerator Dosimetry and Experience*, CONF-651109 (National Technical Information Service, Springfield, Virginia).

SMITH, A.R. (1966). *A Tantalum Fast Neutron Integrator*, UCRL-17051 (Lawrence Berkeley Laboratory, Berkeley, California).

SMITH, A.R. and THOMAS, R.H. (1976). "The production of ^{11}C by the interaction of 375 MeV/amu Ne^{10+} ions with carbon," Nucl. Instrum. Methods **137**, 459–461.

SMITH, A.R., MCCASLIN, J.B. and PICK, M.A. (1964). *Radiation Field Inside a Thick Concrete Shield for 6.2 BeV Incident Protons*, UCRL-11331 (Lawrence Radiation Laboratory, Berkeley, California).

SMITH, A.R., STEPHENS, L.D. and THOMAS, R.H. (1977). "Dosimetry for radiobiological experiments that use energetic heavy ions," Health Phys. **32**, 343–350.

SMITH, A.R., SCHIMMERLING, W., KANSTEIN, L.L., MCCASLIN, J.G. and THOMAS, R.H. (1981). "Neutron flux-density and secondary-particle spectra at the 184-inch synchrocyclotron medical facility," Med. Phys. **8**, 668–676.

SOLON, L.R., Ed. (1957). *Conference on Shielding of High-Energy Accelerators*, TID-7545 (National Technical Information Service, Springfield, Virginia).

SPANIER, J. and GELBARD, E.M. (1969). *Monte Carlo Principles and Neutron Transport Problems* (Addison-Wesley, Reading, Massachusetts).

SSC (1986). Superconducting Super Collider Central Design Group. *Conceptual Design of the Superconducting Super Collider*, SSC-SR-2020, Jackson, J.D., Ed. (Lawrence Berkeley Laboratory, Berkeley, California).

STAPLETON, G.B. and THOMAS, R.H. (1972). "Estimation of the induced radioactivity of the ground water system in the neighborhood of a proposed 300 GeV high energy accelerator situated on a chalk site," Health Phys **23**, 689–699.

STAPLETON, G.B. and THOMAS, R.H. (1989). "Radiation control at the Continuous Electron Beam Accelerator Facility (CEBAF), a new high power CW electron accelerator installation," pages 89 to 92 in *Fourth International Symposium of the Society for Radiation Protection-Theory and Practice*, CONF-8906120 (National Technical Information Service, Springfield, Virginia).

STAPLETON, G.B., O'BRIEN, K. and THOMAS, R.H. (1994). "Accelerator skyshine: Tyger, tyger, burning bright," Part. Accel. **44**, 1–15.

STEPHENS, L.D. and ACETO, H., JR. (1963). "Variation of a fission-neutron fluence and spectrum from a fast reactor measured over large distances,"

pages 535 to 545 in *Neutron Dosimetry, Dosimetry and Standardization*, Vol. 1, STI/PUB/69 (International Atomic Energy Agency, Vienna).

STEPHENS, L.D. and MILLER, A.J. (1969). "Radiation studies at a medium energy accelerator," pages 459 to 485 *Proceedings of the Second International Conference on Accelerator Dosimetry and Experience*, CONF-691101 (National Technical Information Service, Springfield, Virginia).

STEPHENS, L.D. and SMITH, A.R. (1958). *Fast Neutron Surveys Using Indium Foil Activation,* UCRL-8418 (Lawrence Berkeley Laboratory, Berkeley, California).

STEPHENS, L.D., THOMAS, R.H. and THOMAS, S.B. (1975). "Population exposure from high-energy accelerators," Health Phys. **29**, 853–860.

STEPHENS, L.D., THOMAS, R.H. and THOMAS, S.B. (1976). "A model for estimating population exposures due to the operation of high-energy accelerators at the Lawrence Berkeley Laboratory," Health Phys. **30**, 404–407.

STEPHENSON, R.M. (1958). *Introduction to Nuclear Engineering*, 2nd ed. (McGraw-Hill, New York).

STEVENS, A.J. (1992). *Maximum Energy Deposition Densities in the Internal Dump*, AD/RHIC/RD-41 (Brookhaven National Laboratory, Upton, New York).

STEVENS, A.J. (1994a). *Radiation Field in the Vicinity of the Collider Center*, AD/RHIC/RD-77 (Brookhaven National Laboratory, Upton, New York).

STEVENS, A.J. (1994b). *Analysis of Radiation Levels Associated with the Operation of the RHIC Transfer Line*, AD/RHIC/RD-83 (Brookhaven National Laboratory, Upton, New York).

STEVENS, P.N., TRUBEY, D.K., GARRETT, C.W. and SELPH, W.E. (1973). "Radiation transport," in *Reactor Shielding for Nuclear Engineers*, Schaeffer, N.M., Ed., TID-25951 (National Technical Information Service, Springfield, Virginia).

STEVENSON, G.R. (1971). *Evaluation of Neutron Dose Equivalent Around Nimrod,* RP/PN/56 (Rutherford Appleton Laboratory, Oxfordshire, United Kingdom).

STEVENSON, G.R. (1976). *The Radiation Environment of Proton Accelerators and Storage Rings*, CERN-76-04 (European Organisation for Nuclear Research, Geneva).

STEVENSON, G.R. (1979). *A User Guide to the MUSTOP Program*, CERN-HS-RP-TM-79-37 (European Organisation for Nuclear Research, Geneva).

STEVENSON, G.R. (1981). *A Description of the TOMCAT Muon Transport Program*, CERN-HS-RP-IR-81-28 (European Organisation for Nuclear Research, Geneva).

STEVENSON, G.R. (1983). *Dose and Dose Equivalent from Muons*, CERN-TIS-RP-099 (European Organisation for Nuclear Research, Geneva).

STEVENSON, G.R. (1984). "The estimation of dose equivalent from the activation of plastic scintillators," Health Phys. **47**, 837–847.

STEVENSON, G.R. (1986). *Shielding of Extended Targets at Proton Energies of Greater Than 3 GeV*, CERN-TIS-IR-86-04 (European Organisation for Nuclear Research, Geneva).

STEVENSON, G.R. and SQUIER, D.M. (1973). "An experimental study of the attenuation of radiation in tunnels penetrating the shield of an extracted beam of the 7 GeV proton synchrotron NIMROD," Health Phys. **24**, 87–93.

STEVENSON, G.R. and THOMAS, R.H. (1984). "A simple procedure for the estimation of neutron skyshine from proton accelerators," Health Phys. **46**, 115–122.

STEVENSON, G.R., KUEI-LIN, L. and THOMAS, R.H. (1982). "Determination of transverse shielding for proton accelerators using the Moyer model," Health Phys. **43**, 13–29.

STEVENSON, G.R., FASSO, A., SANDBERG, J., REGELBRUGGE, A., BONIFAS, A., MUELLER, A. and NIELSEN, M. (1983). *Measurements of the Dose and Hadron Yield from Copper Targets in 200 GeV/c and 400 GeV/c Extracted Proton Beams. An Atlas of the Results Obtained*, CERN-TIS-RP-112 (European Organisation for Nuclear Research, Geneva).

STEVENSON, G.R., AARNIO, P.A., FASSO, A., RANFT, J., SANDBERG, J.V. and SIEVERS, P. (1986). "Comparison of measurements of angular hadron energy spectra, induced activity, and dose with FLUKA82 calculations," Nucl. Instrum. Methods **A245**, 323–327.

STOKES, R.H., CRANDALL, K.R., STOWALL, J.E. and SWENSON, D.A. (1979). "RF quadrupole beam dynamics," IEEE Trans. Nucl. Sci. **NS-26**, 3469–3471.

STORM, E. and ISRAEL, H.I. (1967). *Photon Cross Sections from 0.001 to 100 MeV for Elements 1 through 100*, LA-3753 (Los Alamos National Laboratory, Los Alamos, New Mexico).

STORM, E. and ISRAEL, H.I. (1970). "Photon cross sections from 1 keV to 100 MeV for elements Z = 1 to Z = 100," Nucl. Data Tables **A7**, 565–681.

STRAKER, E.A., STEVENS, P.N., IRVING, D.C. and CAIN, V.R. (1976). *MORSE-CG, General Purpose Monte-Carlo Multigroup Neutron and Gamma-Ray Transport Code with Combinatorial Geometry*, RSICC Report CCC-203 (Oak Ridge National Laboratory, Oak Ridge, Tennessee).

SUGIYAMA, S. and TOMIMASU, T. (1967). "High energy x-ray albedo for Pb, Cu and duralumin," Nucl. Instrum. Methods **53**, 346–348.

SULLIVAN, A.H. (1982). *Dose Rates from Radioactivity Induced in Thin Foils*, CERN-HS-RP-IR-82-46 (European Organisation for Nuclear Research, Geneva).

SULLIVAN, A.H. (1985). "A method for estimating muon production and penetration through a shield," Nucl. Instrum. Methods **A239,** 197–201.

SULLIVAN, A.H. (1989). "The intensity distribution of secondary particles produced in high-energy proton interactions," Radiat. Prot. Dosim. **27**(3), 189–192.

SULLIVAN, A.H. (1992). *A Guide to Radiation and Radioactivity Levels Near High Energy Particle Accelerators* (Nuclear Technology Publishing, Asford, Kent, United Kingdom).

SULLIVAN, A.H. and BAARLI, J. (1963). *An Ionization Chamber for the Estimation of the Biological Effectiveness of Radiation*, CERN-63-17 (European Organisation for Nuclear Research, Geneva).

SULLIVAN, A.H. and OVERTON, T.R. (1965). "Time variation of the dose-rate from radioactivity induced in high-energy particle accelerators," Health Phys. **11**, 1101–1105.

SWANSON, W.P. (1978). "Calculation of neutron yields released by electrons incident on selected materials," Health Phys. **35**, 353–367.

SWANSON, W.P. (1979). "Improved calculation of photoneutron yields released by incident electron," Health Phys. **37**, 347–358.

SWANSON, W.P. (1985). "Details of calculations: Bremsstrahlung" Appendix B in *Aladdin Upgrade Design Study: Shielding*, Swanson, W.P., DeLuca, P.M., Jr., Otte, R.A. and Schilthelm, S.W., Eds. (National Technical Information Service, Springfield, Virginia).

SWANSON, W.P. (1986). "Photoproduction of tritium in helium cryostats at electron accelerators," Appendix 10 in *Workshop on Radiation Safety*, TN-0058 (Thomas Jefferson National Accelerator Facility, Newport News, Virginia).

SWANSON, W.P. and THOMAS, R.H. (1990). "Dosimetry for radiological protection at high-energy particle accelerators," pages 1 to 161 in *The Dosimetry of Ionizing Radiation, Volume III*, Kase, K.R., Bjarngard, B. and Attix, F.H., Eds. (Academic Press, New York).

SWANSON, W.P., DELUCA, P.M., JR., OTTE, R.A. and SCHILTHELM, S.W., Eds. (1985). *Aladdin Upgrade Design Study*, Synchrotron Radiation Center, University of Wisconsin (National Technical Information Service, Springfield, Virginia).

SYCHEV, B.S., MAL'KOV, V.V., KOMOCHKOV, M.M. and ZAITSEV, L.N. (1966a). "Transmission of high-energy neutrons through iron-water mixture," Atomic Energy **20**, 323–327.

SYCHEV, B.S., MAL'KOV, V.V., KOMOCHKOV, M.M. and ZAITSEV, L.N. (1966b). "Transmission of high-energy neutrons through heavy-weight concrete shielding," Atomic Energy **20**, 355–356.

TAIT, W.H. (1980). *Radiation Detection* (Butterworths, Boston).

TAKA, T. (1984). "Analysis of oil from cyclotron diffusion pumps," Health Phys. **46**, 1311.

TESCH, K. (1966). "Dosisleistung und toleranzflussdichte hochenergetischer elektronen-und gammastrahlen," Nukleonik **8**, 264–266.

TESCH, K. (1970). "Neutron dosimetry in the energy range between 10 and 100 MeV," Nucl. Instrum. Methods **83**, 295–299.

TESCH, K. (1982). "The attenuation of the neutron dose equivalent in a labyrinth through an accelerator shield," Part. Accel. **12**, 169.

TESCH, K. (1983). "Comments on the transverse shielding of proton accelerators," Health Phys. **44**, 79–82.

TESCH, K. (1984). "Measurement of doses between 10^{-2} and 10^8 Gy with glass dosimeters," Radiat. Prot. Dosim. **6**(1–4), 347–349.

TESCH, K. (1985). "A simple estimation of the lateral shielding for proton accelerators in the energy range 50 to 1000 MeV," Radiat. Prot. Dosim. **11**(3), 165–172.

TESCH, K. and DINTER, H. (1986). "Estimation of radiation fields at high energy proton accelerators," Radiat. Prot. Dosim. **15**(2), 89–107.

THERIOT, D., AWSCHALOM, M. and LEE, K. (1971). *Muon Shielding Calculations: Heterogeneous Passive and Active Shields, Applications to Experimental Beams and Areas,* Vol. 2, CERN-71-16 (European Organisation for Nuclear Research, Geneva).

THOMAS, R.H. (1964). *Energy Loss of High Energy Muons*, UCID-10010 (Lawrence Berkeley Laboratory, Berkeley, California).

THOMAS, R.H. (1966). "Radiation hazards of the new generation of accelerators," Nucleonics **24**, 64–69.

THOMAS, R.H. (1970). "The Bevatron," pages 71 to 77 in *Engineering Compendium on Radiation Shielding, Volume 3, Shield Design and Engineering*, Jaeger, R.G., Blizard, E.P., Chilton, A.B., Grotenhuis, M., Hoenig, A., Jaeger, T.A. and Eisenlohr, H.H., Eds. (Springer-Verlag, New York).

THOMAS, R.H. (1972). "Radioactivity in earth induced by high energy electrons," Nucl. Instrum. Methods **102**, 149–155.

THOMAS, R.H. (1974). "Neutron dosimetry at high energy particle accelerators: A review," pages 327 to 353 in *Neutron Monitoring for Radiation Protection Purposes,* Vol. 1, STI/PUB/318 (International Atomic Energy Agency, Vienna)

THOMAS, R.H., Ed. (1976). *Environmental Surveillance Program of the Lawrence Berkeley Laboratory*, LBL-4678 (Lawrence Berkeley Laboratory, Berkeley, California).

THOMAS, R.H. (1978a). *The Radiological Impact of High-Energy Accelerators on the Environment,* LBL-8101 (Lawrence Berkeley Laboratory, Berkeley, California).

THOMAS, R.H. (1978b). *Environmental Radiation from Particle Accelerators*, PUB-300 (Lawrence Berkeley Laboratory, Berkeley, California).

THOMAS, R.H. (1982). "The value of $\overline{w}(E)$ in nitrogen for high-energy ions," Radiat. Res. **90**, 437–440.

THOMAS, R.H. (1985). "Dosimetric aspects," pages 182 to 222 in *Some Issues Important in Developing Basic Radiation Protection Recommendations*, NCRP Annual Meeting Proceedings No. 6 (National Council on Radiation Protection and Measurements, Bethesda, Maryland).

THOMAS, R.H. (1992). "Radiological protection at particle accelerators: An overview," pages 825 to 828 in *Proceedings of the Eighth World Congress of International Radiation Protection Association* (National Technical Information Service, Springfield, Virginia).

THOMAS, R.H. (1998). "Editorial: The seven deadly sins of dosimetry in radiation protection," Radiat. Prot. Dosim. **78**(2), 87–90.

THOMAS, R.H. and MCCASLIN, J.B. (1983). "General shielding for the 20 TeV Hadron Collider Facility: Hadron considerations," in *Report of the 20-TeV Hadron Collider Technical Workshop*, Tigner, M., Ed. (Cornell University, New York).

THOMAS, R.H. and PEREZ-MENDEZ, V., Eds. (1980). *Advances in Radiation Protection and Dosimetry in Medicine* (Plenum Press, New York).

THOMAS, R.H. and RINDI, A. (1979). "Radiological environmental impact of high-energy accelerators," Crit. Rev. Environ. Control **9,** 51–95.

THOMAS, R.H. and STEVENSON, G.R. (1985). "Radiation protection around high energy accelerators," Radiat. Prot. Dosim. **10**(1–4), 283–301.

THOMAS, R.H. and THOMAS, S.V. (1984). "Variance and regression analyses of Moyer model parameter data—a sequel," Health Phys. **46**, 954–957.

THOMAS, R.H., SHAW, K.B., SIMPSON, P.W. and MACEWAN, J.E. (1962). *Neutron Surveys Around the Rutherford Laboratory 50 MeV Proton Linear Accelerator*, NIRL/M/30 (Rutherford Appleton Laboratory, Oxfordshire, United Kingdom).

THOMAS, R.H., LYMAN, J.T. and DE CASTRO, T.M. (1980). "A measurement of the average energy required to create an ion pair in nitrogen by high-energy ions," Radiat. Res. **82**, 1–12.

THOMSON, J.J. (1897). "Cathode rays," Phil. Mag (Series 5) **44**, 293.

THORNGATE, J.H. and GRIFFITH, R.V. (1985). "Neutron spectrometers for radiation monitoring at Lawrence Livermore National Laboratory," Radiat. Prot. Dosim. **10**(1–4), 125–135.

TIGNER, M., Ed. (1983). *Report of the 20-TeV Hadron Collider Technical Workshop* (Cornell University, New York).

TOMMASINO, L. and HARRISON, K.G. (1985). "Damage track detectors for neutron dosimetry: I. Registration and counting methods," Radiat. Prot. Dosim. **10**(1–4), 207–217.

TOMMASINO, L., ZAPPAROLI, G., DJEFFAL, S. and GRIFFITH, R.V. (1984). "A simple and sensitive fast neutron dosimeter using CR-39," pages 141 to 155 in *Proceedings of the 10th DOE Workshop on Personnel Neutron Dosimetry*, PNL-SA-12352, CONF-8308140 (Battelle Pacific Northwest Laboratory, Richland, Washington).

TSAI, Y.S. (1971). *SLAC Users Handbook C.3-1* (Stanford Linear Accelerator Center, Menlo Park, California).

TSAI, Y.S. (1974). "Pair production and bremsstrahlung of charged leptons," Rev. Mod. Phys. **46**, 815–851.

TSAI, Y.S. and WHITIS, V. (1966). "Thick-target bremsstrahlung and target considerations for secondary-particle production by electrons," Phys. Rev. **149**, 1248–1257.

TUYN, J.W.N. (1982). "Radiation protection monitoring around high energy proton accelerators using thermoluminescence dosemeters," Radiat. Prot. Dosim. **2**(2), 69–74.

TUYN, J.W.N., DELTENRE, R., LAMBERET, C. and ROUBAUD, G. (1984). "Some radiation protection aspects of heavy ion acceleration," pages 673 to 676 in *IRPA6: Radiation Risk Protection, Proceedings of the Sixth International Congress, Compacts*, Vol. 2 (International Radiation Protection Association, Fontenay-aux-Roses, Cedex, France).

UNSCEAR (1982). United Nations Scientific Committee on the Effects of Atomic Radiation. *Ionizing Radiation: Sources and Biological Effects, UNSCEAR 1982 Report to the General Assembly*, E.82.IX.8 (United Nations Publications, New York).

URA (1968). Universities Research Association. *National Accelerator Laboratory Design Report* (Universities Research Association, Batavia, Illinois).

UWAMINO, Y., NAKAMURA, T., OHKUBO, T. and HARA, A. (1986). "Measurement and calculation of neutron leakage from a medical electron accelerator," Med. Phys. **13**, 374–384.

VAN GINNEKEN, A. and AWSCHALOM, M. (1974). *Hadronic Cascades, Shielding, Energy Deposition. Volume 1. High Energy Particle Interactions in Large Targets* (Fermi National Accelerator Laboratory, Batavia, Illinois).

VAN GINNEKEN, A., YURISTA, P. and YAMAGUCHI, C. (1987). *Shielding Calculations for Multi-TeV Hadron Colliders*, FERMILAB-FN-447 (Fermi National Accelerator Laboratory, Batavia, Illinois).

VARFOLOMEEV, A.A. and DRABKIN, L.B. (1966). *Calculation of Electromagnetic Showers in Lead with an Initial Energy of 6 GeV*, IAE-1201 [Translation: Oak Ridge National Laboratory Report ORNL-TR-1923] (Institute of Atomic Energy, Moscow).

VARIAN (1975). Varian Associates. *Linatron High-Energy X-Ray Applications* (Varian, Inc., Palo Alto, California).

VOELKEL, U. (1965). *Electronen-Photonen Kaskaden in Blei fuer Primaer Teilchen der Energie 6 GeV*, Internal Note 65/6 (Deutches Elektronen-Synchrotron, Hamburg).

VOELKEL, U. (1967). *A Monte Carlo Calculation of Cascade Showers in Copper Due to Primary Photons of 1 GeV, 3 GeV and 6 GeV, and to a 6 GeV Bremsstrahlung Spectrum*, DESY-67/16 (Deutches Elektronen-Synchrotron, Hamburg).

VYLET, V. (2002). "Response matrix of an extended Bonner sphere system," Nucl. Instrum. Methods **A476**, 26–30.

VYLET, V., LIU, J.C., ROKNI, S.H. and THAI, L.X. (1997a). "Measurements of neutron spectra at the Stanford Linear Accelerator Center," Radiat. Prot. Dosim. **70**(1–4), 425–428.

VYLET, V., LIU, J.C. and ROKNI S. (1997b). "Measurements of non-equilibrium neutron spectra at SSRL," *Proceedings of the Thirtieth Midyear Topical Meeting of the Health Physics Society* (Health Physics Society, McLean, Virginia).

WALLACE, R., MOYER, B.J., PATTERSON, H.W., SMITH, A.R. and STEPHENS, L.D. (1961). "The dosimetry of high-energy neutrons produced by 6.2-GeV protons accelerated in the Bevatron," pages 579 to 588 in *Selected Topics in Radiation Dosimetry*, IAEA Publication STI/PUB/25 (International Atomic Energy Agency, Vienna).

WALZ, D.R. and SEPPI, E.J. (1967). *Radiolysis and Hydrogen Evolution in the A-Beam Dump Radioactive Water System*, SLAC-TN-67-29 (Stanford Linear Accelerator Center, Menlo Park, California).

WARREN, G.J., BUSICK, D.D. and MCCALL, R.C. (1969). "Radioactivity produced and released from water at high energies," in *Proceedings of the Second International Conference on Accelerator Dosimetry and Experience*, CONF-691101 (National Technical Information Service, Springfield, Virginia).

WEINSTEIN, M., HAJNAL, F., MCLAUGHLIN, J.E. and O'BRIEN, K. (1970). *Neutron Dose Equivalents from Multisphere Accelerator-Shield Leakage Spectra,* HASL-223 (National Technical Information Service, Springfield, Virginia).

WESTENDORP, W.F. and CHARLTON, E.E. (1945). "A 100 MeV induction electron accelerator," J. Appl. Phys. **16**, 581.

WIEGAND, C.W. (1949). "High-energy neutron detector," Rev. Sci. Instrum. **19**, 790–792.

WILSON, R.R. (1952). "Monte Carlo study of shower production," Phys. Rev. **86**, 261–269.

WILSON, J.H. and KARCHER, R.H. (1966). *Shielding Effectiveness of Soils Against Initial Radiations*, HN-186 (Holmes and Narver, Inc., Los Angeles).

WINICK, H. (1989). "Storage ring synchrotron radiation sources," Synchrotron Radiat. News **2**, 25.

WINICK, H., Ed. (1994). *Synchrotron Radiation Sources: A Primer* (World Scientific, River Edge, New Jersey).

WOLLENBERG, H.A. and SMITH, A.R. (1969). "Energy and flux determinations of high-energy nucleons," pages 586 to 594 in *Proceedings of the Second International Conference on Accelerator Dosimetry and Experience*, CONF-691101 (National Technical Information Service, Springfield, Virginia).

WOLLENBERG, H.A. and SMITH, A.R. (1973). "Fission track detectors-experiment 12," in *Accelerator Health Physics*, Patterson, H.W. and Thomas, R.H., Eds. (Academic Press, New York).

WOODLEY, R.G. (1970). "Open irradiation facilities for botanical and genetic research," page 89 in *Compendium on Radiation Shielding, Volume 3, Shield Design and Engineering*, Jaeger, R.G., Blizard, E.P., Chilton, A.B., Grotenhuis, M., Hoenig, A., Jaeger, T.A. and Eisenlohr, H.H., Eds. (Springer-Verlag, New York).

WYCKOFF, J.M. and CHILTON, A.B. (1973). "Dose due to practical neutron energy distributions incident on concrete shielding walls," page 694 to 699 in *Proceeding of the Third International Congress of the International Radiation Protection Association*, Snyder, W.S., Ed., CONF-730907 (National Technical Information Center, Springfield, Virginia).

YAGODA, H.J. (1949). *Radioactive Measurements with Nuclear Emulsions* (John Wiley and Sons, New York).

YAMASHITA, M., STEPHENS, L.D. and PATTERSON, H.W. (1966). "Cosmic-ray-produced neutrons at ground level: Neutron production rate and flux distribution," J. Geophys. Res. **71**, 3817–3834.

YOSHIZAWA, N., ISHIBASHI, K. and TAKADA, H. (1995). "Development of high energy transport code HETC-3STEP applicable to the nuclear reaction with incident energies above 20 MeV," J. Nucl. Sci. Technol. **32**, 601–607.

YUDA, T., MASAIKE, A., KUSUMEGI, A., MURATA, Y., OHTA, I. and NISHIMURA, J. (1970). "Electron-induced cascade showers in lead, copper, and aluminum," Nuovo Cimento **65A**, 205–228.

YURISTA, P. and COSSAIRT, J. (1983). *Concrete Shielding Exterior to Iron*, FERMILAB-TM-1204 (National Technical Information Service, Springfield, Virginia).

ZAITSEV, L.N., KOMOCHKOV, M.M. and SYCHEV, B.S. (1971). *Fundamentals of Shielding for Accelerators* (Atomizdat, Moscow).

ZANSTRA, H. (1935). "Ein kurzes verfahren zur Bestimmung des Saettigungsstromes nach der Jaffe'schen Theorie der Kolonnenionisation," Physica **2**, 817–824.

ZAZULA, J.M. (1987). "Derivation of accelerator shielding parameters from adjoint high energy neutron transport calculations," pages 434 to 443 in *Proceedings of the Topical Conference on Theory and Practices in Radiation Protection and Shielding*, Vol. 2, CONF-870405 (American Nuclear Society, LaGrange Park, Illinois).

ZERBY, C.D. and MORAN, H.S. (1962). *Monte-Carlo Calculation of the Three-Dimensional Development of High-Energy Electron-Photon Cascade Showers*, ORNL-3329 (Oak Ridge National Laboratory, Oak Ridge, Tennessee); also published in abbreviated form in J. Appl. Phys. **34**, 2445–2457.

ZERBY, C.D. and MORAN, H.S. (1963). "Monte-Carlo calculation of the three-dimensional development of high-energy electron-photon cascade showers," J. Appl. Phys. **34**, 2445–2457.

ZIELCZYNSKI, M. (1963). "Recombination method for determination of linear energy transfer (LET) of mixed radiation," pages 397 to 404 in *Neutron Dosimetry*, Vol. 2, STI/PUB/69 (International Atomic Energy Agency, Vienna).

ZIELCZYNSKI, M. (1965). "Use of columnar recombination to determine the biological effectiveness of radiation," Nukleonika **7**(1–12), 213–223.

ZIELCZYNSKI, M. (1971). "Integral signal methods for determination of dose equivalent," pages 60 to 74 in *Radiation Dosimetry*, Vol. 2, Miric, I., Ed. (Institute of Nuclear Sciences, Cavtat, Yugoslavia).

ZIELCZYNSKI, M., LEBEDEV, V.N. and SALATSKAYA, M.I. (1965). "Instrument for determination of recommended relative biological effectiveness of radiation," Instrum. Exp. Tech. **6**, 1217–1220.

The NCRP

The National Council on Radiation Protection and Measurements is a nonprofit corporation chartered by Congress in 1964 to:

1. Collect, analyze, develop and disseminate in the public interest information and recommendations about (a) protection against radiation and (b) radiation measurements, quantities and units, particularly those concerned with radiation protection.

2. Provide a means by which organizations concerned with the scientific and related aspects of radiation protection and of radiation quantities, units and measurements may cooperate for effective utilization of their combined resources, and to stimulate the work of such organizations.

3. Develop basic concepts about radiation quantities, units and measurements, about the application of these concepts, and about radiation protection.

4. Cooperate with the International Commission on Radiological Protection, the International Commission on Radiation Units and Measurements, and other national and international organizations, governmental and private, concerned with radiation quantities, units and measurements and with radiation protection.

The Council is the successor to the unincorporated association of scientists known as the National Committee on Radiation Protection and Measurements and was formed to carry on the work begun by the Committee in 1929.

The participants in the Council's work are the Council members and members of scientific and administrative committees. Council members are selected solely on the basis of their scientific expertise and serve as individuals, not as representatives of any particular organization. The scientific committees, composed of experts having detailed knowledge and competence in the particular area of the committee's interest, draft proposed recommendations. These are then submitted to the full membership of the Council for careful review and approval before being published.

The following comprise the current officers and membership of the Council:

Officers

President	Thomas S. Tenforde
Vice President	Kenneth R. Kase
Secretary and Treasurer	William M. Beckner
Assistant Secretary	Michael F. McBride

470

Members

John F. Ahearne	Thomas F. Gesell	David S. Myers
Larry E. Anderson	Ethel S. Gilbert	Bruce A. Napier
Benjamin R. Archer	Joel E. Gray	Carl J. Paperiello
Mary M. Austin-Seymour	Andrew J. Grosovsky	Ronald C. Petersen
Harold L. Beck	Raymond A. Guilmette	R. Julian Preston
Eleanor A. Blakely	Roger W. Harms	Jerome S. Puskin
William F. Blakely	John W. Hirshfeld, Jr.	Allan C.B. Richardson
John D. Boice, Jr.	David G. Hoel	Henry D. Royal
Thomas B. Borak	F. Owen Hoffman	Marvin Rosenstein
Andre Bouville	Roger W. Howell	Lawrence N. Rothenberg
Leslie A. Braby	Kenneth R. Kase	Michael T. Ryan
David Brenner	Ann R. Kennedy	Jonathan M. Samet
Antone L. Brooks	David C. Kocher	Stephen M. Seltzer
Jerrold T. Bushberg	Ritsuko Komaki	Roy E. Shore
John F. Cardella	Amy Kronenberg	Edward A. Sickles
Stephanie K. Carlson	Charles E. Land	David H. Sliney
S.Y. Chen	Susan M. Langhorst	Paul Slovic
Chung-Kwang Chou	Richard W. Leggett	Daniel J. Strom
Kelly L. Classic	Howard L. Liber	Thomas S. Tenforde
Mary E. Clark	James C. Lin	Lawrence W. Townsend
James E. Cleaver	Jill A. Lipoti	Lois B. Travis
J. Donald Cossairt	John B. Little	Robert L. Ullrich
Allen G. Croff	Jay H. Lubin	Richard J. Vetter
Francis A. Cucinotta	C. Douglas Maynard	Daniel E. Wartenberg
Carter Denniston	Claire M. Mays	David A. Weber
Paul M. DeLuca	Cynthia H. McCollough	F. Ward Whicker
John F. Dicello, Jr.	Barbara J. McNeil	Chris G. Whipple
Sarah S. Donaldson	Fred A. Mettler, Jr.	J. Frank Wilson
William P. Dornsife	Charles W. Miller	Susan D. Wiltshire
Stephen A. Feig	Jack Miller	Gayle E. Woloschak
H. Keith Florig	Kenneth L. Miller	Marco A. Zaider
Kenneth R. Foster	William F. Morgan	Pasquale D. Zanzonico
John F. Frazier	John E. Moulder	Marvin C. Ziskin

Honorary Members

Lauriston S. Taylor, *Honorary President*
Warren K. Sinclair, *President Emeritus*; Charles B. Meinhold, *President Emeritus*
S. James Adelstein, *Honorary Vice President*
W. Roger Ney, *Executive Director Emeritus*

Seymour Abrahamson	Patricia W. Durbin	Robert J. Nelsen
Edward L. Alpen	Keith F. Eckerman	Wesley L. Nyborg
Lynn R. Anspaugh	Thomas S. Ely	John W. Poston, Sr.
John A. Auxier	Richard F. Foster	Andrew K. Poznanski
William J. Bair	R.J. Michael Fry	Chester R. Richmond
Bruce B. Boecker	Robert O. Gorson	Genevieve S. Roessler
Victor P. Bond	Arthur W. Guy	William L. Russell
Robert L. Brent	Eric J. Hall	Eugene L. Saenger
Reynold F. Brown	Naomi H. Harley	William J. Schull
Melvin C. Carter	William R. Hendee	J. Newell Stannard
Randall S. Caswell	Donald G. Jacobs	John B. Storer
Frederick P. Cowan	Bernd Kahn	John E. Till
James F. Crow	Roger O. McClellan	Arthur C. Upton
Gerald D. Dodd	Dade W. Moeller	Edward W. Webster
	A. Alan Moghissi	

Lauriston S. Taylor Lecturers

Charles B. Meinhold (2003) *The Evolution of Radiation Protection: From Erythema to Genetic Risks to Risks of Cancer to ?*
R. Julian Preston (2002) *Developing Mechanistic Data for Incorporation into Cancer Risk Assessment: Old Problems and New Approaches*
Wesley L. Nyborg (2001) *Assuring the Safety of Medical Diagnostic Ultrasound*
S. James Adelstein (2000) *Administered Radioactivity: Unde Venimus Quoque Imus*
Naomi H. Harley (1999) *Back to Background*
Eric J. Hall (1998) *From Chimney Sweeps to Astronauts: Cancer Risks in the Workplace*
William J. Bair (1997) *Radionuclides in the Body: Meeting the Challenge!*
Seymour Abrahamson (1996) *70 Years of Radiation Genetics: Fruit Flies, Mice and Humans*
Albrecht Kellerer (1995) *Certainty and Uncertainty in Radiation Protection*
R.J. Michael Fry (1994) *Mice, Myths and Men*
Warren K. Sinclair (1993) *Science, Radiation Protection and the NCRP*
Edward W. Webster (1992) *Dose and Risk in Diagnostic Radiology: How Big? How Little?*
Victor P. Bond (1991) *When is a Dose Not a Dose?*
J. Newell Stannard (1990) *Radiation Protection and the Internal Emitter Saga*
Arthur C. Upton (1989) *Radiobiology and Radiation Protection: The Past Century and Prospects for the Future*
Bo Lindell (1988) *How Safe is Safe Enough?*
Seymour Jablon (1987) *How to be Quantitative about Radiation Risk Estimates*
Herman P. Schwan (1986) *Biological Effects of Non-ionizing Radiations: Cellular Properties and Interactions*
John H. Harley (1985) *Truth (and Beauty) in Radiation Measurements*
Harald H. Rossi (1984) *Limitation and Assessment in Radiation Protection*
Merril Eisenbud (1983) *The Human Environment—Past, Present and Future*
Eugene L. Saenger (1982) *Ethics, Trade-Offs and Medical Radiation*
James F. Crow (1981) *How Well Can We Assess Genetic Risk? Not Very*
Harold O. Wyckoff (1980) *From "Quantity of Radiation" and "Dose" to "Exposure" and "Absorbed Dose"—An Historical Review*
Hymer L. Friedell (1979) *Radiation Protection—Concepts and Trade Offs*
Sir Edward Pochin (1978) *Why be Quantitative about Radiation Risk Estimates?*
Herbert M. Parker (1977) *The Squares of the Natural Numbers in Radiation Protection*

Currently, the following committees are actively engaged in formulating recommendations:

SC 1   Basic Criteria, Epidemiology, Radiobiology and Risk
        SC 1-4 Extrapolation of Risks from Non-Human Experimental Systems to Man
        SC 1-7 Information Needed to Make Radiation Protection Recommendations for Travel Beyond Low-Earth Orbit
        SC 1-8 Risk to Thyroid from Ionizing Radiation
        SC 1-10 Review of Cohen's Radon Research Methods

SC 9   Structural Shielding Design and Evaluation for Medical Use of X Rays and Gamma Rays of Energies Up to 10 MeV
SC 46   Operational Radiation Safety
    SC 46-13 Design of Facilities for Medical Radiation Therapy
    SC 46-16 Radiation Protection in Veterinary Medicine
    SC 46-17 Radiation Protection in Educational Institutions
    SC 57-15 Uranium Risk
    SC 57-17 Radionuclide Dosimetry Models for Wounds
SC 64   Environmental Issues
    SC 64-22 Design of Effective Effluent and Environmental Monitoring Programs
    SC 64-23 Cesium in the Environment
SC 72   Radiation Protection in Mammography
SC 85   Risk of Lung Cancer from Radon
SC 87   Radioactive and Mixed Waste
    SC 87-3 Performance Assessment of Near Surface Radioactive Waste Facilities
    SC 87-5 Risk Management Analysis for Decommissioned Sites
SC 89   Nonionizing Radiation
    SC 89-3 Biological Effects of Extremely Low-Frequency Electric and Magnetic Fields
    SC 89-5 Biological Effects of Radiofrequency Electromagnetic Fields
SC 91   Radiation Protection in Medicine
    SC 91-1 Precautions in the Management of Patients Who Have Received Therapeutic Amounts of Radionuclides
    SC 91-2 Radiation Protection in Dentistry
SC 92   Public Policy and Risk Communication
SC 93   Radiation Measurement and Dosimetry

In recognition of its responsibility to facilitate and stimulate cooperation among organizations concerned with the scientific and related aspects of radiation protection and measurement, the Council has created a category of NCRP Collaborating Organizations. Organizations or groups of organizations that are national or international in scope and are concerned with scientific problems involving radiation quantities, units, measurements and effects, or radiation protection may be admitted to collaborating status by the Council. Collaborating Organizations provide a means by which the NCRP can gain input into its activities from a wider segment of society. At the same time, the relationships with the Collaborating Organizations facilitate wider dissemination of information about the Council's activities, interests and concerns. Collaborating Organizations have the opportunity to comment on draft reports (at the time that these are submitted to the members of the Council). This is intended to capitalize on the fact that

Collaborating Organizations are in an excellent position to both contribute to the identification of what needs to be treated in NCRP reports and to identify problems that might result from proposed recommendations. The present Collaborating Organizations with which the NCRP maintains liaison are as follows:

Agency for Toxic Substances and Disease Registry
American Academy of Dermatology
American Academy of Environmental Engineers
American Academy of Health Physics
American Association of Physicists in Medicine
American College of Medical Physics
American College of Nuclear Physicians
American College of Occupational and Environmental Medicine
American College of Radiology
American Dental Association
American Industrial Hygiene Association
American Institute of Ultrasound in Medicine
American Insurance Services Group
American Medical Association
American Nuclear Society
American Pharmaceutical Association
American Podiatric Medical Association
American Public Health Association
American Radium Society
American Roentgen Ray Society
American Society for Therapeutic Radiology and Oncology
American Society of Emergency Radiology
American Society of Health-System Pharmacists
American Society of Radiologic Technologists
Association of Educators in Radiological Sciences, Inc.
Association of University Radiologists
Bioelectromagnetics Society
Campus Radiation Safety Officers
College of American Pathologists
Conference of Radiation Control Program Directors, Inc.
Council on Radionuclides and Radiopharmaceuticals
Defense Threat Reduction Agency
Electric Power Research Institute
Federal Communications Commission
Federal Emergency Management Agency
Genetics Society of America
Health Physics Society
Institute of Electrical and Electronics Engineers, Inc.
Institute of Nuclear Power Operations
International Brotherhood of Electrical Workers
National Aeronautics and Space Administration
National Association of Environmental Professionals

National Electrical Manufacturers Association
National Institute for Occupational Safety and Health
National Institute of Standards and Technology
Nuclear Energy Institute
Office of Science and Technology Policy
Paper, Allied-Industrial, Chemical and Energy Workers International
  Union
Product Stewardship Institute
Radiation Research Society
Radiological Society of North America
Society for Risk Analysis
Society of Chairmen of Academic Radiology Departments
Society of Nuclear Medicine
Society of Radiologists in Ultrasound
Society of Skeletal Radiology
U.S. Air Force
U.S. Army
U.S. Coast Guard
U.S. Department of Energy
U.S. Department of Housing and Urban Development
U.S. Department of Labor
U.S. Department of Transportation
U.S. Environmental Protection Agency
U.S. Navy
U.S. Nuclear Regulatory Commission
U.S. Public Health Service
Utility Workers Union of America

The NCRP has found its relationships with these organizations to be extremely valuable to continued progress in its program.

Another aspect of the cooperative efforts of the NCRP relates to the Special Liaison relationships established with various governmental organizations that have an interest in radiation protection and measurements. This liaison relationship provides: (1) an opportunity for participating organizations to designate an individual to provide liaison between the organization and the NCRP; (2) that the individual designated will receive copies of draft NCRP reports (at the time that these are submitted to the members of the Council) with an invitation to comment, but not vote; and (3) that new NCRP efforts might be discussed with liaison individuals as appropriate, so that they might have an opportunity to make suggestions on new studies and related matters. The following organizations participate in the Special Liaison Program:

Australian Radiation Laboratory
Bundesamt für Strahlenschutz (Germany)
Canadian Nuclear Safety Commission
Central Laboratory for Radiological Protection (Poland)
China Institute for Radiation Protection

Commisariat à l'Energie Atomique
Commonwealth Scientific Instrumentation Research Organization
  (Australia)
European Commission
Health Council of the Netherlands
International Commission on Non-ionizing Radiation Protection
Japan Radiation Council
Korea Institute of Nuclear Safety
National Radiological Protection Board (United Kingdom)
Russian Scientific Commission on Radiation Protection
South African Forum for Radiation Protection
World Association of Nuclear Operations

The NCRP values highly the participation of these organizations in the Special Liaison Program.

The Council also benefits significantly from the relationships established pursuant to the Corporate Sponsor's Program. The program facilitates the interchange of information and ideas and corporate sponsors provide valuable fiscal support for the Council's program. This developing program currently includes the following Corporate Sponsors:

3M Corporate Health Physics
Amersham Health
Duke Energy Corporation
ICN Biomedicals, Inc.
Landauer, Inc.
Nuclear Energy Institute
Philips Medical Systems
Southern California Edison

The Council's activities are made possible by the voluntary contribution of time and effort by its members and participants and the generous support of the following organizations:

3M Health Physics Services
Agfa Corporation
Alfred P. Sloan Foundation
Alliance of American Insurers
American Academy of Dermatology
American Academy of Health Physics
American Academy of Oral and Maxillofacial Radiology
American Association of Physicists in Medicine
American Cancer Society
American College of Medical Physics
American College of Nuclear Physicians
American College of Occupational and Environmental Medicine
American College of Radiology
American College of Radiology Foundation
American Dental Association

American Healthcare Radiology Administrators
American Industrial Hygiene Association
American Insurance Services Group
American Medical Association
American Nuclear Society
American Osteopathic College of Radiology
American Podiatric Medical Association
American Public Health Association
American Radium Society
American Roentgen Ray Society
American Society of Radiologic Technologists
American Society for Therapeutic Radiology and Oncology
American Veterinary Medical Association
American Veterinary Radiology Society
Association of Educators in Radiological Sciences, Inc.
Association of University Radiologists
Battelle Memorial Institute
Canberra Industries, Inc.
Chem Nuclear Systems
Center for Devices and Radiological Health
College of American Pathologists
Committee on Interagency Radiation Research and Policy
   Coordination
Commonwealth Edison
Commonwealth of Pennsylvania
Consolidated Edison
Consumers Power Company
Council on Radionuclides and Radiopharmaceuticals
Defense Nuclear Agency
Eastman Kodak Company
Edison Electric Institute
Edward Mallinckrodt, Jr. Foundation
EG&G Idaho, Inc.
Electric Power Research Institute
Electromagnetic Energy Association
Federal Emergency Management Agency
Florida Institute of Phosphate Research
Florida Power Corporation
Fuji Medical Systems, U.S.A., Inc.
Genetics Society of America
Health Effects Research Foundation (Japan)
Health Physics Society
Institute of Nuclear Power Operations
James Picker Foundation
Martin Marietta Corporation
Motorola Foundation
National Aeronautics and Space Administration
National Association of Photographic Manufacturers

National Cancer Institute
National Electrical Manufacturers Association
National Institute of Standards and Technology
New York Power Authority
Picker International
Public Service Electric and Gas Company
Radiation Research Society
Radiological Society of North America
Richard Lounsbery Foundation
Sandia National Laboratory
Siemens Medical Systems, Inc.
Society of Nuclear Medicine
Society of Pediatric Radiology
U.S. Department of Energy
U.S. Department of Labor
U.S. Environmental Protection Agency
U.S. Navy
U.S. Nuclear Regulatory Commission
Victoreen, Inc.
Westinghouse Electric Corporation

Initial funds for publication of NCRP reports were provided by a grant from the James Picker Foundation.

The NCRP seeks to promulgate information and recommendations based on leading scientific judgment on matters of radiation protection and measurement and to foster cooperation among organizations concerned with these matters. These efforts are intended to serve the public interest and the Council welcomes comments and suggestions on its reports or activities from those interested in its work.

NCRP Publications

Information on NCRP publications may be obtained from the NCRP website (http://www.ncrp.com) or by telephone (800-229-2652, ext. 25) and fax (301-907-8768). The address is:

NCRP Publications
7910 Woodmont Avenue
Suite 400
Bethesda, MD 20814-3095

Abstracts of NCRP reports published since 1980, abstracts of all NCRP commentaries, and the text of all NCRP statements are available at the NCRP website. Currently available publications are listed below.

NCRP Reports

No.	Title
8	*Control and Removal of Radioactive Contamination in Laboratories* (1951)
22	*Maximum Permissible Body Burdens and Maximum Permissible Concentrations of Radionuclides in Air and in Water for Occupational Exposure* (1959) [includes Addendum 1 issued in August 1963]
25	*Measurement of Absorbed Dose of Neutrons, and of Mixtures of Neutrons and Gamma Rays* (1961)
27	*Stopping Powers for Use with Cavity Chambers* (1961)
30	*Safe Handling of Radioactive Materials* (1964)
32	*Radiation Protection in Educational Institutions* (1966)
35	*Dental X-Ray Protection* (1970)
36	*Radiation Protection in Veterinary Medicine* (1970)
37	*Precautions in the Management of Patients Who Have Received Therapeutic Amounts of Radionuclides* (1970)
38	*Protection Against Neutron Radiation* (1971)
40	*Protection Against Radiation from Brachytherapy Sources* (1972)
41	*Speci cation of Gamma-Ray Brachytherapy Sources* (1974)
42	*Radiological Factors Affecting Decision-Making in a Nuclear Attack* (1974)

479

44 *Krypton-85 in the Atmosphere—Accumulation, Biological Signi cance, and Control Technology* (1975)
46 *Alpha-Emitting Particles in Lungs* (1975)
47 *Tritium Measurement Techniques* (1976)
49 *Structural Shielding Design and Evaluation for Medical Use of X Rays and Gamma Rays of Energies Up to 10 MeV* (1976)
50 *Environmental Radiation Measurements* (1976)
52 *Cesium-137 from the Environment to Man: Metabolism and Dose* (1977)
54 *Medical Radiation Exposure of Pregnant and Potentially Pregnant Women* (1977)
55 *Protection of the Thyroid Gland in the Event of Releases of Radioiodine* (1977)
57 *Instrumentation and Monitoring Methods for Radiation Protection* (1978)
58 *A Handbook of Radioactivity Measurements Procedures*, 2nd ed. (1985)
60 *Physical, Chemical, and Biological Properties of Radiocerium Relevant to Radiation Protection Guidelines* (1978)
61 *Radiation Safety Training Criteria for Industrial Radiography* (1978)
62 *Tritium in the Environment* (1979)
63 *Tritium and Other Radionuclide Labeled Organic Compounds Incorporated in Genetic Material* (1979)
64 *In uence of Dose and Its Distribution in Time on Dose-Response Relationships for Low-LET Radiations* (1980)
65 *Management of Persons Accidentally Contaminated with Radionuclides* (1980)
67 *Radiofrequency Electromagnetic Fields—Properties, Quantities and Units, Biophysical Interaction, and Measurements* (1981)
68 *Radiation Protection in Pediatric Radiology* (1981)
69 *Dosimetry of X-Ray and Gamma-Ray Beams for Radiation Therapy in the Energy Range 10 keV to 50 MeV* (1981)
70 *Nuclear Medicine—Factors In uencing the Choice and Use of Radionuclides in Diagnosis and Therapy* (1982)
72 *Radiation Protection and Measurement for Low-Voltage Neutron Generators* (1983)
73 *Protection in Nuclear Medicine and Ultrasound Diagnostic Procedures in Children* (1983)
74 *Biological Effects of Ultrasound: Mechanisms and Clinical Implications* (1983)
75 *Iodine-129: Evaluation of Releases from Nuclear Power Generation* (1983)
77 *Exposures from the Uranium Series with Emphasis on Radon and Its Daughters* (1984)
78 *Evaluation of Occupational and Environmental Exposures to Radon and Radon Daughters in the United States* (1984)
79 *Neutron Contamination from Medical Electron Accelerators* (1984)

80 *Induction of Thyroid Cancer by Ionizing Radiation* (1985)
81 *Carbon-14 in the Environment* (1985)
82 *SI Units in Radiation Protection and Measurements* (1985)
83 *The Experimental Basis for Absorbed-Dose Calculations in Medical Uses of Radionuclides* (1985)
84 *General Concepts for the Dosimetry of Internally Deposited Radionuclides* (1985)
85 *Mammography—A User's Guide* (1986)
86 *Biological Effects and Exposure Criteria for Radiofrequency Electromagnetic Fields* (1986)
87 *Use of Bioassay Procedures for Assessment of Internal Radionuclide Deposition* (1987)
88 *Radiation Alarms and Access Control Systems* (1986)
89 *Genetic Effects from Internally Deposited Radionuclides* (1987)
90 *Neptunium: Radiation Protection Guidelines* (1988)
92 *Public Radiation Exposure from Nuclear Power Generation in the United States* (1987)
93 *Ionizing Radiation Exposure of the Population of the United States* (1987)
94 *Exposure of the Population in the United States and Canada from Natural Background Radiation* (1987)
95 *Radiation Exposure of the U.S. Population from Consumer Products and Miscellaneous Sources* (1987)
96 *Comparative Carcinogenicity of Ionizing Radiation and Chemicals* (1989)
97 *Measurement of Radon and Radon Daughters in Air* (1988)
99 *Quality Assurance for Diagnostic Imaging* (1988)
100 *Exposure of the U.S. Population from Diagnostic Medical Radiation* (1989)
101 *Exposure of the U.S. Population from Occupational Radiation* (1989)
102 *Medical X-Ray, Electron Beam and Gamma-Ray Protection for Energies Up to 50 MeV (Equipment Design, Performance and Use)* (1989)
103 *Control of Radon in Houses* (1989)
104 *The Relative Biological Effectiveness of Radiations of Different Quality* (1990)
105 *Radiation Protection for Medical and Allied Health Personnel* (1989)
106 *Limit for Exposure to "Hot Particles" on the Skin* (1989)
107 *Implementation of the Principle of As Low As Reasonably Achievable (ALARA) for Medical and Dental Personnel* (1990)
108 *Conceptual Basis for Calculations of Absorbed-Dose Distributions* (1991)
109 *Effects of Ionizing Radiation on Aquatic Organisms* (1991)
110 *Some Aspects of Strontium Radiobiology* (1991)
111 *Developing Radiation Emergency Plans for Academic, Medical or Industrial Facilities* (1991)
112 *Calibration of Survey Instruments Used in Radiation Protection for the Assessment of Ionizing Radiation Fields and Radioactive Surface Contamination* (1991)

113 *Exposure Criteria for Medical Diagnostic Ultrasound: I. Criteria Based on Thermal Mechanisms* (1992)
114 *Maintaining Radiation Protection Records* (1992)
115 *Risk Estimates for Radiation Protection* (1993)
116 *Limitation of Exposure to Ionizing Radiation* (1993)
117 *Research Needs for Radiation Protection* (1993)
118 *Radiation Protection in the Mineral Extraction Industry* (1993)
119 *A Practical Guide to the Determination of Human Exposure to Radiofrequency Fields* (1993)
120 *Dose Control at Nuclear Power Plants* (1994)
121 *Principles and Application of Collective Dose in Radiation Protection* (1995)
122 *Use of Personal Monitors to Estimate Effective Dose Equivalent and Effective Dose to Workers for External Exposure to Low-LET Radiation* (1995)
123 *Screening Models for Releases of Radionuclides to Atmosphere, Surface Water, and Ground* (1996)
124 *Sources and Magnitude of Occupational and Public Exposures from Nuclear Medicine Procedures* (1996)
125 *Deposition, Retention and Dosimetry of Inhaled Radioactive Substances* (1997)
126 *Uncertainties in Fatal Cancer Risk Estimates Used in Radiation Protection* (1997)
127 *Operational Radiation Safety Program* (1998)
128 *Radionuclide Exposure of the Embryo/Fetus* (1998)
129 *Recommended Screening Limits for Contaminated Surface Soil and Review of Factors Relevant to Site-Speci c Studies* (1999)
130 *Biological Effects and Exposure Limits for "Hot Particles"* (1999)
131 *Scienti c Basis for Evaluating the Risks to Populations from Space Applications of Plutonium* (2001)
132 *Radiation Protection Guidance for Activities in Low-Earth Orbit* (2000)
133 *Radiation Protection for Procedures Performed Outside the Radiology Department* (2000)
134 *Operational Radiation Safety Training* (2000)
135 *Liver Cancer Risk from Internally-Deposited Radionuclides* (2001)
136 *Evaluation of the Linear-Nonthreshold Dose-Response Model for Ionizing Radiation* (2001)
137 *Fluence-Based and Microdosimetric Event-Based Methods for Radiation Protection in Space* (2001)
138 *Management of Terrorist Events Involving Radioactive Material* (2001)
139 *Risk-Based Classi cation of Radioactive and Hazardous Chemical Wastes* (2002)
140 *Exposure Criteria for Medical Diagnostic Ultrasound: II. Criteria Based on All Known Mechanisms* (2002)
141 *Managing Potentially Radioactive Scrap Metal* (2002)
142 *Operational Radiation Safety Program for Astronauts in Low-Earth Orbit: A Basic Framework* (2002)
143 *Management Techniques for Laboratories and Other Small Institutional Generators to Minimize Off-Site Disposal of Low-Level Radioactive Waste* (2003)
144 *Radiation Protection for Particle Accelerator Facilities* (2003)

Binders for NCRP reports are available. Two sizes make it possible to collect into small binders the "old series" of reports (NCRP Reports Nos. 8-30) and into large binders the more recent publications (NCRP Reports Nos. 32-144). Each binder will accommodate from five to seven reports. The binders carry the identification "NCRP Reports" and come with label holders which permit the user to attach labels showing the reports contained in each binder.

The following bound sets of NCRP reports are also available:

Volume I. NCRP Reports Nos. 8, 22
Volume II. NCRP Reports Nos. 23, 25, 27, 30
Volume III. NCRP Reports Nos. 32, 35, 36, 37
Volume IV. NCRP Reports Nos. 38, 40, 41
Volume V. NCRP Reports Nos. 42, 44, 46
Volume VI. NCRP Reports Nos. 47, 49, 50, 51
Volume VII. NCRP Reports Nos. 52, 53, 54, 55, 57
Volume VIII. NCRP Report No. 58
Volume IX. NCRP Reports Nos. 59, 60, 61, 62, 63
Volume X. NCRP Reports Nos. 64, 65, 66, 67
Volume XI. NCRP Reports Nos. 68, 69, 70, 71, 72
Volume XII. NCRP Reports Nos. 73, 74, 75, 76
Volume XIII. NCRP Reports Nos. 77, 78, 79, 80
Volume XIV. NCRP Reports Nos. 81, 82, 83, 84, 85
Volume XV. NCRP Reports Nos. 86, 87, 88, 89
Volume XVI. NCRP Reports Nos. 90, 91, 92, 93
Volume XVII. NCRP Reports Nos. 94, 95, 96, 97
Volume XVIII. NCRP Reports Nos. 98, 99, 100
Volume XIX. NCRP Reports Nos. 101, 102, 103, 104
Volume XX. NCRP Reports Nos. 105, 106, 107, 108
Volume XXI. NCRP Reports Nos. 109, 110, 111
Volume XXII. NCRP Reports Nos. 112, 113, 114
Volume XXIII. NCRP Reports Nos. 115, 116, 117, 118
Volume XXIV. NCRP Reports Nos. 119, 120, 121, 122
Volume XXV. NCRP Report No. 123I and 123II
Volume XXVI. NCRP Reports Nos. 124, 125, 126, 127
Volume XXVII. NCRP Reports Nos. 128, 129, 130
Volume XXVIII. NCRP Reports Nos. 131, 132, 133
Volume XXIX. NCRP Reports Nos. 134, 135, 136, 137
Volume XXX. NCRP Reports Nos. 138, 139
Volume XXXI. NCRP Report No. 140

(Titles of the individual reports contained in each volume are given previously.)

NCRP Commentaries

No.	Title
1	*Krypton-85 in the Atmosphere—With Speci c Reference to the Public Health Signi cance of the Proposed Controlled Release at Three Mile Island* (1980)
4	*Guidelines for the Release of Waste Water from Nuclear Facilities with Special Reference to the Public Health Signi cance of the Proposed Release of Treated Waste Waters at Three Mile Island* (1987)
5	*Review of the Publication, Living Without Land lls* (1989)
6	*Radon Exposure of the U.S. Population—Status of the Problem* (1991)
7	*Misadministration of Radioactive Material in Medicine— Scienti c Background* (1991)
8	*Uncertainty in NCRP Screening Models Relating to Atmospheric Transport, Deposition and Uptake by Humans* (1993)
9	*Considerations Regarding the Unintended Radiation Exposure of the Embryo, Fetus or Nursing Child* (1994)
10	*Advising the Public about Radiation Emergencies: A Document for Public Comment* (1994)
11	*Dose Limits for Individuals Who Receive Exposure from Radionuclide Therapy Patients* (1995)
12	*Radiation Exposure and High-Altitude Flight* (1995)
13	*An Introduction to Ef cacy in Diagnostic Radiology and Nuclear Medicine (Justi cation of Medical Radiation Exposure)* (1995)
14	*A Guide for Uncertainty Analysis in Dose and Risk Assessments Related to Environmental Contamination* (1996)
15	*Evaluating the Reliability of Biokinetic and Dosimetric Models and Parameters Used to Assess Individual Doses for Risk Assessment Purposes* (1998)
16	*Screening of Humans for Security Purposes Using Ionizing Radiation Scanning Systems* (2003)
17	*Pulsed Fast Neutron Analysis System Used in Security Surveillance* (2003)
18	*Biological Effects of Modulated Radiofrequency Fields* (2003)

Proceedings of the Annual Meeting

No.	Title
1	*Perceptions of Risk*, Proceedings of the Fifteenth Annual Meeting held on March 14-15, 1979 (including Taylor Lecture No. 3) (1980)
3	*Critical Issues in Setting Radiation Dose Limits*, Proceedings of the Seventeenth Annual Meeting held on April 8-9, 1981 (including Taylor Lecture No. 5) (1982)

4   *Radiation Protection and New Medical Diagnostic Approaches,* Proceedings of the Eighteenth Annual Meeting held on April 6-7, 1982 (including Taylor Lecture No. 6) (1983)

5   *Environmental Radioactivity,* Proceedings of the Nineteenth Annual Meeting held on April 6-7, 1983 (including Taylor Lecture No. 7) (1983)

6   *Some Issues Important in Developing Basic Radiation Protection Recommendations*, Proceedings of the Twentieth Annual Meeting held on April 4-5, 1984 (including Taylor Lecture No. 8) (1985)

7   *Radioactive Waste*, Proceedings of the Twenty-first Annual Meeting held on April 3-4, 1985 (including Taylor Lecture No. 9) (1986)

8   *Nonionizing Electromagnetic Radiations and Ultrasound,* Proceedings of the Twenty-second Annual Meeting held on April 2-3, 1986 (including Taylor Lecture No. 10) (1988)

9   *New Dosimetry at Hiroshima and Nagasaki and Its Implications for Risk Estimates*, Proceedings of the Twenty-third Annual Meeting held on April 8-9, 1987 (including Taylor Lecture No. 11) (1988)

10 *Radon*, Proceedings of the Twenty-fourth Annual Meeting held on March 30-31, 1988 (including Taylor Lecture No. 12) (1989)

11 *Radiation Protection Today—The NCRP at Sixty Years*, Proceedings of the Twenty-fifth Annual Meeting held on April 5-6, 1989 (including Taylor Lecture No. 13) (1990)

12 *Health and Ecological Implications of Radioactively Contaminated Environments*, Proceedings of the Twenty-sixth Annual Meeting held on April 4-5, 1990 (including Taylor Lecture No. 14) (1991)

13 *Genes, Cancer and Radiation Protection,* Proceedings of the Twenty-seventh Annual Meeting held on April 3-4, 1991 (including Taylor Lecture No. 15) (1992)

14 *Radiation Protection in Medicine,* Proceedings of the Twenty-eighth Annual Meeting held on April 1-2, 1992 (including Taylor Lecture No. 16) (1993)

15 *Radiation Science and Societal Decision Making,* Proceedings of the Twenty-ninth Annual Meeting held on April 7-8, 1993 (including Taylor Lecture No. 17) (1994)

16 *Extremely-Low-Frequency Electromagnetic Fields: Issues in Biological Effects and Public Health,* Proceedings of the Thirtieth Annual Meeting held on April 6-7, 1994 (not published).

17 *Environmental Dose Reconstruction and Risk Implications,* Proceedings of the Thirty-first Annual Meeting held on April 12-13, 1995 (including Taylor Lecture No. 19) (1996)

18 *Implications of New Data on Radiation Cancer Risk*, Proceedings of the Thirty-second Annual Meeting held on April 3-4, 1996 (including Taylor Lecture No. 20) (1997)

19 *The Effects of Pre- and Postconception Exposure to Radiation*, Proceedings of the Thirty-third Annual Meeting held on April 2-3, 1997, Teratology **59**, 181–317 (1999)

Lauriston S. Taylor Lectures

No.   Title

11 *How to be Quantitative about Radiation Risk Estimates* by Seymour Jablon (1988) [available also in *New Dosimetry at Hiroshima and Nagasaki and its Implications for Risk Estimates*, see above]

12 *How Safe is Safe Enough?* by Bo Lindell (1988) [available also in *Radon*, see above]

13 *Radiobiology and Radiation Protection: The Past Century and Prospects for the Future* by Arthur C. Upton (1989) [available also in *Radiation Protection Today*, see above]

14 *Radiation Protection and the Internal Emitter Saga* by J. Newell Stannard (1990) [available also in *Health and Ecological Implications of Radioactively Contaminated Environments*, see above]

15 *When is a Dose Not a Dose?* by Victor P. Bond (1992) [available also in *Genes, Cancer and Radiation Protection*, see above]

16 *Dose and Risk in Diagnostic Radiology: How Big? How Little?* by Edward W. Webster (1992) [available also in *Radiation Protection in Medicine*, see above]

17 *Science, Radiation Protection and the NCRP* by Warren K. Sinclair (1993) [available also in *Radiation Science and Societal Decision Making,* see above]

18 *Mice, Myths and Men* by R.J. Michael Fry (1995)

19 *Certainty and Uncertainty in Radiation Research* by Albrecht M. Kellerer (1995). Health Phys. **69**, 446–453.

20 *70 Years of Radiation Genetics: Fruit Flies, Mice and Humans* by Seymour Abrahamson (1996). Health Phys. **71**, 624–633.

21 *Radionuclides in the Body: Meeting the Challenge* by William J. Bair (1997). Health Phys. **73**, 423–432.

22 *From Chimney Sweeps to Astronauts: Cancer Risks in the Work Place* by Eric J. Hall (1998). Health Phys. **75**, 357–366.

23 *Back to Background: Natural Radiation and Radioactivity Exposed* by Naomi H. Harley (2000). Health Phys. **79**, 121–128.

24 *Administered Radioactivity: Unde Venimus Quoque Imus* by S. James Adelstein (2001). Health Phys. **80**, 317–324.

25 *Assuring the Safety of Medical Diagnostic Ultrasound* by Wesley L. Nyborg. Health Phys. **82**, 578–587 (2002)

26 *Developing Mechanistic Data for Incorporation into Cancer and Genetic Risk Assessments: Old Problems and New Approaches* by R. Julian Preston. Health Phys. **85**, 4–12 (2003).

Symposium Proceedings

No.	Title

1 *The Control of Exposure of the Public to Ionizing Radiation in the Event of Accident or Attack*, Proceedings of a Symposium held April 27-29, 1981 (1982)

2 *Radioactive and Mixed Waste—Risk as a Basis for Waste Classi cation,* Proceedings of a Symposium held November 9, 1994 (1995)

3   *Acceptability of Risk from Radiation—Application to Human Space Flight,* Proceedings of a Symposium held May 29, 1996 (1997)
4   *21st Century Biodosimetry: Quantifying the Past and Predicting the Future,* Proceedings of a Symposium held on February 22, 2001, Radiat. Prot. Dosim. **97**, No. 1 (2001)

NCRP Statements

No.   Title

1   "Blood Counts, Statement of the National Committee on Radiation Protection," Radiology **63**, 428 (1954)
2   "Statements on Maximum Permissible Dose from Television Receivers and Maximum Permissible Dose to the Skin of the Whole Body," Am. J. Roentgenol., Radium Ther. and Nucl. Med. **84**, 152 (1960) and Radiology **75**, 122 (1960)
3   *X-Ray Protection Standards for Home Television Receivers, Interim Statement of the National Council on Radiation Protection and Measurements* (1968)
4   *Speci cation of Units of Natural Uranium and Natural Thorium, Statement of the National Council on Radiation Protection and Measurements* (1973)
5   *NCRP Statement on Dose Limit for Neutrons* (1980)
6   *Control of Air Emissions of Radionuclides* (1984)
7   *The Probability That a Particular Malignancy May Have Been Caused by a Speci ed Irradiation* (1992)
8   *The Application of ALARA for Occupational Exposures* (1999)
9   *Extension of the Skin Dose Limit for Hot Particles to Other External Sources of Skin Irradiation* (2001)

Other Documents

The following documents of the NCRP were published outside of the NCRP report, commentary and statement series:

Somatic Radiation Dose for the General Population, Report of the Ad Hoc Committee of the National Council on Radiation Protection and Measurements, 6 May 1959, Science **131** (3399), February 19, 1960, 482–486

Dose Effect Modifying Factors In Radiation Protection, Report of Subcommittee M-4 (Relative Biological Effectiveness) of the National Council on Radiation Protection and Measurements, Report BNL 50073 (T-471) (1967) Brookhaven National Laboratory (National Technical Information Service, Springfield, Virginia)

Index

489